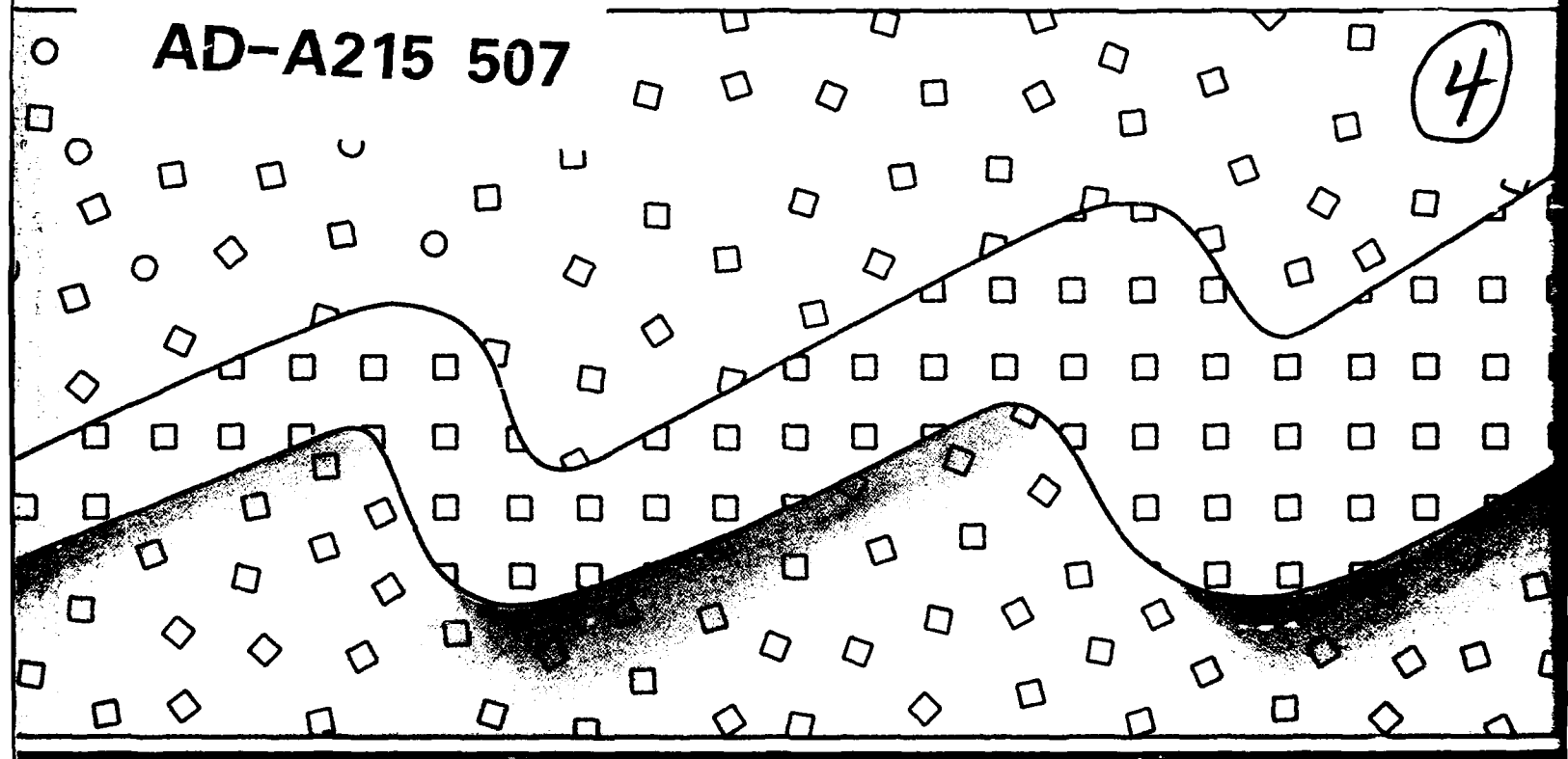


DTIC File Copy

# 'Aha Huliko'a

**AD-A215 507**

(4)



UNCLASSIFIED

SECURITY CLASSIFICATION OF THIS PAGE

## REPORT DOCUMENTATION PAGE

1a REPORT SECURITY CLASSIFICATION Unclassified			1b RESTRICTIVE MARKINGS		
2a SECURITY CLASSIFICATION AUTHORITY			3 DISTRIBUTION/AVAILABILITY OF REPORT Approved for public release; distribution unlimited		
2b DECLASSIFICATION/DOWNGRADING SCHEDULE					
4 PERFORMING ORGANIZATION REPORT NUMBER(S)			5 MONITORING ORGANIZATION REPORT NUMBER(S)		
6a NAME OF PERFORMING ORGANIZATION Hawaii Institute of Geophysics		6b OFFICE SYMBOL (If applicable)	7a NAME OF MONITORING ORGANIZATION Office of Naval Research		
6c ADDRESS (City, State, and ZIP Code) 2525 Correa Road Honolulu, Hawaii 96822			7b ADDRESS (City, State, and ZIP Code) Department of the Navy 800 N. Quincy Street Arlington, Virginia 22217		
8a NAME OF FUNDING/SPONSORING ORGANIZATION		8b OFFICE SYMBOL (If applicable)	9 PROCUREMENT INSTRUMENT IDENTIFICATION NUMBER N00014-89-J-1226		
8c ADDRESS (City, State, and ZIP Code)			10 SOURCE OF FUNDING NUMBERS		
			PROGRAM ELEMENT NO	PROJECT NO 4229013-01	TASK NO WORK UNIT ACCESSION NO
11 TITLE (Include Security Classification) Parameterization of Small-Scale Processes					
12 PERSONAL AUTHOR(S) Müller, Peter and Henderson, Diane (eds.)					
13a TYPE OF REPORT Workshop Proceedings		13b TIME COVERED FROM 12/1/88 TO 1/30/89		14 DATE OF REPORT (Year, Month, Day) September 1989	
15 PAGE COUNT 362					
16 SUPPLEMENTARY NOTATION Proceedings, 'Aha Huliko'a, Hawaiian Winter Workshop, January 1989, Honolulu, Hawaii					
17 COSATI CODES			18 SUBJECT TERMS (Continue on reverse if necessary and identify by block number)		
FIELD	GROUP	SUB-GROUP	general circulation models, eddy resolving models, parameterization, subgrid-scale processes, parameter sensitivity, mixing (diapycnal, isopycnal, interior,		
19 ABSTRACT (Continue on reverse if necessary and identify by block number) These proceedings contain the lectures given at the fifth 'Aha Huliko'a Hawaiian Winter Workshop on the "Parameterization of Small-Scale Processes" and a summary of the workshop, which appeared in EOS (Transactions, American Geophysical Union). The lectures and the summary cover the major aspects and issues of representing subgrid-scale mixing processes in oceanic general circulation models.					
20 DISTRIBUTION/AVAILABILITY OF ABSTRACT <input checked="" type="checkbox"/> UNCLASSIFIED/UNLIMITED <input type="checkbox"/> SAME AS RPT <input type="checkbox"/> DTIC USERS			21 ABSTRACT SECURITY CLASSIFICATION Unclassified		
22a NAME OF RESPONSIBLE INDIVIDUAL			22b TELEPHONE (Include Area Code)		22c OFFICE SYMBOL

18. Subject Terms (continued)

boundary), diffusion, stirring, finestructure, microstructure,  
dissipation

# Parameterization of Small-Scale Processes

PETER MÜLLER  
DIANE HENDERSON  
editors

PROCEEDINGS  
'Aha Huliko'a  
Hawaiian Winter Workshop  
University of Hawaii at Manoa  
January 17-20, 1989

Sponsored by the U.S. Office of Naval Research,  
the Hawaii Institute of Geophysics,  
and the Department of Oceanography, University of Hawaii



Cover, title page: Nancy Hulbirt, Brooks Bays

## FOREWORD

The fifth 'Aha Huliko'a<sup>†</sup> Hawaiian Winter Workshop was held from January 17 to 20, 1989 at the East-West Center in Honolulu, Hawaii. The topic was the "Parameterization of small-scale processes" in oceanic general circulation models.

The workshop brought together numerical modelers, theoreticians and observers to address the question of whether or not observations of small-scale processes are consistent with their parameterization in numerical models. The participants were tasked both to evaluate recent developments and to offer suggestions for future research. Their lectures are published in these proceedings, as submitted in camera-ready form by the authors. The order of the papers loosely follows the agenda of the workshop, covering general circulation models and their sensitivity to diffusion coefficients, observations of mixing in the ocean, laboratory and atmosphere, and discussions of major issues such as interior versus boundary mixing or the rate control of mixing. Also included is a summary of the meeting, which appeared in the Transactions of the American Geophysical Union. The workshop, made possible by a grant from the United States Office of Naval Research, was hosted by the Hawaii Institute of Geophysics and the Department of Oceanography of the University of Hawaii. The excellent facilities of the East-West Center and the capable staff directed by James McMahon contributed greatly to the success of the meeting. The local organization and logistical arrangements were expertly made by Crystal Miles. This proceedings volume came into existence through the help of Nancy Hulbirt and Marilyn Hope Balcerzak, and through the creative and dedicated research of the scientists who gathered in Hawaii and provided the articles that follow.

Peter Müller  
Diane Henderson

Department of Oceanography  
Hawaii Institute of Geophysics  
School of Ocean and Earth Science  
and Technology  
University of Hawaii  
Honolulu, HI 96822

<sup>†</sup>'Aha Huliko'a is a Hawaiian phrase meaning an assembly that seeks into the depth of a matter.

<b>Session For</b>	
GRA&I	<input checked="" type="checkbox"/>
TAB	<input type="checkbox"/>
Announced	<input type="checkbox"/>
Classification	
By	
Distribution/	
<b>Availability Codes</b>	
Dist	Avail and/or Special
A-1	

This work is related to Department of the Navy Grant N-00014-89-J-1226 issued by the Office of Naval Research. The U.S. Government has a royalty-free license throughout the world in all copyrightable material herein.



Participants, 'Aha Huliko'a 1989

Left to right from the front:

Mike Gregg, Trevor McDougall, Mel Briscoe, Dirk Olbers, Peter Rhines, Dave Evans  
 Greg Holloway, Ruediger Gerdes  
 Jim Ledwell, Roy Schmitt, Peter Müller  
 Alan Brandt  
 Anne-Marie Treguier, Chris Garrett, Frank Henyey  
 Jim Moum, Ann Gargett, Dave Fritts, Frank Bryan, Norm McFarlane  
 Fernando Santiago-Mandujano, Niklas Schneider, George Mellor, Joe Fernando  
 Crystal Miles, Ren-Chieh Lien, Eric Kunze, Rob Pinkel  
 Peter Killworth  
 Not pictured: Bill Holland

## TABLE OF CONTENTS

Foreword		iii
Participants		v
Experiences with Various Parameterizations of Sub-Grid Scale Dissipation and Diffusion in Numerical Models of Ocean Circulation	William R. Holland	i
Effects of Variable Diffusivity in the GFDL Model	Ann Gargett, Patrick Cummins and Greg Holloway	11
The Role of Numerical Advection Schemes in General Circulation Models	Ruediger Gerdes	21
On the Parameterisation of Deep Convection in Ocean Models	Peter D. Killworth	59
Boundary Control over the Large-Scale Circulation	Peter Rhines and Parker MacCready	75
A High-Resolution Simulation of the Wind- and Thermohaline-Driven Circulation in the North Atlantic Ocean	Frank O. Bryan and William R. Holland	99
Small-Scale Mixing: A First-Order Process?	Michael C. Gregg	117
Shear and Salt Fingers	R.W. Schmitt, K.L. Polzin, and J.M. Toole	127
Measuring Turbulent Fluxes in the Ocean—The Quest for $K_\rho$	James N. Moum	145
A Strategy for Open Ocean Mixing Experiments	James R. Ledwell	157
Observations of the Vertical Gradient of Isopycnal Vertical Displacement	Robert Pinkel, Jeffrey Sherman, and Steven Anderson	165
Diffusion Parametrizations for the Climatological Circulation of the North Atlantic and the Southern Ocean	Dirk Olbers	181
Turbulent Mixing across Density Interfaces: A Review of Laboratory Experiments and Their Oceanographic Implications	Harindra J.S. Fernando	205

Gravity Wave Saturation, Turbulence, and Diffusion in the Atmosphere: Observations, Theory, and Implications	David C. Fritts	219
Parameterization of Orographic Gravity Wave Drag in Atmospheric General Circulation Models	Norman McFarlane	235
Why Eddy Diffusivity Doesn't Work	Frank S. Henyey	245
Retrospect on Oceanic Boundary Layer Modeling and Second Moment Closure	George L. Mellor	251
The Effect of Internal Waves on Vertical Geostrophic Shear	Eric Kunze and Peter Müller	273
Dianeutral Advection	Trevor J. McDougall	289
Are Diapycnal Fluxes Linked to Lateral Stirring Rates?	Chris Garrett	317
Relating Turbulence Dissipation Measurements to Ocean Mixing	Greg Holloway	329
Parameterization of Small-Scale Processes	Peter Müller and Greg Holloway	341

# EXPERIENCES WITH VARIOUS PARAMETERIZATIONS OF SUB-GRID SCALE DISSIPATION AND DIFFUSION IN NUMERICAL MODELS OF OCEAN CIRCULATION

William R. Holland

National Center for Atmospheric Research, Boulder, Colorado 80307

## ABSTRACT

The parameterization of small spatial scale processes not explicitly included in numerical models of ocean circulation has been at the very heart of ocean model development for two decades. Although computational power has increased dramatically during this time and more and more scales of motion have been included as higher grid resolution has become possible, it is still necessary to determine how sensitive any calculation is to the nature of the sub-grid scale friction and diffusion. This is due to the fact that in many calculations the details of the finest scales of motion and particularly the nature of the dissipation create a sensitivity in the larger scale motions. In this review, we shall look at some of these sensitivity questions and speculate about the future course of development of large scale ocean circulation models.

## INTRODUCTION

There are a number of examples and a variety of earlier experiences that can provide a useful background for a discussion about how any given sub-grid scale parameterization scheme can affect our 'perceptions' about ocean circulation. Among these we shall discuss three: (i) an early attempt to determine the large scale property distributions in an ocean general circulation model; (ii) the development of eddy-resolving models to include explicitly the effects of mesoscale eddies in the redistribution of vorticity, momentum, and various passive and non-passive tracers; and (iii) explicit attempts to carry out detailed sensitivity studies to assess the dependence of results on the eddy viscosities and diffusivities by a direct comparison with certain observations.

The importance of knowing the sub-grid scale details clearly depends upon the problem. For example, local (regional) models may not need to include 'heat diffusion' since such processes might not be important locally for the time scales of interest, while global climate models would need to include such mixing processes (either explicitly or implicitly) in order to close the three dimensional system. On the other hand, it might be necessary to include vertical momentum mixing in a non-eddy-resolving local model in order to account for the effect of turbulent mesoscale eddies in transferring momentum downward (by eddy form drag). Thus the need for and relative importance of a good sub-grid scale parameterization depends upon the problem being examined.

It is probably necessary to distinguish between two kinds of sub-grid phenomena: one that can be 'modeled' with better resolution (and numerics and physics, e.g., mesoscale

eddies) and one that must be 'parameterized' because the phenomenon responsible is too small scale or short-lived to be explicitly included in a larger scale context (e.g., salt fingers or breaking internal waves). However, it should be kept in mind that it still may be useful to build numerical models of the details of such fine scale processes, so-called process models, in order to learn how we might defensibly create a sub-grid scale parameterization of those processes. An interesting example from the atmospheric research community is the case of the parameterization of momentum transfer by gravity wave breaking in atmospheric general circulation models (McFarlane, 1987) and the explicit modeling of such processes in simpler process models, e.g., two dimensional flow over mountains (Durran and Klemp, 1983). See also Fritts (1984), who gives a review of the theory and observations for this situation.

How can we choose a better sub-grid scale parameterization for oceanic general circulation models? One way is to run ever finer resolution models that can explicitly resolve previously parameterized sub-grid scale effects. This has been the direction taken in creating the so-called eddy-resolving models. To accomplish this, modelers have had to increase the horizontal resolution from order 100 kms to 10 kms. Can increased vertical resolution and further increases in horizontal resolution lead to further explicit mixing effects that will make the results of such calculations less sensitive to the sub-grid scale mixing parameterization? As yet, we do not know, but higher resolution numerical experiments do allow us to compare explicit mixing by resolved processes with various parameterizations.

A second approach to 'choosing' a better sub-grid scale parameterization is to mount a concerted search for model fits to observations. These would require exhaustive sensitivity studies in which a 'best' match between a given set of observations and a particular model, with its sub-grid scale parameters, is made. This is typically what has been done (but never exhaustively), for example when the distribution of properties such as temperature, salinity and various passive tracers is said to look 'good' or 'not good' or when the depth of the thermocline is said to be 'too deep' or 'too shallow.' For the eddy problem, Schmitz and Holland (1982, 1986) have examined the correspondence of modeled eddy kinetic energy patterns with 'reality' in order to choose the friction parameters that govern their eddy-resolved model. While this does not give us directly an understanding of the processes behind the sub-grid mixing, it does allow for a better simulation of behavior on the larger scales.

Finally, in choosing a better parameterization, the direct observation of small scale behavior (for example the mixing due to internal wave breaking, double diffusive effects, or convective overturning) is a vital necessity in order to ascertain which mixing processes could be order one in importance and to steer the modeler toward sensible mixing parameterizations.

In order to accomplish such steps, therefore, we need

- Enhanced computer power
- Further model development
- Observational programs directed at the small scales
- Simplified analytical and numerical process 'models'



With such resources, a hierarchy of models with different resolutions and complexity, each investigating the sub-grid scale range of the last, could provide the connecting link that would best be able to tell us how to describe those processes not explicitly calculated in any given model.

## OCEAN GENERAL CIRCULATION MODELS (OGCMs)

Enormous advances have been made in the development and application of sophisticated numerical models of the oceanic circulation in the last two decades. Basin scale models have traditionally come in two varieties—ocean general circulation models (OGCMs), which include much of the detail of the ocean (e.g., realistic coastline, topography, observed winds and surface temperature) but no mesoscale eddies, and eddy-resolving general circulation models (EGCMs), which include higher resolution to allow for important mesoscale processes. The EGCMs are capable of including mesoscale eddies (which contain a large component of the ocean's energy budget) but at the expense of physical and geometrical simplicity. Global ocean models, used for example in coupled climate models, have only been run in the OGCM mode. Recently, with the availability of more and more powerful computers, these two lines have begun to converge, and basin and even global eddy models with high horizontal and vertical resolutions and realistic configurations are being developed (see the article on the WOCE Community Modeling Effort by F. Bryan and W. Holland in this volume).

Both kinds of models, of course, parameterize sub-grid scale processes. The OGCMs must parameterize processes due to mesoscale eddies as well as processes at even finer scales. The EGCMs were developed precisely because this parameterization process is difficult (perhaps even impossible to accomplish in a realistic way) in OGCMs due to the complexity of the turbulent mesoscale mixing processes that occur throughout the global ocean. The OGCM results are sensitive to the details of the sub-grid scale parameterization, as we shall discuss. Whether the EGCMs will also show a similar degree of sensitivity remains to be seen as eddy models with higher and higher resolution are exercised. Most likely the importance of knowing the details of the sub-grid scale processes will depend upon the particular ocean problem being studied.

It is useful to discuss some experiences with OGCMs that illustrate how the large scale circulation can be fundamentally influenced by the choice of the sub-grid scale parameterizations. We shall do this with two examples, one a study of tracer distributions (Holland, 1971) and the other a study that focuses upon thermohaline overturning (Bryan, 1987). Both studies use the well-known model developed at GFDL and show that, even when the form of the sub-grid scale parameterization is kept fixed (Laplacian diffusion of heat and momentum), the circulation depends in an important way upon the size of the diffusion coefficients.

In the first attempt to model tracer distributions in an OGCM, Holland (1971) carried out a single numerical experiment that included, in a simple way, dissolved oxygen and radiocarbon as passive tracers. The steady state, three dimensional circulation, and the distributions of temperature and salinity were predicted—as well as these passive tracers—for a simple sector model of basin-scale flow. The aim was to use the distribution of properties to aid in developing an understanding of the complex, large scale processes found in the model. The results showed some surprising behavior that ran counter to traditional thinking about the three-dimensional circulation, particularly the

abyssal flow as suggested by Stommel (1958). In the model, the meridional circulation consisted of a small region of sinking at high latitudes and an upwelling of water at lower latitudes. In contrast to the assumption by Stommel, however, the upwelling did not occur broadly spread over the oceanic interior but rather mostly in the western boundary current region. An explanation was found (see Veronis, 1975) to lie in the particular choice of the size of the lateral coefficients of momentum and heat diffusion in the model. These were  $A_m = 5 \times 10^4 \text{ m}^2/\text{s}$  and  $A_h = 5 \times 10^3 \text{ m}^2/\text{s}$  respectively. The reader is referred to the above publications for details, but the simple explanation is as follows. When the lateral coefficient of heat diffusion is too large, relative to the lateral coefficient of momentum diffusion (the viscosity), the temperature contrast across the western boundary current, required by the thermal wind relation, can be maintained only by a vertical upwelling of cold water adjacent to the boundary. The three-dimensional circulation conspires to pump much of the water sinking to abyssal depths in high latitudes back to the surface in the boundary layer, leaving little to feed the interior. Numerical experiments were carried out (Holland, unpublished) to confirm that, with a smaller heat diffusivity ( $A_h = 1 \times 10^3 \text{ m}^2/\text{s}$ ), the circulations found in Holland (1971) were modified to have a deep western boundary undercurrent that did feed the interior, where upwelling occurred. Note the possible implications that the presence or lack of such an interior upwelling would have for thermocline maintenance, according to a balance such as that suggested by Munk's Abyssal Recipes (Munk, 1966). Note also that the large diffusion of heat in the western boundary layer was due in part to the fact that the lateral diffusion occurred in that model in constant  $z$  surfaces, and that isopycnal lateral mixing would have very significantly reduced the upwelling in the boundary layer.

The lesson of this work is that the large scale, steady circulation produced in an OGCM can be quite sensitive to the particular choice of diffusion parameters, so much so that very different regimes of flow are possible even with the same physics and same boundary conditions. Following the finding of the results outlined above, almost all subsequent OGCM studies made use of quite large lateral viscosities and as small heat diffusivities as possible on a given grid, to create a flow regime more like the classical one. However, in some sense, we still do not know whether such a boundary upwelling process might be relevant. Ocean modelers and observers must keep these model sensitivities in mind when making inferences from model results. In fact, it clearly spells out the need for extensive sensitivity studies, a costly process that has been little exercised to date.

A second example concerning this sensitivity question is the recent study by Bryan (1987), which explicitly set out to examine the sensitivity of the thermocline structure, meridional overturning, and meridional heat flux to the size of the coefficient of vertical heat diffusion. In this context, a number of numerical experiments were carried out, demonstrating a quite strong dependence of the behavior of the model ocean on this parameter. The amount of meridional (overturning) mass transport increased in amplitude from  $8 \times 10^6$  to  $30 \times 10^6 \text{ m}^3/\text{s}$  as the vertical heat diffusivity was varied from  $0.1 \times 10^{-4}$  to  $2.5 \times 10^{-4} \text{ m}^2/\text{s}$ , exhibiting a  $1/3$  power dependence. The poleward heat transport increased by almost an order of magnitude with the same change. Thus there can be little doubt that, in these OGCM calculations (and perhaps EGCMs as well), the choice of sub-grid scale parameterization is of great importance. Numerical model results (much like observational data) require some presentation of 'error bars,' or better 'sensitivity bars,' to indicate the sensitivity of these results to unknown small scale processes.

## EDDY-RESOLVING GENERAL CIRCULATION MODELS (EGCMs)

Studies of eddy/mean flow interactions in basin-scale, eddy-resolving numerical models have been carried out for more than a decade. Early work focused on the origin of mesoscale eddies as a result of instabilities in the boundary currents and their seaward extensions as well as instabilities of the gyre interior (Holland and Lin, 1975a,b; Holland, 1978). More recent work has begun to refine the picture and examine various theoretical and observational issues. These include studies of the homogenization of potential vorticity (Holland et al., 1984), eddy mixing and gyre equilibration (Rhines and Holland, 1979; Holland and Rhines, 1980), the penetration scale of the Gulf Stream (Holland and Schmitz, 1985), and comparison of model eddy statistics with observations (Schmitz and Holland, 1982, 1986; Holland, 1985).

Such models provide us with two perspectives on the parameterization problem. First, we can explicitly look at the mixing properties in numerical experiments with such models and determine whether any reasonably simple parameterization, in terms of large scale variables, will work. Or will it be necessary to explicitly resolve these mesoscale processes to get a 'right' large scale answer? Second, such models provide a tool by which we can tune our models by seeking a 'best fit' to observations of the mean flow and eddy statistics as we vary the sub-grid viscosity that parameterizes the even finer scale processes not resolved by the eddy resolution.

Using a two layer, quasigeostrophic, wind-driven ocean model with mesoscale resolution, Holland and Rhines (1980) calculated the eddy diffusivities found in a single numerical experiment, by relating the horizontal eddy fluxes of potential vorticity and heat to the mean gradients of these quantities. A horizontal map of the upper layer diffusivity for the eddy mixing of mean potential vorticity showed extremely complicated patterns of positive and negative diffusivities, with positive values as large as  $4000 \text{ m}^2/\text{s}$  and negative values as large as  $-9600 \text{ m}^2/\text{s}$ . The deep ocean was dominated by a relatively simple pattern of large positive diffusivities ( $2800 \text{ m}^2/\text{s}$ ) under the Gulf Stream and small positive values ( $100 \text{ m}^2/\text{s}$ ) in the distant reaches of the gyre. For heat diffusion (at the interface between the two layers), the pattern was also found to be complex, with no simple relationship to the mean temperature field. Maximum negative values of the horizontal heat diffusivity were  $7200 \text{ m}^2/\text{s}$  and maximum positive values were  $4800 \text{ m}^2/\text{s}$ . Such large values confirm the importance of mesoscale processes in determining the large scale flow and distribution of properties, and the complexity of the patterns suggests that it would be difficult to parameterize these processes accurately. Thus, at the present time, it seems unlikely that an accurate, workable parameterization scheme for mesoscale eddies, one that will lead to a correct simulation of large-scale ocean fields, is possible. Fortunately, for the mesoscale problem, computer power is finally reaching such a level that mesoscale resolution can be explicitly included in large-scale models, even global ones.

In a separate study, McWilliams et al. (1978) examined the flows in a quasigeostrophic, partially blocked channel, with application to the role of mesoscale processes in the Antarctic Circumpolar Current. They found that the eddies contributed very importantly to the mean balances by transferring momentum downward from the surface layer, where the momentum is added by the wind, to the deep ocean. If this process were to be parameterized in a coarse resolution (eddyless) model, vertical viscosities as large as  $1 \text{ m}^2/\text{s}$  would be needed, where the eddies were active, throughout the water column. This is several orders of magnitude larger than values typically used in OGCM calculations.

For a simple channel geometry, the horizontal eddy viscosity and the horizontal thermal diffusivity within the mean zonal jet were estimated to be  $-3000 \text{ m}^2/\text{s}$  and  $+900 \text{ m}^2/\text{s}$ , respectively. Again note the importance of negative eddy viscosities, where the eddies serve to sharpen up the mean zonal jet rather than broaden it, a situation not easily parameterized by an eddy viscosity hypothesis.

As mentioned above, another use for eddy-resolving (or indeed any) models is the ability to reproduce observations of the mean and eddy statistics of the ocean. This often involves running a large number of numerical experiments in which the parameterized, sub-grid diffusivities are varied to give a 'best' result. Schmitz and Holland (1982, 1986) and Holland (1985) have been pursuing such an approach and have found the need for quite high vertical and horizontal resolutions in the models. This has led recently to the development of regional models (e.g., for the Gulf Stream) that have horizontal resolutions as high as  $1/8$  degree of latitude and longitude and five layers in the vertical. In such numerical experiments, still underway, it has been found that quite small explicit viscosities (order 25 to  $100 \text{ m}^2/\text{s}$ ) give a best representation of the three dimensional structure of eddy kinetic energy in the Gulf Stream region. Such small values suggest the need for even better resolutions than those used thus far, perhaps as high as  $1/12$  and even  $1/24$  degree for the energetic Gulf Stream.

## DISCUSSION

Advances in computer power are leading to a blurring of the distinction between OGCMs and EGCMs. Instead, a hierarchy of models is being developed that span the range of important scales, each model type focusing upon a given range of space and time scale phenomena. Global, single basin, regional and very high resolution local models all have a role to play. Each can 'handle' only its own scales in a sensibly sized numerical experiment and must parameterize the smaller scales and link to the larger scales through boundary conditions, embedding or other techniques. Global models with eddy resolution (say  $1/3$  degree) will be able to be run for decadal time scales, even centuries, in the decade of the 1990's. But better resolved models (say  $1/6$  or  $1/12$  degree) will be restricted to single basins or even smaller regional domains, if they are intended to be run, for example, for multiyear time scales to examine seasonal or interannual behavior.

It is likely that ocean modeling research for the next few years will involve a continued vigorous expansion of effort and will require much greater computational resources than those currently available. This is due to the fact that models are becoming more sophisticated, model studies will require higher resolution, more investigators are moving toward using large models, and more kinds of problems are being attacked with numerical techniques. We cannot here make the same careful assessment of computational needs carried out in the early 1980's (see the National Research Council publication *An Assessment of Computational Resources Required for Ocean Circulation Modeling*, National Academy of Sciences Press, 1982). However, we can indicate something of the scale of this need by the following examples. During the decade of the 1980's, global ocean models progressively improved their horizontal resolution from 4 degrees latitude/longitude to 2 degrees to 1 degree, with comparable enhancements in vertical resolution. In the next five years, such models will use  $1/3$  degree and  $1/6$  degree resolutions to include the crucial effects of mesoscale processes. For basin scale calculations, the most recent ambitious numerical experiments used  $1/3$  degree resolution

but will progress to 1/6 and 1/12 degree resolutions in the next few years. For regional calculations, model studies currently using 1/6 degree resolution will progress to 1/12 and 1/24 degree resolution and even finer. Each of these factors of two enhancement requires eight times the computer power for a given length of simulation, all other things being equal. Thus it is easy to see that even at the current level of effort, in terms of numbers of people and numbers of projects, the oceanographic modeling community could easily use two orders of magnitude increased computer power over currently available resources. By the mid-1990's, when the satellites are fully functioning and WOCE is in full swing, even greater needs are likely.

Attached is a table, using information taken from the U.S. Planning Document for WOCE Modeling, showing the kinds of computer usage that could effectively occur as substantial new resources become available. Fortunately, the prognosis is good. These are examples, categorized by resolution and domain size, of what can be done in the near future. The table shows the required resources for such experiments, in terms of wall clock hours that can be supplied by prospective new computer systems expected to be available in the next few years (based upon currently available information from computer manufacturers).

As with the mesoscale eddy problem, these higher resolution models will allow for the explicit inclusion of smaller and smaller scale phenomena in any single calculation. However there will still be a need to include even smaller scale effects. By a careful use of the above hierarchy of models, it might be possible to understand how best to do this, but the effectiveness of using mesoscale eddy models as a basis for understanding how to

TABLE 1. Wall clock hours for parallel, vector 25 year integrations.

Machine (Availability)	Number of Processors	Peak, multitasked Vectorized Speed (billions ops/sec)	Horizontal Grid Spacing	Number of Levels	North Atlantic	Global Ocean
Cray X-MP48 (1986)	4	0.94	1/2 x 1/2 1/3 x 2/5	20 20	125 290	1250 2900
ETA 10 8/256G (1988)	8	3.3	1/3 x 1/3	30	60	600
Cray Y-MP832 (1989)	8	2.7	1/4 x 1/4	40	707	7070
Cray 3 (1990)	16	16-32	1/4 x 1/4	40	60-120	600-1200
ETA 30 (1991)	16	30	1/6 x 1/6	40	125	1250
Supercomputing (1992)	64	64-128	1/6 x 1/6 1/2 x 1/2	40 40	50-100 400-800	500-1000 4000-8000
Cray 4 (1992-94)	64	180	1/8 x 1/8	40	83	830

include eddy effects in OGCM-type calculations is unclear. Mesoscale effects are so inhomogeneous and so tenuously connected to the larger scale currents that a simple parameterization seems unlikely. In the end, we probably have to include them explicitly.

What about the scales of mixing (e.g., vertical mixing by breaking internal waves; salt fingers) that are impossible to include explicitly in large scale models? Such effects must be parameterized. Then it seems that only by systematic sensitivity studies that allow us to compare the large scale model results with reality can we begin to choose effective parameters for our parameterization. This will require that the models be realistic in other respects, for example models that use real geometry, bathymetry, and wind and thermohaline forcing, as the test-bed for parameter choices. In addition, this ought to stimulate the collection of certain critical observations that can most definitively pin down these elusive parameters, observations both of the large scale fluxes and of the sub-grid scale fluxes that take place when mixing occurs.

## REFERENCES

- Bryan, F.: 1987. Parameter sensitivity of primitive equation ocean general circulation models. *J. Phys. Oceanogr.*, 17, 970-985.
- Durran, D. and J.B. Klump: 1983. A compressible model for the simulation of moist mountain lee waves. *Mon. Wea. Rev.*, 111, 2341-2361.
- Fritts, D.C.: 1984. Gravity wave saturation in the middle atmosphere: a review of theory and observations. *Geophys. Space Phys.*, 22, 275-308.
- Holland, W.R.: 1971. Ocean Tracer distributions. Part I. A preliminary numerical experiment. *Tellus*, 23, 371-392.
- Holland, W.R.: 1978. The role of mesoscale eddies in the general circulation of the ocean: Numerical experiments using a wind-driven quasigeostrophic model. *J. Phys. Oceanogr.*, 8, 363-392.
- Holland, W.R.: 1985. Simulation of mesoscale ocean variability in midlatitude gyres. Issues in Atmospheric and Oceanic Modeling, Part A, Climate Dynamics, *Advances in Geophysics*, 28, 497-523.
- Holland, W.R. and L.B. Lin: 1975a. On the origin of mesoscale eddies and their contribution to the general circulation of the ocean. I. A preliminary numerical experiment. *J. Phys. Oceanogr.*, 5, 642-657.
- Holland, W.R. and L.B. Lin: 1975b. On the origin of mesoscale eddies and their contribution to the general circulation of the ocean. II. A parameter study. *J. Phys. Oceanogr.*, 5, 658-669.
- Holland, W.R., T. Keffer, and P.B. Rhines: 1984. Dynamics of the oceanic general circulation: the potential vorticity field. *Nature*, 308, 698-705.
- Holland, W.R. and P.B. Rhines: 1980. An example of eddy induced ocean circulation. *J. Phys. Oceanogr.*, 10, 1010-1031.
- Holland, W.R. and W.J. Schmitz, Jr.: 1985. The zonal penetration scale of model midlatitude jets. *J. Phys. Oceanogr.*, 15, 1859-1875.
- McFarlane, N.A.: 1987. The effect of orographically excited gravity wave drag on the general circulation of the lower stratosphere and troposphere. *J. Atmos. Sci.*, 44, 1775-1800.
- McWilliams, J.C., W.R. Holland, and J. Chow: 1978. A description of numerical Antarctic Circumpolar Currents. *Dyn. Atmos. Oceans*, 2, 213-291.
- Munk, W.: 1966. Abyssal recipes. *Deep-Sea Res.*, 13, 707-730.

- Rhines, P.B. and W.R. Holland: 1979. A theoretical discussion of eddy-driven mean flows. *Dyn. Atm. Oceans*, 3, 289-325.
- Schmitz, W.J. Jr. and W.R. Holland: 1982. A preliminary comparison of selected numerical eddy-resolving general circulation experiments with observations. *J. Mar. Res.*, 40, 75-117.
- Schmitz, W.J. Jr. and W.R. Holland: 1986. Observed and modeled mesoscale variability near the Gulf Stream and Kuroshio extension. *J. Geophys. Res.*, 91, 9624-9638.
- Stommel, H.: 1958. The abyssal circulation. *Deep-Sea Res.*, 5, 80-82.
- Veronis, G.: 1975. The role of models in tracer studies. *Numerical Models of Ocean Circulation*. National Academy of Science, Washington, D.C., 133-146.

## EFFECTS OF VARIABLE VERTICAL DIFFUSIVITY IN THE GFDL MODEL

Ann Gargett, Patrick Cummins and Greg Holloway

Institute of Ocean Sciences, Sidney, B.C. V8L 4B2, Canada

## ABSTRACT

The sensitivity of the GFDL ocean model to stratification-dependent diapycnal diffusivity  $K_d \propto N^{-1}$  has been examined. Provided that the value of  $K_d$  in the upper ocean is small (of order  $0.1 \text{ cm}^2 \text{ s}^{-1}$ ), model diagnostics such as meridional heat flux, meridional stream function, and direction of deep interior flow are relatively insensitive to changes in the deep diffusivity. However, use of  $K_d \propto N^{-1}$  significantly changes the model's deep ocean density stratification, suggesting that the specific parameterization chosen for  $K_d$  may be important in problems which are sensitive to deep ocean characteristics.

## INTRODUCTION

The question of the sensitivity of ocean models to the particular form and magnitude of diffusion coefficients is of considerable interest to microscale observers, who naturally wish to know the broader significance of the scales they measure. Moreover it is central to the question of how much faith we should place in present numerical ocean models, particularly those used in the predictive sense required by climate concerns. However, while the perceived need for sensitivity studies is great, it is not clear how best to proceed with them. Models with sufficient horizontal resolution to resolve mesoscale eddies (hence eliminating the need to parameterize the associated stirring and mixing effects) are presently being run but are so computationally intensive that the thermohaline circulation is not calculated (Semtner and Chervin, 1988) and/or does not achieve steady-state (F. Bryan, this volume). Thus it is not yet possible to carry out an exploration of the effects of different parameterizations of  $K_d$ , the diapycnal eddy diffusivity for mass, in eddy-resolving ocean models. If we back off to non-eddy-resolving models which parameterize the effects of eddies on the mass field by a horizontal eddy diffusivity  $K_h$ , assumed to be much larger than  $K_d$ , it becomes possible to carry out extensive investigation of the  $(K_d, K_h)$  parameter space. Unfortunately, there is no guarantee that the observed sensitivity to  $K_d$  in such models will necessarily carry over to eddy-resolving models. In this Catch-22 situation, we are left with the reality that the models presently being coupled with atmospheric models for climate studies are of the non-eddy-resolving variety. Thus it seems necessary to investigate the parameter-space sensitivity of such coarse resolution models.



This paper reports preliminary results of an investigation of the effects of a non-constant  $K_d$  on the widely distributed GFDL model (Cox, 1984). In particular, we examine the stratification-dependent diffusivity proposed by Gargett (1984):  $K_d = a_0 N^{-1}$ , with  $a_0 = 10^{-3} \text{ cm}^2 \text{ s}^{-2}$ . To facilitate comparison with Bryan's (1987) investigation of the effects of different constant values of  $K_d$ , we chose a model configuration which is roughly similar in both physical configuration and forcing.

The standard GFDL code was implemented in a flat-bottomed ocean basin of dimension  $60^\circ$  in both latitude and longitude. Resolution was  $1.5^\circ$  in both horizontal directions, while the 5 km depth range was divided into 15 levels, weighted to provide increased resolution in the upper ocean. The model is forced by a steady double-gyre zonal wind stress, resulting in the standard double-gyre form for the barotropic stream function (Fig. 1). The surface layer T (temperature) and S (salinity) are required to relax to the zonally constant meridional profiles shown in Figure 1, with relaxation time constant of 25 days. Convection is incorporated by setting  $K_d$  to a very large value ( $10^4 \text{ cm}^2 \text{ s}^{-1}$ ) where unstable density gradients were detected (in place of the standard 'convective adjustment' algorithm). The diffusion tensor was rotated to parallel the local isopycnal slope (Redi, 1982), with a view to reducing implicit mixing across isopycnals due to horizontal diffusion  $K_h$  acting in regions of sloping isopycnals: the isopycnal diffusivity  $K_p = 1 \times 10^7 \text{ cm}^2 \text{ s}^{-1}$  in all experiments. Unfortunately, a non-zero value of  $K_h$  must be retained in order to maintain numerical stability, so the experiments are not free

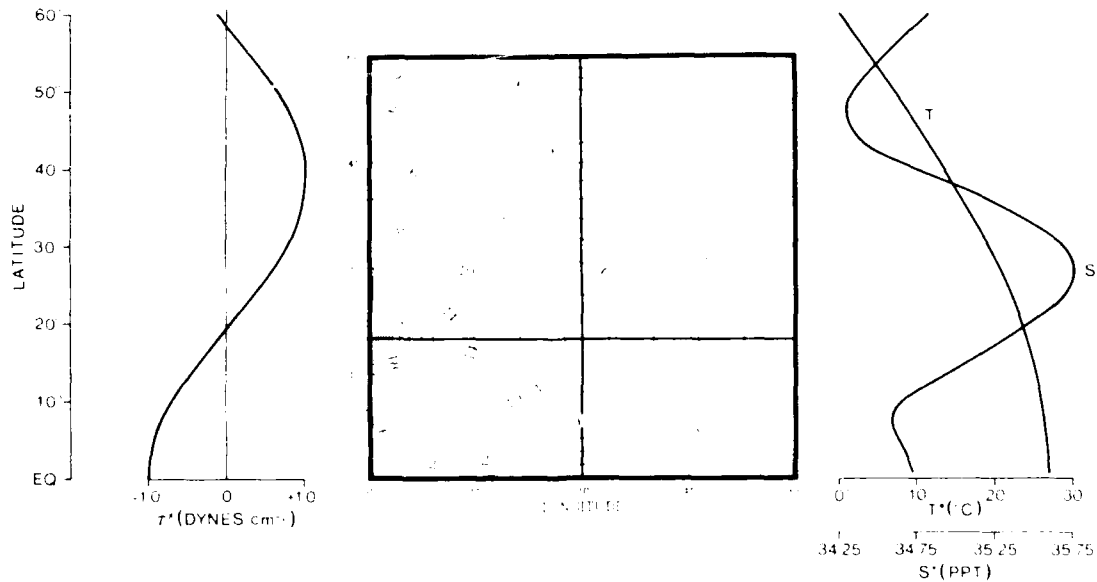


Fig. 1. Two-gyre barotropic stream function resulting from the GFDL model forced by the zonally constant wind stress shown at the left. Thermohaline forcing is by relaxation of surface layer T and S to zonally constant values shown at the right. Heavy lines mark standard sections used to display N-S and E-W variation of model results.

from effects of  $K_h$ . Table 1 gives the values of  $K_d$ ,  $K_\rho$  and  $K_h$  used in the three experiments which are reported here.

Experiment 1 was started from rest and spun up using the accelerated convergence mechanism of Bryan (1984). After  $\sim 1000$  years of equivalent real time (ERT), the system reached a quasi-steady-state, in which the time trends of area-averaged deep ocean temperatures were less than  $(5 \times 10^{-3})^\circ\text{C}/\text{century}$ . Subsequent experiments, initiated from the end state of Exp. 1, took a few hundred years ERT to regain quasi-steady-state after change of  $K_d$ .

Table 1. Values of diapycnal diffusivity  $K_d$ , isopycnal diffusivity  $K_\rho$ , and horizontal diffusivity  $K_h$  used in model runs.  
 $a_0 = 1 \times 10^{-3} \text{ cm}^2\text{s}^{-2}$ .

EXP	$K_d \text{ (cm}^2\text{s}^{-1}\text{)}$	$K_\rho \text{ (cm}^2\text{s}^{-1}\text{)}$	$K_h \text{ (cm}^2\text{s}^{-1}\text{)}$
1	0.2	$1 \times 10^{-7}$	$1 \times 10^{-7}$
2	$a_0 N^{-1}$	$1 \times 10^{-7}$	$1 \times 10^{-7}$
3	$a_0 N^{-1}$	$1 \times 10^{-7}$	$0.33 \times 10^{-7}$

#### EFFECTS OF $K_d = a_0 N^{-1}$

Implementation of the stratification-dependent diapycnal diffusivity  $K_d = a_0 N^{-1}$  was straightforward and produced no problems. The resulting distribution of  $K_d$ , shown in Figure 2, has low values in near-surface ( $z \approx 500\text{m}$ ) mid-ocean regions; with increasing depth (decreasing stabilities), values rise, reaching  $0(1 \text{ cm}^2\text{s}^{-1})$  near 1 km and  $5\text{--}7 \text{ cm}^2\text{s}^{-1}$  in the bottom kilometer of the basin. Even higher values near the northern wall are associated with low stabilities downstream of the region (in the northeast part of the domain) where convection drives the thermohaline cell. These low stabilities are advected south in a western boundary undercurrent, where they are visible in the section at  $20^\circ\text{N}$  (not shown).

Although the field of  $K_d$  varies by nearly two orders of magnitude from the once-canonical value of  $1 \text{ cm}^2\text{s}^{-1}$ , the effect of such variation on the advective heat flux carried by the ocean (a quantity of primary importance to global climate models) is relatively slight. As seen in Figure 3, using  $K_d = a_0 N^{-1}$  (Exp. 2) instead of the constant  $0.2 \text{ cm}^2\text{s}^{-1}$  (Exp. 1) decreases the poleward heat flux by at most  $\sim 30\%$  over the mid-latitude band of interest. The poleward heat flux is calculated by averaging the product  $vT$ , where  $v$  is meridional velocity and  $T$  is temperature, over both the vertical and longitudinal directions. The insensitivity of  $\langle vT \rangle$  occurs because changes in the  $T$  and  $v$  fields tend to partially compensate. Experiment 2 results in an ocean which is slightly colder above the main thermocline ( $z \approx 750\text{m}$ ) and substantially warmer (by  $\sim 0.5^\circ\text{C}$ ) below. By

itself this change would lead to considerably lower poleward heat flux; however it is accompanied by an increase of ~20% in the strength of the main meridional overturning cell (Fig. 4) which nearly compensates for the T field changes.

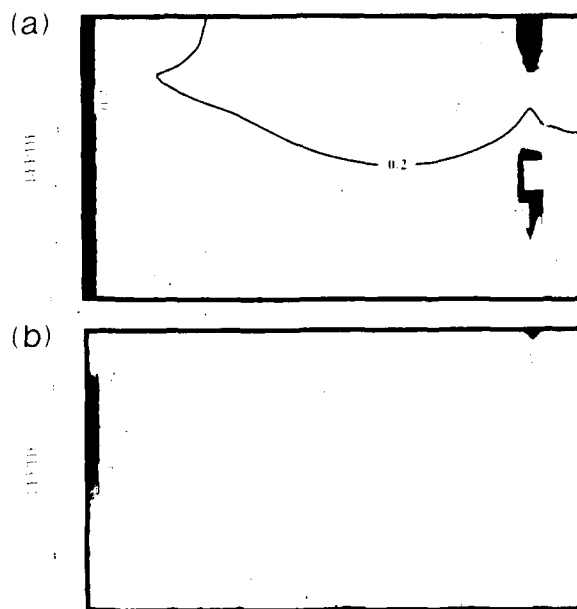


Fig. 2. Field of diapycnal diffusivity  $K_d = a_0 N^{-1}$  associated with the steady state of Experiment 2 (Table 1): units are  $(\text{cm}^2 \text{s}^{-1})$ . (a) Expansion of upper 1000m. (b) Entire water column.

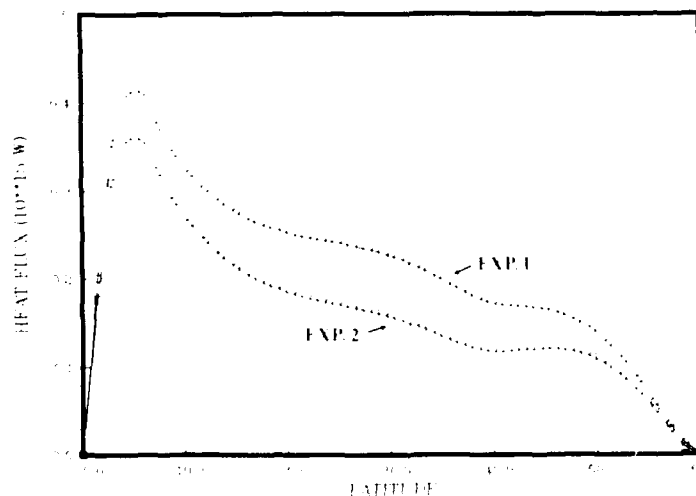


Fig. 3. Over mid-latitudes, implementation of  $K_d = a_0 N^{-1}$  (Exp. 2) yields a poleward heat flux approximately 30% lower than that associated with constant  $K_d = 0.2 \text{ cm}^2 \text{s}^{-1}$  (Exp. 1).

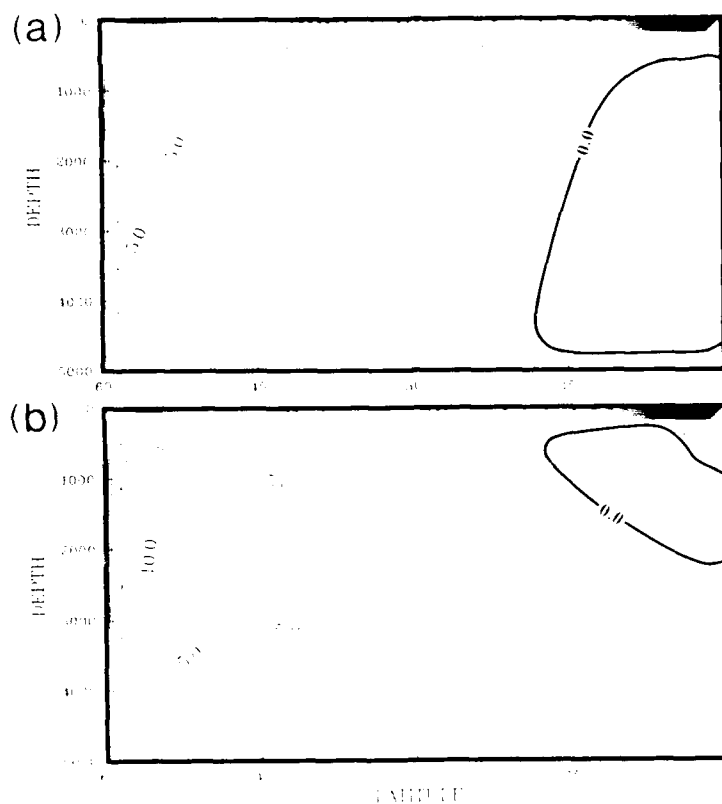


Fig. 4. The zonally averaged meridional overturning stream functions for (a) Exp. 1 and (b) Exp. 2. Dashed contours indicate clockwise flow, solid contours counterclockwise flow: contour interval is  $2.5 \times 10^6 \text{ m}^3 \text{ s}^{-1}$ .

Another point of interest is whether the meridional flow in mid-gyre remains poleward (Stommel and Arons, 1950) or whether a diapycnal diffusivity proportional to  $N^{-1}$  reverses the direction of this flow, a possibility suggested in Gargett (1984). The answer is that the meridional flow of Exp. 2 not only remains poleward in direction, but increases in magnitude relative to Exp. 1, as seen in Figure 5. While the strong surface flows of Exp. 2 (Fig. 5(b)) are comparable to those in Exp. 1 (Fig. 5(a)), the region of significant poleward flow in the deep ocean moves out from the western boundary and extends throughout the deep interior of the gyre. The vertical boundary between the northward-flowing surface western boundary current and the western boundary undercurrent (WBUC) deepens by  $\sim 500\text{m}$  and the region of equatorward flow associated with the WBUC extends much further into the interior (more than halfway across the domain in the near bottom layers). Why does the equatorward interior flow derived by Gargett (1984) not emerge in the model? Recall that the conditions which led to equatorward flow were geostrophy of the velocity field and a vertical advection/diffusion balance for the density field. It is the latter assumption which fails. While the computed model velocity fields obey geostrophy (within 20%) nearly everywhere in the domain, the density field does not achieve steady-state by balancing  $w\bar{\rho}_z$  with  $(K_d\bar{\rho}_z)_z$  in the deep interior.

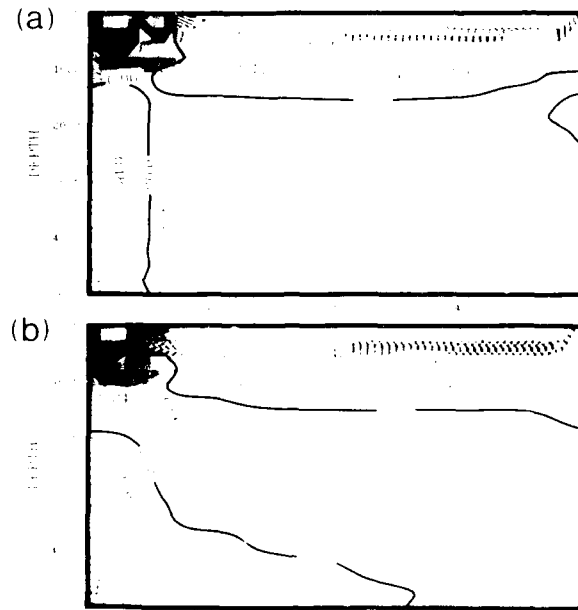


Fig. 5. E-W sections of meridional velocity within the subtropical gyre (20°N) for (a) Exp. 1 and (b) Exp. 2: contour interval is  $0.003 \text{ cm s}^{-1}$ . In both experiments, deep interior flow is poleward.

The preceding comparisons between Experiments 1 and 2 lead to the conclusion that a stratification-dependent diffusivity of the form suggested by Gargett (1984) doesn't matter much to the poleward heat flux carried by the model ocean, to the meridional overturning cell, or to the meridional sense of the deep circulation. ("Much" is of course a relative term: to some applications, 30% change in, say, poleward heat flux, might be important.) Are we thus able to conclude that the possible depth or stratification dependence of  $K_d$  need not concern basin-scale modellers, provided only that the constant value used is chosen to produce an appropriate thermocline depth? Insofar as we are interested in the deep ocean (of major importance to the problem of the ocean as  $\text{CO}_2$  sink, for example), the answer to this question is no. One of the major shortcomings of the GFDL model with constant  $K_d$  is the vertical uniformity of the deep water density field. Figure 6(a) shows the E-W section across the "subtropical gyre" at 20°N for Exp. 1. Below ~2 km depth, the vertical density gradient has a nearly uniform low value. A N-S section at 30° longitude (Fig. 6(b) shows that weak uniform deep gradients occur throughout the domain. In contrast, Exp. 2 yields a significantly more strongly stratified deep ocean (Fig. 6(c) and 6(d)). Both this stronger stratification and higher deep water temperatures (previously mentioned in discussing the heat flux) move Exp. 2 in the direction of the real ocean, suggesting that an inappropriate representation of diapycnal processes is at least partially responsible for the incorrect deep ocean stratification produced by the GFDL model.

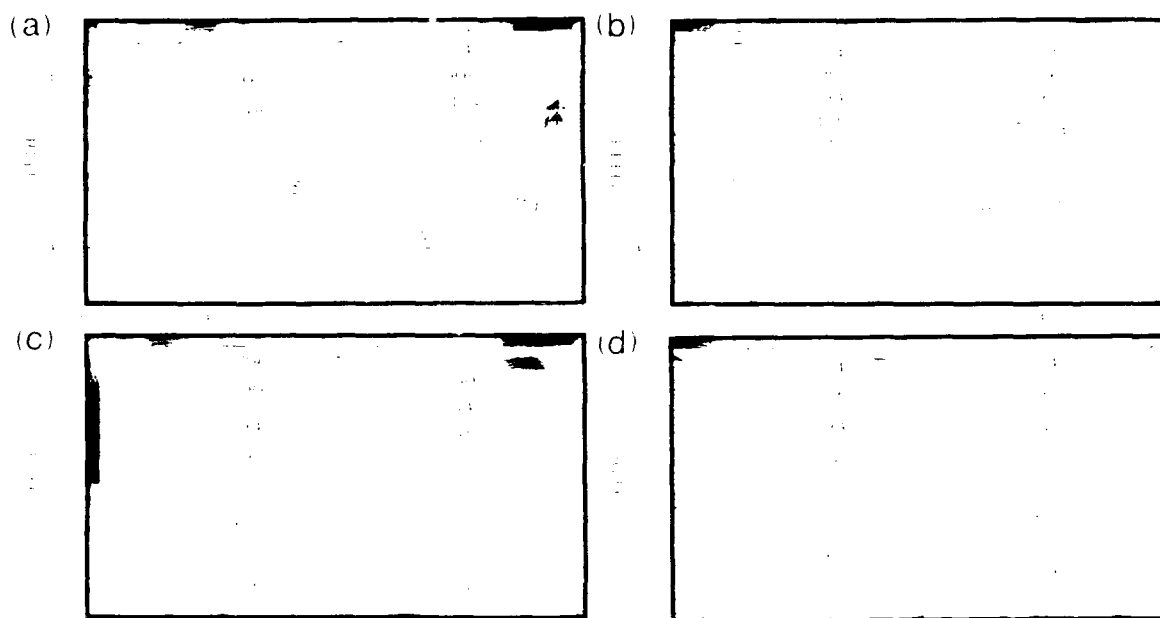


Fig. 6. Contours of  $\log [-\rho_z/\rho_o \text{ (m}^{-1}\text{)}]$ , where  $\rho_z$  is the vertical density gradient and  $\rho_o$  a reference density, show significant differences in intermediate and deep water stabilities between Exp. 1 ((a) and (b)) and Exp. 2 ((c) and (d)).

#### THE EFFECTS OF $K_h$ : IMPLICIT DIFFUSION

An unexpected benefit of implementing  $K_d = a_o N^{-1}$  was a dramatic reduction in unwanted implicit diapycnal diffusion associated with  $K_h \neq 0$ . As mentioned previously, a non-zero value of  $K_h$  yields diapycnal mixing in the presence of sloping isopycnals. A measure of the relative importance of this implicit diffusivity to that explicitly included in the model is given by a normalized diffusivity diagnostic defined as

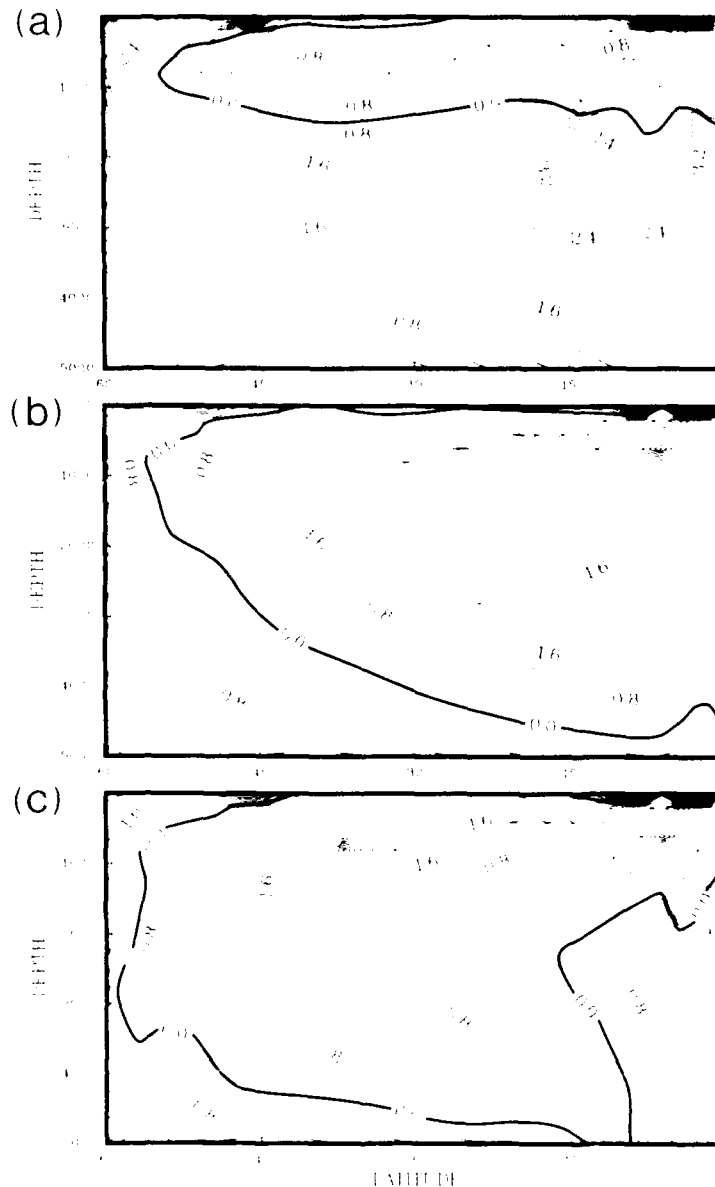
$$\text{NDD} = \frac{K_h m^2}{K_d} = \frac{K_h}{K_d} \frac{\nabla_h \rho \cdot \nabla_h \rho}{\rho_z^2},$$

where  $K_h$ ,  $K_d$  are the explicit horizontal and diapycnal diffusivities and  $m$  is the isopycnal slope (referenced to local pressure). N/S sections of the logarithm of NDD (Fig. 7(a) and (b)) show enormous changes between Exps. 1 and 2, particularly in the 1-4 km depth range where the explicit diapycnal fluxes of Exp. 1 are dominated by implicit diffusion.

In Exp. 1, only the upper kilometer of the subtropical gyre has diapycnal fluxes determined by the explicit diffusivity ( $\log \text{NDD} < 0$ ,  $\text{NDD} < 1$ ), while in Exp. 2 much of the intermediate and deep water is effectively free from implicit diffusion. While some of the observed change in NDD results from increased  $K_d$  at depth in Exp. 2, this can account for only about one order of magnitude. The rest of the change (approximately three

orders of magnitude at some depths) results from decreases in  $m^2$ , the mean square isopycnal slope.

Encouraged by the decrease in implicit diffusion in Exp. 2, we attempted a further reduction of implicit diffusion effects by decreasing  $K_h$  (to  $0.33 \times 10^7 \text{ cm}^2 \text{ s}^{-1}$ ) in Exp. 3. The model retained stability at this lower value of  $K_h$ , but the result was not a straightforward reduction in implicit diffusion. Instead (Fig. 7(c)), while Exp. 3 shows lower NDD



near the northern boundary, in much of the mid-depth interior, particularly near the equator, NDD has actually increased. What apparently happens is that reduction of  $K_h$  reduces the rate at which  $\nabla_h \rho$  is removed, thus increasing  $m^2$ ; the increase in  $m^2$  is larger than the decrease in explicit  $K_h$ , hence NDD increases. While readily "understood" in this way, such a result is counterintuitive to those (most?) of us whose intuition has developed around linear systems, and illustrates the complexity of "the" sensitivity problem in nonlinear systems. Determining "the" sensitivity of any ocean model to sub-grid-scale processes is immensely complicated by the degree of interdependence between horizontal and vertical (or isopycnal and diapycnal) sub-grid-scale parameterizations.

Moreover, considering the range of possible parameterizations of just diapycnal fluxes, it seems unlikely that it will be possible to determine appropriate forms of these fluxes by using observables to constrain the models. The problem is that the same model may give very much the same result using very different values and/or forms for the various diffusivities involved. As an example, Figure 8 is a comparison of the meridional overturning stream function resulting from our Exp. 3 (with  $K_d = a_0 N^{-1}$ ,  $K_\rho = K_h = 0.33 \times 10^7 \text{ cm}^2 \text{ s}^{-1}$ ) and one of Bryan's (1987) runs (with  $K_v = 0.1 \text{ cm}^2 \text{ s}^{-1}$ ,  $K_h = 1 \times 10^7 \text{ cm}^2 \text{ s}^{-1}$  and  $K_\rho = 0$ ): allowing for the different meridional extent of the basins, the two studies give results

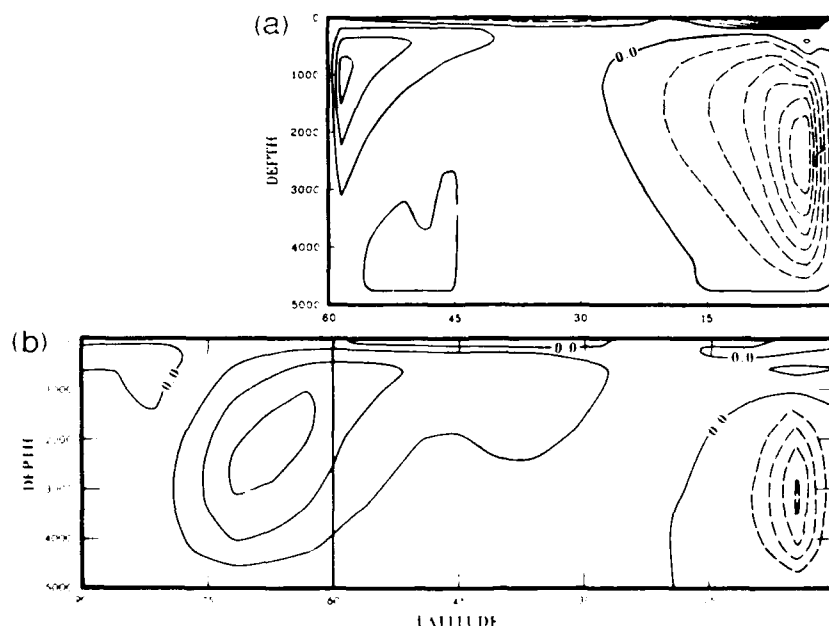


Fig. 8. Zonally-averaged meridional overturning stream function for (a) Exp. 3 of this work and (b) Bryan's (1987) Exp. 2. The contour interval is  $2.5 \times 10^6 \text{ m}^3 \text{ s}^{-1}$ ; dashed line is clockwise, solid line is counter-clockwise flow. The similarity of the two results (apart from the difference in meridional extent of the domain) illustrates that the GFDL model can produce similar results with very different choices for the diffusivities used to parameterize mixing.



which are remarkably similar in both form and magnitude. If we are to learn anything about appropriate parameterizations from models, it is clearly necessary to look for diagnostic fields which are more sensitive to these parameterizations than, for example, the meridional overturning stream function (or the meridional heat flux) and/or to carry various passive tracers as well as the active tracers T and S. It also seems clear that any contribution which the observational community can make as to appropriate forms of diffusivities/fluxes will provide welcome restrictions for model sensitivity studies.

#### REFERENCES

- Bryan, F.: 1987. On the parameter sensitivity of primitive equation ocean general circulation models. *J. Phys. Oceanogr.*, 17, 970-985.
- Bryan, K.: 1984. Accelerating the convergence to equilibrium of ocean-climate models. *J. Phys. Oceanogr.*, 14, 666-673.
- Cox, M.: 1984. A primitive equation, 3-dimensional model of the ocean. GFDL Group Tech. Rep. No. 1, Geophysical Fluid Dynamics Laboratory, Princeton University, Princeton, N.Y.
- Gargett, A.E.: 1984. Vertical eddy diffusivity in the ocean interior. *J. Mar. Res.*, 42, 359-393.
- Redi, M.H.: 1982. Oceanic isopycnal mixing by coordinate rotation. *J. Phys. Oceanogr.*, 12, 1154-1158.
- Semtner, A.J., Jr. and R.M. Chervin: 1988. A simulation of the global ocean circulation with resolved eddies. *J. Geophys. Res.*, 93(C12), 15502-15522.
- Stommel, H. and A.B. Arons: 1960. On the abyssal circulation of the world ocean - I Stationary planetary flow patterns on a sphere. *Deep Sea Res.*, 6, 140-154.

## THE ROLE OF NUMERICAL ADVECTION SCHEMES IN GENERAL CIRCULATION MODELS

Ruediger Gerdes

Geophysical Fluid Dynamics Laboratory, Princeton University  
Princeton, New Jersey 08540

### ABSTRACT

Numerical advection schemes are compared in the context of primitive equation models of the Atlantic circulation at two different horizontal resolutions. The results are interpreted in terms of the effective vertical and horizontal mixing rates. For low horizontal resolution the discussion concentrates on large scale properties like zonally integrated meridional transports and water mass distributions. For higher horizontal resolution the circulation and tracer distributions on the gyre scale are examined in more detail.

### INTRODUCTION

This paper discusses numerical models of basin scale phenomena as they are used for studying climate dynamics, the formation and spreading of the major water masses, and the simulation of various tracer distributions. Typically the resolution in such models does not exceed  $1^\circ$  in the horizontal and a few hundred meters in the vertical in deeper layers. The momentum and vorticity balances for the resulting flow are very nearly geostrophic except in certain boundary layers like the western boundary current and the surface Ekman layer. For this type of model it therefore seems appropriate to put most modeling effort in the equations for temperature and salinity where advection and diffusion determine the representation of water masses in the model as well as the density structure that in turn determines the flow field.

Several systematic studies have dealt with the sensitivity of this class of models to variations of the turbulent closure parameters (e.g. Bryan and Lewis, 1979, Meehl et al., 1982, F. Bryan, 1987). Here results from models with different numerical representations of the advection operator in the thermohaline equations are compared to investigate the sensitivity of the models with respect to numerical formulations.

However, advection and diffusion cannot completely be separated in finite difference models. Numerical advection schemes of second or higher order of accuracy do not preserve the monotonicity of the solutions so that unphysical oscillations or negative concentrations of positive definite tracers can occur. Explicit diffusion is necessary to get stable solutions. Figure 1 illustrates the problem of unphysical oscillations. It shows the temperature distribution from one of the models (the standard case--to be discussed below) at 159 m depth. Small

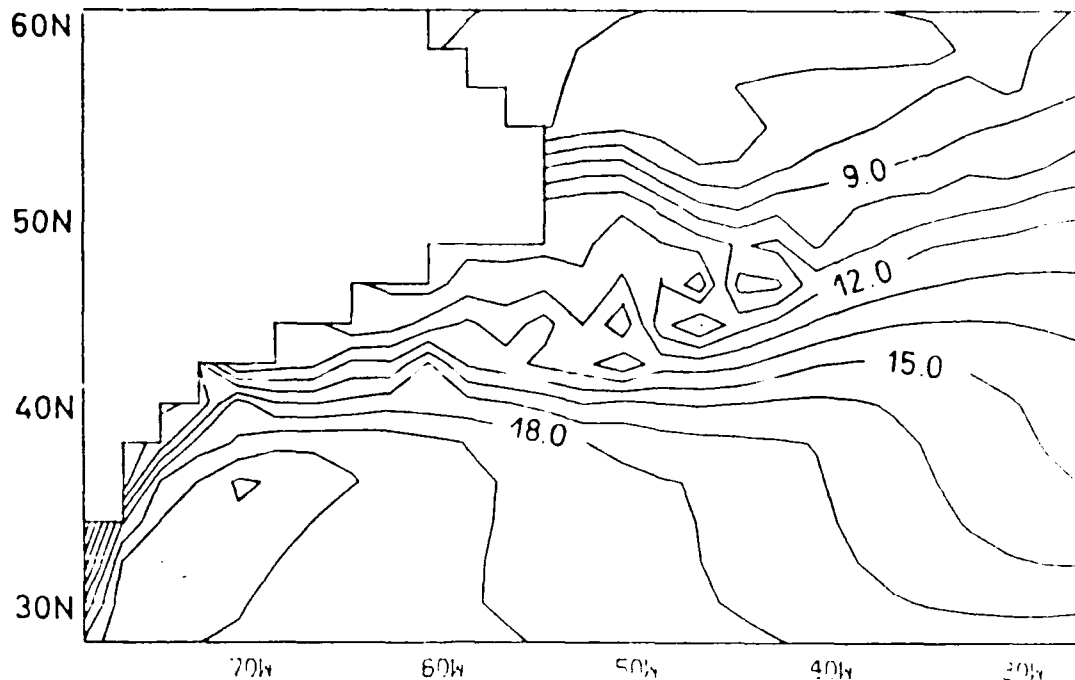


Figure 1. Temperature at 159 m depth for the standard case at 2° horizontal resolution after 2700 years. Contour interval 1 K.

scale features appear in the region of the Gulf Stream off the American coast. These features are due to numerical dispersion of the temperature front associated with the stream. The noise seems to be confined to this region, however, and probably does not harm the solution in the remaining parts of the model domain.

Under certain circumstances the numerical dispersion, however, may affect the whole water mass distribution in the model on a large scale. The salinity section along 30°W (Fig. 2) is dominated by a huge water mass with salinities up to 36.8 psu. The source of this saline water mass at the equator is a single grid point in the Guinea basin below a sharp halocline associated with river run-off. This front disperses and produces an extreme anomaly with salinities out of the physically meaningful range. The anomaly is distributed by the equatorial current system and diffusion over large distances until it becomes a major water mass in that simulation. Other examples of this well known numerical effect can be found in Killworth (this volume).

In the context of the central differences formulation, there are in general two ways to overcome the problem: Increasing the mixing or increasing the resolution. The first way might have a large impact on the quantities that are to be modeled and the second might not be feasible to the necessary extent (especially in the horizontal) because of limited computer resources available.

We therefore considered several alternative advection schemes for the temperature and salinity equations and tested them in simple

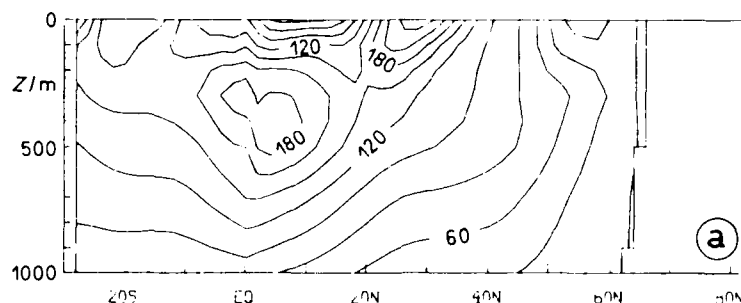


Figure 2. Salinity section along 30°W after 620 years of integration with the standard case at 2° horizontal resolution. The vertical Austausch coefficient  $A_{nv}$  is  $0.3 \times 10^{-4} \text{ m}^2 \text{ s}^{-1}$  in this experiment. Contour interval 0.1 psu, labels are for  $(S-35) \times 100$ .

configurations resembling typical oceanic situations. With an oceanic general circulation model (GCM) we conducted simulations with the central differences scheme, the upstream scheme, and the Flux Corrected Transport (FCT) algorithm that will be described briefly in the next section. A more detailed description and further results will be presented in a forthcoming paper by Gerdes, Koeberle, and Willebrand (1989) and in Gerdes (1988). The upstream and FCT schemes are of lower order of accuracy than the central differences scheme and contain some amount of implicit diffusion. The implicit diffusion varies spatially because it depends (among other quantities) on the velocity of the flow. While the obvious result of the comparison will be an estimate of the sensitivity to numerical advection schemes we may also interpret the results as the produce of subgrid scale mixing that varies in space (and in time).

The differences between consistent (and convergent) numerical schemes vanish in the limit of infinitesimal grid spacing. Hence we expect the sensitivity with respect to different numerical schemes to depend on the resolution--and to eventually vanish when the resolution becomes fine enough. The initial set of experiments with a 2° horizontal resolution was repeated in a similar configuration at doubled horizontal and somewhat increased vertical resolution. Despite the increase of computing power available for oceanographic studies it is still very time consuming to conduct sensitivity studies of the stationary state at this higher resolution. The high resolution cases were in fact only integrated for several decades and are not exactly comparable with the coarse resolution cases. The discussion will therefore concentrate on somewhat different properties for the different sets of experiments. The high resolution cases are covered in detail in Gerdes (1988).

The following section describes the configuration and parameters of the experiments with the coarse resolution models. A brief qualitative discussion of the properties of the different advection schemes is included. Then a few results are presented from the coarse resolution experiments, which are discussed further in terms of the effective

vertical mixing rates. The following three sections present the experiments at the finer resolution. The final section is intended to synthesize the results from both sets of experiments and to draw some conclusions about the suitability of large scale models of this type to study the effects of physically motivated mixing concepts.

#### DESCRIPTION OF THE COARSE RESOLUTION MODEL

Three experiments at  $2^\circ \times 2^\circ$  horizontal resolution will be presented here (Table 1). An integration with the primitive equation model described by Cox (1984) serves as a control experiment and will here be referred to as the standard case. It is based on the central differences advection scheme and employs Laplacian friction and diffusion terms to parameterize the effects of motions which are not resolved by the numerical grid. The advection scheme does not contain implicit diffusion although explicit diffusion is necessary to damp numerical noise that is generated by the numerical dispersion associated with this advection scheme.

Table 1. Overview of the experiments with the coarse resolution model.

Experiment	Advection scheme	Explicit mixing	Integration time
standard	central differences	horizontal/vertical $A_H = 10^3 \text{ m}^2\text{s}^{-1}$ $A_V = 0.65 \times 10^{-4} \text{ m}^2\text{s}^{-1}$	2700 years
upstream	upstream differences	none	2700 years
FCT	FCT algorithm	iso/diapycnal $A_L = 10^3 \text{ m}^2\text{s}^{-1}$ , $A_D = 0$	1500 years

In the upstream case the model is modified by replacing the central differences scheme with the first order upstream scheme for the advection of temperature and salinity. The first order accuracy implies that the scheme approximates a different differential operator to a higher order of accuracy. This operator can be represented by the second order central difference scheme plus a Laplacian diffusion. The mixing coefficient of the diffusion, however, is of a special form where the dominant part for each coordinate direction is proportional to the absolute value of the velocity component and the grid size for that direction. The effective diffusivity with this scheme hence becomes spatially and temporally variable. Vigorous horizontal mixing is to be expected in strong currents, especially in the western boundary current.

Diffusivities in the interior and on deeper levels tend to be relatively small ( $O(10^2 \text{ m}^2\text{s}^{-1})$ ) for a velocity of 0.1 m/s at the given resolution of  $2^\circ$ . The vertical diffusivity is expected to increase with depth since the vertical grid size increases (compare Table 2). The vertical velocity also tends to increase with depth thus contributing to the increase in vertical mixing.

The main advantage of the upstream scheme is that the monotonicity of advected quantities is strictly preserved. Unphysical oscillations like those shown in Figures 1 and 2 cannot occur. Furthermore this scheme is computationally efficient and easy to implement.

The third experiment employs the FCT scheme (Zalesak, 1979) for the advection of tracers. The solution lies between the central differences solution and the upstream solution in this implementation of the FCT algorithm. Starting with the upstream solution a certain amount of antidiffusive flux (the difference between the advective flux from the central differences and from the upstream scheme) is applied. The amount

Table 2. Vertical grid and parameters common to the coarse resolution models.

Level	$\Delta z$	depth of grid point	depth of box bottom
1	50	25.0	50.0
2	63	81.5	113.0
3	92	159.0	205.0
4	140	275.0	345.0
5	213	451.5	558.0
6	313	714.5	871.0
7	435	1088.5	1306.0
8	566	1589.0	1872.0
9	689	2216.5	2561.0
10	790	2956.0	3351.0
11	864	3763.0	4215.0
12	915	4672.5	5130.0

Horizontal resolution	$\Delta\theta = 2^\circ$ $\Delta\lambda = 2^\circ$
Horizontal and vertical viscosities	$A_{MH} = 4 \times 10^4 \text{ m}^2\text{s}^{-1}$ $A_{MV} = 10^{-2} \text{ m}^2\text{s}^{-1}$
Time constant for the Newtonian damping	$1/\gamma = 30 \text{ days}$
Time step for $\theta$ , S	$\Delta t^{\theta S} = 1 \text{ day}$
Time step for velocity	$\Delta t^{UV} = 2 \text{ h}$

of antidiffusive flux added is subject to the constraint that no new extrema should be generated by advection. The scheme may realise the central differences limit (with zero diffusion) at one grid point and the upstream limit (with the implicit diffusion described above) at another grid point. Our tests with the FCT scheme in idealized applications (C. Koeberle, 1988; pers. comm.), as well as the actual amount of implicit diffusion in the ocean model, show that the implicit mixing is largely reduced by the FCT algorithm compared to the upstream scheme. Usually the overall effect of this locally determined diffusion is also much less than the effect of the necessary explicit mixing with the central differences scheme where usually a single coefficient is chosen to avoid numerical dispersion effects everywhere. We may regard the implicit diffusion of the FCT algorithm as the minimum diffusion that is necessary to preserve the monotonicity of the advected quantities required by the second law of thermodynamics.

The experiments were performed in an Atlantic ocean geometry with closed walls at 30°S and 80°N. No attempt has been made to include artificial sources for the shut-off water masses like the Mediterranean water mass, the Antarctic Intermediate water mass and the Antarctic Bottom water. The estimated effect of the closed walls compared to the total changes during the integrations is found to be relatively small.

Winter distributions of potential temperature and salinity from Levitus' atlas (1982) have been used to initialize the experiments and to provide reference values for the Newtonian damping in the uppermost level which parameterizes heat and freshwater fluxes through the surface. Annual mean wind stress fields have been taken from the climatology of Hellerman and Rosenstein (1983).

The standard and upstream cases were integrated for 2700 years. This was not quite sufficient to reach a steady state with the standard case where temperatures and salinities approached their steady state values on the time scale of the vertical diffusion. The FCT experiment was stopped after 1500 years of simulated time, which also did not suffice to reach steady state in the deepest levels. However, we decided that the differences to the other experiments were already established at that stage of the calculation.

Otherwise the parameters were kept identical among the experiments (Table 2). The explicit diffusion of the standard case was modeled with a horizontal Austausch coefficient  $A_H = 10^3 \text{ m}^2 \text{ s}^{-1}$  and a vertical coefficient  $A_V = 0.65 \times 10^{-4} \text{ m}^2 \text{ s}^{-1}$ . The latter value turned out as the smallest value that could prevent the occurrence of the salt anomaly shown in Fig. 2. The choice of this value hence is solely based on numerical considerations.

The upstream case contains no explicit diffusion while the FCT case includes explicit isopycnal diffusion. The same value as for  $A_H$  has been chosen for the isopycnal mixing coefficient  $A_L$ . The explicit diapycnal mixing was set to zero in this case. The isopycnal mixing scheme was implemented as described by Cox (1987) with minor modifications to make sure that the mixing scheme did not contribute to the diapycnal mixing. However, it proved necessary to include mixing in the coordinate

direction within a layer a single grid distance wide along all boundaries except for the surface. At certain grid points the isopycnal mixing scheme would otherwise generate anomalies that violate the second law of thermodynamics (Gerdes et al., 1989).

### RESULTS FROM THE COARSE RESOLUTION MODEL

In the experiments with the 2° model we concentrate on the large scale properties of the simulation. The meridional temperature section of Fig. 3 illustrates the water mass distribution at the end of the integrations. The initial distribution is also included as Fig. 3(d) to demonstrate the deviation from the initial conditions as well as from the observed climatology. The results of the upstream and standard cases are remarkably similar and in comparison with the observations are characterised by a broadening of the tropical thermocline. This accounts for an increase in temperature of 3 to 4K around 600 m depth.

The FCT model yields a much sharper thermocline in the upper 300 m and also a much sharper subarctic front, which actually is more pronounced than in the observed field. Below 500 m, however, the isotherms are essentially flat and the upward rise at the equator is missing. This rise can be seen in the standard and upstream cases and it is a very prominent feature of the observed temperature distribution. A quantitative estimate for the thermocline thickness is given in Table 3.

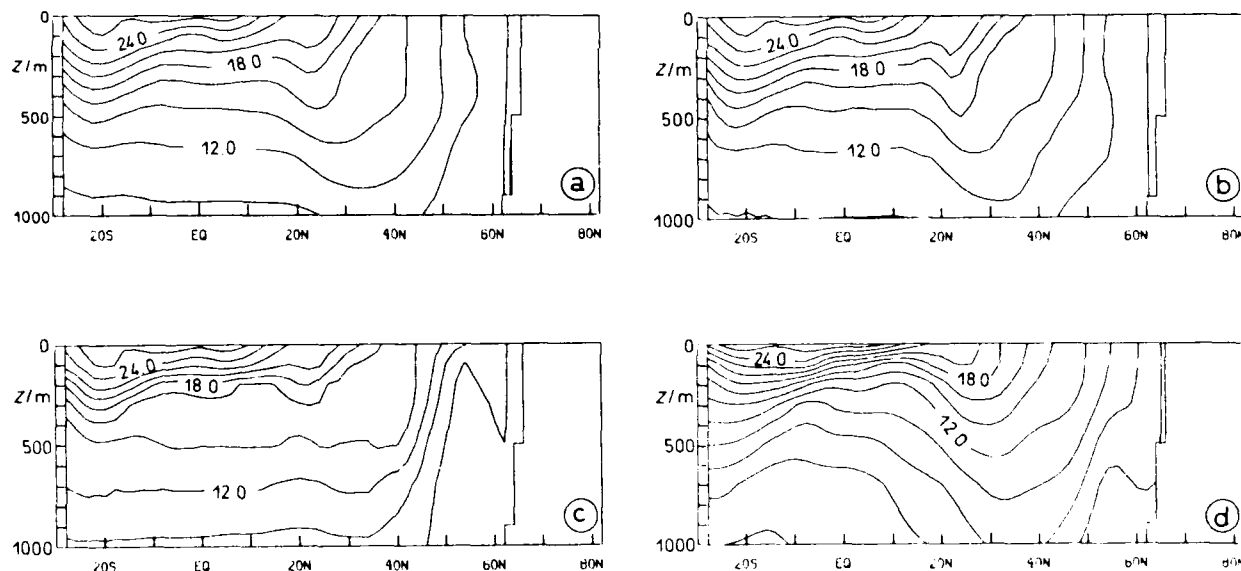


Figure 3. Temperature section along 30°W for the (a) standard, (b) upstream, and (c) FCT coarse resolution experiments. The initial conditions according to Levitus (1982) are included as (d). Contour interval 2 K.

The stream function of the zonally integrated mass transport (Fig. 4) gives an impression of the large scale transport patterns in the models. The upper layers, especially in the tropics, are dominated by shallow circulation cells. The near surface flow of these cells is essentially determined by the Ekman transport. The cells are very similar in all



Table 3. Characteristic results from the coarse resolution models. See text for the definition of the thermocline thickness  $d$  and the effective vertical Austausch  $A_{\text{veff}}$ ;  $w^*$  is the average upwelling velocity at 113 m depth between  $10^\circ\text{S}$  and  $10^\circ\text{N}$ . The diagnostic case is the result of the upstream model after two months of integration.

	standard	upstream	FCT	diagnostic
thermocline depth (m)	173	186	131	149
$A_{\text{veff}}$ ( $10^{-4} \text{ m}^2 \text{ s}^{-1}$ )	0.65	0.81	0.28	0.42
$dw^*$ ( $10^{-4} \text{ m}^2 \text{ s}^{-1}$ )	0.95	1.17	0.31	0.76
Maximum meridional mass transport (Sv)	14.7	20.0	12.8	19.9
Maximum northward heat transport (PW)	0.56	0.51	0.37	1.21

experiments since they are basically prescribed by the external forcing. There are, however, considerable differences in the total equatorial upwelling. In the standard and upstream cases a flow of approximately 4 Sv ascends from deeper layers and adds to the near surface transport in the anticyclonic cell north of the equator. Opposed to these two cases the FCT case exhibits virtually no deep equatorial upwelling. This corresponds to the differences among the models in the general structure of the thermocline in low latitudes as described above.

The FCT case furthermore has the lowest overturning rate (12.8 Sv, compare Table 3) in the northern thermohaline driven cell. This cell is stronger by 2 Sv in the standard case and amounts to 20 Sv in the upstream case. While the motion below 2500 m is very weak in the standard and FCT cases, the deepest levels are well ventilated by the overturning motion in the upstream case. The differences between the standard and upstream cases are in fact almost completely confined to these deeper levels (Fig. 4(d)). The deep ventilation in the upstream case has been further localized to take place solely in the North American basin while the other deep basins communicate with the upper levels neither by advection nor diffusion (which are closely related with the upstream scheme). The temperature of the latter remains very close to the initial values throughout the whole integration.

The levels below 2500 m in the standard case warm very slowly to a vertically homogenous temperature at a rate that is consistent with the explicitly prescribed vertical mixing rate. This indicates a purely diffusive adjustment of these deep levels. The differences in the regimes for the deepest levels result in different timescales for the adjustment to a steady state.

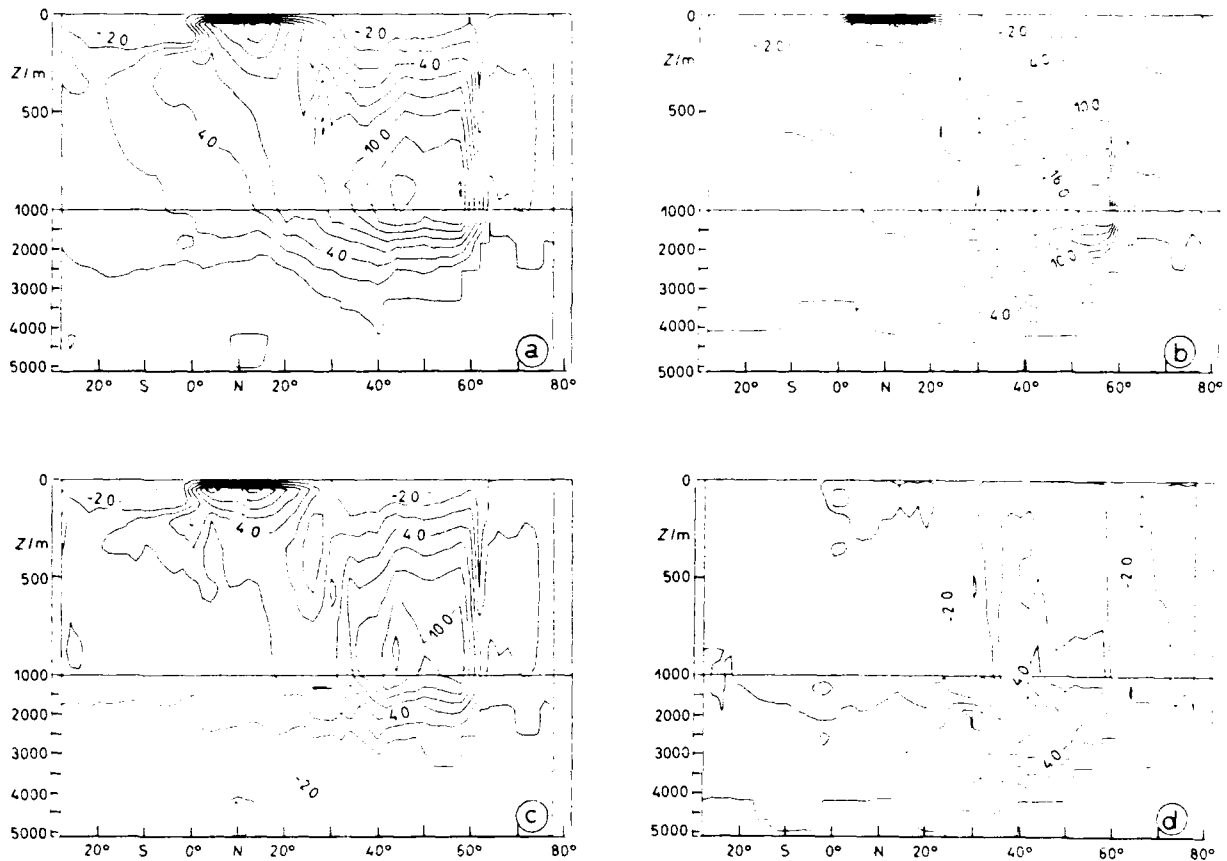


Figure 4. Stream function of the zonally integrated mass transport for the (a) standard, (b) upstream, and (c) FCT coarse resolution experiments. The difference between the upstream and standard cases is plotted in (d). Contour interval 2 Sv.

The poleward heat transport (Fig. 5) at lower and middle latitudes is closely related to the strength of the overturning motion. At higher latitudes the correlation of northward velocity and zonal temperature anomaly, the gyre component of the heat transport (K. Bryan, 1962), becomes increasingly important. Upstream and standard cases accordingly exhibit roughly the same maximum heat transport of around 0.5 PW while the heat transport is significantly reduced with the FCT scheme. In the latter a maximum of only 0.35 PW is reached slightly north of the equator. The enhancement of the deep cell in the upstream case has no impact on the heat transport since the temperature differences between northward and southward flow are small at great depths. The upstream heat transport is in fact slightly less than that of the standard case except for the secondary maximum near 50°N where the gyre component already dominates the heat transport. The subarctic gyre is most intense in the upstream case (33 Sv compared to 28 Sv in the standard case and 26 Sv for the FCT case).

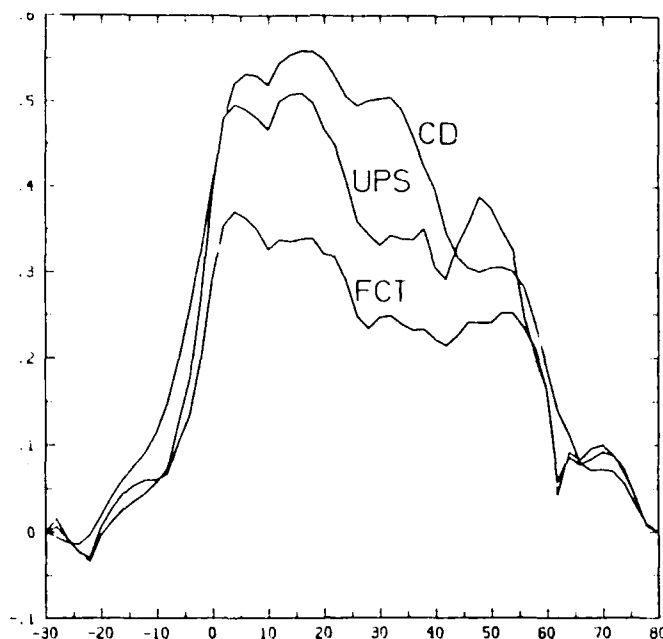


Figure 5. Northward heat transport for the coarse resolution models (CD: standard, UPS: upstream case).

## DISCUSSION

In a sensitivity study with the same basic model (Cox, 1984), F. Bryan (1987) has demonstrated that both the strength of the overturning and the thickness of the thermocline are determined by the vertical diffusivity in the model. Experimentally both of these quantities were found to increase approximately as the cube root of the vertical diffusivity. Thermocline thickness and maximum meridional volume transport for our experiments are summarized in Table 3 together with the maximum northward heat transport. Two estimates for the effective vertical mixing coefficient are given. The first estimate relies on a scaling argument (based on a vertical advective-diffusive balance and the thermal wind relation) which results in a proportionality between the mixing coefficient and the cube of the thickness  $d$  of the thermocline (see Bryan, 1987). The thermocline thickness  $d$  is defined as

$$d = \int_H^0 (T - T_H) dz / (T_S - T_H)$$

where  $T_S$  and  $T_H$  are the temperatures at the surface and at the depth  $z = -H$  respectively. The values in Table 3 are based on  $H = 500$  m and the mean temperature profile for the area between  $10^\circ\text{S}$  and  $10^\circ\text{N}$ . The second estimate is given by the thickness  $d$  times the mean upwelling velocity in the equatorial belt between  $10^\circ\text{S}$  and  $10^\circ\text{N}$ . Both estimates indicate a slightly higher mixing in the upstream case compared to the standard case while the mixing in the FCT case is considerably reduced.

The relation between the overturning and the effective mixing is consistent with the relation found for different explicit vertical mixing rates for the standard case by F. Bryan (1987).

The estimates for the equatorial thermocline presented above do not take into account the lateral fluxes into the equatorial belt. The horizontal fluxes vanish in a horizontal integral. A more appropriate measure for the overall effective mixing might therefore be given by the ratio of the horizontal averages of the vertical diffusive flux and the vertical gradient of temperature respectively. The vertical distributions of this ratio for the upstream and FCT cases are displayed in Fig. 6. In the upstream case the ratio increases from 0.5 near the surface to  $5 \times 10^{-4} \text{ m}^2 \text{ s}^{-1}$  near 3000 m depth. The very low mixing below corresponds to the isolation of deep basins from upper parts of the model ocean. The FCT scheme realizes a lower ratio but below 1000 m it also exceeds the value chosen for the explicit mixing of the standard case. Only above 400 m is the effective mixing considerably smaller than in the standard case.

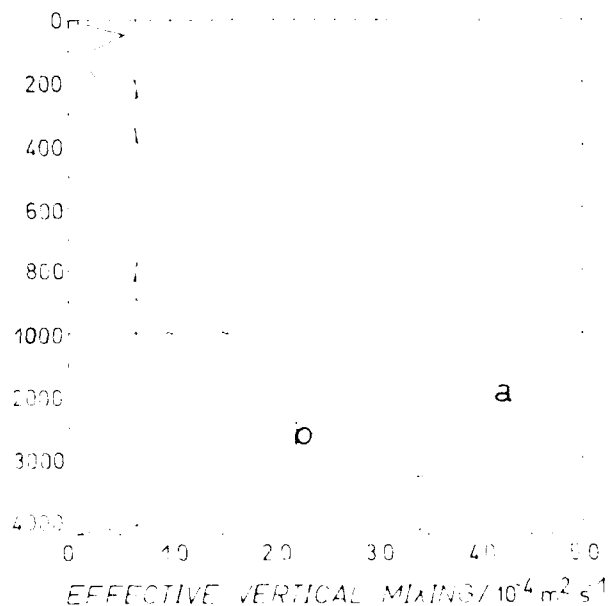


Figure 6. Effective vertical mixing rates in the coarse resolution (a) upstream (UPS) and (b) FCT experiments. The constant mixing rate of the standard case is indicated by the solid line.

Since the mixing rates of the FCT experiment represent minimum diffusivities under the constraint of monotonicity of the advected quantities this indicates that  $0.65 \times 10^{-4} \text{ m}^2 \text{ s}^{-1}$  is still too small to preserve the monotonicity with the central differences advection scheme.

With respect to the results for thermocline thickness and meridional overturning this demonstrates that the large mixing rates at great depths are less important than the rather subtle differences in the upper few hundreds of meters. The large diffusivities of the FCT case

below 1000 m (compared to the standard case) apparently do not contribute to a larger meridional overturning.

A diagnostic model serves to provide for a comparison based on observed fields. In this case the diagnostic model is just the upstream model that was integrated for 2 months allowing the velocity field to adjust to the basically unaltered density field of the initial state. The estimates for the effective vertical mixing in the diagnostic case lie halfway between the upstream and FCT cases while the maximum meridional mass transport is nearly equal that of the upstream case. The much larger heat transport in the diagnostic case compared to the upstream case illustrates the rearrangement of temperature and transport patterns that have taken place during the integration of the upstream model. The results of this diagnostic model reveal a basic problem with mixing rates that are not related to the physical conditions, which vary spatially and probably also with respect to time. The regional variability is demonstrated by the distributions of mixing coefficients implied from the climatology by inverse calculations (Olbers et al., 1985; Olbers, this volume). With the constant vertical mixing coefficient used in the standard case here (and in Bryan's (1987) experiments) it seems impossible to model both the thermocline thickness and the meridional overturning correctly at the same time. Neither is the effective mixing of the upstream or FCT advection schemes related to the physical conditions that actually determine the effective mixing for the stationary large scale averaged quantities in the ocean (corresponding to the model resolution). It is therefore not surprising that the upstream and FCT cases yield no quantitative improvement over the standard case. The upstream and standard cases are very similar with respect to the quantities discussed here while the FCT case yields a reasonable equatorial thermocline but unrealistically small overturning, equatorial upwelling and heat transport.

A prerequisite for the implementation of physically enhanced mixing parameterizations is a numerically necessary mixing that is small compared with the physically motivated mixing. This requirement can be met by all schemes considered here, provided the resolution is fine enough. However, the implicit mixing of the first order upstream scheme decreases very slowly with increasing resolution making it inferior to the central differences scheme (with appropriate explicit mixing) and the FCT scheme at higher resolution. The latter provides a guaranty against unphysical oscillations and negative concentrations combined with low overall mixing rates. However, the FCT scheme is more costly in terms of computer time (roughly a factor of 3 compared with the two other schemes).

#### DESCRIPTION OF THE FINE RESOLUTION MODEL

Three experiments similar to the coarse resolution experiments described above were conducted at the horizontal resolution of  $1^\circ \times 1^\circ$ . The vertical resolution was increased from 12 to 18 levels with vertically varying grid sizes (see Table 4). The same type of thermohaline forcing

Table 4. Vertical grid distances and parameters used for the fine resolution models.

Level	$\Delta z$	depth of gridpoint	depth of box bottom
1	20.0	10.0	20.0
2	26.0	33.0	46.0
3	34.0	63.0	80.0
4	44.0	102.0	124.0
5	56.5	152.3	180.5
6	73.5	217.3	254.0
7	93.5	300.8	374.5
8	120.0	407.5	467.5
9	152.5	543.8	620.0
10	193.0	716.5	813.0
11	242.0	934.0	1055.0
12	301.0	1205.5	1356.0
13	371.5	1541.8	1727.5
14	452.5	1953.8	2180.0
15	542.5	2451.3	2722.0
16	637.5	3041.3	3360.0
17	728.5	3724.3	4088.5
18	800.0	4488.5	4888.5

Horizontal resolution

$\Delta\theta = 1^\circ$

$\Delta\lambda = 1^\circ$

Horizontal and vertical viscosities

$A_{MH} = 5 \times 10^3 \text{ m}^2 \text{ s}^{-1}$

$A_{MV} = 10^{-3} \text{ m}^2 \text{ s}^{-1}$

Horizontal diffusivity (standard case)

$A_{HH} = 10^3 \text{ m}^2 \text{ s}^{-1}$

Vertical diffusivity (standard case)

$A_{VH} = 0.3 \times 10^{-4} \text{ m}^2 \text{ s}^{-1}$

Isopycnal diffusivity (FCT case)

$A_I = 10^3 \text{ m}^2 \text{ s}^{-1}$

Diapycnal diffusivity (FCT case)

$A_D = 0.3 \times 10^{-4} \text{ m}^2 \text{ s}^{-1}$

Time constant for the Newtonian damping

$1/\lambda = 20 \text{ days}$

Time step for  $\theta, S$ 

$\Delta t^{\theta S} = 6 \text{ h}$

Time step for velocity

$\Delta t^{UV} = 1 \text{ h}$

was applied although with slightly reduced damping time scale. We used annual mean wind stress distributions from Isemer and Hasse (1987) instead of the Hellerman and Rosenstein (1983) wind stresses for these calculations. The domain was reduced to the North Atlantic from the equator to  $66^{\circ}\text{N}$ , and the Gulf of Mexico was excluded from the domain. Restoring zones as described by Sarmiento (1986) were implemented near the northern and southern closed walls. These restoring zones prevent the very rapid breakdown of the large scale meridional overturning motion which was associated with the coarse resolution models. The overturning motion there collapsed from initially 20 Sv to around 8 Sv within a decade. It recovered to the (near) steady state value of Table 3 on a much larger time scale.

In spite of the reduction of the domain the computational cost at the doubled resolution was still so large that no steady state solution could be achieved. The models were integrated for only 40 years. The results therefore are not directly comparable with the results discussed above and our analysis will focus on somewhat different properties.

The primary aim of the fine resolution experiments is to assess the influence of diapycnal mixing due to horizontal diffusion. The vertical diffusion may act as a source as well as a sink for available potential energy (APE) (Bryan and Lewis, 1979). In our experiments APE actually was increased by increasing the vertical diffusion. Horizontal diffusion on the other hand always acts as a sink for APE. The effect of decreasing the diapycnal diffusion due to horizontal diffusion may therefore be different from the effect of decreasing the vertical diffusion. The FCT case is supposed to realize the least diapycnal diffusion due to horizontal mixing. However, as we shall see below, this is not everywhere the case.

The standard case contains an explicit vertical diffusivity which is numerically necessary with the central difference advection scheme. The same explicit vertical diffusivity was also implemented in the FCT case. Note that this is different from the coarse resolution FCT case where the explicit diapycnal mixing was set to zero. The effects of the vertical diffusivity are assumed to be small over the relatively short integration period. Besides the explicit vertical mixing, the FCT case employs an explicit isopycnal mixing scheme. This scheme is implemented as described for the coarse resolution model above and introduces no diapycnal diffusion except for the effects of the nonlinear equation of state. No additional diffusive boundary layers as in the coarse resolution model were implemented since no unphysical anomalies due to the isopycnal mixing scheme occurred in the higher resolution case.

An upstream model without any explicit mixing is also considered here. Two additional experiments, one with the central differences advection scheme and horizontal mixing rates decreasing exponentially with increasing depth, and a second with the FCT scheme without any explicit mixing were also conducted in the same configuration. The additional FCT case confirmed the assumption that the explicit mixing in the FCT model

has virtually no influence on the density distribution, which was almost identical in both cases after 40 years of integration. The individual tracers, however, exhibit differences in certain areas like the upper parts of the eastern subtropical gyre and the boundary between subpolar mode water and Mediterranean water at middle depth. Further results from these two additional experiments will not be discussed here.

## RESULTS FROM THE FINE RESOLUTION MODEL

### A) Horizontal mixing rates

The implicit mixing rates occurring with the FCT and upstream schemes were determined by computing the ratio of the diffusive flux of temperature in each coordinate direction and the temperature gradient in this direction. A meridional average over the center of the subtropical gyre (20 to 40°N) for the 102 and 934 m levels is displayed in Fig. 7. For the upstream case we find zonal mixing coefficients exceeding the explicit mixing of the standard case from the western boundary to 30°W. The meridional mixing coefficient reaches very high values in the western boundary layer but stays below  $10^3 \text{ m}^2\text{s}^{-1}$  elsewhere except near 20°W. The eastern maximum indicates the southward branch of the subtropical recirculation. At 934 m depth (and below) the mixing rates still exceed  $10^3 \text{ m}^2\text{s}^{-1}$  in the west but are much smaller outside of the boundary layer.

The mixing is considerably reduced with the FCT scheme. At 102 m depth the meridional and zonal boundary layer values are 3.5 and  $2 \times 10^3 \text{ m}^2\text{s}^{-1}$  respectively while a typical interior value is  $3 \times 10^2$ . In deeper levels  $10^3 \text{ m}^2\text{s}^{-1}$  is hardly reached in the boundary layer and values drop to around  $10^2$  in the interior.

From the results of the FCT case we must, as in the coarse resolution experiments, conclude that the explicit mixing of the standard case is too weak to yield monotonic tracer distributions. We indeed observed numerical dispersion effects in the horizontal temperature maps of the standard case as shown for the coarse resolution model (Fig. 1). The FCT scheme provides stronger mixing in the western boundary layer. Higher diapycnal mixing than in the standard case is to be expected in this area. This is contrary to the idea behind the design of the experiments. Zonal density sections and maps of isopycnal slope, however, reveal that the density gradients in the FCT case are slightly less than in the standard case near the western boundary only in the upper 100 to 150 m (Fig. 8). The density gradients in the FCT case exceed those found for the standard case below 150 m depth. This may partially be caused by the orientation of the mixing in the FCT case along the current axis and therefore essentially along lines of constant density. The zonal mixing in the FCT case falls below the mixing rate of the standard case rapidly as depth increases.



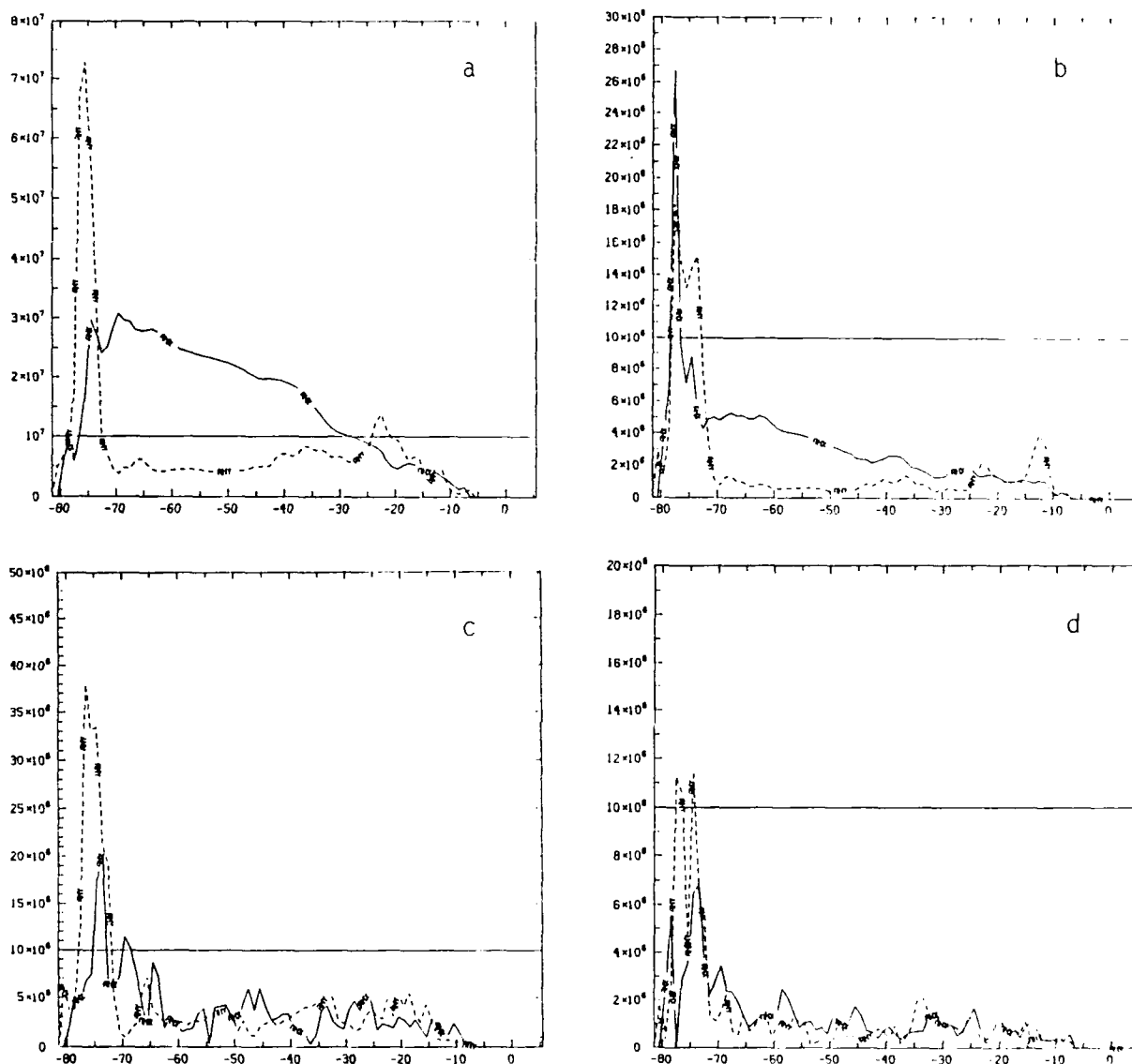


Figure 7. Effective horizontal mixing rates (AHX zonal - solid line; AHY meridional - dashed line) for the fine resolution upstream (a: 102 m depth, b: 934 m depth) and FCT (c: 102 m, d: 934 m) cases. The curves represent a meridional average between  $20$  and  $40^\circ\text{N}$ . The mixing rate of the standard case is indicated by the horizontal line.

The high effective diffusivity of the upstream case that also prevails at greater depths has, on the contrary, a profound effect on the results of this simulation.

We may summarize the situation as follows: The standard case has a relatively high amount of horizontal mixing everywhere except for the upper 100 to 200 m in the western boundary current. The FCT case realizes a weak horizontal mixing extreme except for the uppermost parts

of the western boundary layer. The upstream case combines very strong mixing in the boundary layer and along the Gulf Stream/North Atlantic current (NAC) (the large zonal mixing rates between 70 and 30°W in Fig. 7(a)) with weak mixing in the interior and especially in the deep interior. With respect to the interior the upstream case lies closer to the FCT case than to the standard case.

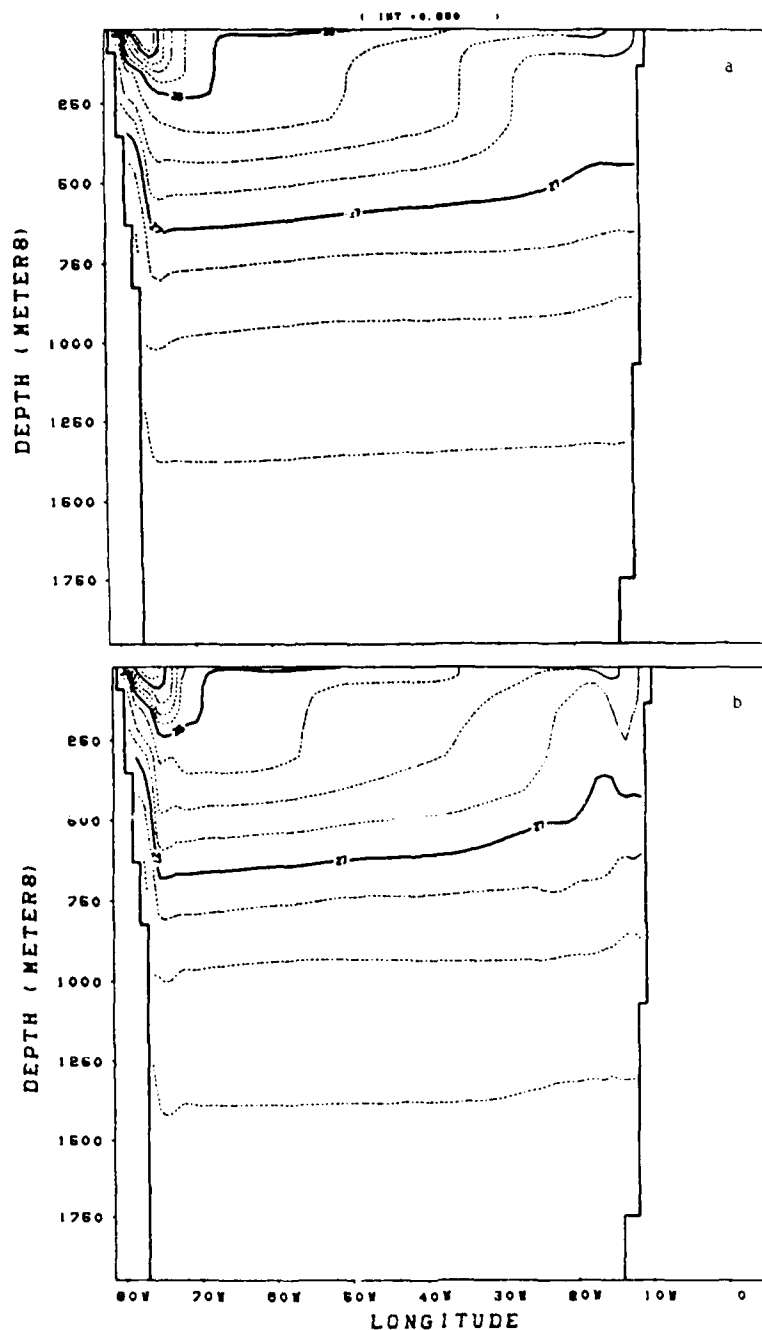


Figure 8. Zonal section of potential density along 29.5°N for the fine resolution (a) standard and (b) FCT experiments. Contour interval 0.25 kg m<sup>-3</sup>.

## B) Potential vorticity

Cox and Bryan (1984) compare the meridional distribution of potential vorticity ( $q = -f\sigma_z$ ) for two experiments with a model similar (and with parameters similar) to our standard case. Their experiments were conducted with an idealized domain and simple surface forcing functions. In their first experiment the ocean is driven only by a surface buoyancy flux while in the second it is driven by surface buoyancy and wind forcing. With buoyancy forcing only, a rather simple structure emerges. The potential vorticity is greatest in subtropical latitudes close to the surface and decreases toward the equator ( $f$  decreasing), towards the northern wall and towards deeper layers ( $\sigma_z$  decreasing). The most important change due to the additional wind forcing is the intrusion into the subtropical thermocline of weakly stratified (mode) water originating from the midlatitude mixed layer. The low potential vorticity of the mode water splits the formerly monotonic structure in the two distinct maxima of the shallow tropical thermocline and the deeper thermocline of middle latitudes. The same basic features as in the second experiment of Cox and Bryan are visible (Fig. 9) in the three models considered here and also in the initial distribution taken from Levitus (1982). The shallow low latitude thermocline differs from the observations in that it intersects the surface between 20 and 30°N while the observations indicate a northward descent of the thermocline. This is due to the lack of enhanced mixing near the surface under statically stable conditions. This prevents the formation of a mixed layer in locations where buoyancy is gained through the surface fluxes. The introduction of an appropriate mixed layer model would very probably remove this unrealistic feature from the model results.

The formation region of the mode water, which for our purposes may be characterized as having a potential vorticity of below  $0.6 \times 10^{-11} \text{ m}^{-1}\text{s}^{-1}$ , the area covered by it, and the depth and latitudinal extent of the core differ among the models. A feature common to the models but distinct from the observations is the variation of potential vorticity on isopycnal surfaces in the North Equatorial Current (NEC). Isopycnals in the model (e.g., the 26.5 surface) intersect the potential vorticity minimum of the mode water whereas isopycnal and potential vorticity lines are almost parallel in the observed fields. This discrepancy has been explained by Cox (1985) as due to the vigorous mixing of potential vorticity by the eddy field that is not resolved (and in this respect obviously only poorly parameterized) in the models considered here. Note also the generally steeper slope of the isopycnal in the models in this area which hints at a missing sink for available potential energy. The most likely sink for APE is the baroclinic instability process that is indicated by the change of the potential vorticity gradient on density surfaces. Instability does not develop in the standard and upstream cases because the damping on the resolved unstable waves is too strong. Waves of approximately 1000 km length are generated in the FCT case in the NEC region. Their energy, however, is much too small to affect the mean density structure. (See Gerdes, 1988 for details.)

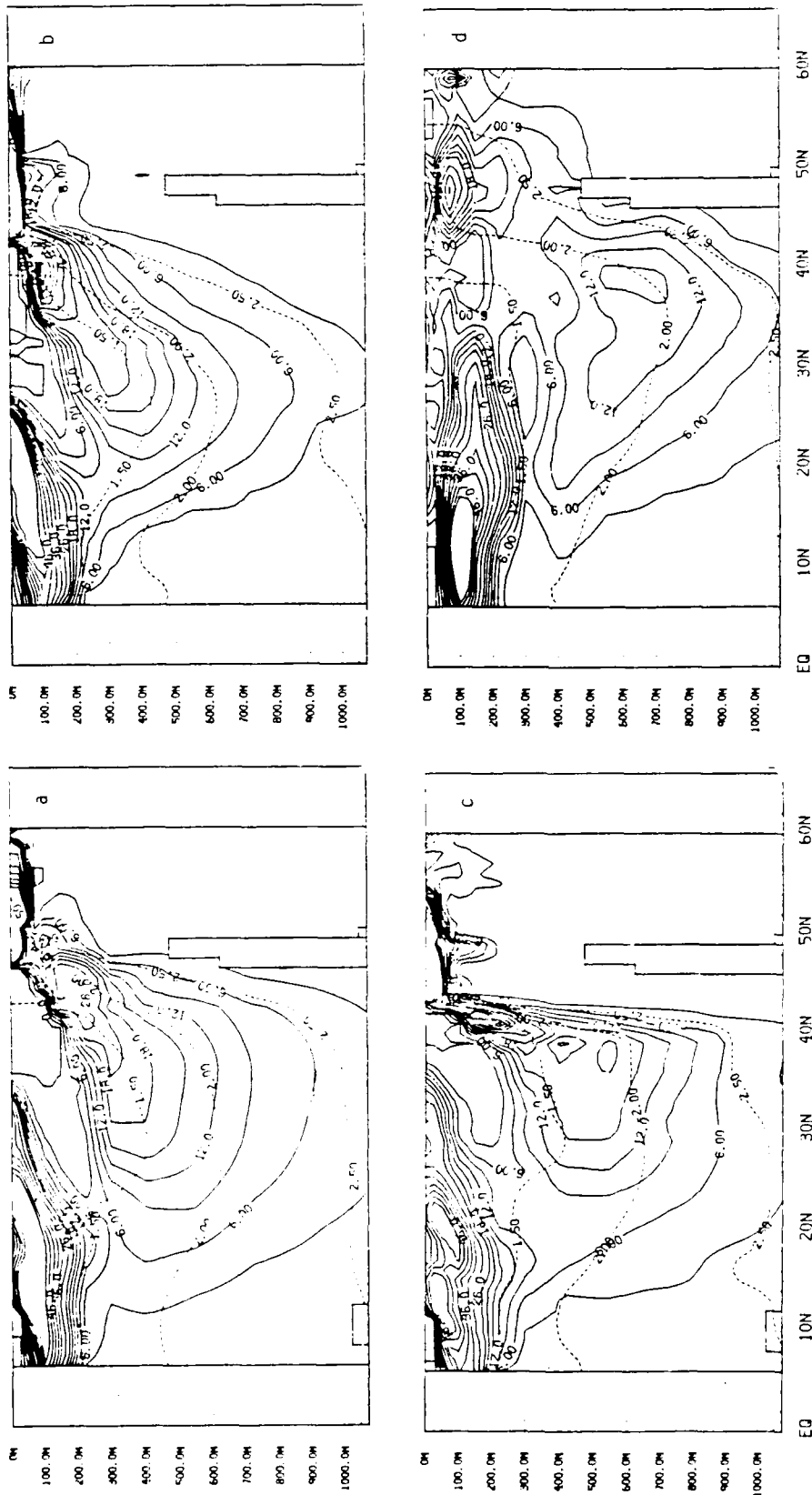


Figure 9. Meridional section of potential vorticity ( $-f\sigma_2$ ) along  $44.5^\circ\text{W}$  for the fine resolution (a) standard, (b) upstream, and (c) FCT cases; (d) is computed from the initial density field. Units are  $10^{-11} \text{ m}^2 \text{ s}^{-1}$  and the contour interval is 3 units between 0 and 21 and 5 units above 21. The isopycnals 26.5, 27.0, and 27.5 are plotted as broken lines.

The models developed remarkable differences in the main thermocline structure in spite of the relatively short integration period. Its depth increases from the upstream case (300 m) to the standard case (350 to 400 m), reaching its maximum of about 500 m in the FCT case. The position of the associated maximum in potential vorticity shifts northward in the same sequence. The FCT case comes closest to the observations although its main thermocline is still 100 to 200 m too shallow and slightly displaced to the south.

Another conspicuous feature of the section (Fig. 9) is a third maximum in the potential vorticity north of the main thermocline and at shallower depths. It can be found at 40°N and between 100 and 150 m in the upstream case, slightly northward and deeper in the standard case, and covering a greater depth range at 40°N in the FCT case. A similar feature is present in the observed field at 150 m depth although considerably farther to the north. This maximum is due to the advection of highly stratified water in the western boundary current and its extension. It penetrates much deeper into the interior as in the simplified case of Cox and Bryan (1984) where it is not recognizable at a similar distance from the western boundary as the section of Fig. 9.

#### C) Upper layer circulation

The Gulf Stream/NAC system is the outstanding feature of the density and velocity maps at 301 m depth (Figs. 10 and 11). The stream does not separate from the coast and follows the continental slope towards the Grand Banks. In the upstream and FCT cases the current continues into the interior of the basin, virtually unaffected by this topographic feature. The Labrador current which joins the zonal jet east of Newfoundland reinforces the current. The confluence of subarctic and subtropical water masses intensifies the already very sharp front in the FCT case.

The zonal current splits into two branches when it hits the Mid-Atlantic Ridge (MAR). These branches, however, rejoin and most of the current contributes to the cyclonic circulation in the eastern part of the subarctic gyre. Part of the water eventually sinks near the northern boundary.

The path of the current clearly emerges from the density distributions in Fig. 10(b) and (c) as a zonal front reaching from the western boundary to 40°W in the upstream case and even farther east in the FCT case. The front parallels the flow path northward and westward along the eastern edge of the subpolar gyre. The effect of the western boundary region becomes apparent in comparison of the high and low boundary layer mixing regimes of the upstream and FCT cases respectively. The intense mixing in the boundary layer in the upstream case produces a very broad front (and current) leaving the boundary layer compared to the very tight front of the FCT case. In the interior where both cases have relatively low mixing rates the behaviour is qualitatively similar. The zonal current to the west of the MAR transports a density signal that

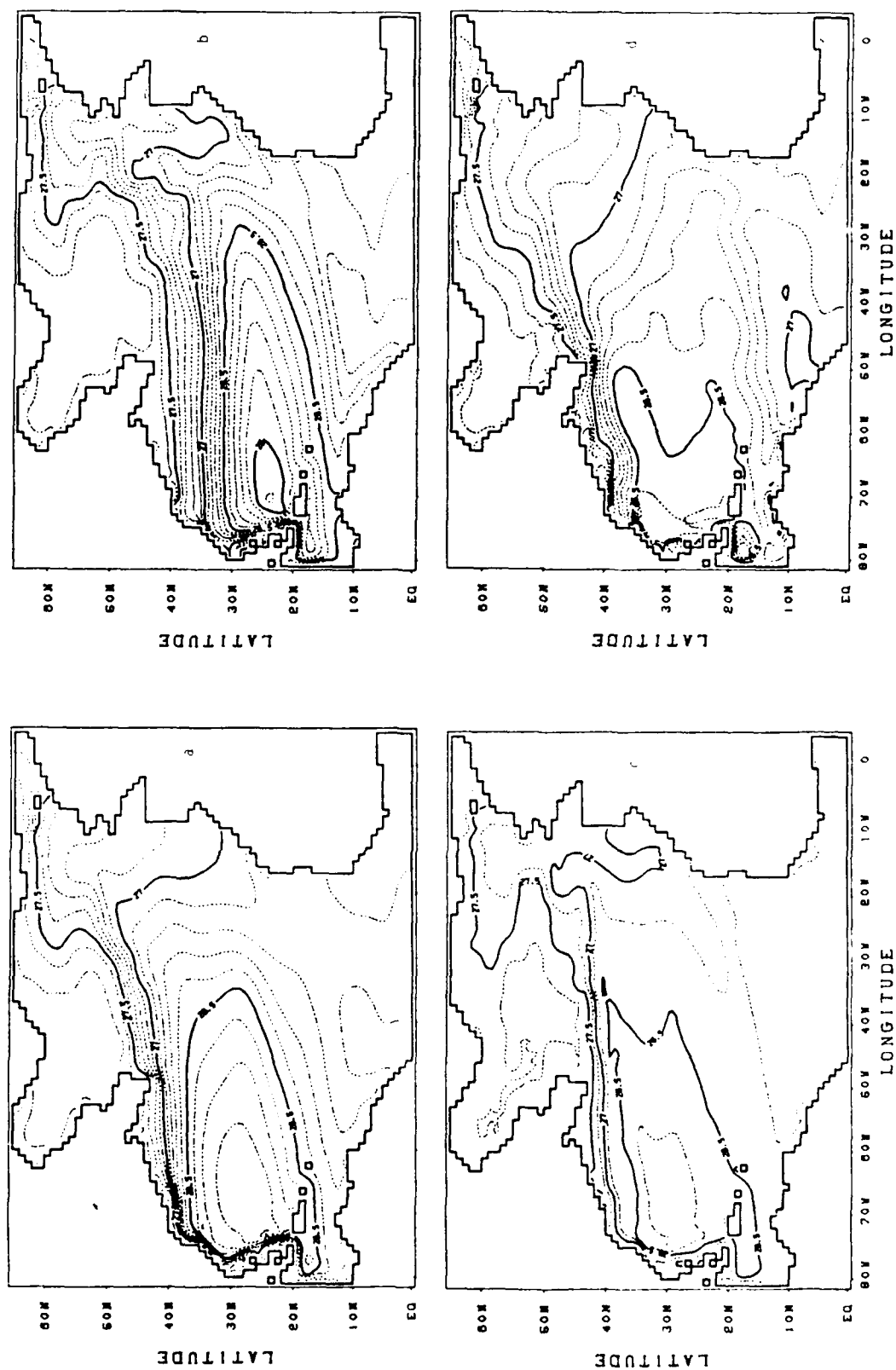


Figure 10. Potential density at 301 m depth for the fine resolution (a) standard, (b) upstream, and (c) FCT cases. The initial distribution is given in (d). The contour interval is 0.1  $\text{kg m}^{-3}$  for (a), (b), and (d), and 0.25  $\text{kg m}^{-3}$  for (c).

has been formed in the western boundary layer and stays virtually unchanged for around  $30^\circ$  of latitude. The large zonal mixing coefficient in the upstream case in the NAC region seen in Fig. 7(a) does not affect the zonally oriented front. This situation arises because the direction of the current nearly coincides with one coordinate direction.

The standard case exhibits a somewhat different behaviour. The originally tight front that leaves the western boundary layer spreads meridionally to almost three times its upstream width at  $40^\circ\text{W}$ . The confluence of NAC and Labrador current intensifies the front east of Newfoundland as in the FCT case. Its position, however, is farther north and the direction is to the northeast instead of the zonal orientation in the FCT case. With this the standard case more closely resembles the observed distributions (compare Fig. 10(d)). The area of cold water in the western part of the subarctic domain is smaller than in the other cases. This is also the case for higher levels and leads to the smallest heat gain in this area of the three experiments. The unrealistic heat gain is very pronounced in the two other cases where a large area of the western subarctic gyre gains heat while the estimates for the actual heat flux through the surface indicate heat loss of up to  $100 \text{ W m}^{-2}$  (Isemer and Hasse, 1987).

Figure 11 contains a velocity field generated by the FCT model after 2 months of simulated time which serves as a diagnostic model. The density field did not change much but the initial adjustment of the velocity field to the density distribution, the boundary conditions, and the wind forcing has already taken place. The result is in fact very similar to that of the diagnostic calculations of Olbers et al. (1985) for the North Atlantic. However, it exhibits common shortcomings of all models considered here, namely the Gulf stream following the coast and the lack of a westward flow north of it. The diagnostic case confirms that the standard case reproduces the basic patterns of the flow field better than the two other cases. Note, however, that the depth of the main thermocline, which is also related to the diapycnal diffusion in the Gulf stream/NAC region, is reproduced best in the FCT case. At this point it is a matter of speculation whether the larger diapycnal diffusion in the standard case along the Gulf Stream/NAC is a realistic process or if the error in the Newfoundland basin is reduced for the wrong reason. The distributions in the Newfoundland basin in the World Ocean Circulation Experiment's Community Modeling Effort (CME) simulation are in much better agreement with observations than in any of the models considered here (F. Bryan, this volume). We may therefore expect that an analysis of the CME results will give some clues about the relevance of diapycnal processes in this crucial area.

## DISCUSSION

### A) Thermocline depth

It is tempting to explain the differences in main thermocline depths among the models as a transition from an advective-diffusive limit to a

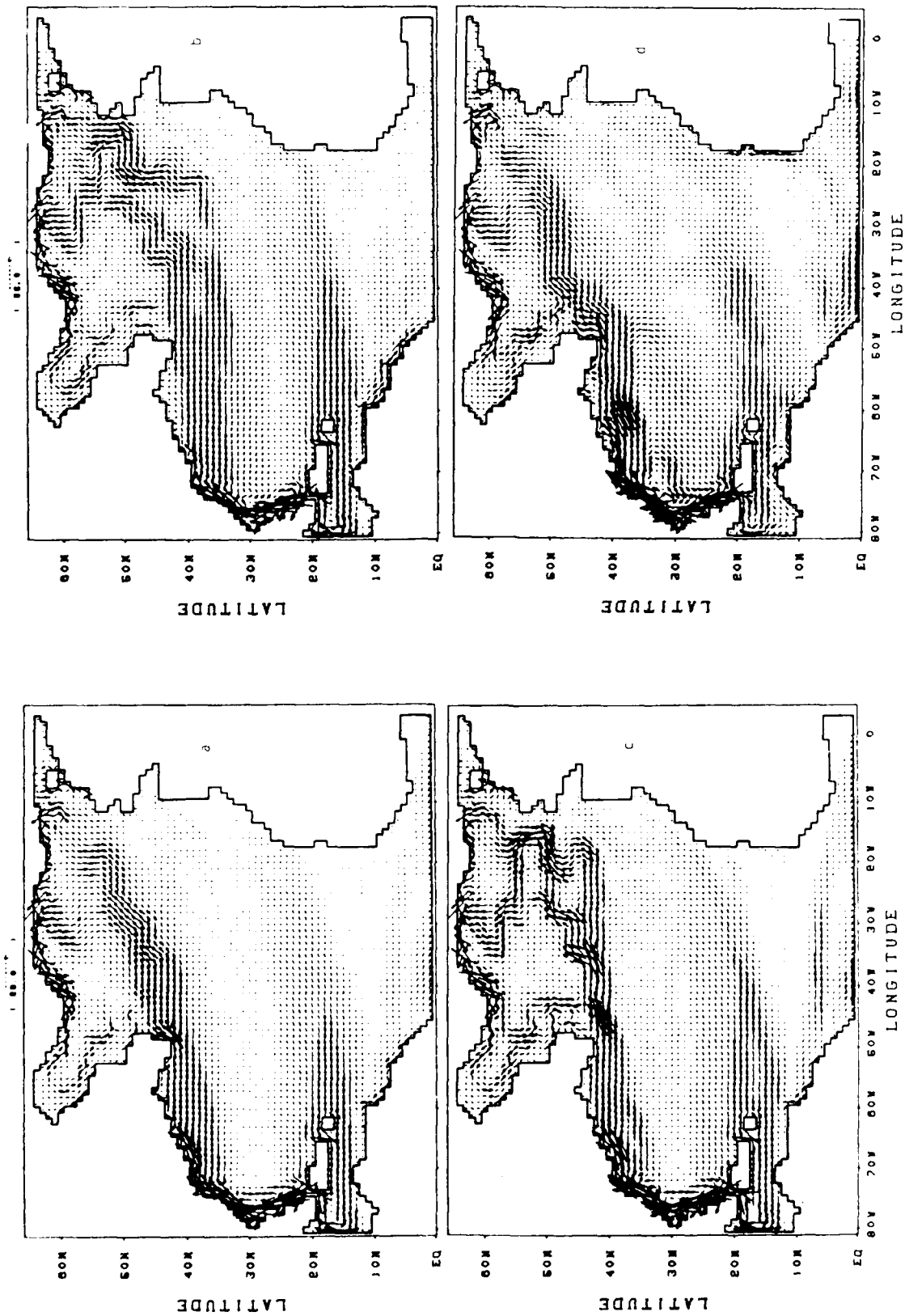


Figure 11. Velocity vectors at 301 m depth for the fine resolution (a) standard, (b) upstream, and (c) FCT cases; (d) is from the FCT model after 2 months of integration. The scaling of the vectors is given by the arrow above each panel.



purely advective regime. Scaling of the Sverdrup relation and the thermal wind equation yields (see e.g., Welander, 1986)

$$d = \rho_0 \beta L^3 W / (g \Delta \rho)$$

as an estimate for the depth of the thermocline where the symbols have their usual meaning:  $W$  denotes the scale for the vertical velocity. An advective-diffusive balance is assumed for  $W = A_{\text{VH}}/d$  while the purely advective balance corresponds to  $W = w_E$  where  $w_E$  is the Ekman pumping velocity in the subtropical gyre. With the first choice and  $L = 6 \times 10^6$  m,  $\Delta \rho / \rho_0 = 10^{-3}$ ,  $\beta = 2 \times 10^{-11} \text{ m}^{-1} \text{ s}^{-1}$  and  $g = 10 \text{ m s}^{-2}$ ,  $d$  turns out to be 270 m while  $W = w_E = 10^{-6} \text{ m s}^{-1}$  yields 450 m. This would imply a transition from an advective-diffusive balance in the upstream case to a more and more advectively dominated balance in the standard and FCT cases and finally in the actual ocean. However, the upstream scheme does not allow for an advective-diffusive balance, the ratio of the advective term and (implicit) diffusive term being approximately  $H/\Delta$  with  $\Delta$  the vertical grid size. This ratio is particularly big for motions with vertical scales  $H$  large compared to the grid distance. Hence we have to discard the possibility of an interior advective-diffusive balance in any of the experiments. The interior dynamics as well as the external forcing are identical in all cases and we should expect the effects of processes in the various boundary layers to be critical. Among the boundary layers are the western boundary layer, the mixed layer and the Gulf Stream/NAC as an internal boundary current (Huang and Flierl, 1987).

The upstream and FCT cases exhibit the largest differences in thermocline depth. From Fig. 7 we know that the effective horizontal mixing rates are widely apart in the western boundary layer whereas both schemes provide very weak mixing in the interior and across the internal boundary current. For depths below the mixed layer at most locations the horizontal density maps (Fig. 10) have already demonstrated the vastly different effect of the western boundary layer mixing on the density signal leaving the coast. The low mixing away from the boundary layer assures that this signal stays unaltered along the (zonal) stream lines. It therefore determines the density structure at this depth at the northern edge of the subtropical gyre right to the MAR.

The situation is different in the standard case where the western boundary layer mixing is comparable to that of the FCT case but the mixing is much stronger across the internal boundary current. This causes the considerable spreading of the isopycnals. The different roles of diffusion in this area could also be verified by direct evaluation of the thermodynamical balances for the individual experiments.

The mixed layer may also be regarded as a boundary layer where the dynamics of the models differ. The deviations of the predicted mixed layer temperatures and salinities from the reference fields used for the Newtonian damping are governed by the ratio of the advective time scale to the damping time scale. For small ratios the advection is the

dominant process and the mixed layer properties are close to their upstream values. If the ratio is large, then the properties in the mixed layer are almost equal to the reference values. The destruction of APE by the large horizontal mixing rates in the upstream case, for instance, retards the flow in the western boundary current and makes the influence of the reference values more pronounced than in the other cases. This clearly contributes to the effect of the diapycnal mixing and allows for additional diapycnal flow. The depth of the mixed layer also depends on the rate of the (lateral) advection. However, the effect of the mixed layer processes seems to be confined to the uppermost levels and not to be very important for the depth of the thermocline.

In summary it appears that the localized relatively large diapycnal mixing that is present in the standard and upstream cases is the reason for the similarly shallow thermoclines we notice for these experiments. The scenario of different diapycnal diffusion in the western boundary layer, transport of the emerging density signal, and different mixing in the internal boundary current shaping the potential vorticity distribution on the northern edge of the subtropical gyre also is consistent with the short time scale of the changes. The short time scale of adjustment in the indirectly ventilated zones of the subtropical gyre has already been noted by Cox and Bryan (1984). They find that the ages of particles on a certain density surface differ by less than a factor of two between the pool zone and the well ventilated zones. This surprisingly fast adjustment was attributed to the intense mixing in the western boundary current. Ierley and Young (1983) investigate the influence of a frictional western boundary layer in a 2-layer quasigeostrophic model of the wind-driven circulation and conclude that the boundary layer determines the vertical structure of the wind-driven flow in the Sverdrup interior. However, the effect of enhanced diapycnal diffusion in the boundary layer was not addressed in that study. The role of western boundary layer mixing and advection for passive tracers has been discussed by Musgrave (1985) and Young (1984). Their results, however, cannot readily be applied to our cases since the mixing strongly influences the flow field.

#### B) Mode water

One conspicuous effect of the different diapycnal mixing across the internal boundary current is the penetration scale of this current into the interior. The path and the longitudinal extent of this current at the boundary between subtropical and subpolar gyres influences several processes in both gyres.

The model solutions do not contain subtropical mode water as described by McCartney (1982). The mode water discussed with the potential vorticity section of Fig. 9 is formed by convection south of the Gulf Stream/NAC, remote from the North American coast. The area and depth of deep convection south of the stream vary with the position and apparently also with the intensity of the stream. In the upstream case mixed layer depths of more than 200 m are present predominantly around

30°N (Fig. 12). The corresponding area in the standard case stretches from 30°N in the west to 45°N in the east. The structure is more zonally oriented in the FCT case with largest depths around 35°N in most of the area. The maximum mixed layer depth increases from the upstream to the standard and FCT cases. Compared to the observations, large mixed layer depths occur too far to the south and also to the west in the models. The southern location corresponds to the more southerly path of the stream as shown in Fig. 11. Because of the lower surface reference density in the weak current region south of the NAC, the density of the mode waters is expected to be lower than observed. The density surfaces drawn in Fig. 9 indeed show a smaller density in the area of the mode waters. This is most pronounced in the upstream case where the mixed layer is displaced farthest to the south.

The differences in the mixed layer properties result in different ventilation patterns among the models as may be seen in Fig. 13 showing the vertically integrated transport between the potential density surfaces 26.6 and 26.8. The intense current moves the outcrop line in the FCT case eastward compared to the standard case. The inflow of weakly stratified water from the mixed layer into the density layer (note the thickness of the layer of 300 to 400 m) occurs farther to the east and south in the FCT case.

The differences between the models, however, seem rather subtle regarding the differences of each model compared with the diagnostic case (Fig. 13(c)). There water from the mixed layer enters the density layer at 40°N and between 45 and 40°W. It is carried eastward after subduction instead of southward and then westward as predicted in the models.

The outcrop lines of the 26.6 and 26.8 surfaces that are included in Fig. 12 indicate that the 'window' through which water from the deep mixed layer can enter the enclosed density layer indeed moves from around 45°W in the diagnostic case to around 30°W and 25°W in the standard and FCT cases respectively. The general mechanism of subpolar mode water formation and subduction is well represented by the models but the location of subduction depends sensitively on the mixed layer depth distribution. The latter is closely related to the buoyancy loss associated with the NAC.

### C) Mid-depth circulation and vertically integrated mass transport

The influence of the large zonal extent of the NAC on the surface heat flux in the Newfoundland basin and the inflow of subtropical water masses in the subpolar domain have already been discussed above. The actual transport into the subpolar basin furthermore differs among the models with larger transports in the FCT and upstream cases than in the standard case. The deep return flow mainly takes place along the eastern flank of the MAR and leads into a zonal westward flow south of the Azores (Fig. 14). This flow is much more intense and more confined in the upstream and FCT cases. The differences even show up in the stream

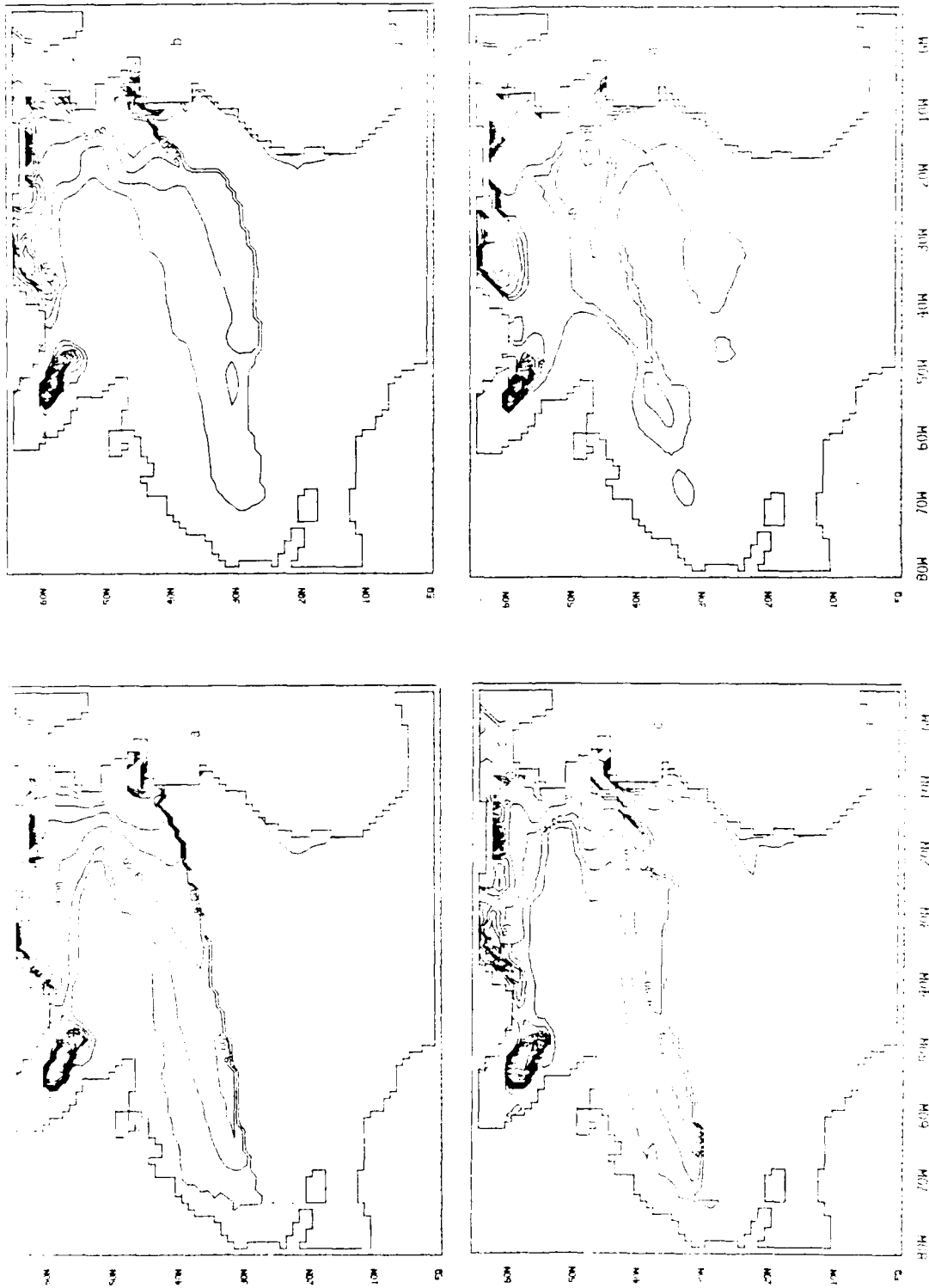


Figure 12. Mixed layer depth in units of 100 m for the fine resolution (a) standard, (b) upstream, and (c) FCT cases; (d) is computed from the initial density field. The mixed layer depth is based on a density criterion with  $\Delta\sigma = 0.05 \text{ kg m}^{-3}$ .

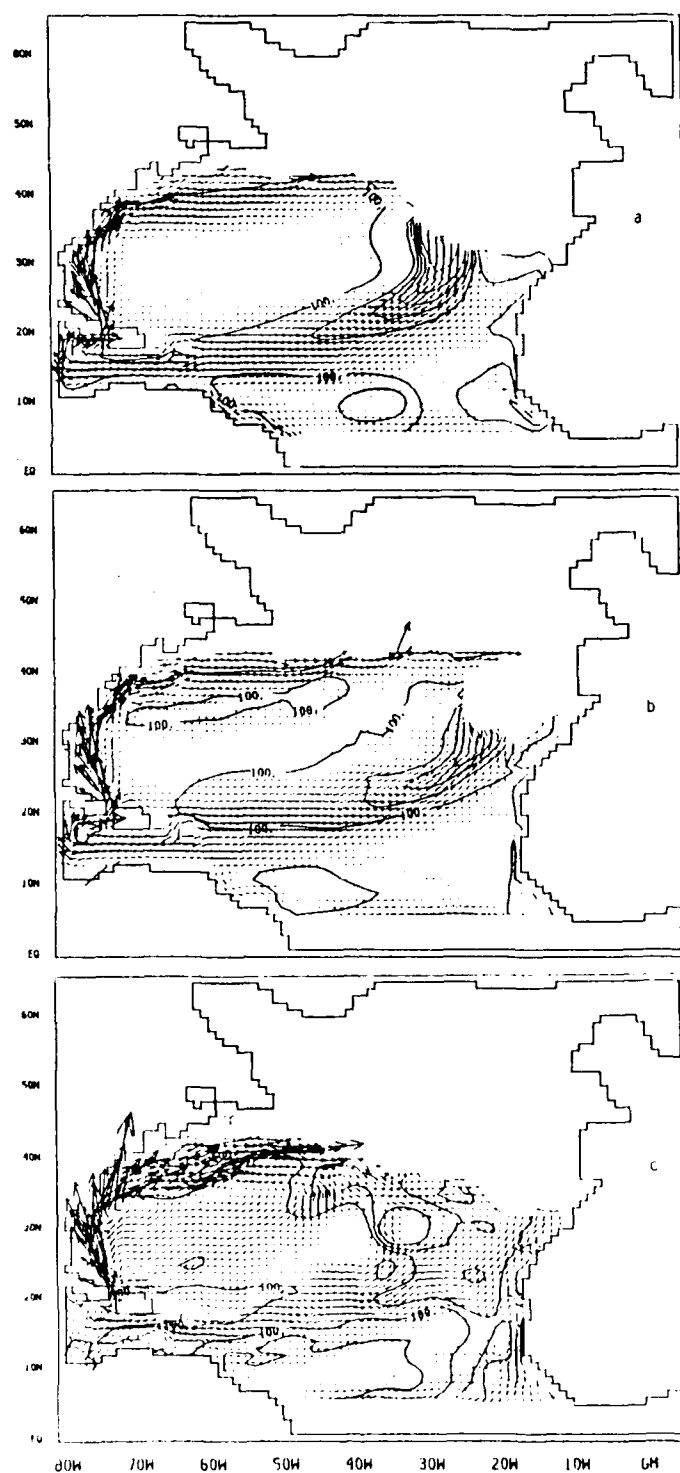


Figure 13. Vectors for the vertically integrated transport between the surfaces  $\sigma_{1500} = 26.6$  and  $26.8$  for the fine resolution (a) standard, (b) FCT, and (c) diagnostic cases; (c) is from the FCT model after 2 months of integration. Vectors are plotted only if both surfaces lie below the uppermost grid point.

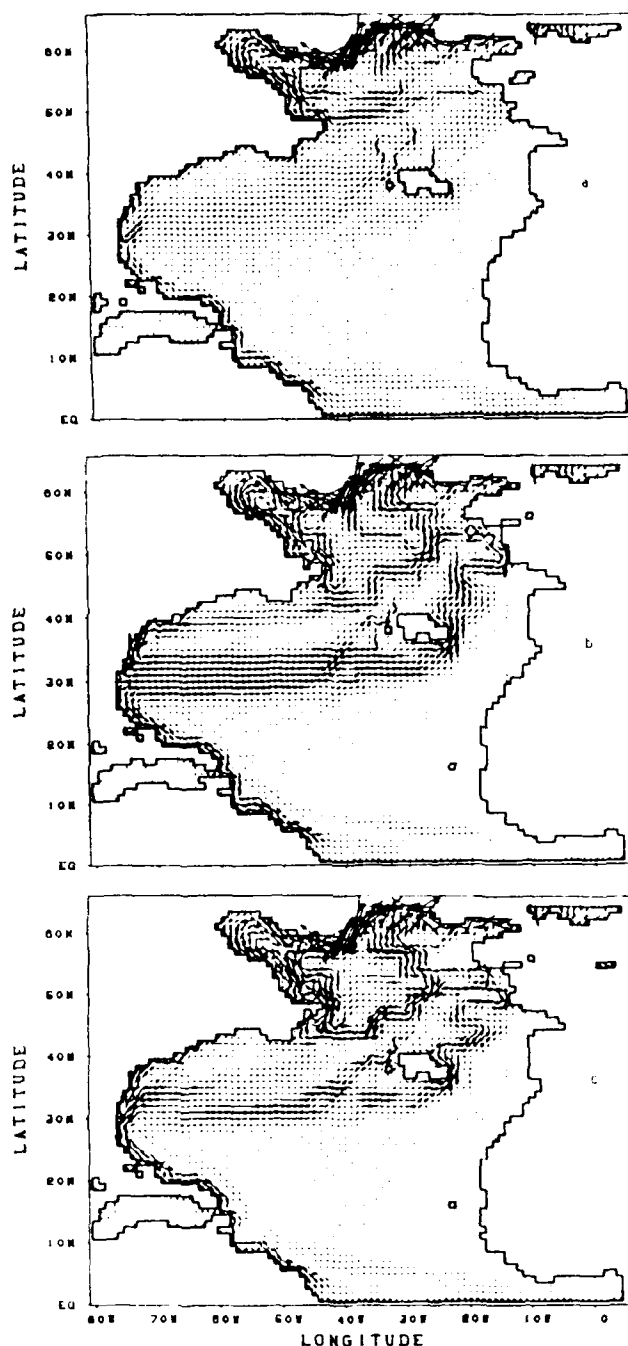


Figure 14. Velocity distribution on the surface  $\sigma_{1500} = 34.80$ . The depth of the surface is roughly 1500 m with very small variations except for the western part of the subpolar gyre where the surface is much shallower. This surface corresponds to the  $\sigma_0 = 27.75$  surface in the western part of the subtropical gyre. The  $\sigma_0$  surface, however, exhibits much larger depth variations than the  $\sigma_{1500}$  surface. The latter is a better approximation to a neutral surface than the former. (Compare You and McDougall, 1989)

function for the vertically integrated mass transport (Fig. 15). The patterns and the figures for the upstream and FCT cases are remarkably similar, including the anticyclonic cell which reinforces the subtropical gyre north of 30°N. Topographic influences are visible east of the Azores where a narrow current flows southward. The vorticity balance of the external mode is much more influenced by the bottom pressure torque term than in the standard case (compare Gerdes, 1988), which approximately obeys a purely wind-driven Sverdrup balance.

The southward flow along the eastern flank of the MAR carries low potential vorticity, low salinity (although saltier than the Labrador Sea water on the same density surface) water close to the high potential vorticity, high salinity Mediterranean water. The interaction of these water masses is rather different in the three experiments as may be seen from the salinity distribution on the  $\sigma_{1500} = 34.80$  surface (Fig. 16). The low interior mixing in the upstream case prohibits the entrainment of Mediterranean water in the flow. The Mediterranean water is shifted to the south and east compared to its initial position. The downstream salinity in the western basin is virtually unchanged from the value imposed in the deep mixed layer in the northeast corner of the domain. Isopycnal and horizontal mixing in the FCT and standard case respectively blends the two water masses, and intermediate salinities are found downstream in the western basin. The balance in the salinity equation is shown for the 1954 m level in Fig. 17. While advective-diffusive balances are found for the standard and FCT cases the contributions from horizontal and vertical advection balance in the upstream case. Note, however, the relatively strong vertical mixing in the upstream case.

Although the diffusion of salinity is similar in the FCT and standard cases, the diffusion of density is not. The isopycnal diffusion of the FCT case by definition does not affect the density distribution. The implicit horizontal mixing of the FCT scheme is by construction not stronger than with the upstream scheme and hence much weaker than in the standard case. The potential vorticity distribution on  $\sigma_{1500} = 34.80$  (not shown) of the upstream and FCT cases exhibits a separation of water masses like the salinity distribution for the upstream case. The standard case exhibits, on the contrary, a much smoother transition. This explains the confinement of the FCT and upstream flows compared to the standard case.

## CONCLUSIONS

Numerical dispersion that occurs with the central differences advection scheme may have a large impact on the results of an GCM on a global scale (Fig. 2). To suppress these effects vertical mixing with an Austausch coefficient of  $0.65 \times 10^{-4} \text{ m}^2 \text{ s}^{-1}$  was necessary in the coarse resolution model. We have to be concerned about this numerically necessary Austausch coefficient because it still lies in the range of vertical mixing rates where critical results of the model depend sensitively on the mixing. Lower order advection schemes like the upstream and FCT schemes preserve the monotonicity of the tracers

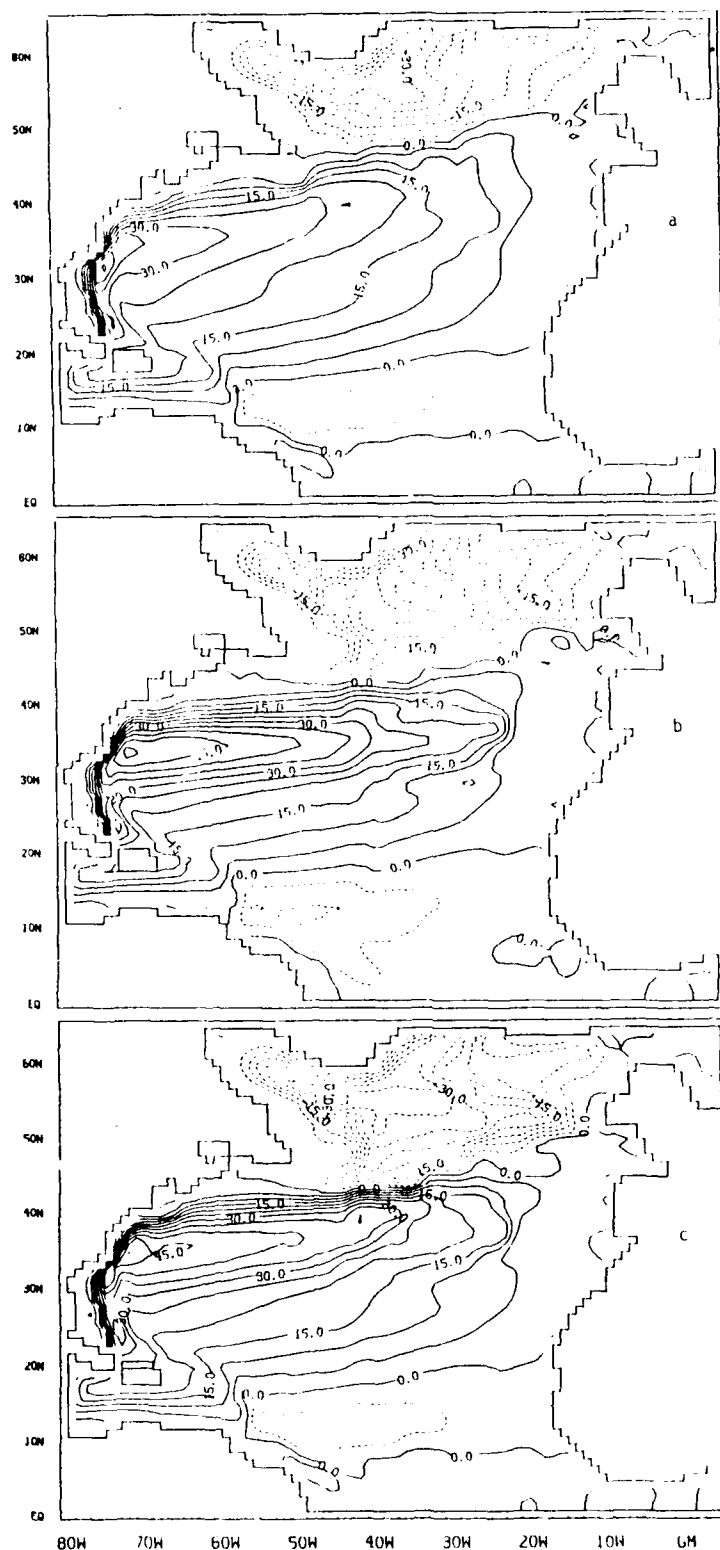


Figure 15. Stream function of the vertically integrated mass transport for the fine resolution (a) standard, (b) upstream, and (c) FCT cases. Contour interval 5 Sv.



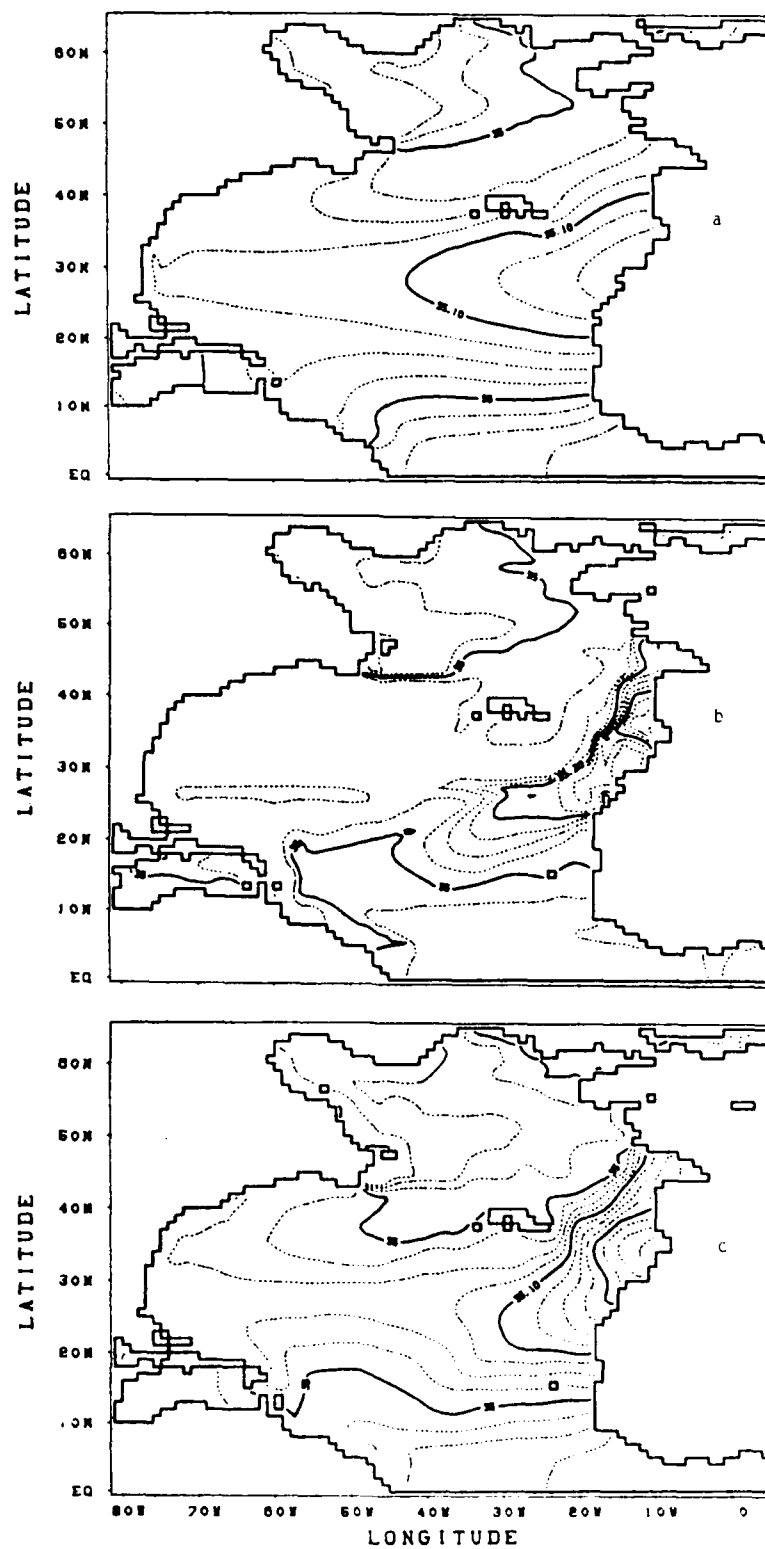


Figure 16. Salinity on  $\sigma_{1500} = 34.80$  for the fine resolution (a) standard, (b) upstream, and (c) FCT cases. Contour interval 0.005 psu.

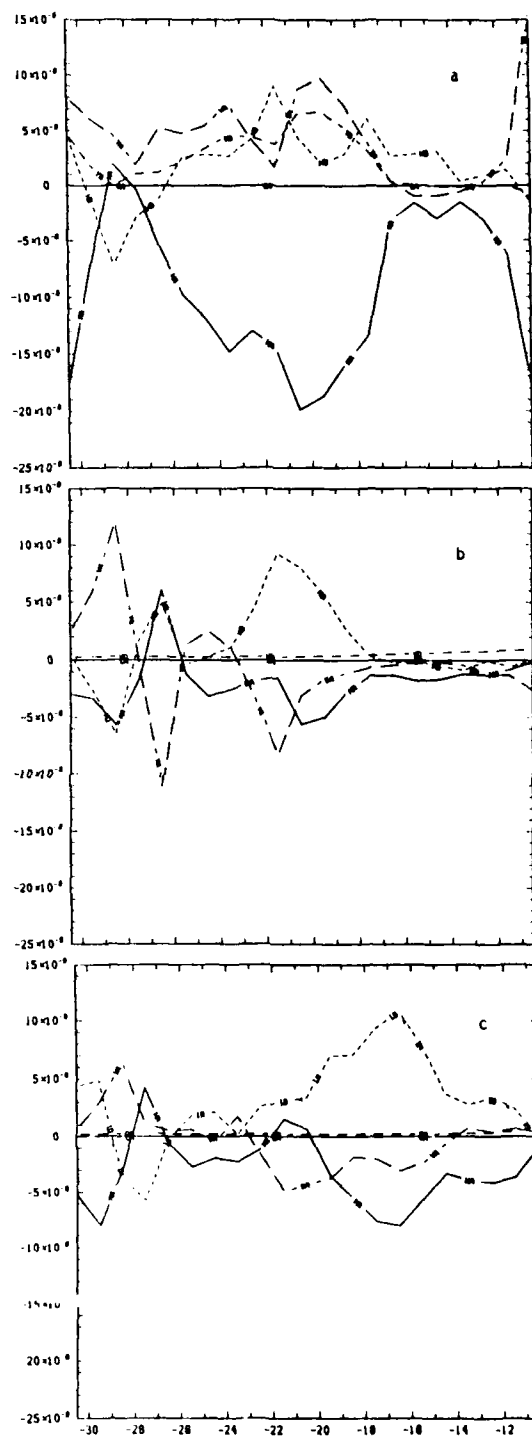


Figure 17. Average change of salinity during one timestep (in psu/s) for the fine resolution (a) standard, (b) upstream, and (c) FCT cases at 1954 m depth between 30 and 10°W due to HA: horizontal advection, VA: vertical advection, HD: horizontal diffusion, VD: vertical diffusion, ID+IM: isopycnal and implicit diffusion.

contrary to the second order central differences scheme. The lower order of accuracy is equivalent to an implicit mixing contained in these schemes which is especially high with the upstream scheme. The FCT algorithm may be regarded as a method to determine the numerically necessary minimum diffusivity.

Numerical properties of advection schemes limit our ability to choose physically meaningful turbulence closure scheme in oceanic GCMs. The effective vertical diffusion of the upstream and FCT advection schemes vary with depth as demonstrated in Fig. 6 for the coarse resolution cases. The trends in the magnitude of meridional heat and mass transports as well as in the thermocline depth are consistent with those found by F. Bryan (1987) in a series of experiments with different, but constant, vertical Austausch coefficients. However, this is only true as long as the diffusivities in the upper few hundreds of meters are considered. The very large diffusivity of the FCT case in the lower layers (compared with the standard case) does not increase the meridional transports in the FCT case over those of the standard case. On the contrary, the meridional transports are smaller in the FCT case. This corresponds to the relatively weak mixing in the upper 300 to 400 m. Similar conclusions were reached by Gargett (this volume) from experiments utilizing a vertical Austausch coefficient depending on static stability.

As the horizontal resolution is increased, the dependence of the results on the numerical advection scheme is not necessarily reduced. The velocity in boundary layers that are essentially one grid size wide increases by roughly the same factor by which the grid distance is decreased. The magnitude of the implicit diffusion of the upstream scheme remains constant in this situation. The reduction of implicit diffusion in the interior, where velocities do not increase, has only minor effects since the balance is already purely advective in the coarse resolution case. Diapycnal diffusion due to horizontal diffusion is negligible in the interior due to the small isopycnal slopes there.

The diapycnal component of horizontal diffusion is important in boundary layer regions like the western boundary current, the North Atlantic current, separating subarctic and subtropical water masses, and the boundary between subpolar mode water (from the outcrop of deep density surfaces in the northeast) and the Mediterranean water mass. The mixed layer is indirectly affected by the differences in diapycnal mixing.

The sensitivity of the higher resolution models to differences in the diapycnal diffusion due to horizontal diffusion shows up in the inflow of subtropical water in the subarctic gyre, the ventilation of the subtropical thermocline and the vertically integrated transport in the central parts of the subtropical gyre region. The NAC plays a crucial role for the distribution of properties in the interior of both gyres. The reduction of diapycnal mixing in the FCT case means less destruction of APE than in the other models and results in a strong internal boundary current which penetrates into the interior much farther than observed. This behaviour is reminiscent of the jets considered by

Schmitz and Holland (1986) which penetrate further when they are more stable against baroclinic instability.

While it seems feasible (at reasonable cost) to increase the vertical resolution to a degree where implicit vertical diffusion or necessary explicit diffusion are no longer relevant compared to the physical diffusion, this does not hold for the horizontal resolution. The numerically necessary diffusivities at  $1^\circ$  horizontal resolution are still uncomfortably high in the western boundary layer. Note that from this perspective the horizontal mixing rate for the standard case is too low. Further refinement of the grid leads into a physically unstable regime without a steady solution. The computational costs grow like the cube of the inverse grid size (as opposed to a linear increase for the vertical resolution in most practical applications) and the logistical problems of handling model output become considerable.

However, certain aspects of the FCT solution, namely the maintenance of fronts in the western boundary layer, Gulf stream extension and North Atlantic current, which are more intense than in the climatological averaged data, and an internal boundary current crossing almost the whole basin, indicate too low overall mixing in this experiment. The preparation of the available climatology, however, is not free of arbitrarily introduced smoothing that corresponds to horizontal diffusion in the model. This arbitrary smoothing also enters the estimates of mixing rates from inverse models (Olbers et al., 1985; Olbers, this volume). Regional climatological data sets that take advantage of the higher density of observations in the western boundary layer region of the North Atlantic would be desirable to assess more accurately the mixing corresponding to a mean state. Some insights on how much diapycnal diffusivity is actually due to eddy processes (directly and indirectly) may eventually be gained from the eddy resolving models like the CME.

We are at the moment quite capable of incorporating in large scale numerical models physically motivated models of the vertical diffusivity. One has to be aware that this requires adequate vertical resolution. The results will, however, be obscured somewhat by the diapycnal diffusion due to inevitable horizontal diffusion that will appear rather localized. This interferes with the higher diapycnal diffusivities indicated by inverse models in the same regions.

The easiest way to overcome these difficulties seems to be to wait for another considerable increase in computing power to appear. This may be available in several years (Holland, this volume) and would allow us to conduct sensitivity studies at high vertical and horizontal resolution. Another alternative may be the use of higher resolution in certain areas, employing curvilinear grids (Blumberg and Mellor, 1987) or adjustable grids. Models formulated in isopycnal coordinates serve the same purpose since the numerically necessary diffusion is along density surfaces (Bleck and Boudra, 1986). However, these models have not yet been thoroughly tested in realistic configurations and in comparison with the more established models.

## ACKNOWLEDGMENT

The parts of this paper about the coarse resolution model are based on a work by C. Koeberle, J. Willebrand and the current author. This work was conducted at the Institut für Meereskunde an der Universität Kiel. It was supported by the Deutsche Forschungsgemeinschaft Bonn, Federal Republic of Germany, SFB 133 and by the Nationales Klimaforschungsprogramm under contract KF 21218 - TV 4.

## REFERENCES

- Bleck, R., and D.B. Boudra: 1986. Wind-driven spin-up in eddy-resolving ocean models formulated in isopycnic and isobaric coordinates. *J. Geophys. Res.*, 91, 7611-7621.
- Blumberg, A.F., and G. Mellor: 1987. A description of a three-dimensional coastal ocean circulation model. In: *Three dimensional coastal ocean models*, N.S. Heaps (Ed.), 1-16.
- Bryan, F.: 1987. Parameter sensitivity of primitive equation ocean general circulation models. *J. Phys. Oceanogr.*, 17, 970-985.
- Bryan, K.: 1962. Measurements of meridional heat transport by ocean currents. *J. Geophys. Res.*, 67, 3403-3414.
- Bryan, K., and L.J. Lewis: 1979. A water mass model of the world ocean. *J. Geophys. Res.*, 84, 2503-2517.
- Cox, M.D.: 1984. A primitive equation, 3-dimensional model of the ocean. GFDL Ocean Group Technical Report No.1, GFDL/Princeton University.
- Cox, M.D.: 1985. An eddy resolving numerical model of the ventilated thermocline. *J. Phys. Oceanogr.*, 15, 1312-1324.
- Cox, M.D.: 1987. Isopycnal diffusion in a z-coordinate ocean model. *Ocean modelling*, 74, 1-5. (Unpublished manuscript)
- Cox, M.D., and K. Bryan: 1984. A numerical model of the ventilated thermocline. *J. Phys. Oceanogr.*, 14, 674-687.
- Gerdes, R.: 1988. Die Rolle der Dichtediffusion in numerischen Modellen der Nordatlantischen Zirkulation. *Ber. Inst. f. Meeresk.*, Kiel, 179, pp.176.
- Gerdes, R., C. Koeberle, and J. Willebrand: 1989. The role of numerical advection schemes in general circulation models. In preparation.
- Hellerman, S., and M. Rosenstein: 1983. Normal monthly wind stress over the world ocean with error estimates. *J. Phys. Oceanogr.*, 13, 1093-1104.
- Huang, R.X., and G.R. Flierl: 1987. Two-layer models for the thermocline and current structure in subtropical/subpolar gyres. *J. Phys. Oceanogr.*, 17, 872-884.
- Isemer, H.-J., and L. Hasse: 1987. The Bunker climate atlas of the North Atlantic Ocean. Volume 2: *Air Sea Interaction*. pp.256.
- Levitus, S.: 1982. Climatological atlas of the world ocean. NOAA Technical Paper 3, pp. 173.
- McCartney, M.S.: 1982. The subtropical recirculation of mode waters. *J. Mar. Res.* 40 (Suppl.), 427-464.
- Meehl, G.A., W.M. Washington, and A.J. Semtner: 1982. Experiments with a global ocean model driven by observed atmospheric forcing. *J. Phys. Oceanogr.*, 12, 301-312.

- Musgrave, D.L.: 1985. A numerical study of the roles of subgyre-scale mixing and the western boundary current on homogenization of a passive tracer. *J. Geophys. Res.*, 90, 7037-7043.
- Olbers, D.J., M. Wenzel, and J. Willebrand: 1985. The inference of North Atlantic circulation patterns from climatological hydrographic data. *Rev. Geophys.*, 23, 313-356.
- Sarmiento, J.L.: 1986. On the north and tropical Atlantic heat balance. *J. Geophys. Res.*, 91, 11677-11689.
- Schmitz, W.J., and W.R. Holland: 1986. Observed and modeled mesoscale variability near the Gulf Stream and Kuroshio extension. *J. Geophys. Res.*, 91, 9624-9638.
- Welander, P.: 1986. Thermohaline effects in the ocean circulation and related simple models. In: *Large scale transport processes in oceans and atmosphere*. J. Willebrand and D.L.T. Anderson (Eds.), 163-200.
- You, Y., and T.J. McDougall: 1989. Neutral surfaces and potential vorticity in the world's oceans. Submitted for publication.
- Young, W.R.: 1984. The role of the western boundary layer in gyre-scale ocean mixing. *J. Phys. Oceanogr.*, 14, 478-483.
- Zalesak, S.T.: 1979. Fully multidimensional flux-corrected transport algorithm for fluid. *J. Comput. Phys.*, 31, 335-362.

## ON THE PARAMETERISATION OF DEEP CONVECTION IN OCEAN MODELS

Peter D. Killworth

Deacon Laboratory of the Institute of Oceanographic Sciences, Wormley, Godalming, Surrey

Address: Hooke Institute for Atmospheric Research, Department of Atmospheric, Oceanic and Planetary Physics, Clarendon Laboratory, Parks Road, Oxford OX1 3PU

### ABSTRACT

Large-scale oceanographic models either ignore deep convection entirely (e.g. quasigeostrophic models) or parameterise it by nonpenetrative convection of temperature and salinity. The processes involved are discussed, and a critical examination of the present methods is given. It is concluded that (a) the mixing by deep convection is non-penetrative; (b) the convective method used in the Cox code is inadequate, with various straightforward methods available for its improvement; (c) there is no need to mix dynamical quantities during the mixing of tracers by convection; (d) that convection can conceal erroneous tracer values caused by inadequate vertical resolution, and act as a false source of dense water; and (e) it is important to maintain identical timesteps for temperature and momentum during the process.

### INTRODUCTION

Oceanic deep convection is a difficult process to observe. Its occurrences appear to be transitory in both space and time, and take place under poor to appalling weather conditions. Thus until the recent advent of vertical Acoustic Doppler Current Profilers, SeaSoars, thermistor chains, etc., ocean modellers have been forced to deduce their physics from the semi-classical (and small) set of observations available.

These observations fall into two categories, summarised by Killworth (1983). The early data were almost entirely of shelf-slope convection, as typified by dense water formation in the Weddell Sea. Here, brine release by the formation of sea ice in winter creates a wide, shallow reservoir of dense water which, with the help of the prevailing circulation, moves off the shelf and begins to descend the slope. En route, it entrains surrounding fluid; the balance between entrainment, friction, dynamics, and thermodynamics is subtle in this and similar areas (Smith, 1975; Killworth, 1977).

Most ocean models do not yet include the effects of ice formation (but see Semtner, 1976, and later papers), and so will not be able to reproduce this convection. Additionally, the patent need for fine vertical resolution in the vicinity of the bottom-trapped plume of dense water and correct treatment of its dynamics also mitigate against the use of most oceanographic models save those which use sigma coordinates; these, too, have their own problems. Thus it seems unlikely that large-scale ocean models will successfully reproduce bottom water formation on the shelf and slope during the next decade.

The second category of deep convection is open-ocean convection. Typical examples include the northwest Mediterranean, or Medoc (the MEDOC group, 1970), the Labrador Sea (Clarke and Gascard, 1983), the Weddell Sea chimney (Gordon, 1978; Killworth, 1979) and polynya (Martinson et al., 1981). In such cases it is believed that some preconditioning mechanism causes a localised area of ocean to be able to respond, by vigorous vertical

convection, to surface cooling, stirring, or ice and brine formation. This convection typically takes place in a narrow chimney, of width 10 to 50 km, and is often accompanied by vigorous eddying at the chimney's edges. At the end of the convective period, a sinking and spreading phase occurs which is not well documented (e.g., Sankey, 1973). Events are believed to last for a period of a few weeks, and are thus statistically rare.

During the period of convection, it is clear that all passive tracers are well-mixed in the vertical (cf., for example, Clarke and Coote, 1988). This at least holds for spatial scales more than a few kilometers; but recent towed thermistor data by Scott (personal communication) near Iceland, appears to show smaller chimneys, on the scale of a few km, within which the mixing is far from complete. The Labrador Sea data (Clarke and Gascard, 1983) show similar small-scale features.

There is little evidence concerning the mixing of dynamical quantities, e.g. horizontal momentum. Recent observations in the Mediterranean by Schott et al. (1988) indicate continuous vertical velocities of the order of  $5 \text{ cm s}^{-1}$  during convective events, in good agreement with earlier observations (e.g. Voorhis and Webb, 1970; Clarke and Gascard, 1983). The structure of the horizontal velocities, however, is less well understood, largely because of the eddying activity.

The scale of many of these convective events is such that fine-scale models will shortly be able to resolve them. Thus, although running a large-scale eddy-resolving model to thermal equilibrium is still beyond oceanographers' resources, such models should be able to reproduce isolated chimney events with some degree of realism. Accordingly, the time is ripe to examine the way models treat convection in a critical manner. In this paper, we shall first discuss briefly the type of convection believed to occur in open-ocean events, and then discuss its implementation in ocean models, including comments on the role of asynchronous integrations.

## THE TYPE OF CONVECTION

Models for mixed layer dynamics are legion; those for deeper convection are rare. Anati (1970) has performed one of the few examinations of deep convective data to discover the role of wind stirring in the Medoc chimney of 1969. Having good estimates of the surface fluxes, and several sets of T-S data in the vertical, he was able to look at heat content and depth of mixed layer to find out the role of wind stirring in the convection. The two extremes he considered were: nonpenetrative convection (where the fluid mixes downwards when statically unstable, but only until the density structure becomes neutrally stable; in other words the mixed layer ends at a depth where the ambient density is exactly that of the mixed layer, as in Fig. 1b); and fully penetrative convection (where all the wind energy is used to mix the column further down than the nonpenetrative value would yield, as in Fig. 1a). He assumed the processes to be only vertical, which is probably a good estimate given that the geostrophic flow is largely around, not into, the convecting chimney.

Anati found that it was impossible to adjust the penetrative convection model to fit his data, whereas the nonpenetrative model gave excellent agreement with data no matter how it was applied (Anati permitted fits using the observed depth, or the observed time, or combinations thereof). The only disagreement in the nonpenetrative case was that the centre of the chimney region initially deepened slightly more rapidly than predicted, and the edges of the chimney consistently deepened at about 80% of the speed predicted from the one-dimensional model. Anati attributed this to advection of unmixed water from outside the chimney. This was later confirmed by Killworth (1976) in a two-dimensional model of the area; he found that the centre sank at 98% of the predicted rate, while the edge of the chimney deepened at 81 to 86% of the predicted one-dimensional rate. The differences were indeed induced by ageostrophic flow advecting less dense water into the convecting chimney. A typical solution is shown in Fig. 2.

As noted above, there is little observational evidence to suggest how the mixed water escapes into the surrounding water. In an unpublished study (1976) I used a general circulation model to emulate the breakup of



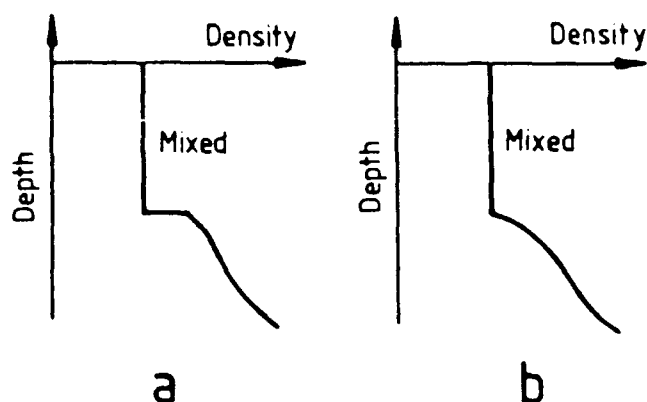


Fig. 1. A schematic of the two forms of convection considered here; (a) shows penetrative convection, where surface stirring acts to mix the density beyond a simple neutral stability; (b) shows non-penetrative convection, where there is no excess energy allowed to stir through the depth of neutral stability.

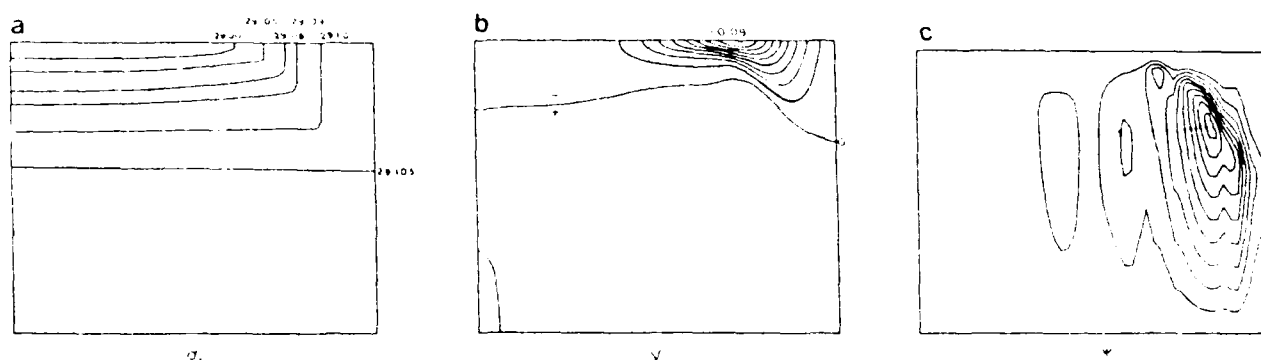


Fig. 2. Solution of a two-dimensional model of the sinking chimney in the Medoc region, after 10 days of convection, showing (a)  $\sigma_t$ ; (b) azimuthal velocity, contour interval  $0.01 \text{ m s}^{-1}$ ; and (c) stream function in the plane of viewing, contour interval  $0.04 \text{ m}^2 \text{ s}^{-1}$ . The axes are depth (vertically upwards), shown between surface and 2500 m, and radius of the chimney horizontally, out to 125 km.

the Medoc chimney after the cessation of surface cooling. Eddies were formed, in agreement with the linear theory (Killworth, 1976), but these had not acted to break up the chimney after three weeks of integration. That study was on an  $f$ -plane, however; studies of 'Meddies', etc. (McWilliams, 1985; Kase, personal communication; Davey and Killworth, 1989) suggest that the beta term may well play an important role in determining the fate of newly formed dense water. It is again unlikely that eddy-resolving models will be able to handle chimney breakup well, since the natural scales for subcoherent vortices can be as small as a few kilometers.

#### HOW CONVECTION IS HANDLED IN MODELS

Anati's (1970) findings are convenient for large-scale modellers, who have consistently used the parameterisation pioneered by Bryan (1969) and later co-workers. (Models of the surface mixed layer are of course more complicated. While it is not impossible that turbulence closure schemes such as Mellor-Yamada could be used for deep convection, to date such schemes have tended to be restricted to surface and local area modelling.) The Bryan parameterisation is very simple, at least as stated:

1. Predict the temperature and salinity at a new time step.
2. Examine each fluid column in turn. If there are regions of static instability, mix the fluid, conserving temperature and salinity within the unstable region. Continue checking the column until it is neutrally stable or better.

Some questions are still begged by this parameterisation. At present, for example, temperature rather than potential temperature is mixed. However, modifications would be easy to make.

The difficulty is that the above scheme is not what is actually done by the program codes currently in use (Semtner, 1974; Cox, 1984). These codes eschew the 'official' scheme, which can in principle take up a large fraction of computing time, and use a quicker and simpler approach:

1. Choose a number of iterations (NCON), defaulting to unity.
2. Examine each fluid column in turn. First, going down the water column, compare the density at each odd-numbered grid point with the density at the point immediately below. Mix these if they are unstable. Second, going down the water column, compare the density at each even-numbered grid point with the density at the point immediately below. Mix these if they are unstable. Repeat steps 1 and 2 NCON times for each fluid column.

This algorithm clearly takes only a predictable amount of computation time: hence its attraction. It relies on the assumption that after a 'sufficient' number of timesteps, the effects of surface cooling or densification will have propagated downwards through the water column. However, examination of circulation model results (e.g. those of Cox and Bryan, 1984) show large areas with static instability in the surface layers even in steady-state solutions. Willebrand (personal communication) has noted that the above algorithm needs an infinite NCON to converge. It is necessary to find out how inaccurate the algorithm can be.

We pose the following model problem:

$$T_t = T_{zz} + 1 \quad (1)$$

representing the nondimensional vertical heat diffusion equation for temperature  $T$ , with uniform (assumed advective) heating everywhere in the vertical, of magnitude unity. This heating is countered exactly by surface cooling:

$$T_z = -1, z = 0 \quad (2)$$

together with an insulated bottom:

$$T_z = 0, z = -1 \quad (3)$$

If  $T$  has the initial value 0 everywhere, then the only steady solution is one of overturning everywhere:

$$T = 0. \quad (4)$$

Fig. 3a shows steady solutions using eight gridpoints in the vertical, for varying values of NCON. Even for NCON as large as 10 - which formally at least permits the influence of the surface cooling to reach the lowest gridpoint every time step - the solution is statically unstable everywhere. Increased vertical resolution (Fig. 3b) makes the effect worse rather than better.

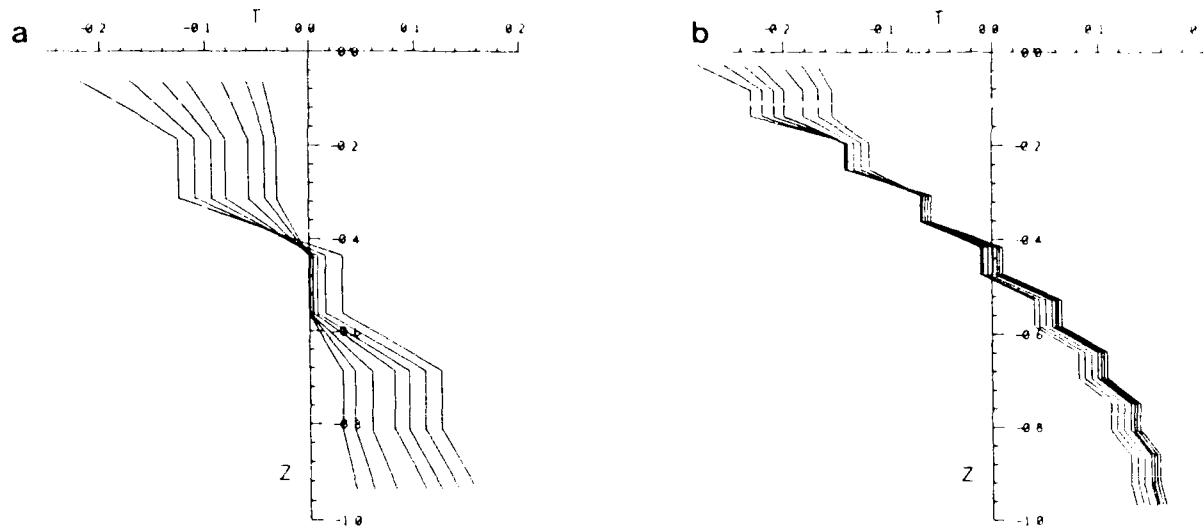


Fig. 3. Steady solution to the simple convection problem (1) to (4), using NCON passes of the standard convection algorithm. Reading from left to right at the top, NCON = 1, 2, 3, 4, 6, 8, 10. (The correct solution is identically zero.) (a) using 8 grid points; (b) using 18 grid points.

What matters, of course, are the relevant dimensional sizes involved. If we take a typical cooling amplitude  $Q$ , then temperature naturally scales with  $QH/(K\rho c_p)$ , where  $K$  is the diffusivity. For  $Q$  as low as  $4 \text{ W m}^{-2}$ ,  $H = 4 \text{ km}$ , and  $K = 10^{-4} \text{ m}^2 \text{ s}^{-1}$ , a temperature scale of  $40^\circ\text{C}$  is obtained, giving a surface error of  $90^\circ$ ! If the heating were produced by a uniform advective term  $vT_y$ , with  $v$  of order  $2 \text{ mm s}^{-1}$ , and  $T_y$  as  $2^\circ$  in  $1000 \text{ km}$ , a surface error of  $150^\circ$  is found.

So even if there is much cancellation of terms (one would expect the majority of the advective effect to be surface concentrated, for example, or at least above the thermocline) there is a large potential for error using the traditional algorithm. We conclude, therefore, that vertical mixing should be done exactly; several suitable algorithms exist for the purpose. (It is less clear that  $T$  should be mixed; one might prefer a formulation based on mixing potential temperature, if mixing over a wide depth range occurs.)

An alternative method would be to increase  $K$  dramatically when there is instability. The current models, however, use an explicit diffusion scheme, which would involve an unacceptably small time step. If the diffusion time over the entire depth is of order the advective time, given by  $H/w$ , where  $w$  is a few  $\text{cm s}^{-1}$ ,  $K$  would have to be  $2.5 \times 10^2 \text{ m}^2 \text{ s}^{-1}$ , and the time step would be around a second. It would not be difficult to modify existing codes to make the vertical diffusion implicit (although see next section). Alternatively, the suggested parameterisation discussed by Gargett (this volume) has this effect; but the explicit timestep must again be limited to ensure numerical stability.

#### WHAT SHOULD BE MIXED?

When deep convection occurs, it is clear that all passive tracers should be mixed. The question arises as to active tracers, typically horizontal momentum. Are water particles exchanging position vertically at a rate sufficient to combat the restructuring by thermal wind balance, which occurs on a timescale of  $f^{-1}$ ? It is interesting to note that laboratory models and calculations (e.g. Gill et al., 1979) allow for momentum as well as density mixing in the vertical. (The more naturally conserved potential vorticity is not well-defined in convective situations, and so would be hard to mix in a sensible way.)

Estimates of the competition between vertical mixing of momentum and thermal wind tendencies are frustratingly equivocal. Suppose we take a typical vertical velocity scale  $w$  to be  $5 \text{ cm s}^{-1}$  as noted earlier. This moves a water particle 200m in one hour, so that in mid- to high-latitudes, a water particle moving unidirectionally (an assumption for which there is no direct evidence observationally in general) would move about a kilometer in a time  $f^{-1}$ , where  $f$  is the Coriolis parameter. Put another way, estimates of vertical advection of horizontal momentum, divided by Coriolis force, are of order  $w/fh$ , where  $h$  is a vertical length scale. Using the above figures, this ratio is about 1/2 for  $h = 1 \text{ km}$ , or 1/10 for a depth of 5 km. Thus the effects of vertical stirring may or may not be relevant.

It is thus logical to examine the results of imposing two extremes on momentum stirring. One extreme, as currently used, assumes no momentum mixing; the other, probably unjustified, assumes 100% momentum mixing, i.e. averaging  $u$  and  $v$  vertically wherever there is convective overturn.

The effects of mixing or not mixing momentum are likely to have little effect on the resulting density structure. If we consider the advection of momentum,  $\mathbf{u} \cdot \nabla \rho$ , there will be no vertical component if overturning is taking place since  $\rho_z$  is identically zero. Let us first consider no momentum mixing. Then the horizontal velocities  $u$  and  $v$  are, under most realistic circumstances, largely dominated by thermal wind balance, so that  $v \propto -\rho_x$ ,  $u \propto \rho_y$ , and the advective terms vanish identically. More formally, if we pose a mixed layer of depth  $D(x,y)$ , whose density is  $\rho_m(x,y)$ , with a stably stratified layer below it, above a flat bottom at depth  $H$ , we may write

$$v = v_D - g\rho_{mx}(z + D)/f \quad (5)$$

$$u = u_D + g\rho_{my}(z + D)/f \quad (6)$$

where  $u_D(x, y)$ ,  $v_D(x, y)$  are the velocities at the base of the overturned layer. Using a streamfunction  $\psi$  for the depth integrated flow, we have

$$v_D = (1/D) \left[ \psi_x - \int_{-H}^{-D} v \, dz + g\rho_{mx}D^2/2f \right] \quad (7)$$

$$u_D = (1/D) \left[ -\psi_y - \int_{-H}^{-D} u \, dz - g\rho_{my}D^2/2f \right] \quad (8)$$

Substituting, we find the horizontal advection of density is

$$\mathbf{u} \cdot \nabla \rho = J(\rho_m, \psi)/D - (1/D) \left[ \rho_{mx} \int_{-H}^{-D} u \, dz + \rho_{my} \int_{-H}^{-D} v \, dz \right] \quad (9)$$

where  $J$  represents the horizontal Jacobian, and all other terms cancel identically. In other words, the density in the overturned region is advected solely by the geostrophic component of flow not associated with the mixed region.

If now we pose the other extreme, in which  $u$  and  $v$  are well-mixed in the overturned domain, then the advection is given by precisely the same formula (9) - although, of course, the values of velocity below the layer etc., may well differ, as would  $\psi$  if the bottom were not flat. However, the point is that there is no a priori reason to expect strongly differing density structures between the two extreme mixing cases.

The velocity structure itself will differ because of advection of momentum - normally small - or viscosity. It is more difficult to estimate the latter terms, especially since total  $u$ ,  $v$  mixing will yield velocity jumps at the base of the overturned region. However, order of magnitude estimates suggest these to be small also. Thus the evidence suggests that results which either permit or do not permit velocity mixing should be similar.

Two tests of this fairly handwaving result have been made.

#### A two-level thermocline model

Killworth (1985) described a simple numerical two-level thermocline model, applicable to a two-gyre ocean basin of size 4000 km. The model is basically a flat-bottomed two-level Cox (1984) general circulation model, with 20 grid points in each direction. The dynamics of each level are geostrophic north-south, and have a small linear drag added east-west in order to provide a simplistic western boundary layer. It is straightforward to deduce the depth-averaged flow, which is Sverdrupian, and divergent. There is a prescribed surface mixed layer, which generates an Ekman pumping velocity and a surface density field. The density of each layer is computed by a full time-dependent advective-diffusive equation, where one-sided differences are used in the vertical to avoid an erroneous numerical mode (see the second model discussed below). Full details are to be found in the paper cited.

Two versions of the model have been run to a steady state.

Version A - the model described in Killworth (1985) - permits only density mixing when convection occurs. There may be mixing from the mixed layer downwards (when the relevant points below it are given the same density as the mixed layer) or from the first to the second level (when the densities of the two levels are averaged). Version B is identical, save for mixing of  $u$  and  $v$  between levels 1 and 2 whenever density is mixed there. Note that the flat bottom means that the density structure has no effect on the barotropic flow.

Figs. 4 and 5 show the results of versions A and B respectively; the reader is invited to detect the differences between the two cases by eye! The only noticeable difference concerns the small convective region north of the western boundary current (about 11 or 12 grid points north of the southern boundary). This became totally steady in version A, but the precise location of convection changed very slowly, without ever settling down, in version B, although the stratification always remained extremely weak there. This is reminiscent of the results of Bryan (1986b), to be discussed later.

Both cases show a pronounced subtropical gyre, and a much weaker, less well-defined, subpolar gyre. The western boundary current separates from the coast and moves northeast, eventually impinging on the eastern boundary. In common with many more complex models, there are insufficient dynamics to divert the incoming eastward flow, so that a strong downwelling occurs at the northeastern boundary, aiding the convective process. This deep convection, combined with momentum mixing, has the effect of replacing the relatively strong baroclinic  $u$  flow with the weaker barotropic circulation (compare the upper level velocity vectors in the northeast between Figs. 4 and 5). However, the predominant geostrophic dynamics prevents these differences from altering the momentum away from the overturned regions.

#### An eight-level Cox general circulation model

In order to examine the effects of including nongeostrophic dynamics and a scale-selective dissipation, and also to permit convection to reach to a varying number of gridpoints, a version of the Cox (1984) model was run in a similar situation to the two-level model above. The model was contained in a basin of the same size, with depth intervals ranging from 50 m at the surface to 1400 m at depth, with a zonal wind stress designed to produce an Ekman pumping identical to that used in the two-level model. (This will also yield Ekman fluxes into the north and south boundaries, an effect not present in the earlier model.) The density was prescribed at the surface by giving a surface temperature which, using a simple linear equation of state  $\rho/\rho_0 = -\alpha T$ , gave the same surface

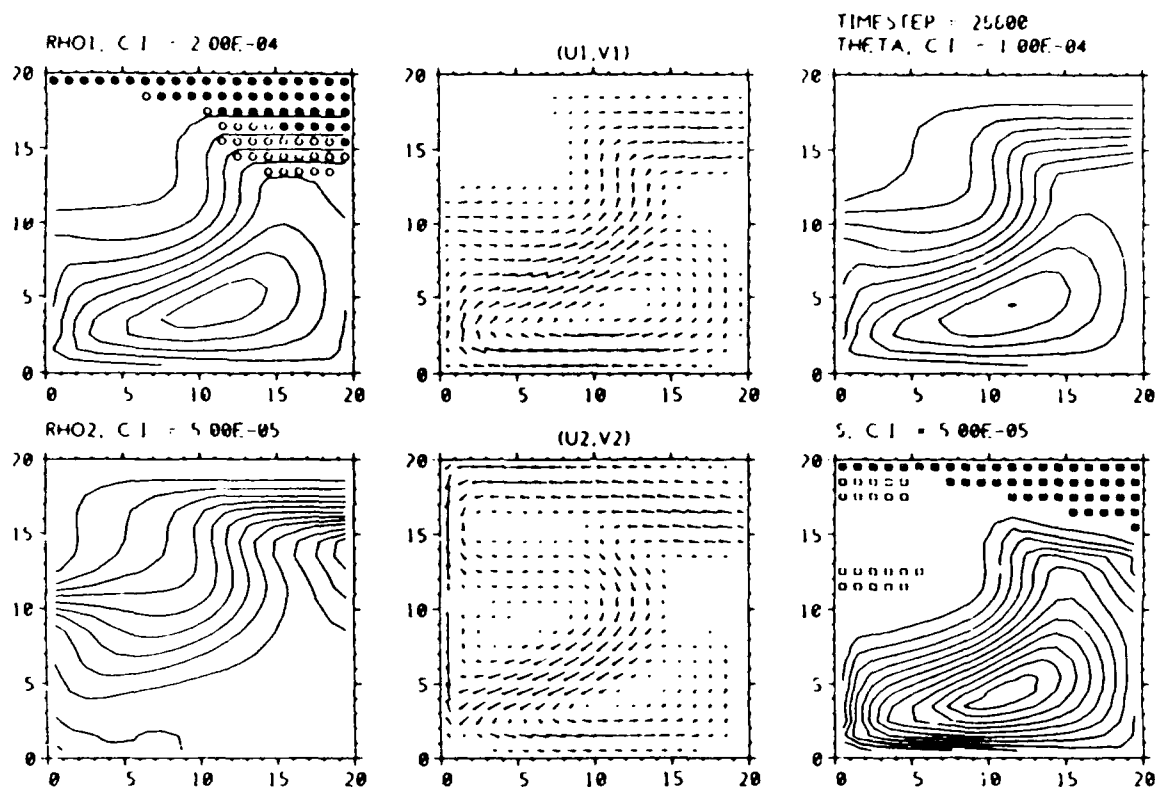


Fig. 4. Results of version A (only density mixing) of the two-level thermocline model. In all cases, axes are east and north; both directions span 4000 km. Top to bottom, and left to right, the panels show: upper level density, contour interval (c.i.)  $2 \times 10^{-4}$ ; lower level density, c.i.  $5 \times 10^{-5}$ ; upper level velocity (a vector of length one gridpoint has magnitude  $10 \text{ cm s}^{-1}$ ); lower level velocity (a vector of length one gridpoint has magnitude  $1 \text{ cm s}^{-1}$ ); the depth averaged temperature, c.i.  $10^{-4}$ ; and (half) the density difference between the two levels, c.i.  $5 \times 10^{-5}$ . In the first frame, a circle denotes convection from mixed layer to surface level; a cross further denotes convection to the bottom. In the last frame, a square denotes convection from upper to lower level, with the cross as before.

density as before. The horizontal grid spacing remained the same. The horizontal viscosity (diffusivity) was  $10^5$  ( $10^3$ )  $\text{m}^2\text{s}^{-1}$ , with vertical eddy coefficients both  $10^{-4} \text{ m}^2\text{s}^{-1}$ . Four passes through the overturning algorithm were used, with the addition that any convection involving the prescribed surface value of temperature had the 'average' value replaced by the surface value. This considerably speeded up convergence, and largely overcame the objections raised earlier. 'Asynchronous' integration was used (see later), in order to reach a steady state. Two versions (A and B) were again run to a steady state, and the results compared.

Fig. 6 shows results from version A. The agreement with the two-level version is quite good, considering the limitations implicit in the latter. The western boundary current is now unidirectional in the top layer along the entire boundary, although current vectors are visible across to the northeastern boundary as before, where there is intense downwelling, with the water returning at mid-depth. Again, there is only a very weak subpolar gyre; the anticyclonic subtropical gyre is rather less well-defined than in the two-level case, although showing up clearly in the near-surface density field. Deep convection is again confined to the northern boundary, with southward extensions at the east. Only very near-surface is there convection in the vicinity of the western boundary current; this occurs only over a single vertical grid interval.

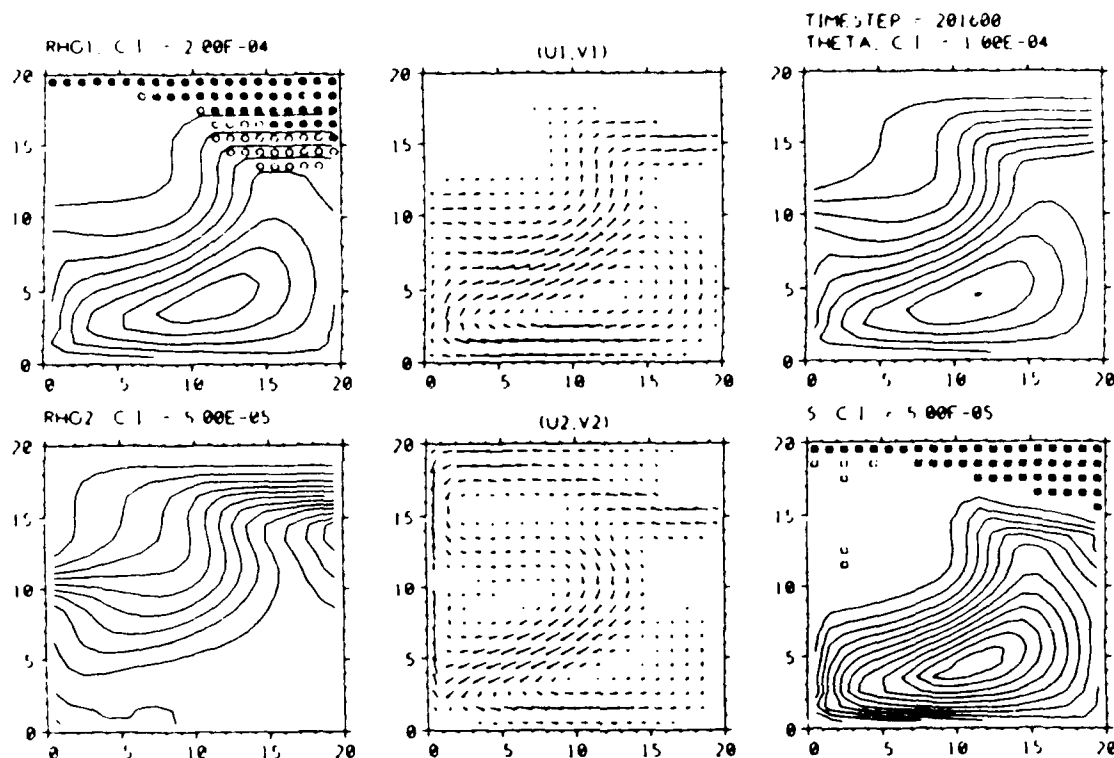


Fig. 5. As Fig. 4, but for version B (density and momentum mixing).

Fig. 7 gives a single example of the version B results, which show as before a striking degree of similarity to those without momentum mixing. More quantitatively, Fig. 8 shows some of the differences between the two cases. The velocity differences are confined to overturning regions, and the temperature (i.e. density) changes are minimal.

Two features of these results should be noted.

First, as in the two-level case, version B again possessed a quasi-random vacillation as to exactly which grid points overturn in the middle of the gyre circulation. Second, note the negative temperatures at depth. All prescribed surface values are positive, and the temperature satisfies an advective-diffusive balance. How, then, can negative temperatures occur?

We note that the vertical cell Peclet number ( $w\Delta z/K$ ) far exceeds the critical value of 2 near the eastern boundary, caused by the strong downwelling, and exceeds it elsewhere also. When this occurs, the numerical solution of a vertical advective-diffusive balance includes an erroneous steady plus-minus pattern in the absence of convection. This is the reason why the two-level model used one-sided differences, which do not suffer from this effect. Such a pattern would be immediately noticeable, except that static instability is induced when the pattern occurs in the density field. The resultant overturning disguises the plus-minus pattern, while inducing a source of negative temperature into the basin at depth. Thus users should be aware that convection may be induced numerically by features other than genuine physics, and may conceal shortcomings in the model which can only be handled properly by increased vertical resolution.

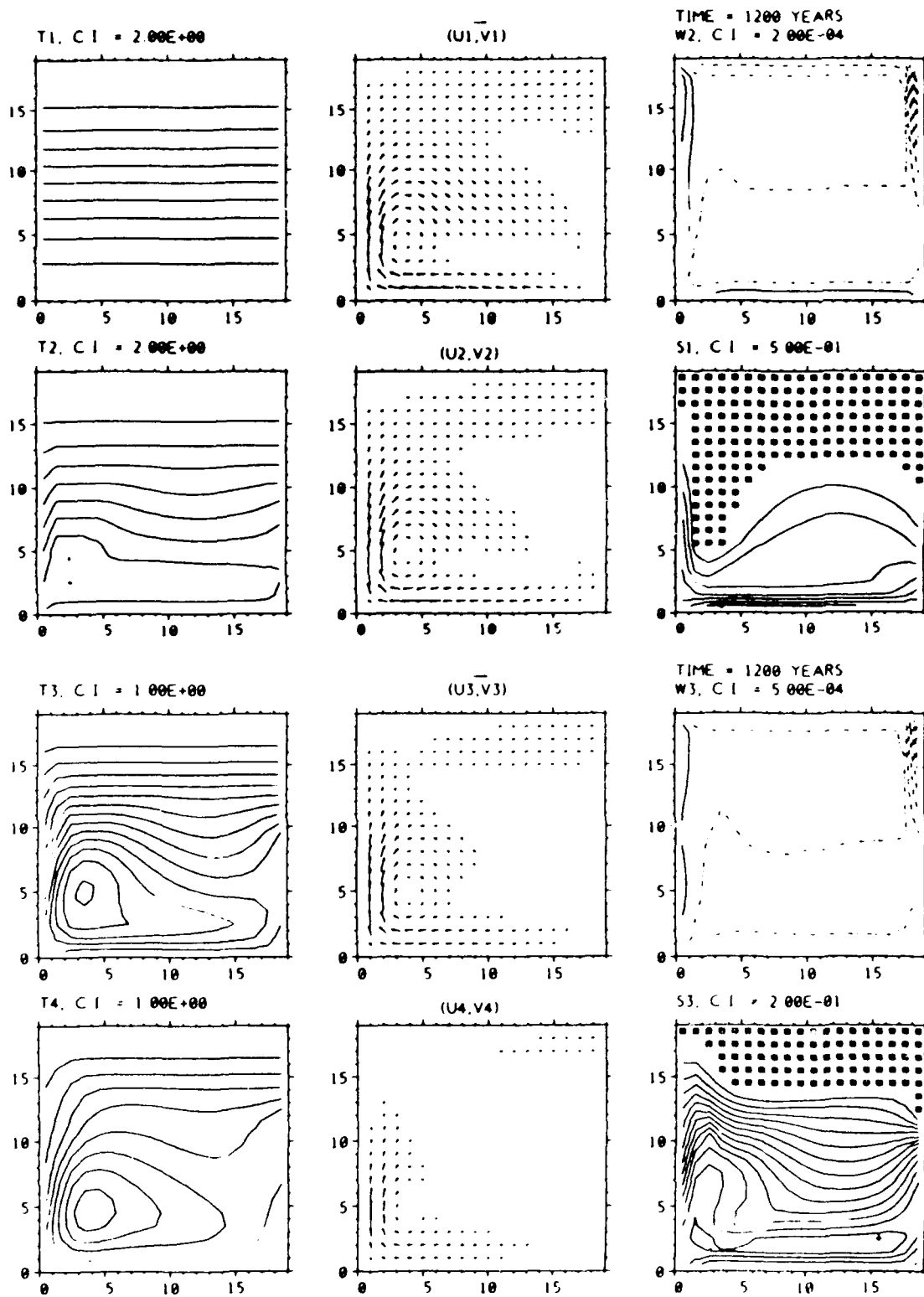
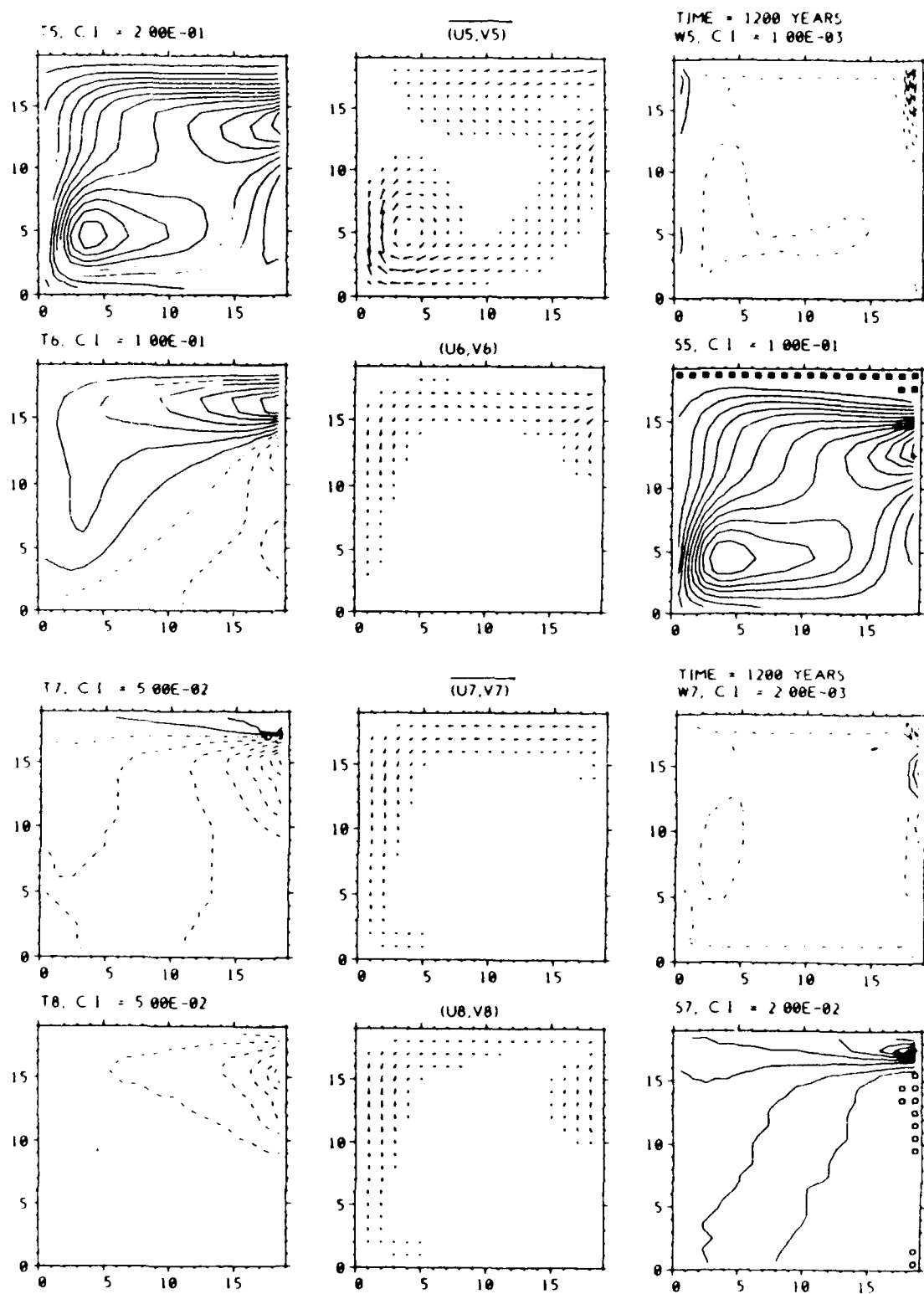


Fig. 6. The results of version A (only density mixing) from the eight-level Cox model. Each set of panels shows two successive levels, indicated on the diagram. Reading up-down and left-right, these are: upper and lower temperatures, upper and lower velocity vectors, vertical velocity at the base of the lower level, and (half of) the temperature difference between the two levels. Contour intervals (c.i.) are indicated; dashed contours





indicate negative values, dash-dotted the zero contour. The single velocity vector shown has a magnitude of  $10 \text{ cm s}^{-1}$ . A small square indicates convection between the two levels shown; a cross within the square indicates that convection has reached that level from the surface.

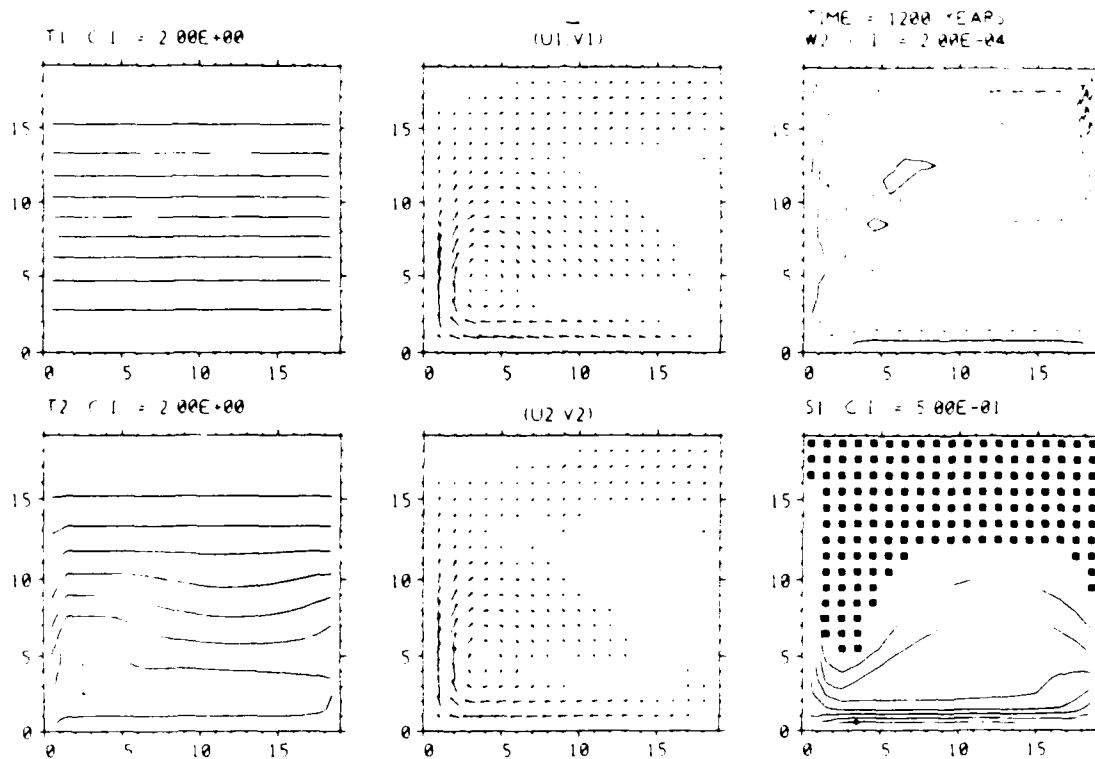


Fig. 7. A single example of the results of version B (density and momentum mixing) from the eight-level Cox model. See Fig.6 for details.

In summary, we find that solutions are largely independent of whether momentum is mixed when density is mixed. Accordingly, there is no reason to modify the manner in which deep convection handles momentum, at least from the data presented here. If the Bryan overturning formulation is used, NCON should almost certainly take values of order half the number of vertical grid points. Note also that numerical results should be treated with care since convection may obscure faulty numerics.

#### TIME VARIATION IN CONVECTIVE SITUATIONS

The previous studies were confined to steady, or nearly steady, situations. Convective events, on the small scale, are spasmodic and thus strongly time-dependent. Even coarse resolution climate models possess regions of deep convection, and such models are naturally time-dependent. We examine here the effects of time dependence on longer-term models which possess deep convection. Numerical restrictions mean that such models are coarse for the foreseeable future.

There have been several recent numerical models of single or double ocean basins which have examined the multiple equilibria problem. Although these are not our primary interest here, the results serve to emphasize the importance of 'asynchronous' timesteps on convective phenomena. This integration method uses an accelerative technique of Bryan (1984) (q.v. also Killworth et al., 1984) which uses a much larger T-S timestep than that used for dynamical variables. This is because diffusive effects determine the time scale for the abyssal circulation to settle to a steady state. The main dynamical effect of asynchronous integration is to slow down wave speeds.

Bryan (1986b; more fully discussed in 1986a) integrated to a steady state a model which was symmetric about the equator. He found difficulties in reaching a steady state when surface conditions were specified using a Haney (1971) condition, which imposes a flux of tracer proportional to the difference between the surface tracer value and a reference value for that latitude. His solution became statistically steady, but with a high degree of variability in high latitude regions, caused by intermittency in the depth of convection there. Figs. 8 and 9 show the mean salt flux at the surface, and its standard deviation, found by Bryan. This intermittency, judging from our results mentioned above, may be generic to coarse resolution calculations, and may not be due to boundary conditions - recall that the 8-level model used a specified surface temperature, not a Haney forcing.

Bryan then replaced the Haney forcing with the diagnosed surface salt flux, while retaining it for heat. Were the solution truly steady, this would not change the solution, of course. However, a gross modification to the solution, termed by Bryan a 'halocline catastrophe', occurred. The halocline strengthened and spread equatorward, interrupting deep convection and weakening the meridional circulation, on a time scale of around 80 years. Although he was able to find conditions under which this did not occur, Bryan suggests that this behaviour may occur in many models of ocean circulation, as well as the real ocean. It should be noted that Bryan's model used very asynchronous time steps; for temperature and salinity, steps of 5 to 8 days, while for velocity 20 minutes. It is not clear whether similar behaviour would occur with synchronous running.

His study then examined multiple equilibria. Bryan first created a two-hemisphere basin, by reflecting the steady solution about the equator, and continuing the run to confirm the steadiness. He then injected salinity anomalies into one hemisphere, and ran to a steady solution, generating an asymmetric solution to a problem with symmetric surface boundary conditions. This second solution involved a breakdown in deep convection in the unperturbed hemisphere.

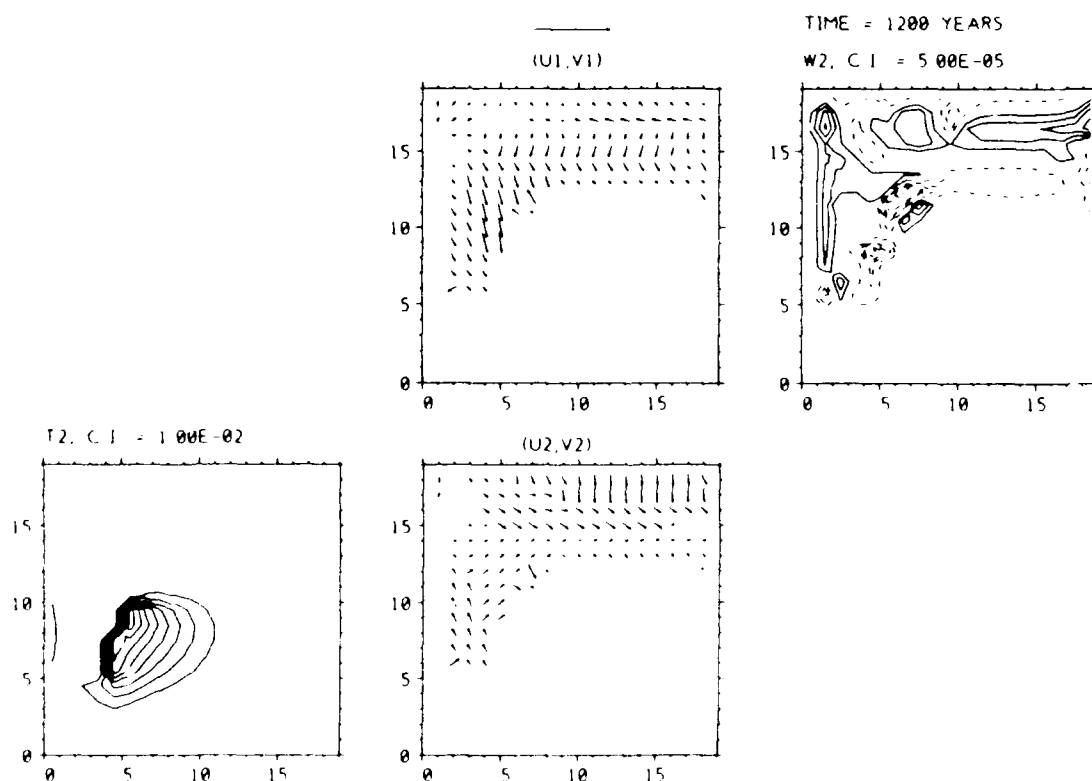


Fig. 8. An example of the differences (version A - version B). The four panels show the temperature at the second level, the velocity differences in the first two levels, and the difference between the vertical velocities at the base of level 2. Other details as Fig. 6. Note how differences are almost entirely confined to regions of convection, as expected.

Later work by Marotzke et al. (1988), using a two-dimensional simulation of a similar problem, found that convection was not needed to produce two-basin asymmetric solutions; indeed, their convective and nonconvective solutions appear very similar. There was no question of asynchronicity in their model, which derived velocity fields diagnostically.

The importance of asynchronicity was briefly discussed by Marotzke (1989), who monitored the variability of a single-basin experiment, and changed from a one-day timestep in periods of slow change to two-hour timesteps when there was rapid change. He noted (private communication) that his results changed significantly if this was not done. He ran a Cox (1984) model, using an algorithm for convection guaranteeing complete mixing, i.e. static stability. The boundary conditions are again a Haney heat flux, and a specified (diagnosed) salinity flux. The injection of a light salt anomaly in the near-polar surface waters leads to a sluggish, reversed meridional circulation which persists for around 7000 years. However, static instability in these regions can set in and spread to most of the basin in a period of just a few decades, with heat losses reaching  $130 \text{ W m}^{-2}$ . This situation is then followed by a very slow return to the previous circulation. The period of this oscillatory behaviour depends mainly on the vertical diffusion.

It is clear that the evidence that asynchronous integration can modify the longer-term temporal behaviour of a convecting system is far from complete. However, enough evidence exists that we may recommend that asynchronous timestepping should be avoided in climate models, if there is any likelihood of rapid changes of meridional flow induced by convective events.

#### ACKNOWLEDGMENTS

My thanks to Peter Muller and Crystal Miles for making the workshop such a pleasant experience, and to Jeff Blundell for producing Cox models at the drop of a hat.

#### REFERENCES

- Anati, D.: 1970. On the mechanism of the deep mixed layer formation during Medoc '69. *Cah. Oceanogr.*, 22, 427-443.
- Bryan, F.O.: 1986a. Maintenance and variability of the thermohaline circulation. Ph.D. Thesis, Princeton University, 254pp.
- Bryan, F. O.: 1986b. High-latitude salinity effects and interhemispheric thermohaline effects. *Nature*, 323, 301-304.
- Bryan, K.: 1969: A numerical model for the study of the circulation of the world ocean. *J. Comp. Phys.*, 4, 347-376.
- Bryan, K.: 1984. Accelerating the convergence to equilibrium of ocean-climate models. *J. Phys. Oceanogr.*, 14, 666-673.
- Clarke, R.A. and A.R. Coote: 1988. The formation of Labrador Sea water, Part III. The evolution of oxygen and nutrient concentration. *J. Phys. Oceanogr.*, 18, 469-480.
- Clarke, R.A. and J.-C. Gascard: 1983. The formation of Labrador Sea water, Part I. Large-scale processes. *J. Phys. Oceanogr.*, 13, 1764-1778.

- Cox, M.D.: 1984. A primitive equation, 3-dimensional model of the ocean. GFDL Ocean Group Technical Report No. 1, GFDL/Princeton University.
- Cox, M.D. and K. Bryan: 1984. A numerical study of the ventilated thermocline. *J. Phys. Oceanogr.*, 14, 674-687.
- Davey, M.K. and P.D. Killworth: 1989. Flows produced by discrete sources of buoyancy. *J. Phys. Oceanogr.*, in press.
- Gill, A.E., J.M. Smith, R.P. Cleaver, R. Hide, and P.R. Jonas: 1979. The vortex created by mass transfer between layers of a rotating fluid. *Geophys. Astrophys. Fl. Dyn.*, 12, 195-220.
- Gordon, A.L.: 1978. Deep Antarctic convection west of Maud Rise. *J. Phys. Oceanogr.*, 8, 600-612.
- Haney, R.L.: 1971. Surface thermal boundary conditions for ocean general circulation models. *J. Phys. Oceanogr.*, 1, 241-248.
- Killworth, P.D.: 1976. The mixing and spreading phases of MEDOC. I. In: *Progr. in Oceanogr.*, 7, Mrs. J.C. Swallow, ed., Pergamon Press, Oxford.
- Killworth, P.D.: 1977. Mixing on the Weddell Sea continental slope. *Deep-Sea Res.*, 24, 427-448.
- Killworth, P.D.: 1979. On 'chimney' formations in the ocean. *Journal of Physical Oceanography*, 9, 531-554.
- Killworth, P.D.: 1983. Deep convection in the world ocean. *Rev. Geophys. and Space Phys.*, 21, 1-26.
- Killworth, P.D.: 1985. A two-level wind and buoyancy driven thermocline model. *J. Phys. Oceanogr.*, 15, 1414-1432.
- Killworth, P.D., J.M. Smith, and A.E. Gill: 1984. Speeding up ocean circulation models. *Ocean Modelling*, 56, 1-3. (Unreferenced ms.)
- Marotzke, J.: 1989. Instabilities and multiple steady states of the thermohaline circulation. In: *Modelling the ocean general circulation and geochemical tracer transport*, D.L.T. Anderson and J. Willebrand, eds., NATO ASI series, Reidel, in press.
- Marotzke, J., P. Welander and J. Willebrand: 1988. Instability and multiple steady states in a meridional-plane model of the thermohaline circulation. *Tellus*, 40A, 162-172.
- Martinson, D.G., P.D. Killworth and A.L. Gordon: 1981. A convective overturn model for the Weddell Polynya. *J. Phys. Oceanogr.*, 11, 466-488.
- McWilliams, J.C.: 1985. Submesoscale coherent vortices in the ocean. *Rev. Geophys.*, 23, 165-182.
- MEDOC group: 1970. Observation of formation of deep water in the Mediterranean Sea. *Nature*, 221, 1037-1040.
- Sankey, T.: 1973. The formation of deep water in the Northwestern Mediterranean. In: *Progr. in Oceanogr.*, 6, B.A. Warren, ed., Pergamon Press, Oxford.

- Schott, F., K. Leaman and R. Zika: 1988. Deep mixing in the Gulf of Lions, revisited. *J. Geophys. Res. Letters*, 15, 800-803.
- Semtner, A.J.: 1974. An oceanic general circulation model with bottom topography. Unpublished ms., Princeton University.
- Semtner, A.J.: 1976. Numerical simulation of the Arctic Ocean circulation. *J. Phys. Oceanogr.*, 6, 409-425.
- Smith, P.C.: 1975. A streamtube model for the bottom boundary currents in the ocean. *Deep-Sea Res.*, 22, 853-874.
- Voorhis, A. and D.C. Webb: 1970. Large vertical currents observed in a western sinking region of the Northwest Mediterranean. *Can. Oceanogr.*, 22, 571-580.

## BOUNDARY CONTROL OVER THE LARGE-SCALE CIRCULATION

Peter Rhines and Parker MacCready

School of Oceanography, WB-10, University of Washington, Seattle WA  
98195

### ABSTRACT

Several examples are given in which the oceanic bottom boundary exerts important control over the large scale circulation (1) through the influence of the boundary shape, (2) from viscous stress exerted by the boundary, and (3) from spin-up processes and boundary layer divergence.

The most important new results are:

- the control exerted by the shape of an ocean basin on the vertical velocity (the 'hypsometric' effect) and its prediction of anticyclonic deep circulations with equatorward interior flow;
- the discussion of the angular momentum of ocean gyres;
- the discussion of the important role of normal viscous stress in free-slip boundary conditions [The two-dimensional free-slip boundary condition is

$$u_t \partial u / \partial n = K u_n; u_n = 0$$

for the tangential ( $s$ -) velocity  $u_t$  and normal ( $n$ -) velocity  $u_n$ ;  $K$  is the curvature of the boundary. This shows that the vorticity at the boundary is  $2Ku_n$ ].

- the shut-off of Ekman circulations by buoyancy forces in lab experiments on stratified spin-up in a bowl-shaped basin.

### INTRODUCTION

It is said: "The ocean has no sidewalls, just a bottom."

There is a tendency to imagine that the general circulation and many aspects of more (and smaller scale) motion near the oceanic boundary are independent of the oceanic boundary. Circulation models tend to use free-slip boundary conditions with vertical sidewalls, and even 'free-slip' conditions for higher order turbulence employed typical 'wall' boundary conditions. This is done to minimize the effects of lateral viscosity. But, in the last 10 years, it has become clear that the lateral viscosity is important in a general circulation

theory of the general circulation, it is remarkable how little study they have received in the context of numerical models. As these models advance, it will be important to represent boundary stress and mixing as an interaction with the sea floor. Our prejudice is that, until we get the potential vorticity dynamics of the boundary currents right, the relevance to reality of an entire model must be questioned.

Here we discuss several examples in which the detailed nature of boundary shape and boundary stresses exert important control over the general circulation.

## 1. RELATION BETWEEN BOUNDARY SHAPE AND THE DEEP CIRCULATION

The simple balance between vertical advection and diffusion of temperature and salinity, of the kind advocated in Munk's abyssal 'recipe', suggests a tight diagnostic relationship between stratification and vertical velocity. There are reasons to believe that this is not so. Acceptable scaling of the thermohaline equations allows significant slantwise advection, in which a large component of  $w$  is adiabatic. Then the cross-isopycnal mixing and advection can take the form of either 'direct' or 'indirect' 'meridional' circulation, to use terminology from atmospheric dynamics, with regions of densification having  $w < 0$  and release of APE in the former, and  $w > 0$  and conversion from KE to APE in the latter. One looks for other possible controls on  $w$ .

*Hypsometric Control.* The question is whether mixing does what it **can** or does what it **must**. Other controls exist over the vertical/meridional circulation. Suppose, for example, the thermohaline circulation is driven by a heavy plume of abyssal water entering through a topographic gap, or over a sill. In a bowl-shaped ocean basin, such that upward vertical motion is more or less uniformly distributed across the basin, conservation of mass requires that

$$(wA)_z = 0 \quad (1)$$

providing there is no entrainment by the plume. Here  $w$  is the vertical velocity averaged over the upward flow (excluding the downward flowing heavy plume) and  $A(z)$  the cross-sectional area as a function of depth. It follows that

$$w_z = -QA_z/A^2$$

Where  $Q = wA$  is the net volume flux of the source. On an  $f$ -plane the result is an average vertical vorticity, which can grow toward Rossby number,  $\epsilon \sim 1$ , being restrained only by friction. This follows Kelvin's theorem,

$$D/Dt (\int \mathbf{u} \cdot d\mathbf{z}) = -2\Omega DA_z/Dt$$



Where  $D/Dt$  is meant to emphasize that we follow the rising fluid and  $\Omega$  is the scalar magnitude of  $\Omega$ . Here  $A_1$  is exactly the projection of  $A$  on the equatorial plane perpendicular to  $\Omega$ ; it is approximately  $A \cos(\text{latitude})$  provided that disks of fluid are nearly horizontal.

For an f-plane, with steady  $w$ ,

$$D/Dt(\int \mathbf{u} \cdot d\mathbf{l}) = 2\Omega A w_z.$$

With the  $\beta$ -effect,  $f = 2\Omega \sin(\text{latitude})$ , we have the same integral constraint on  $\int \mathbf{u} \cdot d\mathbf{l}$ , yet a local balance

$$\beta v = f w_z = f Q A_z / A^2.$$

In a bowl-shaped basin  $A_z$  is large and positive, typically, at depths below 3500 m. Whether the upward motion is diapycnal or lies along isopycnal surfaces, the resulting vortex stretching induces an average anticyclonic flow. The negative  $w_z$  is opposite in sense to the  $w(z)$  profile assumed in the classic thermocline literature. The Stommel-Arons assumption has  $w$  increase from zero at the sea floor to a maximum in the thermocline, and it produces cyclonic general circulation. This may be thought to be the f-plane tendency which, with the  $\beta$ -effect, becomes lopsided, a poleward interior flow connecting to equatorward western boundary currents.

We would look for the hypsometric effect typically in the very deep waters, although there is the possibility that upward momentum transport may carry the anticyclone to mid-depths.

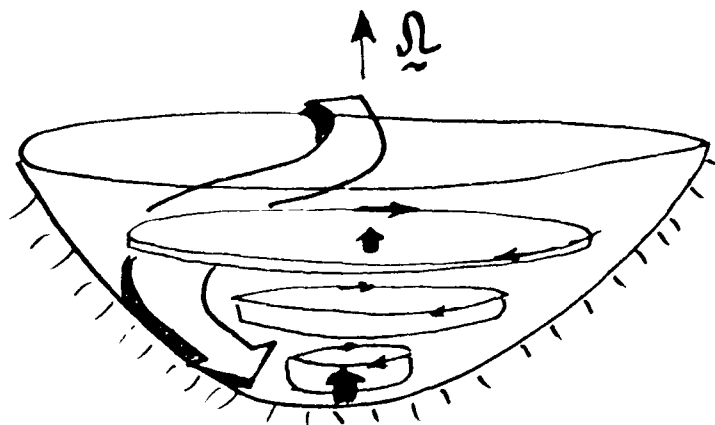


Figure 1. The horizontal divergence experienced by fluid forced to rise in a topographic basin, driven by a source of heavy abyssal water. The source tends to move in the 'Kelvin wave' sense, cyclonically, while the rest of the fluid moves anticyclonically.

We have carried out f-plane laboratory experiments to verify this effect

in a continuously stratified fluid. There are several subtle points about the 'obviously correct' Eq. (1). First, if the fluid is unstratified, there is no enhancement of the circulation by variations in  $A(z)$  at all. This is because the radial flow is confined to Ekman layers, while the interior has  $\partial w / \partial z = 0$ , owing to Taylor-Proudman 'stiffness'. Thus the interior swirl flow is set simply by the radial outflow in the boundary layer, and the hypsometric effect is absent.

Second, with continuous stratification on an  $f$ -plane, a confined deep source of fluid may tend, at least initially, to fill a region of aspect ratio  $f/N$ , which will be far smaller than the width of a typical ocean basin. By gradual interior spindown processes, the fluid will eventually drive the entire basin into motion. The long-term behaviour depends strongly on the nature of the sink of fluid: in the laboratory one can easily let the free surface rise; it does so uniformly and this broad sink essentially validates the use of Eq. (1). With a point sink the result would be very different.

When carried onto a  $\beta$ -plane, baroclinic Rossby waves tend to spread the influence of the source widely, and if the sink is again broadly distributed (for example, a uniform rising motion into the thermocline) then Eq. 1 is again validated.

This emphasizes that such flows are more truly **sink-driven** rather than **source-driven**. Thus we take the view complementary to Kawase's (1987). In the laboratory experiments that accompany this work the anticyclonic tendency was overwhelming; the entering heavy source plumes did move very slowly cyclonically, but the rest of the fluid in the basin moved in the opposite sense. In a right circular cylinder, where there is no hypsometric effect, the experiments showed a local cyclonic circulation of the inflowing source fluid, yet no measurable rotation of the remaining fluid in the container.

Rossby-radius effects and lack of  $\beta$  make the experiment incomplete insofar as the general circulation goes, but the transliteration to oceanic scaling suggests that the poleward flowing side of the anticyclone will intensify into a western boundary current, leaving the interior filled with equatorward flow. The Kelvin circulation integral still controls the amplitude, but it is now dominated by the currents in the boundary layer. Thus the strength of the broad interior flow depends on the level of friction at the boundary!

*Effect of Entrainment.* The descending plume is subject to mixing with the interior, and to entrainment of mass from the interior (note that these are distinct effects, depending on the effective Prandtl number, or ratio of buoyancy mixing to momentum mixing, of the process). The entrainment process is very difficult to scale down to laboratory experiments, for example, being sensitive to the detail of the injected jet. Instead one wants to develop a picture of the response of the rest of the circulation to various entrainment profiles. If now we let the volume flux of the plume, as it descends down the sloping bottom, be

described by a function  $Q(z)$ , then we have

$$w_z = Q/A - \int_0^z Q(z') dz' \quad A_z/A^2$$

These plume entrainment laws may be combined with other kinds of boundary mixing to provide models of the interior vertical motion.

## 2. WHEN DO DETAILED BOUNDARY DISSIPATION RATES MATTER FOR THE LARGE-SCALE CIRCULATION?

In the Urtexts of fluid dynamics we have examples where (it is suspected) large-scale flow of a fluid evolves independently of detailed dissipation rates or scales. The classic example is 3-dimensional turbulence in a homogeneous, non-rotating fluid. Kolmogorov's and G.K. Batchelor's portrayal of the flow is one in which inertial cascades carry energy to small scale where it is dissipated without detailed back-effect on the large eddies. Turbulence does what it is told to do by the large scales. Similar arguments have been made for vorticity in geostrophic flows, although the slowness of the cascade rate with our steep wavenumber spectra weakens the argument.

Some of our ocean mixing problems may have this same character, but there are many examples in which detailed dissipation has an effect at lowest order. Indeed, if midocean mixing is negligible for some purposes, it will be because it is sufficiently small that water mass properties, potential vorticity, angular momentum and energies are preserved there, and changed by dissipation elsewhere: principally at top and bottom boundaries and internal fronts.

One quickly realizes that it is deceptive to look for a 'yes-no' answer to the sub-title question. With respect to mixing, the analogous result is that: small scale turbulent transport of momentum and density is probably unimportant to the  $O(1 \text{ yr})$  timescale dynamics of the wind-driven circulation. They are certainly crucially important to the  $O(1000 \text{ yr})$  creation and maintenance of the vertical stratification of the oceans (though this is difficult to prove). In between, there is a vast range of circulation phenomena for which the answer is uncertain. It helps to be more specific.

*Energy Integrals.* Energy and enstrophy have sinks in the interior, away from boundaries, so that there is not an *a priori* need for special boundary dissipation. There is a fascinating interplay between vorticity,  $\omega = \nabla \times u$ ,

$$\begin{aligned} \epsilon_{1,1} &= (\partial u_1 / \partial x_2 - \partial u_2 / \partial x_1) / 2 \\ &= (\epsilon_{1,2k} \omega_k) / 2 \end{aligned}$$

and the rate of strain,

$$e_{1,1} = (\partial u_1 / \partial x_1 + \partial u_2 / \partial x_2) / 2$$

in the formulas for mechanical energy dissipation. Here  $\xi_{ij}$  and  $e_{ij}$  are, respectively, the antisymmetric and symmetric parts of the strain tensor  $\partial u_i / \partial x_j$ . The viscous force is identically

$$\nu \nabla^2 \mathbf{u} = \nu [-\nabla \mathbf{x} \omega + \nabla (\nabla \cdot \mathbf{u})],$$

which for an incompressible fluid depends only upon gradients of the vorticity. Yet, we also know from the basic decomposition of the rate-of-strain tensor into symmetric and antisymmetric parts that the viscous stress depends not on the vorticity but on the pressure and strain components. The complete stress,  $\sigma_{ij}$ , is the sum of the pressure and the viscous 'deviatoric' stress,  $\tau$ ,

$$\begin{aligned}\sigma_{ij} &= -p \delta_{ij} + \tau_{ij} \\ \tau_{ij} &= 2\mu(e_{ij} - \Delta \delta_{ij}/3)\end{aligned}$$

where  $\Delta = \nabla \cdot \mathbf{u} = e_{mm}$  and  $\delta_{ij}$  is the Kronecker delta. When the energy equation is formed, we find that (e.g., Jeffreys 1963, Batchelor 1967, Panton 1984)

$$\partial(\frac{1}{2}\rho |\mathbf{u}|^2)/\partial t + \nabla \cdot (\frac{1}{2}\rho \mathbf{u} |\mathbf{u}|^2) = -\mathbf{u} \cdot \nabla p + \mathbf{u} \cdot (\nabla \cdot \boldsymbol{\tau}) + \rho \mathbf{u} \cdot \nabla \Phi$$

where  $\Phi$  is the geopotential. Note that working against the geopotential depends on the reference frame through  $\Phi$  (so that an observer rotating with the Earth, watching the energetics of producing a vortex by vertical stretching or squeezing, will always see an increase in kinetic energy, while an observer in a non-rotating frame will see an increase or decrease in KE depending on the sign of the vertical stretching).

A confusing point, which occurs also in eddy-mean energy conversions, is that the sink term in the mechanical energy equation differs from the source term in the first law of thermodynamics (the internal energy equation) by a divergence expression. This means that dissipation of mechanical energy is not 'localizable'; it is meaningless to try to say just where it occurs, because the heating it produces may be very far away. The required spatial flux term carries the energy from the dissipation point to the point of heating.

Thus, we write (see Batchelor, 1967, p. 152)

$$\begin{aligned}\partial/\partial x_j (u_i \sigma_{ij}) &= u_i \partial \sigma_{ij} / \partial x_j + \sigma_{ij} \partial u_i / \partial x_j \\ &\equiv D + Q.\end{aligned}$$

The rate at which surface forces are doing work on a volume element they surround (term 1) is equal to the gain in kinetic energy of the fluid element (force times velocity,  $D$ ) plus the work done in deforming the element (stress times rate of strain,  $Q$ ), the latter without a change in the average velocity. The corresponding internal energy equation is

change in internal energy,  $E = \text{heating} + \text{pressure work}$

or

$DE/Dt = Q + \text{terms due to conduction of heat,}$   
 phase change, chemical reaction, and  
 radiation.

There are interesting ways to rewrite both  $D$  and  $Q$ . We have for the mechanical energy sink

$$\iiint D \, dV = \iiint \mu \mathbf{u} \cdot \nabla \mathbf{x} \omega \, dV$$

with an incompressible fluid, which seems to site the dissipation in regions of strong vorticity gradient. Careful manipulation of the definition of  $Q$  gives

$$\iiint Q \, dV = \iiint \left( -(2/3)\mu \nabla^2 + 2\mu e_{ik} e_{ik} \right) dV \quad (2)$$

Now

$$e_{ik} e_{ik} = \xi_{ik} \xi_{ik} + \partial u_k / \partial x_i \, \partial u_i / \partial x_k$$

and

$$\begin{aligned} \iiint \partial u_k / \partial x_i \, \partial u_i / \partial x_k \, dV &= \iint n_k u_i \, \partial u_k / \partial x_i \, dS \\ &\quad - \iiint u_i \partial / \partial x_k (\partial u_k / \partial x_i) \, dV \end{aligned}$$

with  $n_k$  being the outward unit normal vector at the boundary. Then

$$\begin{aligned} \iint n_k u_i \, \partial u_k / \partial x_i \, dS &= \iint n_k u_i (-2\xi_{ik} + \partial u_i / \partial x_k) \, dS \\ &= -\iint 2n_k u_i \, \xi_{ik} \, dS + \iint \partial(u_i u_i) / \partial n \, dS \\ &= \iint \epsilon_{ikm} u_i n_k \omega_m \, dS + \iint \partial|\mathbf{u}|^2 / \partial n \, dS \end{aligned}$$

where  $\partial/\partial n$  is differentiation along the outward normal vector and  $\xi_{ik} = -\epsilon_{ikm} \omega_m / 2$  by definition. Collecting terms we have

$$\iiint Q \, dV = \mu \iint \partial|\mathbf{u}|^2 / \partial n \, dS + 2\mu \iint (\mathbf{u} \cdot \mathbf{n} \mathbf{x} \omega) \, dS + \mu \iiint |\omega|^2 \, dV \quad (3)$$

for the dissipative heating of the fluid. We have followed here the detail of Jeffreys (1963, p. 89-90) yet corrected an error (a factor of 2) in that derivation, and an incorrect definition of the vorticity vector.<sup>1</sup> Two test cases (to be sure of the derivation) are a solid body rotation, for which the strain and  $Q$  vanish, and a plane Couette flow.

<sup>1</sup>If the fluid is compressible there are the additional terms  $2\mu \iiint (-\Delta^2/3 + D\Delta/Dt - \partial\Delta/\partial t) \, dV$  in the dissipative heating.

$u = \alpha y$ , for which  $Q = \mu \alpha^2$ .

Thus, in a plane Couette flow the uniform viscous shear stress transmits momentum from one plane boundary to the other, and the local viscous force vanishes. Meanwhile the dissipation of mechanical energy,  $D$ , vanishes yet the fluid heats up everywhere at a rate  $\mu \alpha^2$ ! Kinetic energy is fluxed in by the divergence term at just the required rate, also  $\mu \alpha^2$ .

The problem of localizing the dissipation is important also in the case of surface gravity waves, which are nearly irrotational. The free-slip boundary condition requires the vorticity to be non-zero at the fluid surface (contrary to another error in Jeffreys, op. cit., p. 90), and yet the vorticity is very small beneath a thin boundary layer at the surface. The dissipation,  $D$ , virtually vanishes except in this boundary layer, yet the corresponding dissipative heating occurs throughout the depth of the orbital velocity.

*Enstrophy Integrals.* In a one-layer, flat-bottom  $\beta$ -plane ocean, (relative) enstrophy conservation is

$$\frac{1}{2} \frac{d}{dt} \iint |\omega|^2 dS = -\beta \iint v\omega dS - R \iint |\omega|^2 dS \\ - \nu \iint |\nabla \omega|^2 dS + \iint \omega F dS$$

where  $R$  is linear bottom friction,  $\nu$  is Navier-Stokes kinematic viscosity,  $v = \psi_x$ ,  $\omega = |\omega|$ , and  $F$  is external potential vorticity forcing. This shows the production of relative enstrophy by downgradient potential vorticity flux (second term), and dissipation by  $R$  and  $\nu$ , and production by  $F$ . The 'western intensification integral' (Rhines, 1977) is the identity relation of the potential vorticity flux to the dominant location of the kinetic energy:

$$\beta \iint v\omega dS = \beta \int K \sin \theta_b dl.$$

Here  $\theta_b$  is the angle of the boundary with respect to east, and  $K$  is kinetic energy,  $\frac{1}{2} |\mathbf{u}|^2$ ; the relation follows an integration by parts. In absence of friction or forcing, the enstrophy will increase if kinetic energy lies on the western sides of the ocean, and decrease if it lies on the eastern side. Both Rossby wave reflection laws and the linear frictional western boundary currents are manifestations of this integral relation [for the latter set  $\partial/\partial t = 0$  and note that the dominant balance is between frictional terms and the intensification integral, direct generation being  $O(\delta^2/L^2)$  smaller,  $\delta$  being the boundary current width and  $L$  the basin width].

There are interesting unsolved problems in the stratified generalization of these integrals, particularly in the manner in which geostrophic turbulence cascades both achieve, and sometimes are prevented from achieving, maximal dissipation of potential enstrophy (e.g., Salmon et al., 1976, Bretherton et al., 1976). The bottom

topographic contribution to potential vorticity, represented as a  $\delta$ -function sheet (Rhines, 1979), unifies the modal potential vorticity equation but produces singular behavior in potential enstrophy.

*Potential vorticity (pv) integrals.* Haidvogel and Held, 1980, suggest from numerical experiments that the meridional heat- and potential vorticity flux in a thermally maintained channel flow is only weakly dependent on the lateral subgrid friction coefficient. The preferred tendency for the eddy transport of potential vorticity to be directed down-gradient can be viewed through the production-dissipation equations for enstrophy (or, density-variance, respectively), Rhines and Holland, 1979.

**EGCM results.** Volume-integrated budgets of potential vorticity have been used to diagnose general circulation models. Locally, or in subregions of the flow these can give very useful results (for instance, on eddy form drag and vorticity flux in regions bounded by an Eulerian mean streamline). When integrated out to rigid boundaries, the budgets are less obviously interesting, for they are very sensitive to detailed dynamics near the boundary. Both Lozier and Rhines have looked at such budgets for the Holland-class ocean EGCM (3 layers x 200 x 241 mesh with stretched grid near the western boundary, see Lozier, 1989). With Navier-Stokes friction, the integrated potential vorticity balance for an individual layer is

$$H\partial(\int q \, dx dy)/\partial t = - H\int q \, \mathbf{u} \cdot \mathbf{n} \, dl + \nu H\int \partial^2 \zeta / \partial n^2 \, dl \\ + (\int \mathbf{t} \cdot \mathbf{d}l) - [RH \int \partial \psi / \partial n \, dl] \quad (4)$$

where the curly brackets apply only in the uppermost layer,  $\mathbf{t}$  being the wind-stress vector, and the square brackets apply in the bottom-most layer;  $q$  is potential vorticity,  $H$  is the mean layer depth and  $R$  the linear bottom friction coefficient derived from Ekman theory (but, see section 3!).

When the integration is carried out over the area of a single mean gyre (as in Holland and Rhines, 1980) the 'box pv diagnostics' show:

**upper layer:** the expected 'flow' of pv into the basin from wind-curl in the subpolar gyre and out of the subtropical gyre (800 units); eddy transport across the gyre boundary into the subtropics (530 units), and lateral frictional exchange with the both northwestern and southwestern boundaries ( $\pm 215$  units). Other fluxes are small.

**middle layer:** this is the 'isovortical' region (no external source or bottom sink) that characterizes all the 'inner layers' of a many-layer model. Here, unexpectedly, 48 units enter diffusively at the northern boundary, 6 at the northwestern boundary, -8 at the southwestern boundary, and -45 at the southern boundary. The inter-gyre exchange is 49 units. Other residuals are small. The small net contribution of the western boundary is the result of near cancellation

among the pairs of counterrotating mean gyres.

**bottom layer:** Here the inter-gyre fluxes are: eddy, 146 units, bottom friction 75 units, lateral friction 10 units. At the western boundary the lateral friction source is 115 units, and bottom friction 35-38 units. Northern and southern wall sources are lateral friction, 35 units, bottom friction, 42-45 units.

The unexpected role of the north and south boundaries comes from small but intense eddy driven mean gyres there. This emphasizes that integrated potential vorticity budgets may be greatly altered by a small change in dynamics near the boundary: after all, we are looking at the force balance on a thin strip of fluid at the boundary. We expect such results to be very sensitive to changes in boundary conditions. The integrands of the terms in Eq. (4) along the boundaries carry more information. They show, for example that the western boundary flux of  $pv$  is strong locally, grows with the transport of the boundary current, and is subject to cancellation between multiple gyres. Similar remarks apply to the large inter-gyre eddy flux of  $pv$  measured at the 'Gulf Stream front'. This down-gradient flux is related to force-balance on the Eulerian mean jet. As such it is sensitive to the balance between baroclinic and barotropic instability types in the meander field. Inspection of the integrand of the budget along the mid-latitude line shows that this important flux is dominated by the region within 50 km of the boundary: it is the statistical result of the wandering of the separatrix between the gyres.

With higher order friction parameterizations one must invent new coastal boundary conditions; indeed, with 'super-slip' conditions, allowing no vorticity flux through the wall, the above budgets would be totally altered.

Lozier and Riser (1989), in related work, look at the detailed  $nv$  balance on Lagrangian particles moving through the western boundary current of this numerical model. This gives us a first portrayal of the input-output sense of the boundary current: the dissipative sublayer and nearly  $pv$ -conserving layer further seaward. The former tends to carry fluid from the outer Sveinrup-balanced streamlines, while the latter tends to carry fluid involved in the inertial recirculation and homogenized part of the gyre. Similar Lagrangian portraits will be essential to future models and, fortuitously, they can now begin to be compared with observations (Bauer and Rossby, 1989; Hall and Fofonoff, 1989).

*PV-integral diagnostics using a marked-fluid contour.* Area-integrated vorticity is Kelvin's circulation integral,

$$\Gamma = \int \mathbf{u} \cdot d\mathbf{l},$$

and meteorologists are beginning to look at the behavior of  $\Gamma$  in stratospheric sudden warming models (essentially large-amplitude,



breaking Rossby waves on a polar dome of potential vorticity), McIntyre and Palmer (1984). There are two interesting problems with this. First, the rate of dissipation of  $\Gamma$  is unclear: can it be dissipated by cascade on the inertial timescale (like enstrophy or energy), or does its averaged nature (it is the area averaged vorticity) make it more slowly dissipated? By distorting the contour into a long, thin region, viscous interaction between 'opposing' elements of circulation can occur. Equally as important, when the bounding fluid contour can crinkle up (it is a material line),  $\Gamma$  ceases to indicate either the Eulerian or Lagrangian mean fluid circulation. In the simplest example of  $\beta$ -plane induction of zonal flow by barotropic Rossby waves, the Lagrangian and Eulerian mean velocities are both westward, and given by

$$\langle u \rangle = -\beta \eta^2 / 2$$

where  $\eta$  is the north-south particle displacement from a 'rest latitude' (Rhines, 1977). Remarkably, the Kelvin circulation integral  $\Gamma$  is given by

$$\Gamma = +\beta \eta^2 / 2$$

which is equal but eastward! The integral  $\Gamma$  is peculiar, since it involves a projection of the velocity on the bounding contour, rather than the total velocity. With Navier-Stokes friction we have

$$d\Gamma/dt = -2\Omega \, dA/dt + 2\mu \int \partial \xi_{ik} / \partial x_k \, dx_i$$

where  $A$  is now the enclosed area, projected on the plane perpendicular to the rotation axis,  $\Omega$ . The viscous term is the diffusion of vorticity through the boundary, which is significant even at a 'free-slip' boundary. It will play a central role in the discussion of angular momentum below.

*Angular momentum integrals.* The limited usefulness of globally integrated potential vorticity budgets leads us to look for a more robust momentum-like quantity appropriate to ocean circulation. Consider an idealized two-dimensional flow, with horizontal velocity given by a streamfunction,  $\mathbf{u} = \mathbf{z} \times \nabla \psi$ . Let the position vector be  $\mathbf{r}$ . If we integrate the angular momentum,

$$H = \iint \mathbf{r} \times \mathbf{u} \, dS$$

out to a bounding streamline, where  $\psi = \psi_b$ , there results

$$H|_z = \iint (x\psi_x + y\psi_y) \, dx dy \\ - \iint (\psi - \psi_b) \, dx dy$$

Thus the streamfunction is (-) the density of angular momentum in a two-dimensional gyre. The choice of origin is immaterial; let  $\mathbf{r} = \mathbf{r}_0 + \mathbf{r}'$  and note that  $\iint \mathbf{r}_0 \times \mathbf{u} \, dS$  vanishes. One must watch this

property carefully in more complicated cases (like the 3-dimensional circulation on a sphere). For sub-grid parameterizations it may be interesting to allow a microscopic angular momentum of the particles (or unresolved eddies), which then can contribute to the flux of  $H$ .

It will be interesting to try out  $H$  as a diagnostic for ocean circulation. It may be a robust descriptor of the 'spin' of a single gyre (note that it is not particularly sensitive to the width of a boundary current, for example).

With Navier-Stokes friction the integrated angular momentum budget in the simplest case of 2-dimensional incompressible flow is

$$\begin{aligned} dH/dt = & - \int (\mathbf{r} \times \mathbf{u}) \mathbf{u} \cdot \mathbf{n} \, d\ell + \iint (2\Omega)_z \mathbf{r} \cdot \mathbf{u} \, dS + \int p \mathbf{r} \times \mathbf{n} \, d\ell \\ & + \int \mathbf{r} \times \nabla \tau \, dS + \iint \mathbf{r} \times \mathbf{F} \, dS \end{aligned}$$

where  $\tau$  is the viscous stress tensor and  $\mathbf{F}$  an external force (like wind stress or bottom friction). If the outer boundary is a streamline,  $\psi = \text{const.}$ , the first RHS integral vanishes and the second RHS integral is

$$\Omega \int \psi \, d(y^2 - x^2) = 0$$

also. In this case

$$dH/dt = \int p \mathbf{r} \times \mathbf{n} \, d\ell + \int \mathbf{r} \times (\tau \cdot \mathbf{n}) \, d\ell + \iint \mathbf{r} \times \mathbf{F} \, dS. \quad (5)$$

The  $H$  can be changed by pressure torque on the bounding streamline (for instance, inward propagation of Rossby waves) or the moment of viscous stresses at the outer contour, or the moment of external forces;  $\tau \cdot \mathbf{n}$  means  $\tau_{ij} n_j$ . For Navier-Stokes friction the viscous term may be expressed in terms of velocity:

$$\begin{aligned} \iint \mathbf{r} \times \tau \cdot \mathbf{n} \, dS &= \mu \epsilon_{ijk} \iint r_j \nabla^2 u_k \, dx dy \\ &= \mu \epsilon_{ijk} \left( \iint \frac{\partial}{\partial x_\ell} (r_j \frac{\partial u_k}{\partial x_\ell}) \, dx dy \right. \\ &\quad \left. - \iint \frac{\partial r_j}{\partial x_\ell} \frac{\partial u_k}{\partial x_\ell} \, dx dy \right) \\ &= \mu \int \mathbf{r} \times \frac{\partial \mathbf{u}}{\partial n} \, d\ell - \mu z \int \mathbf{u} \cdot d\ell \end{aligned} \quad (6)$$

since  $\partial r_j / \partial x_\ell = \delta_{j\ell}$ ;  $\mathbf{n}$  is an outward pointing unit vector at the boundary, and  $\mathbf{z}$  is a vertical unit vector. It is a familiar idea that something like Rossby wave generation by flow along a bumpy coast can exert wave-drag, in just the same way that flow over a bumpy bottom can (Charney and Flierl, 1981). The role of viscous stresses needs more discussion. Note the two terms describing the viscous stress, one involving the Kelvin circulation itself.

*Free-slip boundaries and normal viscous stress.* Free slip boundary conditions (indeed, super- and hyper-slip, with higher order momentum diffusion) are widely used in ocean circulation modelling. This

boundary condition seems, by its weak damping, to allow the apparent 'Reynolds number' of the simulation to be larger. It is also well known that the boundary condition puts increased demands on bottom frictional dissipation. Perhaps the maxim given at the head of this paper should invalidate any consideration of sidewalls, but they are widely used. Here we consider how that side boundary condition affects vorticity and angular momentum.

**Paradox:** Let us take as our definition of this boundary condition the vanishing of the shear-stress at the wall. Consider the following interesting paradox:

A simple 2-dimensional flow in an infinite channel, given by

$$u = \cos y$$

has free slip boundary conditions

$$\partial u / \partial y = 0 \text{ at } y = 0, \pi.$$

This amounts to a problem of vorticity diffusion, with  $\omega = 0$  on  $y = 0, \pi$  and  $\omega(y, t=0) = a \sin y$ . (Note, below, that in general, vanishing vorticity is not equivalent to free slip.) The solution is simply

$$\omega = \exp(-t) \sin y.$$

The free slip wall, as we saw earlier, allows a flux of vorticity and the motion dies away exponentially quickly. But that means the angular momentum, say

$$H = \rho \iint \mathbf{r} \times \mathbf{u} \, dS$$

also vanishes, yet it is not apparent that there are any torques acting on the fluid! Here  $\mathbf{r}$  is a position vector referenced from any fixed point.

The problem is clarified if we look at an entirely closed domain: suppose now that a rectangular box of width  $\pi/b$  and length  $\pi/a$  has a single 'gyre' of flow:

$$\partial(V^2\psi)/\partial t + J(\psi, V^2\psi) = \nu \nabla^4 \psi$$

$$\psi(x, y, t) = c(t) \sin ax \sin by$$

where  $\partial^3\psi/\partial y^3 = 0$  on  $by = 0, \pi$  and  $\partial^2\psi/\partial x^2 = 0$  on  $ax = 0, \pi$  are the free-slip boundary conditions. Once again the advection  $J()$  vanishes identically and there is simple viscous decay,

$$\psi = c_0 \exp(-\nu(a^2+b^2)t) \sin ax \sin by$$

where  $c_0$  is the initial amplitude at  $t=0$ . The paradox remains. Where

does the angular momentum,  $\mathbf{r} \times \mathbf{u}$ , go? Because the box now has corners, it is tempting to conclude that the pressure 'form drag' exerts the necessary torque, but in this simple fluid without potential vorticity gradients, there are no wave modes to allow the necessary phase shifts. We can calculate the pressure from

$$\partial \mathbf{u} / \partial t + \mathbf{u} \cdot \nabla \mathbf{u} = -\nabla p / \rho + \nabla u.$$

By substituting the solution, we find that the first and last terms balance exactly, leaving essentially a Bernoulli pressure relation:

$$\mathbf{u} \cdot \nabla \mathbf{u} = -\nabla p / \rho.$$

Hence

$$p / \rho + \frac{1}{2} |\mathbf{u}|^2 = \text{function of } \psi,$$

and this symmetric pressure field exerts no torque on the boundary.

The missing element is the normal viscous stress. Even though the shear stress vanishes at the wall, the normal stress does not. Equation (6) gives the necessary terms: we find that for the above solution in a box, the (vertical) angular momentum is

$$H = \rho \iint \psi \, dx \, dy = 4\mu c(t) / ab$$

$$\partial H / \partial t = -4\mu c(t) (a^2 + b^2) / ab$$

Where  $c(t) = c_0 \exp(-\nu(a^2 + b^2)t)$ . The two RHS integrals, describing the torque exerted by normal viscous stress, are

$$\mu \int \mathbf{r} \times \partial \mathbf{u} / \partial n \, d\ell = 0$$

$$\mu \int \mathbf{u} \cdot \partial \ell = 4c(b/a + a/b) = -4\nu(t) (a^2 + b^2) / ab.$$

The normal viscous stress provides the required torque to destroy the angular momentum, and that torque is here simply proportional to the Kelvin circulation integral about the boundary. This resolves the paradox, and shows the subtlety of the first problem for an infinite channel: if this is approached by taking  $a \rightarrow 0$  in the rectangular box solution, then all is well. Gentle viscous normal stresses with long moment-arms achieve the destruction of angular momentum. The case  $a = 0$  taken without this limiting process is thus singular, and somewhat indeterminate.

What are the properties of normal viscous stress? In elastic solids, normal stresses seem clear, yet we seem to think more about shear stress in fluids. We write the rate-of-strain in terms of antisymmetric tensor (relating to vorticity), trace (the compression) and the symmetric strain tensor,  $e_{ij}$ . Because the vorticity contributes no local deformation of fluid elements, the entire viscous stress arises from the

strain tensor,  $e_{ij}$  (and the compression,  $\Delta$ , which we neglect here). The diagonal elements relate to normal stress, and the off-diagonal elements, to shear stress; in two dimensions

$$e_{ij} = 1/2 \begin{vmatrix} 2u_x & v_x + u_y \\ v_x + u_y & 2v_y \end{vmatrix}$$

Notice that the distinction between shear stress and normal stress is a property of the coordinate system more than of the flow itself (although a 'pure' shearing motion is characterized by the persistence in time of the direction of shear). When the coordinates are aligned with the principal axes of strain, off-diagonal shear vanishes. This is summed up in Mohr's Circles (or Circle, in 2 dimensions), which we may borrow from solid mechanics (e.g., Fung, 1969). These are a graphical representation of the way normal and shear stresses trade off with one another, during a coordinate rotation. Thus, the pure strain field

$$\psi = xy$$

has vanishing shear  $\partial u/\partial y$  and  $\partial v/\partial x$ , yet for any other choice of rotated coordinates there will be a gradient of velocity normal to the velocity vector.

Pressure is the isotropic part of the stress, and normal viscous stress is the deviation from isotropy (the sum  $e_{ii}$  vanishes), causing the deformation without compression. If we put a rigid but slippery plane boundary along the x-axis of the pure strain solution, there will be a viscous force exerted on it (equal and opposite on both sides), which is distinct from pressure. (Since the viscous force,  $\nu \nabla^2 u$ , vanishes for this pure strain, the pressure field obeys a Bernoulli relation,  $p/\rho + \frac{1}{2}|u|^2 = \text{const.}$ ; for slow flows variations in the pressure force along the wall are less than the normal viscous stress.) When you pour honey from a jar, the descending, thinning, accelerating stream involves a similar deformation of fluid elements under gravity. It is the normal viscous stress that holds the column together. When the honey hits a horizontal surface it spreads somewhat as in the pure strain flow, exerting a normal viscous stress (less than its total weight) on the boundary.

Free-slip boundary conditions can be visualized at the level of a simple perfect gas, as causing elastic rebound of molecules. Symmetry arguments show that such a boundary can be placed along the x-axis of the  $\psi = xy$  straining flow without any effect on the macroscopic flow (the rebounding molecules replacing molecules crossing  $y = 0$ ). Yet a normal viscous stress exists there, exerting a force on the boundary, as a natural part of the free-slip problem.

More relevant to ocean modelling, G.I. Taylor and Stan Richardson of Cambridge did a simple calculation in about 1968 (I can't find a published version in the literature), that relates to our boundary

conditions. The no-slip condition is usually justified by thermodynamic arguments which seem none too precise. They wondered whether microscopic roughness of the boundary, together with a free-slip boundary condition, might give a different macroscopic boundary condition. The relevant low-Reynolds number calculation is to solve

$$\nu \nabla^4 \psi = 0$$

with vanishing shear stress on a sinusoidal boundary. The result, at a distance of several times the amplitude of the corrugations, is no-slip!

It would be oversimplifying to suggest this as a result relevant to a rough coast. But clever sub-models can illuminate the question of sidewall boundary conditions, acknowledging that the ocean has neither sidewalls, nor a smooth boundary.

One such sub-question is the way in which bottom friction provides the vorticity source for flow around islands and capes, which makes the satellite photographs look like moderate Reynolds number flow around 2-dimensional obstacles. Stratification keeps the flows relatively planar, if not 2-dimensional. The classical fluid dynamics of vorticity shedding from the sidewall boundary layer is replaced by the bottom frictional generation of vorticity in shallow water (Geyer and Signell, 1989).

A classical free-slip boundary problem is the damping of surface gravity waves. If we move with the phase speed, the flow is nearly irrotational, yet viscous. The boundary condition is that along the sinusoidal boundary the shear stress vanish. (Ignoring surface tension, the normal stress at the boundary must be balanced by the pressure.) There are numerous errors in the literature. In particular one sometimes reads that the free slip condition is equivalent to the vanishing of vorticity at the wall. This is true only with plane boundaries!

Consider the viscous evolution of a 2-dimensional symmetric swirl in a cylinder with free slip wall at radius  $r=a$ . We know that viscosity will wipe out straining motions, leaving a solid body rotation with the same angular momentum as the initial flow (for all the viscous boundary terms in the angular momentum equation vanish). Yet this final solid body flow has definite, non-zero vorticity at the outer wall, which is related to the velocity gradient there.

It is useful in this context to write the components of the rate-of-strain tensor referred locally to polar coordinates,  $(r, \theta)$ :

$$e_{rr} = \partial u_r / \partial r, \quad e_{\theta\theta} = r^{-1} \partial u_\theta / \partial \theta + u_r / r,$$

$$e_{r\theta} = \frac{1}{2} r \partial (u_\theta / r) / \partial r + \frac{1}{2} r^{-1} \partial u_r / \partial \theta.$$

The appropriate free-slip condition is

$$\mu \partial(u_\theta/r)/\partial r = 0; u_r = 0 \text{ at } r=a.$$

The free-slip boundary condition for a general boundary can be written as

$$\partial u_s / \partial n - \kappa u_s = 0$$

where  $\kappa$  is the curvature of the boundary, as measured in the direction of the tangential velocity vector, and  $u_s$  is that tangential vector component of velocity. Notice that for two-dimensional flows the vorticity at the boundary is

$$\partial u_s / \partial n + \kappa u_s$$

and hence the vorticity at a free-slip wall is constrained to be twice the tangential velocity times the curvature:

$$\omega = 2\kappa u_s.$$

Leal (1989) describes similar effects at the edges of bubbles. In three dimensions the expression for free slip is

$$2\partial(\mathbf{u} \times \mathbf{n}) / \partial n + \omega = 0.$$

This is related to the force per unit area exerted by an incompressible fluid across a surface element anywhere in the fluid (Batchelor, 1967, p. 178), which is

$$-pn + \mu(2\mathbf{n} \cdot \nabla \mathbf{u} + \mathbf{n} \times \omega).$$

Even in a square box, where  $\kappa$  vanishes almost everywhere, the area-average vorticity at the wall is non-zero, owing to the delta-function behavior of  $\kappa$  in the corners.

The fascinating thing about the swirl in a cylinder is that a bump on the boundary, no matter how small, will cause the fluid eventually to come to rest. It does so, just as did the fluid in the boxes and channels described above, by breaking the symmetry and letting normal viscous stresses act.

*Bottom topography: is inviscid form-drag non-diffusive?* The generalized Rossby-wave drag is important to the basic force balance of the circulation, both as an internal vertical flux of momentum, and as a momentum sink at the sea-floor (Rhines and Holland, 1979). It is best understood through redistribution of mean-state potential vorticity. Generally portrayed as an inviscid wave-drag, it relies on simple 'flow over a corrugated boundary'. But take note, that energy dissipation is a key ingredient. If the flow is driven by an imposed force (e.g., wind), without dissipation the forcing will continue to pump energy into the wave field, whose amplitude grows without bound. A simple example is the one-layer version of the Charney-deVore problem (zonal flow over

sinusoidal topography on a  $\beta$ -plane), where the forced  $\sin x$  wave has amplitude depending both on a resonance denominator and inversely on the bottom-friction coefficient.

This, in combination with observational studies of flow past seamount chains, alerts us to the possibility that the drag and vorticity flux attributed in models to the western boundary sidewall friction may in part be occurring in the ocean interior, through pressure forces on bottom topography.

### 3. STRATIFIED SPIN-UP: THE EFFECT OF A SLOPING BOUNDARY (OR SLOPING ISOPYCNALS )

There has been much recent discussion of boundary mixing (Garrett, this volume). The arguments concentrate on mixing in an otherwise quiescent ocean, and the 'self-propelled' Eddington-Sweet class of circulations that follow. Rather in the spirit of adding wind-stress to upper ocean mixed-layer studies, we want to explore the nature of mixing and secondary circulation where there is a pre-existing interior mean flow and some externally imposed momentum dynamics. This falls in the set of problems known generically as 'stratified spin-up'. Both observations at sea and numerical simulations of the development of the stratified bottom boundary layer have been carried out by Weatherly and Martin (1978).

The ocean is, in one sense, a weakly stratified fluid. A pattern of vertical-velocity forcing with horizontal scale  $L$  greater than about 50 km will penetrate, according to linear  $f$ -plane theory, through the full depth. Thus the energy-containing mesoscale eddies and all larger-scale circulations have quick, geostrophic-adjustment response that penetrates throughout the fluid. At high latitudes and in the deep ocean the stratification is still weaker, with the gravest Rossby radius of deformation 10 km or less.

Does this mean that the oceans are dominated by viscous bottom drag, and are sluggish and overdamped? We know that the  $\beta$ -effect can break the 'Prandtl-ratio' (or equivalently, 'Rossby-radius') rules and cause circulations to develop with  $L$  far in excess of  $NH/f$ ; these involve generalized baroclinic Rossby waves which attempt to destroy east-west density gradients (Rhines and Young, 1982). A typical vertical penetration height then becomes  $(f/N) (U/\beta)^{1/2}$  which is  $(U/\beta L^2)^{1/2}$  times the Prandtl penetration scale:  $U$  is here the large-scale mean velocity. Indeed, the dominant picture of both the wind-driven circulation and the thermohaline circulations involves long-distance penetration of flow structures which are of order 1 km deep, easily over thousands of Rossby radii in the horizontal. This is evidence of the workings of  $\beta$ .

Our textbook accounts of spin-up concentrate on the homogeneous fluid case, in which thin boundary layers drive an interior circulation by inviscid vortex stretching; in the simplest case, without external forcing, this secondary flow brings the interior fluid to rest in a time



$$E^{-\frac{1}{2}}\Omega^{-1}$$

where  $E = \nu/\Omega H^2$  is the Ekman number ( $H$  is the depth of the fluid). This is  $H/\delta$  half-pendulum days, where  $\delta = (\nu/\Omega)^{\frac{1}{2}}$  is the Ekman layer thickness. During the spin-up, the excursion of a fluid particle in the boundary layer is  $\epsilon E^{-\frac{1}{2}}L$ , where  $L$  is the horizontal scale of the flow and  $\epsilon$  is the Rossby number,  $U/\Omega L$ ;  $\epsilon L$  is the lateral excursion of a fluid particle in the interior. This spin-up time is of order 100 seconds for a laboratory experiment 10 cm deep, with  $\Omega$  of order unity. If we imagine the oceanic Ekman layer to be 10 m thick, the oceanic spindown time is typically 250 days.

There are many difficulties in applying these elegant ideas to stratified fluids. Work in the late 1960's by Holton (1965), Walin (1969), and Buzyna and Veronis (1971) and others seemed to provide an answer: the stratification typically is negligible in the boundary-layer equations (if  $NH/fL \sim 1$ ,  $E^{\frac{1}{2}} \ll 1$ ), leaving essentially Ekman layer dynamics to force the quasi-geostrophic, but stratified, interior. Ekman pumping drives vertical velocity through a Prandtl penetration depth  $fL/N$ , achieving fast spin-up only in this region. Then (St-Maurice and Veronis, 1975), the remainder of the flow spins up over a longer diffusive timescale. The adjustment is now modal, with each Fourier component of Ekman pumping having its own spin-up time.

This seemed to solve the problem, and we read in textbooks that the correct boundary conditions for quasi-geostrophic large-scale flow are

$$w_i(x,y,0) = (E^{\frac{1}{2}}/2\epsilon) \omega_0(x,y,0) + u_0 \cdot \nabla(h_b/\epsilon D)$$

where  $w_i$  is the interior vertical velocity just above bottom,  $z = -h_b$ , and  $\omega_0$  is the interior vertical vorticity. The final term is the usual effect of flow up a topographic slope. Below we describe how this formula is largely incorrect.

A central difficulty with the stratified case is that *the interior potential vorticity of every fluid particle must be diffusively changed* to achieve spin-up (except in contrived circumstances). This contrasts the homogeneous-fluid paradigm. Typically the demands of buoyancy adjustment and Ekman pumping are in conflict (as is often the case in the surface forcing of the oceans by the atmosphere).

Laboratory experiments have verified the predictions of 'fast' spin-up for flat-bottom, cylindrical containers, typically with a 1% change in rotation of the tank (i.e.,  $\epsilon = 0.01$ ). St-Maurice and Veronis (1975) find that higher order diffusive effects must be included to give quantitatively accurate spin-up times.

Over a sloping bottom, typical of the sea-floor, we find that the scaling arguments leading to neglect of stratification within the Ekman layer hold true only for a short time. As fluid is forced up or down the slope, there is a growing restoring force from the buoyancy. How

long can the Ekman flow persist before this force exceeds the pressure force driving the layer? The buoyancy force along the boundary grows with time, until at time  $\tau_s$  it is comparable with the driving pressure gradient: the force balance parallel with the boundary (in the upslope direction) is

$$\underline{-\cos \alpha \partial p / \partial r - g \rho' \sin \alpha} + \nu \partial^2 v / \partial z^2 - f u \cos \alpha = 0$$

The underlined terms are comparable at time  $t \approx \tau_s$  given by

$$\begin{aligned} f \tau_s &= 2f^2 (N \sin \alpha)^{-2} \\ &\approx 2f^2 / (N\alpha)^2 \quad \text{for } \alpha \ll 1 \end{aligned}$$

where we have used

$$\rho' \approx U t \rho_r \approx U t \rho_z \tan \alpha.$$

We find that at moderate or small Reynolds number, after this time has elapsed, the Ekman flux is extinguished, and the flow aligns with topographic contours. The pumping of the interior flow ceases and spin-up occurs by simple diffusion of momentum. Estimates of the 'shut-down' time,  $\tau_s$ , are:

deep ocean:  $\alpha \sim 10^{-3}$ ,  $N \sim 10^{-3} \text{ sec}^{-1} \rightarrow \tau_s \sim 5 \text{ years}$

continental rise/ rough interior:  $\alpha \sim 10^{-2}$ ,  $N \sim 3.5 \times 10^{-3} \text{ sec}^{-1} \rightarrow \tau_s \sim 2 \text{ days}$

So classic Ekman pumping and 'fast' spin-up occur only if the spin-up time is less than  $\tau_s$ , or

$$E^{\frac{1}{2}} \gg (N\alpha/f)^2 \text{ for steady flows.}$$

For an oscillatory flow with frequency  $\sigma$ , this is

$$\sigma \gg N^2 \alpha^2 / f.$$

This implies a frequency-dependent bottom friction in the ocean, with rapid oscillations much more strongly damped than slow oscillations.

We carried out experiments with uniform stratification, in a spherical-cap bowl 92 cm wide. Velocity measurements and a time-lapse film of the experiments were shown at the Hawaii meeting, which showed the contrast between spin-up times and surfaces of principal shear in the stratified and homogeneous cases, respectively. The 100-sec e-folding time for a zonally symmetric circulation contrasts with 20 to 30 min. e-folding time with stratification. The flow parameters were in the range  $NH/fl \sim 0.5$ ,  $N/f \sim 3$ ,  $f \sim 1 \text{ s}^{-1}$ ,  $\epsilon \sim 0.05-0.30$ ,  $E \sim 10^{-4}$ .

There is an important asymmetry, where down-slope Ekman flux thrusts light fluid under heavy, leading to more mixing than in the up-slope Ekman layer. Although there are limitations to the Reynolds numbers that can be achieved in the laboratory, we found intrusive penetrations of mixed fluid into the interior at the higher values of  $\epsilon$ , for down-slope boundary layers.

*Flat bottom case.* The shut-off of Ekman pumping due to buoyancy forces is not an effect limited to sloping bottom topography: the key is to have intersection of the isopycnals and the boundary. This occurs both at the sea surface and a level bottom, owing to thermal-wind shear. Corresponding to the above formulas we substitute for  $\alpha y$  the geostrophic slope  $fU_z/N^2$  of the isopycnals, and find

$$f\tau_s \sim (N/U_z)^2 = Ri$$

where  $Ri$  is the Richardson number of the geostrophic flow. This estimate of the time required for buoyancy forces to build up in the Ekman layer suggests the importance of lateral stratification in wind-driven upper mixed layers and deep flows over abyssal plains. Uplift of boundary fluid into the interior has been seen at sea by Armi and d'Asaro (1980).

At large Reynolds number we observed instabilities and mixing that led to intrusions into the stratified interior. This regime, while difficult to reach in the laboratory, is an important area for future study.

The shut-off of Ekman pumping by buoyancy forces reduces boundary momentum sinks even beyond the diminished level found in classical stratified spin-up theory. This liberates nonaxisymmetric flows (for example, a field of geostrophic turbulence) from the strong damping found with homogeneous fluid.

The experiments are described in a paper in preparation for *J. Fluid Mech.*

#### ACKNOWLEDGMENT

This work has been supported by the Office of Naval Research, grant N00014-86-K-0690 and the National Science Foundation, grant OCE 86-13725. We are grateful to the CSIRO Marine Laboratories, Australia for providing laboratory facilities during our 1988 visit. Greg Holloway and Michael McIntyre made important comments.

## REFERENCES

- Armi, L. and E. d'Asaro, 1980: Flow structures in the benthic ocean, *J. Geophys. Res.* 85, 469-481.
- Batchelor, G. K., 1967: *An Introduction to Fluid Mechanics*, Cambridge.
- Bower, A. S. and T. Rossby, 1989: Potential vorticity balances and horizontal divergence along particle trajectories in Gulf Stream meanders east of Cape Hatteras, *AGU abstract, EOS*, 70, 15, 366.
- Bretherton, F.P. and D. P. Haidvogel, 1976: Two-dimensional turbulence above topography, *J. Fluid Mech.*, 78, 129-154.
- Buzyna, G. and G. Veronis, 1971: Spin-up of a stratified fluid: theory and experiment. *J. Fluid Mech.* 50, 579- 608.
- Charney, J.C. and G.R. Flierl, 1981: Oceanic analogues of large-scale atmospheric motions, in *Evolution of Physical Oceanography*, B. Warren and C. Wunsch, eds., MIT press, 504-548.
- Fung, Y.C., 1969: *A First Course in Continuum Mechanics*, Prentice-Hall, Englewood Cliffs, NJ.
- Geyer, W.R. and R.P. Signell, 1989: Measurements of tidal flow around a headland. (submitted to J.G.R.)
- Jeffreys, Sir H., 1963: *Cartesian Tensors*, Cambridge University Press.
- Kawase, M., 1987: Establishment of deep ocean circulation driven by deep-water production, *J. Phys. Oceanogr.*, 17, 2294-2317.
- Haidvogel, D.P. and I.M. Held, 1980: Homogeneous quasigeostrophic turbulence driven by a uniform temperature gradient, *J. Atmos. Sci.*, 37, 2644-2660.
- Hall, M.M. and N.P. Fofonoff, 1989: Potential density transport and potential vorticity in the Gulf Stream, *AGU abstract, EOS*, 70, 15, 366.
- Holland, W.R. and P.B. Rhines, 1980: An example of eddy-induced ocean circulation, *J. Phys. Oceanogr.*, 10, 1010-1031.
- Holton, J.R., 1965: The influence of viscous boundary layers on transient motions in a stratified rotating fluid, I, *J. Atmos. Sci.*, 22, 402-411.
- Leal, L.G. 1989: Vorticity transport and wake structure for bluff bodies at finite Reynolds number, *Phys. Fluids A*, 1, 124-131.
- Lozier, S., 1989: Potential vorticity dynamics of a quasigeostrophic ocean: a Lagrangian perspective, Ph.D. dissertation, School of Oceanography, Univ. of Washington.
- Lozier, S. and S. Riser, 1989: Potential vorticity dynamics of boundary currents in a quasigeostrophic ocean, *J. Phys. Oceanogr.*, in press.
- McIntyre, M.E. and T.N. Palmer, 1984: *J. Atmos. Terres. Phys.*, 46, 825-849.
- Panton, R.L., 1984: *Incompressible Flow*, Wiley and Sons, New York, 780 pp.
- Rhines, P.B., 1977: The dynamics of unsteady currents, in *The Sea*, VI, E. Goldberg, ed., Wiley Interscience, NY, 189-318.
- Rhines, P.B., 1979: Geostrophic turbulence, *Ann. Rev. Fluid Mech.*, 11, 404-441.
- Rhines, P.B. and W.R. Holland, 1979: A theoretical discussion of eddy-driven mean flows, *Dyn. Atmos. Ocean*, 3, 289-325.
- Rhines, P.B. and W.R. Young, 1982: A theory of the wind-driven

- circulation; I. Mid-ocean gyres, *J. Mar. Res. Suppl.* to 40, 559-596.
- Salmon, R., G. Holloway and M. Hendershott, 1976: The equilibrium statistical mechanics of simple geostrophic models. *J. Fluid Mech.*, 75, 691-703.
- St-Maurice, J.P. and G. Veronis, 1975: A multi-scale analysis of the spin-up problem, *J. Fluid Mech.*, 68, 417-445.
- Walsh, G., 1969: Some aspects of time-dependent motion of a stratified rotating fluid, *J. Fluid Mech.*, 36, 289-307.
- Weatherly, G. and Martin, 1978: On the structure and dynamics of the benthic boundary layer, *J. Phys. Oceanogr.*, 8, 557-570.

## A HIGH RESOLUTION SIMULATION OF THE WIND- AND THERMOHALINE-DRIVEN CIRCULATION IN THE NORTH ATLANTIC OCEAN

Frank O. Bryan and William R. Holland

National Center for Atmospheric Research, P.O. Box 3000, Boulder, Colorado, 80307

### ABSTRACT

*A simulation of the general circulation of the North Atlantic Ocean has been carried out using a thermodynamic primitive equation numerical model with sufficient horizontal resolution to explicitly include the hydrodynamic instability processes responsible for eddy formation. The model is forced with climatological, seasonally varying, wind stress and surface heat and salt fluxes. The role of eddies in the general circulation, including their interactions with thermodynamic processes such as poleward heat transport and thermocline ventilation are being investigated. While the simulation has some obvious deficiencies, the overall quality of the solution is very good, leading us to believe that the next level of model development should be directed at more accurate representations of diapycnal processes and the incorporation of more realistic surface forcing.*

### INTRODUCTION

The ubiquity of mesoscale motions and their importance in the general circulation are well established facts in oceanography. The role that ocean eddies play in global climate is still an open question however. The sparsity of current measurements precludes direct estimates of the eddy contribution in basin- to global-scale heat budgets. The dichotomy that has existed in ocean modeling over the last decade has also prevented us from answering this question. On one hand are models with active thermodynamics and moderate to high vertical resolution, but low horizontal resolution. These have been developed in an attempt to represent the large-scale hydrographic structure and climatic properties (water mass formation rates, heat and freshwater transports, sea surface temperature anomalies, etc.) of individual ocean basins or the world ocean. The strong dissipation required to maintain numerical stability in these low resolution models inhibits physically realistic hydrodynamic instabilities as well. Thus, the only source of variability in this type of simulation is time dependence in the imposed atmospheric forcing (or open boundary conditions if they exist). This class of models has been moderately successful in simulating the mean circulation and hydrographic structure of the world ocean, e.g., Bryan (1979), Meehl et al. (1982), and the variability of the upper ocean circulation where the variability is primarily wind forced, e.g., Sarmiento (1986), Philander et al. (1987). On the other hand are models with high horizontal resolution, but low vertical resolution, and generally incomplete treatment of thermodynamic processes. These have been developed in order to investigate the dynamics of time-dependent circulation systems including mesoscale eddies and their interactions with the mean flow. This class of models has shown some success in representing the distributions of eddy variability and the structure of western boundary currents of the

subtropical gyre circulations systems, e.g., Holland et al. (1983), Holland (1985, 1986). Studies carried out with these models have provided insights leading to major advances in the theory of the ocean general circulation. The majority of these calculations have been carried out using the quasigeostrophic equation system. This system does not contain the high frequency gravity waves, and is hence much more economical to integrate than the primitive equation system. However, thermohaline processes are difficult to incorporate into these models and they are limited to non-global domains.

The advent of the current generation of supercomputers has facilitated the convergence of these two modeling approaches. Basin- to global-scale simulations which include both a complete representation of the thermodynamic processes responsible for water mass formation and sufficient horizontal resolution to allow the hydrodynamic instabilities responsible for eddy formation have become feasible. In this paper we describe such a calculation for the circulation in the North Atlantic basin. In addition to addressing basic questions about the role of mesoscale motions in the ocean general circulation and climate, this experiment is meant to serve as a benchmark to judge our progress in basin-scale modeling. The results of this experiment and their analysis will help guide future development efforts by indicating which aspects of the models are most in need of improvement and which are most successful and by providing a reference solution against which to compare successive experiments. These analyses are still underway, so only a preliminary overview of the results will be presented here.

## MODEL CONFIGURATION

The basic model used in this experiment is the primitive equation model developed at the NOAA Geophysical Fluid Dynamics Laboratory by Bryan (1969) and Cox (1984). This model has been used extensively for a variety of ocean modeling problems. The equations of motion are formulated using second-order finite-differences on the Arakawa B-grid (Arakawa and Lamb, 1977) and conserve total heat content (or arbitrary scalar tracer content), mass, energy, and tracer variance in the absence of explicit dissipation or forcing. The horizontal resolution is  $1^\circ 3'$  in latitude and  $2^\circ 5'$  in longitude. This gives equal grid spacing in the north-south and east-west directions of 37 km at  $34^\circ$  latitude. Note that this is approximately equal to the radius of deformation for the first baroclinic mode in mid-latitudes, so that the resolution is just barely adequate to represent many of the eddying processes. There are 30 discrete levels in the vertical, with a spacing of 35 m at the surface and smoothly stretching to 250 m by 1000 m depth. Below 1000 m the vertical grid spacing is a constant 250 m. The computational domain is the North Atlantic basin from  $15^\circ\text{S}$  to  $65^\circ\text{N}$  latitude, including the Caribbean Sea and Gulf of Mexico, but excluding the Mediterranean Sea (Figure 1). Cuba and Hispaniola are treated as true islands, requiring special treatment of the boundary conditions on the barotropic streamfunction. Bottom topography is represented in the model as stacked grid boxes, so that the bottom lies on the interface between two grid levels. The topography is derived from a digital terrain data set with  $5'$  latitude-longitude resolution using a simple nearest neighbor approach. The only smoothing performed is to remove single grid point holes or spikes.

Since this is the first experiment of its kind, we had little guidance in choosing parameterization schemes. Several criteria were considered when making these choices. First, we wanted this experiment to represent the state-of-the-art in general circulation modeling. As this is to be the first experiment in a series and will provide a reference

point for comparing future solutions, it was desirable to keep the parameterizations in this initial experiment fairly simple. The horizontal dissipation mechanism is a highly scale-selective, biharmonic operator with a coefficient of  $-2.5 \times 10^{19} \text{ cm}^4 \text{ s}^{-1}$  for both momentum and tracers. The vertical dissipation mechanism is the more traditional second order operator with constant coefficients of  $30 \text{ cm}^2 \text{ s}^{-1}$  for momentum and  $0.3 \text{ cm}^2 \text{ s}^{-1}$  for tracers. Additional dissipation of momentum is provided by a quadratic bottom drag. A Kraus-Turner type, surface mixed-layer parameterization is included as a purely vertical process, that is, there is no horizontal communication of mixed-layer depth or turbulence levels between adjacent grid points. A conventional adjustment scheme is used to treat free convective mixing.



Figure 1. Three-dimensional perspective view of the bottom topography used in the experiment.

The surface boundary conditions are all based on seasonal climatological data sets. The wind stress and wind work values are taken from the Hellerman and Rosenstein (1983) climatology. The surface thermal boundary conditions are specified by a linear bulk formula described by Han (1984). In this scheme the heat flux is a linear function of the difference between the model-predicted, sea surface temperature and a prescribed "effective" atmospheric temperature that includes corrections for effects like direct solar radiation. The proportionality coefficient varies temporally and spatially, and is primarily a function of surface wind speed. Due to the lack of reliable data sets for precipitation over the ocean, the surface boundary condition for fresh water flux is implemented as a linear damping of salinity in the first model level towards the Levitus (1982) seasonal climatology. Linear interpolation between monthly or seasonal means is used to obtain necessary values for all surface forcing fields at each model time step. The restriction of the model domain to a less than global one decreases the computational burden considerably but introduces the complication of open boundaries. In this experiment these are treated by closing the boundaries to inflow or outflow but introducing narrow "buffer zones" adjacent to them. In these buffer zones the temperature and salinity are damped towards their (seasonally varying) climatological values on a time scale of 25 days at the outer edge (approximately 150 km from the



walls), linearly decreasing to 5 days adjacent to the wall. The damping terms in these buffer zones must provide the heat and salt sources and, for example, sinks to convert southward flowing North Atlantic Deep Water to northward flowing surface waters at the southern boundary.

The experiment was initialized with temperature and salinity for January conditions from the Levitus (1982) climatology. Due to the rather strong smoothing used to construct this data set, a number of frontal features are seriously distorted in the initial condition. For example, the cold slope water north of the Gulf Stream, west of 40°W is almost completely missing from the initial condition.

The model contains over two million grid points, and requires approximately 50 Cray XMP CPU hours for each year of integration. The evolving model solution was sampled at three-day intervals during the final five years of the simulation. The resulting archive of 600 samples requires over 50 Gigabytes of mass storage. Regional and temporal subsamples of the archive, as well as various statistics derived from it, are being made available to interested investigators.

## RESULTS

The complexity of the solution and the volume of data required to describe it prevent a thorough description of the results in any single paper. Indeed, many investigators are involved in the analysis of this experiment since such a wide variety of phenomena are represented in the solution. In this section we will give an overview of the largest scale features of the circulation and some of the processes relevant to the climate problem.

### Mean Circulation, Water Masses and Variability

During the relatively short integration, there is little drift of the basic hydrographic structure away from that described by the initial conditions. The level mean temperatures for depths less than 2000 m warm slightly during the integration, and those below 2000 m cool slightly. The mean, sea surface temperature (SST) for January over the last 15 years of the simulation is shown in Figure 2a, and the difference between the model January mean SST and the Levitus (1982) climatology is shown in Figure 2b. Over most of the basin, the model differs from the climatology by less than 1°C. The largest differences are found in the Gulf Stream region. The model Gulf Stream is displaced to the north of the mean observed position between 50°W and 75°W. This results in large positive differences on the inshore side of the Gulf Stream. The differences between the climatological SST's and the model predictions for other months show similar patterns. A 1° resolution version of the model has a similar pattern as well, with the exception that the region of anomalously warm SST along the western boundary has a larger areal extent. This is an indication that surface temperatures and heat storage away from regions of strong currents are determined primarily by local vertical processes, as suggested by Gill and Niiler (1973), and that the specification of the surface heat flux and mixed layer parameterization in the model are reasonably accurate.

The model is also successful in simulating the formation of both subtropical and subpolar mode waters. Meridional temperature sections in the upper layers of the western basin are shown in Figure 3 for January and July during the final year of the integration. During winter the mixed layer extends to 300 m depth on the south side of

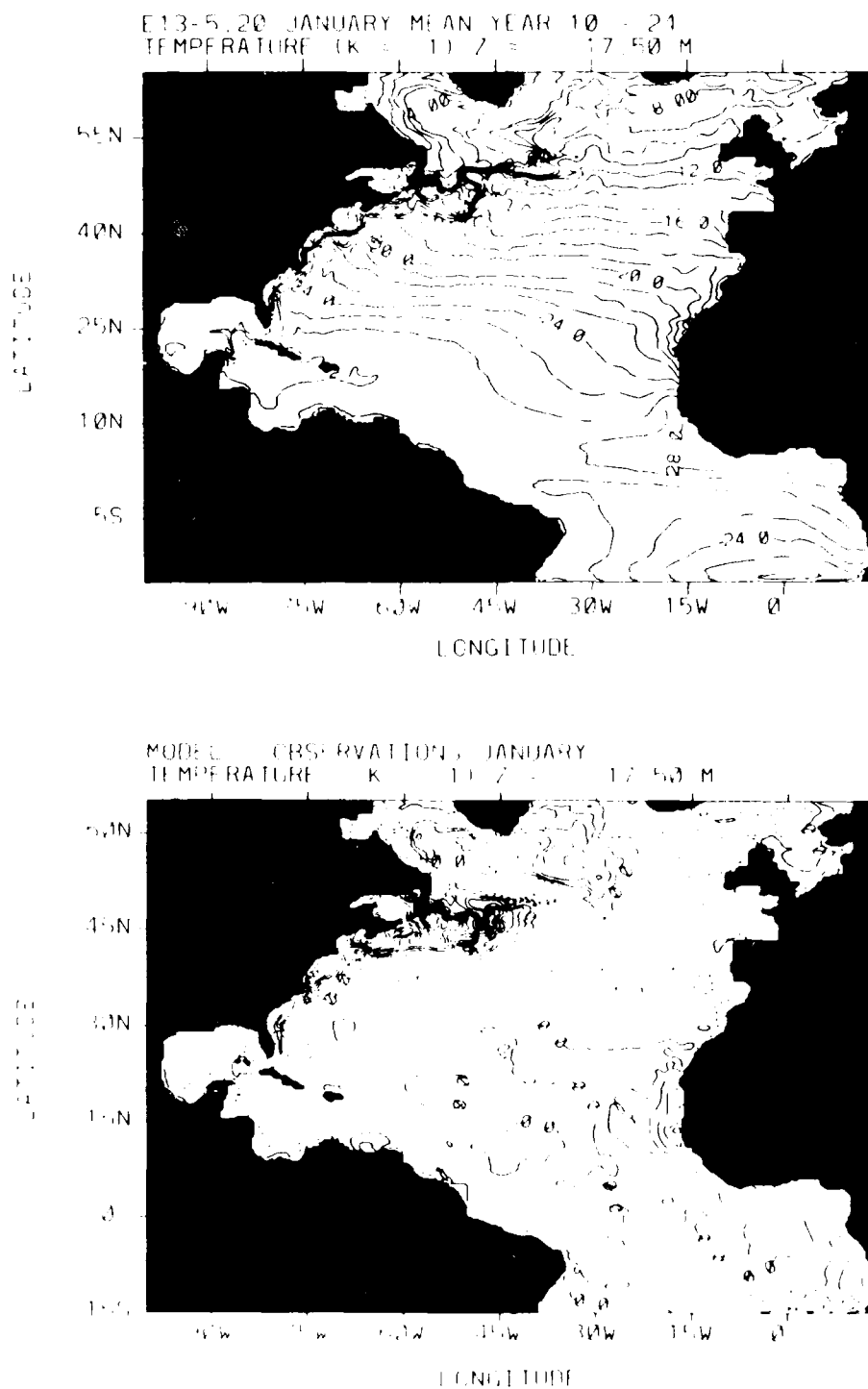


Figure 2. (a) Mean January sea surface temperature from the final 15 years of the experiment. (b) Difference between the model mean January sea surface temperatures and the Levitus (1982) January climatology.

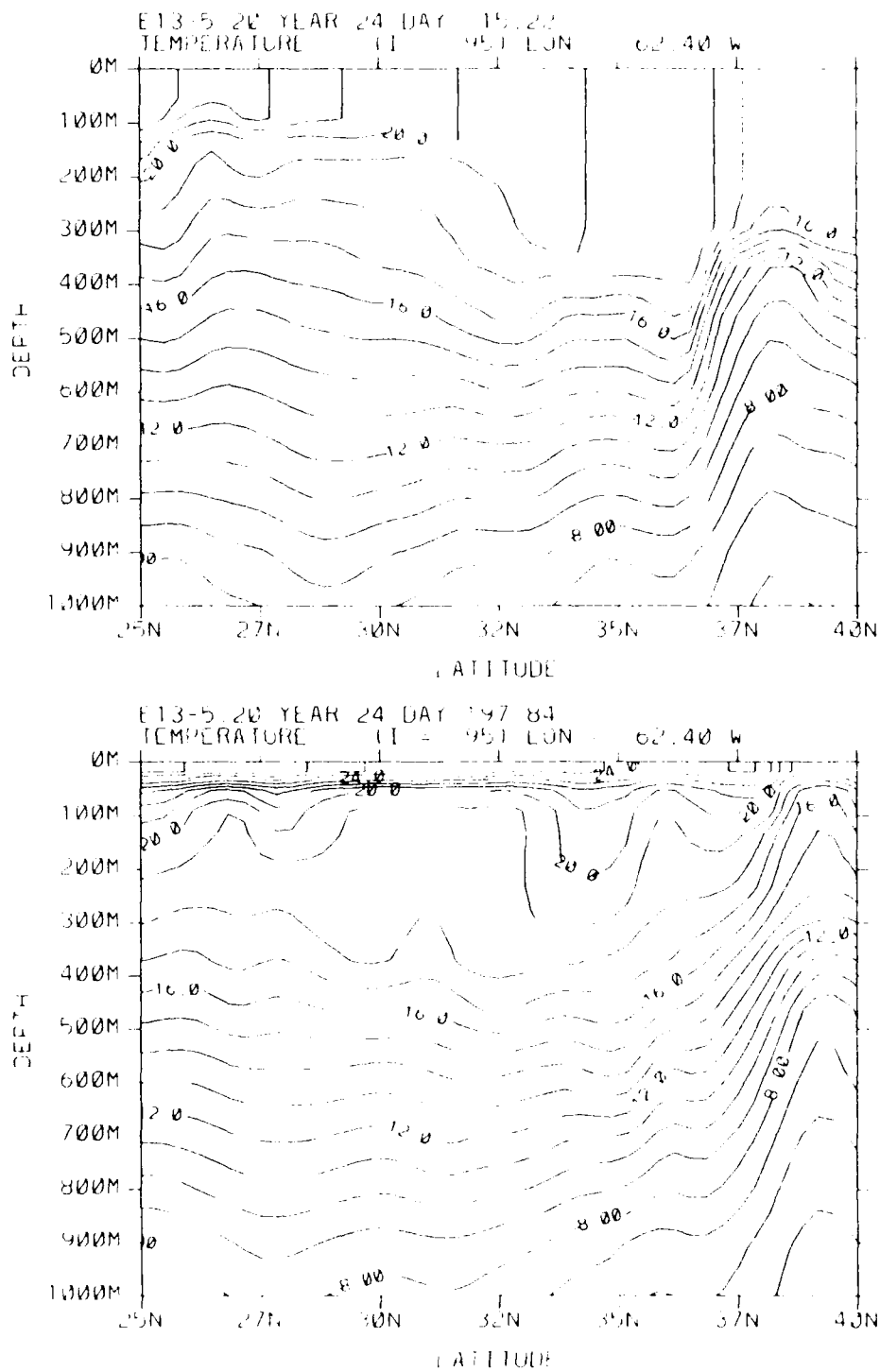


Figure 3. (a) Meridional temperature section in the upper 1000 m along 62.4°W longitude for mid-January during the last year of the experiment. (b) As in (a) for mid-July.

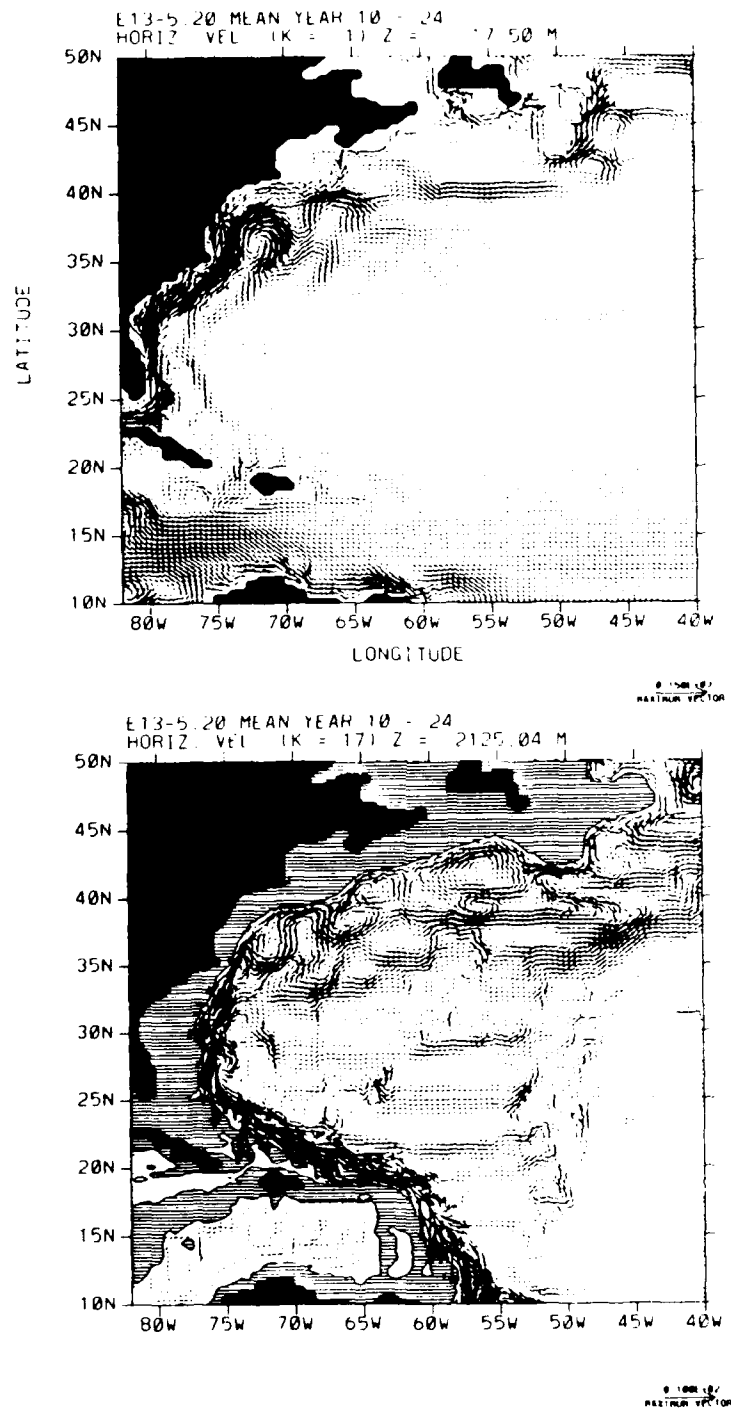


Figure 4. (a) Mean horizontal velocity at the first model level (17.5 m) for January. Vector in the lower right represents 150 cm s<sup>-1</sup>. (b) Mean horizontal velocity at 2125 m for January. Vector in the lower right represents 10 cm s<sup>-1</sup>. Areas with cross hatching indicate topography shallower than 2250 m.

the Gulf Stream (36° to 37°N). During summer, a seasonal thermocline forms at approximately 50 m depth, leaving behind a thick layer of 18° water, or subtropical mode water. This process is the primary ventilation mechanism in the western part of the basin. A second distinct mode water with a temperature around 12°C forms further east along the North Atlantic Current, and a subpolar mode water with a temperature around 4°C forms in the Labrador Sea.

The shifted position of the Gulf Stream is apparent in the January mean surface currents shown in Figure 4a. Whereas the Gulf Stream is observed to separate from the coast at Cape Hatteras, in the model it follows the coast for several hundred kilometers further north. The separation in the model is dominated by a very tight and nearly stationary anticyclonic gyre that is not observed in reality. This type of error in the western boundary current separation region is common in experiments with primitive equation models, yet the dynamical processes involved are still unclear. The lack of a strong theoretical understanding of the physics of boundary current separation compounds the difficulty of trying to understand this aspect of the model solution. South of Cape Hatteras the simulation of the western boundary current is much more realistic. The mean barotropic transport just south of Cape Hatteras is approximately 50 Sverdrups. The core of the southward flowing North Atlantic Deep Water is located between 2000 and 3000 m depth. As shown in Figure 4b, a coherent deep western boundary current can be identified everywhere south of Cape Hatteras. Between Cape Hatteras and the Grand Banks, a weaker westward flow can be seen following the continental slope. In any instantaneous realization the flow at this level, north and east of Cape Hatteras, is dominated by the eddy field.

The time series for the volume transport through the Florida Straits is shown in Figure 5. The well-documented seasonal variation of the transport (see Leaman et al., 1987), with a maximum in summer and a sharp drop in fall, is reproduced by the model. Both the amplitude and the phase of the variability agree well with the observations. The model solution also shows a large amount of interannual variability. The annual mean transport is somewhat too low however. This is not too surprising, given that the model resolves the Florida Straits with only three grid points in the zonal direction.

With the emergence of satellite altimetry it has become possible to accurately map the distribution of eddy variability in the ocean. This provides one of the few basin- to global-scale measurements of variability with which to compare the models. The distribution of the standard deviation of the surface elevation in the model is shown in Figure 6. The peak values in the Gulf Stream region are approximately 30 cm. This compares favorably with the estimates of Koblinsky (1988) derived from the GEOSAT altimeter. The secondary maximum in variability off the coast of Brazil is also reproduced by the model. The sea level variability in the interior, away from the western boundary, is too low by a factor of two however. This may be due to the lack of subseasonal frequencies in the wind forcing.

#### Heat Transport and Meridional Circulation

A primary quantity of climatic interest is the poleward heat transport and, especially for this study, the contribution of the eddies. The mean seasonal cycle of the total northward heat transport is shown in Figure 7. The most prominent signal is the large variability in the tropics, where the heat transport reaches a maximum of  $1.3 \times 10^{15}$  W in January and a minimum of  $-0.7 \times 10^{15}$  W in August. This is associated with the

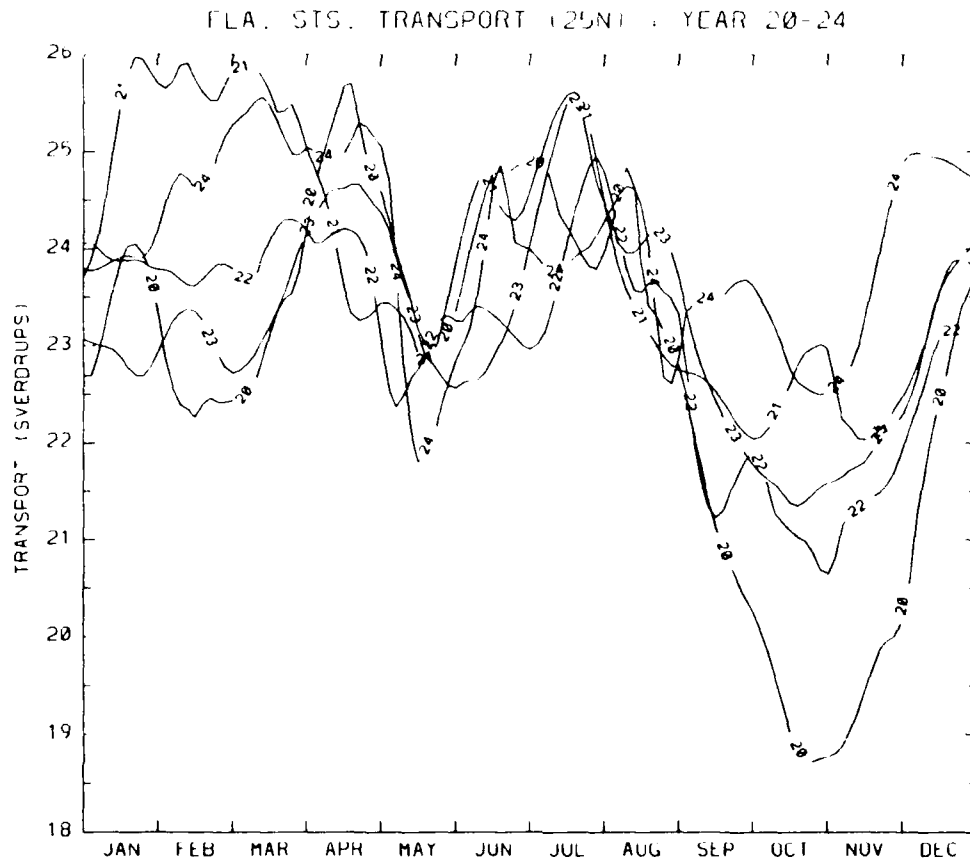


Figure 5. Barotropic transport in the Florida Straits during the final 5 years of the experiment.

seasonal onset of the North Equatorial Counter Current, as discussed below. The annual mean transport reaches a maximum of  $0.6 \times 10^{15}$  W at  $35^\circ\text{N}$  latitude. Hall and Bryden (1982) estimate the transport across  $24^\circ\text{N}$  to be  $1.2 \pm 0.3 \times 10^{15}$  W whereas the model prediction for the mean annual transport across this latitude is  $0.55 \times 10^{15}$  W.

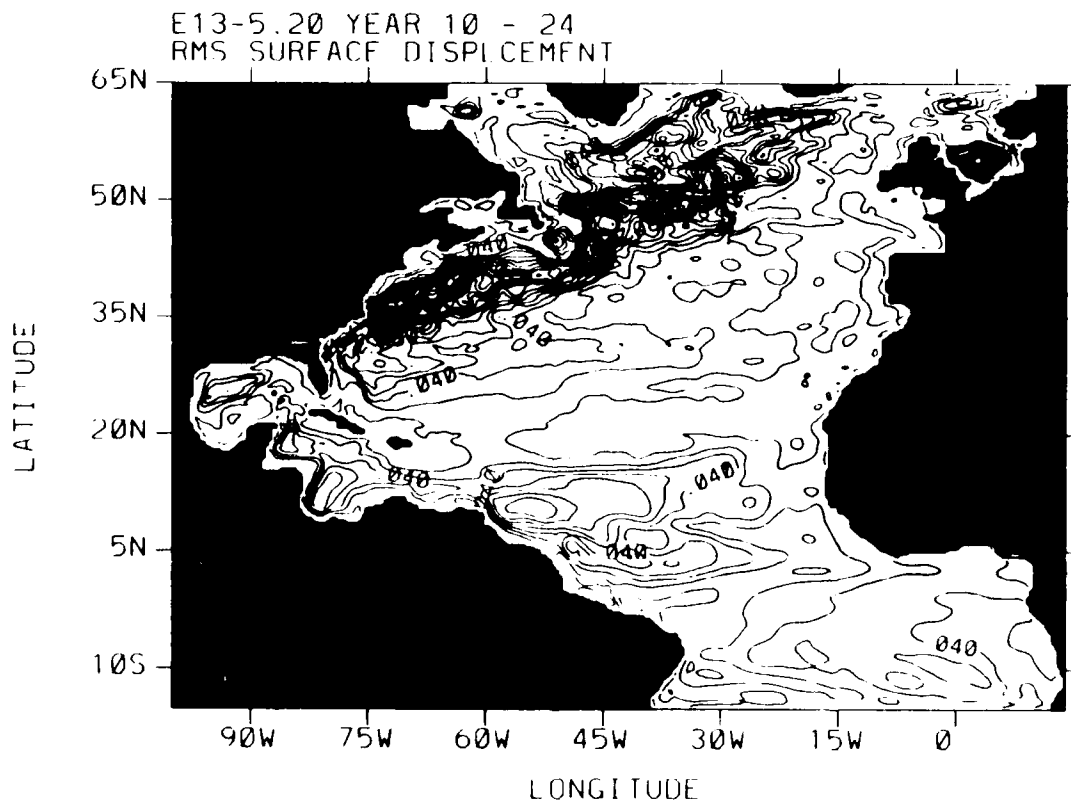
The primary contribution to the heat transport comes from the meridional overturning mode of the circulation. The sensitivity of this aspect of the circulation to various sub-grid scale parameterizations is well-documented in Bryan (1987). The net overturning in the model (Figure 8) is somewhat lower than estimates based on observations. This difference is easily accounted for by the uncertainty in the strength of vertical mixing processes. In this limited area model the specification of the open boundary conditions also affects the total overturning in the basin. While the water mass properties appear to be set correctly in the buffer zones, the exchange of water entering and leaving them appears to be too weak. Thus, while the gain and loss of heat within the basin appear to agree well with observations, the net heat transport through the basin is too small.

The contributions of the mean flow and the eddies to the northward heat transport are shown in Figure 9. The eddy contribution is largest in the latitude band of the Gulf Stream but never exceeds 10% of the contribution of the mean flow. In sharp contrast to the situation in the atmosphere, it appears that transient eddies in the ocean do not make a large direct contribution to the total poleward heat transport.

### An Example of Wave-Mean Flow Interaction

The equatorial circulation system in the Atlantic has a large seasonal cycle and is the most energetic part of the basin outside of the Gulf Stream region. The model successfully simulates the seasonal formation of the North Equatorial Counter Current (NECC) during summer and fall as well as the development of "equatorial long waves" (see Philander et al., 1986) on the NECC, as shown in Figure 10. These waves are the result of baroclinic instability and are responsible for the equatorward heat transport between  $0^\circ$  and  $10^\circ\text{N}$  seen in Figure 7. Note that the isotherms tilt up towards the equator in this region, so that the eddy heat flux is indeed down gradient.

The circulation in this region is particularly sensitive to variations in the dissipation, and this sensitivity reveals an interesting example of wave-mean flow interaction processes. A one year sensitivity experiment in which the vertical viscosity was reduced from  $30 \text{ cm}^2\text{s}^{-1}$  to  $10 \text{ cm}^2\text{s}^{-1}$  was run starting from the conditions at the beginning of year 20 of the standard case. The strength of the Equatorial Undercurrent increased by approximately 50 percent and it penetrated farther to the east. The amplitude of the waves on the NECC also grew significantly, and the wave field penetrated several more wavelengths to the east (Figure 11). Since these eddies are responsible for the equatorward heat transport, we might expect this to increase as well. The maximum magnitude of the total heat transport was essentially the same in the two cases, however.



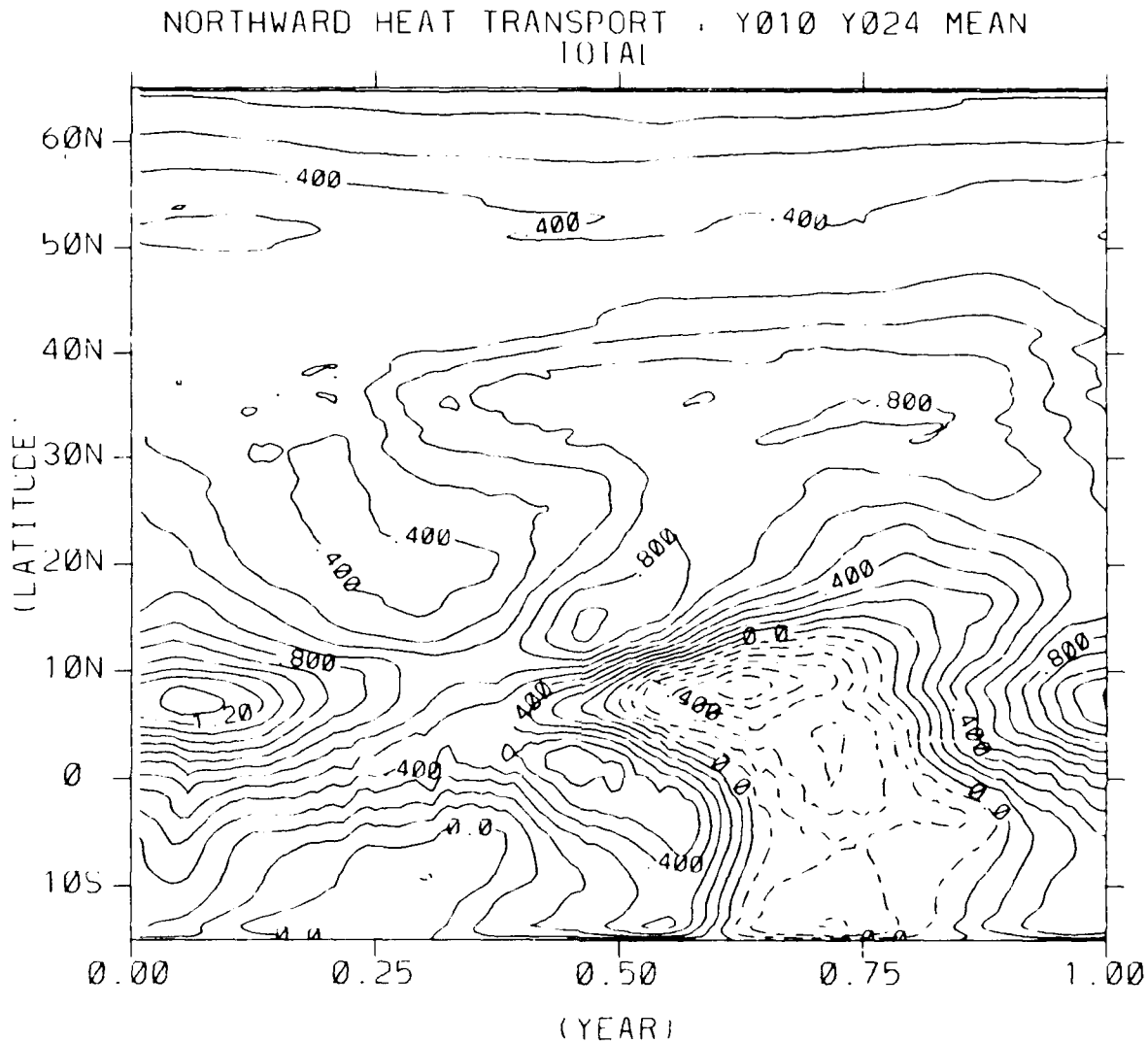


Figure 7. Mean annual cycle of meridional distribution of northward heat transport. Units are  $10^{15}$  W.

The resolution to this paradox is apparent in Figure 12. The southward heat transport by the eddies is opposed by a northward heat transport due to a shallow meridional overturning cell, which is itself partially driven by the eddies (analogous to the Ferrell cell in the atmosphere). In the low dissipation case, the increase in the direct heat transport by the eddies is almost exactly canceled by the changes in the heat transport by the mean flow due to the change in the driving of the mean flow by the eddies. This provides very clear example of strong eddy interactions with a climatically important process.

## CONCLUSIONS

The experiment described here represents the current state-of-the-art in ocean general circulation modeling. It is clear that the physical processes responsible for both water mass formation and eddy formation can be successfully simulated in models of this class.



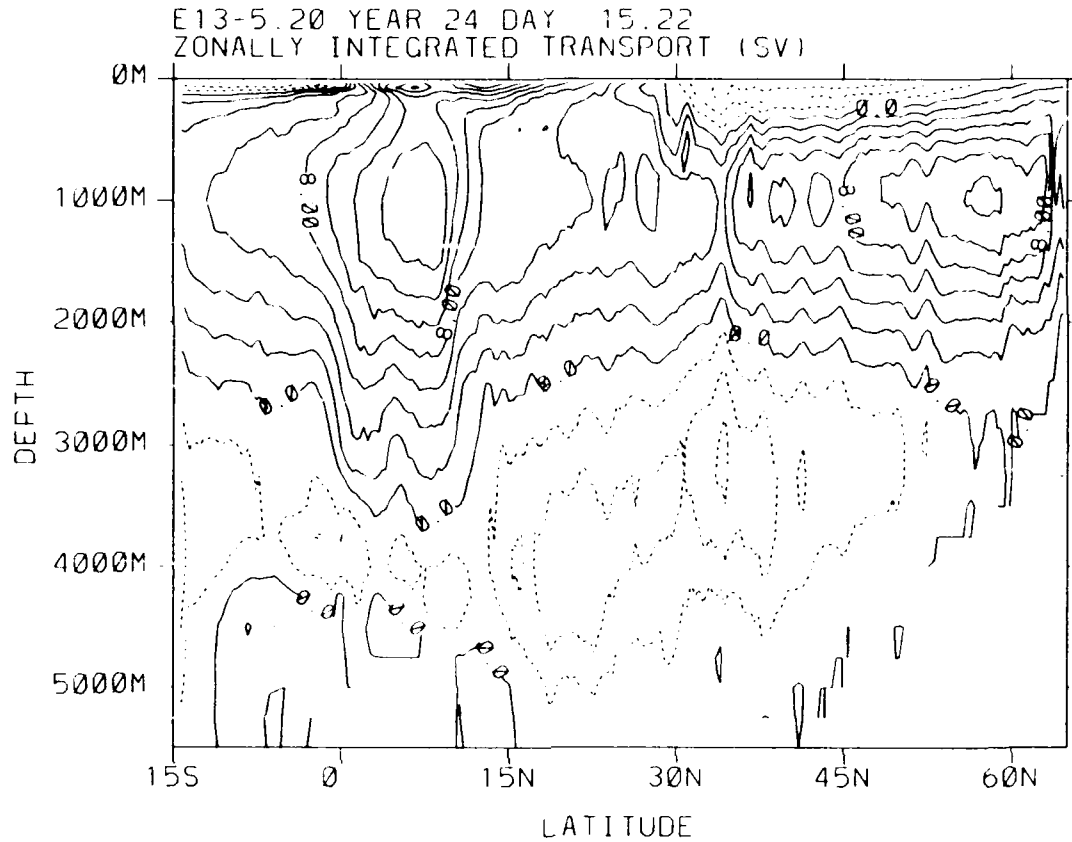


Figure 8. Streamfunction for the zonally integrated transport during mid-January of the final year of the integration.

The major area of difficulty remaining in the model is the simulation of the western boundary current near the separation point. Experience with quasigeostrophic models of the mid-latitude circulation suggest that even higher resolution will be required to overcome these difficulties. We have seen that both the eddies and the mean flow are very sensitive to the magnitude of the dissipation provided by sub-grid-scale parameterizations, and thus many more experiments of this type will be required before we can quantify our confidence in the simulations. Further, as we are now able to explicitly resolve most of the important scales involved in quasigeostrophic eddies, the class of motions that are regarded as "sub-grid-scale" has been redefined. It appears that the next major level of model development should be directed towards improving our understanding and the parameterization of the truly small scale processes responsible for diapycnal mixing and momentum dissipation.

This experiment provides one of the first estimates of the contribution of mesoscale eddies to ocean heat transport. The direct contribution of the eddies to the heat transport was 10% or less of the contribution of the mean flow. In at least one region however, we saw that the eddies had strong interactions with the mean flow itself, and thus strong indirect effects on climatically important aspects of the ocean circulation.

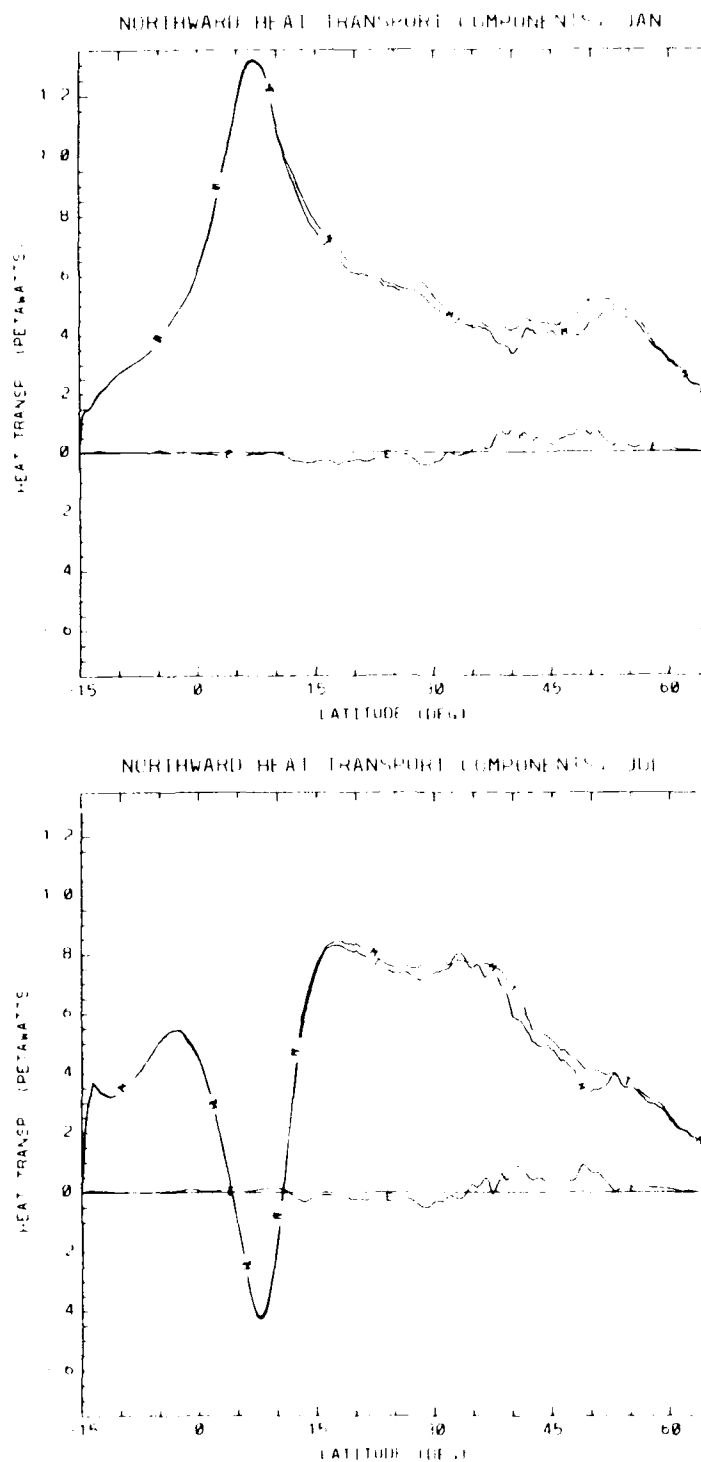


Figure 9. Total heat transport (T), the contribution of the time mean flow to the total heat transport (M), and the eddy contribution to the total heat transport (E) for January (top) and July (bottom).

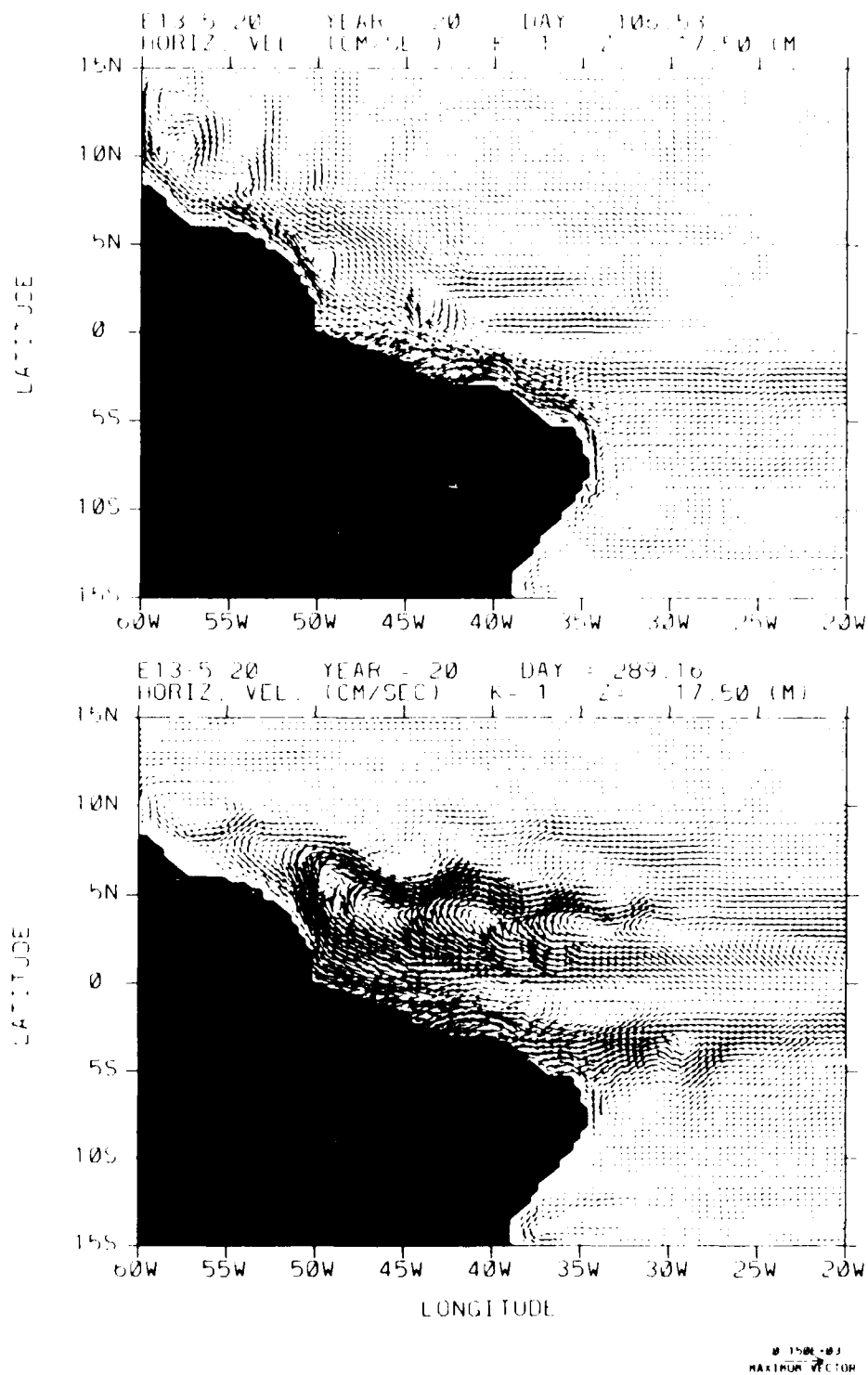


Figure 10. a) Horizontal velocity at 17.5 m in the western equatorial region for mid-April during the year 20 of the standard experiment. Vector in the lower right represents  $150 \text{ cm s}^{-1}$ . b) As above for mid-October.

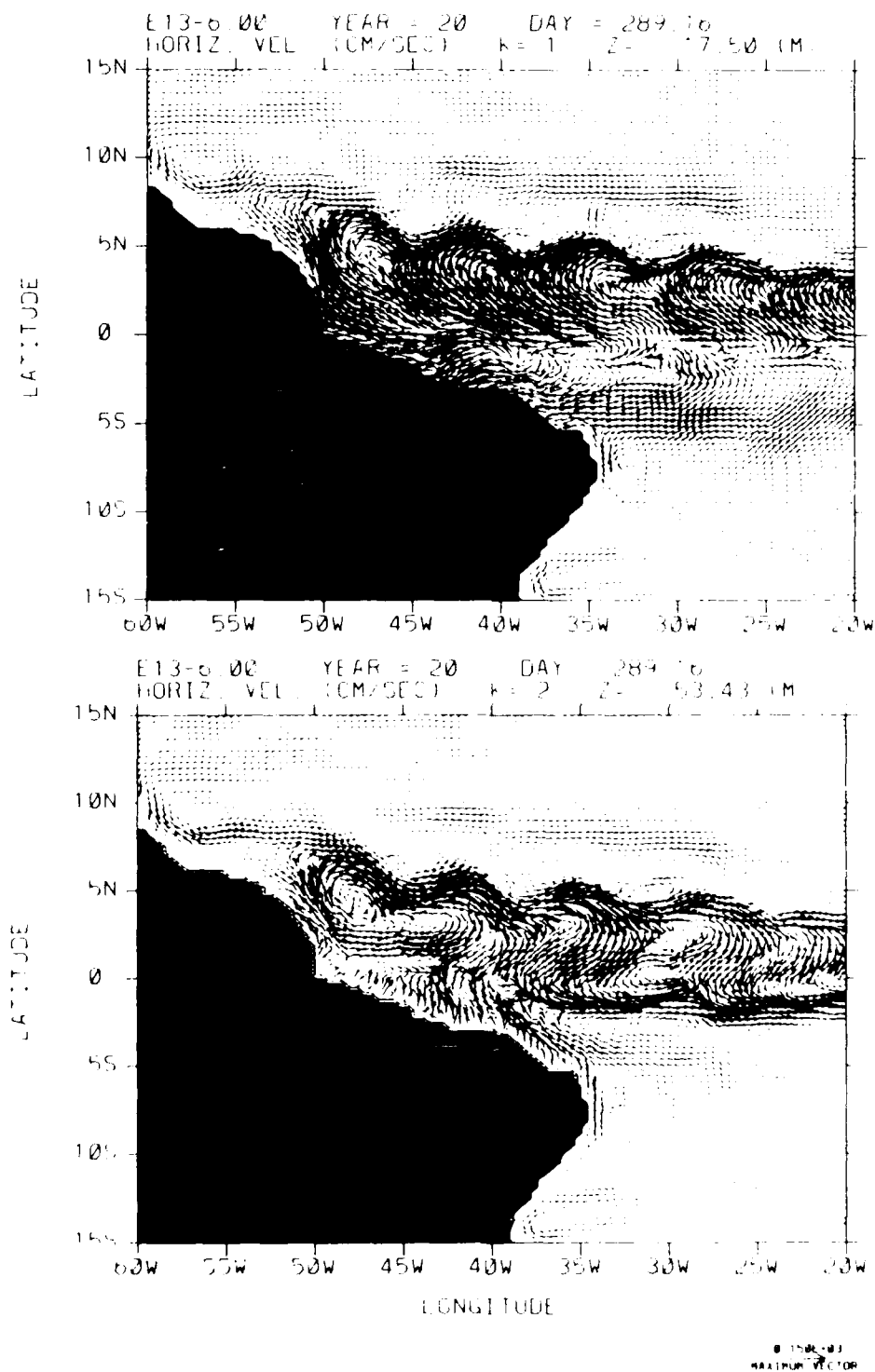


Figure 11. a) Horizontal velocity at 17.5 m in the western equatorial region for mid-October during year 20 of the case with decreased vertical viscosity. Vector in the lower right represents  $150 \text{ cm s}^{-1}$ . b) As above except at 53.4 m.

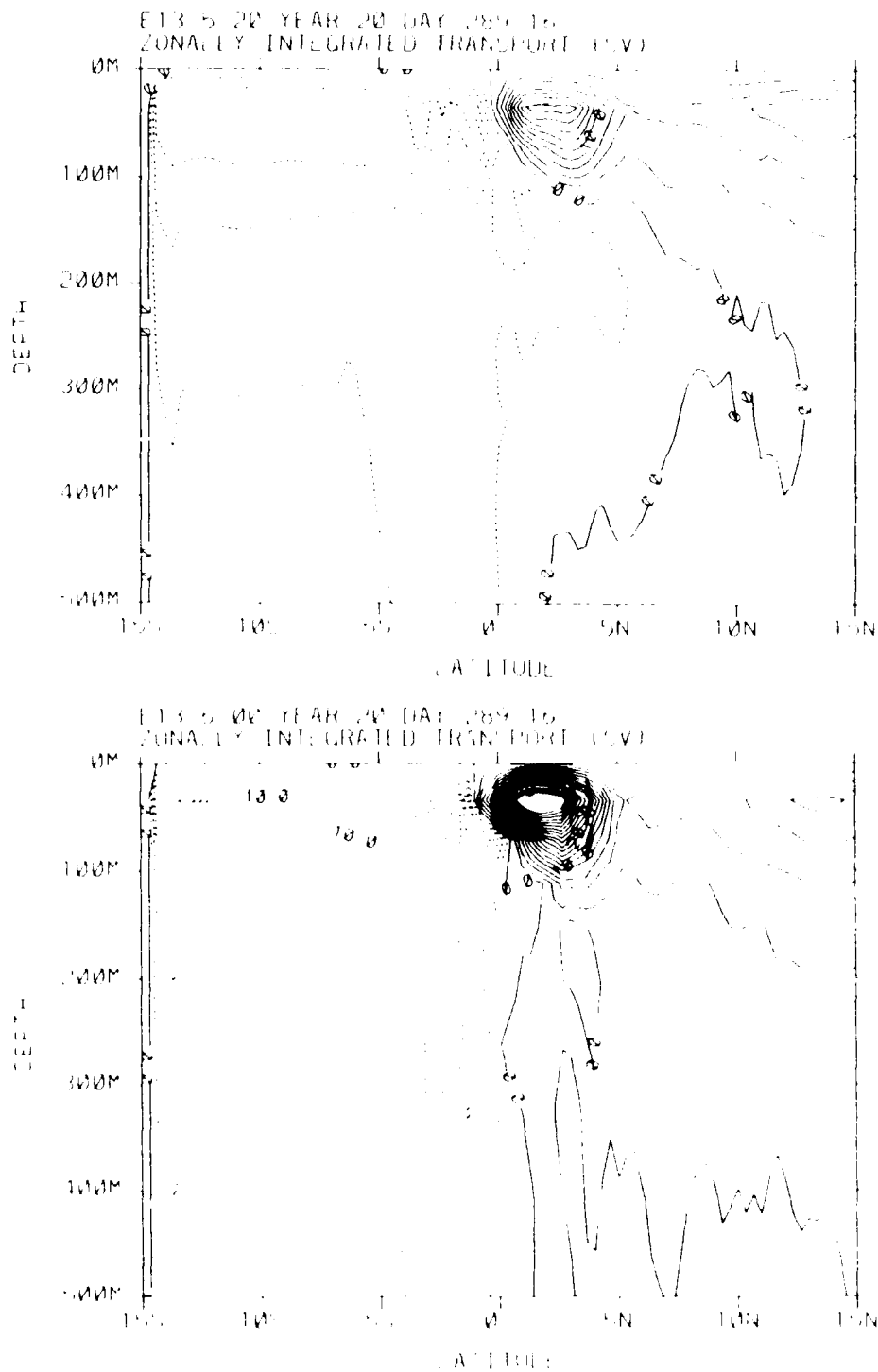


Figure 12. a) Zonally integrated transport in the equatorial region during mid-October for the standard experiment. b) As above for the case with reduced vertical viscosity.

## REFERENCES

- Arakawa, A. and V.R. Lamb: 1977. Computational design of the basic dynamical processes of the UCLA general circulation model. In: *Methods in Computational Physics*, 17, J. Chang (Ed.), Academic Press.
- Bryan, F.: 1987. Parameter sensitivity of primitive equation ocean general circulation models. *J. Phys. Ocean.*, 17, 970-985.
- Bryan, K.: 1969. A numerical method for the study of the circulation of the world ocean. *J. Comput. Phys.*, 4, 347-376.
- Bryan, K.: 1979. Models of the world ocean circulation. *Dynamics of Atmospheres and Oceans*, 3, 327-338.
- Cox, M.D.: 1984. A primitive equation three dimensional model of the ocean. *GFDL Ocean Group Technical Report No. 1*, Geophysical Fluid Dynamics Laboratory/NOAA.
- Gill, A.E. and P.P. Niiler: 1973. The theory of the seasonal variability in the ocean. *Deep-Sea Res.*, 20, 141-177.
- Hall, M.M. and H.L. Bryden: 1982. Direct estimates and mechanisms of ocean heat transport. *Deep-Sea Res.*, 29, 339-360.
- Han, Y.-J.: 1984. A numerical world ocean general circulation model. Part II A baroclinic experiment. *Dynamics of Atmospheres and Oceans*, 8, 141-172.
- Hellerman, S. and M. Rosenstein: 1983. Normal monthly wind stress over the world ocean with error estimates. *J. Phys. Oceanogr.*, 13, 1093-1104.
- Holland, W.R., D.E. Harrison, and A.J. Semtner, Jr.: 1983. Eddy resolving numerical models of large-scale ocean circulation. In: *Eddies in Marine Science*, A.R. Robinson (Ed.), Springer-Verlag, 379-403.
- Holland, W.R.: 1985. Simulation of mesoscale ocean variability in mid-latitude gyres. In: *Issues in Atmospheric and Oceanic Modeling, Part A: Climate Dynamics*, S. Manabe (Ed.) Reviews of Geophysics, 28, Academic Press, 479-523.
- Holland, W.R.: 1986. Quasi-geostrophic modelling of eddy-resolved ocean circulation. In: *Advanced Physical Oceanographic Numerical Modeling*, J.J. O'Brien (Ed.), NATO ASI Series C: Mathematical and Physical Sciences, 186, Reidel, 203-231.
- Koblinsky, C.: 1988. GEOSAT vs. SEASAT. *EOS Trans. Amer. Geophys. Union*, 69, 1026.
- Leaman, K.D., R.L. Molinari, and P.S. Vertes: 1987. Structure and variability of the Florida Current at 27°N: April 1982-July 1984. *J. Phys. Oceanogr.*, 17, 565-583.
- Levitus, S.: 1982. Climatological Atlas of the World Ocean, *NOAA Prof. Paper 13*, U.S. Govt. Print. Office. 173 pp.
- Meehl, G.A., W.M. Washington, and A.J. Semtner: 1982. Experiments with a global ocean model driven by observed atmospheric forcing. *J. Phys. Oceanogr.*, 12, 301-312.
- Philander, S.G.H., W.J. Hurlin, and R.C. Pacanowski: 1986. Properties of long equatorial waves in models of the seasonal cycle in the Tropical Atlantic and Pacific Oceans. *J. Geophys. Res.*, 91, 14207-14211.
- Philander, S.G.H., W.J. Hurlin and A.D. Siegel: 1987. Simulation of the seasonal cycle of Tropical Pacific Ocean. *J. Phys. Oceanogr.*, 17, 1986-2002.
- Sarmiento, J.L.: 1986. On the North and Tropical Atlantic heat balance. *J. Geophys. Res.*, 91, 11677-11689.

## SMALL-SCALE MIXING: A FIRST-ORDER PROCESS?

M.C. Gregg

Applied Physics Laboratory and School of Oceanography, College of Ocean and Fishery Sciences, University of Washington, Seattle, Washington 98105

## ABSTRACT

To within a factor of 2, observations from diverse sites in the mid-latitude thermocline demonstrate that  $\langle \varepsilon_{IW} \rangle = 7 \times 10^{-10} \langle N^2/N_0^2 \rangle \langle S_{10}^4/S_{GM}^4 \rangle \text{ W kg}^{-1}$ , where  $\langle \varepsilon_{IW} \rangle$  is the average rate of turbulent dissipation due to internal waves,  $N_0 = 0.0052$ , and  $S_{GM}$  is the root mean square shear larger than 10 m calculated with the Garrett and Munk model. When the observed shear matches the Garrett and Munk level, this scaling yields a vertical eddy diffusivity of  $5 \times 10^{-6} \text{ m}^2 \text{ s}^{-1}$ , independent of depth. Levels this low suggest that small-scale mixing is not a major process forming the thermocline and can be omitted from dynamical models, although it must be important for water mass modification occurring over decades. In some places, however, intense shear produces much higher mixing. Owing to the strong sensitivity to shear, the occurrence of significant mixing can be parameterized in models only by including the climatology of internal waves.

## INTRODUCTION

Since Munk's (1966) Abyssal Recipes, small-scale mixing has been considered a major factor in the creation and formation of the thermocline. Subsequent modelers have strengthened this belief by stressing the need for turbulent transport similar to Munk's vertical eddy diffusivity of  $K_v = 1 \times 10^{-4} \text{ m}^2 \text{ s}^{-1}$ . A recent example is Frank Bryan's (1986) sensitivity study using primitive equations. These modelers assume that one eddy coefficient represents the fluxes generated by small-scale turbulence, at least when the fluxes are averaged over several years and the 100 km grid scale used for models of the general circulation. Recently, however, Ann Gargett (1984) and Gargett and Holloway (1984) argue that  $K_v$  varies inversely with the buoyancy frequency  $N$ , producing a vertical gradient in diffusivity that profoundly affects the interior circulation of ocean basins.

Within this general context, our observational strategy has been to ask

- When and where is turbulence important?
- How can turbulent transport be parameterized?
- What is the energy flux through the internal wave spectrum?

The first question is being answered gradually as data from diverse places and seasons are reported. Below are some observations that span the full range of probable importance.

Except for the preliminary  $\overline{u_3' T'}$  measurements of Jim Moum, the second question is being addressed indirectly.  $K_p$  is calculated using simple models and measurements of  $\chi_T \equiv 6\kappa_T(\partial T'/\partial x_3)^2$  and  $\varepsilon \equiv 7.5\nu(\partial u_1'/\partial x_3)^2$ . The vertical eddy coefficient for heat,  $K_T$ , is inferred by assuming a simple balance between local production and diffusive smoothing of temperature fluctuations (Osborn and Cox, 1972), which yields

$$K_T = \frac{\chi_T}{2\kappa_T(\partial \overline{T}/\partial x_3)^2} \quad [\text{m}^2 \text{ s}^{-1}] \quad (1)$$

A similar approach (Osborn, 1980) gives the vertical buoyancy flux in terms of

$$K_p \leq \frac{0.2\varepsilon}{N^2} \quad [\text{m}^2 \text{ s}^{-1}] \quad (2)$$

The assumptions leading to these expressions appear reasonable, and the two approaches seem to give consistent values. No one, however, has verified either formula by comparison with changes in average properties. Furthermore, at this meeting Holloway continued to assert that inferring diffusivities from  $\varepsilon$  may be quite wrong. Although his arguments seem implausible to me, they cannot be dismissed. In any event, the lack of any confirmation of these inferential techniques is disquieting.

Because we think that breaking internal waves produce most of the small-scale mixing, the first two questions lead to the third. Things are somewhat better with this question, since it can be addressed more directly—by relating  $\varepsilon$  observations to the intensity of internal waves. The major observational questions reduce to assessing isotropy and the statistical adequacy of the sampling. Working for the past nine years, we have compiled six sets of simultaneous observations of shear and  $\varepsilon$ , allowing us to address the last question with new data. The results, however, apply as well to the first two questions.

## INTERNAL WAVE SCALING OF TURBULENT DISSIPATION

By comparing simultaneous observations of  $\varepsilon$ ,  $N$ , and shear calculated over 10 m intervals, we find that

$$\langle \varepsilon_{10} \rangle = 7 \times 10^{-10} \langle N^2/N_0^2 \rangle \langle S_{10}^4/S_{GM}^4 \rangle \quad [\text{W kg}^{-1}] \quad (3)$$

where  $N_0 = 5.2 \times 10^{-3} \text{ s}^{-1}$ ,  $S_{10}$  is the observed 10 m shear, and  $S_{GM}$  is the corresponding shear in the Garrett and Munk spectrum. Thus,  $\varepsilon_{10}$  varies as the fourth power of the shear and the square of the buoyancy frequency.



Taking  $u_1$  and  $u_2$  as the eastward and northward velocity components, the shear components are computed as

$$S_{x_1} \equiv \sqrt{2.11} \frac{\Delta u_1}{\Delta x_3}, \quad S_{x_2} \equiv \sqrt{2.11} \frac{\Delta u_2}{\Delta x_3} \quad (4)$$

where  $\Delta x_3 = 10$  m. The factor of  $\sqrt{2.11}$  corrects for the attenuation of the first-difference filter and makes the shear variance comparable to that obtained by integrating a spectrum to  $0.6 \text{ rad m}^{-1}$ . Then,

$$S_{10}^4 = (S_{x_1}^2 + S_{x_2}^2)^2 \quad (5)$$

For comparison, the variance of the 10 m shear in the Garrett and Munk model is

$$S_{GM}^2 = (3\pi/2)j_* E_{GM} b N_0^2 k_3^C (N/N_0)^2 = 1.91 \times 10^{-5} (N/N_0)^2 \quad [\text{s}^{-2}] \quad (6)$$

Garrett and Munk did not estimate the fourth moment, but they did assume that  $S_{x_1}$  and  $S_{x_2}$  are statistically independent and normally distributed. We examined two of our data sets and found that both conditions are satisfied. Applying normal probability statistics, H. Scim (personal communication, 1988) showed that the average of the fourth moment is twice the square of the variance. We also verified this by comparing  $2 \langle S_{10}^2 \rangle$  with  $\langle S_{10}^4 \rangle$ . Therefore, for the reference shear we use

$$\langle S_{GM}^4 \rangle = 2 \langle S_{GM}^2 \rangle^2 \quad (7)$$

The functional form of  $\langle \varepsilon_{IW} \rangle$  is the same as that predicted by McComas and Müller (1981) and by Henyey et al. (1986), provided the shear varies as  $S_{GM}^2 \propto E_{GM}$ , as it does in Eq. (6).

McComas and Müller assumed that nonlinear interactions among internal waves are weak and calculated the flux of energy through the spectrum due to two resonant mechanisms: parametric subharmonic instability and induced diffusion. Supposing that all of this flux is dissipated, they estimated

$$\varepsilon_{MM} = \left( \frac{27\pi}{32\sqrt{10}} + 1 \right) \pi^2 j_*^2 b^2 \int N^2 E_{GM}^2 \quad [\text{W kg}^{-1}] \quad (8)$$

where  $j_* = 3$  and  $b = 1300$  m are parameters in the Garrett and Munk model.

Henyey et al. recognized that interactions within the internal wave spectrum are not necessarily weak, but argued that the primary interactions occur between widely different wavenumbers. Since most of the energy in the internal wave spectrum is at low

wavenumber, they followed the evolution of energy at high wavenumbers by using the ray-tracing equations. After several further assumptions, they obtained

$$\varepsilon_{HWF} = (1.67/\pi) j_*^2 b^2 f \cosh^{-1}(N/f) N^2 E_{GM}^2 \quad [\text{W kg}^{-1}] \quad (9)$$

Thus, the two predictions have the same  $f N^2 E_{GM}^2$  dependence. Neglecting the  $\cosh^{-1}(N/f)$  factor, which varies little, Eq. (3) is twice  $\varepsilon_{HWF}$  and about one third  $\varepsilon_{MM}$ .

### COMPARISON WITH OBSERVATIONS

The need to scale with  $S_{10}$  as well as with  $N$  is demonstrated in Fig. 1. Three cruise averages of  $\langle \varepsilon \rangle / \nu \langle N^2 \rangle$  are compared in the left panel. We made the PATCHEX observations in the outer reaches of the California Current when the internal wave shear was nearly identical with the Garrett and Munk levels (Gregg and Sanford, 1987).

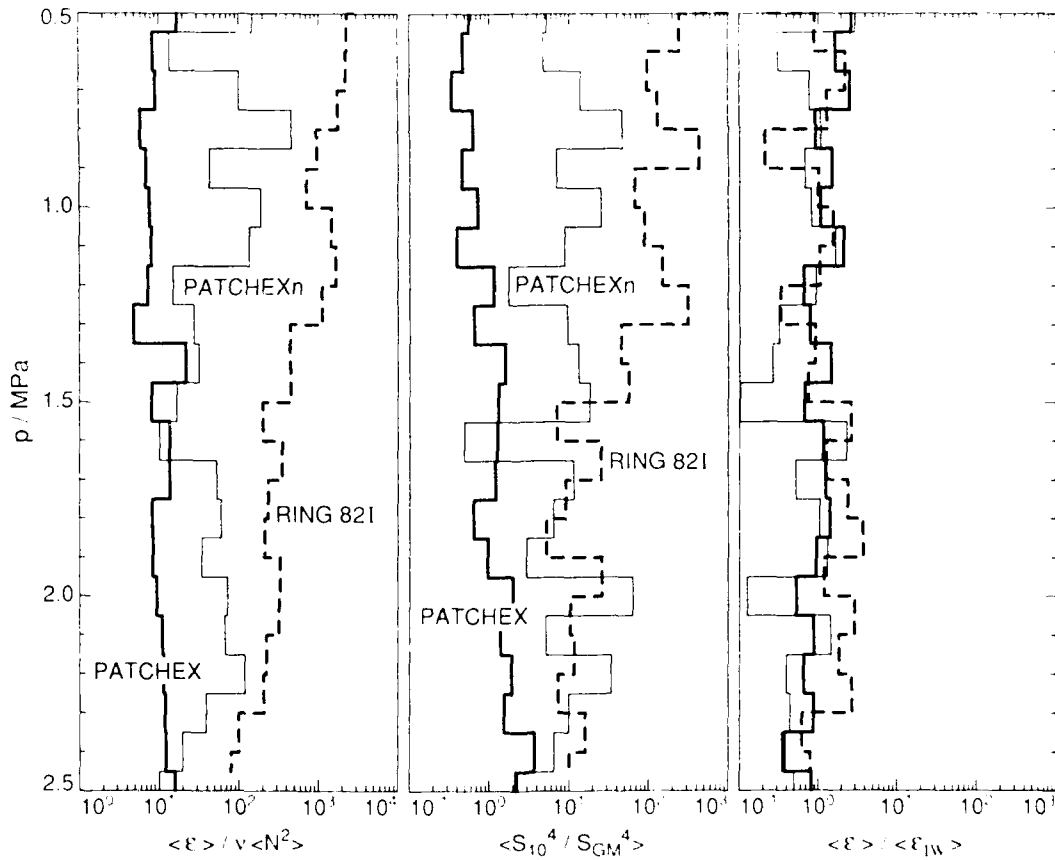


Fig.1. Scaling comparisons for three mid-latitudes averages. Including shear scaling greatly reduces the large differences remaining when  $\varepsilon$  is scaled only with  $N$ .

Becoming bored with Garrett and Munk's energy level, we left PATCHEX a few days early and headed for a mature coastal jet off Crescent City. Although neither the shear nor  $\varepsilon$  showed signatures in the coastal jet, both were much higher than at PATCHEX. We collected the RING82I data south of New England while waiting for an outbreak of cold air (Larson, 1988). Even before the arrival of the storm trailing the cold air behind it, both shear and dissipation were very high: averaged vertically,  $\langle \varepsilon \rangle / \nu \langle N^2 \rangle$  for RING82I was 58 times the similar average for PATCHEX, compared with 9 times higher for PATCHEX north.

Applying the full scaling greatly reduces the variability in dissipation rates (Fig. 1, right panel). Averaged vertically,  $\langle \varepsilon \rangle / \langle \varepsilon_{IW} \rangle$  is 1.52 for RING82I, 1.11 for PATCHEX north, and 1.00 for PATCHEX (Table 1). The very high dissipation rates for RING82I resulted from internal energy levels of  $4.3E_{GM}$ , compared with  $3.2E_{GM}$  for PATCHEX north. We also have a fourth data set from mid-latitudes, DRIFTER (not shown in the figures, but listed in Table 1). Its vertical average is  $\langle \varepsilon \rangle / \langle \varepsilon_{IW} \rangle = 0.5$ , on the low side, but within the factor of 2 claimed for the scaling.

Since these four sets of profiles were taken at  $31^\circ$ – $42^\circ$ N, the variation in  $f$  is much smaller than the statistical scatter of the data. Consequently, we used  $34^\circ$ N, the latitude of PATCHEX, in computing  $\varepsilon_{IW}$  for them. Three of these data sets were taken

Table 1. Vertical averages. Excluding CSALT,  $\langle \varepsilon \rangle / \nu N^2$  varies from 0.21–58.3 times the PATCHEX value, compared with 0.5–1.5 for  $\langle \varepsilon \rangle / \langle \varepsilon_{IW} \rangle$ , strongly demonstrating the need to scale with shear as well as with buoyancy frequency. For CSALT,  $\langle \varepsilon \rangle / \langle \varepsilon_{IW} \rangle$  is larger than predicted, consistent with salt fingers producing turbulence in addition to that generated by internal waves. For TROPIC HEAT 2, we use a conditional average calculated by setting to zero all raw  $\varepsilon$ 's less than  $10^{-10} \text{ W kg}^{-1}$ . Averaging all the data, including values dominated by noise, gives  $\langle \varepsilon \rangle / \nu N^2 = 5.1$  and  $\langle \varepsilon \rangle / \langle \varepsilon_{IW} \rangle = 1.99$  and 2.16, with and without  $f$ -scaling, respectively.

Cruise	$\frac{\langle \varepsilon \rangle}{\nu N^2}$	$\left\langle \frac{S_{10}^2}{S_{GM}^2} \right\rangle$	$\left\langle \frac{S_{10}^4}{S_{GM}^4} \right\rangle$	$\frac{\langle \varepsilon \rangle}{\langle \varepsilon_{IW} \rangle}$	$\frac{\langle \varepsilon \rangle}{\langle \varepsilon_{IW} \rangle}$ <i>f</i> -scaling
PATCHEX (1.0-9.5)	13.1	0.98	1.02	1.00	1.08
RING82I (0.5-2.5)	763.4	4.31	43.66	1.52	1.35
PATCHEXn (1.0-9.5)	123.4	3.17	9.89	1.11	1.08
DRIFTER (0.5-2.0)	14.8	1.54	2.19	0.50	0.53
TROPIC HEAT 2 (1.0-9.5)	2.7	0.86	0.80	0.96	2.33
CSALT (1.0-7.0)	17.2	0.70	0.64	3.52	8.44

in diffusively stable profiles below the shallow salinity minimum in the eastern Pacific. RING82I, however, sampled a profile that was diffusively unstable, to the diffusive regime above 1.5 MPa and to salt fingering below 1.5 MPa. In addition, many strong thermohaline intrusions were found. Nevertheless, Larson (1988) found no relationship between the intrusions and the dissipation. Furthermore, he determined that the dissipation rates are much larger than can be attributed to double diffusion. Consequently, we attribute the primary dissipation in all of these profiles to internal waves.

Two additional sets of observations were made, both near 12°N: CSALT in the thermohaline staircase east of Barbados (Gregg and Sanford, 1987), and TROPIC HEAT 2 in the central Pacific. Vertical averages give  $\langle \varepsilon \rangle / \langle \varepsilon_{IW} \rangle = 3.5$  for CSALT (Table 1), more than twice any of the others. Multiplying  $\langle \varepsilon_{IW} \rangle$  by  $f/f_{34^\circ}$  to include the  $f$ -scaling (Fig. 2) raises this to 8.4. By contrast, although TROPIC HEAT 2 was taken

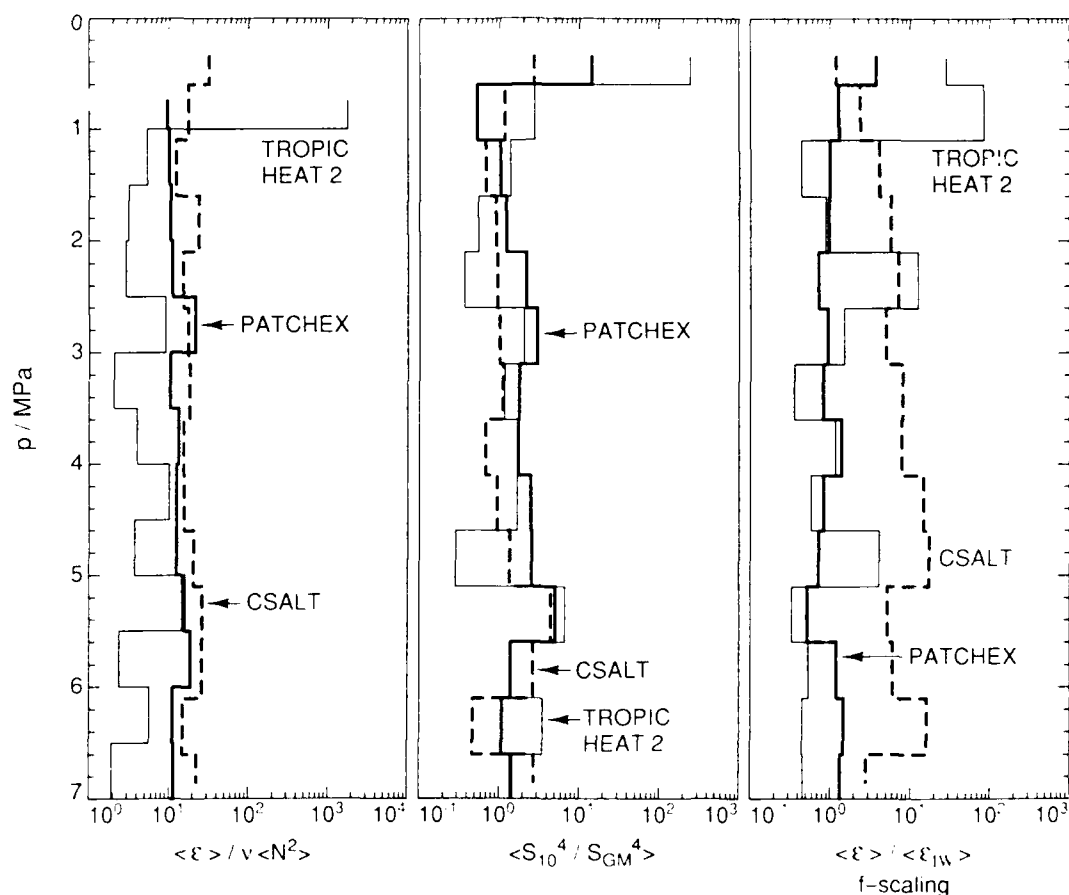


Fig.2. Comparisons including the  $f$ -scaling for two sites at 12°N and PATCHEX, at 31°N. Although both low-latitude sites are higher than predicted by the scaling, the discrepancy is much larger for CSALT than for TROPIC HEAT 2, presumably due to the salt fingering that forms the thermohaline staircase in the CSALT profiles.

at the same latitude, its vertical average is  $\langle \varepsilon \rangle / \langle \varepsilon_{IW} \rangle = 0.96$  and 2.3, without and with the  $f$ -scaling. Therefore, both are higher than expected for that latitude, but CSALT is much higher.

Although these data do not confirm a decrease in dissipation toward the equator, we cannot conclude that the prediction is wrong, because both profiles are diffusively unstable to salt fingering. The existence of the staircase and other evidence observed during CSALT is consistent with weak salt fingers in the interfaces. Although we found no staircases during TROPIC HEAT 2, the profile is diffusively unstable to salt fingers between 2 and 6 MPa. The major difference between the two profiles is the density ratio,  $R_\rho \equiv (\alpha \partial \bar{T} / \partial x_3) / (\beta \partial \bar{s} / \partial x_3)$ , which is 4 for TROPIC HEAT 2 and 1.6 for CSALT. Schmitt (1979) argues that fingers become more intermittent as  $R_\rho$  increases, and are therefore less likely to form staircases. Whether this also implies lower buoyancy fluxes is uncertain, as Kunze (1987) argues that the fluxes increase with  $R_\rho$ . Therefore, it is possible that 1)  $\varepsilon_{IW}$  decreases toward the equator as predicted, 2) salt fingering in the tropical halocline obscures the decrease, and 3) dissipation due to the salt fingering varies with  $R_\rho$ .

## CONCLUSIONS AND DISCUSSION

From the summaries in Table 1 and Fig. 3, we conclude that

- In the mid-latitude thermocline, to within a factor of 2, the average dissipation rate scales as  $\langle \varepsilon_{IW} \rangle = 7 \times 10^{-10} \langle N^2 / N_0^2 \rangle \langle S_{10}^4 / S_{GM}^4 \rangle \text{ W kg}^{-1}$ . The functional form matches predictions by McComas and Müller (1981) and Henyey et al. (1986), but the magnitude is one third of McComas and Müller's estimate and twice that of Henyey et al.
- Two sets of observations at 12°N had higher dissipation rates than expected when the  $f$ -scaling in the predictions is included. One of the sets was taken through the thermohaline staircase east of Barbados, making salt fingers a likely source of the additional dissipation. Although the second set did not have a staircase, much of the profile was diffusively unstable to salt fingers, and we cannot exclude them as an extra source of dissipation.

By virtue of its success with data as disparate as PATCHEX and RINGS21, it seems likely that the scaling is at least approximately correct for mid-latitudes. What are the implications?

When the internal wave shear matches the Garrett and Munk value, Eq. (2) gives  $K_\rho \leq 5 \times 10^{-6} \text{ m}^2 \text{ s}^{-1}$ , independent of  $N$ . This diffusivity is close to  $K_\rho \approx 10^{-5}$ , increasing the evidence in support of Garrett's (1984) 'zeroth-order view' of internal waves and mixing. Although this may well demonstrate that we have a first-order understanding of the important dynamics linking internal waves and mixing, we should not ignore the possibility that we may have the right answer for the wrong reasons. Had the scaling not worked, plausible excuses are close at hand, beginning with the linear interactions used by McComas and Müller and the ad hoc assumptions made by

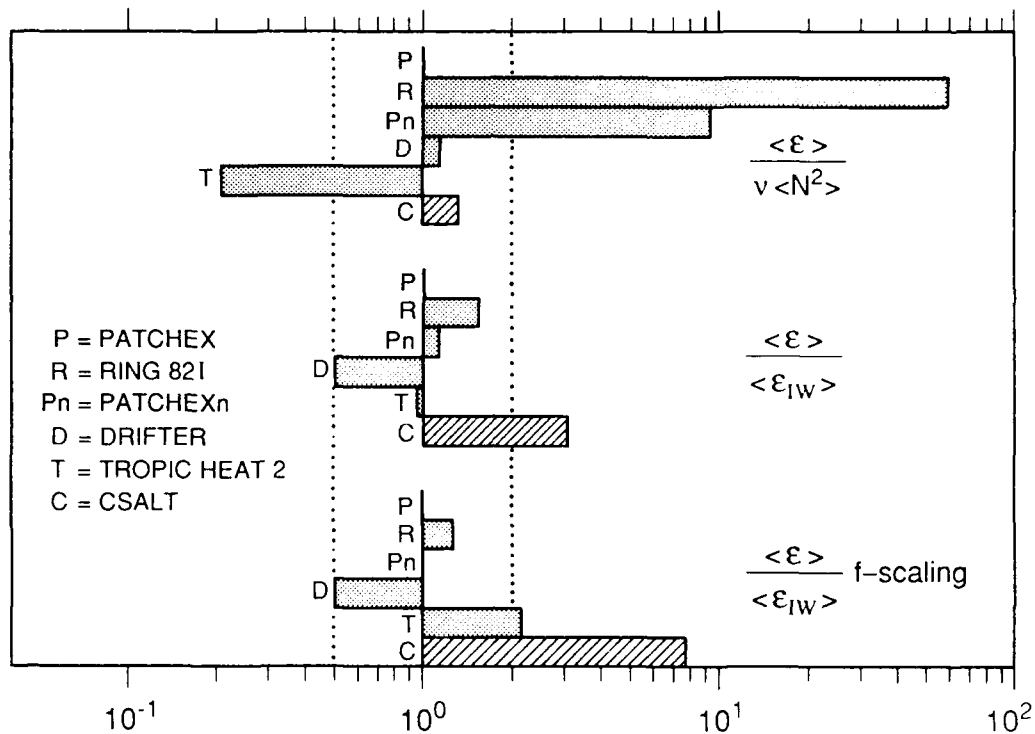


Fig. 3. Summary of vertical averages of the scalings.

Henye et al., including the discrepancies between the Garrett and Munk spectrum and Pinkel's (1985) observations, and ending with Holloway's questioning of the entire basis for inferring diffusivity from dissipation rates. Thus, in spite of the success of the  $\langle \epsilon_{IW} \rangle$  scaling, too many issues remain unresolved for us to be fully confident that we now have a first-order understanding of the dynamics.

The scaling gives a constant and small diffusivity when internal waves are at the background level modeled by Garrett and Munk. How well must we know that constant? Is  $K_p \leq 5 \times 10^{-6}$  so low that it can be set to zero in dynamical models? If so, small-scale mixing is not a first-order dynamical process in these places, although, over decades, it may modify water masses. If mixing in most of the thermocline is of secondary importance, then working out the details is not a high priority problem for oceanography, even though it is interesting fluid mechanics. To sort this out, we need numerical sensitivity studies. However, present models cannot run with such low diffusivities; owing to their large grid spacings, the models require higher diffusivities for numerical stability. While waiting for the next generation of computers, we should focus on confirming the dissipation scaling, Eq. (3), and testing our formulas, Eqs. (1) and (2).

Ledwell's (this volume) tracer release offers the only prospect for testing Eqs. (1) and (2) in the open ocean, but the dissipation scaling indicates that we will have severe sampling problems. The preliminary plans are to release the tracer along parallel

tracks tens of kilometers long and to sample it at intervals no shorter than 6 months. After a year, the tracer streaks will extend at least 500 km. If internal wave breaking is the major process mixing the tracer vertically, then the variability of the internal wave field establishes the sampling requirements for microstructure, or for  $S_{10}$ . Horizontal coherence lengths for internal waves are about 10 km (D'Asaro and Perkins, 1984). Although the energy levels do not necessarily change over short distances, they may—as we learned to our dismay when we found a very energetic inertial feature 50 km away after making the DRIFTER microstructure observations. Since we may need to profile continuously for 1–2 days to estimate  $\epsilon$  and  $\chi_T$  to within a factor of 2 at one place, no conceivable amount of sampling can give adequate averages over a 500 km box until we know much more about the spatial variability of internal waves. To compound the difficulties, Briscoe and Weller (1984) report an annual cycle in the energy of high-frequency waves and episodic bursts of low-frequency waves. Thus we must conclude that ship-based microstructure observations will be inadequate for a decent statistical comparison with the tracer. Therefore, the primary data must come from floats or moorings. As one approach, I am working with Russ Davis to add temperature microstructure to the bobbing floats (ALICE) that he is building with Doug Webb.

Although we have doubts about the importance of small-scale mixing accompanying background internal wave levels, there is little question about its significance when internal waves rise above the background. For instance, in PATCHEX north  $K_\rho = 5 \times 10^{-5} \text{ m}^2 \text{ s}^{-2}$  throughout the upper kilometer; and in RING82I,  $K_\rho \approx 5 \times 10^{-4}$  from 0.5–1.5 MPa and  $\approx 8 \times 10^{-5}$  from 1.5–2.5 MPa. Based on observed changes over the winter in another warm-core ring, Terry Joyce (personal communication, 1989) inferred diffusivities similar to those we measured in 82I. Since diffusivities this large produce important water-mass changes, they need to be incorporated into numerical models by including the variability of internal wave shear. Until now, the hope was that the vertical fluxes of all processes between mesoscale and microscale could be parameterized by simple eddy coefficients that were either constant or, more recently, varied only with  $N$ . It now seems that we cannot get off so simply and that we must deal with the intermediate processes, at least where small-scale mixing is large.

*Acknowledgments.* This work was funded by the *Mixing to Mesoscale* University Research Initiative funded at the University of Washington by the Office of Naval Research (Contract N00014-86-K-0690). Contribution 1801 of the School of Oceanography.

## REFERENCES

- Briscoe, M. G., and R. A. Weller, 1984: Preliminary results from the Long-Term Upper-Ocean Study (LOTUS). *Dyn. Atmos. Oceans*, **8**, 243-265.
- Bryan, F. O., 1986: Maintenance and variability of the thermohaline circulation. Ph.D. dissertation, Princeton Univ., Princeton, N.J., 271 pp.
- D'Asaro, E.A., and H. Perkins, 1984: A near-inertial internal wave spectrum for the Sargasso Sea in late summer. *J. Phys. Oceanogr.*, **14**, 489-505.
- Gargett, A. E., 1984: Vertical eddy diffusivity in the ocean interior. *J. Mar. Res.*, **42**, 359-393.
- Gargett, A. E., and G. Holloway, 1984: Dissipation and diffusion by internal wave breaking. *J. Mar. Res.*, **42**, 15-27.
- Garrett, C. J. R., 1984: Parameterizing the effects of internal waves: Simple things we need to know. In *Internal Gravity Waves and Small-Scale Turbulence, Proceedings, Hawaiian Winter Workshop*, P. Müller and R. Pujulet, Eds., 171-181. Hawaii Institute of Geophysics, Honolulu.
- Gregg, M. C., and T. B. Sanford, 1987: Shear and turbulence in thermohaline staircases. *Deep-Sea Res.*, **34**, 1689-1696.
- Henye, F. S., J. Wright, and S. M. Fløtté, 1986: Energy and action flow through the internal wave field: an eikonal approach. *J. Geophys. Res.*, **91**, 8487-8495.
- Kunze, E., 1987: Limits on growing, finite-length salt fingers: A Richardson number constraint. *J. Mar. Res.*, **45**, 533-556.
- Larson, N. G., 1988: Viscous Dissipation and Mixing Mechanisms in Gulf Stream Warm-Core Ring 82-I. Ph. D. dissertation, School of Oceanography, Univ. Washington, Seattle, 153 pp.
- McComas, C. H., and P. Müller, 1981: The dynamic balance of internal waves. *J. Phys. Oceanogr.*, **11**, 970-986.
- Munk, W. H., 1966: Abyssal recipes. *Deep-Sea Res.*, **13**, 707-730.
- Osborn, T. R., 1980: Estimates of the local rate of vertical diffusion from dissipation measurements. *J. Phys. Oceanogr.*, **10**, 83-89.
- Osborn, T. R., and C. S. Cox, 1972: Oceanic fine structure. *Geophys. Fluid Dyn.*, **3**, 321-345.
- Pinkel, R., 1985: A wave number-frequency spectrum of upper ocean shear. *J. Phys. Oceanogr.*, **15**, 1453-1469.
- Schmitt, R. W. Jr., 1979: The growth rate of super-critical salt fingers. *Deep-Sea Res.*, **26**, 23-40.



## SHEAR AND SALT FINGERS

R. W. Schmitt, K. L. Polzin and J. M. Toole

Woods Hole Oceanographic Institution  
Woods Hole, MA 02543

### ABSTRACT

The Central Waters of the North Atlantic subtropical gyre are characterized by a remarkably constant density ratio ( $R_\rho$ ) on large scales. However, when computed over smaller scales, significant finestructure in  $R_\rho$  is seen. One possible source for this finestructure is the action of inertial period shear acting on isopycnal gradients of salinity. Data from the High Resolution Profiler are examined to explore this mechanism, which appears to be viable, though it cannot explain all of the variance in  $R_\rho$ .

Given the finestructure in  $R_\rho$ , one would also expect modulation of the intensity of salt fingering, since it is a strong function of the density ratio. Evidence for such modulation is seen in the HRP data in the form of increased thermal microstructure when  $R_\rho$  is low and the stratification is strong. A distinct relationship between the theoretical salt finger growth rate and the dissipation rate of thermal variance is found in the data, which supports a simple model of intermittent fingering. Development of such relationships between microstructure and finestructure is an important step toward parameterization of the effects of salt fingers on the thermohaline structure of the ocean.

### 1. INTRODUCTION

The double-diffusive instabilities (salt fingers and diffusive interfaces) are thought to dominate vertical mixing in certain limited regions of the ocean (thermohaline staircases in the arctic, tropical Atlantic and Mediterranean out-flow). It is possible that elevated thermal dissipation levels in these regions make them important contributors to the global destruction of thermal variance. However, it is more probable that intermittently occurring salt fingers in the "Central Waters" (CW) of the subtropical thermocline make the larger contribution to global dissipation, by virtue of their vast extent. If salt fingers do elevate mixing levels in the main thermocline, it has been suggested that the associated nutrient fluxes could have a significant impact on biological productivity in the euphotic zone (Hamilton, Lewis and Ruddick, 1989).

The problem of assessing the role of salt fingers in the CW is potentially complex, since shear instability can also contribute to mixing there. An approach taken by Schmitt and Evans (1978) was to assume that fingers are intermittently active on the high gradient interfaces

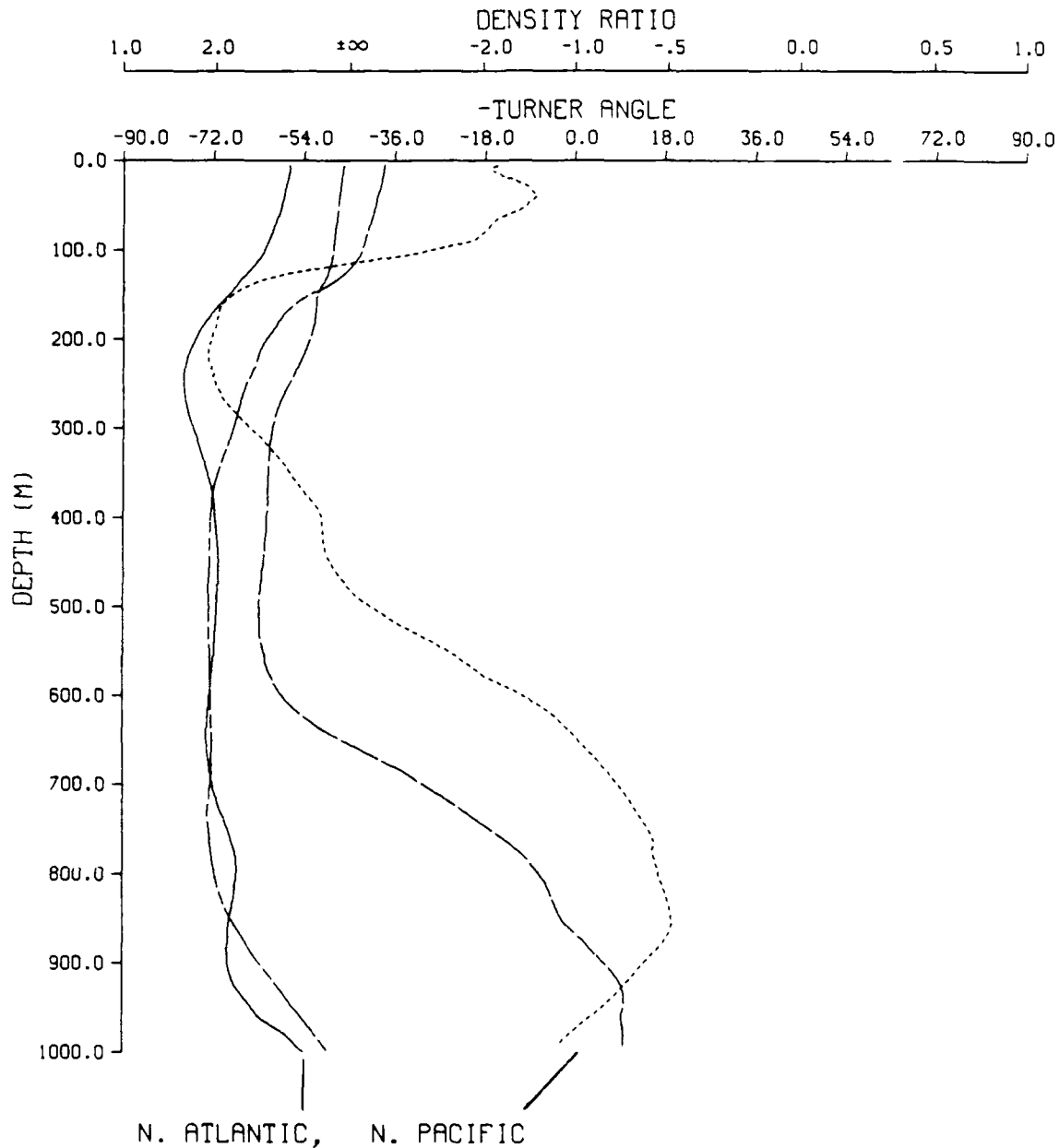


Figure 1. Density ratio ( $R_\rho$ ) computed over 100 m vertical intervals for 4 CTD stations at  $24^\circ\text{N}$  in the eastern N. Atlantic ( $- = 30^\circ\text{W}$ ), western N. Atlantic ( $- - - = 70^\circ\text{W}$ ), eastern N. Pacific ( $- \cdot - = 140^\circ\text{W}$ ), and western N. Pacific ( $- - - = 150^\circ\text{E}$ ). The scale for  $R_\rho$  (top) is linear in  $\arctan(R_\rho)$ ; the equivalent scale in the negative Turner Angle is also given. Salt fingers are possible for  $1 \leq R_\rho \leq 100$ , the left quadrant of the scale. The central half of the scale represents a diffusively stable stratification with  $-\infty < R_\rho < 0$ . The "diffusive" instability (cold, fresh over warm, salty) is possible for  $0 < R_\rho \leq 1$ .  $R_\rho$  profiles show less variability in the salt finger regime (North Atlantic) than in diffusively stable thermoclines (below salt minimum in the North Pacific). A value of  $R_\rho$  near 2.0 is often found in finger-favorable thermoclines, possibly a consequence of increased salt fingering for  $R_\rho$  below 2.0 (Schmitt, 1981).

produced by internal wave strain. Presumably, unstable buoyancy fluxes do not become sufficiently large to maintain a thermohaline staircase in the constantly strained and sheared internal wave field. Schmitt and Evans (1978) estimated the salt flux by applying the laboratory 4/3 power law to the "interfaces", a procedure which must be viewed as suspect since measurements from C-SALT (Lueck, 1987; Gregg and Sanford, 1987; Schmitt, 1988) indicate that this will overestimate the flux. However, an alternative flux law, based on the "Stern number" (Stern, 1969) or interface thickness (Kunze, 1987) is consistent with the C-SALT fluxes. This would reduce the Schmitt and Evans estimates for the Central Waters modestly, but would make a more dramatic difference to flux estimates in thermohaline staircases (Schmitt, 1981). Even with this revision in flux estimates the staircases have a salt diffusivity ( $K_s$ ) of  $\sim 10^{-4} \text{ m}^2/\text{s}$ , and in the central waters  $K_s$  would still be  $\sim 10^{-5} \text{ m}^2/\text{s}$ . Since recent estimates of mixing rates in a diffusively stable regime (Gregg and Sanford, 1988) have a diffusivity of only  $\sim 10^{-6} \text{ m}^2/\text{s}$ , even these reduced finger fluxes may still be significant.

How then, do we go about developing a more sophisticated understanding of Central Water salt fingers? In this paper we examine two aspects of the problem. 1) the effect of finescale shears on the local density ratio and 2) an apparent finescale predictor of microscale dissipation in fingering-favorable regions. Both aspects result from the examination of fine- and microstructure data acquired with a recently developed instrument, the High Resolution Profiler (HRP, Schmitt *et al.*, 1988). Section 2 treats the shear effect, which is more fully developed elsewhere (Schmitt, Polzin and Toole, in preparation). Section 3 examines the relationship between the finescale salt finger potential and the observed thermal dissipation. The apparent relationship is an important step toward the development of a parameterization of salt finger fluxes. In Section 4 we estimate the vertical diffusivity from the observed thermal dissipation rate. Results are summarized in section 5.

## 2. THE EFFECT OF SHEAR ON THE DENSITY RATIO

The Central Waters of the world's subtropical gyres are characterized by a remarkable constancy of the large scale density ratio  $R_\rho = \alpha\theta_z/\beta S_z$ ,

$$\text{where } \alpha = \frac{-1}{\rho} \frac{\partial \rho}{\partial \theta} \bigg|_{p,s}, \quad \beta = \frac{1}{\rho} \frac{\partial \rho}{\partial S} \bigg|_{p,\theta}$$

and  $\theta_z, S_z$  are the vertical gradients of temperature and salinity. Schmitt (1981) hypothesized that this feature was due to salt fingers. The finger properties of having a greater transport of salt than heat and a strong dependence of mixing rate on  $R_\rho$  are the key elements of the mechanism. A detailed confirmation of the model will require the development of a parameterization of the effects of fingers on larger scales. However, the model is consistent with microstructure studies, and no other mechanism has been proposed to account for the dramatic difference in  $R_\rho$  profiles between salt fingering water masses and diffusively stable regimes (Figure 1). The fingering-favorable regions tend to have nearly constant  $R_\rho$ , often near a value of 2.0, while diffusively stable regions tend to have arbitrary values of  $R_\rho$ .

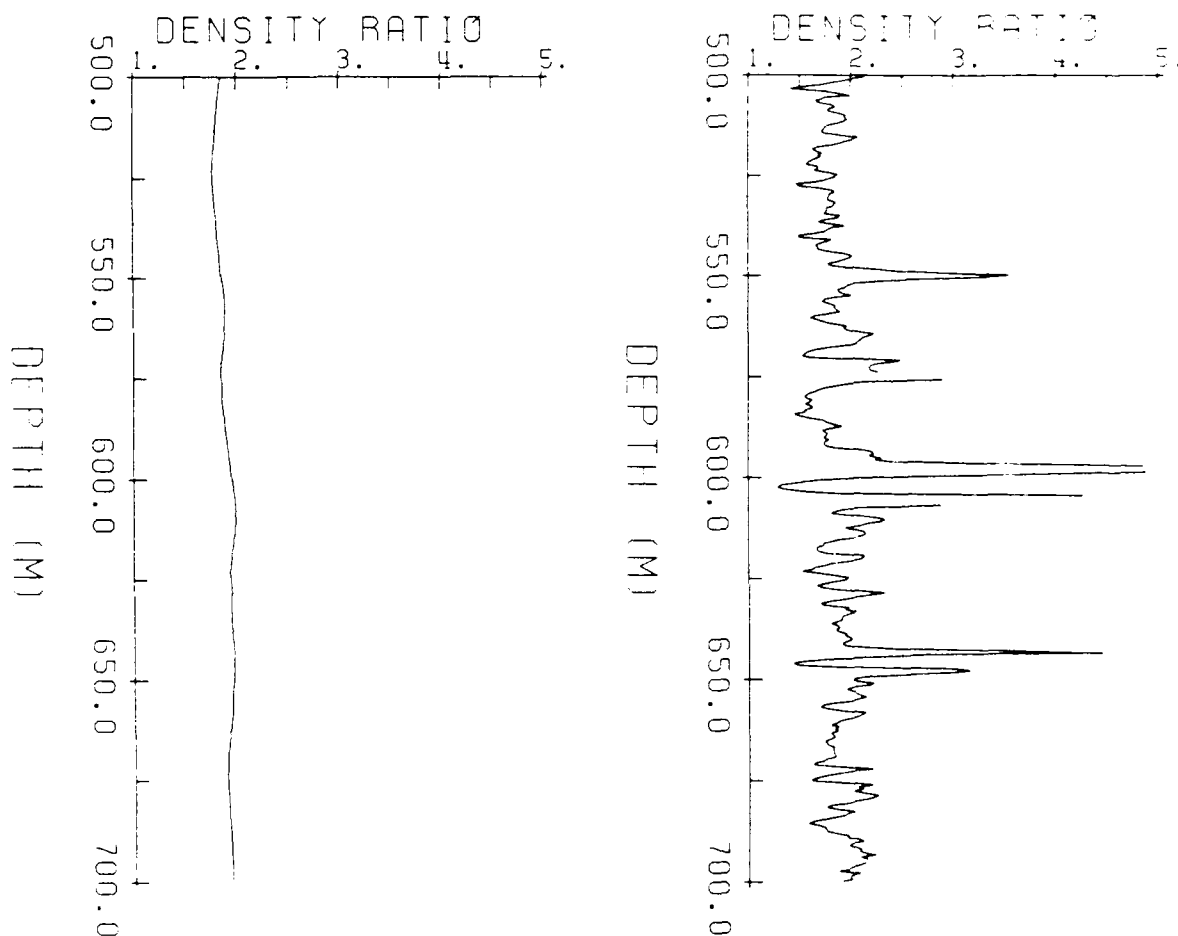


Figure 2.a. Profile of  $R_\rho$  computed using least square fits over a sliding vertical interval of 50db. Data are from HRP Dive 28, at  $28^\circ 41'N$ ,  $68^\circ 30'W$  in the Sargasso Sea.

Figure 2.b. Profile of  $R_\rho$  computed using least square fits over an interval of 3db. Great variability in  $R_\rho$  is seen at small scales which should modulate the intensity of salt fingers.

While the density ratio over 50 m scales and greater is rather constant in the Central Waters, one can find sizable variations in  $R_\rho$  when the scale of the computation is reduced (Figure 2). Given that  $R_\rho$  is the ratio of two gradients, it is hardly surprising that variance increases with a decreasing computation scale, especially given the potential problems with sensor lag corrections and variable fall rate for a wire lowered CTD. However, free fall profilers have a steady fall rate and there are processing techniques for accurately matching the data from temperature and conductivity sensors (Horne and Toole, 1980). We have used such a profiler in the Sargasso Sea during the Frontal Air-Sea Interaction Experiment (FASINEX). The instrument, the High Resolution Profiler (HRP) is described by Schmitt *et al.* (1988). The HRP carries a CTD, acoustic velocimeters to measure the vertical shear of horizontal currents, accelerometers to monitor body motion, and microscale temperature, conductivity and velocity sensors. This suite of sensors provides the ability to compare microstructure levels with finescale Richardson numbers, density ratios, etc. With its steady fall rate and internal recording, we believe that the finescale salinity profiles obtained with the HRP approach the limits of resolution possible with standard 16 bit oceanographic sensors. The raw finescale data is recorded at 10 Hz; temperature, salinity and horizontal velocity are derived from the raw data and pressure sorted into 1/2 db intervals (about 10 raw data points per 1/2 db). In the remaining analysis we use a vertical interval of 3 db to compute gradients and averages from the pressure sorted data.

The variability in  $R_\rho$  seen in Figure 2 is most likely real and not due to noise in the measurement. What, then, is its origin? If the Schmitt (1981) mechanism is operative then such fluctuations should decay with time, and should not be remnants of mixing processes that occurred at the boundary of the water mass. The most likely source of finescale variability in  $R_\rho$  is the finescale vertical shear due to inertial-internal waves acting on horizontal gradients in water mass properties. That is, shear can readily change  $R_\rho$  by advecting warmer, saltier (or colder, fresher) water over a given parcel of water, if there are gradients in temperature and salinity on density surfaces. A detailed treatment of this effect is given in Schmitt, Polzin and Toole (in preparation). Using the "neutral surface" formalism of McDougall (1987) it is possible to derive the following expression for the rate of change of  $R_\rho$ .

$$\frac{\partial R_\rho}{\partial t} + \mathbf{V}^n \cdot \nabla_n R_\rho + \mathbf{e} \frac{\partial R_\rho}{\partial z} = \frac{(R_\rho - 1)}{S_z} \mathbf{V}_z^n \cdot \nabla_n S + \text{diffusive terms}, \quad (1)$$

where  $\mathbf{V}^n$  is the neutral surface (isopycnal) velocity,  $\mathbf{V}_z^n$  is its vertical shear, and  $\mathbf{e}$  is the diapycnal velocity. Some of the diffusive terms are treated in Schmitt (1981) and will not be the focus of the present discussion. The term of interest is the shear term on the right hand side of the equation. It neatly expresses the potential for vertical shear acting on isopycnal gradients of salinity for changing the density ratio.

As seen in Figure 1, large scale vertical and horizontal gradients of  $R_\rho$  are weak in the North Atlantic Central Water, so the advective terms should be small. If we disregard mixing, then there is no diapycnal velocity. Thus, we can examine the (reversible) effects of inertial-internal

waves on  $R_\rho$  with the simpler equation:

$$\frac{\partial R_\rho}{\partial t} = \frac{(R_\rho - 1)}{S_z} \mathbf{V}_z \cdot \nabla S \quad (2)$$

where we have dropped the neutral surface notation, though it still applies.

$R_\rho$  has the inconvenient range of  $\pm \infty$  making the calculation of variances, etc., unduly influenced by large  $R_\rho$  values. Alternative transformations of equation 2 are possible. One is to rearrange (2) as:

$$\frac{\partial \ln (R_\rho - 1)}{\partial t} = \frac{\mathbf{V}_z}{S_z} \cdot \nabla S \quad (3)$$

for  $R_\rho > 1$ , and

$$\frac{\partial \ln(1 - R_\rho)}{\partial t} = \frac{\mathbf{V}_z}{S_z} \cdot \nabla S$$

for  $R_\rho < 1$ . Another option is to use the Turner Angle of Ruddick (1983) defined by the two-component arctangent:

$$Tu = \arctan \left( \alpha \frac{\partial \theta}{\partial z} - \beta \frac{\partial S}{\partial z}, \alpha \frac{\partial \theta}{\partial z} + \beta \frac{\partial S}{\partial z} \right).$$

So that  $R_\rho = -\tan(Tu + 45^\circ)$ . Equation 2 can be expressed as:

$$\frac{\partial Tu}{\partial t} = \frac{(R_\rho - 1)}{2R_\rho^2 S_z} \mathbf{V}_z \cdot \nabla S \quad (4)$$

Since equation 3 is simpler, we will use the natural logarithm of the absolute value of  $R_\rho - 1$  as our variable, i.e.,  $\ln |R_\rho - 1|$ .

Our hypothesis is that near-inertial frequencies are the primary source of finescale vertical shear. If we separate the salinity and velocity fields into mean  $(-)$  and fluctuating components  $(')$  we obtain the following expression for fluctuations in  $\ln |R_\rho - 1|$ :

$$\begin{aligned} \frac{\partial (\ln |R_\rho - 1|)}{\partial t} &= \frac{1}{S_z} (\bar{\mathbf{V}}_z \cdot \nabla S' + \mathbf{V}'_z \cdot \bar{\nabla S} + \mathbf{V}'_z \cdot \nabla S') \\ &\quad - \frac{S'_z}{\bar{S}_z^2} (\bar{\mathbf{V}}_z \cdot \bar{\nabla S} + \mathbf{V}'_z \cdot \bar{\nabla S} + \bar{\mathbf{V}}_z \cdot \nabla S' + \mathbf{V}'_z \cdot \nabla S') \end{aligned} \quad (5)$$

We expect the mean vertical shear to be small on the finescale wavelengths of interest here ( $\sim 10$  m) and assume  $\bar{\mathbf{V}}_z = 0$ . For this analysis we will also neglect terms of higher order in

the fluctuating quantities since there appears to be no reason to expect correlation between them. Thus, the dominant effect should be due to the action of finescale shears on the mean horizontal salinity gradient:

$$\frac{\partial \ln |R_\rho - 1|'}{\partial t} \approx \frac{V_z'}{\bar{S}_z} \cdot \nabla \bar{S}. \quad (6)$$

If we assume that the shears have an inertial period so that the components are given by:

$$u_z = V_z^0(z) \sin(ft), \quad v_z = V_z^0(z) \cos(ft)$$

we can integrate (6) over one inertial period to obtain an expression for perturbations in  $\ln |R_\rho - 1|$ :

$$(\ln |R_\rho - 1|)' = \frac{1}{f \bar{S}_z} V_z^0(z) \left[ \cos(ft) \frac{\partial \bar{S}}{\partial x} - \sin(ft) \frac{\partial \bar{S}}{\partial y} \right]. \quad (7)$$

Squaring equation 7 and time averaging leads to an expression for the variance in  $\ln |R_\rho - 1|$ :

$$\overline{(\ln |R_\rho - 1|)^2} = \frac{1}{f^2 \bar{S}_z^2} \frac{\overline{(V_z^0(z))^2}}{2} \left( \frac{\partial \bar{S}^2}{\partial x} + \frac{\partial \bar{S}^2}{\partial y} \right). \quad (8)$$

This indicates that the vertical wavenumber spectra of vertical shear and  $\ln |R_\rho - 1|$  should have similar structure, and be related in magnitude by the factor  $\frac{\nabla \bar{S}^2}{2f^2 \bar{S}_z^2}$ .

We have examined the spectra of shear and  $\ln |R_\rho - 1|$  for dives of the High Resolution Profiler during FASINEX. These profiles were obtained in the Sargasso Sea near an upper ocean front. The region of interest for this analysis is well below the strong variability near the surface, in the depth range of near uniform  $R_\rho$  between 300 and 800 m. However, modest variations in salinity along isopycnals lead us to believe that the above mechanism should be operative.

The vertical wavenumber spectra of  $\ln |R_\rho - 1|$  and vertical shear are shown in Figure 3 a,b. Both have a similar shape, flat from low wavenumbers up to  $\sim 20$  m wavelength beyond which the spectral densities decrease. The shear spectra falls off more sharply than the usual  $K^{-1}$  (Gargett *et al.*, 1981) at wavelengths smaller than 10 db. This is due to the 3 db least square fit used to estimate the shear; a first difference operator is more commonly used.

How does the observed variance in  $\ln |R_\rho - 1|$  compare with that expected from equation 8? For the latitude of these dives ( $28^\circ N$ ) and a mean vertical salinity gradient of  $2.6 \times 10^{-3} / \text{km}$ , a horizontal (isopycnal) salinity gradient with a magnitude of  $0.03^\circ / \text{km}$  would appear to be necessary, given the spectral levels of  $\ln |R_\rho - 1|$  and shear for vertical wavelengths between 100 and 20 m. We can examine the variation of salinity vs. density for

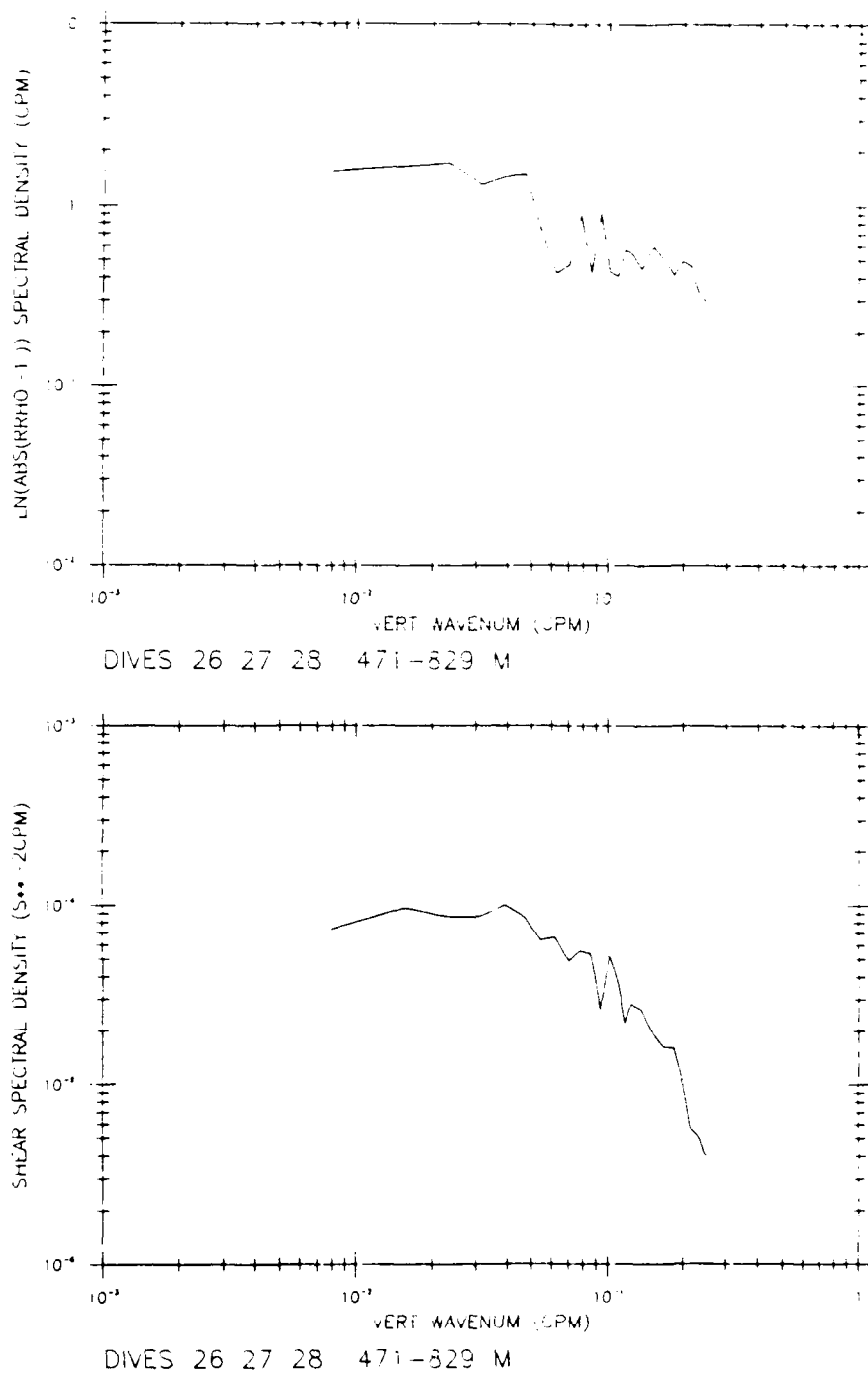


Figure 3.a. Vertical wavenumber spectrum of  $\ln |R_p - 1|$  for the pressure range 471-829 db for three HRP dives.  $R_p$  was computed from least square straight line fits over 3 db.

Figure 3.b Vertical wavenumber spectrum of vertical shear (both components) computed by least squares regression over 3 db, for the same intervals as Figure 3.a.



the three dives used in the spectral estimates (Figure 4). Variations of about  $0.05^\circ/\text{‰}$  are seen on potential density surfaces. These dives are separated by as much as 30 km, suggesting that the observed salinity gradients may be a factor of 20 too low. However, other dives in the area, which are more closely spaced, show that  $0.01^\circ/\text{‰}$  variations over 1 km or less are quite common. Thus, the salinity gradients on density surfaces are not smooth, but rather streaky. This fluctuation in intensity could easily be caused by the horizontal stirring of mesoscale eddies. Even if the maximal gradient is of order  $0.01^\circ/\text{‰}/\text{km}$  it still suggests that the inertial wave shears are inadequate to explain more than about  $1/3 - 1/2$  of the variance in  $R_\rho$ . A lack of coherence between  $V'_z$  and  $\ln |R_\rho - 1|$  is also found; this could be due to streakiness in the salinity field, varying salt gradient direction with depth, and the bandwidth of inertial-internal waves which contribute to the vertical shear. Spectra from other dives with weaker horizontal salinity gradients have reduced variance in  $\ln |R_\rho - 1|$  but only by a factor of 2 or so. This suggests that the other terms in equation 5 beside the  $V'_z \cdot \nabla S$  term, as well as the advective terms in equation 1, must also be contributing to the finestructure in  $R_\rho$ . These results are reminiscent of the Georgi (1978) estimate that internal wave displacements were inadequate to explain thermohaline intrusions. However, it is unclear whether these modest  $R_\rho$  fluctuations could be caused by the double-diffusive intrusion mechanism of Stern (1967) and Toole and Georgi (1981).

### 3. THE MODULATION OF MICROSTRUCTURE BY $R_\rho$ .

Having identified some plausible mechanisms for generating finestructure in the density ratio, we can ask whether such fluctuations lead to variations in the intensity of microstructure, since theory (Schmitt, 1979a) and experiment (Schmitt, 1979b) indicate that salt fingers are strongly dependent on  $R_\rho$ . There is ample precedent for expecting that it will; Schmitt and Georgi (1982) found a correlation of optical microstructure with  $R_\rho$ , and Mack (1985) found an increase in the occurrence of temperature gradient zero crossings when  $R_\rho$  approached one. We first examine some profiles in detail before looking at the parametric dependence of microstructure indicators.

Using a 3db vertical window for averaging and gradient calculations we have plotted vertical profiles of buoyancy frequency ( $N$ ), density ratio ( $R_\rho$ ), Richardson number ( $Ri$ ), thermal dissipation rate ( $\chi$ ) and theoretical salt finger growth rate (Figure 5). The data are from the interval 800-900 db in Dive 28.  $N$ ,  $R_\rho$  and  $Ri$  are computed from the finescale CTD and velocity data from the HRP. The finger growth rate is computed from the formula given by Schmitt (1979a) for the fastest growing finger; an approximate form is

$$\lambda = (\kappa/\nu)^{1/2} N [(1 - 1/R_\rho)^{-1/2} - 1] \quad (9)$$

(Schmitt and Evans, 1978; Stern, 1975). Thus, the growth rate increases when  $N$  is high and when  $R_\rho$  approaches 1. Schmitt and Evans (1978) argued that internal wave strain caused variations in  $N$  (in a constant  $R_\rho$  thermocline) which modulated the salt finger intensity. Given the finestructure in  $R_\rho$  (possibly caused by the previously described shear mechanism) and the non-linear dependence of growth rate on  $R_\rho$ , it seems in fact, that  $N$  variations are of

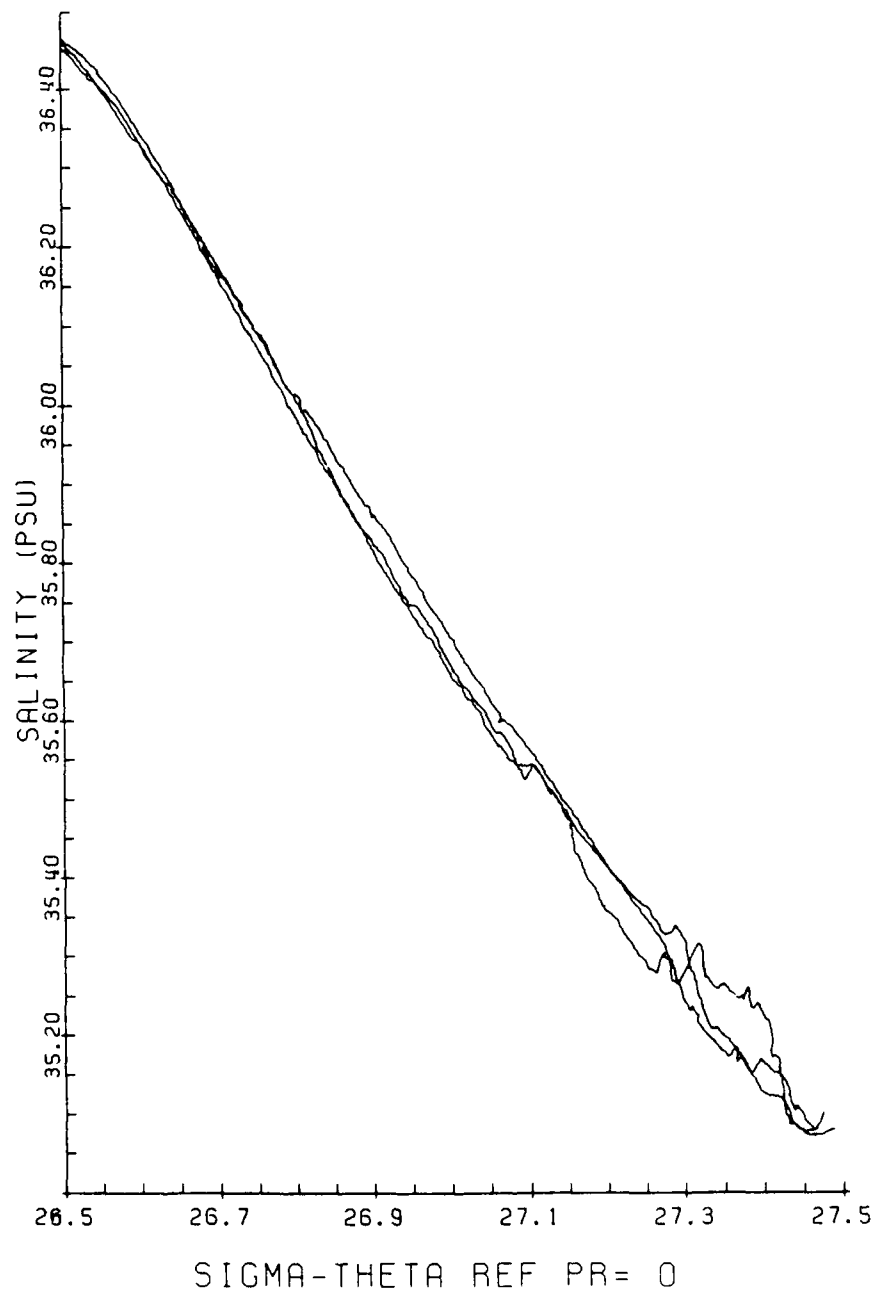


Figure 4. Salinity versus potential density for High Resolution Profiler dives 26, 27 and 28.

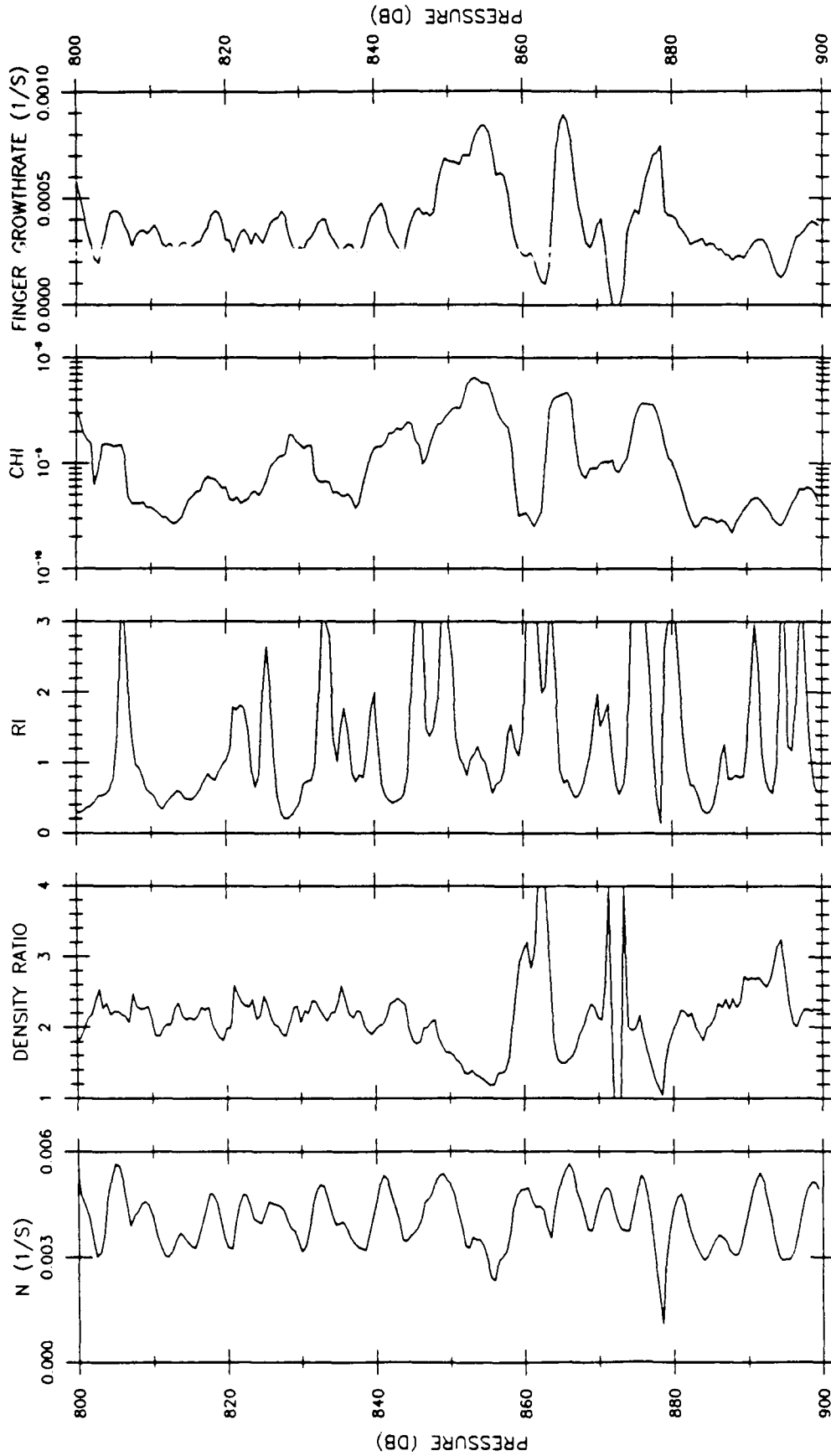


Figure 5: Vertical profiles of buoyancy frequency (N), density ratio ( $R_\rho$ ), Richardson number ( $Ri$ ), vertical component of thermal dissipation rate ( $\chi$ ,  $K^2/s$ ) and salt finger growth rate, for the interval 800-900 db in HRP dive 28. A 3 db window is used for gradient calculations and averaging.

secondary importance. Close examination of the profiles reveals incidences of both positive and negative correlation between  $N$  and  $\lambda$ .

The contribution of vertical gradients to the thermal dissipation rate ( $\chi_z$ ,  $K^2/s$ ) was computed from the conductivity microstructure probe by using a local regression against CTD temperatures. A similar profile is obtained with the temperature probe; the conductivity was used because it resolves more of the thermal variance spectrum. The profile of  $\chi_z$  can be compared with the other variables to identify probable sites of shear instability and salt fingering. For instance, at 828 db the Richardson number drops below  $1/4$  and there is a corresponding increase in  $\chi_z$ . Deeper in the water column, at 854, 866 and 878 db, we find sites with higher salt finger growth rate and  $\chi_z$  elevated by an order of magnitude. The deeper of these also has a low Richardson number, so the mechanism is ambiguous at that site. The others, though, have Richardson numbers in the range of 0.5 - 1.0, the usual range for the median value of  $Ri$  on these scales. Thus, in this 100 m segment of North Atlantic Central Water we find only a few meters which have  $Ri < 1/4$ , while nearly the whole segment is unstable to salt fingering. The sections of the profile with the strongest microstructure generally have large salt finger growth rates, so it appears that fingering may be the more important mixing mechanism.

To further explore the apparent relationship between dissipation rate and finger growth rate we have generated scatter plots of the two variables (Figures 6.a, 6.b). The first, Figure 6.a shows the relationship between 3 db averaged thermal dissipations (as computed from the fast response thermistor) and the salt finger growth rate, for all the data from Dive 28 which went to 1000 m depth. There is considerable scatter, especially at low salt finger growth rates, but a clear positive correlation is seen. Part of the scatter may be due to shear instability events which could occur at any finger growth rate. Accordingly we have selected a subset of the data which have a Richardson number greater than 1.5; this corresponds roughly to the upper quartile of Richardson number observations. A scatter plot of conductivity derived  $\chi_z$  estimates against salt finger growth rate for the high Richardson number data from Dives 25-30 is shown in Figure 6.b. The cluster of points suggests a linear relationship between the log of  $\chi_z$  and the finger growth rate. The evidence perhaps favors a minimum  $\chi_z$  level for a given growth rate; points are more likely to scatter above the main grouping than below it. This might be due to prior shear instability events or tilting of fingers by vertical shear, thus increasing the variance seen by a vertical profiler (Kunze, Williams and Schmitt, 1987).

Why should the log of  $\chi_z$  be proportional to the finger growth rate? A very simple model that allows this is one in which the time allowed for finger growth is fixed by processes external to the fingering, that is, by the internal wave strains and shears which modulate the intensity of the salinity gradient. In such a situation, the amplitude of the fingers will be proportional to  $\exp(\lambda\tau)$ , where  $\tau$  is the time allowed for growth. This is exactly the model used by Gargett and Schmitt (1982) to generate salt finger spectra from the Schmitt (1979a) theory for comparison with towed microstructure observations. The fluxes (and the dissipation) scale as  $\exp(2\lambda\tau)$ . If applied to the data of Figure 6.b we expect to see a relation between  $\chi_z$  and  $\lambda$  such that

$$\chi_z = \chi_0 \exp(2\lambda\tau). \quad (10)$$

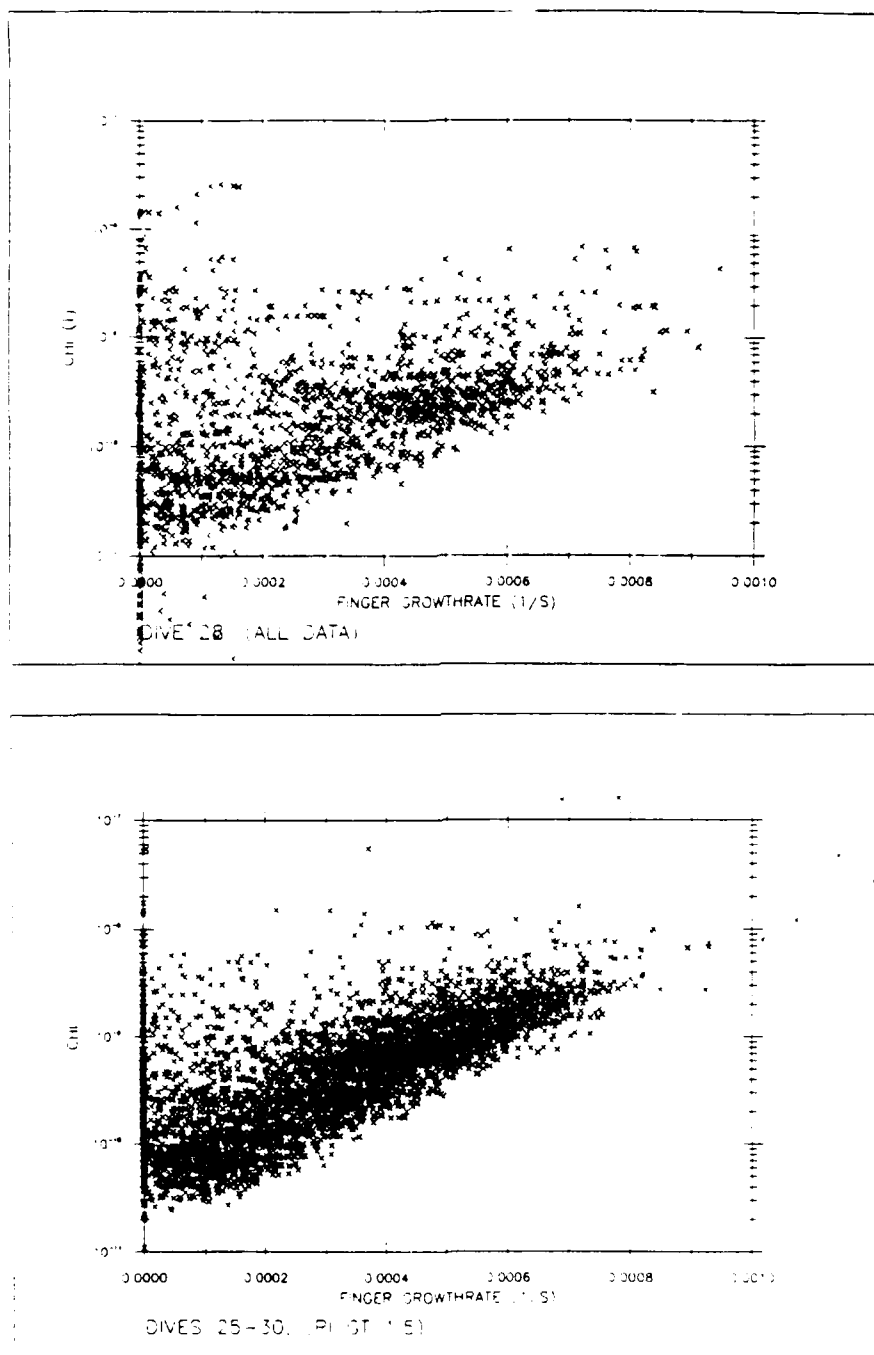


Figure 6.a.  $\chi_z$  ( $K^2/s$ ) as derived from the fast response thermistor plotted against salt finger growth rate. A log scale is used for  $\chi_z$  and a linear scale for the growth rate. All data from overlapping 3 db intervals from HRP dive 28 are shown.

Figure 6.b.  $\chi_z$  ( $K^2/s$ ) as derived from the micro-conductivity probe plotted against salt finger growth rate. Only those 3 db intervals with a Richardson number greater than 1.5 in dives 25-30 are shown.

Values for  $\chi_0$  of  $3 \times 10^{-11}$  K<sup>2</sup>/s and for  $\tau$  of  $\sim 1$  hour give a reasonable fit to the main trend in the data. Since the mean buoyancy period is about 1/2 hour in the main thermocline, it appears that these data are consistent with the spectral level reported by Gargett and Schmitt (1982), where a few buoyancy periods of growth were required to match theoretical and observed spectra.

The foregoing simplistic model for the salt finger intensity can surely be improved upon. An approach we are taking with the FASINEX HRP data is to search for a general dependence of  $\chi$  upon  $N$ ,  $R_\rho$  and other variables for comparison with salt finger models such as that of Kunze (1987). It seems likely that a purely kinematic explanation for the correlation seen in Figure 6 can be ruled out, as  $\chi_z$  is poorly correlated with  $N$ , yet well correlated with  $R_\rho$ . The complex issues of appropriate averaging intervals and conditional sampling of the data set carry this task beyond the scope of the present paper and we reserve these discussions for future publications.

#### 4. IMPLICATIONS FOR MIXING IN THE CENTRAL WATER

The thermal dissipations derived from the HRP data can be used to estimate the vertical eddy diffusivities. The Osborn and Cox (1972) model can be used for the thermal diffusivity, however, there are two caveats for its application to salt fingering portions of the water column. The first problem is uncertainty in the orientation of the fingers; if the fingers are perfectly vertical then a vertically traversing probe could underestimate the dissipation by an order of magnitude. However, the shears that are present in the thermocline should tilt the fingers (Kunze, Williams and Schmitt, 1987), so that the normal assumption of isotropy may be reasonable. The second problem arises if the fingers are not in a steady state, but growing, as the foregoing analysis implies. Gargett and Schmitt (1982) estimate that the flux could be underestimated by as much as 56% because of the unsteady terms in the growing finger model. Since both of these uncertainties would increase the vertical diffusivity, the following estimates should be considered lower bounds.

The vertical contribution to  $\chi$  can be related to the vertical diffusivity for heat by the relation:

$$K_\theta = \frac{3\chi_z}{2(\bar{\theta}_z)^2}, \quad (11)$$

where the factor of 3 assumes isotropy and the factor of 1/2 is required from the definition of  $\chi$ . The diffusivity for salt (and nutrients) is obtained from the definitions of the salt finger flux ratio,

$$\gamma = \frac{\alpha F_\theta}{\beta F_s}$$

and the density ratio,  $R_\rho = \alpha\theta_z/\beta S_z$ . The effective diffusivities for heat and salt are obtained by dividing the fluxes by the mean gradients, thus the ratio of salt to heat diffusivities is:

$$\frac{K_s}{K_\theta} = \frac{R_\rho}{\gamma} \quad (12)$$

In salt finger theory and experiments,  $\gamma = 0.5 - 0.7$  at low density ratios. Thus, we expect the salt diffusivity to be 3-4 times as large as the heat diffusivity for  $R_\rho$  near 2.

For the present data set,  $\overline{\chi_z} \approx 2 \times 10^{-9} \text{ K}^2/\text{s}$  in the low  $\overline{R}_\rho$  portion of the main thermocline. The mean vertical temperature gradient is about  $2 \times 10^{-2} \text{ K/m}$ . Equation (11) yields a thermal diffusivity estimate of  $K_\theta \approx 7.5 \times 10^{-6} \text{ m}^2/\text{s}$ ; the corresponding salt diffusivity is  $K_s \approx 2.25 - 3 \times 10^{-5} \text{ m}^2/\text{s}$ . The actual diffusivity could be higher if the isotropy factor is greater or if time dependent effects are important. Given that the estimate of vertical diffusivity in a diffusively stable thermocline is only  $3 \times 10^{-6} \text{ m}^2/\text{s}$  (Gregg and Sanford, 1988), it appears that salt fingers could easily be the dominant mixing mechanism in the North Atlantic Central Water. Note that the salt diffusivity estimate of Schmitt and Evans (1978) was also  $\sim 10^{-5} \text{ m}^2/\text{s}$  for this water mass, despite an uncertain estimation technique.

## 5. SUMMARY

We have examined two aspects of salt finger mixing in the Central Waters: the effects of finescale shear on the density ratio in the presence of horizontal salinity gradients, and the relationship between thermal dissipation and salt finger growth rate. We have also estimated the effective vertical diffusivity due to salt fingers, finding it to be notably higher than estimates in non-double-diffusive regions. These investigations were made possible by the small scales resolvable by the High Resolution Profiler. It appears that a parameterization of salt fingering based on finescale CTD data may be possible. However, to be effective, a vertical resolution of 0.1 m should be retained in processed CTD data.

Identification of the shear mechanism as a source of finestructure in  $R_\rho$ , and therefore the salt finger intensity, raises some interesting questions about the relationship between vertical mixing and isopycnal stirring. The mechanism is an example of shear dispersion in which vertical gradients are intensified by the action of shear on horizontal gradients (Young, Rhines and Garrett, 1982). In this case we can see that the vertical mixing achieved will depend on the value of  $R_\rho$ , with more mixing when  $R_\rho$  is driven toward 1, less mixing when  $R_\rho$  is increased. One can imagine that this would lead to a rectification of the shear dispersion, in which more horizontal mixing is achieved during the low  $R_\rho$  portion of an oscillatory excursion than during the high  $R_\rho$  portion. Also, a thermohaline intrusion, in which a salinity compensated temperature inversion is found, can be viewed merely as a case of  $R_\rho$  being driven through unity. Intrusions are relatively rare in the Central Water and it seems likely that the increased salt fingering found when  $R_\rho \rightarrow 1$  is a significant factor in limiting their occurrence.

The shear mechanism is also important for maintaining relatively low  $\overline{R}_\rho$  in the CW on large scales. That is, aside from air-sea interaction effects (Schmitt and Olson, 1985; Gordon, 1981) and particular vertical variations in the intensity of horizontal mixing, the action of the mean vertical shear on the mean isopycnal salinity gradient is the only mechanism for decreasing  $R_\rho$ . This is required to balance the tendency for salt fingers to increase  $R_\rho$ . It appears that estimates of the shear term from mean hydrographic survey data may be used to place an

upper bound on the eddy diffusivity for salt in a suitably "constant  $R_\rho$ " portion of the Central Water (Schmitt, in preparation).

The Central Waters of the World Ocean, in which the large scale density ratio is rather constant, may represent a situation in which the small scale physics controls the thermohaline stratification for a vast portion of the main thermocline. Much remains to be done to understand the mechanism; however, there seems to be sufficient evidence to suggest that it has global significance. One can argue that Central Water salt fingers play a role in regulation of climate, since modification of evaporation and precipitation patterns is a likely consequence of global warming. This affects the surface buoyancy flux (Schmitt, Bogden and Dorman, 1989) and could change the rate of salt finger mixing in the thermocline. The modified heat and salt transports themselves may have feed-back effects as would any change in biological productivity due to increased nutrient transport rates (Hamilton, Lewis and Ruddick, 1989).

Thus, there is ample motivation for further study of salt fingering in the Central Water. There is an obvious need for improved theoretical, numerical and laboratory modeling of the process, especially with regard to the effects of internal waves. The problem also provides a clear focus for a coordinated field program. Large scale surveys, direct microstructure measurements, and novel tracer release techniques (J. Ledwell, this volume) would be valuable components of such a program.

#### ACKNOWLEDGMENTS:

The authors thank V. Green for word processing and E. Ralph for programming assistance. This work was supported by the Office of Naval Research, contract N00014-82-C-0019, NR083-004. This is FASINEX contribution number 73.

#### REFERENCES

- Gargett, A. E., and R. W. Schmitt: 1982. Observations of salt fingers in the central waters of the eastern North Pacific. *Journal of Geophysical Research*, **87**(C10), 8017-8029.
- Gargett, A. E., P. J. Hendricks, T. B. Sanford, T. R. Osborn, and A. J. Williams III: 1981. A composite spectrum of vertical shear in the upper ocean, *Journal of Physical Oceanography*, **11**, 1258-1271.
- Georgi, D. T.: 1978. Finestructure in the Antarctic Polar Front Zone: Its characteristics and possible relationship to internal waves. *Journal of Geophysical Research*, **83**, 4579-4588.
- Gordon, A. L.: 1981. South Atlantic thermocline ventilation. *Deep-Sea Research*, **28**, 1236-1264.
- Gregg, M. C. and T. B. Sanford: 1987. Shear and turbulence in thermohaline staircases. *Deep-Sea Research*, **34**, (10), 1689-1696.
- Gregg, M. C. and T. Sanford: 1988. The dependence of turbulent dissipation on stratification in a diffusively stable thermocline. *Journal of Geophysical Research*, **93**, (C10), 12381-12392.



- Hamilton, J. M., M. R. Lewis and B. R. Ruddick: 1989. Vertical fluxes of nitrate associated with salt fingers in the world's oceans. *Journal of Geophysical Research*, **94**, (C2), 2137-2145.
- Horne, E. P. W. and J. M. Toole: 1980. Sensor response mismatches and lag correction techniques for temperature salinity profilers. *Journal of Physical Oceanography*, **10**, (7), 1122-1130.
- Kunze, E.: 1987. Limits on growing, finite length salt fingers: a Richardson number constraint. *Journal of Marine Research*, **45**, 533-556.
- Kunze, E., A. J. Williams III, and R. W. Schmitt: 1987. Optical microstructure in the thermohaline staircase east of Barbados. *Deep-Sea Research*, **34**, 10, 1697-1704.
- Lueck, R.: 1987. Microstructure measurements in a thermohaline staircase. *Deep-Sea Research*, **34**, 10, 1677-1688.
- McDougall, T. J.: 1987. Neutral surfaces. *Journal of Physical Oceanography*, **17**, (11), 1950-1964.
- Mack, S. A.: 1985. Two-dimensional measurements of ocean microstructure: The role of double diffusion. *Journal of Physical Oceanography*, **15**, (11), 1581-1604.
- Osborn, T. R. and C. S. Cox: 1972. Oceanic fine structure, *Geophysical Fluid Dynamics*, **3**, 321-345.
- Ruddick, B.: 1983. A practical indicator of the stability of the water column to double-diffusive activity. *Deep-Sea Research*, **30**, 1105-1107.
- Schmitt, R. W.: 1979(a). The growth rate of super-critical salt fingers. *Deep-Sea Research*, **26A**, 23-40.
- Schmitt, R. W.: 1979(b). Flux measurements on salt fingers at an interface. *Journal of Marine Research*, **37**(3), 419-436.
- Schmitt, R. W.: 1981. Form of the temperature-salinity relationship in the Central Water: Evidence for double-diffusive mixing. *Journal of Physical Oceanography*, **11**, (7), 1015-1026.
- Schmitt, R. W.: 1988. Mixing in a thermohaline staircase. *Small-scale Turbulence and Mixing in the Ocean*, ed. J. Nihoul and B. Jamart, Elsevier, Netherlands, 435-452.
- Schmitt, R. W., P. S. Bogden and C. E. Dorman: 1989. Evaporation minus precipitation and density fluxes for the North Atlantic. *Journal of Physical Oceanography*, in press.
- Schmitt, R. W., and D. L. Evans: 1978. An estimate of the vertical mixing due to salt fingers based on observations in the North Atlantic Central Water. *Journal of Geophysical Research*, **83**, (C6), 2913-2919.
- Schmitt, R. W. and D. T. Georgi: 1982. Finestructure and microstructure in the North Atlantic Current. *Journal of Marine Research*, Supplement to **40**, 659-705.

- Schmitt, R. W., and D. B. Olson: 1985. Wintertime convection in warm core rings: thermocline ventilation and the formation of mesoscale lenses. *Journal of Geophysical Research*, **90**(C5), 8823-8837.
- Schmitt, R. W., J. M. Toole, L. Koehler, C. Mellinger, and K. W. Doherty: 1988. The development of a fine- and microstructure profiler. *Journal of Atmospheric and Oceanic Technology*, **5**, (4), 484-500.
- Stern, M. E.: 1967. Lateral mixing of water masses. *Deep-Sea Research*, **14**, 747-753.
- Stern, M. E.: 1969. The collective instability of salt fingers. *Journal of Fluid Mechanics*, **35**, 209-218.
- Stern M. E.: 1975. Ocean circulation physics. Academic Press, New York, p192-195.
- Toole, J. M. and D. T. Georgi: 1981. On the dynamics and effects of double-diffusively driven intrusions. *Progress in Oceanography*, **10**, 123-145.
- Young, W. R., P. B. Rhines, and C. J. R. Garrett: 1982. Shear-flow dispersion, internal waves and horizontal mixing in the ocean. *Journal of Physical Oceanography*, **12** (6), 515-527.

## MEASURING TURBULENT FLUXES IN THE OCEAN – THE QUEST FOR $K_\rho$

J. N. Moum

College of Oceanography, Oregon State University, Corvallis, Oregon 97331-5503

### Abstract

Simultaneous measurements of vertical velocity fluctuations,  $w'$ , and temperature fluctuations,  $T'$ , on scales of three-dimensional turbulence yield a direct measure of the turbulent heat flux,  $J_q$ . The scales contributing most significantly to  $J_q$  are 10s of centimeters or about 10 times larger than the scales contributing to the turbulent kinetic energy dissipation for the data examined. A limited sample indicates that, instantaneously,  $J_q$  is almost as frequently positive (countergradient) as negative (downgradient). In contrast, instantaneous estimates of  $J_q$  from microstructure measurements of  $\epsilon$  or  $\chi$  are always, by definition, downgradient.

### 1. Introduction

A primary goal of ocean microstructure measurements has been to estimate the vertical fluxes of mass, heat, momentum, etc., due to three-dimensional turbulence processes in the water column. Although *direct* measurements of the turbulent fluxes (or transports) have not previously been made, estimates based on the measurements of  $\chi$  (dissipation of temperature variance) and  $\epsilon$  (dissipation of turbulent kinetic energy) have been widely used. It has been almost twenty years since Osborn and Cox (1972) proposed estimating the turbulent diffusion coefficient for heat from temperature microstructure measurements of  $\chi$  and ten years since Osborn (1980) suggested a method by which velocity microstructure measurements of  $\epsilon$  could be used to estimate the turbulent diffusion coefficient for mass,  $K_\rho$ . These estimates have been compared to each other (Oakley, 1982; Moum, *et al.*, 1989) but not to *direct* measurements of the turbulent transport; the applicability of these methods remains untested.

Recent estimates of  $K_\rho$  from microstructure measurements in the main thermocline indicate that there is a considerable range of variability. These estimates vary by a factor of 20, from being insignificant for numerical models (Gregg and Sanford, 1988) to being definitely important (Moum and Osborn, 1986). What is the source of this discrepancy? The possibilities include:

- i) limited sampling - measurements in the deep ocean are considerably more difficult and time-consuming than upper ocean measurements. It is quite

possible that the temporal variability of turbulent mixing in the main thermocline has not been resolved.

ii) lack of understanding of the applicability of our estimates of  $K_\rho$ .

The purpose of this paper is to present preliminary results of an attempt to directly measure turbulent heat fluxes from simultaneous measurements of the vertical velocity fluctuation,  $w'$ , and temperature fluctuation,  $T'$ . The results are compared to estimates from measurements of  $\epsilon$  and the presentation is prefaced by a discussion of the methods of estimating  $K_\rho$  from  $\epsilon$  and  $\chi$ . These methods have been reviewed recently by Caldwell (1983) and Gregg (1987); it is important to note precisely how these relate to the turbulent heat flux,  $J_q \equiv \rho C_p \overline{w'T'}$ .

## 2. Estimating $K_\rho$ from $\chi$ : Osborn and Cox (1972)

The equation describing the evolution of temperature variance in a three dimensional stratified turbulence field is

$$\frac{\partial \overline{T'^2}}{\partial t} + U_i \frac{\partial \overline{T'^2}}{\partial x_i} + \frac{\overline{u'_i \partial T'^2}}{\partial x_i} + 2 \overline{u'_i T'} \frac{\partial T}{\partial x_i} = D \frac{\partial}{\partial x_i} \frac{\partial \overline{T'^2}}{\partial x_i} - \chi \quad (1)$$

where  $T'$  refers to the small scale fluctuations of temperature,  $D$  is the thermal diffusivity due to molecular processes,  $\chi = 2D(\overline{\partial T'/\partial x_i \cdot \partial T'/\partial x_i})$  and the overbar denotes an appropriate average. From profiler measurements, only the vertical component  $(\partial T'/\partial z)^2$  is obtained so that by necessity it is assumed that  $(\overline{\partial T'/\partial x_i \cdot \partial T'/\partial x_i}) = (1-3)(\overline{\partial T'/\partial z})^2$ , the coefficient  $(1-3)$  being a function of the degree of isotropy of the turbulence. The turbulent eddy coefficient for heat is defined by  $\overline{w'T'} \equiv -K_T \frac{\partial T}{\partial z}$ . Since the only measurable terms are  $\chi$  and the vertical temperature gradient, it is conveniently assumed that all of the other terms are unimportant and that the balance reduces simply to

$$\overline{w'T'} \frac{\partial T}{\partial z} = -\frac{\chi}{2}$$

so that

$$K_T = \frac{\chi/2}{(\partial T/\partial z)^2}.$$

The quantity  $(\overline{\partial T'/\partial z})^2/(\partial T/\partial z)^2$  is termed the Cox number,  $C_x$ , so that

$$K_T = (1-3)DC_x. \quad (2)$$

## 3. Estimating $K_\rho$ from $\epsilon$ : Osborn (1980)

The turbulent kinetic energy (TKE) equation is given by:

$$\begin{aligned} \frac{\partial}{\partial t} \overline{q^2} + U_j \frac{\partial}{\partial x_j} \overline{q^2} + \frac{\partial}{\partial x_j} \overline{u'_j q^2} + \frac{1}{\rho} \frac{\partial}{\partial x_i} \overline{(u'_i p')^2} &= -\overline{u'_i u'_j} \frac{\partial U_i}{\partial x_j} - \frac{g}{\rho} \overline{w' \rho'} - \epsilon \\ &= P + J_h - \epsilon \end{aligned} \quad (3)$$

where TKE is defined by  $q^2 \equiv \overline{u_i u_i}/2$ ,  $U$  represents mean or large scale velocities and  $u$  represents fluctuations. Terms on the LHS are neglected for practical purposes; they have not been measured. Some scaling arguments have been proposed to support this neglect. It is not clear, however, under what range of conditions the LHS may be considered unimportant. The RHS is a combination of mechanical production of TKE,  $P$ ; buoyancy flux suppression (or in some cases, production) of TKE,  $J_b$ ; and the rate of viscous dissipation of TKE,  $\epsilon$ . The flux Richardson number,  $R_f$ , is defined as the ratio of buoyancy flux to mechanical production:  $R_f \equiv J_b/P$ . The eddy diffusivity for mass,  $K_\rho$ , is defined as

$$K_\rho \equiv -\frac{\overline{w' \rho'}}{\partial \rho / \partial z}, \text{ yielding } J_b = -K_\rho N^2,$$

where  $N^2 = -g/\rho \cdot \partial \rho / \partial z$  is the local buoyancy frequency. A practical assumption has been that  $R_f$  has some constant value. Osborn (1980) intended only to define an upper bound for  $R_f$  based on laboratory measurements leading to an upper bound for  $K_\rho$ . However the estimate is not really useful without using *some* value for  $R_f$ .  $R_f$  has not been measured directly in the ocean, of course, since measurements of  $\overline{w' \rho'}$  and  $\overline{u_i' u_j'}$  have not been made. An indirect estimate follows from a comparison of  $\chi$ - and  $\epsilon$ -estimates of  $K_\rho$ . With the above forms for  $R_f$  and  $K_\rho$ , the reduced form of the TKE equation,  $P + J_b = \epsilon$  yields

$$K_\rho = \gamma \frac{\epsilon}{N^2}; \quad \gamma = \frac{R_f}{1 - R_f}. \quad (4)$$

With an assumed upper bound for  $R_f$  of 0.17, the form for  $K_\rho$  becomes  $K_\rho < 0.2 \epsilon/N^2$ . If we further assume that the mixing of temperature and density are described by the same eddy diffusivities, *i.e.*,  $K_\rho = K_T$ , then we can equate the  $\chi$ -estimate (Eq.2) to the  $\epsilon$ -estimate (Eq.4) to get

$$\gamma = (1 - 3) \frac{DC_r N^2}{\epsilon} \quad (5)$$

Simultaneous measurements of  $\chi$  (or  $C_r$ ) and  $\epsilon$  have indicated that

$$\begin{aligned} 0.05 < \gamma < 0.47; \quad 0.05 < R_f < 0.32 \quad (\text{Oakey, 1982}) \\ 0.12 < \gamma < 0.48; \quad 0.11 < R_f < 0.32 \quad (\text{Moum, et al., 1989}). \end{aligned}$$

This large range of variation is troubling and it is difficult to determine what the source of the variability is, given the numerous assumptions made to arrive at our estimates. Undoubtedly, some of the problem lies in the natural intermittency of the turbulence. How much? Perhaps  $\gamma$  is simply not constant, in which case this form for estimating  $K_\rho$  is not a useful prescription. Recently, Oakey (1988) has suggested that  $\gamma$  may depend on the strength of double-diffusive processes.

#### 4. The Direct Approach - Measuring $\overline{w'T'}$

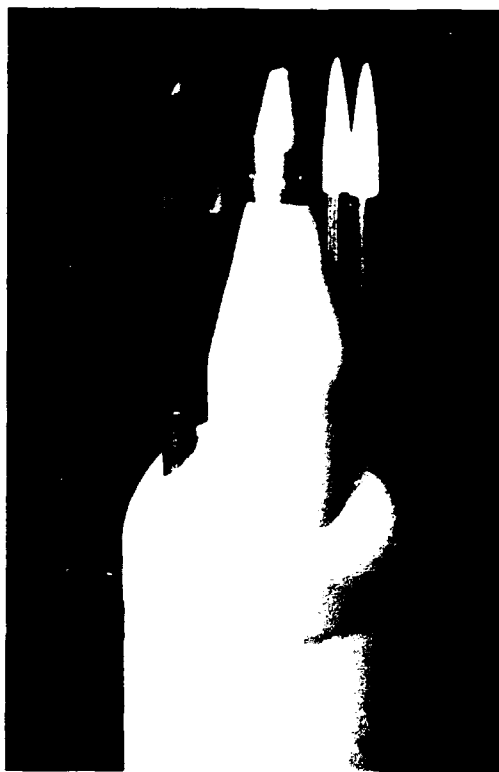


Figure 1. RSVP nosecone showing sensors - 2 airfoil shear probes (far right), a microbead thermistor (far left), a 4-electrode conductivity probe (2nd from left) and the pitot sensor (centre; the holes on the side of the aluminum nose are 2 of 4 static ports). The outer diameter of the nosecone is 5.7 cm and the shear probes protrude 7.6 cm.

##### *a) Method*

The majority of microstructure measurements have been obtained from freely falling profilers although reliable horizontal measurements have been made recently (*e.g.*, Osborn and Lueck, 1985a,b). Velocity microstructure measurements of horizontal velocity components  $u'$ ,  $v'$  are now made routinely using airfoil shear probes (Osborn and Crawford, 1980). However, the critical measurement required to determine the vertical transports due to turbulence is the vertical component,  $w'$ . Moun (1989) has recently demonstrated a technique for detecting  $w'$  in the inertial subrange of ocean turbulence. The measurement is of dynamic pressure using a highly sensitive differential piezoresistive pressure transducer. The sensor, essentially a pitot tube, is mounted on the nose of our profiler, the RSVP (Caldwell *et al.*, 1985), separated spatially from shear probes and fast response thermistor by approximately 1.5 cm (Figure 1). Spectral analysis of the signal indicates that, although hydrodynamic noise limits the range to frequencies less than 30 Hz in

its present incarnation, the sensor is able to resolve the inertial subrange. The equivalent spatial range of scales covered is 2 m to 2 cm, the upper limit due to the highpass filtering effect of the 1.2 m long vehicle itself as it responds (imperfectly) to vertical velocities in the water column.

The calibration procedure is described by Moum (1989) as is the comparison to simultaneous airfoil shear probe velocity microstructure measurements. Briefly, independent calibrations were applied separately to the outputs of both pitot sensor and shear probes. Power spectra were computed and scaled in the inertial subrange. The excellent agreement of the independently scaled spectra is taken to demonstrate the validity of the measurement.

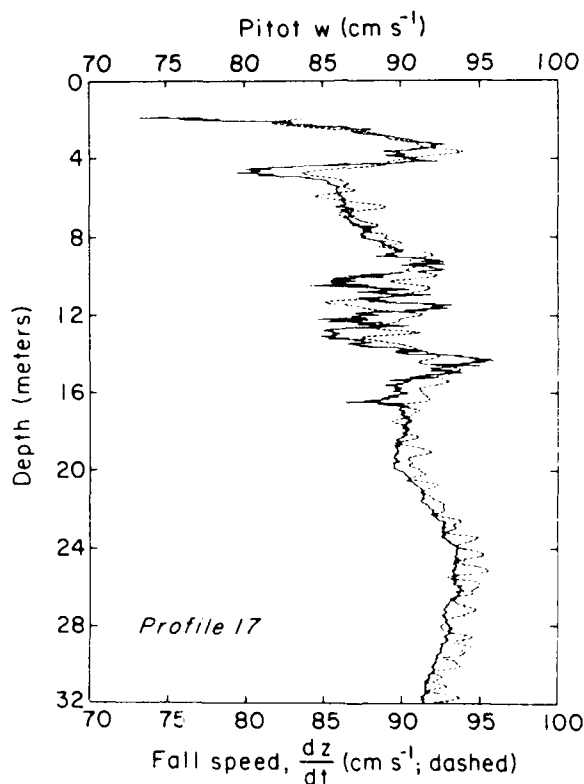


Figure 2. Vertical profile of vehicle fall rate (lowpass-filtered at 2 Hz; dashed line) computed by differencing the depth record obtained from a 500 psi FS pressure sensor and of vertical velocity from the pitot sensor (solid line).

### *b) Preliminary Results*

The measurements discussed here are from a group of twenty consecutive profiles made on 30 April 1987 at the equator and 110°W over a period of approximately two hours, right at sunrise. In the thermocline below the nearly mixed surface layer, a continually mixing turbulent patch of  $\sim 10$  m vertical scale was observed in almost every profile. This feature is qualitatively similar to the mixing events observed in

the thermocline at 140°W in 1984 (Moum *et al.*, 1989). At 140°W the mean depth of the core of the equatorial undercurrent (EUC) is about 120 m and the thermocline mixing events in November 1984 were observed over the depth range 35 to 85 m. In contrast, at 110°W in April 1987, the EUC core was observed to be located at about 50 m depth; thermocline mixing events were observed at depths of 10 to 30 m.

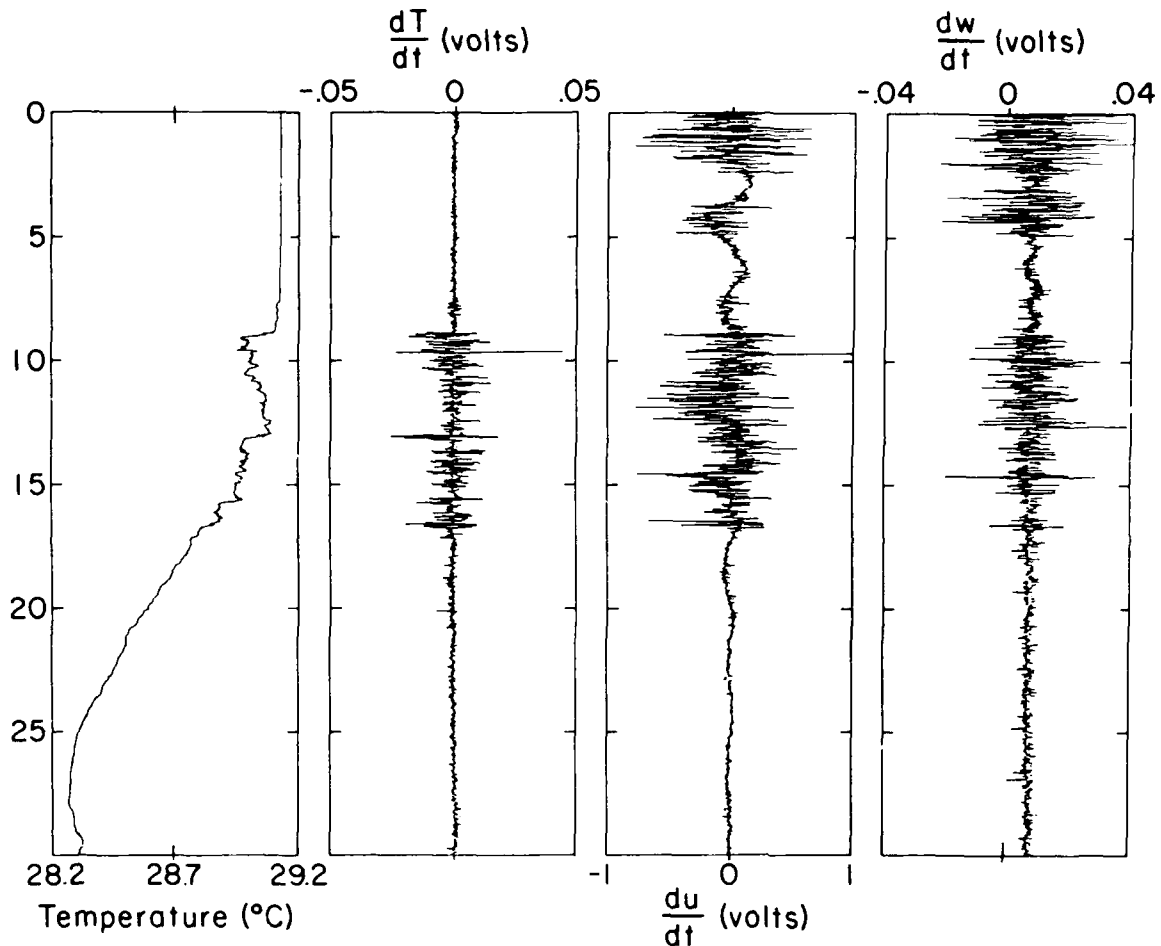


Figure 3 - Vertical profiles (profile 17) of temperature and uncalibrated, differentiated outputs from temperature ( $dT/dt$ ), horizontal velocity from the airfoil shear probes ( $du/dt$ ) and vertical velocity from the pitot sensor ( $dw/dt$ ).

The vehicle fall speed,  $dz/dt$ , was determined by differencing the pressure record. The dashed trace in Figure 2 represents the calibrated fall speed, lowpass filtered at 1/2 Hz. The solid trace is the calibrated velocity signal from the pitot sensor (the method of obtaining calibrated output in light of an inherent dc sensor drift is described by Moum, 1989; it is sufficient to note that we are not concerned here with scales greater than 2 m). The vehicle accelerates as it falls from the surface, reaching terminal fall speed of approximately  $0.9 \text{ m s}^{-1}$  by 10 m depth. Fluctuations about the mean vehicle fall speed are due to:



- a) wave orbital velocities in the surface wave zone;
- b) vehicle tilting at about 1 Hz;
- c) turbulent velocities in the patch observed between 8 and 16 m;
- d) velocities with larger scales (10s of meters) below 20 m.

At present, there is no good model of vehicle response to vertical velocity in the water column. There is undoubtedly a response to scales greater than about 2 m which acts as a highpass filter on the measured vertical velocity. Hence, only velocities on scales smaller than 2 m were considered for further analysis.

Vertical profiles of temperature, temperature derivative and the derivatives of the outputs from one shear probe and the pitot sensor are shown in Figure 3. The actively mixing patch between 8 and 16 m depth is characterized by the irregular temperature profile caused by vertical advection of fluid parcels by turbulent motion, and large values of gradients of temperature and velocity fluctuations (both horizontal and vertical). The pitot sensor obviously senses the turbulent motion in the patch, at least qualitatively. Scaling of the respective horizontal and vertical velocity spectra in the inertial subrange of the turbulence indicates good quantitative agreement as well (Moum, 1989).

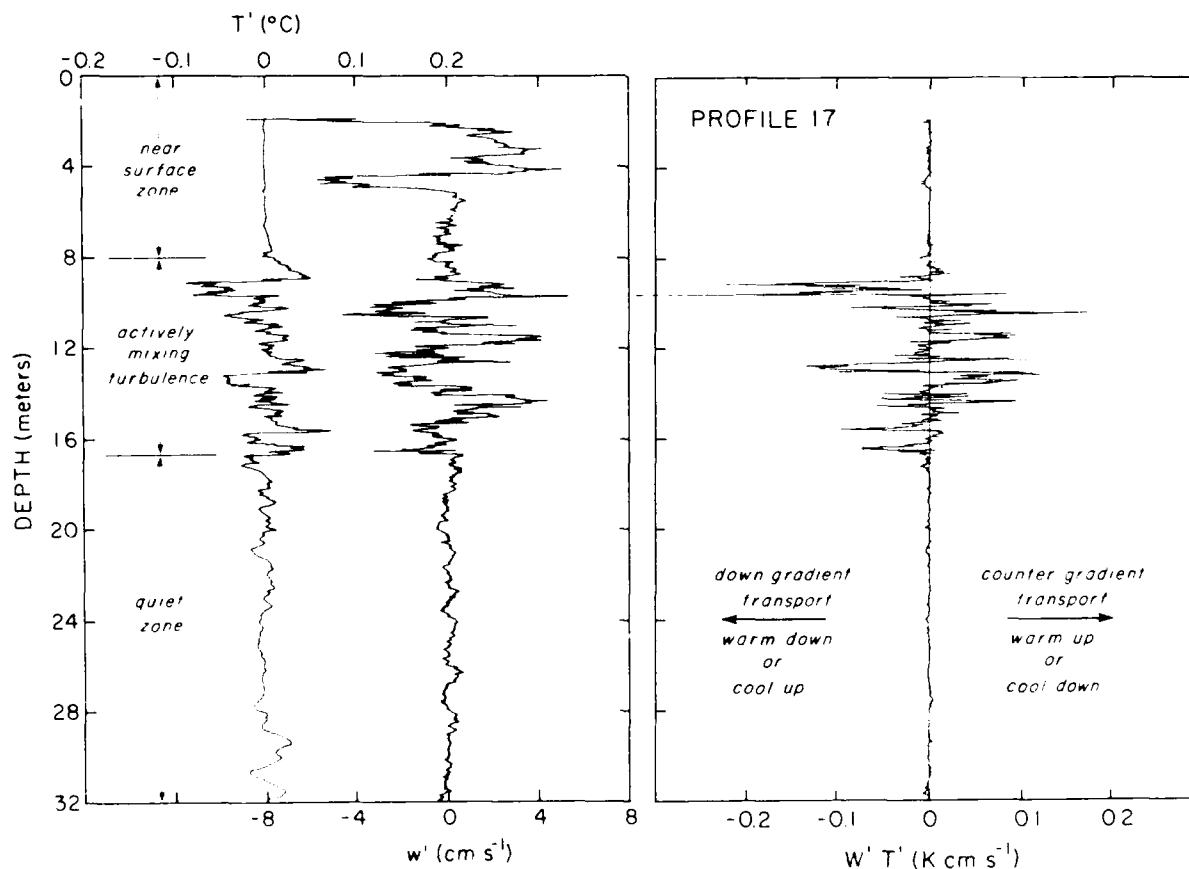


Figure 4. Highpass-filtered (1/2 Hz) temperature and vertical velocity records from profile 17 (left panel). The right panel shows the result of multiplying the two series.

Profiles of temperature and vertical velocity were highpass filtered at 1/2 Hz (or 1.8 m vertically at our nominal fall speed). The resulting vertical profile of  $w'$  and  $T'$  from profile 17 (Figure 4) indicates three distinct regions:

1. Surface to 8 m - well-mixed in temperature,  $\pm 6 \text{ cm s}^{-1}$  variations in  $w'$  due to the effects of vehicle instabilities during initial acceleration and possibly surface wave orbital velocities.
2. 8 to 16 m - within the actively mixing patch defined in Figure 3, variations in  $T'$  are  $\pm 0.05^\circ\text{C}$  over vertical scales of centimeters to 10s of centimeters. Similarly, variations in  $w'$  are  $\pm 4 \text{ cm s}^{-1}$  over vertical scales of centimeters to 10s of centimeters.
3. 16 to 32 m - variations in  $w'$  and  $T'$  are relatively small and occur over a much narrower range of vertical scales. The noise level in  $w'$ , approximately  $2\text{--}3 \text{ mm s}^{-1}$ , is the source of high frequency variability below 16 m.

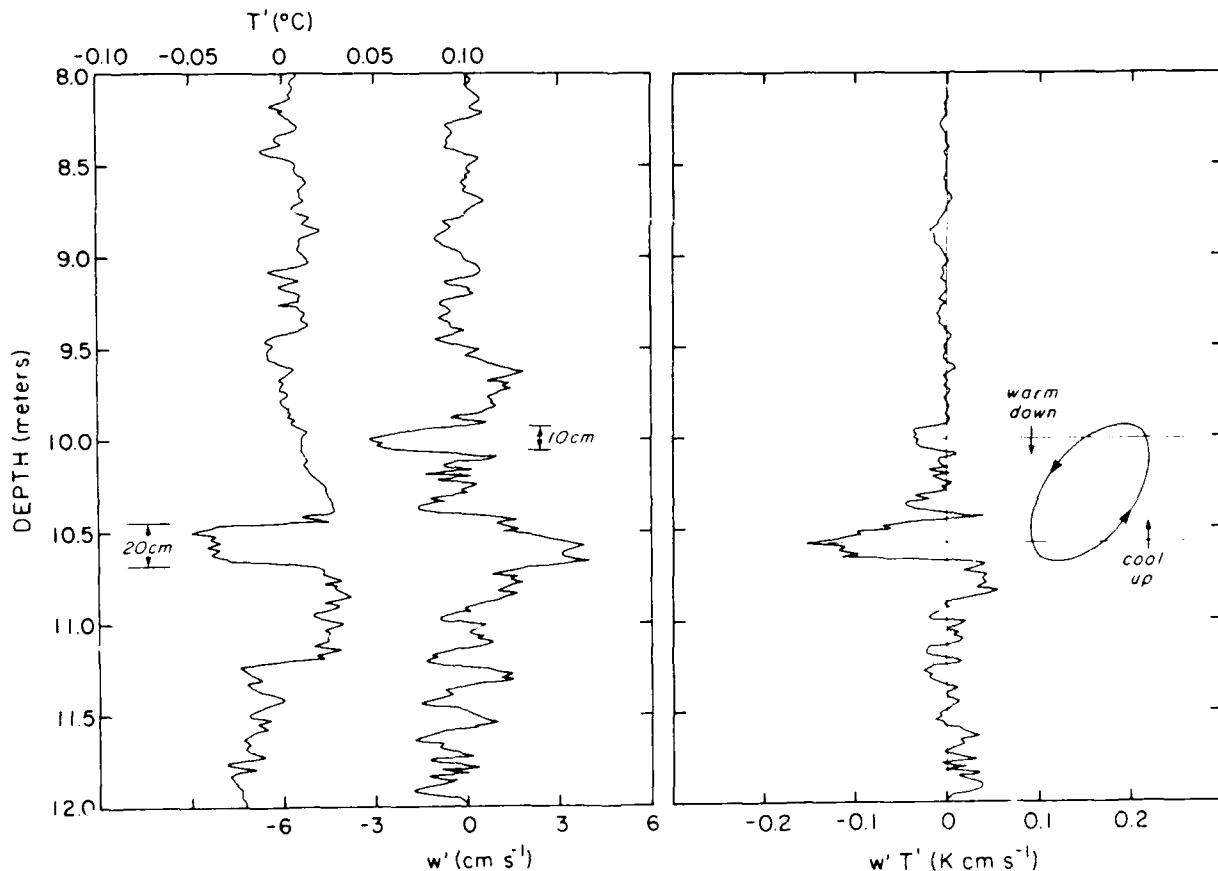


Figure 5. As in Figure 4 but for an expanded vertical section (8–12 m) from a different profile.

The instantaneous turbulent heat flux is defined by  $J_q \equiv \rho C_p w' T'$ . Considering only contributions due to scales of 2 m down to 2 cm, vertical profiles of  $w' T'$  were obtained by simply multiplying the 2 series,  $w'$  and  $T'$ . Our example profile 17 shows clearly the effect of the turbulent patch (Figure 4). Although variability in  $T'$  and  $w'$  occurs in all three regions discussed in Figure 4, only within the turbulent patch do they correlate to effect significant vertical heat transport.

Instantaneous values of  $w' T'$  are both negative and positive. Negative values are due to either vertical advection of warm water downwards or cool water upwards. In the case of a mean temperature profile which decreases with depth this results in down gradient transport. However, numerous instantaneous examples of countergradient transport (due to vertical advection of either warm water upwards or cool water downwards) are also present. The largest contributions to  $w' T'$  occur over vertical scales of 10s of centimeters.

Detailed examination of  $w' T'$  leads to some interesting small scale structure (Figure 5). This particular profile was made approximately 20 minutes after profile 17. The plot has been expanded to focus on the structure between 9.5 and 11 m. A 20 cm thick patch at 10.5 m is approximately 0.05°C cooler than ambient and being rapidly advected upwards at 3 cm s<sup>-1</sup>. A 10 cm thick patch at 10 m is slightly warmer than ambient and advected downwards at about 3 cm s<sup>-1</sup>. Each of these two parcels contribute to a downgradient (negative) heat transport (Figure 5). The structure suggests a coherent overturning eddy, as depicted in Figure 5.

## Discussion

The data considered for this first examination of the statistics of  $w' T'$  come from a particularly energetic mixing regime. The range of  $\epsilon$  was 10<sup>-7</sup> to 10<sup>-6</sup> m<sup>2</sup> s<sup>-3</sup> for the forty patches evaluated here and the mean value of  $\epsilon/\nu N^2$  was in excess of 70,000, which I believe suggests to all that the turbulence is isotropic. The corresponding Kolmogoroff wavelength,  $\eta = 2\pi(\nu^3/\epsilon)^{1/4}$  ranged from 1/2 to 1 cm (with kinematic viscosity,  $\nu = 10^{-6}$  m<sup>2</sup> s<sup>-1</sup>). The peak in the dissipation spectrum is associated with scales of  $\sim 5 - 10\eta$  (Townsend, 1976) or 2 to 10 cm. In comparison to the scales which appear to dominate the turbulent heat transport, the dissipation scales are significantly smaller. Apparently, the dissipation is dominated by structures having scales of centimeters whereas the turbulent transports are dominated by scales of many 10s of centimeters. If this can be consistently demonstrated with more extensive data sets, it relaxes the spatial resolution requirements for instrumentation designed to sense the vertical transports. Rather than requiring full resolution of the dissipation spectrum of the turbulence, it may only be necessary to resolve the inertial subrange.

To some extent, these profiles represent instantaneous snapshots of the turbulent fields of vertical velocity and temperature fluctuations. The largest distinct overturns, on scales of 10s of centimeters, are associated with vertical velocities of several cm s<sup>-1</sup>. A corresponding overturning time scale might be estimated as  $\tau \sim \frac{l}{u} \sim$

O (10 s). This time scale is large compared to the time required for the profiler to traverse 10s of centimeters (9 seconds to traverse the entire 8 m patch of profile 17). By comparison, the local buoyancy period was many 100s of seconds.

These snapshots of turbulent patches indicate that, at any particular instant in time, there is a considerable contribution to countergradient transport by the turbulence. As a measure of this contribution, it is noted that a value of  $w'T' = 0.1$  K cm s<sup>-1</sup> (Figures 4, 5) corresponds to a turbulent heat flux  $J_q \sim 4 \times 10^5$  W m<sup>-2</sup>, where  $\rho \sim 1025$  kg m<sup>-3</sup> and  $C_p \sim 4000$  J kg<sup>-1</sup> K<sup>-1</sup>.

The heat flux resulting from a single turbulent patch is the patch-averaged value  $\langle w'T' \rangle$  (equivalently, this is the integrated variance of the cospectrum of  $w'$  and  $T'$ ). For the patch from 8 to 16 m in profile 17,  $J_q = -240$  W m<sup>-2</sup>, a significant downgradient transport.

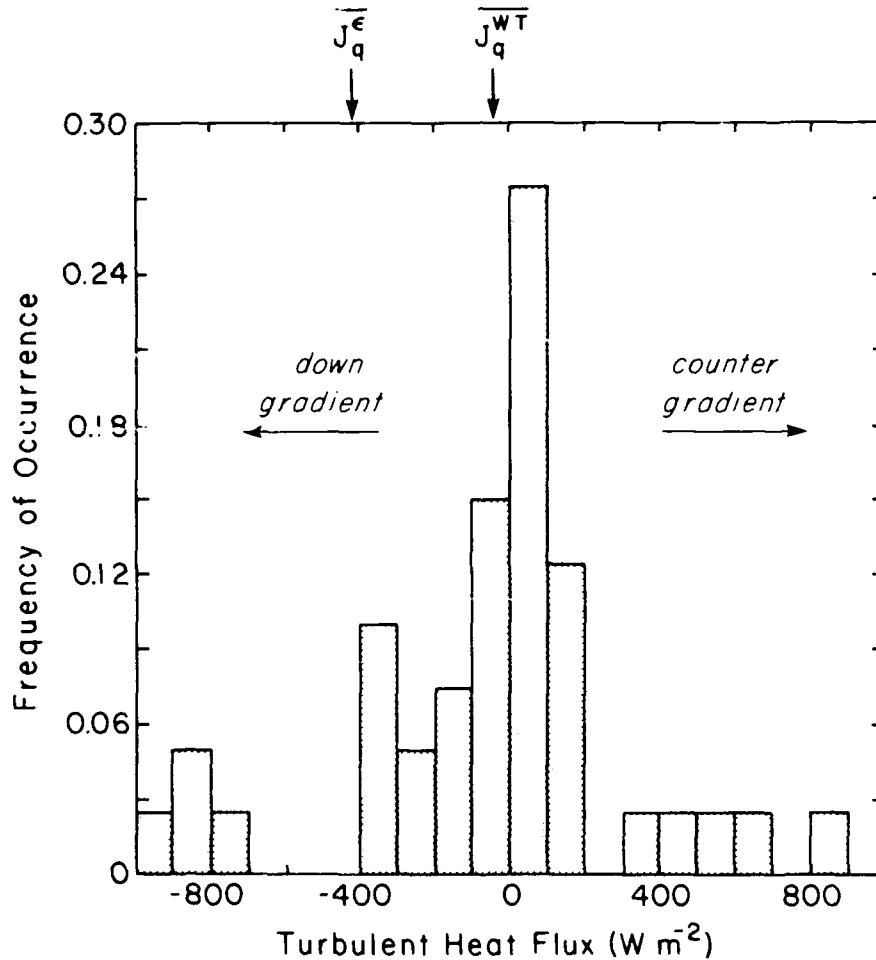


Figure 6. Histogram of patch-averaged estimates of  $J_q$  on  $\overline{w'T'}$ . The sample size was 40. The average value  $J_q^{wT}$  is  $-50$  W m<sup>-2</sup> compared to the average value obtained using the dissipation method,  $J_q^\epsilon$  of  $-420$  W m<sup>-2</sup>.

The degree of irreversible heat transfer in a single estimate of  $\langle w'T' \rangle$  is not clear. Individual occurrences of countergradient transport are likely a result of restratification following the initial overturn. The patch-averaged transport  $\langle w'T' \rangle$  was computed for each of forty patches observed over approximately the same depth range from twenty consecutive profiles. The values are presented as a histogram in Figure 6. The range of  $\langle w'T' \rangle$ , although concentrated at low values, is large. Averaged over all forty patches, the turbulent heat flux was  $-50 \text{ W m}^{-2}$ . In contrast, the eddy coefficient estimate based on  $\epsilon$  and  $R_f = 0.17$  (Eq. 4), leads to an average value of  $J_q = -\rho C_p K_\rho \frac{dT}{dz} \sim -420 \text{ W m}^{-2}$ . Based on individual patch estimates of the heat flux, the  $\epsilon$  estimate gives *downgradient* transport when significant *countergradient* transport actually occurs. This estimate, of course, is always negative instantaneously and does not include restratification effects. It is only meant to hold in an *averaged* sense. The  $w'T'$  correlation, on the other hand, represents the true turbulent heat flux at the time and place of the measurement. Unfortunately, I think that the number of data points is too small to allow a critical examination of the apparent disparity in heat flux estimates. Obtaining an adequate determination of  $\overline{w'T'}$  will require many more realizations.

#### Acknowledgments

Ayal Anis, Richard Dewey and Dave Hebert all made constructive comments on the manuscript, for which I am grateful. This work has been sponsored by NSF grant OCE-8608256 and ONR grant N00011-89-1-1616.

#### References

- Caldwell, D.R.: 1983. Small-scale physics of the ocean. *Rev. Geophys. Space Phys.*, **21**, 1192-1205.
- Caldwell, D.R., T.M. Dillon and J.N. Moum: 1985. The Rapid-Sampling Vertical Profiler: an evaluation. *J. Atmos. Oceanic Technol.*, **2**, 615-625.
- Gregg, M.C.: 1987. Diapycnal mixing in the ocean. *J. Geophys. Res.*, **92**, 5249-5286.
- Gregg, M.C. and T.B. Sanford: 1988. The dependence of turbulent dissipation on stratification in a diffusively stable thermocline. *J. Geophys. Res.*, **93**, 12,381-12,392.
- Moum, J.N.: 1989. Profiler measurements of vertical velocity microstructure in the ocean. *J. Atmos. Oceanic Technol.*, *submitted*.
- Moum, J.N., D.R. Caldwell and C.A. Paulson: 1989. Mixing in the equatorial surface layer and thermocline. *J. Geophys. Res.*, **94**, 2005-2021.
- Moum, J.N. and T.R. Osborn: 1986. Mixing in the main thermocline. *J. Phys. Oceanogr.*, **16**, 1250-1259.
- Oakey, N.S.: 1988. Estimates of mixing inferred from temperature and velocity microstructure. in *Small-scale turbulence and mixing in the ocean*, Elsevier Oceanography series, vol. 46, J.C.J. Nihoul and B.M. Jamart, Eds., Elsevier, 239-247.
- Oakey, N.S.: 1982. Determination of the rate of dissipation of turbulent energy from simultaneous temperature and velocity shear microstructure measurements. *J. Phys. Oceanogr.*, **12**, 12-256-12,271.
- Osborn, T.R.: 1980. Estimates of the local rate of vertical diffusion from dissipation measurements. *J. Phys. Oceanogr.*, **10**, 83-89.
- Osborn, T.R. and C.S. Cox: 1972. Oceanic fine structure. *Geophys. Fluid Dyn.*, **3**, 321-345.
- Osborn, T.R. and W.R. Crawford: 1980. An airfoil probe for measuring turbulent velocity fluctuations in water. *Air-Sea Interaction: Instruments and Methods*, F. Dobson, L. Hasse and R. Davis, Eds., Plenum, 369-386.

- Osborn, T.R. and R.G. Lueck: 1985a. Turbulence measurements from a submarine. *J. Phys. Oceanogr.*, **15**, 1502-1520.
- Osborn, T.R. and R.G. Lueck: 1985b. Turbulence measurements from a towed body. *J. Atmos. Oceanic. Technol.*, **2**, 517-527.
- Townsend, A.A.: 1976. *The Structure of Turbulent Shear Flow*. Cambridge.

## A STRATEGY FOR OPEN OCEAN MIXING EXPERIMENTS

JAMES R. LEDWELL

Lamont-Doherty Geological Observatory of Columbia University  
Palisades, New York 10964

### ABSTRACT

Tracer release experiments to study diapycnal mixing in the open ocean on 500 km x 12 month scales are in prospect. These should be combined with small scale physics measurements to interpret the experiments and to develop relatively inexpensive robotic techniques for diapycnal mixing studies over the coming decades. The robotic techniques may eventually supplant tracer releases as a means of exploring the parameter space in which diapycnal mixing is controlled. Armed with these tools we may be able to develop a nearly complete parameterization for diapycnal mixing throughout the ocean over the next 30 years.

### INTRODUCTION

Why do we care about diapycnal mixing in the ocean? One model may show that the value of the diapycnal mixing coefficient is important to the meridional heat flux (e.g., Bryan, 1987), another may suggest that it isn't (e.g., Gargett, this volume). Classical models such as Stommel and Arons (1960) imply a dominant role for diapycnal mixing in determining the interior abyssal circulation. Yet, for some reasonable depth dependencies of the diffusivity it can be shown that the interior circulation driven by diapycnal mixing through the absolute vorticity balance is virtually nil, or is equatorward rather than poleward.

Are the diapycnal processes at the air-sea interface, together with lateral transport at the surface, sufficient to explain what is known about the circulation and hydrographic structure of the ocean? I suspect not, otherwise there would be no tritium on those density surfaces in the North Pacific which don't outcrop (see, e.g., Gargett et al., 1986). If we were to add diapycnal processes at the topographic boundaries at the bottom and around the rim of the ocean, would it then be sufficient? Maybe, but if so, we need to show that it is so. That is, we at least need to demonstrate that interior diapycnal processes aren't important, and that boundary processes are large enough to account for the observations.

The flow of mass, heat, salt and trace constituents through the density strata of the ocean is one of the most intrinsically fascinating processes for study in the ocean. The storage of these properties under the transient conditions accompanying climatic change on time scales of decades to millenia are important to the prosperity of civilization. I would like to sketch some new field techniques for the study of diapycnal mixing in the ocean on much larger lateral and temporal scales than have been attempted up until now. I would also like to suggest a strategy for combining these techniques in a way that within the next 30 years could reveal the magnitude and spatial distribution of diapycnal mixing in the ocean.

## TRACER RELEASE EXPERIMENTS

One technique under development involves the release of a tracer on an isopycnal surface and the measurement of its subsequent diapycnal and lateral dispersion. Floats released with the tracer to enable tracking will also yield the lateral mixing. Prospective experiments have been described in some detail elsewhere (e.g., Ledwell and Watson, 1988). The tracers being used at present are fluorinated compounds detected by gas chromatography with an electron capture detector. The tracer to be proposed for the first open ocean experiments is sulfur hexafluoride ( $\text{SF}_6$ ). The sensitivity is such that a 12 month x 500 km scale experiment could be performed in the open ocean with just 100 kg of this tracer.

The injection will be performed by towing an injection device as near to an isopycnal surface as possible. The injection pump is shut down when the ambient density is more than a preset distance away from the target density. It is also shut down when any one of a number of transducers indicate malfunction of the injection. The tow speed for injection will be 20 to 40 cm/s. This slow speed enables the initial streak to be spread laterally without creating a large initial dispersion due to the wake. A week or so will be required for injection of a patch with an initial length scale of 30 km or so. The scientific advantage of spreading the initial patch out is that there is less chance of the tracer being in an anomalous spot early on. Technical advantages are that the density anomaly associated with the tracer is diluted by the wake of the injector, and that sections of the initial plume may be readily encountered by cutting across the injection streaks with a sampling ship. A small spot of tracer would be difficult to find, and once found, the danger would be that sampling it would induce artificial mixing of some consequence.

Because the tracer distribution is expected to be streaky, the tracer must be sampled by towing a vertical array of integrating samplers through the patch. The center of the array is kept on the target isopycnal surface in the same way as the injector. A multichamber sampler could be placed at the center of the array, with the chambers filled sequentially to give a lateral resolution of better than 1 km for locating the tracer streaks. The samples can be analyzed on board the ship at a rate of about 10/hour for a single instrument manned by an analyst and an assistant.

Three sampling cruises are planned for the first open ocean tracer release experiment. The first will be carried out shortly after the injection operation from a second ship. This ship will tow the samplers through the patch of recently injected streaks, guided by floats released with the tracer. The patch at this point might be about 50 km across. A second sampling cruise will be performed about six months after injection, or when the anticipated patch is about 250 km across. The samplers will be towable at 5 km/hr, with four 15-km tracks performed per day. Thus, in a month an overall track length of 1500 km could be traced out; i.e., the patch could be crossed approximately five times with virtually unbroken track. Again, the float positions would be used to plan the sampling tracks. A final survey would be performed about a year after the injection, or when the patch size is anticipated to be about 500 km. The sampling track could cross the patch five times again in a month, but this time the tracks would not be continuous, having gaps of 15 km length between the individual tow tracks. An experiment starting in the spring would yield two measures of the diapycnal diffusion, one for the "summer" season and one for the "winter" season.



I should note that it would be better if the tracer could be measured with an in situ instrument at a high sampling rate to examine the details of the tracer patch and to more accurately determine the distribution of the tracer in density space. Although an in situ gas chromatograph for sulfur hexafluoride could be conceived, the expense would be great and the sampling rate would still be relatively low, say 2 min/sample at best. A more promising approach might be to push the sensitivity of in situ fluorometric techniques for the sensing of fluorescent dye, with sampling rates of 1 Hz or better. Either approach would take at least a few years of development, but would be worth pursuing.

The first open ocean tracer release experiment will be proposed for the upper pycnocline of the eastern subtropical North Atlantic. This first experiment may be viewed as a pilot to get the technique into open water. It should also serve as a pilot for float-based and mooring-based small scale measurements. The site has been chosen to take advantage of available resources, both ships and scientific manpower. In particular, the experiment will coincide with the Subduction Experiment presently planned by the U.S. Office of Naval Research, and the site enables heavy participation by the United Kingdom and Canada, as well as the U.S., as part of the World Ocean Circulation Experiment.

An idea of the diapycnal spreading to be expected can be had from Table 1, where I list the square root of the second moment of the vertical distribution,  $\sigma$ , for various values of the diffusivity and for an initial value of  $\sigma_0 = 5$  m. The values in the table are simply calculated from the formula:

$$\sigma^2 = \sigma_0^2 + 2 Kt \quad (1)$$

where  $K$  is the diapycnal diffusivity for the tracer and  $t$  is the time since injection. It is important to design the experiment to minimize the initial dispersion; based on our experience so far, 5 m is a conservative estimate for the stratifications to be encountered in the main pycnocline. For  $K = 0.01$  cm<sup>2</sup>/s,  $\sigma$  does not quite double over the course of a year. This value should probably be viewed as the minimum detectable level of  $K$  for the experiment. The experiment would certainly be valuable, however, even if it only succeeded in setting this upper limit on  $K$ , as 0.01 cm<sup>2</sup>/s is a very low value in the context of the general circulation and water mass transformation.

Two pilot experiments in the basins off the coast of Southern California have been performed to develop the technique. Ledwell et al. (1986) reported the first experiment in Santa Monica Basin (sill depth of 737 m; bottom depth of about 914 m; and area of about 1800 km<sup>2</sup>). The injection was performed on the 5.085°C potential temperature surface, at about 800 m depth. The subsequent spreading of the patch (Fig. 1) yields an estimate of the diapycnal diffusivity of approximately 0.3 cm<sup>2</sup>/s at a buoyancy frequency of about 1.0 cph. Most of the uncertainty in the result is due to changes in the horizontally averaged hydrographic structure from one cruise to another.

The second experiment was started in 1988 in Santa Cruz Basin (sill depth of 1084 m; bottom depth of around 1950 m; area of around 1800 km<sup>2</sup>) on the 4.0681°C potential temperature surface at about 1500 m depth. The buoyancy frequency at the injection depth was about 0.2 cph, i.e., about five times less than for the Santa Monica experiment. Preliminary analysis suggests that the diapycnal diffusivity is greater than 1 cm<sup>2</sup>/s, while lateral processes are much slower than in Santa Monica Basin. One of the primary accomplishments in this experiment was the use of a prototype injector for sulfur hexafluoride which has the capacity required for open ocean experiments.

Table 1. Vertical dispersion,  $\sigma$ , in m, of a tracer patch at various times for different values of  $K$ , assuming  $\sigma_0 = 5$  m.

$K$ ( $\text{cm}_2/\text{s}$ )	Time (days)		
	10	180	330
0.01	5.2	7.5	9.1
0.03	5.5	11	14
0.1	6.5	18	24
0.3	8.8	31	42
1	14	56	76
3	23	97	131
10	42	176	239

#### LIMITATIONS OF THE TRACER RELEASE TECHNIQUE

A single open ocean tracer release experiment, as presently envisioned, requires several months of a full crew on at least a 50-m research vessel. It also requires deployment and tracking of a dozen or so neutrally buoyant floats. The minimum cost is on the order of 3 million 1989 US dollars. Obviously a large number of such experiments cannot be done quickly. Yet the number of independent variables that govern diapycnal mixing is potentially large, among them might be:

depth  
latitude  
buoyancy frequency  
density ratio  
wind forcing of the internal wave field  
mesoscale eddy forcing of the internal wave field  
mean shear  
along-isopycnal T/S variations  
topographic parameters.

Clearly we cannot expect, even in several generations of scientists, to be able to explore this parameter space with tracer release experiments alone. Instead, we must develop relatively inexpensive means of reliably estimating diapycnal mixing averaged over at least as large temporal and spatial scales as achievable with tracer release experiments.

Furthermore, even if tracer release experiments were inexpensive, they would not answer all of the questions on diapycnal mixing. The most important reason is that a dynamically passive tracer may not behave the same as heat or salt, which of course are both dynamically active. It is true that the molecular diffusivity of a tracer of moderate molecular weight is of the same order of magnitude as that of salt, and on this ground the tracer is expected to mimic salt. However, I believe that one must be cautious about even this expectation, especially where the salinity gradient contributes to the stratification, and even more so where salt fingering is occurring.

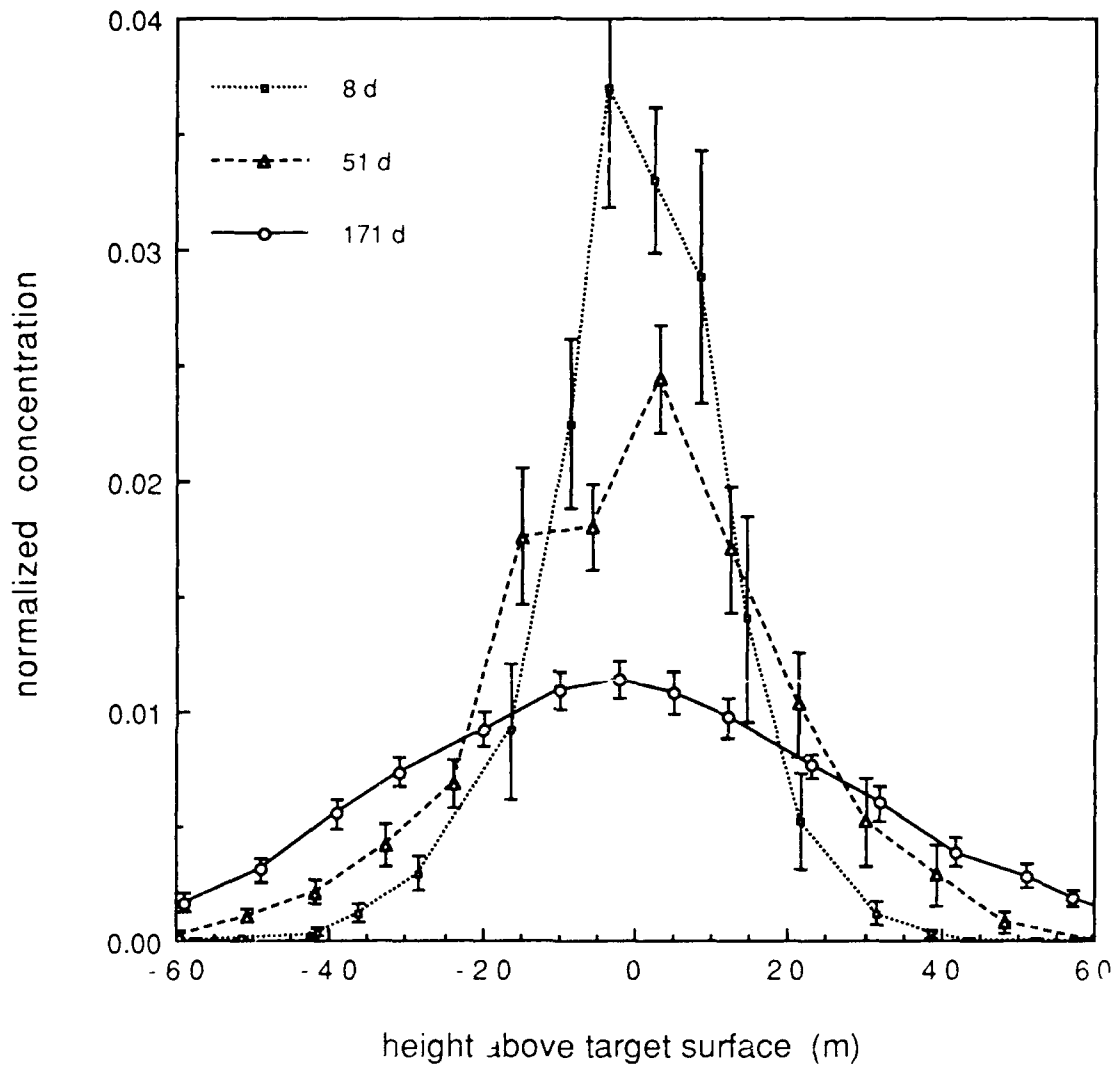


Fig. 1. Vertical spreading of the tracer during the Santa Monica Basin Experiment. Each profile is an average of ten or so individual profiles, with the error bars indicating the variance in shape of the individual profiles. The target surface of the injection was the 5.085°C potential temperature surface. The height is really a transformed coordinate based on the potential temperature profiles and the mean height versus temperature profile for the middle (51 d) survey. The concentration shown is normalized so that the area under each curve is unity. The days after injection given in the key are nominal; in reality each survey cruise was about 10 days long. The diapycnal diffusivity inferred from the spreading is about  $0.3 \text{ cm}^2/\text{s}$ .

Differences between the diffusivity of heat and the tracer are even more likely. Clearly such differences will arise in double diffusive regimes where order of magnitude differences between the diffusivity of heat and salt are expected. Even in diffusively stable regimes the eddy diffusivity may depend on the molecular diffusivity, as recently pointed out by Gargett (1988). Conditions of relatively weak turbulence can arise in which the smallest eddies are large enough that, while temperature variance is effectively dissipated by molecular diffusion on a time scale short compared with the time scale of a mixing event, salinity or tracer variance is not. This effect will lead to a larger eddy diffusivity for heat than for salt or tracer.

## ROBOTIC TECHNIQUES

Hypotheses exist, of course, for the relation of diapycnal mixing to characteristics of the fine structure and microstructure (see, e.g., Gregg, 1987, for a review). Examples of relevant parameters are the kinetic energy dissipation rate, the temperature variance dissipation rate, the fine-scale Richardson number or simply the fine-scale shear (see, Gregg, this volume, for a study of the last). Most of these quantities up to now have been measured using sophisticated profilers which require special cruises for deployment. Measurements are thus very expensive and yield averages for a week or so at one site, or else cover a long section with little temporal averaging.

Nevertheless, it seems likely to me that some of these quantities will soon be accessible to autonomous devices deployed for months at a time. Already a float exists to measure temperature and velocity gradients to estimate Richardson number on 1 to 5 m scale (Williams et al., 1987). There seems little in the way of deploying such floats for six months, especially in view of the success of long term moored deployments. Another technique which may be developed in the next few years is the measurement of temperature variance dissipation from floats which bob up and down through a layer of interest as they roughly follow the lateral flow. Perhaps it will prove feasible to do the same with shear probes to measure the kinetic energy dissipation rate. It is even feasible with presently available battery packs to power neutrally buoyant drones to cruise at speeds of 30 km/day for several months while sampling small scale features. Moored instruments which measure small scale features as they are advected past the sensors by the ambient flow might also prove useful in some situations.

Thus, the coming decade may bring measuring systems that do not require the continual presence of a research vessel, and are therefore considerably less expensive than present techniques. The development of such systems should be encouraged, and mixing experiments involving tracer releases should be coordinated with small scale physics measurements with a view toward exploiting robotic techniques in the future.

## LONG TERM STRATEGY

Neither tracer release experiments, nor the robotic techniques I have alluded to, have been tried in the open ocean in anything close to 12 month x 500 km experiments. While we are still very much in the development stage on all fronts, it is wise to ask where we ought to be headed. I believe our goals should be to construct a climatology of diapycnal mixing in the present ocean, and to be able to predict how diapycnal mixing will vary with hydrographic and dynamic variables. Predictive schemes will be especially useful if they are posed in variables likely to be the products of coupled atmosphere-ocean numerical models to be developed in the next several decades.

It seems to me that the best way to achieve these goals is with a combination of tracer-release experiments and the development of robotic techniques to measure small scale physics. The tracer technique promises direct measurements of diapycnal mixing of a passive tracer, albeit in a relatively modest number of situations. If simultaneous studies of small scale physics are performed on the same spatial and temporal scale as the tracer release experiments, then we can hope to confirm existing hypotheses or to discover new relationships which will ultimately enable the use of the small scale measurements alone for accurate estimates of the diapycnal diffusivities. Then, if these measurements can be made without great expense using robotic techniques, we can explore the parameter space more thoroughly than would be possible with the tracer release technique.

Ultimately we would perform fewer and fewer tracer release experiments, using them only for qualitatively new situations, or where they are uniquely suited to a special situation. Of course, the success of this plan depends on the development of small scale measurements from floats, drones or moorings, and on advances in the interpretation of the small scale measurements. It is important, then, to develop the various techniques together in a series of experiments for which interpretation promises to be straightforward.

I can envision performing three to six mixing experiments during the 1990's, depending on how many nations and scientists become involved. We can hope that by the end of the decade inexpensive robotic techniques will be proven, and their products interpretable. During the first two decades of the next century, the robotic techniques could be deployed in increasingly ambitious programs, with tracer releases used as needed, until at the end of the period we have largely achieved a basic parameterization and understanding of diapycnal mixing in the ocean. I believe that we stand at the threshold of a very exciting time: we can solve within the coming generation a problem which has long been a central enigma of oceanography.

## REFERENCES

- Bryan, F., 1987: Parameter sensitivity of primitive equation ocean general circulation models. *J. Phys. Oceanogr.*, 17, 970-985.
- Gargett, A.E., G. Ostlund, and C.S. Wong, 1986: Tritium time series from Ocean Station P. *J. Phys. Oceanogr.*, 16, 1720-1726.
- Gargett, A.E., 1988, Reynolds number effects on turbulence in the presence of stable stratification. In: *Small Scale Turbulence and Mixing in the Ocean*, J.C.J. Nihoul and B.M. Jamart, eds., pp. 517-528, Elsevier, Amsterdam.
- Gregg, M. C., 1987: Diapycnal mixing in the thermocline: a review. *J. Geophys. Res.*, 92, 5249-5286.
- Ledwell, J.R., A.J. Watson., and W.S. Broecker, 1986: A deliberate tracer experiment in Santa Monica Basin. *Nature*, 323, 322-324.
- Ledwell, J.R., and A.J. Watson, 1988: The use of deliberately injected tracers for the study of diapycnal mixing in the ocean. In: *Small Scale Turbulence and Mixing in the Ocean*, J.C.J. Nihoul and B.M. Jamart, eds., pp. 11-20, Elsevier, Amsterdam.
- Stommel, H., and A.B. Arons, 1960: On the abyssal circulation of the world ocean - I. Stationary planetary flow patterns on a sphere. *Deep-Sea Res.*, 6, 140-154.
- Williams, A.J. 3rd, C.H. Converse, and J.W. Nicholson, 1987: Richardson number float. In: *Current Practices and New Technology in Ocean Engineering - 1987 - OED - Vol 12*, G.K. Wolfe, (Ed.), pp. 25-29, Am. Soc. Mech. Eng., New York.

## OBSERVATIONS OF THE VERTICAL GRADIENT OF ISOPYCNAL VERTICAL DISPLACEMENT

Robert Pinkel, Jeffrey Sherman, and Steven Anderson  
Marine Physical Laboratory of the Scripps Institution of Oceanography,  
University of California, San Diego, La Jolla, CA 92093

### ABSTRACT

The dynamics of the fine scale motion field (1-50 m vertical scales) in the sea remains the subject of conjecture (Gregg, 1987; Munk, 1981). Efforts to investigate these motions experimentally have centered on measurements of the vertical profile of temperature gradient (Gregg, 1977) and shear (Garrett et al., 1981). The vertical wavenumber spectra obtained in these efforts have served as the basis for subsequent theoretical speculation. In this work, a repeated profiling CTD is used to monitor the fine scale density field in both time and depth. Here, the vertical separation between successive isopycnal surfaces is tracked. The quantity obtained is related to the vertical derivative of vertical displacement and will be referred to as the strain. The purpose of this work is to present a simple picture of the fine scale strain field as it evolves in time as well as depth. It is hoped that the observed time evolution of the field will provide additional clues to the underlying dynamics.

When viewed in isopycnal following coordinates, the qualitative nature of the strain field depends strongly on the characteristic vertical scale over which it is estimated. The "20 m strain" field has a strongly wave-like character, dominated by inertial and semi-diurnal tidal motion. The "2 m strain" more closely resembles the classical picture of fine structure. Lenses of low density gradient fluid are separated by sheets of higher gradient water. The lenses are seen to persist from several hours to a fraction of a day. They can propagate with respect to the density field over tens of meters. The low gradient regions evolve into regions of high gradient and vice versa, as a consequence of both spatial and temporal variability in the density field. Histograms of observed isopycnal separation are log-normal, with the skewness of the distributions increasing as the mean separation is decreased. Since all scalar fields in the sea are strained by the same velocity field, fluctuations in the fine scale vertical gradients of a variety of quantities are correlated. This may be of consequence to aspects of large scale modeling.

### INTRODUCTION

The early oceanographic discussions of the fine scale field were based on the assumption that the motions are small scale, perhaps non-linear, internal waves (Garrett and Munk, 1975, 1979; Munk, 1981). Relationships between the shear and strain (the vertical derivative of vertical displacement) fields were derived using internal wave scaling relationships (Munk, 1981; Desaubies and Smith, 1982). More recently, Holloway (1983), Müller (1984) and others have suggested that the small-scale component of so-called quasi geostrophic two-dimensional turbulence is indeed responsible for the variance observed in the ocean. The relationship between strain and shear for this class of motions is unclear.

Interestingly, power spectra of both shear and strain are found to have the same general form, as a function of vertical wavenumber. Spectral density is independent of vertical wavenumber, for wavenumbers less than 0.1 cpm. Between wavenumbers of 0.1 and 1 cpm the spectra have a  $k_z^{-1}$  dependence (Fig. 1).

At present there are a number of arguments used to "explain" the form of the fine scale spectrum of strain and shear over the wavenumber band 0.1-1 cpm. Gargett et al. (1981) use dimensional arguments to set the spectral form and level in this region. They suggest that the rate of turbulent kinetic energy dissipation,  $\epsilon$ , and the local Vaisala frequency,  $N$ , are the sole parameters of importance. Holloway (1983) cites studies in atmospheric dynamics, which suggest that the fine scale field is the result of the non-linear cascade of enstrophy from large to small horizontal scales. Internal waves play no role here. Finally, Fritts (this volume) presents a model for the fine scale spectrum based entirely on an internal wave breaking criterion. Atmospheric radar observations are used to support his argument.

In this work, the objectives are more modest than the resolution of the above uncertainty. Here, we attempt to add insight by extending the fine scale observations into the time as well as depth domains. Repeated profiling CTD (conductivity-temperature-depth) instruments mounted on the research platform Flip are used to observe the time evolution of the density field in the upper 500 m of the sea. The instantaneous density profiles measured by the CTD are assumed to be displaced and strained versions of some monotonic mean density profile, described equivalently by the functions  $\bar{\rho}(z)$  or  $\bar{z}(\rho)$ . The vertical displacement of an isopycnal,  $\eta$ , from its mean depth,  $\bar{z}(\rho)$ , is related to its instantaneous depth,  $z$ , by

$$\eta(t, \rho) \equiv \eta(t, \bar{z}(\rho)) \equiv z(t, \rho) - \bar{z}(\rho)$$

Using this notation one can express the isopycnal depth difference,  $\Delta z$ , and its normalized equivalent, the finite difference strain,  $\gamma$ , as

$$\Delta z(t, \bar{z}; \bar{\Delta z}) = z(t, \rho_1) - z(t, \rho_2)$$

and

$$\gamma(t, \bar{z}; \bar{\Delta z}) = (\eta(t, \bar{z}_1) - \eta(t, \bar{z}_2)) / \bar{\Delta z} = (\Delta z - \bar{\Delta z}) / \bar{\Delta z}$$

Here,  $\bar{z} = (\bar{z}(\rho_1) + \bar{z}(\rho_2)) / 2$  is the mean depth of the isopycnal pair and  $\bar{\Delta z} = \bar{z}(\rho_1) - \bar{z}(\rho_2)$  is the mean separation. It is these quantities,  $\Delta z$  and  $\gamma$ , which are the subject of this investigation.

The first section of this paper describes the measurement approach. Observations of the fine scale strain field are then presented in the depth-time domain. A simple statistical view of the data is given, in which histograms of the strain are seen to be clearly non-Gaussian. A brief discussion of some implications of this non-Gaussianity concludes the work.

## EXPERIMENT DESCRIPTION

The data are derived from sets of density profiles obtained from a profiling CTD system on the Research Platform FLIP. Approximately six thousand profiles, from the surface

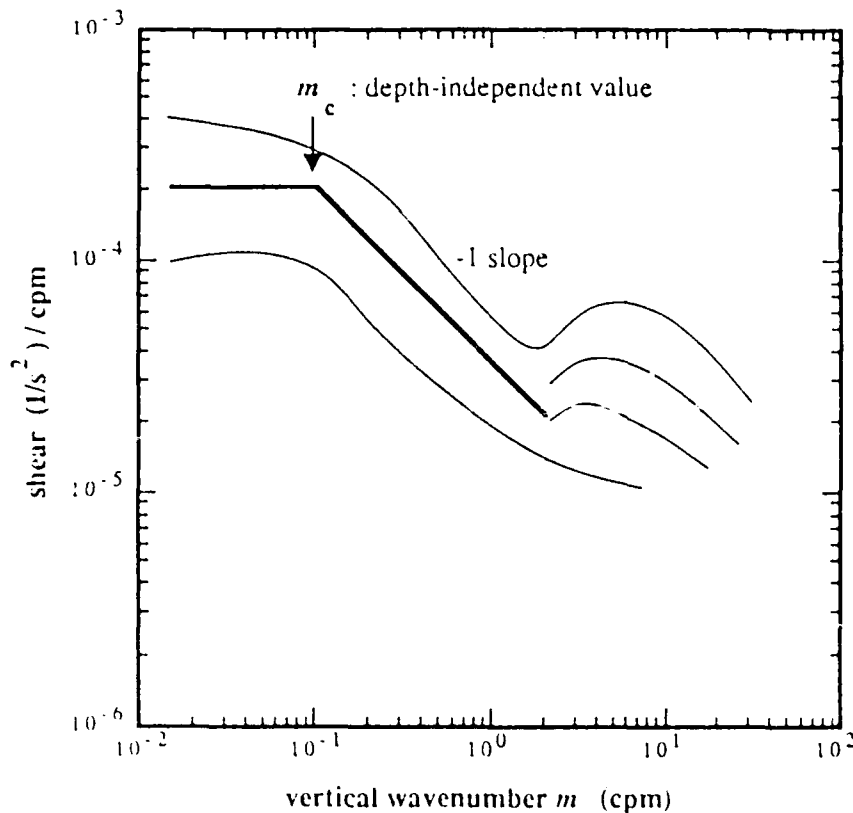


Fig. 1. A schematic representation of the spectrum of shear as a function of vertical wavenumber. The strain spectrum is found to have similar form, although units and the spectral level differ and scale differently with depth. (From Gargett et al., 1981). Note that approximately two thirds of the variance associated with non-overturning events (scales greater than 1m) is found in the 0.1-1 cpm band.

to 320 m, were collected over a 12 day period in the 1983 experiment, MILDEX. Ten thousand profiles were collected from the surface to 560 m in the 1986 PATCHEX Experiment. Both operations commenced at 34°N, 127°W, about 500 km west of Point Conception, California. Water depth at the site is 4 km. In MILDEX, FLIP drifted in a counterclockwise trajectory (Pinkel, Plueddemann and Williams, 1987), covering over 100 km. In the 1986 cruise, FLIP was placed in a two-point taut moor, restricting lateral motion to an area of several hundred meters square.

The CTD's used were Seabird Instruments model SBE-9, modified for high speed operation. The modifications include the construction of an open cylindrical frame to protect and support the instrument, and the addition of a weighted (25 kg lead shot) nose piece to increase the fall rate. Also a static pressure port is interfaced to the digi-quartz pressure sensor, to reduce the magnitude of turbulent pressure fluctuations associated with the high fall rate.

In MILDEX, a single instrument profiled from the surface to 320 m. In PATCHEX, a pair of instruments covered the depth ranges 0-300 m and 260-560 m. The CTD's were cycled every three minutes, corresponding to a drop rate of 3.8 m/s. The Nyquist



frequency, 10 cph, is not sufficient to prevent aliasing of internal wave motions in the upper thermocline (80–150 m). The aliasing of low mode internal wave motions is the dominant high frequency noise in these measurements.

The instruments were sampled at 12 Hz, corresponding to a sampling distance of 32 cm. Given the high fall rate, it was not necessary to pump the conductivity cell to achieve reasonable spatial resolution. The relative phase and amplitude response of the temperature and conductivity sensors was estimated by comparison of temperature and conductivity gradient cross spectra using data from nearly isohaline regions of the water column. The processing method is discussed in greater detail in Sherman (1989). Potential temperature, salinity and potential density profiles were obtained from the response corrected CTD information. Cruise-averaged profiles were computed for both cruises. A set of reference densities, whose mean depths were separated by 1 m, was then chosen. The encounter depth of each of these reference densities was computed for each profile using linear interpolation.

## OBSERVATIONS

In this section the CTD information is first used to describe the large scale isopycnal vertical displacement field. Subsequent plots display strain calculated on progressively finer depth and time scales. The objective here is to contrast qualitatively the nature of the motions at the various scales.

In Fig. 2, we see the isopycnal displacement field of the 1986 PATCHEX experiment. A set of 100 isopycnals is tracked. The mean separation between isopycnals over the 20 day record is 5 m. A low-pass filter with a two hour rectangular window is used to reduce the time variability of the data. During the period between days 4.2 and 4.5, the system was not operating.

Clearly apparent in the motion field is the semi-diurnal baroclinic tide. This has vertical wavelength long compared to the 400 m observation depth and vertical displacements as great as 40 m, crest-to-trough. Some evidence of a spring-neap fluctuation in amplitude is seen, particularly at depth.

The fine vertical scale motions of interest in this study are largely obscured by the tide and the other higher frequency constituents of the wavefield which are so coherent with depth. To view the smaller scale field, it is convenient to form plots of isopycnal depth-difference,  $\Delta z(t)$ . These can be plotted against either the instantaneous mean depth of the isopycnal pair or against the cruise averaged mean depth of the pair,  $\bar{z}$ . In the latter case the time evolution of the field is seen in a "semi-Lagrangian" frame, with  $\bar{z}$  effectively serving as a label for the isopycnal pair. In Fig. 3, the depth-time series of 20 m strain,  $\Delta z(t, \bar{z}; 20)$ , is plotted. This is a record of the instantaneous difference in depth between an isopycnal whose mean depth is 10 m above the depth signified in the ordinate and one whose mean depth is 10 m below. The two hour smoothing nearly obscures the period on day 4 when the no data were taken. Surprisingly, the dominant signals apparent in the 20 m strain are associated with both inertial waves and semi-diurnal motions. The vertical coherence of the tidal strain signal is greatly reduced when compared to the displacement signal. This is to be expected, as the strain is effectively the derivative of displacement with respect to depth. The vertical wave number dependence of the strain spectrum is "less red" than that of displacement by the factor  $k_z^2$ . While the strain field has a lumpy and irregular aspect in general, there are

# ISOPYCNAL VERTICAL DISPLACEMENT MEAN SEPARATION 5 m

SMOOTHED 2 HOURS IN TIME  
START DAY 279.5, 1986  
(NOON 6 OCT., pst)

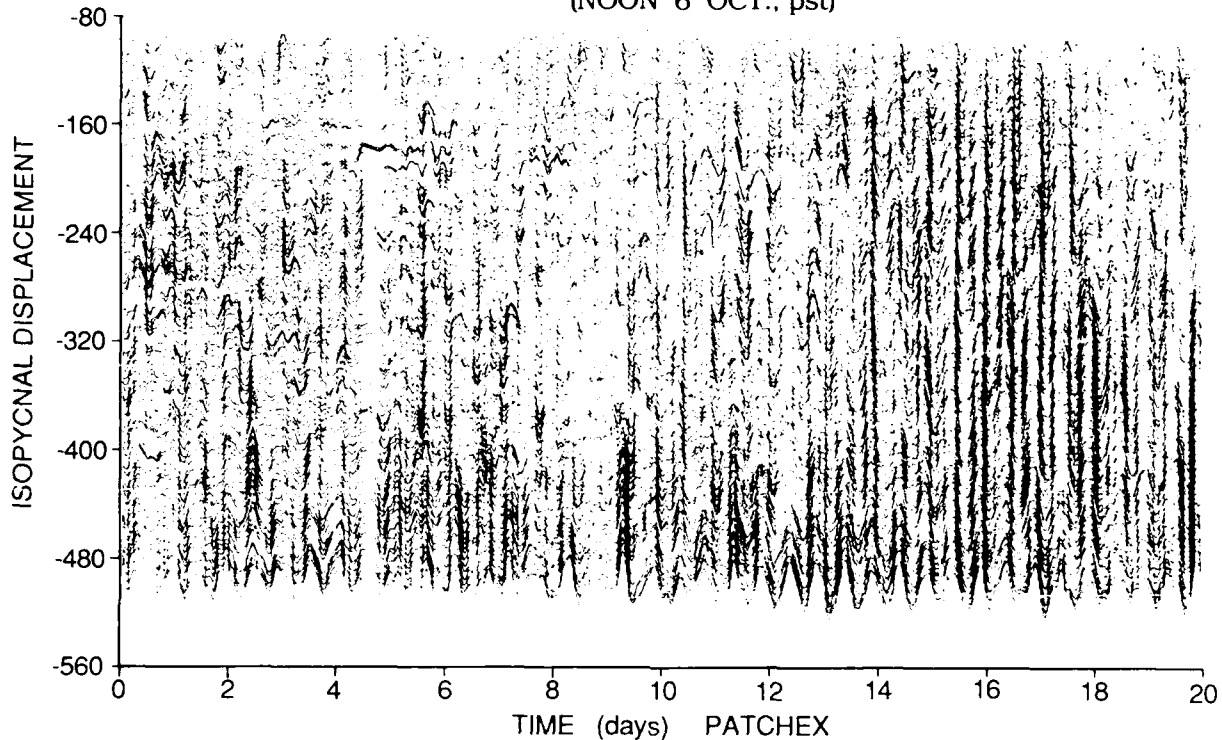


Fig. 2. The vertical displacement field observed in the 1986 experiment, PATCHEX. One hundred isopycnal surfaces, each separated by 5 m in the mean are tracked. The record starts at noon local time, 6 October and is smoothed by a two hour running mean filter. The filtering partially obscures a 6 hour period (days 4.2-4.5) when data were not collected.

periods where both upward (day 3, ~350-450 m, diurnal frequency) and downward (days 15-20, 100-300 m, semi-diurnal frequency) phase propagation are seen.

In some sense it is surprising to see a strong inertial signal in the strain field. Linear inertial motions are not expected to produce a vertical displacement signature. Nevertheless the signal is present. In the 1983 experiment, MILDEX, power spectra of strain (Fig. 10F in Pinkel et al., 1987) also reveal weak inertial as well as tidal peaks. When contrasted with other Southern California observations (Pinkel, 1984) the near inertial fields in MILDEX and PATCHEX are relatively weak. It is likely that the near inertial signal is a ubiquitous feature of the strain field.

The dominant motions in Fig. 3 have vertical scales of tens of meters. Most of the strain variance, as described spectrally in Fig. 1, occurs at far smaller scale. We can focus on the smaller scale motions by considering the depth difference between isopycnals whose mean separation is 5 m rather than 20 m.

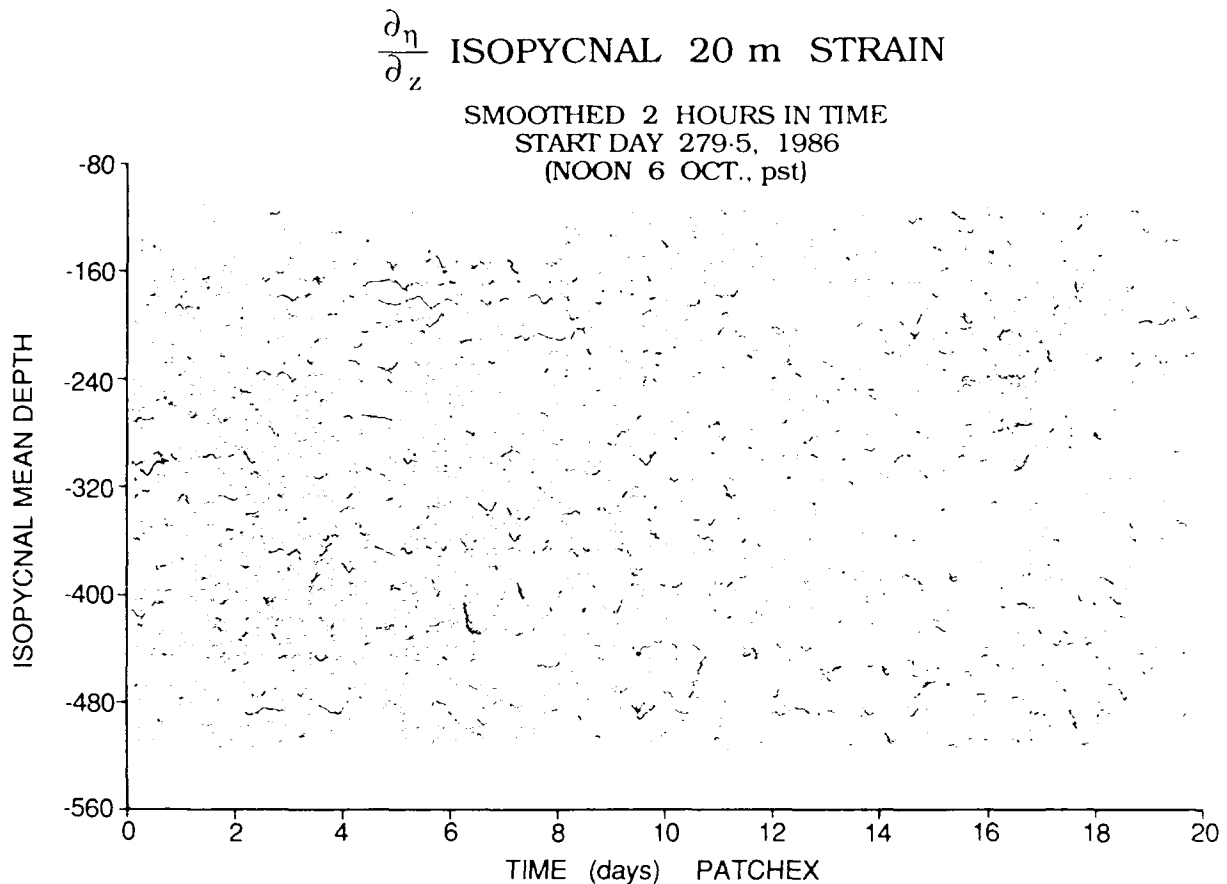


Fig. 3. Twenty-m isopycnal strain or depth difference time series. Vertical excursions of these lines are proportional to the separation between isopycnals whose mean separation is 20 m. Data are smoothed by two hours in time. Successive strain series are offset in depth, in proportion to the mean depth of the isopycnal pair. This removes the effect of the gross vertical advection of the internal wavefield.

In Fig. 4 the logarithm of 5 m isopycnal separation is plotted over a 40 hour period. Here data from the MILDEX experiment are presented. The displacement of the profiles to the right in Fig. 4 corresponds to large isopycnal separation--a layer of depressed local Vaisala frequency. Displacement to the left corresponds to small isopycnal separation--a sheet of enhanced stability. In this display of 15 min averaged strain profiles, there is little evidence of the large scale semi-diurnal signals which are prominent in the preceding figure. Here one sees motions appear as isolated lumps, slowly propagating vertically across isopycnal surfaces. The maximum rate of phase propagation is of order 4 m/hr  $\sim 10^{-1}$  cm/s. Note the downward phase propagation between hours 16 and 19 at a depth of 180 m. It appears that the event reverses direction beyond hour 20, propagating upward. A linear internal wave group with characteristic vertical wavenumber 0.1 cpm and intrinsic frequency midway between the inertial and Vaisala frequencies would have a characteristic horizontal phase speed of

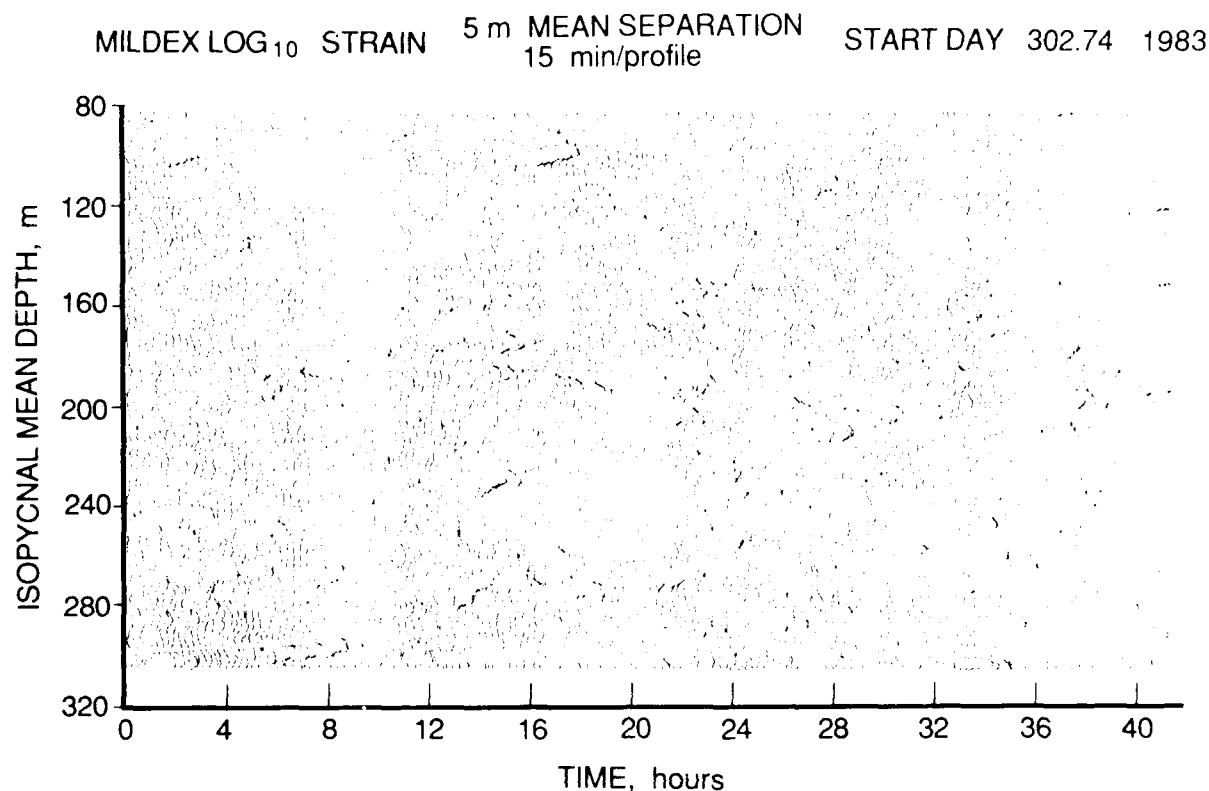


Fig. 4. Five-m strain: the logarithm of instantaneous separation between isopycnals whose mean separation is 5 m. Depth differences are averaged over 15 min. prior to forming these profiles. Data are plotted as a function of isopycnal mean depth. Excursions to the right correspond to large isopycnal separations, or layers. Excursions to the left correspond to small isopycnal separation. The signal consists predominately of isolated events which persist for a fraction of a day, and can propagate significantly with respect to the density field.

$$c = \frac{\omega}{k_H} \sim \frac{N}{k_z} = 1 \text{ cm/s}$$

for  $N = 3.6 \text{ cph}$ .

Here,  $c$  is the phase speed,  $N$  is the local Vaisala frequency and  $k_H$ ,  $k_z$  are horizontal and vertical wavenumbers, respectively. As typical horizontal advection speeds are larger than 1 cm/s, it is likely that spatial as well as temporal variation is being seen.

In Fig. 5, the logarithm of 2 m isopycnal separation is presented. Profiles are presented every 3 minutes for a single day of the PATCHEX experiment. As in Fig. 4, layers or lenses of nearly constant density appear as fine, nearly horizontal lines. Cross isopycnal propagation of these lenses is often seen (0200 at 300 m or 0800 at 320 m, for example). The layers persist for periods of one to five hours. The evolution of these layer-lenses place against a fine-scale background that is remarkably repeatable in detail, except in isolated depth-time regions of rapid and irregular change. The region above 200 m is typically quiescent, with the smallest details in the strain profiles repeatable over periods of an hour or more.

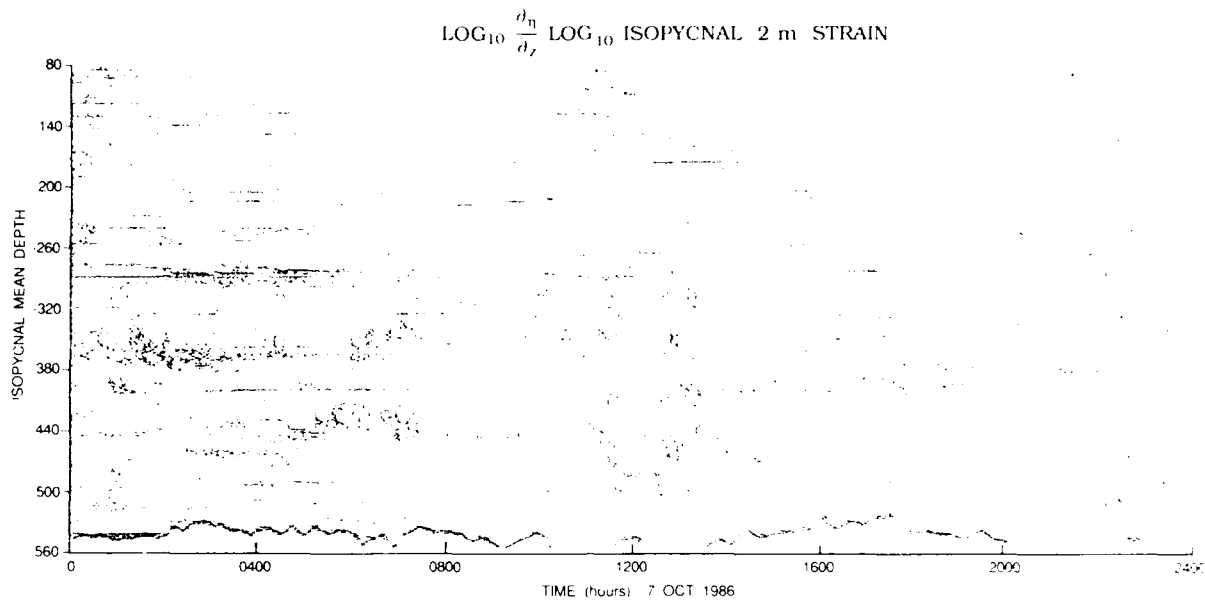


Fig. 5. The logarithm of 2-m strain. Depth difference profiles are presented every 3 min. for a single day from the PATCHEX experiment.

The regions of rapid variation (300–380 m at 0100 for example) stand out strongly in Fig. 5. The physical phenomenon which causes this effect is not clear. It was originally suspected that problems associated with estimating density from the conductivity and temperature sensors on the CTD were responsible for the periods of irregularity. However analogous plots using only temperature data show similar behavior. It remains to investigate the correlation of occurrence of these active patches with the horizontal velocity and shear fields measured using the Doppler sonars on Flip. If patches tend to occur during periods of high horizontal velocity, the advection of small horizontal scale perturbations in the density field must be considered. If they occur during periods of low velocity, instrument wake might be the cause.

### STRAIN STATISTICS

The essential character of the strain field changes markedly as progressively smaller scales are considered. We have seen this in a qualitative sense above. Simple statistics are now presented to emphasize the effect of changing scale. In Fig. 6, the isopycnal depth difference variance is plotted as a function of mean vertical separation,  $\Delta z$ . The square of the mean separation is removed from the variance estimates prior to plotting, in order to emphasize the contribution of the fluctuating components of the signal. Patterns from four depth zones are presented. At mean separations greater than 10 m, the variance is seen to increase roughly linearly with mean separation. This is consistent with a strain spectrum which is essentially white in vertical wavenumber (Appendix) at vertical wavenumbers less than 0.1 cpm. The straight lines, if extrapolated to small separation, would not indicate zero variance at zero mean separation. The actual curves indeed roll down at less than 10 m, to provide a physically sensible result. The roll down is a consequence of the finite variance of the strain spectrum (Appendix).

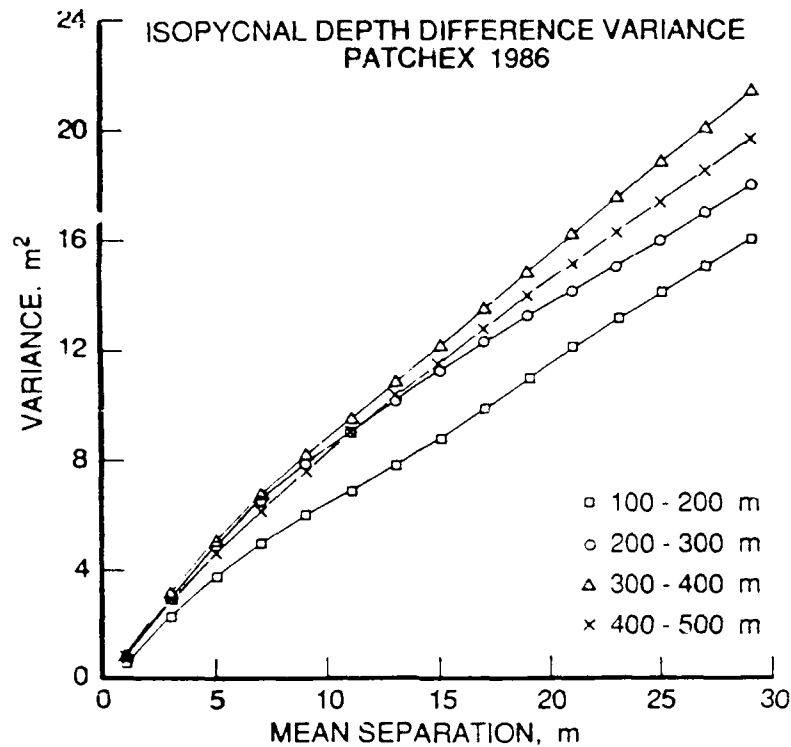


Fig. 6. The variance of isopycnal displacement difference  $\langle \Delta \eta^2 \rangle$  as a function of mean separation  $\Delta z$  from PATCHEX.

At very large mean separations, (not shown in Fig. 6), where the participating isopycnals are uncorrelated, the variance should approach a constant value, equal to twice the variance of the individual isopycnal displacements.

The mean separation and variance are, in fact, not adequate to describe the statistics of the strain measurements. This is seen in Figs. 7, 8, and 9 where representative histograms of isopycnal separation are presented. The "events" recorded in these histograms represent individual encounters of the isopycnal pairs during the first 9000 profiles of the PATCHEX experiment. The events are thus equally sampled in time but not necessarily in depth. Each histogram records the distribution of nearly two million events. However, adjacent events in time are highly correlated. The profiles are repeated 20 times per hour and the correlation time of the strain field is several hours or longer. Thus, the number of independent strain events represented by these histograms is probably a factor of fifty less than the total number of events recorded. The issue of statistical stability is not of great import here, however, as the histograms have clearly converged to stable forms.

One sees at large separation (Fig. 7) near Gaussian forms. The deep data have broader histograms than the shallow, at similar mean vertical separation. This corresponds to the general increase in strain variance with depth, seen in Fig. 6. As mean separation is decreased (Figs. 8, 9), the distributions become progressively more skewed. Also, the difference between the upper and lower depth ranges decreases.

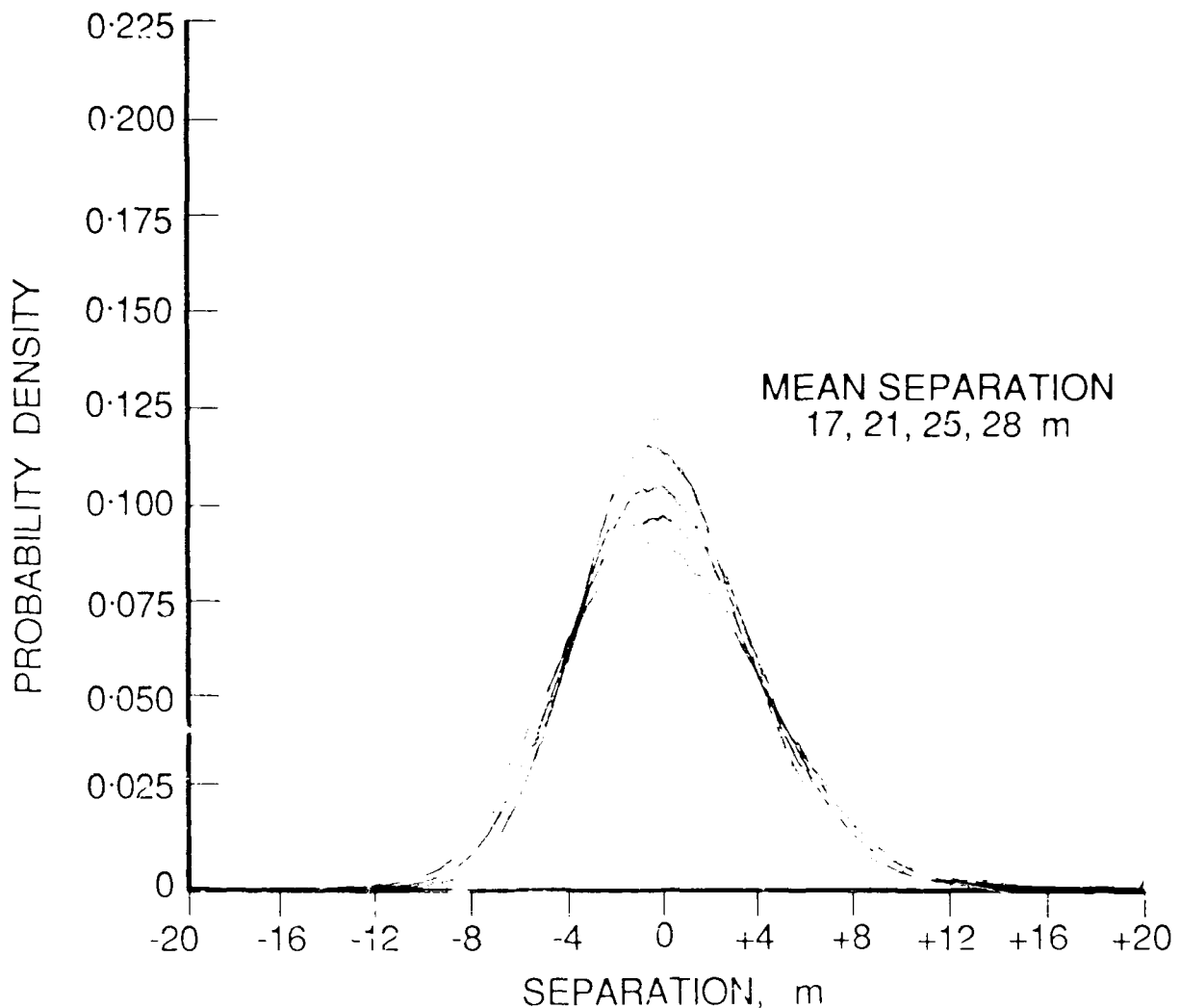


Fig. 7. Probability density of isopycnal separation from PATCHEX. Data from 100-300 m are drawn with a light line, 300-500 m with a heavy line. Note that the PDF's from the shallow region are more sharply peaked (have less variance) than their deep counterparts, at fixed mean separation. The histograms are each based on  $1.8 \times 10^6$  points.

In the algorithm used to calculate isopycnal position, density inversions are removed. Hence, there is no possibility of observing "crossed isopycnals" in this data set. Isopycnals separated by  $\Delta\sigma$  meters, on average, will never be observed closer together than  $-\Delta\sigma$  meters. Thus the distributions are forced into a truncated form at negative separation. Also, the occurrence of closely spaced isopycnals implies the existence of large density gradients. The finite resolution of the CTD significantly smooths the high gradient regions, artificially separating the isopycnals. As a consequence of this effect, a precutoff increase in probability is often seen just preceding the truncation at maximum negative separation. Instrument resolution has little effect on other aspects of histogram form.

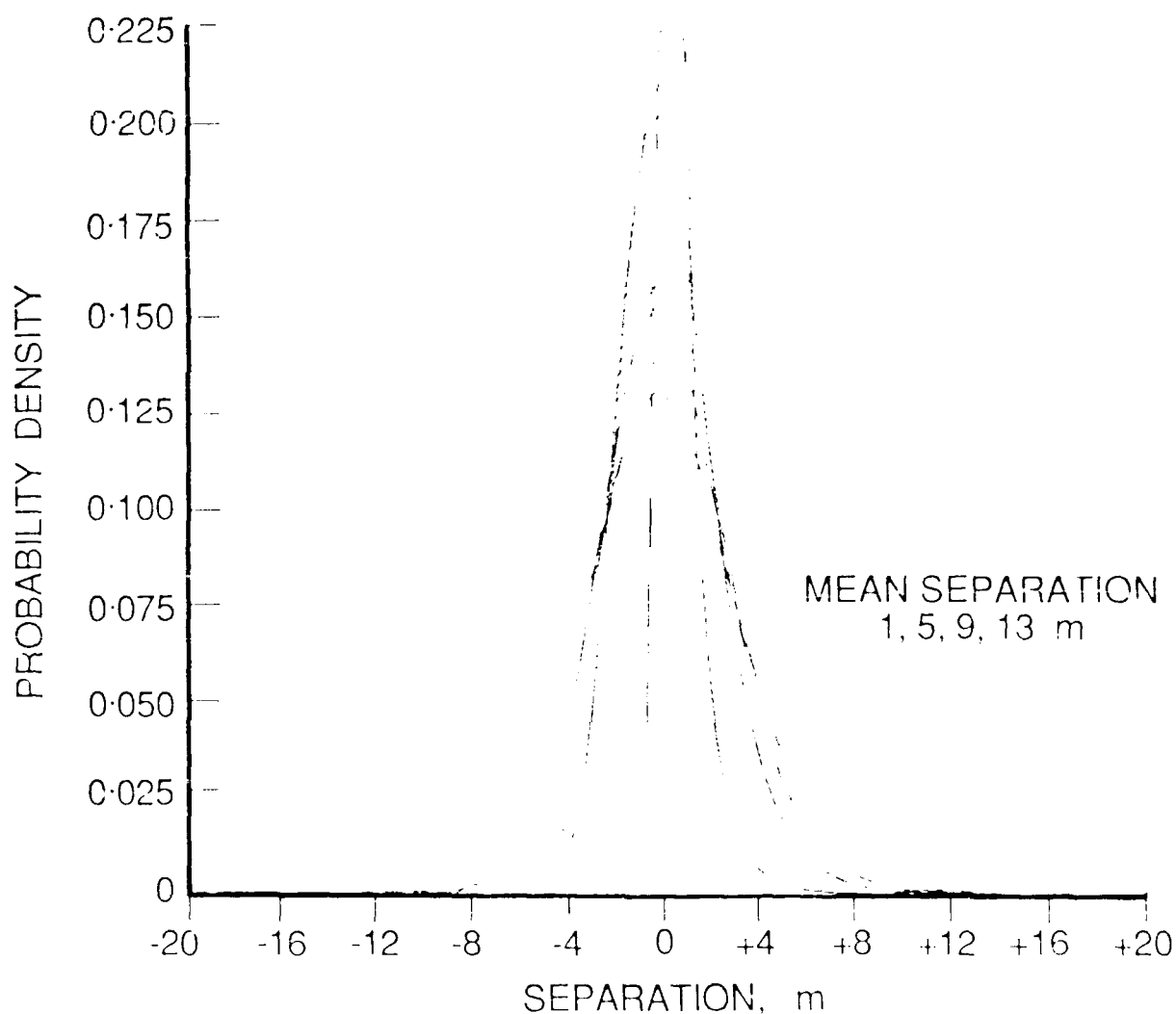


Fig. 8. Probability of isopycnal separation, as in Fig. 7, except for smaller separations. The PDF of 1m separation has been truncated.

## DISCUSSION

These histograms closely approximate a log-normal family of distributions. The log-normality is a reflection of the fact that isopycnals which are closer together than their mean separation tend to remain close together for a relatively long time, as they experience the same motion field. Isopycnals which are farther apart than their mean separation, experience a greater difference in advecting velocities. The relative separation between such isopycnals can be expected to change more rapidly. The sampling format of this experiment, with profiles spaced at equal increments of time, necessarily results in skewed isopycnal separation distributions.



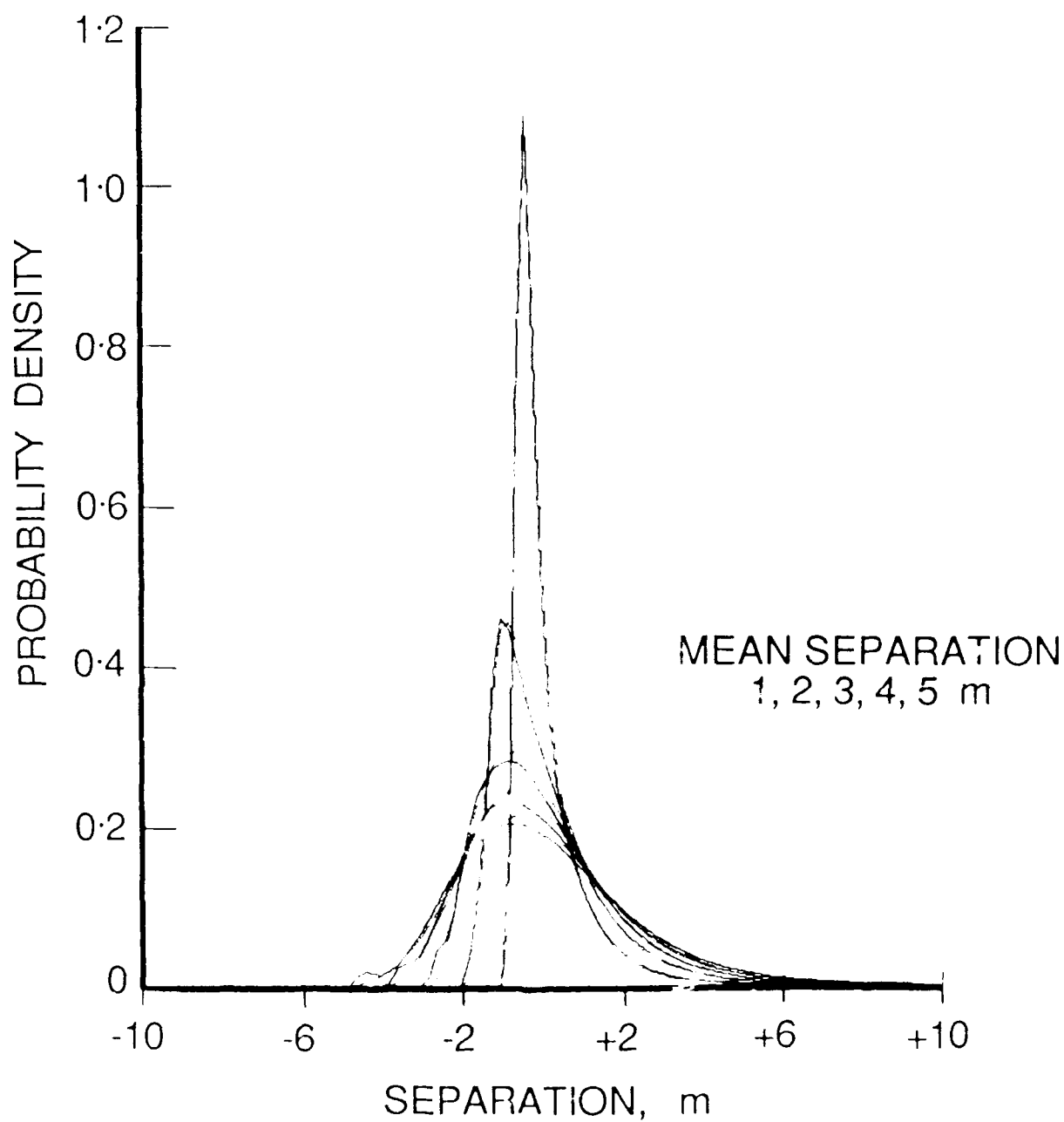


Fig. 9. Probability of isopycnal separation, as in Figs. 7 and 8, for very small mean separations. Note the change in vertical scale relative to the previous figures. The histograms representing the upper and lower depth ranges become more nearly identical as the mean separation is decreased.

The assertion that these skewed distributions are members of a log-normal family can be easily rationalized. Consider a Gaussian vertical velocity field over the time interval  $(-T, T)$  described by the Fourier series

$$w(z, t) = \sum_{n=-\infty}^{\infty} a_n(z) e^{i\omega_n t}$$

$$\text{where } \omega_n = \frac{n\pi}{T}$$

The separation between neighboring isopycnals, each advected by the local velocity field, can be expressed in terms of a Taylor expansion about the mid depth,  $\hat{z}$ .

$$\frac{\partial(\Delta z)}{\partial t} = \frac{\partial w}{\partial z} \Big|_{z=\hat{z}} \Delta z$$

Here  $\Delta z$  is the instantaneous separation.

$$\text{Thus } \frac{\partial(\log(\Delta z / \Delta \hat{z}))}{\partial t} = \frac{\partial w}{\partial z} \Big|_{z=\hat{z}}$$

If the rate of strain component  $\partial w / \partial z$  has Gaussian statistics, the time derivative of log separation will be Gaussian as well. Integrating with respect to time, it is seen that isopycnal separation will be log normal provided the vertical gradient of the vertical "progressive vector"

$$\hat{\eta} = \int_0^t w \, dt'$$

has Gaussian statistics. This indeed appears to be the case.

The log-normality of isopycnal separation has significant consequences for oceanography, in general. In particular, it is easily demonstrated that if a quantity, such as isopycnal separation has a log-normal probability distribution, then so does its inverse,  $\Delta z^{-1}$ .

It is usually the case that properties in the stratified ocean of the ocean vary more rapidly in the cross-isopycnal direction than in an isopycnal plane. If one describes the instantaneous vertical gradient of such properties in density co-ordinates,

$$\begin{aligned} \frac{\partial \Theta}{\partial z}(t, \hat{z}; \Delta z) &= \frac{\Theta(\rho_1) - \Theta(\rho_2)}{\Delta z(t)} \\ &= \frac{\Theta(\rho_1) - \Theta(\rho_2)}{\overline{\Delta z}} \frac{\overline{\Delta z}}{\Delta z(t)} \end{aligned}$$

The instantaneous value of the gradient equals the product of the mean value and the normalized inverse separation. It follows that fluctuations of the vertical gradients of a variety of passive quantities such as temperature or density itself, will have log-normal distributions. Knowledge of the inherent log normality of vertical gradient fluctuations allows one to predict fluctuation statistics in a manner far simpler and more appropriate than did Desaubies and Gregg (1981). There is no need to linearize about small values of the strain.

While these gradient fluctuations may appear as "sub grid scale" effects to large scale modelers, not all aspects of the gradient modulation problem disappear with spatial averaging. In particular, since the vertical gradients of many quantities are modulated by the identical strain field, averages of the products of gradients can be expected to differ significantly from products of the averages.

We note that there is no inference that the layers result from "lateral intrusions" which are small scale manifestations of large horizontal scale inhomogeneity. The lenses can come and go as a consequence of the (perhaps Gaussian) fields of horizontal and vertical velocity. They might represent local constructive interference in the orbital motion of the internal wavefield. The lenses can appear to propagate across isopycnal surfaces, although their persistence time/distance (as with any constructive interference) will be shorter than the characteristic times of the constituent motions which interfere. The lenses will, of course, disappear as a result of lateral divergence of the underlying current field. This divergence need not be driven by gravitational collapse, as discussed by Stommel and Federov (1967) and others. To the extent that the fine structure is truly reversible, there is no implication of dissipative processes.

Finally, it must be emphasized that the log normal nature of these small scale strain observations is very much a consequence of the sampling method employed, i.e. isopycnal following. By definition, one passes through more iso-surfaces per unit distance in high gradient regions than in low. Averages taken along isopycnal surfaces will be biased toward the high gradient regions, to an extent determined by the log normality of the iso-surfaces. In terms of the simple sheet and layer point of view, the waters of the sea are found in the layers, while the isopycnal surfaces congregate in the sheets.

Consistent with this viewpoint, data obtained from horizontal tows (space-series) could also be expected to have skewed distributions of vertical isopycnal separation, at the fine scale. However isopycnal separation data obtained from Lagrangian floats should be more nearly Gaussian. As isopycnals congregate to form high gradient sheets, the floats will tend to be exhausted laterally. Only the isopycnals converge in high gradient regions; the water does not, being incompressible.

#### ACKNOWLEDGMENTS

The authors would like to thank R.E. Davis, G. Holloway, P. Müller and J. Smith for useful discussions. E. Slater, L. Green and M. Goldin designed and operated the CTD profiling system used to collect these data. This program was sponsored by the office of Naval Research.

## APPENDIX

In this work, a finite difference approximation is used to describe the strain field in a semi-Lagrangian frame. The relation between a finite difference and a derivative is well known. It is reviewed here for the sake of completeness. If the isopycnal vertical displacement field,  $\eta(t, \bar{z})$ , is described over the depth interval  $(0, Z)$  by a Fourier series,

$$\eta(t, \bar{z}) = \sum_k A(t, k) e^{ik\bar{z}}$$

then the associated strain field is given by

$$\frac{\partial \eta}{\partial \bar{z}} = i \sum_k k A e^{ik\bar{z}}$$

The strain variance, for a stationary, homogeneous process, is

$$\begin{aligned} \langle \left( \frac{\partial \eta}{\partial \bar{z}} \right)^2 \rangle &= \sum_k k^2 \langle AA^* \rangle \\ &= \sum_k k^2 S(k) \Delta k \\ &= \sum_k \Gamma(k) \Delta k \end{aligned}$$

Here, the brackets refer to either ensemble or time averaging,  $S(k)$  is the power spectral estimate of displacement,  $\Gamma(k)$  is the power spectral estimate of strain and  $\Delta k = 2\pi/Z$  is the resolution bandwidth of the spectral estimates.

The isopycnal depth-difference time series, discussed in the text, is related to

$$\begin{aligned} \Delta \eta(t, \bar{z}; \bar{\Delta z}) &= \eta(t, \bar{z}_1) - \eta(t, \bar{z}_2) \\ &= \sum_k A(k, t) (e^{ik\bar{z}_1} - e^{ik\bar{z}_2}) \\ &= 2 \sum_k A e^{ik\bar{z}} \sin \frac{k \bar{\Delta z}}{2} \end{aligned}$$

$$\text{where } \bar{z} = (\bar{z}_1 + \bar{z}_2) / 2$$

$$\text{and } \bar{\Delta z} = (\bar{z}_1 - \bar{z}_2).$$

The depth-difference variance is

$$\begin{aligned} \langle \Delta \eta^2 \rangle &= 4 \sum_k \langle AA^* \rangle \sin^2 \frac{k \bar{\Delta z}}{2} \\ &= \bar{\Delta z}^2 \sum_k \Gamma(k) \text{sinc}^2 \frac{k \bar{\Delta z}}{2\pi} \Delta k \end{aligned}$$

where  $\text{sinc}(x) = \sin(\pi x) / (\pi x)$

The  $\text{sinc}^2$  function has unit value when  $k\Delta z$  is small compared to  $2\pi$ . It falls to a local zero when  $k\Delta z = 2\pi$ . The  $\text{sinc}^2$  thus serves to low-pass filter the strain spectrum. If the strain spectrum is band limited, i.e.,  $\Gamma(k) = 0$  for  $k > k_0$ , then one can always determine a differencing interval  $\Delta z_0 \ll 2\pi/k_0$  such that the finite difference strain is a good approximation to the total strain field. In general, as one reduces the differencing interval  $\Delta z$ , the filter broadens and less of the spectral variance is filtered out. If the strain spectrum is independent of wavenumber, the observed strain variance will vary like  $\Delta z^{-1}$  as the differencing interval is altered. The isopycnal depth-difference variance,  $\langle \Delta \eta^2 \rangle = \langle (\partial \eta / \partial z)^2 \rangle \Delta z^2$  will thus increase linearly with  $\Delta z$ , as is seen in Fig. 5.

## REFERENCES

- Desaubies, Y.J.F., and M.C. Gregg, 1981: Reversible and irreversible fine structure. *J. Phys. Oceanogr.*, 541-556.
- Desaubies, Y.J.F., and W.K. Smith, 1982: Statistics of Richardson number and instability in oceanic internal waves. *J. Phys. Oceanogr.*, 1245-1259.
- Gargett, A.E., P.J. Hendricks, T.B. Sanford, T.R. Osborn, and A.J. Williams III, 1981: composite spectrum of vertical shear in the upper ocean. *J. Phys. Oceanogr.*, 1258-1271.
- Garrett, C.J.R., and W.H. Munk, 1971: Internal Wave Spectra in the presence of fine structure. *J. Phys. Oceanogr.*, 196-202.
- Garrett, C.J.R., and W.H. Munk, 1972: Space-time scales of internal waves. *Geophys. Fluid Dyn.*, 225-264.
- Garrett, C.J.R., and W.H. Munk, 1975: Space-time scales of internal waves: A progress report. *J. Geophys. Res.*, 291-299.
- Garrett, C.J.R., and W.H. Munk, 1979: Internal waves in the ocean. *Ann. Rev. Fluid Mech.*, 339-369.
- Gregg, M.C., 1977: A Comparison of fine structure spectra from the main thermocline. *J. Phys. Oceanogr.*, 33-40.
- Gregg, M.C., 1987: Diapycnal mixing in the thermocline: A review. *J. Geophys. Res.*, 5249-5286.
- Holloway, G., 1983: A conjecture relating oceanic internal waves and small-scale processes. *Atmosphere-Ocean*, 107-122.
- Müller, P., 1984: Small scale vortical motions, in *Internal Gravity Waves and Small-Scale Turbulence*. Proceedings, Hawaii Winter Workshop, edited by P. Müller and R. Pujale, pp. 249-262, Hawaii Institute of Geophysics, Honolulu.
- Munk, W. H., 1981: Internal waves and small scale processes. In *Evolution of Physical Oceanography*, Scientific Surveys in Honor of Henry Stommel, edited by B.A. Warren and C. Wunsch, 623 pp., MIT Press, Cambridge, Mass.
- Phillips, O.M., 1971: On spectra measured in an undulating layered medium. *J. Phys. Oceanogr.*, 1, 1-6.
- Pinkel, R., 1984: Doppler sonar observations of internal waves: The wavenumber frequency spectrum. *J. Phys. Oceanogr.*, 1249-1270.
- Pinkel, R., A.J. Plueddemann and R.G. Williams, 1987: Internal wave observations from Flip in Mildex. *J. Phys. Oceanogr.*, 1737-1757.
- Sherman, J.T., 1989: Observations of fine-scale vertical shear and strain in the upper-ocean. Ph.D. Thesis, University of California, San Diego.
- Stommel, H., and K.N. Iedrov, 1967: Small scale structure in temperature and salinity near Timor and Mindanao. *Tellus*, 306-325.

# DIFFUSION PARAMETRIZATIONS FOR THE CLIMATOLOGICAL CIRCULATION OF THE NORTH ATLANTIC AND THE SOUTHERN OCEAN

Dirk Olbers

Alfred-Wegener-Institute for Polar and Marine Research,  
2850 Bremerhaven, FRG

## ABSTRACT

This paper is a review of the basic physics and some technical and conceptual problems of estimation procedures which attempt to determine mixing parametrizations for heat and salt from hydrographic data. The review is guided by applications of various different forms of the  $\beta$ -spiral method to the hydrography of the North Atlantic and the Southern Ocean. The results appear reasonable in areas where intense mixing is expected to occur. In regions of low mixing, however, as in the central North Atlantic, the coefficients often are only marginally significant. A fairly distinct pattern of mixing and fairly large diffusivity values are obtained in the Southern Ocean. The data, however, are not able to distinguish between different orientations of the mixing tensor: the question of horizontal versus isopycnal mixing is still open for dispute.

## PROBLEMS

The inference of mixing properties from hydrographic data meets with many difficulties. Some of these are fairly obvious (though not easy to handle), as, e.g., the effects of errors in the data. Other difficulties are of a more subtle nature. Of the various assumptions which have to be made in the course of any estimation procedure, some are hidden so deeply in the approximation of physical principles or the mathematical estimation techniques that they may elude even careful, experienced people. In this section we discuss various causes of possible failure.

### Searching for a small signal

In a diagnostic approach the density and tracer data are given from the hydrographic observations. Any determination of mixing parameters has to make use of the tracer balance

$$u \sigma_x + v \sigma_y + w \sigma_z = D[\sigma] \quad (1)$$

governed by the advection of the tracer  $\sigma$  by the current  $(u,v,w)$  and by the mechanism of mixing, which will be assumed here to be of a diffusive nature. In the applications the tracer  $\sigma$  will be any in adiabatic conditions conserved functional  $\sigma(\theta,S)$  of potential temperature  $\theta$  and

salinity  $S$ , such as potential density or veronicity (for a definition of this tracer see Veronis, 1972 or Olbers et al., 1985). Obviously the estimation of a parametrization of  $D[\sigma]$  by Eq. (1) is inherently coupled to the estimation of the velocities  $u$ ,  $v$  and  $w$  as well, since these are generally not known. The relative roles of advection and diffusion can be found by scaling the above set of equations (see, e.g., Pedlosky, 1978). Taking here vertical diffusion for the purpose of demonstration

$$D[\sigma] = K \sigma_{zz}$$

we obtain for motions of planetary scale the well-known ratio of diffusive to advective terms

$$\text{diffusion} / \text{advection} \approx \delta_d / \delta_a$$

where  $\delta_a = (fa^2W/g\delta\rho)^{1/2}$  is the advective vertical scale ( $a$  = earth radius,  $\delta\rho$  = density scale) and  $\delta_d = K/W$  is the diffusive vertical scale. With a  $K$  of  $10^{-4} \text{ m}^2/\text{s}$ --as proposed by Monk (1966)--and a vertical velocity scale  $W$  of  $10^{-6} \text{ m}^2/\text{s}$  the ratio of diffusive to advective terms becomes 0.1 (or less for smaller values of  $K$ , as presumably appropriate for local conditions). It appears that mixing is only a small contribution to the tracer balance. We must expect that determination of mixing parameters from such a balance might be a delicate problem unless applied in region of strong mixing.

This problem can readily be seen in the diffusivity estimates obtained from the North Atlantic application of the  $\beta$ -spiral method (Olbers et al., 1985). As an example, Fig. 1 displays the diapycnal diffusivity corresponding to the depth range 100 to 800 m determined from the balance of veronicity (the reference velocities used in the tracer balance were determined before from data between 800 and 2000 m, see below). The most obvious feature in this figure is the marked correspondence of large diffusivities with the regions of strong currents where mixing is more likely to occur. In the calm region between the Gulf Stream and North Atlantic Current on the one side and the equatorial current system on the other the diffusivities are low, in fact they are set to zero in many places by the inversion scheme which constrains the diffusivities to be positive. The determination of these low values of mixing (isopycnal values below  $10^2 \text{ m}^2/\text{s}$  and diapycnal values below  $10^{-5} \text{ m}^2/\text{s}$ ) is entirely spoiled by noise in the data. It may as well point toward an inadequate parametrization of the mixing mechanism.

#### The level-of-no-motion problem

The velocities which are necessary to utilize Eq. (1) for the estimation of the diffusion processes are generally determined from the geostrophic and hydrostatic approximations of the momentum balance. These are quite appropriate for the large-scale oceanic currents but hydrographic data only allow us to determine the baroclinic pressure. Without any

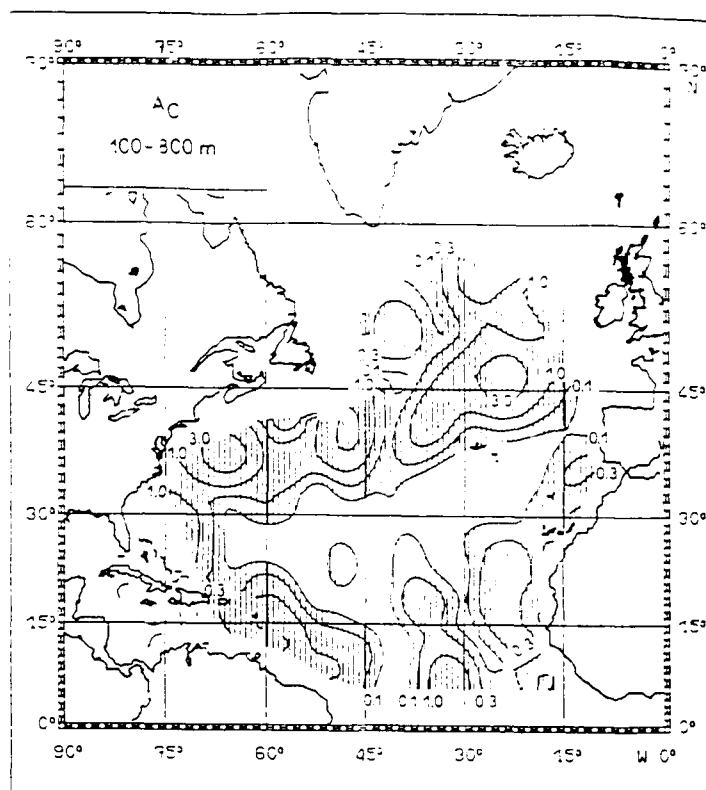


Fig 1. Map of the diapycnal diffusion coefficient in the North Atlantic for the depth range 100-800 m. Units are  $10^{-4} \text{ m}^2/\text{s}$ , contours are logarithmically spaced with interval 0.5.

knowledge about surface topography we are faced with a classical problem of large-scale oceanography--the determination of the absolute velocity profile given the vertical shear by hydrography in form of the thermal wind relations

$$\begin{aligned} u_z &= (g/f) \rho_y \\ v_z &= -(g/f) \rho_x \end{aligned} \quad (2)$$

and the local version of the vortex stretching equation

$$w_z = (\beta v - F)/f \quad (3)$$

Here turbulent diffusion of vorticity is included by a term  $F$ , since all terms retained in Eq. (3) are of higher order than the geostrophic momentum terms in Eq. (2). Integration of these relations from a fixed reference level  $z = z_0$



$$\begin{aligned}
u &= u_0 + (g/f) \int_{z_0}^z dz' \quad \rho_y = u_0 + u' \\
v &= v_0 - (g/f) \int_{z_0}^z dz' \quad \rho_x = v_0 + v' \\
w &= w_0 + (1/f) \int_{z_0}^z dz' (\beta_v - F) \\
&= w_0 + (\beta/f)(z - z_0)v_0 - (1/f) \int_{z_0}^z dz' F + w'
\end{aligned} \tag{4}$$

reveals the set of unknowns--the reference velocities  $u_0$ ,  $v_0$  and  $w_0$ --which any estimation scheme must determine in conjunction with the mixing parameters. Inserting the integrated thermal wind and vorticity Eqs. (4) into the tracer balance Eq. (1) we find the  $\beta$ -spiral equation in the form

$$\begin{aligned}
&u_0 \sigma_x + v_0 [\sigma_y + (\beta/f) (z - z_0) \sigma_z] + w_0 \sigma_z \\
&\quad - D - (1/f) \sigma_z \int_{z_0}^z dz' F \\
&= - (u' \sigma_x + v' \sigma_y + w' \sigma_z)
\end{aligned} \tag{5}$$

Given a parametrization for the diffusion term  $D$  for the tracer and  $F$  for vorticity this equation may be applied at some levels to set up a formally overdetermined inverse problem for the unknown mixing parameters and the reference velocities. A powerful method for solving such a problem is the technique of singular value decomposition (SVD) described for oceanographic aspects, e.g., in Olbers (1989) and Wunsch (1989). The problem may be only formally overdetermined since the rank of the set of equations Eq. (5) may effectively (not mathematically) be less than the number of unknowns. As demonstrated below this occurs frequently in the determination of reference velocities.

### Ill-posedness

One of the most frequent fallacies of an inverse solution arises from the attempt to extract from the data information that is not really contained there, i.e., parameters should be estimated which are not or not well enough constrained by the relations and data considered. At first, it seems that such a mistake can easily be avoided by simple inspection of the data and the relevant physical mechanisms responsible for the shape of the data. And indeed, in low-order problems a close inspection generally will sort out such failures. However, in case of

problems with many data and unknowns the failure may only be found deep in the elements of the inversion tools.

An example of an ill-posed inverse problem is taken here from the North Atlantic application of the  $\beta$ -spiral method (Olbers et al., 1985). In that paper the attempt was made to determine the three unknown reference velocities  $u_0$ ,  $v_0$  and  $w_0$  from about ten relations of the form Eq. (5) with vanishing  $D_0$  and  $F_0$ . The tracer was the potential density at levels between 100 and 800 m depth taken from Levitus' atlas (Levitus, 1982). Accepting the physical assumptions which lead to Eq. (5) and the data accuracy, this problem with three unknowns and ten relations should at first sight give a well-behaved inverse solution. However, the matrix condition (ratio of the smallest to the largest eigenvalue of the  $3 \times 3$  matrix corresponding to Eq. (5)) points out severe problems. The model was applied to the entire North Atlantic south of  $60^\circ\text{N}$ . Over more than half of this area the condition index is less than  $10^{-3}$  (Fig. 2). This indicates that we have tried to estimate some parameter combination which is not constrained by the hydrographic fields. The data structure leading to this singular behaviour in the low index areas of Fig. 2 is

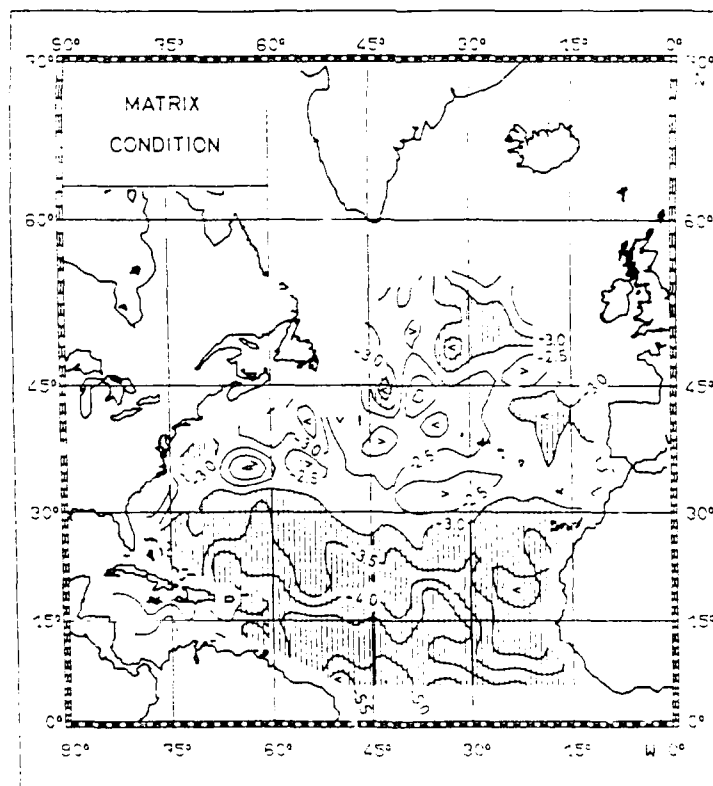


Fig 2. Condition index for the adiabatic form of the set of equations (5) at levels between 100 and 800 m in the North Atlantic. Contours are logarithmically spaced, the area with a condition index below  $10^{-3}$  is shaded.

similar to the one considered below for the circulation in the Southern Ocean: the horizontal gradient of the tracer does not turn rapidly enough with depth, deteriorating the effective rank of the problem.

The next vivid example of singular behaviour occurred during the construction of an inverse model for the Antarctic Circumpolar Current (Olbers and Wenzel, 1989) based on a collection of hydrographic data from the Southern Ocean prepared by Gordon et al. (1982). For our work we used the gridded version of this atlas, for which the temperature and salinity fields are interpolated on a grid with dimensions of  $1^\circ$  of latitude and  $2^\circ$  of longitude on 42 standard levels in the depth range 0 to 7000 m.

As conserved tracer we used potential density referred to the surface. Figure 3 displays the absolute geostrophic circulation in 2000 m depth, obtained by fitting the model to the 100 to 2000 m part of the data. In view of the well-known eastward surface circulation of the Antarctic

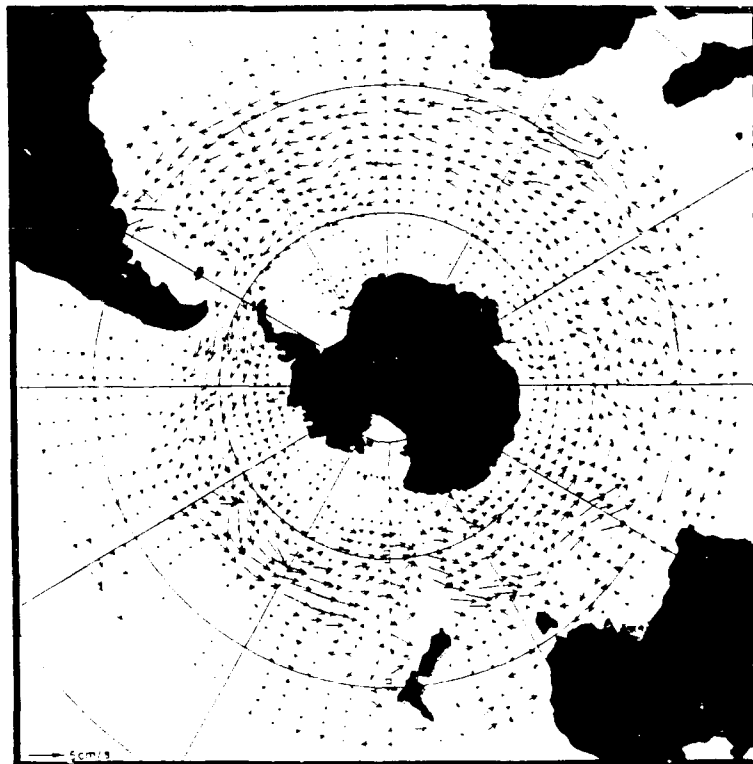


Fig. 3. The absolute horizontal velocity at 2000 m depth in the Southern Ocean, obtained from data for 100–2000 m and an adiabatic  $\beta$ -spiral model. Notice the wrong direction of the current in this ill-conditioned solution.

Circumpolar Current (ACC) the level-of-no-motion in this solution must lie well above 2000 m depth, which entirely contradicts our expectation that the ACC is an almost barotropic eastward current. The matrix condition of the solution has very low values (below  $10^{-3}$ ) in most of the latitudes of the ACC. The separation of the total circulation of Fig. 3 into three components of the eigenvector basis associated with the eigenvalues of Eq. (5) revealed that the contributions from the two large eigenvalues are small and mainly meridional, whereas the contribution from the smallest eigenvalue is almost identical to the total solution.

The reason for this behaviour must be sought in the zonality of the potential density field. Over most of the upper part of the water column the zonal gradient is much smaller than the meridional one so that the reference velocity  $u_0$  is not sufficiently constrained by the  $\beta$ -spiral equation Eq. (5). Unreliable data structures may then be amplified as the consequence of near singular relations and spoil the total solution. Cutting off the contribution from the smallest eigenvalue, as suggested by the SVD approach, leaves us with the sum of the two contributions of the two large eigenvalues, which is still an unsatisfactory circulation. One way out of this dilemma appears to explicitly prescribe  $u_0$  from some a priori knowledge, but  $u_0$  of course is the most essential part of the signal we actually would like to extract from the data. We consider two other possibilities later: taking deeper data and expanding the model by the bottom boundary condition. Both extensions break the zonality and thus yield better condition indices.

Notice that the almost-singularity does not imply invalidity of the physical model Eq. (5); we are just asking too much if we want three independent parameters from this model. Notice further the potential fallacy in such a situation: the inversion always provides a set of parameters (unless the condition index is exactly zero) and only deeper insight into the inverse machinery and possibly a priori information about the expected solution prevents the acceptance of unreliable results.

### Noise

We have mentioned the possible failure of parameter fitting because of noisy observations. Hydrographic data contain errors from different sources. Instrumental noise may be important in great depths and high latitudes where temperature and salinity vary only a few thousandths of a degree or per mille in the entire water column. Individual sections generally contain aliasing by internal waves and small-scale eddies because of undersampling. The presence of data noise arising from such observational limitations apparently may lead to a masking of the mixing signatures so that mixing parameters may become undeterminable. A more fundamental mistake may be introduced if the original data have been processed in some interpolation or objective analysis scheme which necessarily implies smoothing. This may yield a systematic bias of the mixing effects and estimated mixing coefficients will be oversized.

Frequently the data situation is characterized by a considerable amount of ignorance about the possible structure of noise. Often one hardly can get a reliable value for standard deviation. Hydrographic data are a vivid example in this respect since in many areas of the world ocean--particular high latitudes and greater depths--we have only very few observations and these are subject to a heavy seasonal bias. One hardly can construct a climatological mean, not to speak of variances at all.

The relevant quantities in our problem are not temperature and salinity or related scalars but their gradients, since only these enter the physical model. Even though the scalars may be known accurately enough, the gradients may be very small so that they are statistically not distinguishable from zero. Figure 4 exemplifies this situation for Levitus' analysis (Levitus, 1982) in the central North Atlantic. The estimation of the variance structure of this data set is discussed in detail in Olbers et al. (1985). At depths greater than 2500 m horizontal variations of temperature and salinity become smaller than the estimated standard deviation and reliable gradients cannot be given. This of course destroys any further attempt at parameter estimation in this depth range of the particular data. Fortunately, the deep data in the ACC have significant gradients because in contrast to the North Atlantic the current reaches deep and feels the effects of (nonzonal) topography almost everywhere. This will circumvent the singularity revealed above and enable the determination of the zonal velocity.

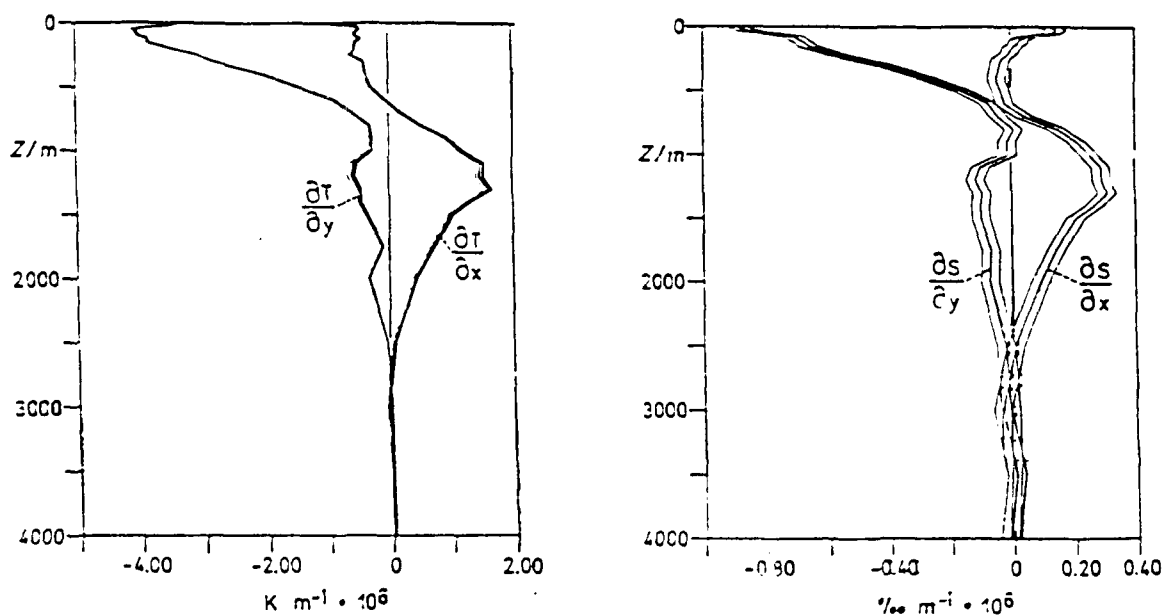


Fig 4. Gradients of temperature (left) and salinity (right) at 35°N, 25°W computed from the Levitus atlas. Strips indicate the estimate of the standard deviation.

If the noise statistics are known it is usually a simple task to study the effect on the estimated parameters by some sort of error propagation analysis. Most inverse techniques are formulated within a statistical framework, and data noise is considered both in the weighting procedure of the model constraints as well as in the evaluation of second order statistics (variances and correlations) of the parameters. In the  $\beta$ -spiral model of the North Atlantic (Olbers et al., 1985) the entire covariance matrix of the parameter was estimated on the basis of a crude model of the data statistic for the analysis scheme of the Levitus atlas. As an example Fig. 5 displays the standard deviation of the diapycnal diffusion coefficient of Fig. 1. The values indicate that in the quiet regions of low eddy activity the estimates of the diffusion coefficient are not significantly different from zero.

Finally we would like to address a problem which at first sight seems to be a mere manipulation of equations and not related to noise at all. Consider, e.g., the physical model described above, which consists of the advective-diffusive balance of a tracer supported by the geostrophic relations and the linearized vorticity balance. Suppose for simplicity that the profiles of the absolute horizontal velocities and the mixing parameters are already known. The remaining task is the determination of

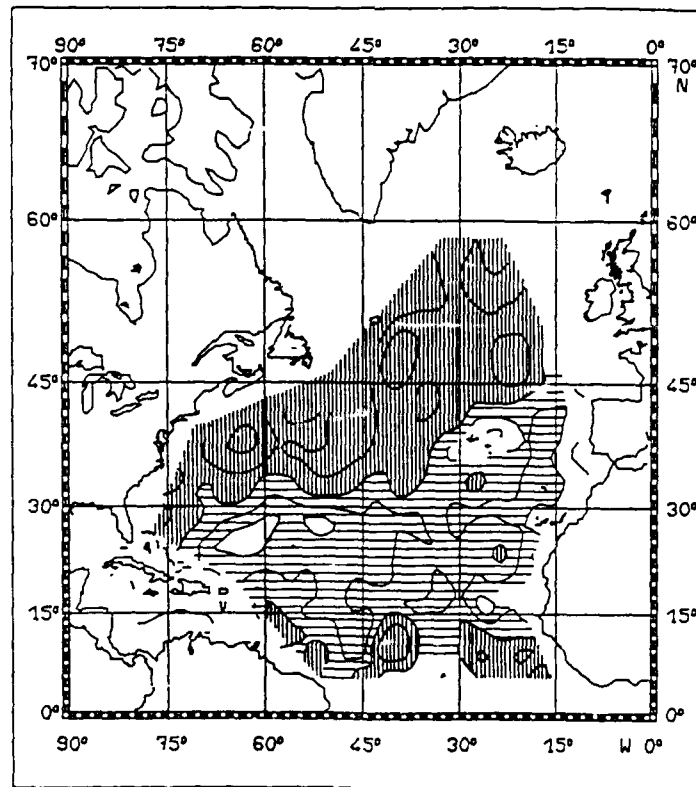


Fig 5. Standard deviations of the diapycnal diffusivities shown in Fig. 1. Hatching indicates values larger than  $10^{-4} \text{ m}^2/\text{s}$  (vertical), values larger than  $10^{-5} \text{ m}^2/\text{s}$  (horizontal) and values below  $10^{-5} \text{ m}^2/\text{s}$  (blank). Contours are logarithmically spaced with interval 0.5.

the profile of the vertical velocity  $w$ . In a straightforward way one would calculate  $w$  at each level, writing the advective-diffusive tracer balance in the form

$$w = (D - u \sigma_x - v \sigma_y) / \sigma_z \quad (6)$$

Alternatively the vorticity balance may be used in the integrated form Eq. (4) with an unknown reference velocity  $w_0$ . This parameter can then be estimated by requiring that the imbalances  $\epsilon(z)$  at all levels  $z$ , given as

$$\epsilon(z) = u \sigma_x + v \sigma_y + (w_0 + w'') \sigma_z - D, \quad (7)$$

be a minimum in a least-square sense. Here  $w''$  represents the remaining terms in the last identity of Eq. (4). At first it can be argued that Eq. (6) should give better results since the tracer balance—apart from the problem of parametrization—appears to be more accurate than the linearized vorticity equation used in Eq. (7). The example in Fig. 6 (taken from Olbers et al., 1985) shows that this need not be true. While the estimate of  $w$  from Eq. (7) looks rather smooth the direct calculation appears very noisy, in particular near the surface.

The relation of this surprising result to the noise structure is as follows. When Eq. (6) is used it is implicitly assumed that the noise originating from the tracer gradient data in this equation is small, in

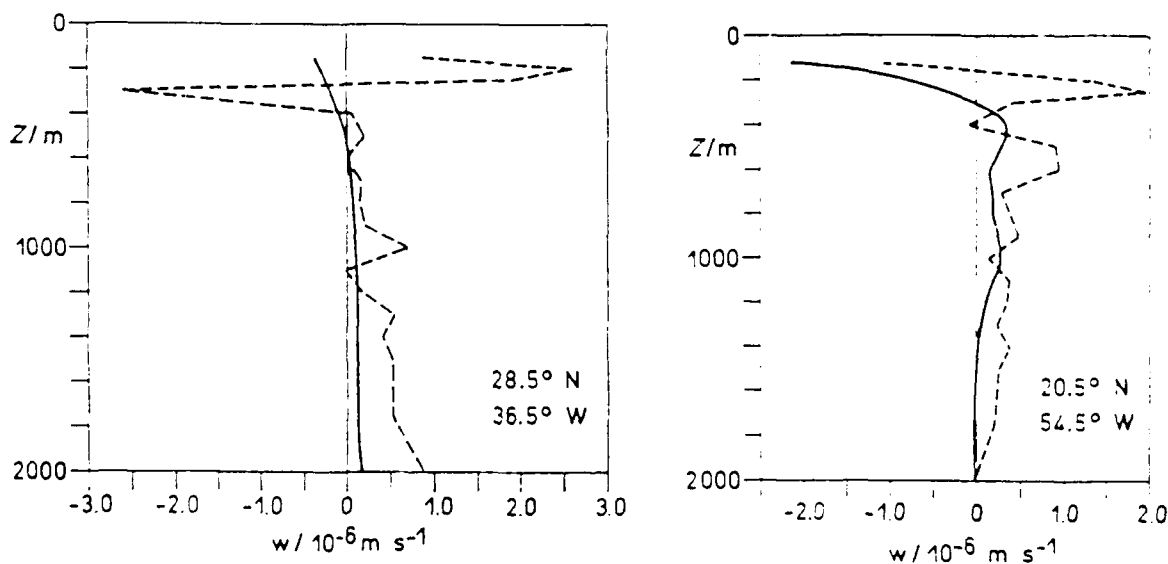


Fig 6. Profiles of the vertical velocity  $w$ . Solid lines represent  $w$  computed from the linear vorticity balance and the least square problem. Eq. (7), and dashed lines give  $w$  computed from the tracer balance, Eq. (6).

fact much smaller than any other term in the equation so that it can entirely be neglected. The method based on Eq. (7), however, allows for noise but denies any noise in the vorticity equation. Obviously, the noise structure in the data does not agree with the assumption leading to Eq. (6): the noise in the tracer balance is not small and the estimate  $w$  collects all of it at every level. The better result of Eq. (7) is due to the consideration of noise--the tracer balance need not be exactly satisfied. Furthermore, the vorticity balance is used here in an integrated form which can be expected to reduce noise amplitudes.

### The parametrization of mixing

So far we have not faced the problem of an adequate parametrization of the mixing effects, i.e., the appropriate form of the functional  $D[\sigma]$  in the tracer balance Eq. (1). In fact, this was one of the topics of the 1989 'Aha Huli' conference, since a comprehensive theory in this field is still lacking. We shall adopt here the traditional parametrization of the turbulent fluxes in terms of the mean gradients  $d_i \sigma$  ( $i = 1, 2, 3$ ) of the tracer  $\sigma$  and write  $D$  in the general diffusive form

$$D[\sigma] = d_i K_{ij} d_j \sigma \quad (8)$$

where  $K_{ij}$  is the diffusion tensor. If this tensor is diagonal in a coordinate system with orthogonal unit vectors  $m_i, q_i, t_i$  with corresponding diffusion coefficients  $K_m, K_q, K_t$  we have

$$K_{ij} = K_m n_i n_j + K_q q_i q_j + K_t t_i t_j \quad (9)$$

The dispute is, of course, about the orientation of the unit vectors and the values of the  $K$ 's. In principle the inverse model should be able to clarify this problem by selecting the different orientations, determining the coefficients and judging the goodness of the fit by some kind of objective measure, if possible even by testing of the different hypotheses within a statistical framework (see, e.g., Müller et al., 1978). In practice, however, we will see that noise, and possibly the bias introduced by data smoothing, wipes out the differences between the interesting cases of mixing models.

According to the traditional convention in modeling, the tensor is considered diagonal in the Cartesian coordinate system with diffusion coefficients representing horizontal (i.e., on geopotential surfaces) and vertical diffusion, respectively. In descriptive oceanography and particularly in water mass analysis, however, it has long been argued (e.g., Montgomery, 1938; Solomon, 1971) that spreading of tracers should preferentially go along isopycnal surfaces because, in a near-adiabatic flow regime, advection and mixing processes should be approximately oriented along the isopycnal surface but for different reasons. In an adiabatic flow, advection conserves potential density exactly so that the velocity vector  $(u, v, w)$  must lie in the local isopycnal (see Eq.



(1) with  $D \equiv 0$ ). Based on a variety of arguments partly discussed below it is widely believed that mixing is favoured along isopycnals, too, so that the mixing tensor should be oriented with respect to these surfaces (Redi, 1982; Olbers et al., 1985).

A main motivation for the preference of isopycnals in mixing processes was sought in the argument that a displacement of a fluid parcel along this surface requires no work against the Archimedean force while a normal displacement would require work. However, this is strictly correct only at the reference level of the potential density and a thorough investigation leads to the replacement of isopycnals by the so-called neutral surfaces (McDougall, 1987). This surface comprises the infinitesimal directions a particle can move without experiencing a buoyant restoring force. By this definition the neutral surface is locally tangent to the isopycnal if the potential density is referred to the local pressure.

A further sensible orientation of the mixing tensor has been suggested by Olbers and Wenzel (1989) analysing the particular form of the work done by the Archimedean force during the displacement  $d\mathbf{x}$

$$dA = \rho (\alpha \text{ grad } \theta - \beta \text{ grad } S) \cdot d\mathbf{x} (\text{grad } \Phi \cdot d\mathbf{x}) \quad (10)$$

The work vanishes on both the neutral surface (where  $\alpha \text{ grad } \theta = \beta \text{ grad } S$ ) and the geopotential surface (since  $\text{grad } \Phi$  and  $d\mathbf{x}$  are normal here), so that from the energetics point of view we seem not to be able to distinguish between isopycnal-neutral-surface mixing and the ordinary lateral mixing form. However, for certain directions of displacement (in fact those of the baroclinic instability mechanism)  $dA$  may as well be positive. This occurs for the angle range between the neutral and the geopotential surfaces where available potential energy is converted if the particle is displaced. The energy conversion is a maximum at half of the angle between the neutral and the geopotential surfaces. So based on the energy argument this should be the direction favoured by mixing. Mixing along this direction implies mixing both along and across neutral surfaces. A canonical parametrization of mixing effects in this framework then appears in the form of a diagonal tensor with three independent coefficients in the coordinate system, given by the intersection of the neutral and the geopotential surfaces (where  $dA = 0$ ), the orthogonal direction in the half angle plane (where  $dA$  is maximum, i.e., maximum energy conversion) and the normal direction (where  $dA$  is minimum, i.e. maximum input of energy is required).

## SOLUTIONS

### The bottom connection

The singularity of the solution exemplified in Fig. 3 had its origin in the zonality of the tracers in the upper part of the water column (100-800 m) of the Southern Ocean data set. To overcome the zonality of the problem the set of  $\beta$ -spiral equations, Eq. (5) must be augmented by

constraints with non-zonal properties. Since the ACC has a strong barotropic component the current must be affected by the bottom topography. At the bottom it has to satisfy the kinematic boundary condition

$$w + \mathbf{u} \cdot \text{grad } H = 0 \quad \text{at the bottom } z = -H \quad (11)$$

Strictly, this applies to the total velocity and not to the geostrophic part alone. If a frictional boundary layer is present each component of the total velocity vector must separately vanish at the bottom and the behaviour of the geostrophic velocity is a matter of the entire dynamical problem. Still, in case of weak frictional effects we expect that the geostrophic velocity adjusts to approximately satisfy Eq. (11) close to the bottom. Considering Eq. (4) this may be written in the form

$$\begin{aligned} w_0 - (\beta/f)(H + z_0)v_0 + \mathbf{u}_0 \cdot \text{grad } H \\ = -w' - \mathbf{u}' \cdot \text{grad } H \quad \text{at } z = -H \end{aligned} \quad (12)$$

Apparently, in this equation  $\mathbf{u}_0$  is no longer multiplied by a small factor since the topography in the Southern Ocean shows almost everywhere strong non-zonal patterns. Adding this constraint to the set of  $\beta$ -spiral Eqs. (5) we thus expect a better condition of the corresponding inverse problem.

Using the identical upper ocean tracer relations as the one before and deep data to incorporate the relation (12) in a suitably weighted form, the resulting matrix condition and reference velocities confirm this presumption. The condition index lies well above  $10^{-3}$  almost everywhere and the reference velocities point eastward in the Atlantic and by and large also in parts of the Indian and Pacific oceans. Corresponding experiments have been made with data from deeper parts of the water column. In fact, the deep structure of the tracer distribution is considerably influenced by the topography and is basically non-zonal. For the results displayed in Fig. 7 only deep data below 2000 m were used in connection with the bottom boundary condition. The reference velocities are in good agreement with our presumption of the circulation in the Southern Ocean.

#### Mass conservation

The estimate of the three-dimensional velocity field obtained by the  $\beta$ -spiral approach does generally not satisfy continuity. This is a consequence of a local estimation procedure which determines velocity profiles from the local gradients of density and tracers without taking care of the neighbouring velocities. One can of course design inverse methods which consider continuity from the beginning. However, with high resolution in a large region as, e.g., the Southern Ocean the number of unknowns will be too large to obtain a manageable problem. Hence we decided to investigate in a separate step how severe the violation of continuity is and how much the  $\beta$ -spiral results must be changed in order

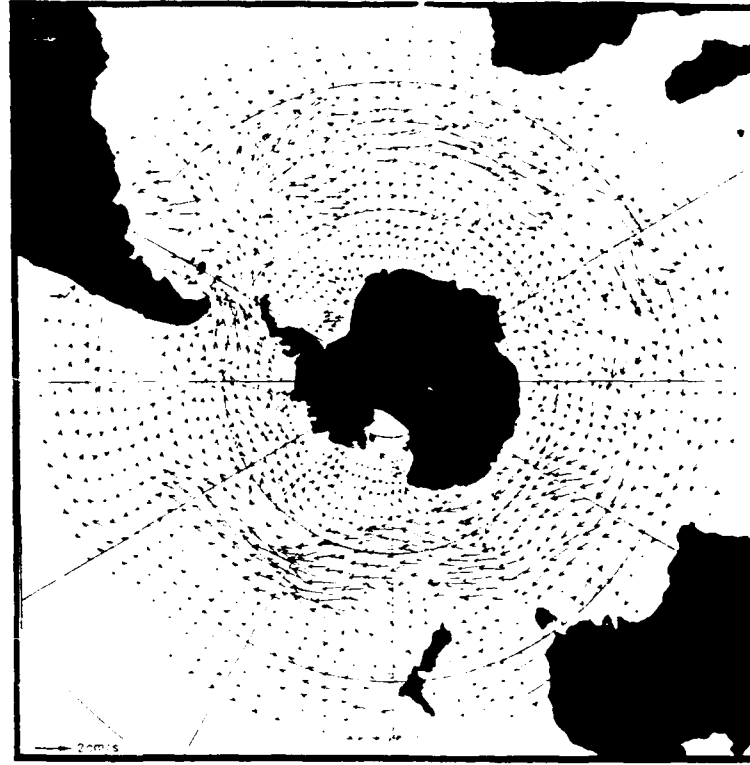


Fig 7. The absolute horizontal velocity at 2000 m depth in the Southern Ocean, obtained from 2000-m bottom data and an adiabatic  $\beta$ -spiral model with inclusion of the kinematic bottom boundary condition, Eq. (12).

to get a mass conserving velocity field. The procedure which we present here has been devised by Wenzel (1986) and applied first to the  $\beta$ -spiral results of the North Atlantic.

Close to the surface we should include the Ekman part to define the total velocity vector by

$$\mathbf{u}^* = \mathbf{u}_g + \mathbf{u}_E \quad (13)$$

where  $\mathbf{u}_g$  is the geostrophic part from the  $\beta$ -spiral. The Ekman part  $\mathbf{u}_E$  can be calculated from the wind stress using the Ekman theory of a frictional wind-driven boundary layer. The simplest way would be to distribute the Ekman mass transport over the (assumed) depth of the Ekman layer.

So consider the task to find a velocity field  $\mathbf{u} = (u, v, w)$  which is free of divergence and as close as possible to a given field  $\mathbf{u}^* = (u^*, v^*, w^*)$ . We have to solve the variational principle

$$\int d^3x \, \| \mathbf{u} - \mathbf{u}^* \|^2 = \min \quad (14)$$

subject to the constraints that  $\text{div } \underline{u} = 0$  (or  $\underline{u} = \text{curl } \underline{A}$  in terms of the vector potential  $\underline{A}$ ) and the kinematic boundary conditions at vertical and lateral boundaries

$$\begin{aligned} w &= 0 && \text{at the surface } z = 0 \\ w + \underline{u} \cdot \text{grad } H &= 0 && \text{at the bottom } z = -H \\ \underline{u}^\perp &= 0 && \text{at closed lateral boundaries} \\ \underline{u}^\parallel &= \underline{u}^{\star\parallel} && \text{at open lateral boundaries} \end{aligned} \tag{15}$$

where  $\underline{u}^\perp$  and  $\underline{u}^\parallel$  are the normal and tangential velocity vectors, respectively. The last condition appears best in view of our task to determine a closely neighbouring velocity field which is free of divergence; and, indeed, it is the canonical boundary condition for the variational principle. The norm in Eq. (14) is taken diagonal with a suitable weighting of the vertical part relative to the horizontal parts. Also the separate levels can be weighted differently. In view of increasing errors in the assumption of a linear vorticity balance without horizontal friction, we chose smaller weights in the surface layers so that there  $w$  will essentially be determined by the continuity constraint.

Eq. (14) yields three coupled second order differential equations for the three components of the vector potential. For further details such as weighting and numerical algorithms, we refer to Wenzel (1986). By and large the mass conservation leads to a smoothing of the circulation. The corrections to the geostrophic velocity are generally small except near the surface where the Ekman pumping dominates the vertical velocity (see Olbers and Wenzel, 1989).

### Strategies

The model described in the preceding section contains about five to ten different parameters which can be determined at each point of the gridded hydrographic data set. Besides the parameters in the dynamical balances--the three reference velocities and the parameters appearing in the term  $F$  for the mixing of vorticity--we have up to three diffusivities in the tracer balance. For the Levitus data we have eliminated the deep part below 2000 m because of insufficient accuracy of the gradients of temperature and salinity while in the Gordon data the upper part above 2000 m turned out to be useless for the determination of reference velocities because of the strong zonality of the tracer fields. In both data sets roughly 10 to 20 levels remain at which the  $\beta$ -spiral constraint, Eq. (5), can be applied. There are many sensible ways to set up the inverse model. In particular, if the mixing parameters should be determined outside the depth range of the applicability of Eq. (5), a strategy must be worked out for an optimum extraction of information from the data. Apparently, a strategy will

always be associated with a particular data set, however, certain elements have proved to be more general:

- a. The depth range for the determination of the reference velocities should be chosen as to maximize the condition index of the matrix to be inverted.
- b. It should be attempted to separate the entire problem into subdivisions each of which only attacks certain subsets of the parameter fitting. As an example, diapycnal and isopycnal diffusivities can be determined successively from separate data structures since isopycnal mixing does not affect the potential density.
- c. The fitting procedure can be iterated by implementing the mass conserving scheme and using the resulting circulation for the determination of mixing effects to obtain smoother parameter patterns.

#### Mixing coefficients

The diapycnal mixing coefficient for the range 100–800 m of the North Atlantic model has been discussed above in Fig. 1. The coefficient decreases with depth, the values for 800–2000 m are smaller by an order of magnitude. The structure of the isopycnal coefficient looks quite similar with peak values of  $10^3 \text{ m}^2/\text{s}$  in the regions of strong currents and undetectably small values in the quiet regions (set to zero by the positiveness constraint of the inverse model). As exemplified in Fig. 5 the values of the coefficients are but marginally statistically significant. This is in particular true for the deeper values. It is mainly the plausible overall pattern that supports our belief in their physical significance.

The situation in the Southern Ocean model is quite different. A first estimate of the reference velocities (with consideration of diapycnal and vorticity diffusion) were determined from the balance of potential density at the levels between 2000 m and the bottom. The mass conserving circulation was determined as described above taking the wind stress data of Hellerman and Rosenstein (1983). This velocity field was then taken to estimate the diffusive part of the solution.

Various parametrizations of the mixing term  $D[\sigma]$  in the tracer balance Eq. (1) were implemented to determine the unknown parameters of the diffusion tensor  $K_{ij}$ . We report here on three sets of experiments:

- the standard model uses potential density (referred to the local pressure) to determine the diabatic coefficient and vorticity to determine the isopycnal coefficient,
- models with either potential density or vorticity to determine the coefficients for horizontal and vertical mixing,

- and two experiments aiming at the differences between the isopycnal form and the half-angle form (based on the argument of the baroclinic instability mechanism) of the mixing tensor.

The differences between these models are quite small and the common pattern is displayed in Fig. 8 showing the regional distribution of the diapycnal and isopycnal diffusivities for the depth intervals 100–800 m. Figure 9 gives the zonal averages of these quantities and the 800–2500 m and 2000 m bottom values. The diapycnal diffusivity has a pronounced peak in the core of the ACC and increases significantly with depth. Along the current path there are some well defined maxima (with values of a few  $10^{-4} \text{ m}^2/\text{s}$  in the upper layer and exceeding  $10^{-3} \text{ m}^2/\text{s}$  in the deep ocean) which generally extend through the entire water column. The isopycnal coefficients reveal a similar horizontal pattern but a slight decrease from top to bottom with values of  $10^3 \text{ m}^2/\text{s}$  in the upper layer dropping down to a few  $10^2 \text{ m}^2/\text{s}$  at greater depth. It appears that the decrease away from the ACC to the northern subtropical gyres is less than towards the southern subpolar gyres (except for the eastern Pacific region).

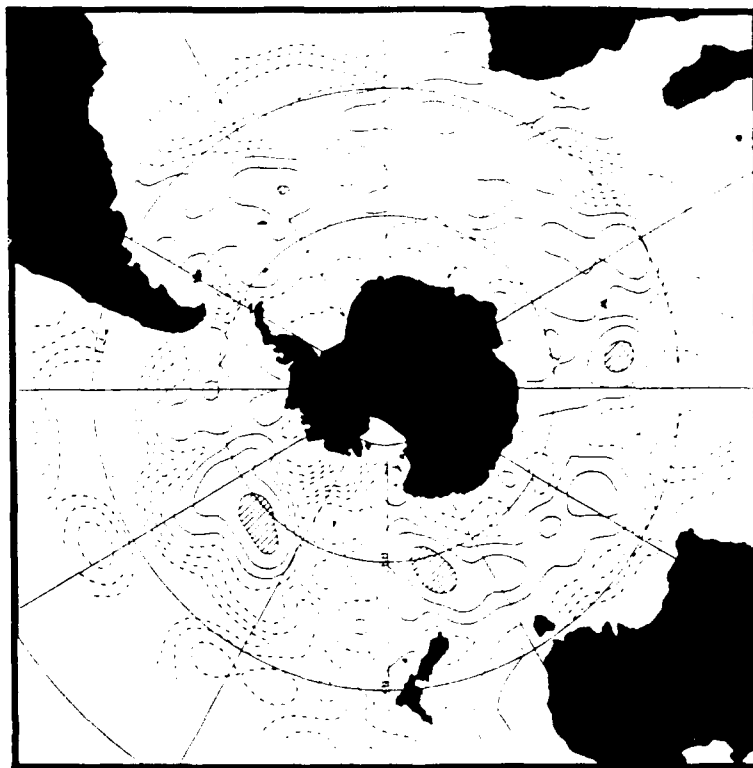


Fig 8a. Map of the diapycnal diffusivities for the depth range 100–800 m. Contours are logarithmically spaced with interval 0.5. Contours  $> 10^{-4} \text{ m}^2/\text{s}$  are full and  $< 10^{-4} \text{ m}^2/\text{s}$  dashed. Areas with values  $> 10^{-3} \text{ m}^2/\text{s}$  are shaded.

The correlation of the pattern of the diffusivities with the current core is quite obvious. It is tempting to search for more connections to environmental conditions such as topography, current speed or eddy kinetic energy. With some intention one could easily find correspondences between areas of large diffusivities and the hot spots of eddy activity as visible in the maps of rms surface topography determined from SEASAT altimetry (Cheney et al., 1983) or the maps of eddy kinetic energy determined from the FGGE drifters (Daniault and Menard, 1985). We are reluctant to value such findings, partly because the current path itself is correlated with all these parameters and partly due to our inability to give sufficiently accurate estimates of the parameter variance.

A comparison between the performance of the isopycnal and the Cartesian (horizontal and vertical) orientation of the mixing tensor can be drawn from Fig. 9 and Fig. 10, the latter being the result of fitting the Cartesian form to potential density conservation. There are no striking differences between the corresponding coefficients, neither in the

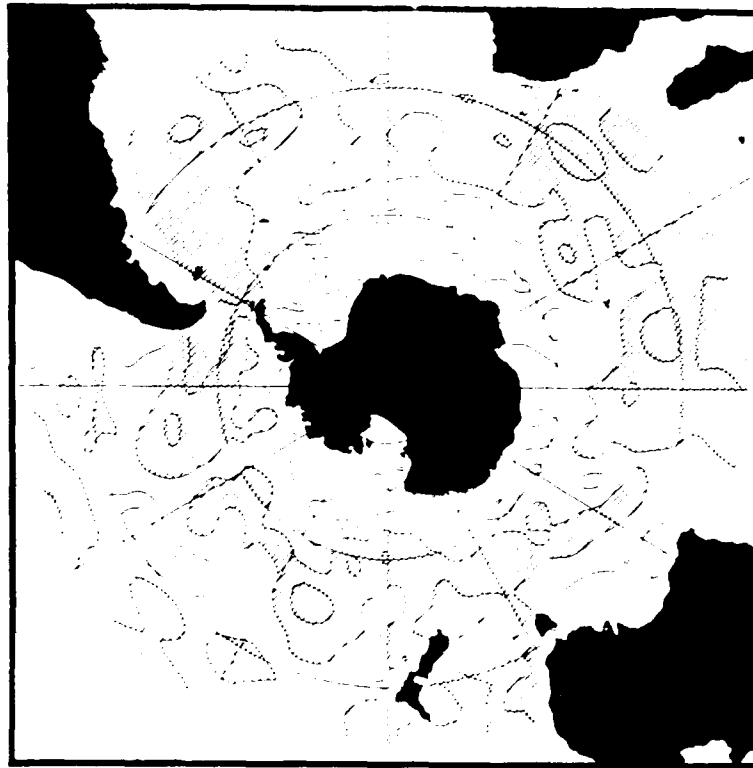


Fig 8b. Map of the isopycnal diffusivities for the depth range 100-800 m. Contours are logarithmically spaced with interval 0.5. Contours  $> 10^2 \text{ m}^2/\text{s}$  are full and  $< 10^2 \text{ m}^2/\text{s}$  dashed. Areas with values  $> 10^3 \text{ m}^2/\text{s}$  are shaded.

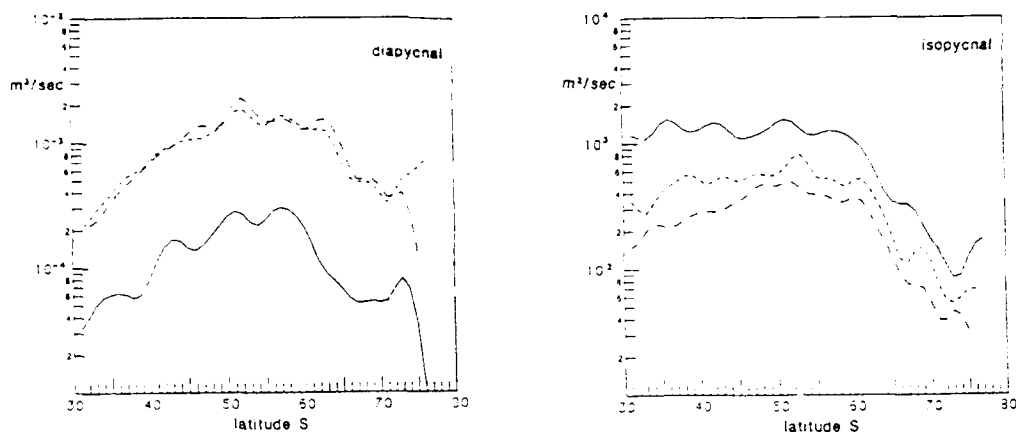


Fig 9. Zonal averages of (a) the diapycnal diffusivities and (b) the isopycnal diffusivity shown in Fig 8. Solid line corresponds to 100-800 m values, narrow dashed to 800-2500 m values and wide dashed to 2000-m bottom values.

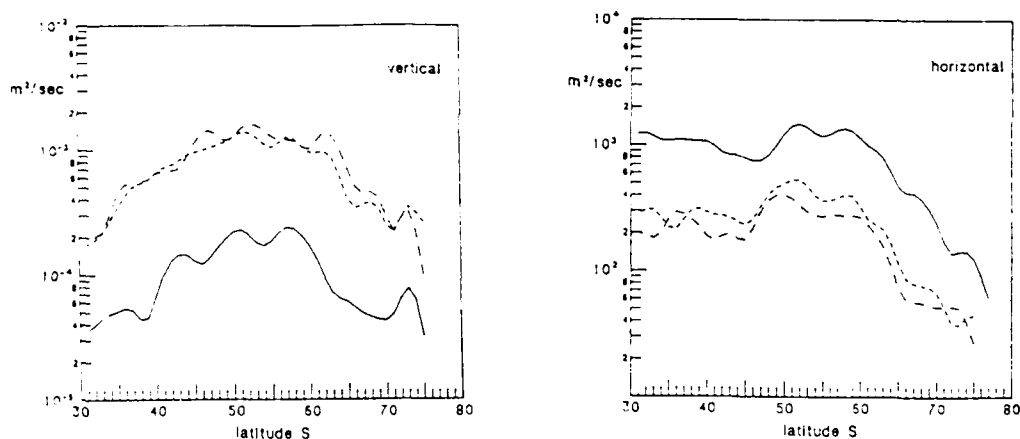


Fig 10. Same as Fig. 9, but for vertical and horizontal diffusivities. Solid lines correspond to 100-800 m values, narrow dashed to 800-2500 m values and wide dashed to 2000-m bottom values.

typical magnitudes nor the overall pattern. What fit should be judged superior, however? Can we decide whether the ocean is mixed along isopycnal or geopotential surfaces? A decent answer to this important question would require the careful statistical framework and an adequate knowledge of the data statistics which are necessary to formulate and test hypotheses about the models we are using (see, e.g., Müller et al. (1978) and Wunsch (1989)). The lack of a sensible model of the covariances of the analysed temperature and salinity fields of Gordon's atlas prevented us from going along this well-established path of inverse techniques.

As a substitute for statistical testing we consider here the skill achieved by the two competing models. The normalized sum of the squared



imbalances of the model equations Eq. (5) is used to form a skill measure comparing the performance of each of the diffusive models in comparison to an entirely advective model. The skill is defined here then as the relative reduction of the squared imbalances of the diffusive model and the squared imbalances of the purely advective model. To make a meaningful decision between different models the number of parameters allowed in the fits must obviously be the same. This is not the case for the results of Figs. 9 and 10 since the isopycnal coefficient drops out of the balance of potential density. Figure 11 shows the skills achieved with an isopycnal and a Cartesian diffusion tensor in the balance of veronicity. There is no apparent distinction between the models in the upper layer (100-800 m). However, in the deep ocean south of 50°S the isopycnal diffusion seems to work slightly better than the Cartesian diffusion, the skill is up to 5% larger. The zonal averages shown here are in fact representative for the areal patterns. We have to conclude that diffusion along isopycnals is a slightly better parametrization of mixing in the Circumpolar Current than diffusion along geopotential surfaces. It may well be, however that these small differences become insignificant when the noise structure of the data is invoked to calculate variances of the skills considered here. In any case, what remains is the quite unexpected result that the isopycnal diffusion tensor is not drastically superior to the Cartesian tensor, even in an oceanic area as the Circumpolar Current where the isopycnal slopes are large.

The last set of model comparisons considered here aimed at the distinction between the half-angle orientation of the mixing tensors, based on the energy conversion arguments discussed above. With the above

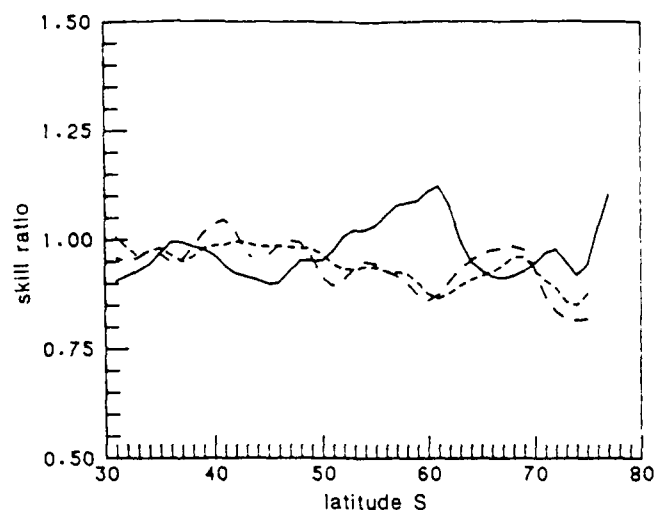


Fig 11. The skill of the two models with Cartesian orientation and isopycnal orientation of the mixing tensor. Solid lines correspond to 100-800 m values, narrow dashed to 800-2500 m values and wide dashed to 2000-m bottom values.

results in mind one would of course not expect any great differences of the half-angle models from any of the other models. Indeed, corresponding isopycnal and half-angle models turned out almost indistinguishable. As an interesting side remark, however, we like to point out that the mixing tensor of this model is anisotropic in the neutral surface so that fair comparison with isopycnal or Cartesian diffusion requires rewriting these mixing tensors in an anisotropic form, too. The result is exemplified in Fig. 12. There is clear evidence for anisotropy in the upper layer, the horizontal coefficient exceeds the maximum gain coefficient by a factor of two. With the orientation of the neutral surfaces in the area of the ACC this means larger diffusivity along the current.

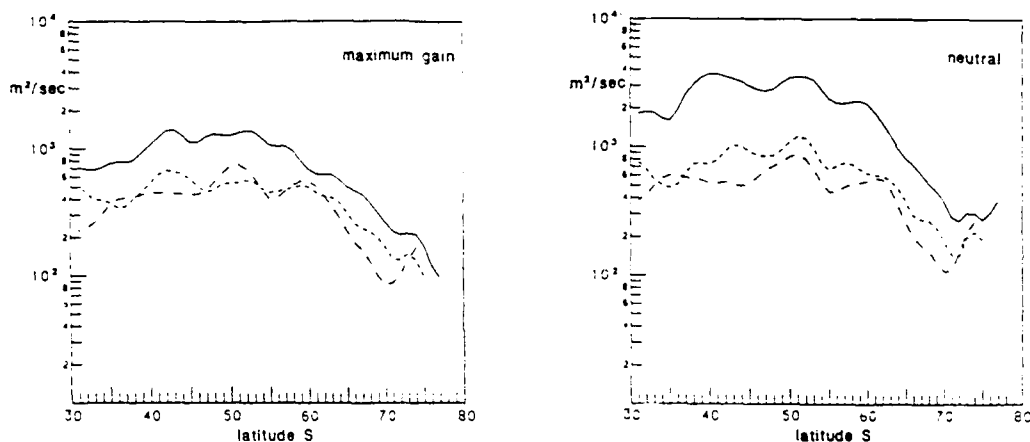


Fig 12. Zonal averages of the diffusivities for an anisotropic model in the half-angle plane, (a) for direction of maximum energy gain and (b) for the neutral direction. Solid lines correspond to 100-800 m values, narrow dashed to 800-2500 m values and wide dashed to 2000-m bottom values.

## SUMMARY

Inverse models have recently been utilized to obtain estimates of the mixing properties in the large scale ocean circulation on the basis of the momentum, vorticity, heat and salt balances. The  $\beta$ -spiral method of Stommel and Schott (1977)—first applied in a strictly adiabatic version in the North Atlantic (see also Schott and Stommel, 1978)—can be extended to diabatic conditions to give estimates of the parameters which control the diffusion of heat and salt. The consideration of the diffusion terms in the balances for tracers and vorticity are conceptually simple (e.g., Olbers et al., 1985; Bigg, 1985; Olbers and Wenzel, 1989). The determination of diffusion coefficients, however, is coupled to the classical level-of-no-motion problem—the determination of absolute velocities from a hydrographic section. The physical model then must incorporate the advective-diffusive balance equations for the

tracers and the momentum balance, usually in some approximated form adequate for a large scale flow.

In terms of the unknown parameters--the diffusion coefficients and the reference velocities--the mathematical relations of such a model are linear so that linear inversion schemes may be used. Still, if large amounts of data and relations are involved the problem may be rather complex since intrinsic interdependencies and inconsistencies are not immediately evident. We have pointed out several problems which may occur in the course of such an inversion, notably the case of improperly formulated constraints leading to an ill-conditioned inverse problem and the effect of different models of the noise in the data (which is rarely known for an hydrographic atlas) leading to drastically different parameter estimates.

The diffusion coefficients obtained by our extended  $\beta$ -spiral approach from the climatological averaged and gridded data of Levitus (1982) and Gordon et al. (1982) show patterns which by and large confirm our conception of the mixing activity in the ocean: larger values occur in areas of strong currents and eddy activity. The peak values, however, appear sometimes fairly large: in the ACC we get diapycnal coefficients up to  $10^{-3} \text{ m}^2/\text{s}$ . In our present position of ignorance about the mixing processes in this region of the ocean we cannot entirely deny the physical reality of these results. It may well be, however, that the effect is largely caused by a bias due to the climatological smoothing of the data. Such a smooth state is of course never realized in the ocean and one may argue that mixing is smaller in any actual configuration. In any case, we must bear in mind that these large coefficients are appropriate to such a state which is not unlike the outcome of most ocean general circulation models. In fact, following our analysis they are the optimal values.

These studies were partly supported by BMFT contract 07KF221/1. This is contribution number 195 of the Alfred Wegener-Institut für Polar- und Meeresforschung.

## REFERENCES

- Bigg, G.R.: 1985. The beta spiral method, *Deep-Sea Res.* 32, 465-484.
- Cheney, R.E., Marsh, J.G. and B.D. Beckley: 1983. Global mesoscale variability from collinear tracks of SEASAT altimeter data, *J. Geophys. Res.* 88, 4343-4354.
- Daniault, N. and Y. Menard: 1985. Eddy kinetic energy distribution in the Southern Ocean from altimetry and FGGE drifting buoys, *J. Geophys. Res.* 90, 11877-11889.
- Gordon, A.L., Molinelli E. and T. Baker: 1982. *Southern Ocean Atlas*, Columbia University Press.
- Hellermann, S. and M. Rosenstein: 1983. Normal monthly wind stress over the world ocean with error estimates, *J. Phys. Oceanogr.* 13, 1093-1104.

- Levitus, S.: 1982. Climatological atlas of the world ocean, NOAA Tech Paper. 3, 173 pp.
- McDougall, T.J.: 1987. Neutral Surfaces, *J. Phys. Oceanogr.* 17, 1950-1963.
- Montgomery, R.B.: 1938. Circulation in upper layers of southern North Atlantic deduced with use of isentropic analysis, *Pap. Phys. Oceanogr. Meteorol.* 6, 55 pp.
- Müller, P., Olbers, D. and J. Willebrand: 1978. The IWEX spectrum, *J. Geophys. Res.* 83, 479-500.
- Munk, W.H.: 1966. Abyssal recipes, *Deep-Sea Res.* 13, 707-730.
- Olbers, D.J., Wenzel, M. and J. Willebrand: 1985. The inference of North Atlantic circulation patterns from climatological hydrographic data, *Rev. Geophys.* 23, 313-356.
- Olbers, D.: 1989. A geometrical interpretation of inverse problems. In: Modeling the ocean circulation and transient tracer transport, D. Anderson and J. Willebrand (Eds.) (in press).
- Olbers, D., and M. Wenzel: 1989. Determining diffusivities from hydrodynamic data by inverse methods with applications to the Circumpolar Current. In: Modeling the ocean circulation and transient tracer transport, D. Anderson and J. Willebrand (Eds.) (in press).
- Pedlosky, J.: 1978. *Geophysical Fluid Dynamics*, Springer Verlag, 624 pp.
- Schott, F. and H. Stommel: 1978. Beta spirals and absolute velocities from different oceans, *Deep-Sea Res.* 25, 961-1010.
- Solomon, H.: 1971. On the representation of isentropic mixing in ocean circulation models, *J. Phys. Oceanogr.* 1, 233-234.
- Stommel, H. and F. Schott: 1977. The beta spiral and the determination of the absolute velocity field from hydrographic station data, *Deep-Sea Res.* 24, 325-329.
- Veronis, G.: 1972. On properties of seawater defined by temperature, *Deep-Sea Res.* 24, 325-329.
- Veronis, G.: 1972. On properties of seawater defined by temperature, salinity, and pressure, *J. Mar. Res.* 30, 227-255.
- Wenzel, M.: 1986. Die mittlere Zirkulation des Nordatlantik auf der Grundlage klimatologischer hydrographischer Daten, *Berichte Institut für Meereskunde Kiel* 157, 109 pp.
- Wunsch, C.: 1989. Tracer inverse problems. In: Modeling the ocean circulation and transient tracer transport, D. Anderson and J. Willebrand (Eds.) (in press).

## **TURBULENT MIXING ACROSS DENSITY INTERFACES: A REVIEW OF LABORATORY EXPERIMENTS AND THEIR OCEANOGRAPHIC IMPLICATIONS**

Harindra J. S. Fernando

Department of Mechanical and Aerospace Engineering, Arizona State University,  
Tempe, AZ 85287-6106

### **ABSTRACT**

Oceanic observations are usually influenced by many intermingled physical processes that interact in such a way that it is difficult to study each process in detail. Laboratory studies are extremely useful to this end and, in particular, can provide fundamental understanding of small-scale oceanic mixing processes. Such understanding is the basis for the development of sound parameterizations for these processes. In this paper, the results of some recent laboratory experiments on turbulent mixing across density interfaces are summarized and their possible oceanic applications are described.

### **1. INTRODUCTION**

An understanding of mixing across density interfaces is imperative in studies of the dynamics of the upper ocean and the lower atmosphere. In the former case, the turbulence generated by wave breaking, velocity shear and surface cooling interacts with the thermocline and erodes it, thereby increasing the depth of the upper mixed layer. In view of the impact of upper-ocean dynamics on global-scale motions, studies of mixed layer deepening have been a center of attention among oceanographers. Although a large number of theoretical, numerical and laboratory studies on mixing across density interfaces have been reported, understanding of the subject is far from complete. As in other turbulence problems, modeling of mixed layer processes requires sound closure hypotheses, which can be conceived only after understanding the underlying physics. In this regard, laboratory experiments are known to be a useful tool.

During (oceanic) thermocline mixing many turbulence generating mechanisms, such as velocity shear, wave breaking and buoyant convection, are simultaneously active so that it is difficult to discern the effects due to a particular turbulence source. In addition, the interaction between two mechanisms may produce a flow situation that prevents probing into the individual contributory mechanisms. In general, laboratory experiments are designed to study a single mixing mechanism with the hope that the resulting fundamental knowledge will be useful in delineating the flow structure in the presence of multiple mechanisms. Laboratory observations also provide useful clues for interpreting various oceanic observations, at least qualitatively. However, direct application of laboratory results to the ocean has to be done with caution as there are vast differences between them; unlike laboratory situations, oceanic phenomena are generally three dimensional and represent the combined effect of different, possibly interacting, physical mechanisms.

The aim of this paper is to note some advances in experimental laboratory research on turbulent mixing across density interfaces and to briefly discuss their geophysical implications. These experiments can be subdivided into three categories, according to the

turbulence generating mechanism. They are: i) experiments with interfacial velocity shear; ii) experiments with shear-free energy sources; and iii) experiments that employ a combination of i) and ii).

## 2. INTERFACIAL MIXING DUE TO SHEAR-FREE TURBULENCE

Laboratory experiments reported in this context fall into two categories, namely, (1) mechanically induced zero-mean-shear turbulence and (2) convective turbulence.

### 2.1 Mechanically-Induced Turbulence

It has been customary to use oscillating-grid induced, spatially decaying turbulence in stratified turbulent mixing studies. Most experiments of this type are one-dimensional mixing-box experiments in which a stratified fluid is agitated by an oscillating grid; hence, the following discussion is limited to this particular case. Both laboratory and oceanic observations show that, sufficiently far from the grid, the nature of the grid-induced turbulence is similar to that generated beneath breaking waves (Kitaigorodskii, 1979; Wang and Wu, 1985; Jones, 1985). The first quantitative experiment was performed by Turner (1968), who studied the rate of entrainment across a density interface  $u_e$  as a function of the interfacial stability. Based on his experimental results, the entrainment law was proposed to be

$$E = u_e/u = c_1 Ri^{-n}, \quad (2.1)$$

where  $n = 3/2$  for salt-stratified fluids and  $n = 1$  for heat-stratified fluids. Here  $E$  is the entrainment coefficient,  $u$  is the r.m.s horizontal velocity near the interface,  $Ri = \Delta b h / u^2$  is the bulk Richardson number,  $h$  is the depth of the mixed layer,  $\Delta b$  is the buoyancy jump across the interface and  $c_1, c_2, \dots$  are henceforth used to denote constants. Since Turner's work, there has been much controversy over the value of  $n$ , which, unfortunately, despite many exhaustive attempts, has not been resolved. Linden (1975) argued that the rate of potential-energy increase of the fluid system due to mixing should be proportional to the kinetic energy flux ( $\sim u^3$ ) available at the interface. This argument has led to an entrainment law with  $n = 1$ , which was found to be in reasonably good agreement with Linden's experiments with salt stratified fluids. Long (1978) argued that only a portion of the energy flux available at the density interface is transported to the interfacial layer that separates the turbulent and non-turbulent layers, and in which the active turbulent mixing takes place. At large  $Ri$ , large scale turbulent eddies near the interface were shown to be anisotropic, with the r.m.s. vertical velocity  $w$  much smaller than the horizontal counterpart. Hannoun, Fernando and List (1988) have demonstrated the validity of Long's hypothesis of anisotropy at large scales. The variation of the turbulent-energy spectra with the normalized distance from the density interface  $\xi/L_0$  where  $L_0$  is the integral length-scale is shown in Figure 1. It is believed that the flattening of the eddies near the interface, as discussed by Hunt and Graham (1978) and Hunt (1984), is the cause of such anisotropy (also see McDougall, 1979). Eddy flattening leads to an intercomponent energy transfer from vertical to horizontal scales, as shown in Figure 2.

According to Long (1978), since  $w \ll u$  and since  $w$  is continuous across the interface, energy flux transferred into the interfacial region is much smaller than the turbulent energy available near the interface. Assuming that mixing occurs due to intermittent breaking of interfacial waves by saturation, which produces mixed turbulent patches at the entrainment interface, Long developed a theory which predicts  $n = 7/4$ . Support for this theory has

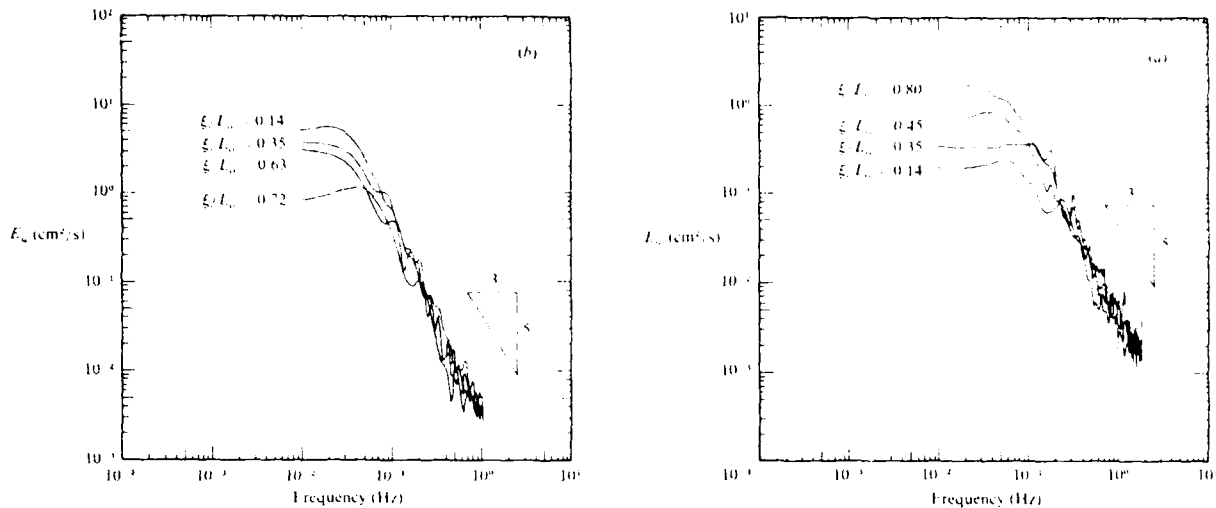


Fig. 1. Frequency spectra of turbulent velocity fluctuations (left) horizontal velocity  $u$  and (right) vertical velocity  $w$ .

been provided by Folsø, Cox and Schenayder (1981), Fernando and Long (1983, 1985a,b) and Noh and Long (1989). E and Hopfinger (1986), however, reconfirmed the earlier finding of Turner (1968) and Hopfinger and Toly (1976), which showed  $n = 3/2$  for salt stratified fluids. They postulated that the results of experiments which show  $n = 7/4$  may have been contaminated by secondary circulations in the test cell. Further support for  $n = 3/2$  behaviour can be seen in Hannoun and List (1988) and Altman and Gargett (1989). Other recent results from Nokes (1988) show that the correct exponent is  $n = 1.21$ , which is as predicted by McDougall (1978) on the basis of a least-square fit to Turner's data. According to Nokes, errors may have been introduced into the E and Hopfinger data due to the use of an empirical formula to evaluate the integral length-scale of turbulence near the interface. One of the problems that arises in data handling of such experiments is the selection of the virtual origin from which the length measurements are made. Different investigators have used different methods to determine its location and the entrainment law appears to be strongly dependent on this selection. In future experiments, it is suggested that a consistent way of determining the virtual origin be used so that the results of various investigators can be compared effectively.

Substantial progress has been made with regard to the understanding of the entrainment mechanism. The experiments of Hannoun and List (1988), performed using advanced laser imaging techniques, have established that turbulent mixing occurs by interfacial wave breaking, as proposed by Long (1978). According to Fernando (1988), however, the wave breaking mechanism is operative only in a specific intermediate  $Ri$  range. At low  $Ri$ , entrainment occurs by the splashing of non-turbulent fluid into the mixed layer by impinging eddies on the interface, as proposed by Linden (1973), whereas, at very high  $Ri$ , wave-breaking events disappear, as reported by Crapper and Linden (1974) and Hannoun and List (1988), and the interface tends to be dominated by molecular diffusive processes.

Once the interface becomes diffusive, there is a sudden decrease in the entrainment rate. Crapper and Linden suggested that the interface becomes diffusive when the Peclet number  $Pe = uL_0/k$ , where  $k$  is the molecular diffusivity of the stratifying agent, falls below 200.

More extensive measurements have, however, revealed that the criterion for the occurrence of diffusive interfaces is

$$Ri_\ell = \Delta b L_0 / u^2 > c_2 Pe^{1/2} \quad (2.2)$$

(Noh and Fernando, 1989). Theoretical arguments suggest  $c_2 = 1.6 Pr$ , where  $Pr$  is the Prandtl number; this result awaits experimental verification. According to Noh and Fernando, transition from an active (wave-breaking) to a molecular-diffusion dominated interface occurs when the rate of decay of internal-wave energy exceeds the rate of energy supply from turbulence. They also showed that the mixed-layer growth under this condition is intermittent. Molecular diffusion takes place at the entrainment interface till the buoyancy gradient is small enough to be engulfed by the mixed-layer eddies; at that time a sudden increase in the mixed layer can be seen. The corresponding entrainment law was shown to be  $E = c_3 Ri^{-2} Pe^{-2}$ .

Another debated, but experimentally less-studied, issue is the radiation of internal waves from the entrainment interface into the outer stratified layer. Based on implicit experimental evidence, Linden (1975) argued that such a wave radiation is important and can have a significant effect on the energy budget at the entrainment interface. Theoretical calculations of Kantha (1979) and Carruthers and Hunt (1986) as well as direct numerical simulations of Riley and Metcalfe (1987) also show that internal wave radiation can be of importance. This supposition has not been corroborated by later laboratory experiments of Fernando and Long (1985b) and E and Hopfinger (1986). Accordingly, internal waves are trapped within the interfacial layer and dissipate energy by breaking, thereby making available only an insignificant amount of energy for the radiation into the outer region.

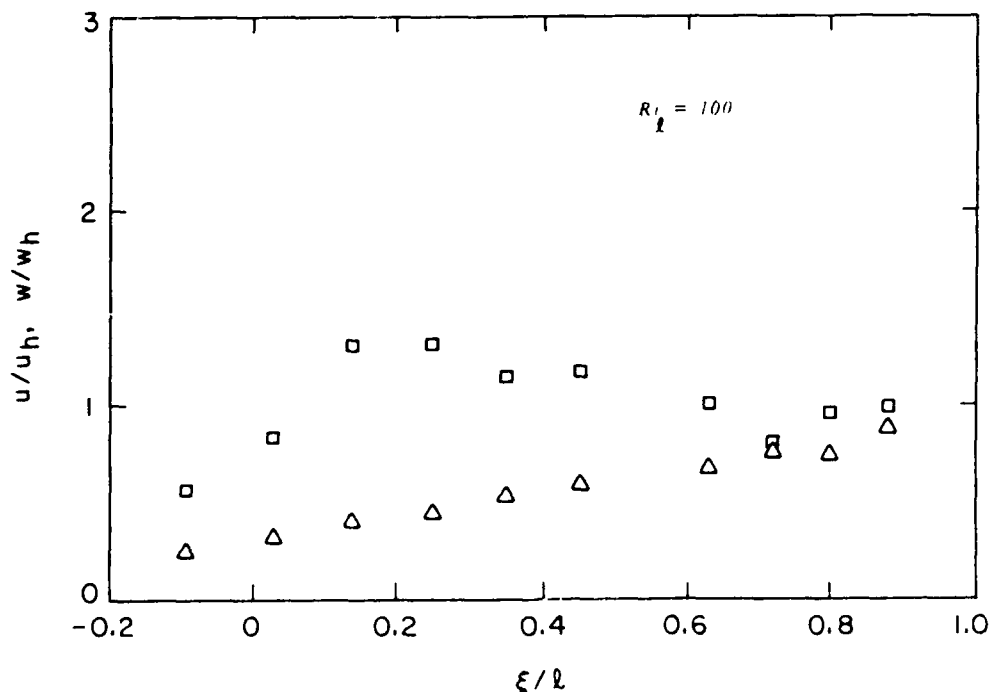
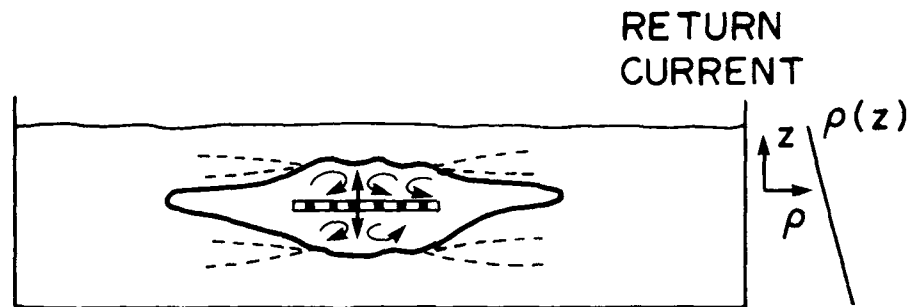


Fig. 2. Variation of r.m.s. turbulent velocities ( $u, w$ ) with the distance from the density interface  $\xi$ . The velocities are normalized using their counterparts measured in the absence of the interface. Squares denote horizontal velocity; triangles denote vertical velocity.



Only a few laboratory experiments have been reported to investigate the effect of two-dimensionality of the mixed-layer deepening process in stratified fluids. (Maxworthy and Monismith, 1988; Fernando and DeSilva, 1989). The latter investigators used an oscillating grid that spans only a finite length of their tank (Figure 3). Even for this simple configuration, the observed flow patterns were very complex. Due to local mixing, a horizontal pressure gradient develops and ejects fluid out of the mixed region to form intrusions. Return currents are set up to provide the make-up fluid, which, in turn, is mixed and ejected into the intrusion. The results of Fernando and DeSilva further show that the entrainment law in this case is much different from that corresponding to the one-dimensional case.



1 b

Fig. 3. A schematic diagram of the mixing experiment in which the development of an isolated mixed region by a "sustained" energy source was studied. The initial density distribution  $\rho(z)$  is also shown.

## 2.2 Convective Turbulence

Mixing at density interfaces due to convective turbulence is important in both oceanic and atmospheric contexts. It is generally believed that, in the upper atmosphere, the turbulence is mainly contributed by convective motions (Deardorff 1970a,b; 1972) and hence, in the laboratory, heating of a stable temperature gradient from below has been used to simulate tropospheric mixing. Convective turbulence that is generated due to oceanic surface cooling can also interact with the thermocline and cause mixing. It should be kept in mind that both heat and salt contribute to oceanic stratification and, due to their widely different diffusivities, double-diffusive effects can become significant. A brief account of double-diffusive mixing is given in Section 5.

Results from convective mixing experiments are generally different from mechanical mixing experiments. According to Deardorff et al. (1969), the entrainment law for convective mixing can be written in the form (2.1) with  $n = 1$ , but more detailed measurements have shown that the possibility  $n = 3/2$  cannot be excluded (Deardorff et al., 1980). In these cases the relevant velocity scale is the convective velocity  $w_*$ , which is proportional to  $u$ , and the Richardson number is defined as  $Ri_t = \Delta b h / w_*^2$ . The data of Deardorff et al. (1980), which shows  $E$  versus  $Ri_t$ , display considerable scatter and the involvement of molecular diffusive effects has been conjectured as its cause (Breidenthal and Baker, 1985).

although Deardorff et al. argued against the involvement of molecular diffusive effects in their experiments. Experiments carried out at Arizona State University clearly indicate that, in the range  $75 < Ri_t < 800$ , the mixed-layer growth occurs in an intermittent fashion, similar to that proposed by Noh and Fernando (1989). The diffusion of heat into the upper layer reduces the interfacial density gradient which, when it falls below a critical value, is susceptible to the direct engulfment by the eddies. This differs from the mechanism proposed by Deardorff et al. based on the splashing of non-turbulent fluid into the mixed layer due to eddies impinging on the interface. More detailed experimental and theoretical modeling efforts are needed to improve understanding of this problem.

### 3. MIXING IN THE PRESENCE OF SHEAR

Although there have been several prior experiments (Macagno and Rouse, 1961; Ellison and Turner, 1959), because of their apparent applications to the oceanic situations, major attention has been focussed on the experiments of Kato and Phillips (1969). These experiments were performed in an annular tank that contained a linearly stratified fluid. The fluid was driven by a rotating surface screen that exerts a constant shear stress. The shear-generated turbulence caused a surface mixed layer to develop and penetrate into the non-turbulent layer. The results show that, over the Richardson number range investigated,  $20 < Ri_* < 200$ , the entrainment law is given by

$$E = c_4 Ri_*^{-1}, \quad (3.1)$$

where  $c_4 = 0.25$ ,  $Ri_* = \Delta b h / u_*^2$  and  $u_*$  is the surface friction-velocity. The later experiments by Scranton and Lindberg (1983), Jones and Mulhearn (1983), and Deardorff and Yoon (1984), however, have established that the Kato-Phillips apparatus does not produce a one-dimensional flow situation. Ekman pumping, introduced by the solid-body rotation of the surface screen, was found to generate secondary circulations which cause uneven entrainment in both the radial and azimuthal directions, thereby tilting the interface. In addition to  $Ri_*$ , parameters such as the aspect ratio of the annulus and the Richardson number  $Ri_u$ , based on the interfacial velocity jump  $\Delta u$ ,  $Ri_u = \Delta b h / (\Delta u)^2$ , were also shown to be important. Although the findings of Kato and Phillips have been employed for the interpretation and prediction of the upper-ocean mixed layer (Denman and Miyake, 1973; Niiler and Kraus, 1977), the above comments suggest that such extrapolations should be done with caution.

To alleviate the problem of secondary circulations due to Ekman pumping, Narimousa et al. (1986) and Narimousa and Fernando (1987) used an Odell-Kovaszny-type disk pump, instead of a surface screen, to drive the mixed layer over the non-turbulent layer. In this case, the interfacial tilt due to non-uniform entrainment was reported to be very small. The results, when plotted using  $\Delta u$  as the velocity scale, collapse satisfactory and yield the entrainment law  $E \sim Ri_u^{-1}$  (Figure 4). If we assume that  $u \sim \Delta u$  (Ellison, 1962), then it is possible to show that the buoyancy flux, production and dissipation rates of turbulent kinetic energy near the interface are of the same order, or the flux Richardson number  $R_f$  at the entrainment interface is a constant. The value of  $R_f$  is generally believed to be 0.2-0.3 (McEwan, 1983) although in some laboratory experiments  $R_f$  has been found to be a function of  $Ri$  (Linden, 1980; Rohr and Van Atta, 1987).

The mixing mechanism for sheared interfaces has not been studied as extensively as the shear-free case. Based on shadowgraph flow visualization, Narimousa and Fernando (1987)

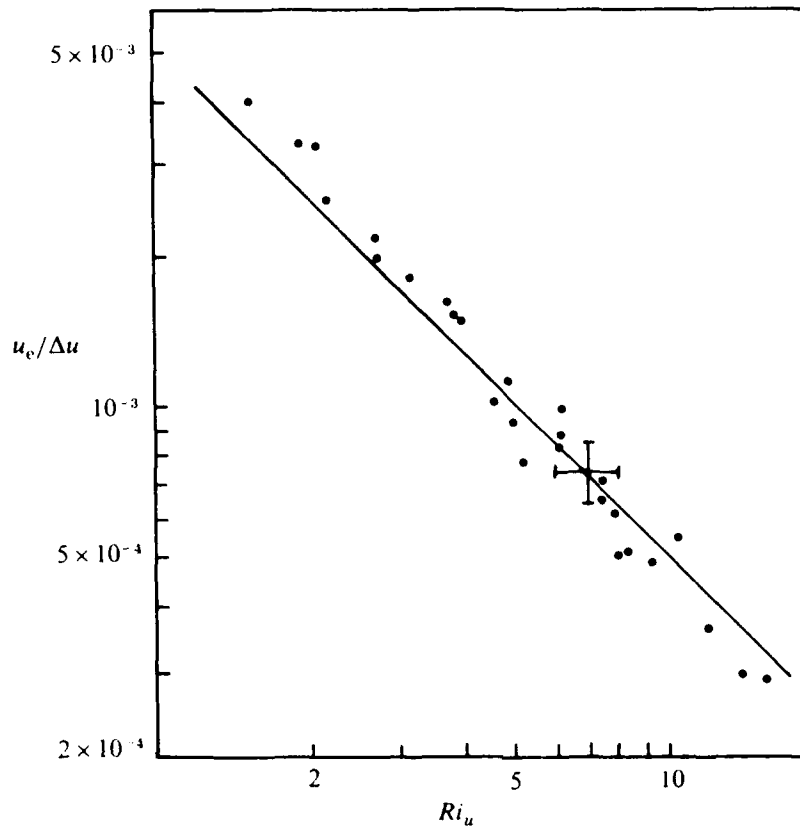


Fig. 4. variation of the entrainment coefficient with the Richardson number for experiments performed with interfacial shear.

identified three entrainment regimes. When  $Ri_u < 5$ , Kelvin-Helmholtz instabilities are responsible for mixing whereas for  $5 < Ri_u < 20$ , interfacial wave breaking is the major entrainment mechanism. When  $Ri_u > 20$ , the interfacial processes become molecular diffusive and only a negligible entrainment can be detected. Since shadowgraph flow visualization has been shown to give an incomplete picture of mixing events (Thorpe, 1985), the above results need to be reinvestigated using more sophisticated visualization techniques.

No systematic studies have been reported on the transition from the active entrainment regime to the molecular-diffusion dominated entrainment regime. Phillips (1977) has suggested that, for sheared interfaces, molecular diffusive effects become important when

$$Ri < Pe^{-1}, \quad (3.2)$$

for which some support can be seen in Narimousa et al. (1986). Kantha, Phillips and Azad (1977) observed that, for a given  $Ri$ , the entrainment coefficient in a linearly stratified system is smaller than that of a two-fluid system. This behavior was explained by assuming that there is an appreciable loss of kinetic energy from the entrainment zone to the outer stratified layer because of internal waves. The results of Narimousa et al. (1986), however, show that the entrainment laws for both two-fluid and linearly stratified systems are the same. Direct measurement of internal wave energy radiation is required to resolve this conflict. Evidence of the radiation of internal waves beneath the equatorial mixed layer have been recently found by Dillon (1989, personal communication).

Since bulk of the turbulent energy generated at the surface decays before arriving at the thermocline, it is possible to surmise that the energetics of thermocline mixing are governed by the local shear-generated turbulence. If so, laboratory experiments with shear will be valuable in parameterizing and understanding oceanic thermocline mixing. For instance, Kelvin-Helmholtz billows of the ocean, observed by Woods (1968), have similarities to laboratory K-H billows generated by Thorpe (1973). Cushman-Roisin (1981) notes good agreement between the published oceanic entrainment data and the laboratory data of Kato and Phillips (1969) although the latter work has been criticized for being influenced by secondary circulations. The values of the coefficient  $c_4$  compiled by Cushman-Roisin are given below.

Investigators	Data	Ri* range	$c_4$
Kato and Phillips (1969)	Laboratory	15-400	2.5
Turner (1969)	South of Bermuda	30	3.2
Denman and Miyake (1973)	Station Papa	150	2.0
Halpern (1974)	Northeast Pacific	80	5.6
Kullenberg (1977)	Coastal Waters-Lakes	10 -104	2.2
Price et al. (1968)	Florida Continental Shelf	300	1.8
Dillon and Powell (1979)	Lake Tahoe	30	1.8-3.2

#### 4. ENTRAINMENT IN THE PRESENCE OF COMBINED FORCING.

Only a few laboratory experiments have been reported to examine the combined effects of shear and zero-mean-shear sources of turbulence. Munoz and Zangrando (1986) investigated interfacial mixing in the presence of interfacial shear and convective turbulence. By assuming that the combined effect can be represented by the velocity scale introduced by Deardorff (1983),

$$u_R = [(c_5 \Delta u)^3 + c_6 w_*^3]^{1/3}, \quad (4.1)$$

they attempted to correlate the data using the non-dimensional parameters  $u_e/u_R$  and  $\Delta b h/u_R^2$ . This attempt was not satisfactory. The effect of shear and oscillating-grid turbulence on a density interface has been studied by Atkinson and Wolcott (1989). Their results are in agreement with a model based on (4.1). Andre and Lacarrere (1985) have proposed an alternative to (4.1), viz.,

$$u_R^2 = [c_7 (\Delta u)^2 + c_8 w_*^2]. \quad (4.2)$$

Although (4.2) has not been employed in interpreting laboratory observations, a model based on (4.2) has been shown to give satisfactory predictions for the daily evolution of the planetary boundary layer (Andre et al., 1978).

## 5. MIXING ACROSS DOUBLE DIFFUSIVE INTERFACES

The migration of double diffusive interfaces due to interfacial mixing is important in an oceanic context. Since most of the related published work has dealt with the diffusive interface of double diffusive convection, here we focus our attention on this particular case. Diffusive interfaces are common in regions where hot, salty water underlies cold, fresh water. The density interfaces, which separate turbulently convecting layers of thermohaline staircases, fall into this category.

Laboratory experiments have been successful in delineating the physics of the formation of thermohaline staircase structures (Turner, 1968; Huppert and Linden, 1979; Fernando, 1987). Fernando (1989) has demonstrated that the thicknesses of the convecting layers  $h^c$  are determined by a balance between kinetic and potential energies of the turbulent eddies within the layers. This result can be written, in terms of local variables pertaining to the layers, as

$$h_c = c_9 (q_h / N_s^3)^{1/2} (1 - R_\rho^{-1})^{-3/4}; \tau^{1/2} R_\rho \ll 1 \text{ or } 0.15 R_\rho \ll 1, \quad (5.1)$$

where the selection of the latter condition depends on the buoyancy transport mechanism at the interface. Here  $R_\rho = \Delta b_s / \Delta b_T$  is the stability ratio,  $\Delta b_s$  and  $\Delta b_T$  are the buoyancy jumps across the convecting layers due to salinity and temperature, respectively,  $q_h$  is the buoyancy (heat) flux through the layers and  $N_s$  is the stability frequency based on the salinity stratification  $N_s^2 = \Delta b_s / h_c$ . The available oceanic data were found to be in good agreement with (5.1).

In the presence of differential turbulence intensities across them, the migration of the interfaces occurs in the direction of decreasing turbulent intensity. It has been argued that the resultant entrainment velocity should be equal to the difference of the entrainment velocities that are evaluated by neglecting the convection in the opposite side (Kelley 1986). Some support for this can be seen from the laboratory experiments of Muench, Fernando and Stegan (1989). These experiments have been performed by heating a two-layer salt stratified fluid from below. The convection is initiated in the bottom layer and then in the top layer through the molecular diffusion of buoyancy across the interface. Since the convection in the lower layer is stronger than that in the top layer, the interface propagates upwards. It was shown that the net entrainment rate can be given by

$$u_e / w_{*1} = 0.25 \text{ Ri}_1^{-1} (1 - q_{h2} / q_{h1}), \quad (5.2)$$

when  $\text{Ri}_1^{-1} (1 - q_{h2} / q_{h1}) > 10^{-3}$  and

$$u_e / w_{*1} = 0.15 \text{ Pe}_1^{-1/2} [(1 - (q_{h2} / q_{h1}))^{1/6} (h_1 / h_2)^{1/3}], \quad (5.3)$$

for  $\text{Ri}_1^{-1} (1 - q_{h2} / q_{h1}) < 10^{-3}$ . Here subscripts 1 and 2 denote quantities pertinent to the lower (strongly convecting) and upper (weakly convecting) layers, respectively. It was noted, however, that, when the interfacial Richardson number  $\Delta b \delta / w_{*1}^2$ , where  $\delta$  is the thickness of the interfacial layer, falls below a critical value, the entrainment law does not

follow either of the above expressions. Instead the interface moves rapidly and assumes a new quasi-equilibrium position. Thereafter the interface moves slowly and the entrainment law obeys (5.1) or (5.2). Muench et al. (1989) noted a good agreement between their Weddell Sea interfacial migration data and laboratory observations.

## 6. CONCLUDING REMARKS

In this paper, a brief account of the results of laboratory studies that have been performed to understand turbulent mixing across density interfaces was presented. It was pointed out that, although laboratory studies cannot be directly extrapolated to oceanic situations, they can provide valuable guidance to the oceanographic community in understanding fundamental physical mechanisms of the oceanic processes. For many reasons, the interpretations and results of laboratory experiments are sometimes ambiguous; some of these factors are wall effects, instrument and flow visualization problems and differences in data-handling procedures. Careful design of the experiments and a unified approach of data handling may alleviate some of these disparities.

## ACKNOWLEDGMENTS

The author would like to thank the organizers of the 'Aha Huliko'a workshop for inviting him to participate in the workshop. Thanks are also due to the Ocean Sciences division of the Office of Naval Research and Fluid Mechanics and Hydraulics program of the National Science Foundation for supporting stratified flow research at Arizona State University, and Professor D.F. Jankowski and G. Oth for their help in numerous ways.

## REFERENCES

- Altman, D., and A.E. Gargett: 1989. Differential property transport due to incomplete mixing in a stratified fluid. *Proceedings 3rd Intl. Symposium on Stratified Flows*. (In press.)
- Andre, J.C., and P. Lacarrere: 1985. Mean and turbulent structure of the oceanic surface layer as determined from one-dimensional third order simulations. *J. Phys. Oceanogr.*, **15**, 121-132.
- Andre, J.C., G. De Moor, P. Lacarrere, G. Therre, and R. Du Vachat: 1978. Modeling the 24-hour evolution of the mean and turbulent structures of the planetary boundary layer. *J. Atmos. Sci.*, **35**, 1861-1883.
- Atkinson, J.F., and S.B. Wolcott: 1989. Interfacial mixing driven by mean shear and an oscillating grid. Submitted for publication.
- Breidenthal, R.E., and M.B. Baker: 1985. On entrainment at stratified interfaces. In J.C. Weil (Editor) *7th Symposium on Turbulence and Diffusion*, 43-46.
- Carruthers, D.J., and J.C.R. Hunt: 1986. Velocity fluctuations near an interface between a turbulent region and a stably stratified layer. *J. Fluid Mech.*, **165**, 475-501.
- Crapper, P.F., and P.F. Linden: 1974. The structure of the turbulent density interfaces. *J. Fluid Mech.*, **65**, 45-83.
- Cushman-Roisin, B.: 1981. Deepening of the wind mixed layer: A model of the vertical structure. *Tellus*, **33**, 564-582.
- Deardorff, J.W.: 1970a. Preliminary results from numerical integrations of the unstable boundary layer. *J. Atmos. Sci.*, **27**, 1209-1211.
- Deardorff, J.W.: 1970b. Convective velocity and temperature scales for the unstable planetary boundary layer and for Rayleigh convection. *J. Atmos. Sci.*, **27**, 1211-1213.

- Deardorff, J.W.: 1972. Numerical investigation of neutral and unstable planetary boundary layer. *J. Atmos. Sci.*, **29**, 91-115.
- Deardorff, J.W.: 1983. A multi-limit mixed layer entrainment formulation. *J. Phys. Oceanogr.*, **13**, 988-1002.
- Deardorff, J.W., and S.C. Yoon: 1984. On the use of an annulus to study mixed-layer entrainment. *J. Fluid Mech.*, **142**, 97-120.
- Deardorff, J.W., G.E. Willis, and D.K. Lilly: 1969. Laboratory Investigation of nonsteady penetrative convection. *J. Fluid Mech.*, **35**, 7-31.
- Deardorff, J.W., G.E. Willis, and B.H. Stockton: 1980. Laboratory studies of entrainment zone of convective mixed layer. *J. Fluid Mech.*, **100**, 41-62.
- Denman, K.L., and M. Miyake: 1973. Upper layer modification at Ocean Station Papa: Observations and Simulation. *J. Phys. Oceanogr.*, **3**(2), 185-196.
- Dillon, T.M., and T.M. Powell: 1969. Observations of a surface mixed layer. *Deep-sea Res.*, **26A**, 915-932.
- E, X., and, E.J. Hopfinger: 1986. On mixing across an interface in stably stratified fluid. *J. Fluid Mech.*, **166**, 227-244.
- Ellison, T.H.: 1962. Laboratory measurements of turbulent diffusion in stratified flows. *J. Geophys. Res.*, **67**, 3029-3031.
- Ellison, T.H., and J.S. Turner: 1959. Turbulent entrainment in stratified flows. *J. Fluid Mech.*, **6**, 423-448.
- Fernando, H.J.S.: 1987. The Formation of layered structure when a stable salinity gradient is heated from below, *J. Fluid Mech.*, **182**, 525-541.
- Fernando, H.J.S.: 1988. The growth of a turbulent patch in a stratified fluid. *J. Fluid Mech.*, **190**, 55-70.
- Fernando, H.J.S.: 1989. Oceanographic implications of laboratory experiments on diffusive interfaces. *J. Phys. Oceanogr.* Accepted.
- Fernando, H.J.S., and R.R. Long: 1983. The growth of a grid generated mixed layer in a two fluid system. *J. Fluid Mech.*, **133**, 351-377.
- Fernando, H.J.S., and R.R. Long: 1985a. On the nature of the entrainment interface of a two-layer fluid subjected to zero-mean-shear turbulence. *J. Fluid Mech.*, **151**, 21-53.
- Fernando, H.J.S., and R.R. Long: 1985b. The deepening of a mixed layer in a linearly stratified fluid. *Phys. Fluids*, **28**, 2999-3004.
- Fernando, H.J.S., and I.P.D. De Silva: 1989. On the collapse of a turbulent patch generated by a continuous energy source. In preparation.
- Folse, R.F., T.P. Cox, and K.R. Schexnayder: 1981. Measurements of the growth of a turbulently mixed layer in a linearly stratified fluid. *Phys. Fluids*, **24**, 396-400.
- Halpern, D.: 1974. Observations of the deepening of the wind mixed layer in northeast Pacific Ocean. *J. Phys. Oceanogr.*, **4**, 454-466.
- Hannoun, I.A., and E.J. List: 1988. Turbulent mixing at a shear free density interface. *J. Fluid Mech.*, **189**, 211-234.
- Hannoun, I.A., H.J.S. Fernando, and E.J. List: 1988. Turbulence structure near a density interface. *J. Fluid Mech.*, **189**, 189-209.
- Hopfinger, E.J., and J.A. Toly: 1976. Spatially decaying turbulence and its relation to mixing across density interfaces. *J. Fluid Mech.*, **78**, 155-175.
- Hunt, J.C.R.: 1984. Turbulence structure in thermal convection and shear-free boundary layers. *J. Fluid Mech.*, **138**, 161-184.
- Hunt, J.C.R., and J.M.R. Graham: 1978. Free stream turbulence near plane boundaries. *J. Fluid Mech.*, **84**, 209-235.
- Huppert, H.E., and P.F. Linden: 1979. On heating a stable salinity gradient from below. *J. Fluid Mech.*, **95**, 431-464.
- Jones, I.S.F.: 1985. Turbulence below wind waves. In "The Ocean surface: wave breaking, turbulent mixing and radio probing," [Eds. Toba, Y. and Mitsuyasu, H.] Reidel, 437-442.

- Jones, I.S.F., and P.J. Mulhearn: 1983. The influence of external turbulence on sheared interfaces. *Geophys. and Astrophys Fluid Dyn.*, **24**, 49-62.
- Kantha, L.H.: 1979. On generation of internal waves by turbulence in the mixed layer. *Dyn. Atm. Oceans.*, **3**, 39-46.
- Kantha, L.H., O.M. Phillips, and R.S. Azad: 1977. On turbulent entrainment at a stable density interface. *J. Fluid Mech.*, **79**, 753-786.
- Kato, H., and O.M. Phillips: 1969. On the penetration of the turbulent layer into a stratified fluid. *J. Fluid Mech.*, **37**, 643-665.
- Kelley, D.: 1986. Interfacial migration in thermohaline staircases. *J. Phys. Oceanogr.*, **17**, 1633-1639.
- Kitaigorodskii, S.A.: 1979. Review of the theories of wind mixed-layer deepening. *In* Marine Forecasting, Elsevier Oceanog. Series, **25**, 1-33.
- Kullenberg, G.: 1977. Entrainment velocity in natural stratified vertical shear flow. *Estuarine and Coastal Mar. Sci.*, **5**, 329-338.
- Linden, P.F.: 1973. The interaction of vortex rings with a sharp density interface: A model for turbulent entrainment. *J. Fluid Mech.*, **60**, 467-480.
- Linden, P.F.: 1975. The deepening of a mixed layer in a linearly stratified fluid. *J. Fluid Mech.*, **71**, 385-405.
- Linden, P.F.: 1980. Mixing across a density interface produced by grid turbulences. *J. Fluid Mech.*, **100**, 691-703.
- Long, R.R.: 1978. A theory of mixing in a stably stratified fluid. *J. Fluid Mech.*, **84**, 113-124.
- Macagno, E.O., and H. Rouse: 1961. Interfacial mixing in stratified flow. *J. Eng. Mech. Div., Proc. Am. Soc. Civil Eng.*, **87**(EM5), 55-79.
- Maxworthy, T., and S.G. Monismith: 1988. Differential mixing in a stratified fluid. *J. Fluid Mech.*, **189**, 571-598.
- McDougall, T.J.: 1978. Some aspects of geophysical turbulence. Ph.D. thesis, University of Cambridge.
- McDougall, T.J.: 1979. Measurements of turbulence in a zero-mean-shear mixed layer. *J. Fluid Mech.*, **94**, 409-431.
- McEwan, A.D.: 1983. The kinematics of stratified mixing through internal wave breaking. *J. Fluid Mech.*, **128**, 47-58.
- Muench, R., H.J.S. Fernando, and G.R. Stegan: 1989. Temperature and salinity steps in northwestern Weddell Sea: remnant convective features? Submitted for publication.
- Munoz, D.R., and F. Zangrando: 1986. Mixing in a double-diffusive, partially stratified fluid. Solar Energy Research Inst., Report SERI/TR-252-2942.
- Narimousa, S., and H.J.S. Fernando: 1987. On sheared density interface of an entraining stratified fluid. *J. Fluid Mech.*, **174**, 1-22.
- Narimousa, S., R.R. Long, and S.A. Kitaigorodskii: 1986. Entrainment due to turbulent shear flow at the interface of a stably stratified fluid. *Tellus*, **38A**, 76-87.
- Niiler, P.P., and E.B. Kraus: 1977. "One dimensional models of the upper ocean." *Modelling and Prediction of the upper layers of the Ocean.* (Ed. E.B. Kraus) Pergamon. 143-177.
- Noh, Y., and H.J.S. Fernando: 1989. The role of molecular diffusion in the deepening of the mixed layer. Submitted for publication.
- Noh, Y., and R.R. Long: 1989. Turbulent mixing in a rotating, stratified fluid. Submitted for publication.
- Nokes, R.I.: 1988. On the entrainment across a density interface. *J. Fluid Mech.*, **134**, 195-204.
- Phillips, O.M.: 1977. *Dynamics of the Upper Ocean.* Cambridge University Press.
- Price, J.F., C.N.K. Mooers, and J.C. Van Leer: 1978. Observation and simulation of storm-induced mixed-layer deepening. *J. Phys. Oceanogr.*, **8**, 582-599.



- Riley, J.J., and R.W. Metcalf: 1987. Direct numerical simulations of turbulent patches in stably stratified fluids. Presented at 3rd Intl. Symp. on Stratified Flows.
- Rohr, J.J., and C.W. Van Atta: 1987. Mixing efficiency in stably stratified growing turbulence. *J. Geophys. Res.* **92**, 5481-5488.
- Scranton, D.R., and W.R. Lindberg: 1983. An experimental study of entraining stress-driven, stratified flow in an annulus. *Phys. Fluids*, **26**, 1198-1205.
- Thorpe, S.A.: 1973. Experiments on instabilities and turbulence in a stratified shear flow. *J. Fluid Mech.* **61**, 731-751.
- Thorpe, S.A.: 1985. Laboratory observations of secondary structures in Kelvin-Helmholtz billows and consequences for ocean mixing. *Geophys. Astrophys. Fluid Dyn.* **34**, 175-199.
- Turner, J.S.: 1968. The behaviour of a salinity gradient heated from below. *J. Fluid Mech.* **33**, 183-200.
- Turner, J.S.: 1969. A note of wind mixing at the seasonal thermocline. *Deep-sea Res. Suppl.* **16**, 297-300.
- Wang, J., and J. Wu: 1985. Wind-induced water turbulence. In: *The Ocean Surface: wave breaking turbulent mixing and radio probing*, [Eds. Toba, Y. and Mitsuyasu, H.] Reidel, 401-406.
- Woods, J.D.: 1968. Wave induced shear instability in summer thermocline. *J. Fluid Mech.* **32**, 791-800.

## GRAVITY WAVE SATURATION, TURBULENCE, AND DIFFUSION IN THE ATMOSPHERE: OBSERVATIONS, THEORY, AND IMPLICATIONS

David C. Fritts

Geophysical Institute and Department of Physics, University of Alaska, Fairbanks, AK 99775-0800

### ABSTRACT

Our understanding of wave processes in the atmosphere has progressed considerably in the last few years. Yet there remain uncertainties concerning wave saturation mechanisms, the factors responsible for spectral shape, and wave influences on transports and small-scale diffusion. This paper will examine the evidence for various saturation mechanisms in the atmosphere, their implications for transport, diffusion, and spectral shape, as well as the possible differences between such processes in the atmosphere and the oceans. Atmospheric observations suggest wave saturation via linear wave field instabilities, consistency with enhanced saturation theory, and the need for an effective turbulent Prandtl number  $Pr > 1$ . Wave transports of energy and momentum will also be discussed.

### INTRODUCTION

In the atmosphere, as in the oceans, internal gravity waves are believed to account for a significant fraction of mesoscale variance and to be largely responsible, via wave field instabilities, for small-scale turbulence and diffusion. Unlike the oceans, however, gravity waves appear to have major effects on the large-scale circulation and thermal structure throughout the atmosphere. These effects are most pronounced in the mesosphere and lower thermosphere, where wave fluxes of energy and momentum drive the mean state far from radiative equilibrium conditions.

The large-scale effects of gravity waves in the middle atmosphere arise from the dissipation of upward propagating wave motions. This dissipation is driven by a tendency for atmospheric gravity waves to grow with increasing height due to the decrease in mean density. Ultimately, wave fluctuations become sufficiently large to cause instability within the wave field, leading to spectral energy transfers, limits on wave amplitudes, turbulence production, and the divergences of wave energy and momentum fluxes.

Our purposes in this paper are 1) to examine our theoretical and observational understanding of the processes contributing to gravity wave saturation in the atmosphere, 2) to consider some of the implications of saturation for small-scale turbulence and diffusion, and 3) to identify some of the similarities and differences between such processes in the atmosphere and in the oceans. We will begin by reviewing the evidence for gravity wave saturation and its effects in the atmosphere. Then evidence for various saturation mechanisms will be examined; these include both essentially linear instabilities of the wave field and systematic nonlinear exchanges of energy among gravity waves or between gravity waves and the vortical mode. Next we review the evidence for a saturated spectrum of gravity waves in the atmosphere and its evolution with height. The implications of saturation and of the observed form of the energy spectrum for wave transports of energy and momentum, turbulence, and diffusion are examined next, followed by a summary of the atmospheric results, and a comparison of their applicability to the oceans.

# EVIDENCE OF GRAVITY WAVE SATURATION IN THE ATMOSPHERE

A large body of evidence now exists which points to the fact that gravity wave amplitudes are strongly constrained as these waves propagate upward in the atmosphere. For conservative wave motions not experiencing reflection, the vertical flux of wave action should be constant, leading to an approximately uniform wave energy density per unit volume (and an energy density per unit mass increasing as  $\sim \rho^{-1}$ ). But observations reveal that wave energy density decays considerably with height relative to these inviscid limits, suggesting processes that act to limit wave amplitudes in some manner.

Radar studies have shown the horizontal wind variance to increase with a scale height  $H_E \sim 12 - 15$  km throughout the lower and middle atmosphere (Balsley and Carter, 1982; Vincent, 1984; Balsley and Garelle, 1985; Meek et al., 1985; Vincent and Fritts, 1987) and revealed an apparent limit on the vertical shear of horizontal wind of  $u_z \sim N$ , where  $u_z$  is the horizontal wind shear and  $N$  is the Brunt-Vaisala frequency (Balsley et al., 1983; Fritts et al., 1988a; Muraoka et al., 1988). Near the tropopause, typical vertical wavelengths are  $\sim 2.5$  km (Fritts and Chou, 1987; Fritts et al., 1988b), with corresponding horizontal wave velocities of  $\sim 5$  m/s. At greater heights, both vertical wavelengths and amplitudes increase in a manner consistent with the observed limit on horizontal wind shears, achieving values of  $\sim 20$  km and 50 m/s near the mesopause. An example of this wave growth with height and of the limits on vertical shears of horizontal motions obtained with an instrumented falling sphere is shown in Figure 1.

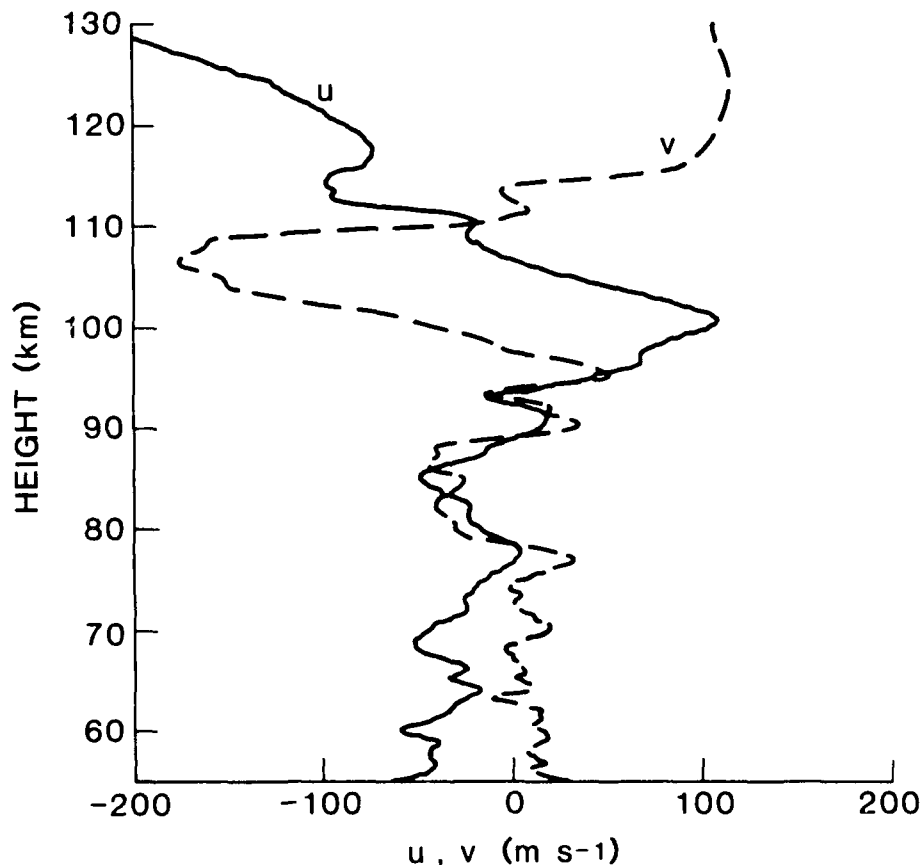


Fig. 1. Zonal and meridional velocities obtained by falling sphere during the STATE experiment during June 1983 at Poker Flat, Alaska. The profiles have a vertical resolution of 250 m.

Temperature and density measurements have also exhibited both a limit on vertical gradients and a growth of fluctuation variance with height consistent with radar wind studies. High-resolution soundings reported by Philbrick et al. (1983) and Fritts et al. (1988b) revealed a clear tendency for temperature gradients to be constrained near adiabatic lapse rates, despite the growth of wave amplitudes and the dominant vertical wavelengths with height. Rayleigh LIDAR observations and density measurements obtained during space shuttle re-entry likewise have shown temperature and density variance to increase with a scale height  $H_E \sim 12$  - 15 km, as noted in the radar data. Thus, there are clear indications both of a decay of wave energy with increasing height and of the importance of processes that act to limit wave amplitudes in some manner. The processes that are the most likely candidates for limiting gravity wave amplitudes in the atmosphere will be examined in the following section.

## SATURATION MECHANISMS FOR ATMOSPHERIC GRAVITY WAVES

The mechanisms by which internal gravity waves are saturated, or constrained in amplitude, have received considerable attention in both the atmospheric and oceanic communities because of their influence on the wave spectrum and their role in generating turbulence and diffusion. In many respects, consideration of these processes in the atmosphere has lagged that in the oceans because of a lack, until recently, of detailed information on the gravity wave spectrum. It has been recognized for thirty years, however, that wave instability would be the likely consequence of upward propagation in an atmosphere with an exponentially decaying density (Hines, 1960). The question, then, is the nature of the instability. Is it a local instability of an essentially linear wave field, is it a systematic nonlinear exchange or cascade of energy through the wave spectrum, or can it even be described without discussing as well the turbulent scales into which energy is transferred and where it ultimately is dissipated? To address these topics reasonably, we will describe first the various linear and nonlinear saturation mechanisms that have been considered theoretically and then discuss the observational support for them.

### a. Linear Instability Mechanisms

Early attention in the atmosphere and oceans focussed on the convective instability of the wave field occurring where parcel velocities exceed the phase speed of the wave motion,  $u' > (c - u)$  (Hodges, 1967; Orlandi and Bryan, 1969), because this is the location where, and the condition under which, a monochromatic gravity wave will yield an inverted potential temperature gradient,  $d\theta/dz < 0$ . This threshold is also the wave amplitude corresponding to  $u'_z = N$  in the WKB approximation for wave motions with intrinsic frequencies  $\omega \gg f$ , which appears to describe reasonably the observed limit on wave shears in the atmosphere and the oceans (though the maximum wave shear does not occur at the level of minimum stability). For these and conceptual reasons, the convective amplitude limit has served as the basis for various parameterizations of wave saturation effects in recent years (Orlandi and Ross, 1973; Lindzen, 1981; Holton, 1982; Fritts, 1984; Garcia and Solomon, 1985; Miyahara et al., 1986). More recently, these ideas have been extended to the possible convective instability along a slanted path by Hines (1988). The assumptions that instability will occur at just this amplitude threshold and will act to limit wave amplitudes near this value are, of course, simplistic. Yet, the apparent success of this theory and the ease with which it may be applied are clear attractions.

The consequences of convective instability, to the extent that it is important in the atmosphere or the oceans, are expected to be local convective overturning of the fluid and local production of velocity and density variance at turbulent scales of motion. As such, we anticipate a direct transfer of energy from (potentially large) gravity wave scales to (small) turbulence scales without necessarily experiencing an energy enhancement at intermediate scales. Both the local nature of the convective instability and this discrete rather than continuous spectral energy transfer may help to distinguish this instability from other possible, and more systematic (nonlinear), forms of energy transfer in the atmosphere.

A second linear instability that is thought to play a significant role in the saturation of gravity waves at certain frequencies is the Kelvin-Helmholtz (KH) instability. This is a dynamical instability that may occur in a stably stratified flow when the local shear and stratification are such that the local Richardson number  $Ri = N^2/u_z^2 < 1/4$ . Like the convective instability, the KH instability is assumed to be local, responding primarily to the local flow conditions, and to provide a means of generation of smaller-scale turbulent motions without a systematic downscale energy transfer.

The KH instability is believed unable to compete with the convective instability for wave motions with high intrinsic frequencies because the thresholds for the two instabilities are nearly identical for  $f/\omega \ll 1$  (Dunkerton, 1984; Fritts and Rastogi, 1985). For frequencies near the inertial frequency, however, the threshold for (or necessary condition for) KH instability occurs at significantly smaller amplitudes because of the enhancement of wave shears relative to density fluctuations as  $\omega \rightarrow f$ . Thus, the KH instability may be a viable saturation mechanism for waves with  $\omega \sim f$ . This suggestion has been confirmed recently by stability analyses of inertio-gravity wave structure in both sheared and unsheared environments (Fritts and Yuan, 1989; Yuan and Fritts, 1989). The maximum growth rates as a function of intrinsic frequency obtained in the absence of mean shear for a minimum  $Ri = 0.1$  are illustrated in Figure 2. As noted previously, the gravity wave structure is most unstable for a transverse KH orientation where  $d\theta/dz$  is a minimum rather than where the shear is maximum.

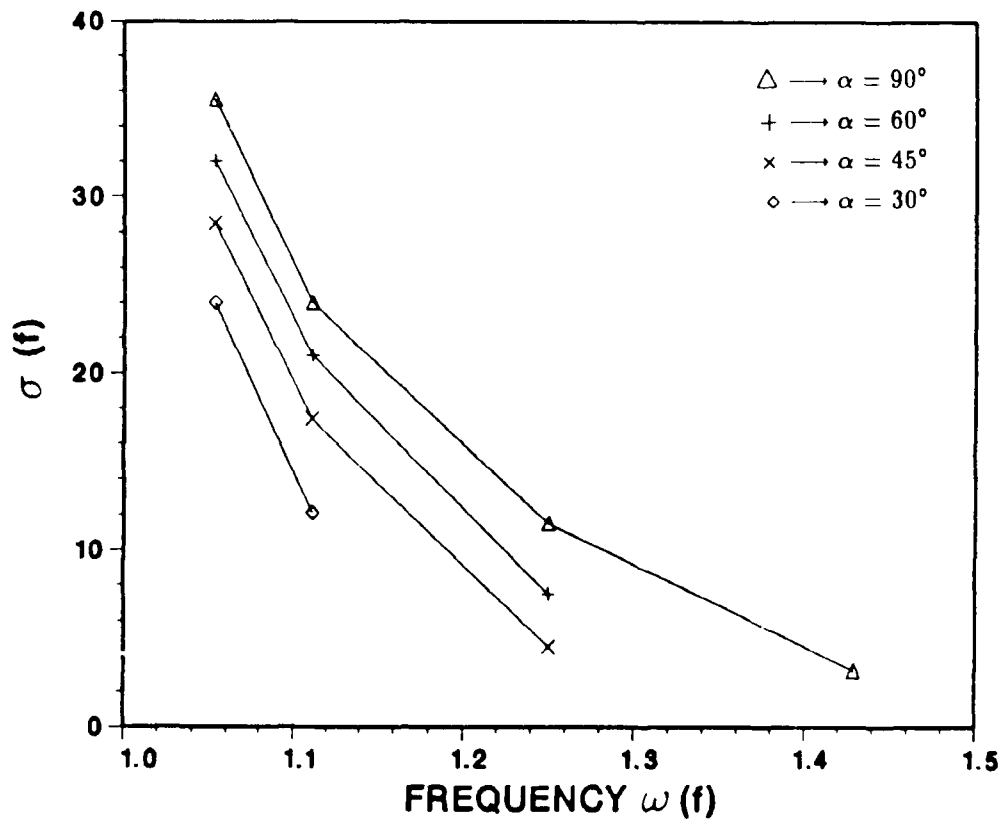


Fig. 2. Maximum KH growth rates as a function of intrinsic frequency for four orientations of the KH instability relative to the inertio-gravity wave. The mean shear is assumed to be zero and the minimum  $Ri = 0.1$ . Both  $\sigma$  and  $\omega$  are in units of  $f$ .

### b. Nonlinear Instability Mechanisms

An attractive alternative in many respects to the seemingly ad hoc assumptions of wave saturation via convective and dynamical instability is the systematic and directly calculable transfer of wave action or energy via nonlinear interactions. In contrast to the linear instability mechanisms discussed above, nonlinear interactions do not, in general, rely on a threshold wave amplitude, but simply operate more efficiently among waves of large amplitude. The nonlinear interactions are of two types, either resonant or non-resonant. Resonant interactions require an approximate quantization of total wavenumber and intrinsic frequency, such that the sum or difference for an interacting pair must match that of a third wave,  $k_1 \pm k_2 = k_3$  and  $\omega_1 \pm \omega_2 = \omega_3$ . The degree to which these resonance conditions must be satisfied is dependent on the strength of the interaction, with only small departures allowed for weak interactions and larger departures permitted for stronger interactions. Thus, resonant interaction theory is most appropriate for interactions among waves of small amplitudes and may not be relevant for large-amplitude wave motions in the middle atmosphere. Non-resonant or off-resonant interactions, in contrast, become more significant at large wave amplitudes, involve direct forcing of non-resonant wave motions, and are poorly approximated by weak (resonant) interaction theory. These interactions were reviewed in an oceanic context by Müller et al. (1986). Our purpose here is to summarize what is known at present about the role of nonlinear interactions in the middle atmosphere.

Resonant interaction theory was initially applied in an oceanic context by Hasselmann (1967) and McComas and Bretherton (1977), who first identified the three resonant interaction triads, induced diffusion, elastic scattering, and the parametric subharmonic instability (PSI). In the atmosphere, these interactions were first considered by Yeh and Liu (1981, 1985) and found to be of potential importance under various circumstances. Elastic scattering was found to operate efficiently for wave motions with small scales and high intrinsic frequencies. Induced diffusion was calculated to have small interaction times for small horizontal or vertical scales. Finally, the PSI appears to operate most efficiently among wave motions with low intrinsic frequencies and small scales.

Other recent studies have attempted to address the roles of resonant and non-resonant interactions under more realistic conditions. Inghester (1987) considered the effects of wave packet localization and non-uniform stratification on the PSI and found them to lead to threshold amplitudes and smaller interaction rates. Dunkerton (1987) examined the influence of the PSI on the momentum flux of the wave field and found, consistent with the study by Fritts (1985), that nonlinearity results in a reduction of wave momentum flux through excitation of other motions but fails to prevent the achievement of linearly unstable wave amplitudes. Dong and Yeh (1988) performed an analysis of the non-resonant interactions between a gravity wave and two vortical modes and obtained a threshold given by  $u' = 2^{1/2} (c - \bar{u})$ , suggesting a means of coupling the gravity wave and vortical motions for sufficiently large wave amplitudes. This amplitude threshold, however, is somewhat larger than the amplitude limits observed in the atmosphere. And Holloway (1988) attempted to provide a theory of nonlinear interactions without distinguishing between waves and turbulence, but was unable to predict amplitude limits that could be compared with observed spectra.

Finally, several studies have attempted to address the role of nonlinearity in limiting wave amplitudes and in initiating wave instability. Fritts (1985) used a quasi-compressible model to compare the effects of convective adjustment and nonlinearity. These simulations showed nonlinear interactions to restrain wave amplitudes somewhat but not to prevent the attainment of amplitudes permitting local convective instability. In a similar study using a fully compressible model, Walterscheid and Schubert (1989) found the form of wave instability to be of a convective nature largely consistent with the linear theory. Related studies of the resonant excitation and breakdown of gravity waves generated by flow over topography have yielded similar results. Thus, there is a body of modelling work that suggests that atmospheric gravity waves are saturated via local convective instabilities (at sufficiently high intrinsic frequencies), resulting in a rapid transfer of energy to turbulent scale of motion, rather than through a systematic nonlinear extraction of energy via wave-wave interactions.

### c. Observations of Wave Saturation

Because of observational constraints, there have been few detailed studies of gravity wave saturation and its effects in the middle atmosphere to date. There are, nevertheless, a number of observations of atmospheric fluctuations that suggest the nature of the wave field instability. In addition, several recent studies have attempted to combine observations using several instrument systems with some success.

One of the better known examples of gravity wave instability and breakdown is the severe downslope wind storm which occurs in the lee of major mountain barriers (Lilly and Kennedy, 1973; Lilly, 1978) under suitable atmospheric flow conditions. Several of these have been probed using aircraft equipped with in situ sensors for wind and temperature fluctuations. These have revealed, consistent with numerical models of this process, that strong turbulence accompanies the formation of convectively unstable regions within the wave field. Studies of wave instability in the laboratory were reviewed by Fritts (1984) and likewise suggest consistency of turbulence production with the predictions of linear theory. In each of these cases, turbulence appears to be strongly localized and associated closely with that portion of the wave field that supports a local convective instability.

Recent studies also have addressed wave instability in the middle atmosphere using a variety of radar, balloon, and rocket measurements of atmospheric parameters. Arecibo radar data were used by Tsuda et al. (1985) to infer a quadrature relationship between echo power, assumed to be an indication of turbulence intensity, and wind shear due to inertio-gravity wave motions in the stratosphere. A similar relationship was noted by Sidi and Barat (1986) in a study of such motions using high-resolution balloon data. In both cases, these observations support the predictions of linear theory that instability should be localized in that region of the wave field in which the local stability and shear are a minimum (Fritts and Rastogi, 1985).

Studies in the mesosphere and lower thermosphere using both ground-based instrumentation and in situ rocket-borne probes likewise have provided evidence of a correlation between regions of wave instability and enhanced turbulence energy levels. High turbulence energies and small inner scales inferred from ion density measurements were observed to be correlated with regions of convective or dynamical instability by Thrane et al. (1987) during the MAP/WINE experiment. Similar enhancements have been observed in spectra of electron density fluctuations (Ulick et al., 1988) and a correlation of regions of likely wave instability and enhanced VHF radar echoes suggesting strong turbulence was obtained (Fritts et al., 1988a) during the STATE experiment. Particularly relevant here is the correlation between the inferred most unstable phase of a large-amplitude, low-frequency wave motion and the radar echo power, or signal-to-noise (S/N). As in the stratosphere, high S/N values obtained near the high-latitude summer mesopause are believed to be an indication of enhanced turbulence intensities. This correlation is shown in Figure 3 and suggests, consistent with observations cited above and linear theory, that turbulence is both localized and associated primarily with that portion of the wave field expected to be unstable on the basis of linear theory. These atmospheric observations are reviewed in more detail by Fritts (1989).

The theoretical and observational studies described above have clear implications for the gravity wave spectrum in the middle atmosphere. The first is that wave propagation appears to be reasonably described by linear theory for the larger vertical scales at which most of the gravity wave energy resides due to the inferred long interaction times and the apparent inability of nonlinear wave-wave or wave-vortical mode interactions to restrain wave amplitudes effectively. As gravity waves achieve large (linearly unstable) amplitudes, however, nonlinearity must play a significant role in the transfer of energy between the wave and turbulence spectra. The resulting turbulence appears to be highly localized within the wave field and to coincide with the most unstable phase of the wave field based on linear theory. At smaller vertical scales, interaction rates are larger, wave scales are closer to the buoyancy scale,  $L_b$  (~500-100 m in the mesosphere), and nonlinear interactions are more likely to play a major role in the evolution of and the energy exchange within the gravity wave and turbulence spectra.

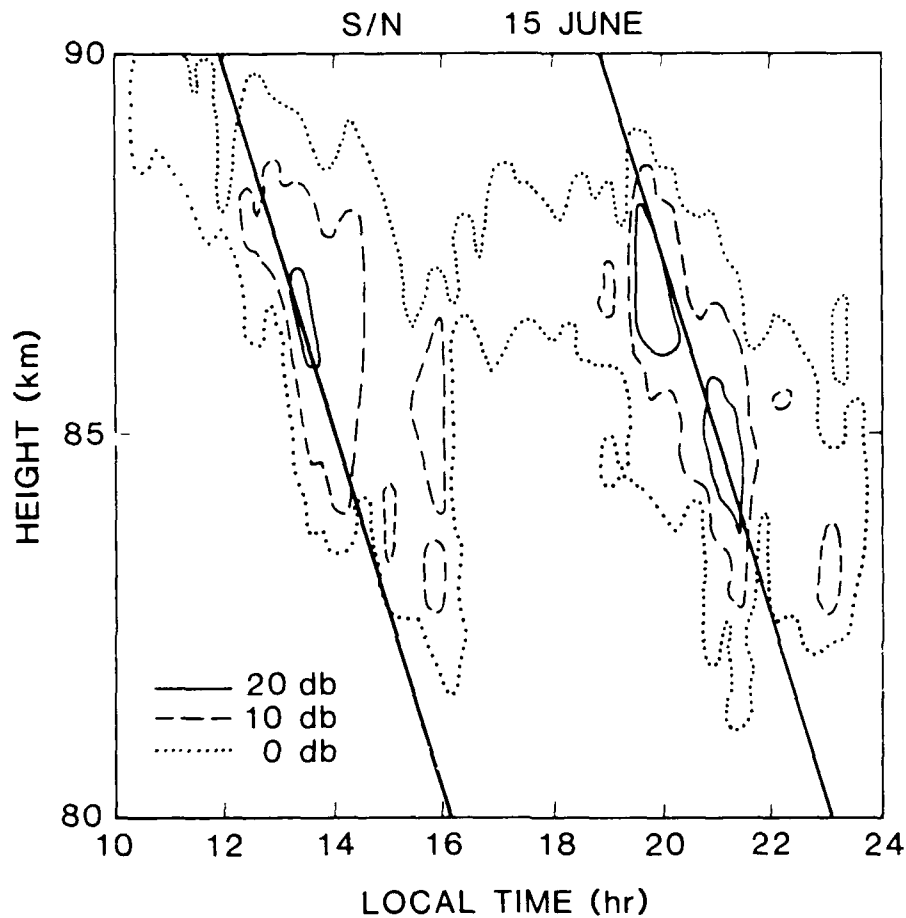


Fig. 3. Signal-to-noise (S/N) contours for 14 hours on 15 July 1983 during the STATE experiment at Poker Flat, Alaska. Slanted solid lines indicate the locations of the inferred most unstable phase of the inertio-gravity wave motion observed with radar and rocket instrumentation. The good correlation of strong S/N enhancements with the unstable wave phase is suggestive of local turbulence associated with dynamical instability of the wave field.

#### A SATURATED GRAVITY WAVE SPECTRUM

A major consequence of the saturation processes described above for the gravity wave spectrum in the atmosphere is the achievement of a near-universal spectral amplitude at large vertical wavenumbers (but below those of inertial range turbulence). All of the competitive theories (linear waves, nonlinear waves, or buoyancy range turbulence) lead to predictions differing at most by a constant amplitude coefficient. What is important is that this saturated spectrum is observed to occur and has a number of important implications. For our purposes here, we will use linear saturation theory to describe the saturated spectrum limits, both because it provides the most intuitive view of the saturation process and because it is the only theory, at present, that provides unambiguous predictions of spectral amplitudes.



Both linear and nonlinear saturation theories predict a power spectral density of horizontal velocity fluctuations that varies as  $F_u^S(m) \approx bN^2/m^3$ , where  $b$  is a constant and  $m$  is vertical wavenumber. The constant  $b$  may be inferred by assuming that the total variance of wave fluctuations is just that required to achieve linear instability of the wave field. This was done by Dewan and Good (1986) by imposing a threshold shear for instability and by Smith et al. (1987) by assuming a threshold of incipient convective instability. Equating the variance of the wave spectrum with that required for an individual wave motion at the threshold amplitude then leads to saturated power spectral densities for horizontal velocity and fractional temperature ( $T'/\bar{T}$ ) fluctuations given by

$$F_u^S(m) \approx \frac{p}{10} \frac{N^2}{m^3} \quad (1)$$

and

$$F_T^S(m) \approx \frac{1}{10} \frac{N^4}{g^2 m^3} \quad (2)$$

The factor  $p$  is the slope of the frequency spectrum of total wave energy,  $F(\omega) \sim \omega^{-p}$  with  $p \approx 5/3$ , and represents the ratio of kinetic to potential energy for a spectrum of motions influenced at low frequencies by rotational effects. These saturated spectral amplitudes are found to be in excellent agreement with observations of the wave field at high vertical wavenumbers (Dewan et al., 1984; Smith et al., 1987; Fritts et al., 1988b; Sidi et al., 1988). Examples of velocity and fractional temperature spectra obtained by Fritts et al. (1988b) with the MU radar and high-resolution balloon soundings in Shigaraki, Japan during March 1986 are shown in Figure 4. In each case, the predicted saturation limit is shown with a straight dashed line for an  $N$  appropriate to the stratosphere. Solid and short-dashed curves show the observed horizontal velocity and fractional temperature spectra in the lower and middle stratosphere, respectively, and long-dashed curves show the corresponding tropospheric spectra.

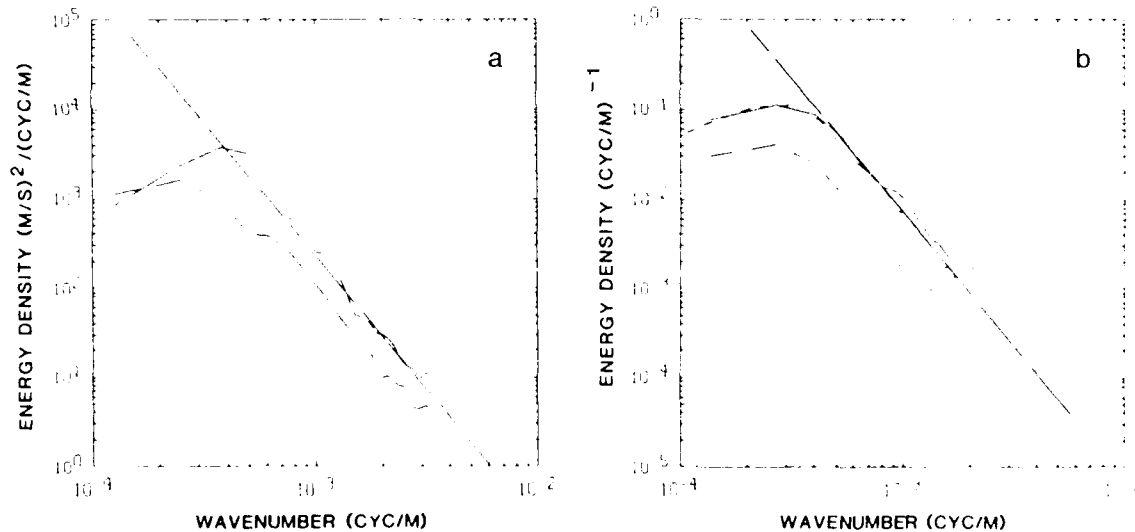


Fig. 4. Horizontal (zonal plus meridional) velocity and fractional temperature spectra in the troposphere and the lower and middle stratosphere obtained during an experiment at the MU radar in Shigaraki, Japan. The straight dashed lines correspond to the saturated spectrum predictions. See text for details.

At low vertical wavenumbers, the motions spectrum must acquire a positive slope in order for the energy density and the vertical fluxes of energy and momentum to remain finite (VanZandt and Fritts, 1989). Evidence of this is seen in Figure 4 where energy densities fall well below saturated spectral amplitudes for  $m < 4 \times 10^{-4}$  cyc/m and in other studies by Smith et al. (1987), Fritts and Chou (1987), and Sidi et al. (1988). A spectral form reminiscent of the oceanic internal wave spectrum (Garrett and Munk, 1972, 1975; Desaubies, 1976; VanZandt, 1982), and which fits atmospheric observations quite well, is

$$F(m) \sim \frac{(m/m_*)^s}{1 + (m/m_*)^{s+3}} \quad (3)$$

Here  $s$  is the asymptotic slope at small  $m$  and will be assumed to have a value near  $s = 1$  in the remainder of this paper. A vertical wavenumber spectrum of this form also allows for the growth of the energy (per unit mass) with increasing height via a decrease of the characteristic wavenumber,  $m_*$ , with height (Smith et al., 1987). In particular, the observed growth with height of wave energy (per unit mass) implies a faster growth of those motions with  $m < m_*$  since motions with  $m > m_*$  are largely constrained by saturation processes. For a gravity wave energy density (per unit mass) that varies as  $E \sim e^{z/H_E}$  with  $H_E \sim 12 - 15$  km, the characteristic vertical wavenumber varies as  $m_* \sim (m^3 F(m)/E)^{1/2} \sim e^{-z/2H_E}$  and the energy density for  $m < m_*$  then varies as  $F(m) \sim E/m_*^{(1+s)} \sim e^{(3+s)z/2H_E}$ . This suggests that motions at small  $m$  increase in amplitude without significant dissipation until they are sufficiently large to contribute to saturation processes.

The saturated spectrum concept offers clear advantages over monochromatic saturation theory because it permits gradual increases of wave drag and diffusion with increasing height rather than sudden transitions in drag and diffusion. Despite its apparent near-universality at large  $m$ , the saturated spectrum also allows for considerable temporal and geographic variability of the motion spectrum and can account for wave field anisotropy, momentum fluxes, and filtering effects. One example of this is the calculation of enhancements of wave drag and diffusion due to increases in  $N$  with height (VanZandt and Fritts, 1989).

Increases in  $N$  by a factor  $R \sim 2 - 3$  are typical near the tropopause and the high-latitude summer mesopause and imply significant changes in gravity wave structure, in saturated amplitudes, and in the corresponding wave spectrum with height. The interesting consequences occur, however, because the amplitudes of conservative wave motions and the amplitude limits imposed by linear saturation theory scale differently with  $N$ . The former vary in such a way to conserve the vertical flux of wave action (or wave energy in an unsheared flow), yielding an energy density per unit mass that varies as  $E \sim m/\rho_0 \sim R$ . But this energy is also shifted to a higher wavenumber  $m = Rm_0$ . Because the spectral energy content,  $mF(m)$ , varies as  $m^{-2}$  for  $m > m_*$ , the WKB-scaled energy density at wavenumber  $m$  increases as  $F^w(m) \sim R^3$ . For fixed  $m$ , in contrast, the saturated spectral energy densities vary as  $F^s(m) \sim N^2 \sim R^2$ . For an increase in  $N$  with height then, a saturated gravity wave spectrum will experience an additional dissipation, relative to that occurring due to either density or mean velocity variations, resulting from the response of wave motions to changes in  $N$  alone.

The influences of these effects on an incident wave spectrum are shown for  $R = 3$  in Figure 5. In the absence of dissipation, the incident spectrum, denoted  $i$ , is transformed to the spectrum denoted  $w$ , but the saturated spectral amplitude moves only from that labeled  $si$  to that labeled  $sf$ . This results in the energy lying between the curves  $f$  and  $w$  being above the saturation limit by a factor  $R$ , requiring dissipation over a depth interval comparable to a vertical wavelength, and implying corresponding increases in wave drag and diffusion. The relaxation of the wave spectrum from  $w$  to  $f$  results in a new characteristic vertical wavenumber,  $m_{*f} = R^{3/4}m_{*i} = R^{-1/4}m_{*w}$  and fractional losses of the energy and momentum fluxes of the wave spectrum of  $(1 - R^{-1/4})$  and  $(1 - R^{-1/2})$ , respectively, for  $s = 1$ . Corresponding estimates of the enhanced turbulent energy dissipation rate and momentum flux divergence vary as  $\Delta \epsilon \sim R(1 - R^{-1/2})$  and  $\Delta \bar{u}_t \sim R(1 - R^{-3/4})$  and appear to be consistent with atmospheric observations and the needs of large-scale models (VanZandt and Fritts, 1989).

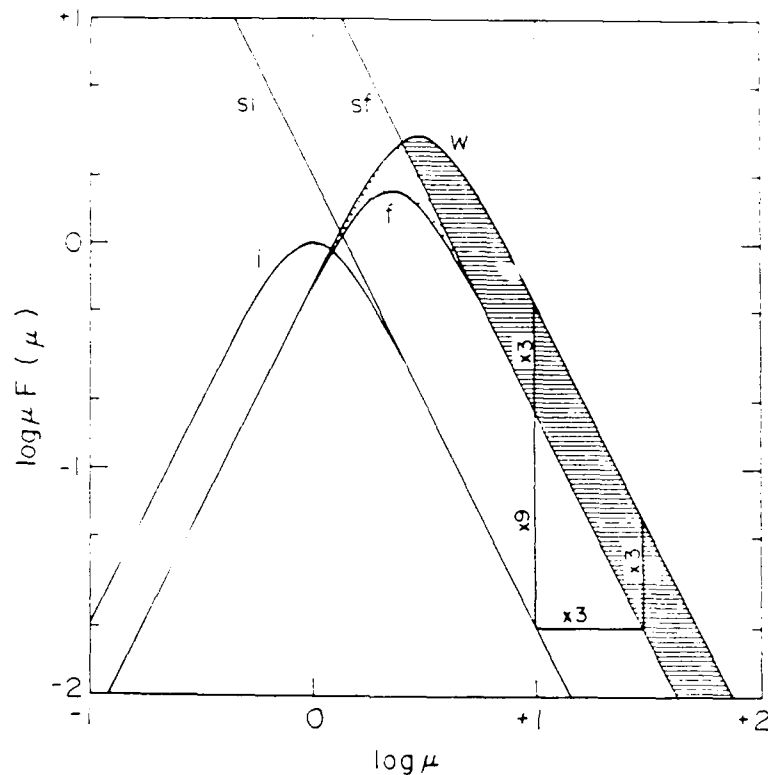


Fig. 5. Energy content spectra,  $\mu F(\mu)$ , where  $\mu = m/m_*$ , below an increase in  $N$  (i), above and WKB scaled (w), and above after adjustment to a new saturation limit (f) for  $R = 3$ . The energy difference between the spectra labeled w and f is that that must be dissipated near the increase in  $N$ . A spectrum of the form given by (3) with  $s = 1$  has been assumed.

It is apparent from the above discussion that the saturated gravity wave spectrum, independent of the processes acting to maintain this spectrum, may provide a convenient description of the manner in which atmospheric gravity waves evolve with height and respond to changes in the mean environment. As such, it offers a means of predicting wave influences arising from wave dissipation and of parameterizing wave effects in large-scale models of the atmosphere. The advantages of this approach remain to be determined, but it offers clear advantages over monochromatic saturation theory and is now being used as the basis for a GCM gravity wave parameterization.

#### IMPLICATIONS OF SATURATION

The saturation processes that act to determine the gravity wave spectrum in the atmosphere have clear implications for wave transports of energy and momentum and for wave generation of turbulence and diffusion. The former depend on the degree to which the wave spectrum is composed of upward-propagating motions and, in the case of the momentum flux, on its azimuthal anisotropy. Turbulence and diffusion, on the other hand, are dependent on the rate at which energy must be removed from the gravity wave spectrum to preserve saturated amplitudes and on the processes by which this is accomplished. We examine these consequences of saturation in an atmospheric context below. The extent to which saturation processes may be relevant in the oceans is considered in the following section.

### a. Fluxes of Energy and Momentum

Gravity wave observations cited above suggest that wave amplitudes are limited by saturation processes to values consistent with that required for linear wave instability,  $u' \approx (c - \bar{u})$  or  $\theta'_z \approx \bar{\theta}_z$ , where the subscripts denote differentiation. If we then use these values to examine the dependence of the energy and momentum fluxes on wave scales and frequencies, assuming  $f^2 \ll \omega^2 \ll 14^2$ , we obtain

$$c_{gz} E \sim \frac{\omega}{N} (c - \bar{u})^3 \quad (4)$$

and

$$\rho_0 \overline{u'w'} \sim \frac{\omega}{N} (c - \bar{u})^2 \quad (5)$$

These expressions suggest that gravity wave fluxes of energy and momentum should be dominated by those motions with high intrinsic frequencies and large horizontal phase speeds (or equivalently, large vertical wavelengths, since with our approximations  $\lambda_z \sim (c - \bar{u})/N$ ). This can be further quantified by assuming a mean frequency spectrum, as above, of  $F(\omega) \sim \omega^{-p}$  with  $p = 5/3$ . Then the flux content form of either the energy or momentum flux spectrum varies as  $\omega F(\omega) \sim \omega^{-2-p}$ . Integrating spectral contributions to the energy or momentum flux reveals that those motions with periods less than 1 hr account for  $\sim 70\%$  of the total flux, demonstrating the domination by the highest frequencies. The importance of the high-frequency motions is even more pronounced if one recognizes that the momentum flux due to low-frequency motions is further reduced by a factor  $\delta_z = (1 - f^2/\omega^2)$  due to transverse motions within the wave field. These estimates are confirmed by recent observations of gravity wave momentum fluxes in the middle atmosphere by Fritts and Vincent (1987) and Reid and Vincent (1987).

Gravity wave momentum fluxes are unimportant, of course, unless the wave motions are dissipated because it is the flux divergence that provides a forcing of the local mean flow. But saturation occurring within the wave spectrum provides this divergence and leads to accelerations of  $\sim 1 - 2$  and  $20 - 200$  m/s/day in the lower stratosphere and in the mesosphere and lower thermosphere, respectively (Palmer et al., 1986; McFarlane, 1987; Fritts and Vincent, 1987; Reid and Vincent, 1987; Reid et al., 1988). In most cases, the mean flux divergence leads to a net drag on the local mean flow, requiring a significant meridional circulation, to provide an approximate force balance. While the required meridional drift in the lower stratosphere is small, it becomes appreciable in the mesosphere,  $\bar{v} \sim 10 - 20$  m/s (Nastrom et al., 1982), and causes correspondingly large departures from radiative equilibrium conditions.

### b. Fluxes of Heat and Constituents

The diffusion implied by gravity wave saturation and turbulence production depends, in some measure at least, on the nature of the dominant saturation process. In the atmosphere, the observations and theory reviewed above suggest that this process is primarily a linear (convective or dynamical) instability of the wave field. Given also that the dominant energy fluxes are accomplished by waves with high intrinsic frequencies and that high frequencies strongly favor the convective over the dynamical instability, we assume, in addition, that saturation occurs largely via convective instability of the wave field. Finally, if we assume that turbulence is initiated only within regions with  $\theta_z < 0$  and that the turbulence decays sufficiently rapidly to be strongly localized in these regions, then it is possible to formulate a model of the fluxes of heat (and constituents) due to gravity wave saturation and to examine the influence of saturated wave amplitudes on the (wave and turbulence) transports of heat and momentum.

Such an approach was taken, first in an Eulerian frame by Fritts and Dunkerton (1985), and later in a Lagrangian frame by Coy and Fritts (1988). The results in each case are the same and may be summarized by the relation for the total heat flux

$$S = -\bar{\theta}_z \bar{v} \left( 1 - 2\beta\alpha + (1 + k^2/m^2)(1 + \gamma) \frac{\alpha^2}{2} \right) \quad (6)$$

where  $\bar{\theta}_z$  is the mean gradient of potential temperature,  $\bar{v}$  is the mean eddy diffusivity,  $k$  and  $m$  are the horizontal and vertical wavenumbers of the wave motion,  $\alpha = u/(c - u)$  is the nondimensional wave amplitude, and  $\beta$  and  $\gamma$  are functions of the distribution of  $v$  throughout the wave field (Fritts and Dunkerton, 1985; Coy and Fritts, 1988).

If we now assume  $v = v_0 ((1 - \cos\phi)/2)^n$  with  $\phi = 0$  in the most stable phase of the wave motion, then  $v$  is a maximum where  $\bar{\theta}_z$  is most negative (assuming  $\alpha > 1$ ) and increasing  $n$  implies an increasing degree of localization of turbulent diffusion within the most unstable phase of the wave. This yields  $\beta = n/(n + 1)$  and  $\gamma = n(n - 1)/(n + 1)(n + 2)$ , which cause  $S$  given by (6) to be less than its value with  $\beta = \gamma = 0$  for all  $\alpha$ . These results are presented graphically in Figure 6, where  $G$  is the coefficient on the right side of (6) and curves are labeled with values of  $n$ . Clearly, the heat flux is large for  $n = 0$ , and is enhanced by the wave motion for the reasons given by Coy and Fritts (1988). As turbulence becomes more localized, however, reductions in the heat flux become more pronounced. Thus, to the extent that this simple model describes the effects of a localized turbulent diffusion arising in response to convective instability, it suggests that the localization should result in a reduction of the overall (wave plus turbulence) heat flux and less efficient mixing due to gravity wave saturation.

Another way to view this process is in terms of the relative efficiency of diffusion of momentum and heat. If we represent this competition by an effective Prandtl number, then it can be shown that this is given by  $Pr = G^{-1}$  (Coy and Fritts, 1988). Thus, localized turbulence suggests a Prandtl number  $Pr \approx 3 - 10$  and implies that turbulence arising from gravity wave saturation will likely not mix the environment as efficiently as previously believed. These predictions have been confirmed by recent studies of the thermal and constituent structures of the middle atmosphere (Strobel et al., 1987; Strobel, 1989).

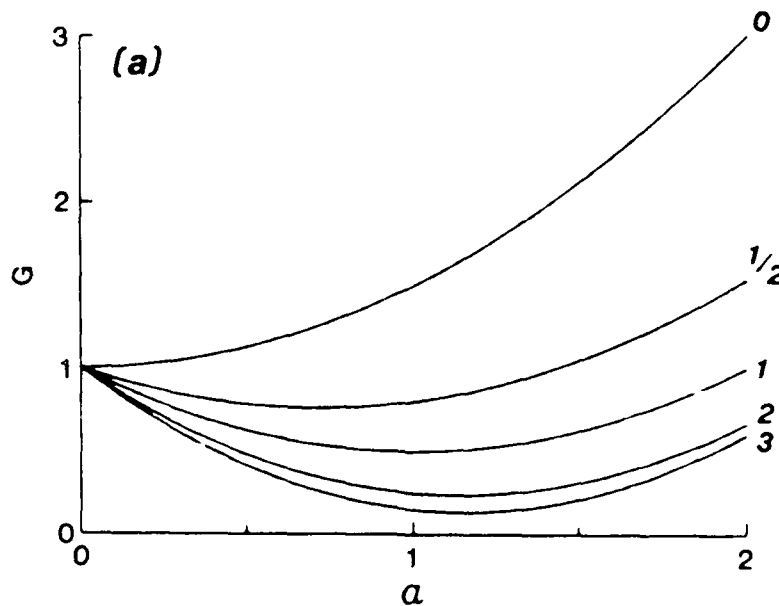


Fig. 6. The coefficient on the right side of (6) as a function of  $\alpha$  for various  $n$ . Note that  $\alpha = 1$  corresponds to the threshold amplitude for convective instability and that the smallest values of  $G$  (and the largest values of  $Pr$ ) occur for wave amplitudes just above this threshold.

## SUMMARY AND COMPARISON WITH OCEANS

This paper has provided a brief review of the processes thought to be responsible for gravity wave saturation in the middle atmosphere and of the consequences of saturation for the form of the wave spectrum, for transports of energy and momentum, and for diffusion of heat and constituents. Both observations and theory suggest that saturation occurs in the middle atmosphere largely as a result of linear instabilities within the wave field, leading to local turbulence production and diffusion. Nonlinear interactions among gravity waves or between gravity waves and the vortical mode no doubt occur, but appear not to control wave amplitudes sufficiently to account for the observed motion spectrum.

The effects of gravity wave saturation include 1) a motion spectrum that achieves a near-universal amplitude at high vertical wavenumbers that scales as  $F(m) \sim N^2/m^3$  as a result of amplitude limits applied to each component of the spectrum and 2) turbulence that acts locally to extract energy from large scales of motion and diffuse heat and constituents. The former implies divergences of the momentum and energy fluxes of the wave spectrum throughout the atmosphere while the latter suggests a turbulent diffusion that is much less efficient than an equivalent mean diffusion because of where turbulence arises within the wave field.

The extent to which these arguments have relevance in the oceans is, of course, a function of the character and the vigor of those processes acting to control amplitudes within the oceanic internal wave spectrum. To address this, we compare several measures of the rate at which energy must flow through the wave and turbulence spectrum in the atmosphere and the oceans in Table 1.

The range and extent of inertial range turbulence are controlled by the rate of energy flow and the strength of viscous dissipation, with  $L_B \sim (\epsilon/N^3)^{1/2}$  and  $l_0 \sim (v^3/\epsilon)^{1/4}$ , such that  $L_B/l_0 \sim \epsilon^{3/4}$ . But more important in a comparison of saturation processes in the atmosphere and oceans are 1) the transition from the gravity wave or buoyancy range to the inertial range and 2) the range of  $m$  over which wave amplitudes are large, because the strength of nonlinear interactions relative to wave time scales increases as  $m$  increases. This is particularly true in the atmosphere where the mean density structure causes wave motions with large vertical scales to increase rapidly in amplitude with time, thus permitting other (linear) instabilities to dominate the saturation process.

Table 1. Turbulence and wave parameters for the middle atmosphere and ocean.

Parameter		Atmosphere (~60 km)	Ocean
kinematic viscosity, $\nu$	(m <sup>2</sup> /s)	$\sim 10^{-1}$	$\sim 2 \times 10^{-6}$
outer scale of inertial range turbulence, $L_B$	(m)	$\sim 500$	$\sim 1$
inner scale of inertial range turbulence, $l_0$	(m)	$\sim 5$	$\sim 0.1$
turbulent energy dissipation rate, $\epsilon$	(m <sup>2</sup> /s <sup>3</sup> )	$\sim 10^{-2}$	$\sim 10^{-9}$
wave kinetic energy density, $E$	(m <sup>2</sup> /s <sup>2</sup> )	$\sim 10^2$	$\sim 10^{-2}$
rate of logarithmic energy decay, $d/dt \ln E$	(s <sup>-1</sup> )	$\sim 10^{-4}$	$\sim 10^{-7}$

The values of  $\epsilon$  and  $E$  cited in Table 1 reveal an enormous difference between the middle atmosphere and the oceans in terms of the rate at which wave energy must be dissipated in order to maintain the turbulent energy flux. A typical decay time for the atmospheric wave spectrum is a few hours while for the oceans it is  $\sim 100$  days. This suggests that the processes acting to extract energy from the wave spectrum must operate very rapidly and at large vertical scales in the atmosphere, but only gradually and at much smaller vertical scales in the oceans. Since a typical decay time for the atmosphere is comparable to typical gravity wave periods and nonlinear wave-wave interactions appear not to have sufficiently large interaction rates at large vertical scales, the middle atmosphere appears to favor the linear convective and/or dynamical instabilities as the dominant saturation processes. In the oceans, on the other hand, decay times exceed wave periods by  $10^2$  to  $10^3$  and thus provide ample opportunities for nonlinear interactions to occur and largely shape the internal wave spectral characteristics. To the extent that these ideas have merit, it should perhaps not be surprising that different processes act to control wave amplitudes and spectral energy transfers in the middle atmosphere and the oceans.

**Acknowledgments** This work was supported by the Air Force Office of Scientific Research (AFSC) under contract F49620-87-C-0024 and by the SDIO/IST and managed by the Office of Naval Research under contract N00014-86-K-0661.

#### REFERENCES

- Balsley, B.B., and D.A. Carter, 1982: The spectrum of atmospheric velocity fluctuations at 8 and 86 km. *Geophys. Res. Lett.*, **9**, 465-468.
- Balsley, B.B., W.L. Ecklund, and D.C. Fritts, 1983: VHF echoes from the high-latitude mesosphere and lower thermosphere: Observations and interpretations. *J. Atmos. Sci.*, **40**, 2451-2466.
- Balsley, B.B., and R. Garelo, 1985: The kinetic energy density in the troposphere, stratosphere and mesosphere: A preliminary study using the Poker Flat radar in Alaska. *Radio Sci.*, **20**, 1355-1362.
- Coy, L., and D.C. Fritts, 1988: Gravity wave heat fluxes: A Lagrangian approach. *J. Atmos. Sci.*, **45**, 1770-1780.
- Desaubies, Y.J.F., 1976: Analytical representation of internal wave spectra. *J. Phys. Oceanogr.*, **6**, 976-981.
- Dewan, E.M., and R.E. Good, 1986: Saturation and the "universal" spectrum for vertical profiles of horizontal scalar winds in the atmosphere. *J. Geophys. Res.*, **91**, 2742-2748.
- Dewan, E.M., N. Grossbard, A.F. Quesada, and R.E. Good, 1984: Spectral analysis of 10m resolution scalar velocity profiles in the stratosphere. *Geophys. Res. Lett.*, **11**, 80-83, and Correction to "Spectral analysis of.", *Geophys. Res. Lett.*, **11**, 624.
- Dong, B., and K.C. Yeh, 1988: Resonant and nonresonant wave-wave interactions in an isothermal atmosphere. *J. Geophys. Res.*, **93**, 3729-3744.
- Dunkerton, T.J., 1984: Inertio-gravity waves in the stratosphere. *J. Atmos. Sci.*, **41**, 3396-3404.
- Dunkerton, T.J., 1987: Effect of nonlinear instability on gravity wave momentum transport. *J. Atmos. Sci.*, **44**, 3188-3209.
- Fritts, D.C., 1984: Gravity wave saturation in the middle atmosphere: A review of theory and observations. *Rev. Geophys. Space Phys.*, **22**, 275-308.
- Fritts, D.C., 1985: A numerical study of gravity wave saturation: Nonlinear and multiple wave effects. *J. Atmos. Sci.*, **42**, 2043-2058.
- Fritts, D.C., 1989: A review of gravity wave saturation processes, effects, and variability in the middle atmosphere. *Pure Appl. Geophys.*, in press.
- Fritts, D.C., and H.-G. Chou, 1987: An investigation of the vertical wavenumber and frequency spectra of gravity wave motions in the lower stratosphere. *J. Atmos. Sci.*, **44**, 3610-3624.
- Fritts, D.C., and T.J. Dunkerton, 1985: Fluxes of heat and constituents due to convectively unstable gravity waves. *J. Atmos. Sci.*, **42**, 549-556.

- Fritts, D.C., and P.K. Rastogi, 1985: Convective and dynamical instabilities due to gravity wave motions in the lower and middle atmosphere: Theory and observations. *Radio Sci.*, **20**, 1247-1277.
- Fritts, D.C., S.A. Smith, B.B. Balsley, and C.R. Philbrick, 1988a: Evidence of gravity wave saturation and local turbulence production in the summer mesosphere and lower thermosphere during the STATE experiment. *J. Geophys. Res.*, **93**, 7015-7025.
- Fritts, D.C., T. Tsuda, T. Sato, S. Fukao, and S. Kato, 1988b: Observational evidence of a saturated gravity wave spectrum in the troposphere and lower stratosphere. *J. Atmos. Sci.*, **45**, 1741-1759.
- Fritts, D.C., and R.A. Vincent, 1987: Mesospheric momentum flux studies at Adelaide, Australia: Observations and a gravity wave/tidal interaction model. *J. Atmos. Sci.*, **44**, 605-619.
- Fritts, D.C., and L. Yuan, 1989: A stability analysis of inertio-gravity wave structure in the middle atmosphere. *J. Atmos. Sci.*, in press.
- Garcia, R.R., and S. Solomon, 1985: The effect of breaking gravity waves on the dynamical and chemical composition of the mesosphere and lower thermosphere. *J. Geophys. Res.*, **90**, 3850-3868.
- Garrett, C.J.R., and W.H. Munk, 1972: Space-time scales of internal waves. *Geophys. Astrophys. Fluid Dyn.*, **3**, 225-235.
- Garrett, C.J.R., and W.H. Munk, 1975: Space-time scales of internal waves: A progress report. *J. Geophys. Res.*, **80**, 291-297.
- Hasselmann, K., 1967: A criterion for nonlinear wave stability. *J. Fluid Mech.*, **30**, 737-739.
- Hines, C.O., 1960: Internal gravity waves at ionospheric heights. *Can. J. Phys.*, **38**, 1441-1481.
- Hines, C.O., 1988: The generation of turbulence by atmospheric gravity waves. *J. Atmos. Sci.*, **45**, 1269-1278.
- Hodges, R.R., Jr., 1967: Generation of turbulence in the upper atmosphere by internal gravity waves. *J. Geophys. Res.*, **72**, 3455-3458.
- Holloway, G., 1988: The buoyancy flux from internal gravity wave breaking. *Dyn. Atmos. Oceans*, **12**, 107-125.
- Holton, J.R., 1982: The role of gravity wave-induced drag and diffusion in the momentum budget of the mesosphere. *J. Atmos. Sci.*, **39**, 791-799.
- Inhester, B., B., 1987: The effect of inhomogeneities on the resonant parametric interaction of gravity waves in the atmosphere. *Ann. Geophys.*, **87**, 209-217.
- Lilly, D.K., 1978: A severe downslope windstorm and aircraft turbulence induced by a mountain wave. *J. Atmos. Sci.*, **35**, 59-77.
- Lilly, D.K., and P.J. Kennedy, 1973: Observations of a stationary mountain wave and its associated momentum flux and energy dissipation. *J. Atmos. Sci.*, **30**, 1135-1152.
- Lindzen, R.S., 1981: Turbulence and stress due to gravity wave and tidal breakdown. *J. Geophys. Res.*, **86**, 9707-9714.
- McComas, C.H., and F.P. Bretherton, 1977: Resonant interaction of oceanic internal waves. *J. Geophys. Res.*, **82**, 1397-1412.
- McFarlane, N.A., 1987: The effect of orographically excited gravity wave drag on the general circulation of the lower stratosphere and troposphere. *J. Atmos. Sci.*, **44**, 1775-1800.
- Meek, C.E., I.M. Reid, and A.H. Manson, 1985: Observations of mesospheric wind velocities. II. Cross sections of power spectral density for 488-8h, 8-1h, 1h-10 min over 60-110 km for 1981. *Radio Sci.*, **20**, 1383-1402.
- Miyahara, S., Y. Hayashi, and J.D. Mahlman, 1986: Interactions between gravity waves and the planetary scale flow simulated by the GFDL "SKYHI" general circulation model. *J. Atmos. Sci.*, **43**, 1844-1861.
- Muller, P., G. Holloway, F. Henyey, and N. Pomphrey, 1986: Nonlinear interactions among internal gravity waves. *Rev. Geophys.*, **24**, 493-536.
- Muraoka, Y., T. Sugiyam, K. Kawahira, T. Sato, T. Tsuda, S. Fukao, and S. Kato, 1988: Formation of mesospheric VHF echoing layers due to a gravity wave motion. *J. Atmos. Terres. Phys.*, **50**, 819-829.
- Nastrom, G.D., B.B. Balsley, and D.A. Carter, 1982: Mean meridional winds in the mid- and high-latitude summer mesosphere. *Geophys. Res. Lett.*, **9**, 139-142.



- Orlanski, I., and K. Bryan, 1969: Formation of the thermocline step structure by large-amplitude internal gravity waves. *J. Geophys. Res.*, **74**, 6975-6983.
- Orlanski, I., and B.B. Ross, 1973: Numerical simulation of the generation and breaking of internal gravity waves. *J. Geophys. Res.*, **78**, 8808-8826.
- Palmer, T.N., G.J. Shutts, and R. Swinbank, 1986: Alleviation of a systematic westerly bias in general circulation and numerical weather prediction models through an orographic gravity wave drag parameterization. *Quart. J. Roy. Met. Soc.*, **112**, 1001-1040.
- Philbrick, C.R., K.U. Grossman, R. Hennig, G. Lange, D. Krankowsky, D. Offermann, F.J. Schmidlin, and U. von Zahn, 1983: Vertical density and temperature structure over Northern Europe. *Adv. Space. Res.*, **2**, 121-124.
- Reid, I.M., R. Ruster, P. Czechowsky, and G. Schmidt, 1988: VHF radar measurements of momentum flux in the summer polar mesosphere over Andenes (69°N, 16°E), Norway. *Geophys. Res. Lett.*, **11**, 1263-1266.
- Reid, I.M., and R.A. Vincent, 1987: Measurements of mesospheric gravity wave momentum fluxes and mean flow accelerations at Adelaide, Australia. *J. Atmos. Terres. Phys.*, **49**, 443-460.
- Sidi, C., and J. Barat, 1986: Observational evidence of an inertial wind structure in the stratosphere. *J. Geophys. Res.*, **91**, 1209-1217.
- Sidi, C., J. Lefrere, F. Dalaudier, and J. Barat, 1988: An improved atmospheric buoyancy wave spectrum model. *J. Geophys. Res.*, **93**, 774-790.
- Smith, S.A., D.C. Fritts, and T.E. VanZandt, 1987: Evidence for a saturated spectrum of atmospheric gravity waves. *J. Atmos. Sci.*, **44**, 1404-1410.
- Strobel, D.F., 1989: Constraints on gravity wave induced diffusion in the middle atmosphere. *Pure Appl. Geophys.*, in press.
- Strobel, D.F., M.E. Summers, R.M. Bevilacqua, M.T. DeLand, and M. Allen, 1987: Vertical constituent transport in the mesosphere. *J. Geophys. Res.*, **92**, 6691-6698.
- Thrane, E.V., T.A. Blix, C. Hall, T.L. Hansen, U. von Zahn, W. Meyer, P. Czechowsky, G. Schmidt, H.-U. Widdel, and A. Neumann, 1987: Small scale structure and turbulence in the mesosphere and lower thermosphere at high latitudes in winter. *J. Atmos. Terres. Phys.*, **49**, 751-762.
- Tsuda, T., K. Hirose, S. Kato, and M.P. Sulzer, 1985: Some findings on correlation between the stratospheric echo power and the wind shear observed by the Arecibo UHF radar. *Radio Sci.*, **20**, 1503-1508.
- Ulick, J.C., M.C. Kelley, K.D. Baker, B.B. Balsley, and W.L. Ecklund, 1988: Comparison of simultaneous MST radar and electron density probe measurements during STATE. *J. Geophys. Res.*, **93**, 6989-7000.
- VanZandt, T.E., 1982: A universal spectrum of buoyancy waves in the atmosphere. *Geophys. Res. Lett.*, **9**, 575-578.
- VanZandt, T.E., and D.C. Fritts, 1989: A theory of enhanced saturation of the gravity wave spectrum due to increases in atmospheric stability. *Pure Appl. Geophys.*, in press.
- Vincent, R.A., 1984: Gravity wave motions in the mesosphere. *J. Atmos. Terres. Phys.*, **46**, 119-128.
- Vincent, R.A., and D.C. Fritts, 1987: A climatology of gravity waves in the mesosphere and lower thermosphere over Adelaide, Australia. *J. Atmos. Sci.*, **44**, 748-760.
- Walterscheid, R.L., and G. Schubert, 1989: Nonlinear evolution of an upward propagating gravity wave: Overturning, convection, and turbulence, submitted to *J. Atmos. Sci.*
- Yeh, K.C., and C.H. Liu, 1981: The instability of atmospheric gravity waves through wave-wave interactions. *J. Geophys. Res.*, **86**, 9722-9728.
- Yeh, K.C., and C.H. Liu, 1985: Evolution of atmospheric spectrum by processes of wave-wave interaction. *Radio Sci.*, **20**, 1279-1294.
- Yuan, L., and D.C. Fritts, 1989: Influence of a mean shear on the dynamical instability of an inertio-gravity wave. *J. Atmos. Sci.*, in press.

## PARAMETERIZATION OF OROGRAPHIC GRAVITY WAVE DRAG IN ATMOSPHERIC GENERAL CIRCULATION MODELS

Norman McFarlane

Canadian Climate Centre, 4905 Dufferin Street, Downsview, Ontario, Canada

### ABSTRACT

Most numerical models designed for numerical weather prediction or atmospheric general circulation studies have become increasingly more sophisticated in the past two decades. Rapid advances in super-computer technology have permitted development of models with relatively high spatial resolution and improved representation of physical processes. For the most part this has resulted in more accurate modelling of atmospheric flow regimes. However, certain systematic deficiencies, related in part to representation of the effects of variations in surface orographic elevation, have remained. Recently it has been found that these systematic errors are substantially reduced when the drag forces resulting from breaking of unresolved, orographically excited, gravity waves are parameterized in the models. In this paper the parameterization techniques currently used are outlined and some examples of the effects of using them in an atmospheric general circulation model are presented.

### INTRODUCTION

Most numerical models used for weather prediction or atmospheric general circulation studies are designed to represent phenomena whose horizontal and vertical length scales are a few hundred kilometers and a few hundred meters respectively. The models all make use of the primitive equations of motion. The range of atmospheric phenomena that are resolved is illustrated to some extent by noting that the density scale height in the troposphere is of the order of 10 km. This is also a representative depth for the synoptic scale dynamical processes in the troposphere. Typical flow speeds are in the range of 10-20 m/sec in the middle troposphere. The potential temperature variation in the vertical is typically such that the buoyancy period ( $2\pi/N$ ;  $N$  = Brunt-Väisälä frequency) is a few hundred seconds. Thus a typical internal wave vertical length scale, given by the product of the buoyancy period and the flow speed, is a few kilometers while a typical Rossby deformation length scale is a few thousand kilometers.

Synoptic-scale storms embedded in the middle latitude westerly flow are baroclinic eddies whose dynamics are quasi-geostrophic in nature. Such eddies are adequately resolved in atmospheric general circulation models.

Substantial refinements of the spatial resolution of global atmospheric models have accompanied advances in super-computer technology in the past decade. In general this has resulted in more accurate modelling of flow patterns. However, certain systematic errors have not only remained but become accentuated with increased horizontal resolution. These errors are associated, at least in part, with inadequate representation of the effects of orography on the atmospheric flow in synoptic and planetary scales. The

errors in question are quite apparent for the northern hemispheric flow during winter and are characterized by excessively strong westerly flow over continental areas in middle and high latitudes. This excessively strong zonal flow regime is accompanied by unrealistically low and broad minima in pressure and temperature fields in northerly regions.

A terrain-following coordinate system is used in most atmospheric models. Although effects of variations in orographic forcing at the surface are formally taken into account in such a coordinate system, all the models employ smoothed representations of orographic height fields. The smoothing procedure may vary somewhat from model to model but is invariably such as to ensure that the smoothed field does not contain scales of variation which are smaller than those explicitly resolved in the model.

Largely as a result of radiative cooling at the surface the atmospheric boundary layer over continents is stably stratified in winter. The boundary layer formulations commonly used in atmospheric models are such as to ensure suppression of vertical transports by turbulent processes in stably stratified flow near the surface. Consequently surface wind stress values (and the associated frictional drag forces) are often rather small in mountainous regions during winter, even though surface roughness may be larger than in other locations. Thus, in the absence of other parameterizations of the effects of unresolved orography, representation of the effects of mountains is accomplished entirely through the effects of (smoothed) variations in the elevation of the lower boundary in the terrain-following coordinate system. Reduction of the barrier effect of mountains associated with smoothing may have a detrimental effect on modelling of flow which is strongly statically stable near the surface. Wallace et al. (1983) were able to reduce systematic errors over continental areas in winter to some extent by simply adding to the smoothed orography a height increment proportional to the local standard deviation about this smoothed mean. Use of such "envelope" orography is less effective, and sometimes detrimental, in summer when the near surface flow is often slightly unstably stratified and surface heat fluxes and wind stresses are relatively large.

A second means of reducing the systematic westerly flow error in models is associated with parameterization of the effects of unresolved internal gravity waves. It is well known that such waves are excited when stably stratified air flows over irregular terrain. The Eliassen-Palm theorem indicates that the vertical momentum flux associated with stationary internal gravity waves is independent of height except in regions where wave dissipation occurs. In such regions wave momentum flux divergence gives rise to drag forces which act on the mean flow. The idea that such mountain wave drag forces may have a significant impact on the larger scale flow is not of recent origin. The linear theory of mountain waves, though analytically difficult in general, has been explored quite extensively for idealised mean flow conditions so that many of the important properties of these waves are now known. A few detailed observational studies of naturally occurring wave events have been carried out within the last two decades. To a substantial extent these studies confirm the usefulness of linear theory in describing the salient features of such wave systems.

Sawyer (1959) suggested, on the basis of linear theoretical calculations, that the effects of mountain wave momentum fluxes should be taken into account in numerical weather prediction models. However, at that time detailed observational studies of mountain waves were not available and sample theoretical calculations had not been done for very realistic conditions of background flow and topographic forcing. Moreover the existing

numerical weather prediction models were far too unsophisticated to provide clear evidence that errors in numerical weather forecasts were due explicitly to neglect of mountain wave drag as opposed to a variety of other physical processes which were either neglected as well or very poorly represented by the coarse spatial resolution employed in the models at that time. A decade later Bretherton (1969) presented results of a theoretical calculation of the linear wave response for realistic mean flow and topographic forcing conditions selected from actual observations of flow conditions over an area in Wales. This paper was an important contribution to the literature on this subject in that it not only demonstrated that wave momentum fluxes of substantial magnitudes could be associated with gravity waves excited in realistic conditions but also included a thorough discussion of the relevant linear wave dynamics and included some discussion of the question of parameterizing their effects in larger scale models.

A large amount of very useful information has been provided by the series of detailed aircraft observations of mountain wave events in the Colorado Rocky mountains documented and analysed in a series of papers by D.K. Lilly and colleagues. These studies have stimulated the development of several high resolution numerical models of stratified flow over ridges. Results from these modelling studies are still being published and have provided valuable insights into the non-linear wave dynamics. Of particular relevance to the parameterization problem is the finding that the onset of convective instability in the waves is of crucial importance in determining locations of vertical momentum flux divergence. The importance of this processes in regard to mountain waves was demonstrated numerically by Clark and Peltier (1977), although the idea that such wave breaking effects may determine gravity wave momentum flux profiles in general has an earlier origin in the literature on middle and upper atmosphere dynamics. The wave saturation hypothesis of Lindzen (1981) was proposed in this context and now forms the basis of the current parameterization schemes.

## PARAMETERIZATION OF OROGRAPHIC WAVE DRAG

### *Basic theoretical ideas*

Most of the orographic gravity wave drag parameterization schemes currently used in atmospheric models are based on those developed independently by McFarlane (1987) and Palmer et al. (1986). These two schemes are fundamentally similar in formulation, and in practice behave in much the same way.

The relevant theoretical ideas can be outlined simply by considering the linear theory for steady unidirectional flow of stably stratified air over a two-dimensional orographic perturbation whose displacement from the larger scale mean terrain height is of the form

$$h(x) = h_0 \cos(kx) \quad (1)$$

where the horizontal coordinate ( $x$ ) is oriented in the direction of the mean flow and  $k$  is a characteristic horizontal wave number for the perturbation.

In this simple monochromatic wave response case the horizontal and vertical velocities ( $u, w$ ) and potential temperature ( $\theta$ ) perturbations can all be represented in terms of a stream line displacement function ( $\delta$ ) such that

$$u = -(1/\bar{\rho}) \partial(\bar{\rho}\bar{u}\delta)/\partial z \quad (2)$$

$$w = \bar{u}\partial\delta/\partial x \quad (3)$$

$$\theta = -\delta\partial\bar{\theta}/\partial z \quad (4)$$

where over bars denote mean flow quantities, assumed to vary only in the vertical ( $z$ ) direction.

The streamline displacement must conform to the orographic perturbation at the lower boundary. This boundary condition is applied at the level of the undisturbed mean terrain ( $z = 0$ ).

It is assumed at the outset that the horizontal scale of the wave response is such that the flow is nearly in hydrostatic balance and that effects of rotation can be ignored. In addition mean flow quantities are assumed to vary more slowly in the vertical than do those associated with the wave. These assumptions imply that

$$N/\bar{u} \gg k \gg f/\bar{u} \quad (5)$$

$$\{N/(\bar{u}\chi)\} |\partial\chi/\partial z| \ll 1 \quad (6)$$

where  $\chi$  is a mean flow quantity.

Under these assumptions an approximate solution to the linear partial differential equation governing the streamline displacement can be obtained using the WKBJ method. Details are given in McFarlane (1987). The result is

$$\delta = A \cos(kx + \phi) \quad (7)$$

$$u = NA \sin(kx + \phi) \quad (8)$$

$$w = -k\bar{u} A \sin(kx + \phi) \quad (9)$$

$$\theta = -A(\partial\bar{\theta}/\partial z) \cos(kx + \phi) \quad (10)$$

where the amplitude ( $A$ ) and phase ( $\phi$ ) of the streamline displacement function are as follows:

$$A^2 = h_0^2 (\bar{\rho}(0) N(0) \bar{u}(0))/\bar{\rho}N\bar{u} \quad (11)$$

$$\phi = \int_0^z (N/\bar{u})dz \quad (12)$$

where the Brunt-Väisälä frequency is defined as

$$N^2 = (g/\bar{\theta}) \partial\bar{\theta}/\partial z \quad (13)$$

The vertical momentum flux, averaged over a horizontal wavelength is

$$\bar{\rho}\bar{u}\bar{w} \approx -(k/2)\bar{\rho}N\bar{u}A^2 \quad (14)$$

As expected, this quantity is independent of height when the wave amplitude is given by equation (11). However, since air density decreases with height in the atmosphere while the mean flow speed and Brunt-Väisälä frequency remain finite it is clear that equation (11) implies that the wave amplitude will eventually become very large. This will also be true in regions where the mean flow speed becomes small. Such behaviour would, of course, lead to violation of the linearization assumptions employed up to this point. More importantly, however, small scale convective and shearing instabilities may occur when the wave amplitude becomes sufficiently large. Such processes act to dissipate wave energy and limit the wave amplitude. These dissipative effects are taken into account in a simple way by invoking a wave amplitude saturation hypothesis.

It is assumed here that the onset of convective instability is the dominant process leading to limitation of wave amplitudes. This process can occur if the total potential temperature (including both mean flow and wave contributions) decreases with height somewhere in the atmosphere. Using equation (10) with the WKBJ assumption that mean flow quantities vary slowly in the vertical over a distance of the order of a vertical wavelength gives the following approximate expression for the vertical potential temperature gradient:

$$\partial(\bar{\theta} + \theta)/\partial z \approx (\partial\bar{\theta}/\partial z) \{1 + (NA/\bar{u}) \sin(kx + \phi)\} \quad (15)$$

This quantity must be negative for the onset of convectivity, a condition which can be satisfied somewhere in the wave if the amplitude is large enough so that the quantity  $NA/\bar{u}$  exceeds unity. The amplitude saturation hypothesis simply assumes that the effects of convective over-turning act to limit the wave amplitude without substantially affecting its phase structure. The mathematical statement of this hypothesis is simply

$$A \leq F_c \bar{u}/N \quad (16)$$

where  $F_c$  is unity for the simple monochromatic wave response considered here.

In practice this saturation condition can be implemented in a simple way by starting at the surface with the wave amplitude defined as

$$A = \text{MIN}(h_0, F_c \bar{u}/N) \quad (17)$$

and the vertical momentum flux defined by (14). The amplitude at any other height can be determined in terms of its value a short distance below by assuming first that the momentum flux does not vary over this short distance. The amplitude so determined is then limited if necessary by invoking the saturation hypothesis (16). The resulting amplitude is then used in equation (14) to specify the vertical momentum flux at the vertical level in question. The drag force on the mean flow which results from divergence of the vertical momentum flux due to the wave produces a local deceleration of the flow such that

$$(\partial\bar{u}/\partial t)_w = -(1/\bar{\rho})\partial(\bar{\rho}\bar{u}\bar{w})/\partial z \quad (18)$$

(the subscript denotes an effect due to wave-drag).

### *Parameterization procedure*

The orographic gravity wave-drag parameterizations currently used in global atmospheric models are based on the simple monochromatic wave model outlined above. The wave-drag force is represented as a local deceleration of that component of the flow which is parallel to the flow at a reference level near the surface. The local deceleration term has the form

$$(\partial V / \partial t)_w = \mathbf{n}(1/\rho L) \partial(\rho N U D^2) / \partial z \quad (19)$$

where  $V$  is the local flow velocity,  $\mathbf{n}$  a unit vector in the direction of the flow at the reference level, and  $U$  is the component of the local velocity in that direction.

The displacement amplitude,  $D$ , is initially defined at the reference level in terms of the variance associated with the unresolved orography in the manner outlined in McFarlane (1987). The length scale,  $L$ , is taken to be a tuneable parameter whose value is fixed for all locations. As discussed in McFarlane (op.cit.),  $(1/L)$  can be thought of as being the ratio of a wave generating efficiency factor and an effective gravity wave length scale. In practice it was chosen to ensure that wave momentum flux values determined by the parameterization for typical large scale flow conditions were in reasonable accord with observed values.

The procedure for determining  $D$  at higher model levels is as outlined above and may be stated as follows:

$$D_j^2 = \text{MIN}\{(\rho N U D^2)_{j+1}/(\rho N U)_j, (F_c U/N)_j^2\} \quad (20)$$

where the index,  $j$ , increases downward from the top of the model. The value of  $F_c$  is fixed and slightly less than unity in the parameterization of McFarlane (1987) but is made to be a function of the local gradient Richardson number in that of Palmer et al. (1986). This, in fact, is the only essential difference between the two schemes.

### **EFFECTS OF WAVE-DRAG ON THE CIRCULATION SIMULATED BY GLOBAL ATMOSPHERIC MODELS**

Although the wave-drag parameterization outlined above is based on a highly simplified model of the wave generation process, its use in atmospheric general circulation models and numerical weather prediction models has resulted in a significant reduction of the systematic westerly flow error which develops in the northern hemisphere in winter. Examples of this are documented in Palmer et al. (1986) and McFarlane (1987). The results of those studies have since been confirmed in other models and this has led to a rather general use of these parameterization schemes in atmospheric models.

Two figures are included here to illustrate the general nature of the improvements which are found with use of the wave-drag parameterization outlined above in the Canadian Climate Centre atmospheric general circulation model. Examples of the zonally averaged westerly flow, which is typically simulated by the model for the December to February period, both with and without the wave-drag parameterization are shown in Figure 1. The climatological flow, as obtained from several years of objectively analysed data from the National Meteorological Center, is also shown for comparison. Figure 2 depicts the zonally averaged mean sea-level atmospheric pressure for the corresponding cases.

The reduction of the excessive westerly flow in the upper troposphere in high northern latitudes is quite apparent in the simulation which included the wave-drag parameterization (Fig. 1B). The flow in this case is in better agreement with observed climatology (Fig. 1C). The improvement in simulated surface pressure fields is perhaps even more dramatic, as illustrated in Figure 2A,B. This effect is also seen at higher levels and coincides with reduction of the erroneous cool bias which develops in polar regions in winter (see McFarlane, 1987, for further details of this effect). The thermal response is, of course, an effect of the non-linear adjustment of the large scale flow toward a thermal wind balance in the presence of the wave-drag forcing of the wind field.

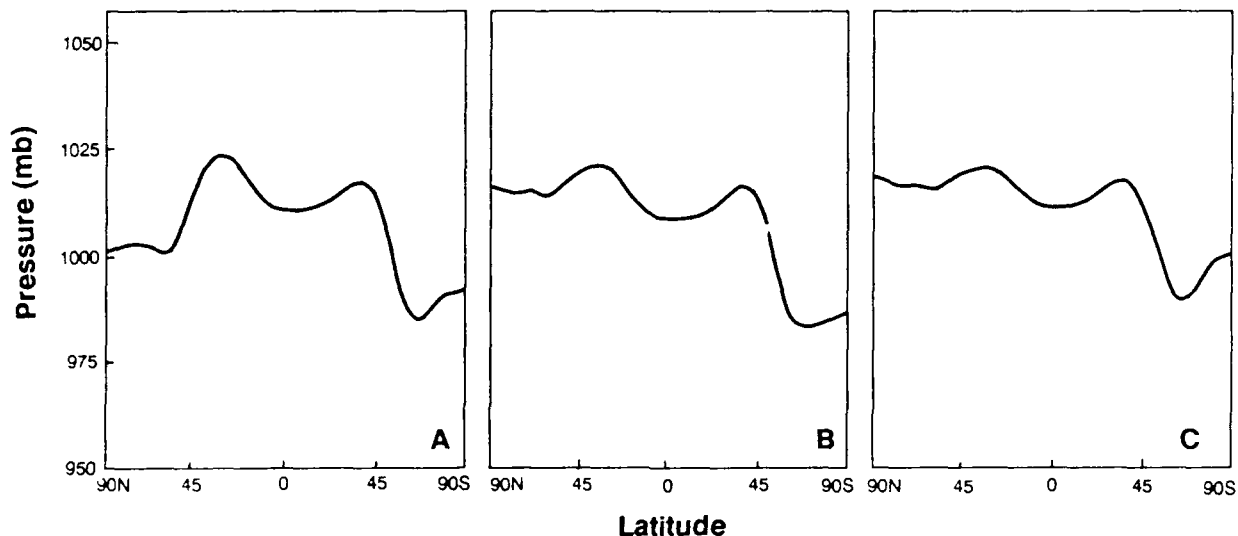


Figure 1. Zonally averaged zonal flow for the December-February season as simulated with the CCC AGCM and from observations. (A) Control (without wave drag); (B) With orographic wave drag; (C) Observed, based on seven years of objectively analyzed data from the U.S. National Meteorological Center. Contours every 5 m/sec.

## DISCUSSION

Although the wave drag parameterization discussed above is based on a highly simplified model of orographic gravity wave dynamics, it captures some of the important effects of those waves on the larger scale atmospheric flow. However, it is over-simplified in many respects. An obvious deficiency is the assumption that the dominant effects can be accounted for in terms of a single gravity wave whose characteristic horizontal wave length is independent of location or mean flow conditions.

In principle it is possible to permit excitation of a spectrum of waves at any particular location in response to variations in the spectral content of the unresolved orography. In practice, however, such a procedure would greatly complicate the implementation of gravity wave parameterizations in models. It is probable that a major effect of horizontal variations in the structure of the unresolved orography has to do with the possibility that an azimuthal spectrum of waves may be excited. Hines (1988) has proposed that such a possibility may be dealt with in a simple way by classifying the local orography as to whether it is predominantly isotropic in structure (rolling terrain) or anisotropic with a



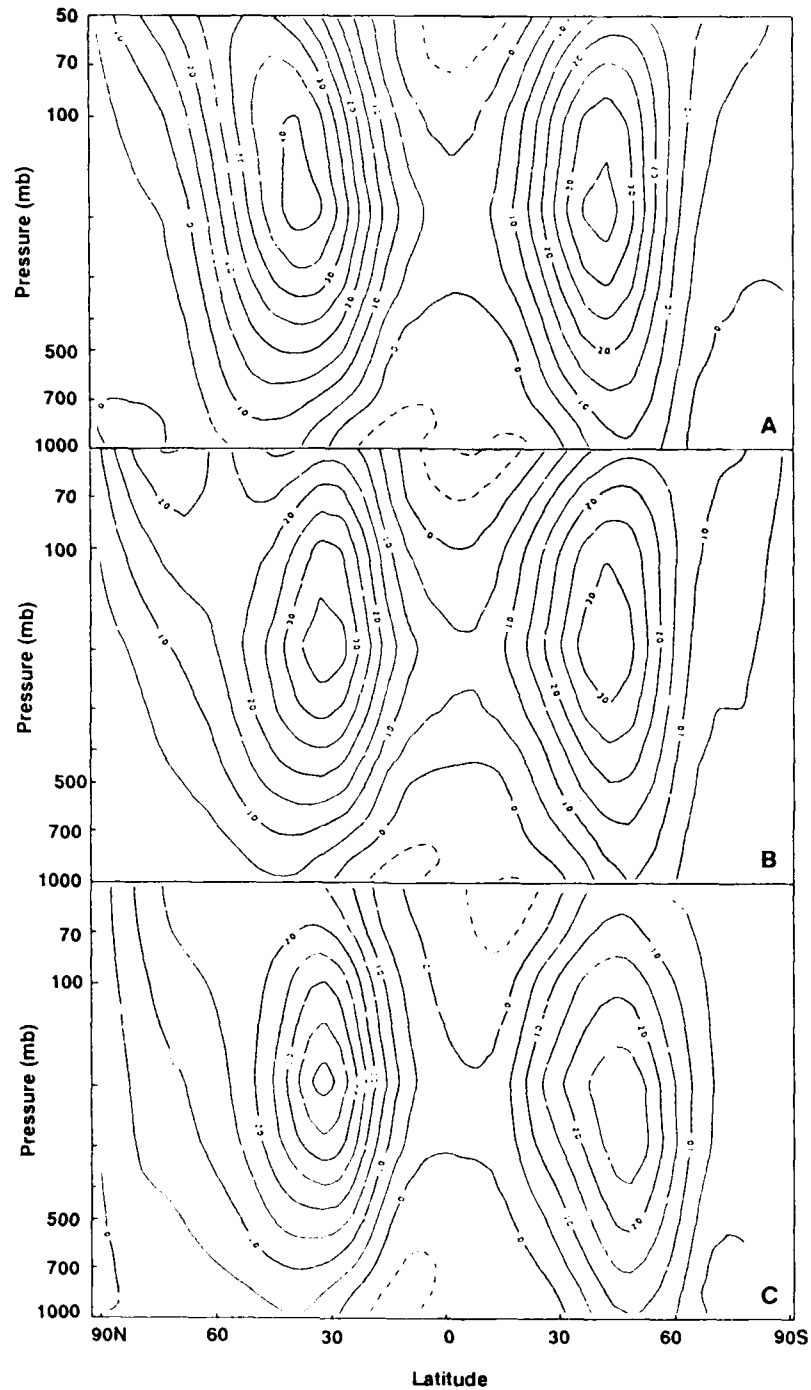


Figure 2. Zonally averaged mean sea level pressure for the December-February season as simulated with the CCC AGCM and from observations. (A) Control (without wave drag); (B) With orographic wave drag; (C) Observed, based on seven years of objectively analyzed data from the U.S. National Meteorological Center.

dominant orientation (a series of ridges). In the case of a single dominant orientation the simple wave-drag schemes presently used might still be applied for that component of the flow which is normal to the dominant ridges.

When the local orography is predominantly isotropic in nature Hines (1988) has proposed use of an azimuthal spectrum consisting of a small number of waves (at least two!), each having a specified orientation with respect to the reference level mean flow. Isotropy of the underlying terrain implies that all waves have the same amplitude and horizontal wavelength at the reference level. However, because they are differently oriented, each of the waves may be differently affected by vertical variations in the mean flow, especially when it changes direction with height.

This, of course, raises the question of how to deal with super-positioning of the waves when applying the saturation hypothesis. In this case, at a given altitude, wave interference may either enhance or inhibit the onset of convective instability. In our view a simple but physically satisfying way of dealing with such a circumstance has not yet been proposed. This problem is also present when the orography is anisotropic but localized in structure (a single dominant ridge, for example). In this case a longitudinal spectrum of waves may be excited and interfere in such a way as to inhibit convective overturning except at preferred locations in the vertical. It is well known, for instance, that for homogeneous flow over bell-shaped ridges convective instability is inhibited below a distance of one half of a vertical wavelength above the surface and occurs preferentially at  $3/4$  of a vertical wavelength (plus integral multiples of a wavelength) above the surface (Lilly and Klemp, 1979).

The validity of linear theory is, at least formally, suspect when wave amplitudes become large enough to induce the onset of convective instability. The presence of more than one wave enhances the likelihood that non-linear effects may be non-negligible. The non-linear dynamics of two-dimensional flow over isolated ridges is now the subject of active research using high resolution numerical models such as that of Clark and Peltier (1977). Recently published work in this field has demonstrated that the combined effects of convective over-turning and non-linearity can in some cases give rise to complicated temporal behaviour in the region between the surface and the level at which convective instability arises, leading to development of a flow regime which is quite different from that implied by linear wave theory, and associated vertical momentum flux profiles which are strongly divergent in the lower levels and substantially larger in magnitude than linear estimates.

This sort of phenomenon occurs in nature as well, examples being the strong down-slope wind storms which occur sporadically in mountainous regions (Chinooks, Bora). Although such events are not frequent, they may have a significant impact on the evolution of the larger scale flow during their lifetime. They are not yet well enough understood to permit parameterization of their effects in larger scale models.

Fortunately the available observational data (e.g., Lilly et al., 1982) suggest that the more frequently occurring mountain wave systems are at least qualitatively in accord with linear theory and this will probably remain as the basis for future work directed toward improvement of the orographic gravity wave models used in the wave-drag parameterizations, although strongly non-linear processes such as those discussed above may eventually be shown to be of sufficient importance that their effects will have to be taken into account in future parameterizations.

The wave saturation concept, though physically appealing, is hypothetical in nature and remains to be confirmed on the basis of observational data, although considerable progress in this regard is being made. Studies such as those of D. Fritts and colleagues (reported elsewhere in these proceedings) do lend some credibility to the wave saturation hypothesis. Studies of this sort may in fact provide the basis for improving wave drag parameterizations in a number of ways including accounting for wave excitation from other sources in the atmosphere.

## REFERENCES

- Boer, G.J., N.A. McFarlane, R. Laprise, J.D. Henderson, J.P. Blanchet, 1984; The Canadian Climate Centre Spectral Atmospheric General Circulation Model. *Atmosphere-Ocean*, 22, 1397-429.
- Bretherton, F.P., 1969; Momentum transport by gravity waves. *Quart. J.R. Met. Soc.*, 95, 213-243.
- Clark, T.L., and W.R. Peltier, 1977; On the evolution and stability of finite amplitude mountain waves. *J. Atmos. Sci.*, 34, 1715-1730.
- Hines, Colin O., 1988, A modelling of atmospheric gravity waves and wave drag generated by isotropic and anisotropic terrain. *J. Atmos. Sci.*, 45, 309-322.
- Lilly, D.K., and J.B. Klemp, 1979; The effects of terrain shape on non-linear hydrostatic mountain waves. *J. Fluid. Mech.*, 95, 241-246.
- Lilly, D.K., J.M. Nicholls, R.M. Chervin, P.J. Kennedy, and J.B. Klemp, 1982; Aircraft measurements of wave momentum flux over the Colorado Rocky Mountains. *Quart. J.R. Met. Soc.*, 108, 625-642.
- Lindzen, R.S., 1981, Turbulence and stress owing to gravity wave and tidal breakdown. *J. Geophys. Res.*, 86, 9707-9714.
- McFarlane, N.A., 1987; The effect of orographically excited gravity wave drag on the general circulation of the lower stratosphere and troposphere. *J. Atmos. Sci.*, 44, 1775-1800.
- Palmer, T.N., G.J. Shutts, and R. Swinbank., 1986; Alleviation of a systematic westerly bias in general circulation and numerical weather prediction models through an orographic gravity wave drag parameterization. *Quart. J. R. Met. Soc.*, 112, 1001-1039.
- Sawyer, J.S., 1959; Introduction of the effects of topography into methods of numerical weather forecasting. *Quart. J. R. Met. Soc.*, 85, 31-43.
- Wallace, J.M., S. Tibaldi, and A.J. Simmons, 1983; Reduction of systematic forecast errors in the ECMWF model through introduction of an envelope orography. *Quart. J. R. Met. Soc.*, 109, 683-717.

## WHY EDDY DIFFUSIVITY DOESN'T WORK

Frank S. Henyey

Areté Associates, La Jolla, California 92037  
and Center for Studies of Nonlinear Dynamics,  
La Jolla Institute, La Jolla, California 92037

### ABSTRACT

Three topics are discussed for which the concept of diffusion is inappropriate for summarizing the effect of small scale flows on larger flows. These three topics are lack of sufficient scale separation, conservation laws, and the mediating effect of intermediate scales to transfer non-diffusive effects from small scales to large.

### INTRODUCTION

In modelling large scale flows in the ocean, one would like to be able to summarize the smaller scale processes in some simple way. A very common way is to use eddy viscosity, or other eddy diffusivities. The small-scale oceanographer is then supposed to supply the correct value of the diffusivity to be used in larger scales. The purpose of this paper is to point out that the use of eddy diffusivities is not an appropriate summary of small-scale phenomena, and a more complete description of these small features is required.

There are three topics that I will discuss to support this view. The first is that there is not a sufficient gap in scales between the small-scale flows one wishes to eliminate and the larger scale flows of interest. The second is the incompatibility of some conservation laws with diffusion. The third is that effects at small scales can be mediated by intermediate scales, leading to non-diffusive behavior.

### NO SCALE GAP

We first discuss the absence of enough scale separation. It is true that if there were enough scale separation, the small scales would provide a diffusivity given by the Green-Kubo formula

$$D = \int_0^{\infty} \langle \mathbf{v}(t) \mathbf{v}(t+\tau) \rangle d\tau \quad (1)$$

where  $\mathbf{v}$  is the velocity followed by a Lagrangian tracer, (or, more generally, the velocity of the quantity being diffused), and the expression is written assuming  $\langle \mathbf{v} \rangle = 0$ . The Green-Kubo formula is exactly what happens with thermal motions, providing the "molecular diffusivity". The thermal fluctuations have a wave number spectrum which is white

$$\begin{aligned} dE(\mathbf{k}) &= \frac{k_B T}{(2\pi)^3} d^3\mathbf{k} \\ &= \frac{k_B T}{(2\pi)^3} k^2 dk d^2\Omega \end{aligned} \quad (2)$$

so that most of the velocity fluctuations are at very small scale. Ocean spectra, on the other hand, often have a negative power of  $k$  rather than a positive power. One cannot assume the scales are separated.

For molecular diffusivity, a cloud of tracer particles becomes diffuse as time goes on; the rms separation between two initially close particles is just  $\sqrt{2}$  times the rms displacement of each one. The same value of the diffusivity applies to both the one-particle and two-particle cases. For "eddy diffusivity", this clearly doesn't work. The separation between particles is generally much smaller than  $\sqrt{2}$  times the distance they have moved. This discrepancy is an indication that there is something wrong.

A way to understand the situation in which diffusivity does not work, is to use the approximation

$$D \approx \int_0^T \langle \mathbf{v}(t) \mathbf{v}(t+\tau) \rangle d\tau \quad (3)$$

where  $T$  is the time scale on which the large-scale phenomena occur. (Thus  $D$  depends on more than the properties of the neglected small scales.) If the resulting value of  $D$  is not close to the infinite time limit, one should not expect diffusive behavior. Consider, for a moment, a small scale circular eddy. The Lagrangian velocity field is oscillating as the particle is carried around the eddy, and the time required for convergence of the Green-Kubo expression is likely to be very much larger than the rotation period of the eddy; if the convergence time is a year, the effect of the eddy cannot be summarized as diffusion for processes with characteristic times of a month. The typical sizes of flows with characteristic times short compared to the Green-Kubo convergence time can be considerably larger than the eddy under consideration.

It is the nature of diffusion that if there isn't any organized flow such as advection, the rms distance moved goes as the square root of the time. For non-diffusive cases, where eddy diffusion would often be used, various models have been worked out to give the time scaling of typical displacements. One of the earliest was Richardson (1926), who obtained  $x \sim t^{3/2}$  for turbulent transport. This scaling has been refined, and other cases investigated by the Montroll school. Shlesinger and co-workers (1986), for example, have improved on Richardson's original work. More relevant to the ocean problems is the recent work by Young et al. (1989). They consider the

transport of a tracer in a sequence of eddies considered to be stationary. Most of the tracer will stay at the outer edges of an eddy and be rapidly transported past the eddy. Some of the tracer, however, works its way into the eddy, where it is trapped for a significant time, and slowly released. If there were to be enough eddies, almost all of the tracer would eventually find itself in some eddy, and the diffusive regime would be recovered, but with a very small diffusivity determined by the trapping time. Most of the tracer would initially be transported significant distances i.e., several eddy diameters at a much higher rate than the ultimate asymptotic diffusion. The power law obtained by these workers depends on the specific model they make for the eddies. Young (1988) has also looked at the more general problem of transport with trapping.

## CONSERVATION LAWS

The second topic concerns conservation laws. I will discuss this topic by means of an example. This example does not divide large scale from small scale, but divides submesoscale from even smaller scales. It concerns the interaction of submesoscale eddies with internal waves. The POLYMODE Local Dynamics Experiment group, McWilliams et al. (1983), find that an eddy viscosity estimated from a correlation between mesoscale horizontal shear and internal wave Reynolds stress implies a lifetime for a submesoscale eddy of 10 days, inconsistent with the observed much longer lifetime. (They speculate that absence of scale separation is responsible for the discrepancy; I will offer another explanation). This puzzle can be resolved by considering conservation laws. The integral of any function  $F(\rho, J)$  of potential density  $\rho$  and potential vorticity  $J$  is conserved if dissipative processes are neglected. In fact,  $F$  is only advected by the water. Since internal waves propagate through the water, they carry zero value of each of these quantities. (Since  $J$  is nonlinear, the internal waves must include their nonlinear interactions in order to make this true.) Thus, interaction with internal waves can change the energy of an eddy, but cannot change the conservation of each  $F$ . If we assume the eddy is energetic relative to the internal waves with which it interacts, the second law of thermodynamics requires a random wave field to reduce the energy of the eddy. Eventually the eddy will have as little energy as it can, consistent with the conservation of each  $F$ .

A theorem known to Kelvin and proved by Arnol'd (1965) (quoted by Vallis et al., 1989) states that a steady flow is a stationary point of the energy with the constraint given by the conservation laws. This stationary point cannot be a local maximum, because a small amount of internal wave energy can always be added. It might be a saddle point, or it might be a minimum. Stability analysis suggests it is often a minimum. Stable solutions (neglecting the  $\beta$  effect) are circular vortices. The observed long-lifetime eddies do appear to be these circular solutions. The observations and the stability analysis are reviewed by McWilliams (1985).

If one attempted to describe the evolution of an eddy in a bath of internal waves using an effective diffusivity, the value of such a diffusivity would rapidly approach zero as the circular conditions were approached. (Nonetheless, the fluctuations that diffusion theory relates to dissipation would not diminish at all). As with the first topic I discussed, the effective diffusivity depends on the larger scale flow as well as on the eliminated smaller scales.

Vallis et al. (1989) look for extremal energy flows by evolving the equations of motion with a modification which dissipates energy but does not modify the vorticity invariants. Perhaps their modified equations (with the energy-dissipating parameter properly chosen) may model the actual large-scale flow in the presence of an internal-wave bath.

## MEDIATION BY INTERMEDIATE SCALES

The third topic that illustrates flaws in the concept of eddy diffusivity involves even smaller scales. The large scales are now on the order of 10 meters, and the small scales are perhaps in the centimeter regime.

It is believed that the properties of the large scales in fully developed 3D turbulence are unaffected by changes in the viscosity. Doing anything to the small scales should, if eddy viscosity ideas apply, change the value of the eddy viscosity, but nothing more. In particular, with enough scale difference between the large scale flows and the small ones summarized by an eddy viscosity, the large scales should be unaffected.

But this is not what happens. It turns out that turbulent drag is reduced by adding very small amounts of long chain polymers to the water (or other fluid). These polymers directly influence rather small scales. I think the drag should be thought about as an energy loss, rather than as a force. The idea is that the interior of the flow dissipates energy, and the boundary layers adjust themselves to make the forces agree with the energetics. With this view, the drag has become inevitable when the largest scales of the flow, which are organized, break down into random flows at the next smaller scales. Doing something to the small scales has influenced the large scales.

The contrary view, widely held, is that the drag reduction is a boundary layer effect, and that the foregoing argument does not apply. Adherents of this view discount the experiments in which attempts were made to keep the polymers out of the boundary layer, and drag reduction still occurred (actually, it works even better).

As a result, experiments have been done avoiding boundaries completely. It appears that the spectrum of turbulence is steeper than without the polymers, with the large scales stronger and the small scales weaker. This is entirely consistent with my view that the energetics is dominant. In the drag reducing case, more energy remains in the larger scales, and less cascades to smaller scales.

This upscale influence must require the presence of the intermediate scales. It seems that the arguments which give rise to molecular diffusivities would apply in the absence of these scales. There is something, as yet not definitively identified, which works its way from scale to scale, upstream against the energy cascade, and changes the strength of that cascade. That something is not eddy viscosity, but something which knows more about the properties of the small scale flow.

## CONCLUSION

The various topics I have treated show that the relevance of small-scale oceanography to large scales is more profound than can be summarized in a handful of parameters. Answers to questions discussed by small-scale modellers, such as whether small-scale flows are internal waves or vortical motions (Müller et al., 1988) have ramifications to larger scale questions such as the evolution of circular vortices.

## REFERENCES

- Arnol'd, V. I.: 1965. Variational principle for three-dimensional steady-state flows of an ideal fluid. *J. Applied Math. and Mech.*, **29**, 1002-1008.
- McWilliams, J.C.: 1985. Submesoscale, Coherent Vortices in the Ocean. *Rev. Geophys.*, **23**, 165-182.
- McWilliams, J.C., E.D. Brown, H.L. Bryden, C.C. Ebbesmeyer, B.A. Elliott, R.H. Heinmiller, B. Lien Hua, K.D. Leaman, E.J. Lindstrom, J.R. Luyten, S.E. McDowell, W. Breckner Owens, H. Perkins, J.F. Price, L. Regier, S.C. Riser, H.T. Rossby, T.B. Sanford, C.Y. Shen, B.A. Taft, and J.C. Van Leer: 1983. The Local Dynamics of Eddies in the Western North Atlantic. *Eddies in Marine Science*, A.R. Robinson (Ed.) (New York: Springer Verlag).
- Müller, P., R.C. Lien, and R. Williams: 1988. Estimates of Potential Vorticity at Small Scales in the Ocean. *J. Phys. Ocean*, **18**, 401-416.
- Richardson, L.F.: 1926. Atmospheric Diffusion shown on a Distance Neighbour Graph. *Proc. Roy. Soc. London Ser. A*, **110**, 709 - 737.
- Shlesinger, M.F., B.J. West, and J. Klafter: 1986. Diffusion in a Turbulent Phase Space. *The Physics of Phase Space*, Y.S. Kim and W.W. Zachary, eds. (New York: Springer Verlag).
- Vallis, G.K., G.F. Carnevale, and W.R. Young: 1989. Extremal energy properties and construction of stable solutions of the Euler equations. *J. Fluid Mech.*, in press.
- Young, W.R.: 1988. Arrested shear dispersion and other models of anomalous diffusion. *J. Fluid Mech.* **193**, 129-149.
- Young, W.R., A. Pumir, and Y. Pomeau: 1989. Anomalous diffusion of tracer in convection rolls. *Physics of Fluids*, **A 1**, 462-469.



# RETROSPECT ON OCEANIC BOUNDARY LAYER MODELING AND SECOND MOMENT CLOSURE

George L. Mellor

Atmospheric and Oceanic Sciences Program, Princeton University,  
Princeton, New Jersey 08542

## ABSTRACT

Models that describe ocean surface and bottom layers are discussed in the context of numerical ocean modeling; second moment turbulence models are emphasized. Here, we deal with the methodology and with errors that have been encountered. Errors relate to: (i) inadequate model resolution and boundary conditions which are, oftentimes, severely filtered, (ii) errors in the surface forcing variables, and (iii) inherent errors in model physics. It is difficult to quantify and even indentify the errors in each category. We begin here to evaluate (i). One finding is that error is reduced if observed, large horizontal scale, internal wave energy is included in the turbulence energy, closure equations.

## 1. INTRODUCTION

This is partially an essay and a tutorial on turbulence modeling of geophysical flows although we hope to bring forward some useful new information. Some of my colleagues and I believe that second moment turbulence closure comes closest to being a "theory" among the various schemes now extant in the ocean modeling community and, consequently, has a greater range of application. This fact is almost self-evident to us, but may not be self-evident to an important segment of the ocean community. I therefore welcome the opportunity presented by this workshop to argue our case; I try to do so with a minimum use of equations although the essence of second moment closure does reside in the relevant equations for which references are cited.

The beginning of second moment closure (henceforth SMC) or second order closure, as it is sometimes called, is now ancient history (Kolmogorov, 1941; Rotta, 1951) and its extension and application to geophysical flows is over fifteen years old (Mellor, 1973; Lewellen and Teske, 1973; Lumley et al., 1978; see also Mellor and Yamada, 1982, and Rodi, 1987, for extensive references). Not too much has happened in recent years to the models per se. However, the number of applications to oceans and atmospheres has mounted steadily as has a developing sense of the role of SMC as it fits into the overall ocean modeling problem. Primarily, SMC provides mixing information in the surface and bottom boundary layers related to shear and buoyancy driven turbulence. It is silent about the smaller but climatologically important mixing processes in the interior ocean which are the subject of much of this workshop.

The basis of SMC modeling, which we will deal with directly in section 3, is that the turbulence structures of one problem, defined by a set of boundary conditions, are similar to another problem, defined by another set of boundary conditions; i.e., there is sufficient degree of universality such that a few non-dimensional constants, imbedded in theoretically derived, second moment equations and conceptually derived hypotheses, can predict a useful range of turbulence problems.

Some attributes of second moment closure are as follows: (i) It embodies hypotheses that absorb empirical constants; they are, however, constants which are well defined in terms of measureable turbulence variables. Second moment closure directly addresses the fact of the fluid being turbulent; then, predicts the consequences. (ii) It accounts for a range of turbulence problems so that, for example, the same theory is useful for oceanic bottom layers (and atmospheric boundary layers) as well as surface layers and, in fact, a larger range of turbulence problems whether they are oceanic or not.

As a consequence of (i) and (ii), one can make use of relatively unambiguous laboratory data and can incorporate laboratory concepts into our thinking. This is fortunate because geophysical flows—albeit the ultimate target for enhanced understanding and simulative skills—are complicated; observational data is the composite result of competing and interacting physical processes. Thus, concepts such as the law-of-the-wall and the roughness parameter might never have been clearly isolated from the geophysical record, *cum sole*. We rely on laboratory data for many other turbulent flow concepts. Conversely, it is hard to create the natural geophysical environment (small Rossby numbers, large Richardson numbers) in the laboratory. Thus, some kind of a theoretical framework is needed.

SMC models, as they are presently formulated, are meant to account for small scale turbulence; in the oceans, this translates into scales of the order of tens of meters. Larger scales should, in principal, be accounted for by well resolved time-dependent, three-dimensional, numerical models or, if not, by sub-grid scale parameterization which specifically accounts for the lack of model resolution. We discuss this matter in section 4.

Numerical ocean models which are supposed to simulate observed data generally suffer from inadequate resolution and boundary conditions which are not sufficiently well known or resolved. Thus, we do not know the error inherent in SMC models except by extrapolation from more sedate applications where competing physical processes are minimal and boundary conditions are well posed. Our expectation is that the inherent error is small. However, we do know that most closure models, including SMC, do not account for mixing due to small scale internal waves or surface waves, scales of the order of tens of meters or less. These are mixed layer scales and may interact with "turbulence". The lack of understanding of this coupling and its level of physical importance is a weakness in need of repair.

## 2. LOCAL VERSUS BULK MODELS

The issue of bulk (or integral) versus local (or differential) models has been around for a long time. There are "localists" and there are "bulkists". Mitigating against local theories is the fact that turbulence length scales are not very small (but, as we later shall argue, small enough) compared to problem scales. It is this very fact that makes turbulence so difficult a subject. (Conversely, the kinetic theory of gases leads rigorously to the Navier-Stokes constitutive equations due to the fact that the molecular mean free path is very small compared to the problem scale. The Navier-Stokes relations are empirically and successfully applied to liquids for the same reason.)

Not too long ago an eminent scientist was heard to express puzzlement over the fact that, while temperature and salinity are well mixed in "mixed layers", velocity or momentum may not be. However, this issue is simple. Let heat and momentum flux be defined according to

$$-\overline{w'\theta'} = K_H \frac{\partial \theta}{\partial z}, \quad -\overline{w'u'} = K_M \frac{\partial U}{\partial z}$$

where the left sides of the above equations are the heat flux and one component of the momentum flux. We approximate  $K_H = K_M$  and further approximate the flux ratio to be constant across the mixed layer and equal to the surface values. Therefore  $(\partial\theta/\partial z)/(\partial U/\partial z) \approx (H/\rho c_p)/(\tau_x/\rho)$ . Take representative surface values for heat flux and stress,  $H = 200 \text{ W m}^{-2}$ ,  $\tau_x/\rho = 4 \times 10^{-4} \text{ m}^2 \text{ s}^{-2}$  so that

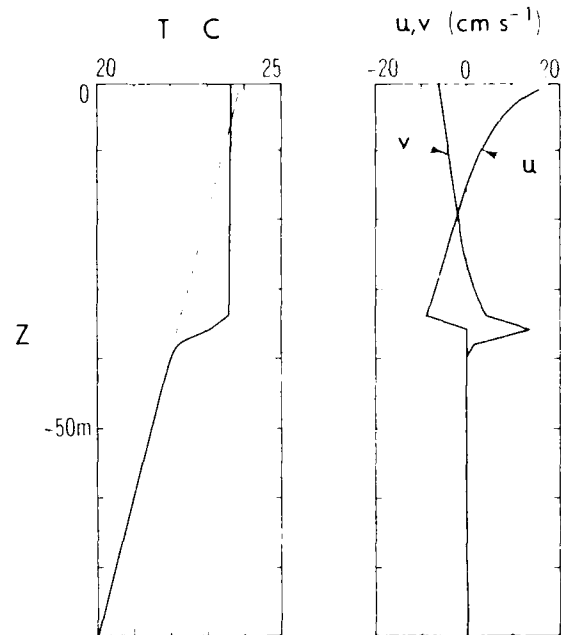
$$\frac{\partial\theta/\partial z}{\partial U/\partial z} \approx 0.1 \frac{^\circ\text{C}}{\text{m s}^{-1}}$$

Thus, a velocity change across the entire layer of, say,  $20 \text{ cm s}^{-1}$  will be accompanied by a temperature change of only  $0.02^\circ\text{C}$ , a simple theoretical result, generally inaccessible to bulk theories. Figure 1 is a model illustration of the cited example after five days from the initial conditions given by the dashed lines. (For the numerical calculations shown in Figs. 1, 9, and 10, the vertical increment was 3 m, the time step 20 min and background diffusivities of  $0.1 \text{ cm}^2 \text{ s}^{-1}$  were added to  $K_M$  and  $K_H$ .) By the way, the term "mixed layer" is poor semantics; nevertheless, it is rooted in oceanographic jargon.

Just how large are turbulence scales?

In Fig. 2, we show non-geophysical ( $f = N = 0$ ), high Reynolds number, boundary layer data obtained in a wind tunnel. The along-flow pressure gradient is first zero ( $x < 18$  feet) and then positive ( $x > 18$  feet). The flow is fully turbulent since the Reynolds number, based on mainstream velocity and boundary layer thickness, is much greater than the transition Reynolds number. Due to the positive (adverse) pressure

Figure 1. An illustrative mixed layer development for a layer forced by a wind stress of  $4 \text{ dynes cm}^{-2}$  and a (warming) heat flux of  $200 \text{ W m}^{-2}$ . The initial temperature and velocity components are given by the dashed lines. The solid curves are after five days of integration. The Coriolis parameter is  $0.727 \times 10^{-4}$  corresponding to  $30^\circ\text{N}$ .



gradient, the flow separates at  $x = 25.5$  feet. The main information in Fig. 2 is that the lateral integral length scale,  $\Lambda = \int_0^{\delta} g dr$ , where the upper limit is taken near the zero crossing of  $g$ , is about  $1/5$  of the boundary layer thickness,  $\delta$ , in the constant pressure gradient part;  $\Lambda$  decreases to about  $1/10 \delta$  in the positive pressure gradient part. Here  $g$  is the lateral correlation plotted in the upper panel in Fig. 2. The integral of the longitudinal correlation function as shown in the lower panel is about twice the former value in accordance with isotropic turbulence theory although the flow is certainly not isotropic.

If we take the lateral (or shear) integral length as the relevant turbulence length scale, then  $\Lambda/\delta = 0.2$  is small but not very small; it does not persuade or dissuade one to adopt a local description of the turbulence. However, if one does adopt an eddy viscosity parameterization based on SCM or even a lower level parameterization, then one does find that, by integrating the mean equations of motion, the flow can be simulated in detail; that is, experimental velocity profiles that, for example, are associated with the data of Fig. 2, can be calculated with quite good accuracy (Kline et al., 1968). Thus, one finds that the length scale of turbulence is small enough to enable local models to yield approximate but good estimates of reality.

Integral or bulk models are often useful in expressing simple ideas; the relation between Ekman transport and wind stress is a notable example. They are useful in one form or other for incorporation into simple theories of oceanic processes. There are quite a few clever bulk models that have evolved since the well known Kraus-Turner (1967) model. Generally, these models make statements about the turbulent entrainment or detrainment of fluid into a pre-defined or assumed mixed layer. Some

of the newer schemes (Garwood, 1977; Niiler 1975) have been shown (Martin 1985; see comments in section 5) to yield quite good estimates of ocean surface temperatures and mixed layer depth. Their disadvantage is that they are one-problem models whose constants are adjusted for the ocean surface boundary layer problem. (However, the latter attribute may be an advantage since the constants can be tuned to the ocean

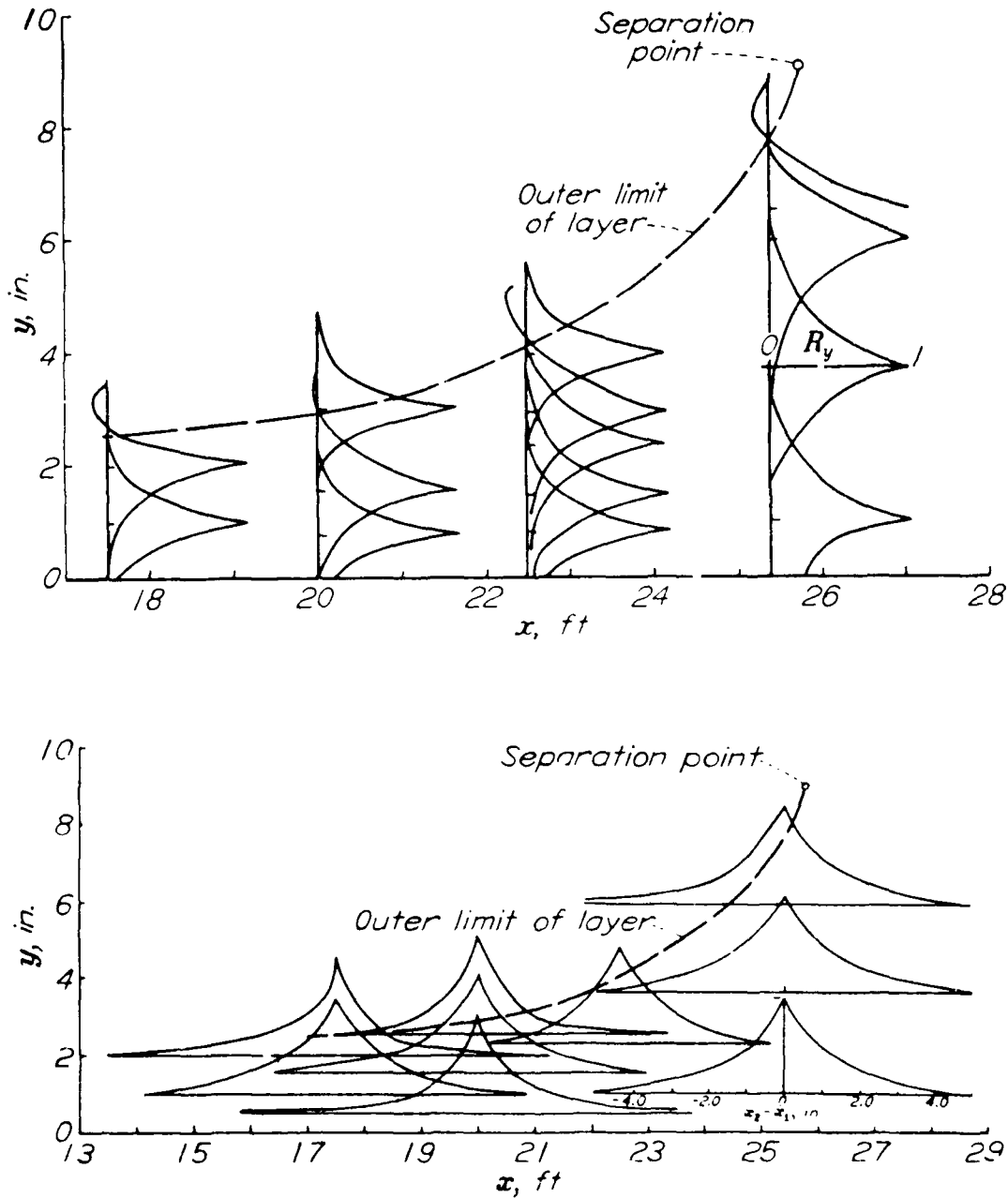


Figure 2. Lateral (or transverse) correlation coefficients,  $g(r_z)$ , are shown in the top panel. Longitudinal correlation coefficients are shown in the bottom panel. They are measured in a cross-stream homogeneous, boundary layer flow. After Schubauer and Klebanoff (1951).

surface problem.) The wind stress, normally considered a boundary condition, is built into the governing differential equations. The models do not, for example, apply to the bottom boundary layer and, therefore, to estuaries or to surface boundary layers of ice covered waters. Furthermore, bulk theories do not yield information on velocity or temperature or other scalar profiles, such as biochemical constituents or turbulence (see Yamada, 1983, for a direct application of turbulence information to the problem of plume dispersion); they do not relate to laboratory turbulent flows where detailed turbulence information is available.

An intriguing new model by Price et al. (1986), relying on a few simple observables, states that local mixing is enabled until three criteria are satisfied: that local static stability be positive or null, the local Richardson number not exceed 0.25 and a bulk Richardson number not exceed 0.65. The authors call it a bulk theory but, operationally, it seems to be a combined local and bulk model. The model would seem to be degenerate in the neutral case and is limited in problem range as are the bulk models.

### 3. SECOND MOMENT TURBULENCE CLOSURE

There now exist quite a few second moment models with application to geophysical flows (Lewellen and Teske, 1973; Lumley et al., 1978; Andre et al., 1978<sup>1</sup>; Therry and Lacarrere, 1983). They differ in detail but it is probable that their performance in simulating mean properties does not differ greatly. We introduced our own model some years ago (Mellor, 1973; Mellor and Yamada, 1974; Mellor and Durbin, 1974). The model development did three things: First, it extended the Rotta and Kolmogorov hypotheses into density stratified regimes. Second, it created rational simplifications so that one need not prognostically solve for all components of the Reynolds stress and heat flux tensors. Third, it demonstrated skill in solving diverse turbulence problems including oceanic problems. Table 1 is a list of fluid problems that have been simulated with the M-Y model and have generally compared well with observational data.

The M-Y model consists of the following:

- 1) A hypothesis by Rotta (1951) for the pressure, velocity gradient covariance term and extended to the pressure, temperature (density) gradient covariance terms. The hypothesis relates these terms to linear

<sup>1</sup>The model of Andre et al. is labeled a *third moment* model by the authors, since closures are constructed for the fourth moment terms in an equation for the diffusional third moments. However, the more important pressure-velocity gradient terms and the dissipation--related to the gradient of the two-point triple correlation (Mellor, 1985)--are still closed at a lower order so that the model is predominantly a second moment model.

TABLE 1. An abbreviated table of turbulent flow problems where the M-Y model has been compared with data. Non-dimensional constants in the model have been obtained from cases 1, 2 and 3. Cases 1 to 10 are non-rotating, neutral flows. (L) signifies laboratory data whereas (F) signifies field data. † signifies that the non-hydrostatic equations and the level 4 model have been used. Three-dimensional ocean and atmospheric simulations are not included. See Mellor and Yamada (1982) and this paper for references.

1.	Velocity and temperature laws of the wall.	(L)
2.	Constant pressure boundary layer.	(L)
3.	Decaying Isotropic Turbulence	(L)
<hr/>		
4.	Decaying, anisotropic turbulence	(L)
5.	Boundary layer flow over a flat plate	(L)
6.	Channel Flow	(L)
7.	Pipe Flow	(L)
8.	Separated and reattached flow on a flat plate	(L) †
9.	Separated and reattached flow over backward facing step.	(L) †
10.	Curved boundary layer flow	(L)
11.	Free convection topped by inversion	(L)
12.	Surface stress forced entrainment	(L)
13.	Near surface PBL (Monin-Obukhoff Similarity)	(F)
14.	1-D, "Wangara" atmospheric boundary layer.	(F)
15.	1-D, Ocean surface mixed layers.	(F)

functions of the Reynolds stress and heat (density) flux and are tensorially unambiguous.

2) The Kolmogorov (1941) hypothesis for the dissipation extended to other dissipation terms involving the fluctuating temperature (density) gradients. The choice here is unambiguous.

3) Fickian type gradient terms for turbulence diffusion terms. The choice here is somewhat ambiguous but these terms play a relatively minor role (they are excluded from the level 2 model).

4) Steps 1 and 2 lead to the definition of four length scales and a non-dimensional constant. It is then assumed that all are proportional to one another or to a "master length scale". There are then five constants to be determined. These constants are unambiguously related to measured laboratory turbulence data for neutral flows.

There is left the specification of the master length scale,  $\ell$ . But assuming that  $\ell = kz$  is valid near a solid surface (the five constants were scaled as a group so that  $\ell$  became asymptotically equal to Prandtl's mixing length as a solid surface is approached), the Monin-

Obukhov similarity variables were derived and compared with near surface wind data obtained from a meteorological tower in Kansas (Businger et al., 1971) as shown in Fig. 3. It was this result (Mellor, 1973) that encouraged further development and application of the model. Apparently, not all SCM models have reproduced this result.

The so-called level 2 and 2 1/2 models both lead to expressions for the vertical diffusivities,  $K_M$  and  $K_H$ , such that

$$K_M = q \ell S_M \quad (1a)$$

$$K_H = q \ell S_H \quad (1b)$$

where  $q^2/2$  is the turbulence kinetic energy,  $\ell$  is the turbulence master scale. The coefficients,  $S_M$  and  $S_H$ , are functions of a Richardson number given by<sup>2</sup>

$$\begin{aligned} S_H [1 - (3A_2B_2 + 18A_1A_2)G_H] \\ = A_2[1 - 6A_1/B_1] \end{aligned} \quad (2a)$$

$$\begin{aligned} S_M [1 - 9A_1A_2G_H] - S_H [(18A_1^2 + 9A_1A_2)G_H] \\ = A_1[1 - 3C_1 - 6A_1/B_1] \end{aligned} \quad (2b)$$

where

$$G_H = -(\ell^2/q^2)(g/\rho_o) \partial\rho/\partial z \quad (2c)$$

is a Richardson number. The five constants in (2a,b) are mostly evaluated from near surface data (law-of-the-wall region) and are found (Mellor and Yamada, 1982) to be  $(A_1, A_2, B_1, B_2, C_1) = (0.92, 16.6, 0.74, 10.1, 0.08)$ . The stability functions,  $S_M(G_H)$  and  $S_H(G_H)$ , are plotted in Fig. 4. The stability functions limit to infinity as  $G_H$  approaches the value 0.0288, a value larger than one expects to find in nature.

<sup>2</sup>In Mellor and Yamada (1982)  $S_M$  and  $S_F$  were also listed as additional functions of either the parameter,  $G_M = \ell^2 [(\partial U/\partial z)^2 + (\partial V/\partial z)^2]/q^2$  or the parameter,  $(Ps + Pb)/\epsilon$  where  $Ps$ ,  $Pb$  and  $\epsilon$  are shear production, buoyancy production, and dissipation respectively. Subsequently, Yamada (1983) found that  $(Ps + Pb)/\epsilon$  could be set to unity without much change in calculated results. Then Galperin et al. (1988) justified this step by recognizing that  $(Ps + Pb)/\epsilon = 1 + O(a^2)$  where  $a^2$  is a non-dimensional measure of the departure from isotropy (Mellor and Yamada, 1974). Within the rules of the level 2 1/2 model, the  $O(a^2)$  term could be neglected. In practice, we have also found negligible differences in performance between the two versions and the newer version does avoid some numerical complexities. However, there is a disadvantage; when one examines the resulting turbulence components, they do not add up to  $q^2$ ; the difference is  $q^2 O(a^2)$ .



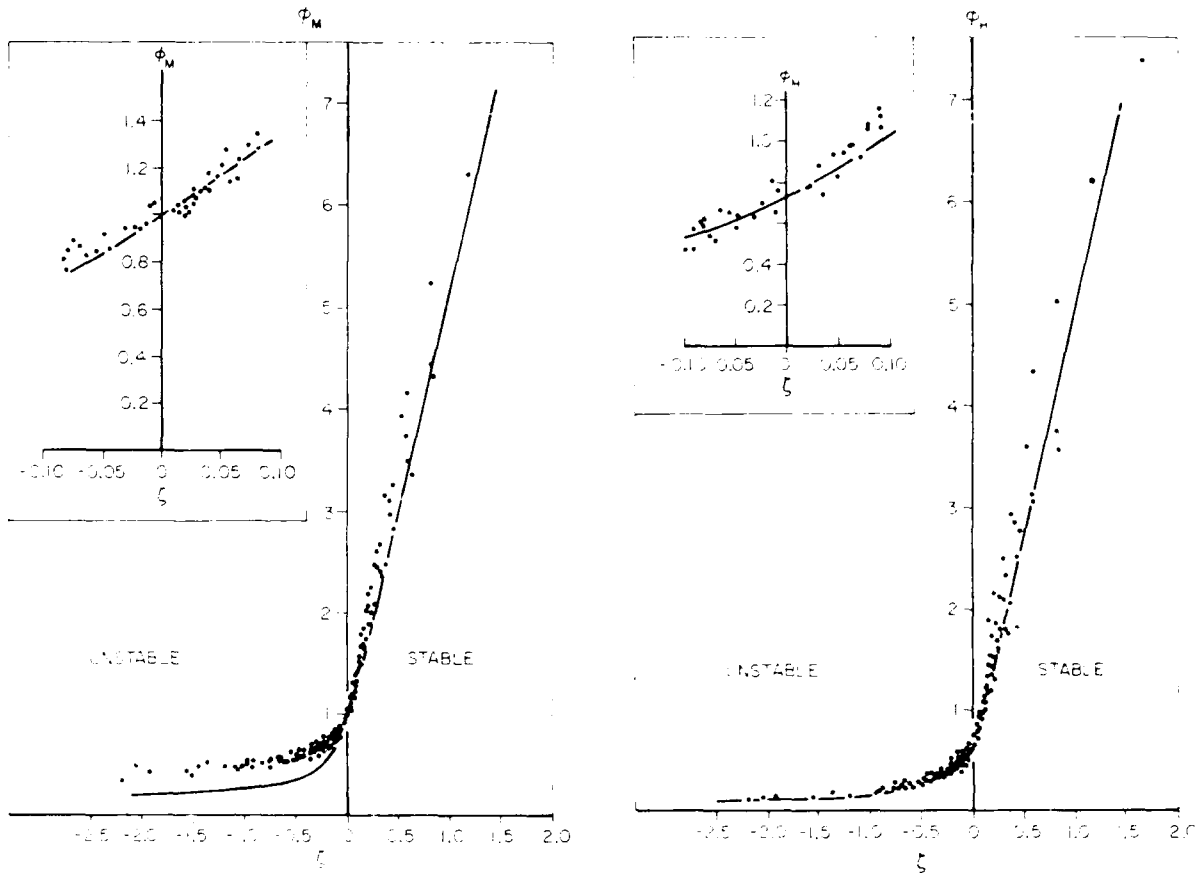


Figure 3. Monin-Obukhov similarity variables. The data is from Businger et al. (1971) whereas the solid lines are calculated by the model (Mellor, 1973).

In the level 2 1/2 version of the model, two prognostic equations are solved for  $q^2$  (twice the turbulent kinetic energy equation) and  $q^2 \ell$  (the master length scale equation which is related to integrals of the 2-point, correlation equations). They are

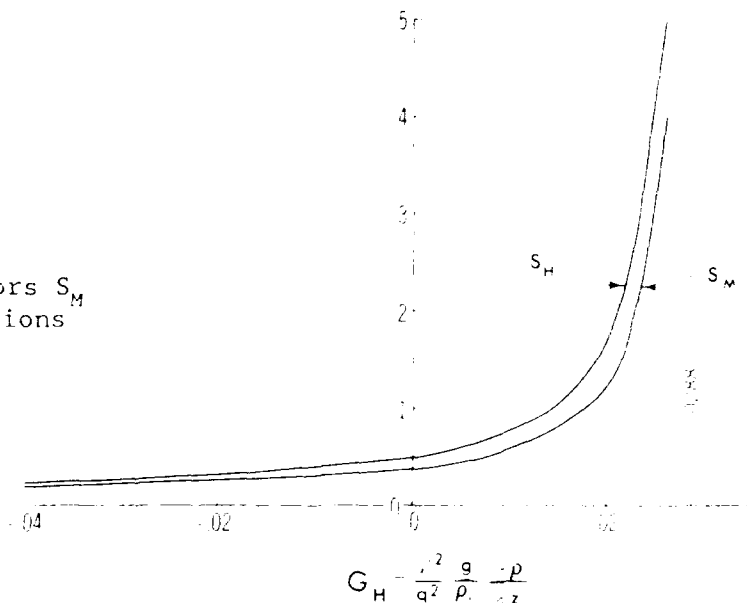
$$\begin{aligned} \frac{\partial q^2}{\partial t} + \frac{\partial U q^2}{\partial x} + \frac{\partial V q^2}{\partial y} + \frac{\partial W q^2}{\partial z} = \frac{\partial}{\partial z} \left[ K_q \frac{\partial q^2}{\partial z} \right] \\ + 2K_M \left[ \left( \frac{\partial U}{\partial z} \right)^2 + \left( \frac{\partial V}{\partial z} \right)^2 \right] + \frac{2g}{\rho_0} K_H \frac{\partial \rho}{\partial z} - \frac{2q^3}{B_1 \ell} + F_q \end{aligned} \quad (3)$$

$$\begin{aligned} \frac{\partial q^2 \ell}{\partial t} + \frac{\partial U q^2 \ell}{\partial x} + \frac{\partial V q^2 \ell}{\partial y} + \frac{\partial W q^2 \ell}{\partial z} = \frac{\partial}{\partial z} \left[ K_q \frac{\partial q^2 \ell}{\partial z} \right] \\ + E_1 \ell \left\{ K_M \left[ \left( \frac{\partial U}{\partial z} \right)^2 + \left( \frac{\partial V}{\partial z} \right)^2 \right] + \frac{g}{\rho_0} K_H \frac{\partial \rho}{\partial z} \right\} - \frac{q^3}{B_1} \bar{W} + F_\ell \end{aligned} \quad (4)$$

$\tilde{W}$  is a "wall proximity" function,  $K_q$  is the vertical turbulence diffusivity, and  $F_q$  and  $F_\ell$  are horizontal diffusion terms (see Mellor and Yamada, 1982). Boundary conditions for (3) and (4) are that  $\ell = \partial q^2 / \partial z = 0$  on bounding surfaces<sup>3</sup>. We note that equation (4) is the most empirical part of the model and has often been replaced by an algebraic equation for  $\ell$ , namely  $\ell = \kappa z \ell_0 / (\kappa z + \ell_0)$  where  $\ell_0 = \alpha \int |z| q dz / \int q dz$ . The early value of  $\alpha = 0.1$  (Mellor and Yamada, 1974) has been revised to  $\alpha = 0.2$  (Mofjeld and Lavelle, 1984; Martin, 1985). This also agrees more nearly with calculated results using (4). We generally use (4) instead of the algebraic relation because it seems to yield credible results for multiple turbulent regions for, say, an ocean with surface and bottom boundary layers separated by an inviscid region or for merged layers. It also expresses the fact that eddy scales are transportable quantities; i.e., they have memory.

Recently, large eddy simulations by Moeng and Wyngaard (1989) have persuasively demonstrated the existence of buoyancy driven turbulence diffusion in convectively driven boundary layers so that we do intend to add such terms to equations (3) and (4) as has been done by Sun and Ogura (1980) in their applications of the M-Y level 2 model. Lumley et al. (1978) and Therry and Lacarrere (1983) have also included such terms in their models. Based on our own past experience, however, we do not expect a large net effect on the mean variables.

Figure 4 The stability factors  $S_M$  and  $S_H$  as obtained from equations (2a,b).



<sup>3</sup>It can be shown from (3) and the law of the wall that the boundary condition,  $\partial q^2 / \partial z = 0$ , is formally equivalent to the alternate condition,  $q^2 = B_1^{-2/3} u_\tau^2$ , on bounding surfaces; here  $u_\tau$  is the friction velocity defined as the square root of the surface stress divided by density and  $B_1$  is a model constant.

Solutions to (3) and (4) together with (1) and (2) yield values of  $K_M$  and  $K_H$  which can be used to solve for the horizontal velocity components, temperature and salinity. Thus,

$$\frac{\partial U}{\partial t} + \frac{\partial U^2}{\partial x} + \frac{\partial UV}{\partial y} + \frac{\partial UW}{\partial z} - fV + \frac{1}{\rho_0} \frac{\partial p}{\partial x} = \frac{\partial}{\partial z} \left[ K_M \frac{\partial U}{\partial z} \right] - F_U \quad (5a)$$

$$\frac{\partial V}{\partial t} + \frac{\partial UV}{\partial x} + \frac{\partial V^2}{\partial y} + \frac{\partial VW}{\partial z} + fU + \frac{1}{\rho_0} \frac{\partial p}{\partial y} = \frac{\partial}{\partial z} \left[ K_M \frac{\partial V}{\partial z} \right] - F_V \quad (5b)$$

$$\frac{\partial p}{\partial z} = -\rho g \quad (5c)$$

$$\frac{\partial \theta}{\partial t} + \frac{\partial \theta U}{\partial x} + \frac{\partial \theta V}{\partial y} + \frac{\partial \theta W}{\partial z} = \frac{\partial}{\partial z} \left[ K_H \frac{\partial \theta}{\partial z} \right] + F_\theta \quad (6a)$$

$$\frac{\partial S}{\partial t} + \frac{\partial SU}{\partial x} + \frac{\partial SV}{\partial y} + \frac{\partial SW}{\partial z} = \frac{\partial}{\partial z} \left[ K_H \frac{\partial S}{\partial z} \right] + F_S \quad (6b)$$

where  $f$  is the Coriolis parameter and  $F_U, F_V, F_\theta, F_S$  are horizontal diffusion terms.

Figure 5 is an example of a two-dimensional simulation of coastal upwelling. Note the surface Ekman layer and the entrainment of mid-depth water in the bottom boundary layer. Figure 6 illustrates the application of the model in a three-dimensional estuarine simulation where there are generally merged surface and bottom layers.

#### 4. SCALES AND HORIZONTAL DIFFUSION

Aside from vertical fluxes, SMC can also supply horizontal fluxes. However, so long as the horizontal scale of variability,  $L_x$ , is large compared with the boundary thickness scale,  $\delta$ , then their effect should be negligible. In fact, neglect of these terms is the *boundary layer approximation* which also yields the *hydrostatic approximation* within surface or bottom boundary layers (and if  $L_x$  is also large compared to the depth, the hydrostatic approximation applies to the entire water column).

If horizontal fluxes are negligible, what are the terms  $F_U, F_V, F_\theta, F_S$  in (5) and (6)? They represent the fact that present day ocean models do not resolve important horizontal physical scales. We really should have  $\Delta x/L_x \ll 1$  or say, optimistically,  $\Delta x/L_x \approx 0.1$  where  $\Delta x$  is a grid increment. In open ocean  $L_x \approx$  the Rossby radius of deformation  $\approx 30$  km, so that we really need  $\Delta x \approx 3$  km, scarcely attainable with present computational power. All we can hope is that, useful information may be numerically obtained with larger  $\Delta x$ .

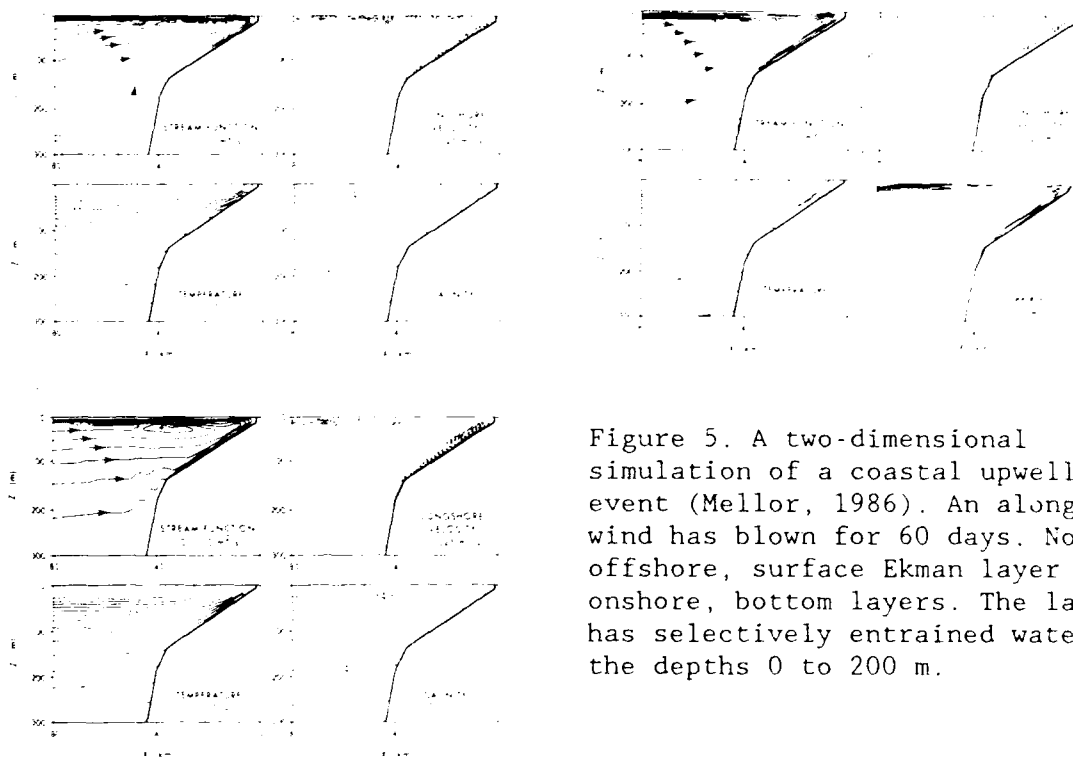


Figure 5. A two-dimensional simulation of a coastal upwelling event (Mellor, 1986). An alongshore wind has blown for 60 days. Note the offshore, surface Ekman layer and onshore, bottom layers. The latter has selectively entrained water from the depths 0 to 200 m.

In much of our own work, when forced by poor resolution, we use the Smagorinsky horizontal diffusivity where, for example,  $F_\theta = \partial(A_H \partial\theta/\partial x)/\partial x + (A_H \partial\theta/\partial y)/\partial y$ ; the diffusivity is given by  $A_H = C(\Delta x \Delta y) |\nabla \mathbf{V} + (\nabla \mathbf{V})^T|$  and  $\mathbf{V} = (U, V)$  is the velocity vector. The constant  $C$  is non-dimensional and the formulation does yield decreased diffusivity as the resolution is increased. However, we have found that the necessary value of  $C$ —it is chosen large enough to suppress objectional grid point noise—also decreases as resolution improves. Thus, a model of the Gulf Stream region where the typical grid size (the grid is curvilinear and variable) is 25 km uses  $C = 0.05^4$ ; a model of the Santa Barbara Channel where the grid is 3 km uses  $C = 0.02$  and a model of New York Harbor where the grid size is 500 m uses  $C = 0$ , the happy limit of no horizontal diffusion. (Note that, in these examples, the physical horizontal scale of variability is also decreasing.) For the Gulf Stream model, we believe that an open ocean grid size of 5 or 10 km would require no horizontal diffusion to suppress numerical noise, and would, at the same time, resolve the important physical processes.

It should be noted that horizontal diffusion represents sub-grid scale parameterizations which can be eliminated with sufficient resolution. On the other hand, SMC represents *ensemble mean* closure (Mellor, 1985)

<sup>4</sup>The Gulf Stream model is actually numerically stable with  $C = 0.01$  when the SMC sub-model is disabled and is stable when  $C = 0$  with the SMC sub-model enabled. However, in the latter case, temperatures and velocities are horizontally noisy.

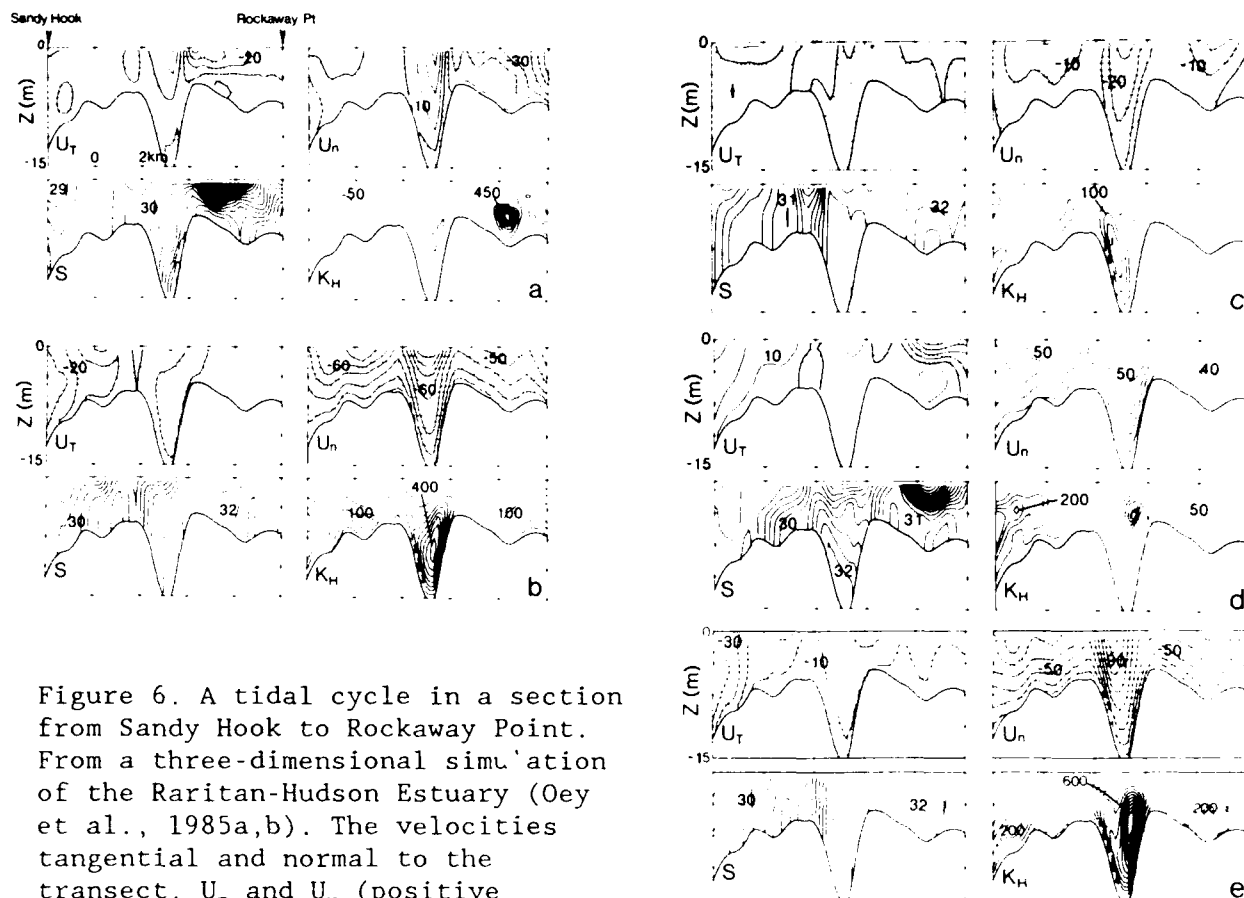


Figure 6. A tidal cycle in a section from Sandy Hook to Rockaway Point. From a three-dimensional simulation of the Raritan-Hudson Estuary (Oey et al., 1985a,b). The velocities tangential and normal to the transect,  $U_T$  and  $U_N$  (positive ebbing), the salinity,  $S$ , and the turbulence mixing coefficient,  $K_H$ , are plotted for different stages of the tidal cycle during August 20, 1980: a) 0300 GMT (near the beginning of flood), b) 0600 GMT, c) 0800 GMT, d) 1100 GMT, e) 1800 GMT.

for scales of turbulence which, in the foreseeable future, we have no hope of resolving. However, this is the arena of LES or large eddy simulation (Deardorff, 1974; Moeng and Wyngaard, 1989). LES is a research tool; it is clearly not useful for ocean simulations for the next 50 years or more. In section 2, we determined an estimate of turbulence integral scales,  $\Lambda = 0.2 \delta$  where  $\delta$  are boundary layer thicknesses. Therefore, we would need  $\Delta x = \Delta y = \Delta z \approx 0.2 \Lambda \approx 0.04 \delta$  to eliminate the need for SMC. For  $\delta \approx 50$  m, one would require 2 m grid cells! Using SMC, we can, as already stated, use  $\Delta x = \Delta y = 5$  or 10 km and a vertical grid size which is about  $0.1 \delta$  or about 5 m in the surface layer but decreasing to hundreds of meters at mid-depth. A resolved bottom boundary layer does, of course, require additional grid points near the bottom. The illustration in Figure 5 used a sigma coordinate system of 21 sigma level with increased resolution in the surface and bottom layers.

## 5. GEOSTROPHIC SHEAR AND INTERNAL WAVES

Martin (1985) compared the Niiler and Garwood bulk models with the M-Y model for data obtained at weather ship stations November (140°W, 30°N) and Papa (145°W, 50°N). Tables 2 and 3 (Martin's Tables 5 and 4) are reproduced here; they show the observed, monthly averaged, surface temperatures and the model errors during the 1961 seasonal cycle. The seasonal change in SST is about 4° at November and about 9° at Papa. Thus, the errors can be as high as 30%. The empirical constants in the Garwood model were tuned to minimize error for these data.

TABLE 2. Observed Monthly Mean SST (°C) for Ocean Stations November and Papa for Year 1961.

Station	Jan	Feb	Mar	Apr	May	Jun	Jul	Aug	Sep	Oct	Nov	Dec	Mean
November	19.2	18.7	18.6	19.3	19.9	20.9	21.6	22.2	22.8	21.7	20.4	19.2	20.4
Papa	5.5	4.9	4.7	5.1	6.0	8.1	11.3	13.5	13.4	11.6	8.6	6.5	8.3

TABLE 3. Difference Between Model-Predicted and Observed Monthly Mean SST (°C) for Model Simulations at November and Papa for Year 1961.

Model <sup>1</sup>	Jan	Feb	Mar	Apr	May	Jun	Jul	Aug	Sep	Oct	Nov	Dec	Mean
<i>November</i>													
MYL2	0.0	0.3	0.3	-0.1	0.2	0.7	0.7	1.4	0.1	0.3	0.4	0.3	0.4
MYL2 <sub>1/2</sub>	0.0	0.3	0.3	-0.1	0.2	0.9	0.8	1.5	0.2	0.3	0.4	0.3	0.4
Niiler	0.0	0.1	0.1	-0.3	-0.1	0.2	-0.1	0.5	-0.6	-0.3	0.0	0.0	-0.1
Garwood	0.0	0.2	0.2	-0.3	-0.1	0.1	-0.2	0.2	-0.7	-0.3	0.1	0.1	-0.1
<i>Papa</i>													
MYL2	-0.1	0.2	0.2	0.0	0.2	0.6	0.8	1.5	1.9	0.0	0.2	0.8	0.5
MYL2 <sub>1/2</sub>	-0.1	0.2	0.2	0.0	0.2	0.7	0.9	1.6	2.2	0.3	0.5	0.9	0.6
Niiler	-0.1	0.2	0.1	-0.2	-0.5	-1.2	-2.0	-2.4	-2.7	-3.0	-2.0	-0.8	-1.2
Garwood	-0.1	0.2	0.2	0.0	-0.1	-0.3	-0.2	-0.3	-1.1	-1.8	-1.0	-0.1	-0.4

Assuming that errors due to missing advective information and errors in the surface forcing are small, then the M-Y model is too warm in the late summer and early fall, indicating that during this heating season the mixed layer is too shallow. A candidate cause of the discrepancy is that there is a great deal more energy in the real ocean than that which is taken into account by wind-driven, one-dimensional models. (Note, however, that bulk models may account for some of the missing physics by adjustment of their empirical constants.)

Figure 7 is a current meter time series obtained during the 1977 Mixed Layer Experiment (MILE) which was near station Papa and is compared to the M-Y level 2 model by Martin et al. (1986). At the eight meter

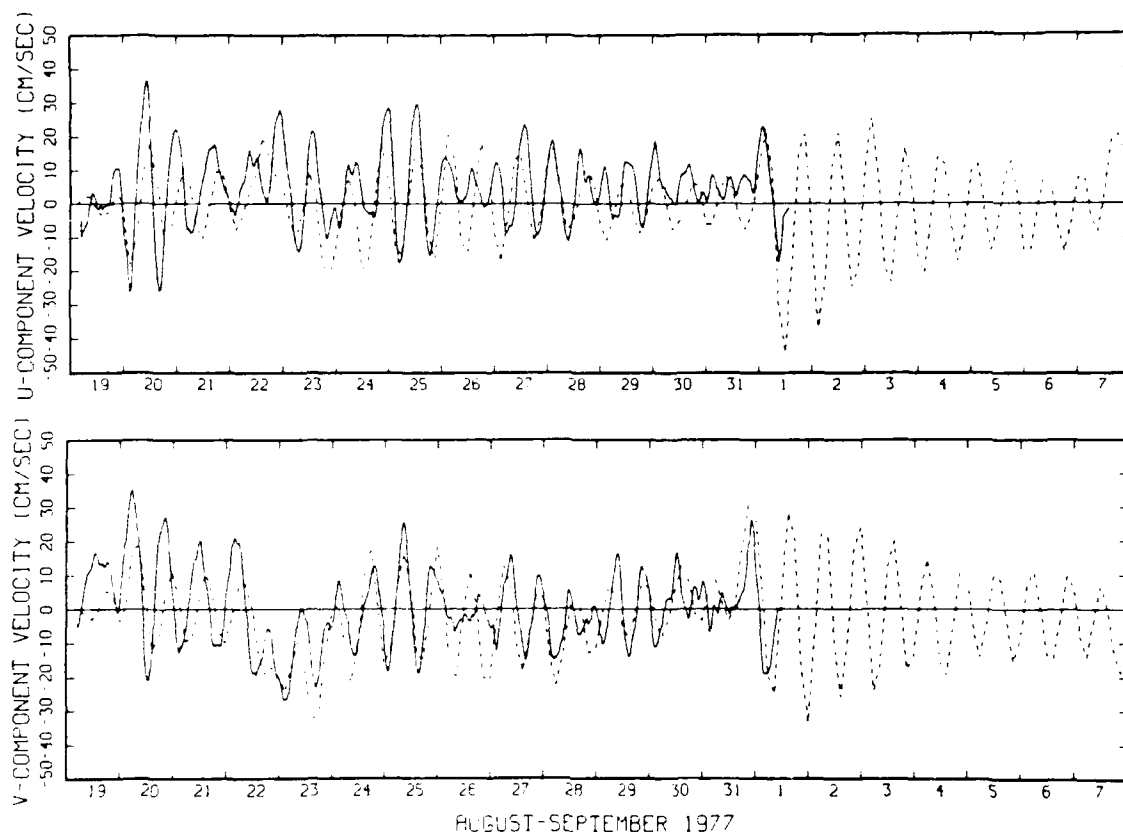


Figure 7. Observed (solid line) and calculated (dashed line), east-west (top panel) and north-south (bottom panel) components of current obtained during the MILE experiment (Martin et al., 1986).

depth, the comparison is acceptable. However, in the same paper are displayed shear profiles some of which are shown here in Fig. 8. Below the mixed layer, one observes significant internal wave shear with values up to  $0.04 \text{ s}^{-1}$ . Most of the energy is concentrated at frequencies near and larger than inertial frequencies (Levine et al., 1983). In principle, this energy would be captured by a well resolved, three-dimensional numerical model driven by a wind stress field which is sufficiently well resolved temporally and spatially to create surface forced internal waves; the model should have sufficient topographical resolution so that barotropic tidal energy can be converted to internal wave energy. Obviously, this utopian situation does not prevail with most model applications and certainly does not with a one-dimensional model ( $\Delta x = \Delta y = \infty$ ).

To assess the sensitivity of our mixed layer model to shears of this magnitude, we have run the model with wind stresses of 1 and 4 dynes  $\text{cm}^{-2}$  and initial conditions which include constant geostrophic shear profiles,  $\partial V_g / \partial z$ , and balancing pressure gradient terms in the momentum equations. We repeat five day calculations where the shear vector is rotated to angles of  $0^\circ$ ,  $90^\circ$ ,  $180^\circ$  and  $270^\circ$  relative to the surface stress vector and the four results are averaged. Figure 9 shows the

averaged mixed layer depth for the two wind stress magnitudes as a function of the geostrophic shear magnitude. We conclude that our model is indeed sensitive to shears of the magnitudes shown in Fig. 8.

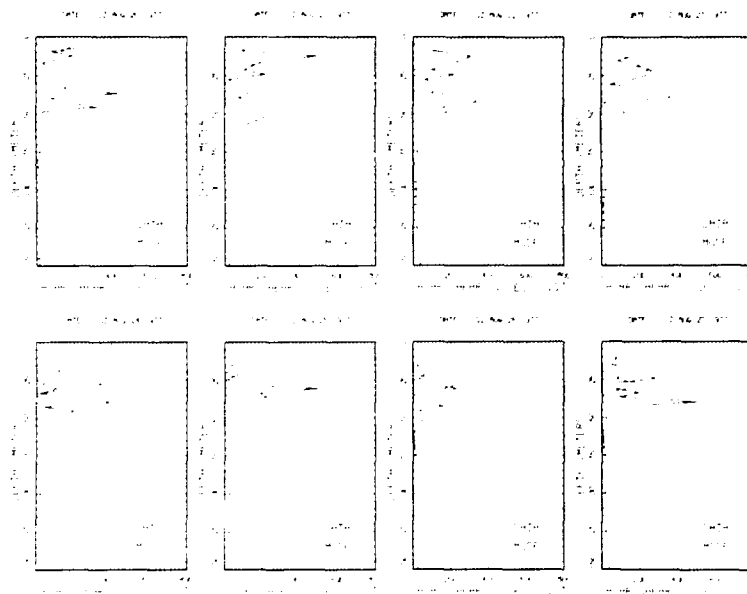


Figure 8. Observed (solid line) and calculated (dashed line) shear profiles at 00Z from August 20 to August 27 obtained during the MILE experiment (Martin et al., 1986).

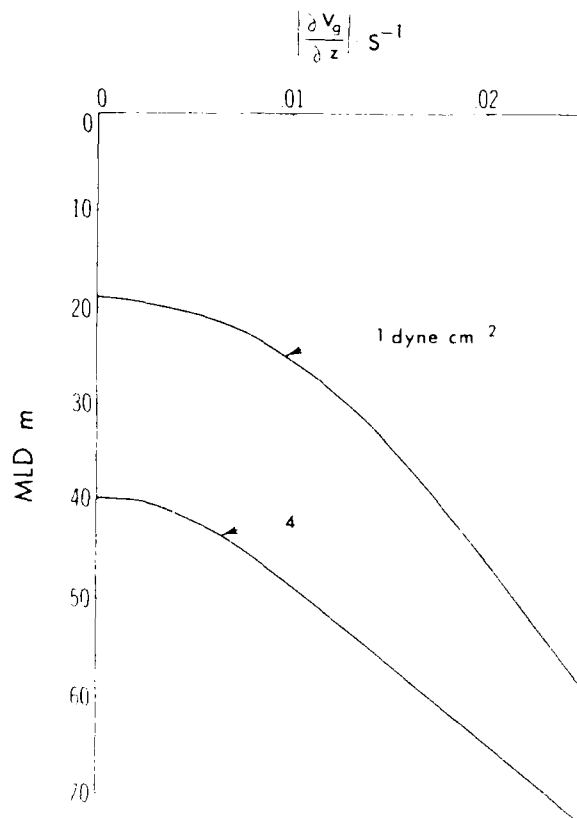


Figure 9. The effect of a superposed geostrophic shear,  $|\partial V_g / \partial z|$ , on mixed layer deepening. The mixed layer depth after 5 days is plotted for wind stresses of 1 and 4 dyne  $\text{cm}^{-2}$ . The initial temperature gradient was a uniform  $0.05^\circ\text{C}/\text{m}$ ; the SST was  $24^\circ\text{C}$  and the salinity was a constant 35 ppt. The Coriolis parameter,  $f = 0.727 \cdot 10^{-4} \text{ s}^{-1}$ .



We now turn to the question of including some kind of correction to the model to account for internal wave energy. Now Levine et al. (1983) show that WKB scaling works fairly well (Garrett and Munk, 1979) with the MILE data (even though the WKB approximation is suspect in the upper ocean). We therefore characterize the square of the internal wave shear by  $0.70 N^2$  (Gill, 1982; p. 299) where  $N$  is the Brunt-Vaisala frequency and where the dimensional constant is estimated from Fig. 8 (using an estimate of the average maximum shear and the maximum frequency). This term is simply added to the shear squared terms in (3) and (4); i.e., the model itself offers a rather obvious way to include the effects of internal wave energy.

We have rerun the 1961, station Papa and November cases (and we thank Paul Martin for supplying us with the initial conditions and surface forcing information), to obtain results shown in Table 4 for the monthly averaged sea surface temperatures. We use our version of the level 2 model (which includes the prognostic equation for  $q^2\ell$  whereas Martin used the algebraic equation to determine  $\ell$  as described in section 3. Thus, Martin's results in Table 2 differ by a small amount from the results in Table 4.)

If we now include internal wave shear in equations (3) and (4), then the surface temperature results are significantly improved. Not shown are the fact that heating season mixed layers are deepened. As alluded to earlier, these comparisons are subject to error or missing information. Nevertheless, whether or not the results were improved, the internal wave shear should, in principal, be included in the model.

TABLE 4. Difference between model and observed monthly mean SST ( $^{\circ}\text{C}$ ) for stations November and Papa for the year 1961. The first row of each station are the control values; the second row corresponds to calculations where internal wave shear energy,  $0.70 N^2$ , has been added to equations (3) and (4).

I.W. Shear Added?	Jan	Feb	Mar	Apr	May	Jun	Jul	Aug	Sep	Oct	Nov	Dec	Mean
<i>November</i>													
No	0.1	0.4	0.4	0.0	0.1	0.9	0.8	1.5	0.0	0.1	0.3	0.3	0.4
Yes	0.1	0.3	0.3	-0.1	0.0	0.4	0.4	1.0	-0.4	-0.1	0.2	0.2	0.2
<i>Papa</i>													
No	0.0	0.3	0.2	0.0	0.3	1.1	1.8	2.4	2.1	-0.6	-0.8	0.0	0.6
Yes	0.0	0.3	0.2	0.0	0.3	0.6	0.0	0.2	-0.4	-1.9	-1.2	-0.2	-0.2

## 6. TIME DEPENDENT WIND STRESS FORCING

Generally, in oceanographic model simulations, boundary conditions are not well resolved temporally. Except at a finite number of points, wind stress is generally available from NMC or FNOC only at twelve hourly intervals. In some applications, the only available winds are

climatological winds; the winds are then too weak to yield the correct mixing and layer deepening. Both Klein (1980) and Adamec and Elsbury (1984) have found that filtering or averaging the wind stress decreases mixed layer deepening.

Klein (1980), using an M-Y level 2 model, directly investigated the effect of wind variability and we pursue his line of enquiry here. Consider a simple surface wind forcing

$$\begin{aligned} \tau_x = \tau_y = 0 & \quad ; t < 0 \\ \tau_x = \tau_{x0} + A_x \sin \sigma t, \tau_y = 0 & \quad ; t > 0 \end{aligned} \quad (7)$$

Martin defined a benchmark problem. The initial temperature gradient was a uniform  $0.05^\circ\text{C}/\text{m}$ ; the SST was  $24^\circ\text{C}$  and the salinity was a constant 35 ppt and  $f = 0.727 \cdot 10^{-4} \text{ s}^{-1}$ . We use these parameters to investigate the effect of wind variability using (7) and the sensitivity to the frequency,  $\sigma$ . Note that (7) represents only a small subset of possible parameter space involving wind variability. We further restrict to the cases where  $A_x = \tau_{x0} = 1 \text{ dyne cm}^{-2}$  and  $4 \text{ dyne cm}^{-2}$ .

Figure 10 shows the mixed layer depths after five days for the two wind stress levels as a function of  $\sigma/f$ . The mixed layer depth is defined as the point where the temperature is  $0.2^\circ\text{C}$  cooler than the surface

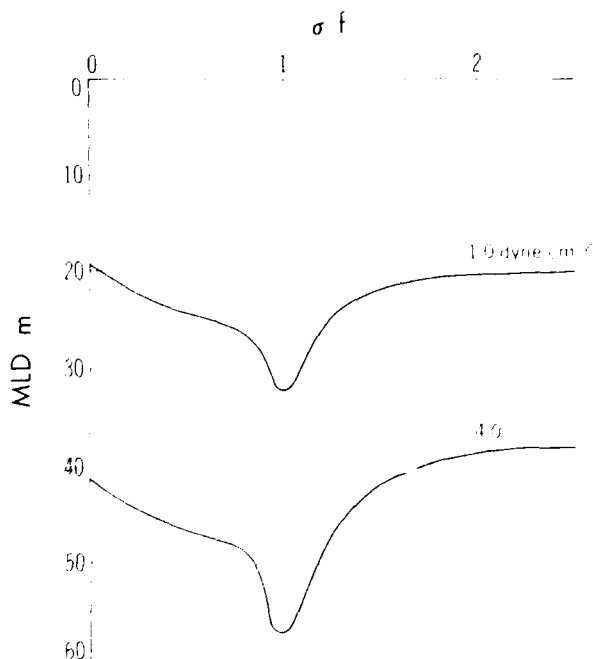


Figure 10. The effect of oscillatory wind forcing on mixed layer depth. The problem definition is the same as in Fig. 9 except that there is no geostrophic shear and the wind stress is given by equation (7) where

$$\tau_{x0} = A_x.$$

temperature. The mixed layer depths agree with Martin's values for  $\sigma = 0$  (for which case, decreasing the depth definition to  $0.1^\circ\text{C}$  has negligible effect). The resonance at  $\sigma = f$  is weaker than obtained by Klein; presumably, this is due to our use of the level 2 1/2 model and the turbulence tendency terms in (3) and (4) which are neglected in the

level 2 model. In Fig. 10, the curves represent the depth of the deepest mixed layer penetration during the five days. (Generally, this occurs at the end of the five days. However, at resonance, the five day point in time occurs after the half cycle of weakest winds so that, according to the temperature criterion, the mixed layer is temporarily shallower than it was a half cycle earlier.)

In the past we have modeled oceans using only climatological winds. To account for the missing information, we have added a simple oscillatory wind while maintaining the climatological mean. This causes analysis problems since one is compelled to filter out the concomitant oscillatory motion rather than display aliased results. A better procedure might be to rationally alter the turbulence model itself to account for the missing information.

We define a factor to account for lack of temporal resolution. We will call the factor,  $\zeta_{FF}$ , a "filter factor" (those who lack piety might call it a fudge factor) or possibly an "inverse filter factor" which is meant to undo the temporal filtering of the forcing wind stress. The filter factor is simple a multiplier of vertical velocity gradients as they appear in (3) and (4). Table 5 lists the mixed layer depths after five days as a function of wind stress and  $\zeta_{FF}$  for the previously defined benchmark problem. Scale analysis shows that  $hf/u_\tau = \text{fcn}(ft, N/f, \zeta_{FF})$  so that a more extensive table could be prepared relating the relevant non-dimensional variables.

As noted above, this whole analysis needs to be extended to include a larger range of wind stress variability parameter space; the study should be coupled with studies on wind velocity and stress variability such as those by Thompson and Marsden (1983) and Sadler et al. (1986) who showed that wind variability is correlated with average wind magnitude. In the meantime, we observe that winds are typically variable in the range,  $0 < \sigma/f < 2$ ; then it is probable that, when one uses climatological winds, a value  $\zeta_{FF} = 1.5$  or larger would yield mixed layer results closer to those observed than the uncorrected results ( $\zeta_{FF} = 1$ ).

TABLE 5. The mixed layer depth after 5 days as a function of wind stress ( $\text{dyne cm}^{-2}$ ) and the filter factor,  $\zeta_{FF}$ , for the problem defined in Figure 1. For fixed initial Brunt-Vaisala frequency and Coriolis parameter the table collapses to  $h/u_\tau$  as a function of  $\zeta_{FF}$ .

$\tau_x$	$\zeta_{FF}$		
	1.0	1.5	2.0
1.0	19.2	24.1	28.2
4.0	40.1	48.6	55.1
16.0	80.2	93.7	109.1

## 7. SUMMARY

The rationale for second moment closure is that it has some theoretical basis, it relates to turbulence data and offers a simulative capability with a broad range of applications.

The role of SMC in numerical ocean modeling and errors that have been encountered are reviewed. In particular, it is recognized that internal wave energy, normally missing in numerical model simulations, can, in the real ocean, enhance mixing; in this paper we incorporate this energy source into the model and differences between model calculations and data from stations Papa and November are reduced. Wind stress filtering reduces mixed layer deepening; ways of reducing the resultant errors are tentatively advanced.

ACKNOWLEDGMENTS. Ideas and stimuli have been contributed to this paper by colleagues; they include Boris Galperin, Lakshmi Kantha, Paul Martin, Peter Niiler, Tony Rosati and others. Support of the Arctic branch of the Office of Naval Research (N0014-84-K-0640) and the Institute for Naval Oceanography (INO-S8751-3-89) is gratefully acknowledged.

## REFERENCES

- Adamec, D. and R.L. Elsbury: 1984. Sensitivity of mixed layer predictions at ocean station Papa to atmospheric forcing parameters. *J. Phys. Oceanogr.*, 14, 769-780.
- Andre', J.C., G. DeMoor, G. Therry, and R. DuVachat: 1978. Modeling the 24-hour evolution of the mean and turbulence structures of the planetary boundary layer, *J. Atmos. Sci.*, 35, 1861-1863.
- Businger, J.A., J.C. Wyngaard, Y. Izumi and E.F. Bradley: 1971. Flux profile relationships in the atmospheric surface layer. *J. Atmos. Sci.*, 28, 181-189.
- Deardorff, J.W.: 1974. Three dimensional numerical study of turbulence in an entraining mixed layer. *Boundary Layer Meteorol.*, 7, 119-226.
- Galperin, B., L.H. Kantha, S. Hassid and A. Rosati: 1988. A quasi-equilibrium turbulent energy model for geophysical flows. *J. Atmos. Sci.*, 45, 55-62.
- Garrett, C.J.R, and W.H. Munk: 1979. Internal waves in the ocean. *Annual Review of Fluid Mechanics*, Vol. 11, Annual Reviews, Inc., 239-369.
- Garwood, R.W.: 1977. An oceanic mixed-layer model capable of simulating cyclic states. *J. Phys. Oceanogr.*, 7, 455-471.
- Gill, A.E. *Atmosphere-Ocean Dynamics*, International Geophysics Series, Vol. 30, New York. Academic Press, 662 p.
- Klein, P.: 1980. A simulation of the effects of air-sea transfer variability on the structure of the marine upper layers. *J. Phys. Oceanogr.*, 10, 1824-1841.
- Kline, S.J., M.V. Morkovin, G. Sovran and D.J. Cockrell: 1968. *Proceedings of the AFOSR Stanford Conference on Computation of Turbulent Boundary Layers*. Dept. of Mech. Eng., Stanford Univ., Stanford, CA.

- Kolmogorov, A.N.: 1941. The local structure of turbulence in incompressible viscous fluid for very large Reynolds number (in Russian). *Dokl. Akad. Nauk SSSR*, 30, 299-303.
- Kraus, E.B. and J.S. Turner: 1967. A one-dimensional model of the seasonal thermocline, 2, The general theory and its consequences. *Tellus*, 19, 98-105.
- Levine, M.D., R.A. deSzoeke and P.P. Niiler: 1983. Internal waves in the upper ocean during MILE. *J. Phys. Oceanogr.*, 13, 240-257.
- Lewellen, W.S. and M.E. Teske: 1973. Prediction of the Monin-Obukhov similarity functions from an invariant model of turbulence. *J. Atmos. Sci.*, 30, 1340-1345.
- Lumley, J.L., O. Zeman and J. Seiss: 1978. The influence of buoyancy on turbulent transport. *J. Fluid Mech.*, 84, 581-597.
- Martin, P.J.: 1985. Simulation of the mixed layer at OWS November and Papa with several models. *J. Geophys. Res.*, 90, 903-916.
- Martin, P.J., A. Warn-Varnas, J.P. French and S.A. Piacsek: 1986. Comparison of model-predicted shear with observations during MILE. NORDA Tech. Note 328, Naval Ocean Research and Development Activity, SSS, Miss. 39529.
- Mellor, G.L.: 1973. Analytic prediction of the properties of stratified planetary surface layers. *J. Atmos. Sci.*, 30, 1061-1069.
- Mellor, G.L.: 1985. Ensemble average, turbulence closure. *Advances in Geophysics*, Vol. 28, Part B, Saltsman and S. Manabe, Academic Press, New York, 432 pp.
- Mellor, G.L.: 1986. Numerical simulation and analysis of the mean coastal circulation off California. *Continental Shelf Res.*, 6, 689-713.
- Mellor, G.L. and P.A. Durbin: 1975. The structure and dynamics of the ocean surface mixed layer. *J. Phys. Oceanogr.*, 5, 718-728.
- Mellor, G.L. and T. Yamada: 1974. A hierarchy of turbulence closure models for planetary boundary layers. *J. Atmos. Sci.*, 31, 1791-1806.
- Mellor, G.L. and T. Yamada: 1982. Development of a turbulence closure model for geophysical fluid problems. *Rev. Geophys. Space Phys.*, 20, 851-875.
- Moeng, C.-H. and J.C. Wyngaard: 1989. Evaluation of turbulent transport and dissipation closures in second-order modeling. *J. Atmos. Sci.*, in press.
- Mofjeld, H.O. and J.W. Lavelle: 1984. Setting the length scale in a second order closure model of the unstratified bottom boundary layer. *J. Phys. Oceanogr.*, 14, 833-839.
- Niiler, P.P.: 1975. Deepening of the wind-mixed layer. *J. Mar. Res.*, 33, 405-422.
- Oey, L.-Y., G.L. Mellor and R.I. Hires: 1985a. A three-dimensional simulation of the Hudson-Raritan estuary. Part I. Description of the model and model simulations. *J. Phys. Oceanogr.*, 15, 1676-1692.
- Oey, L.-Y., G.L. Mellor and R.I. Hires: 1985b. A three-dimensional simulation of the Hudson-Raritan estuary. Part II. Comparison with observation. *J. Phys. Oceanogr.*, 15, 1693-1709.
- Price, J.F., R.A. Weller and R. Pinkel: 1986. Diurnal Cycling. Observations and models of the Upper Ocean response to diurnal heating, cooling and wind mixing. *J. Geophys. Res.*, 91, 8411-8427.

- Rodi, W.: 1987. Examples of calculation methods for flow and mixing in stratified fluids. *J. Geophys. Res.*, 92, 5305-5328.
- Rotta, J.C.: 1951a. Statistische Theorie nichthomogener Turbulenz, 1. *Z. Phys.*, 129, 547-572.
- Rotta, J.C.: 1951b. Statistische Theorie nichthomogener Turbulenz, 2. *Z. Phys.*, 131, 51-77.
- Sadler, J. C., M. Lander, J. Maliekal and A. Hori: 1986. *Surface wind stress from monthly mean winds*. Proceedings of a Coads Workshop, Boulder, CO, January 22-24, 1986, NOAA Tech. Memo. ERL ESG-23.
- Schubauer, P.S. and P.S. Klebanoff: 1951. *Investigation of separation of the turbulent boundary layer*. N.A.C.A. Report 1030, U.S. Govt. Printing Office, Washington DC.
- Sun, W.-Y. and Y. Ogura: 1980. Modeling the evolution of the convective planetary boundary layer. *J. Atmos. Sci.*, 37, 1558-1572.
- Therry, G. and P. Lacarrere: 1983. Improving the eddy kinetic energy model for planetary boundary layer description. *Boundary-Layer Meteorol.*, 25, 67-88.
- Thompson, K.R. and R.F. Marsden : 1983. Estimation of low-frequency wind stress fluctuations over the open ocean. *J. Phys. Oceanogr.*, 13, 1003-1011.
- Yamada, T.: 1983. Simulation of nocturnal drainage flows by a  $q^2$  turbulence closure model. *J. Atmos. Sci.*, 40, 91-106.

## THE EFFECT OF INTERNAL WAVES ON VERTICAL GEOSTROPHIC SHEAR

Eric Kunze

School of Oceanography, WB-10, University of Washington, Seattle, WA 98195

Peter Müller

Department of Oceanography, University of Hawaii, 1000 Pope Rd and Hawaii Institute of Geophysics, Honolulu, HI 96822

### ABSTRACT

Exchange of energy and momentum between internal waves and geostrophic flow is severely constrained by conservation of potential vorticity even at sites of the irreversible processes of dissipation and mixing that occur when internal waves break. For a horizontally isotropic internal wave spectrum, the only noncancelling Reynolds terms are the vertical momentum-flux (or Reynolds-stress) divergences, e.g.,  $\partial \langle u'w' \rangle / \partial z$ . In a unidirectional flow, these do not affect the geostrophic flow. Instead, by analogy to wind-stress forcing, the momentum-flux divergences are balanced by a Coriolis acceleration, producing an 'Ekman' flow to the right of the geostrophic flow. For a first baroclinic mode geostrophic current sheared only in the vertical, this 'Ekman' flow will be  $\sim O(0.01 \text{ cm/s})$ . It will interact with the horizontal geostrophic density gradient to tilt isopycnals into the vertical but without modifying the geostrophic shear. This reduces the buoyancy frequency on timescales of  $\sim O(100 \text{ yrs})$ , similar to the time it would take an eddy diffusivity of  $10^{-4} \text{ m}^2/\text{s}$  to eradicate the pycnocline. This effect can be parameterized for inclusion into numerical models but may not be discernible over the large numerical diffusivities needed to maintain numerical stability.

### INTRODUCTION

While atmospheric scientists are sufficiently confident of their understanding of internal wave interaction with the mean geostrophic shear and its importance in determining the mesosphere circulation to try to parameterize its effect in eddy-resolving numerical models (e.g., McFarlane, 1987), research on this topic in the ocean is far less advanced. While the main source of internal waves in the atmosphere appears to be lee waves, atmospheric forcing dominates in the ocean (Olbers, 1983).

This report describes preliminary results from an examination of the effect of ocean internal waves modelled by the Garrett and Munk spectrum (Garrett and Munk, 1979; Munk, 1981) on realistic geostrophic shear for the case of purely vertical shear.

Exchange of energy and momentum between internal waves and geostrophic flow is strongly constrained by conservation of potential vorticity (Ertel, 1942; Pedlosky, 1979). The potential vorticity of a water parcel can be modified only through irreversible

processes—dissipation and mixing. This constraint is often posed as a nonacceleration theorem (Eliassen and Palm, 1961; Andrews and McIntyre, 1976) which applies to a broad class of phenomena including all waves. Potential vorticity can be defined as

$$\Pi = (2\Omega + \nabla \times \mathbf{V}) \cdot \nabla B \quad (1)$$

where  $\Omega$  is the Earth's rotation vector,  $\mathbf{V}$  is the fluid velocity and  $B = g\delta\rho/\rho_0$  is the buoyancy. For a quasigeostrophic flow  $\mathbf{V}_0$ , the horizontal Coriolis acceleration and vertical velocity can be neglected

$$\Pi = -(f + \zeta_0)N^2 - \frac{\partial V'_x}{\partial z} \frac{\partial B_0}{\partial x} + \frac{\partial U'_y}{\partial z} \frac{\partial B_0}{\partial y} \quad (2)$$

where  $\zeta_0$  is the vertical component of the geostrophic relative vorticity and the buoyancy frequency squared  $N^2 = \partial(B + B_0)/\partial z$  includes both the background stratification  $B(z)$  and anomalies associated with the geostrophic flow  $B_0(x, y, z)$ . The vertical shears  $\partial(U'_y, V'_x)/\partial z$  and horizontal buoyancy gradients  $\partial B_0/\partial(x, y)$  are related through the thermal-wind relations

$$f \frac{\partial V'_x}{\partial z} = - \frac{\partial B_0}{\partial x} \quad ; \quad f \frac{\partial U'_y}{\partial z} = \frac{\partial B_0}{\partial y} \quad (3)$$

so that the geostrophic potential vorticity anomaly can be written

$$\delta\Pi = \zeta_0 N^2 - f(\mathbf{V}_z \cdot \nabla_z \mathbf{V}_z) = fN^2 (\text{Ro} - \text{Ri}^{-1}), \quad (4)$$

demonstrating that potential vorticity anomalies are associated with both horizontal and vertical geostrophic shears. The horizontal and vertical anomalies scale as the Rossby and inverse Richardson numbers, respectively. Under the usual scaling assumptions, the contribution from vertical shear is neglected. However, measurements in the Gulf Stream (Hall, 1985) and Kuroshio (Hall, personal communication, 1989) find comparable contributions from the Rossby and Richardson number terms in (4).

On the other hand, internal waves have no potential vorticity fluctuations associated with them; the terms in (1) cancel. Therefore, interaction between internal gravity waves and geostrophic or quasigeostrophic flow is severely restricted. In the absence of molecular processes, internal gravity waves cannot modify the potential vorticity of fluid parcels; they can at most play a role in the redistribution of potential vorticity as geostrophic flow seeks a lower energy state, e.g., in the process of geostrophic adjustment (Rossby, 1938). With the inclusion of molecular processes, internal waves can affect the geostrophic flow at sites of internal wave breaking due to the enhancement of dissipation and mixing at these sites. Internal wave breaking can result from either random superposition or critical-layers. For a horizontally isotropic internal wave field, random internal wave breaking will deposit no net mean momentum. Critical-layers due to Doppler-shifting by the geostrophic shear, however, select out that portion of the spectrum propagating with the flow, so can lead to a net momentum-flux divergence,  $\partial\langle u'w' \rangle/\partial z$ , which can act on the mean.

Vertical critical-layers result when changes in the geostrophic flow with depth force either (i) the intrinsic frequency toward the lower bound of the internal waveband,  $f_{\text{eff}} = f + \tau/2$  (Fig. 1B) (e.g., Olbers, 1981), or (ii) this lower bound to increase with depth (Fig. 1A) (Mooers, 1975; Kunze, 1985). Horizontal critical-layers occur when



either the intrinsic frequency is Doppler-shifted toward the buoyancy frequency  $N$  by lateral changes in the geostrophic flow (Fig. 1C) (Olbers, 1981), or  $N$  changes laterally (Fig. 1D) (Miropol'skiy et al., 1976). We will focus on vertical critical-layers here. In the absence of horizontal geostrophic shear, the lower bound of the internal waveband is just the planetary value  $f$  independent of depth and the only critical-layer that can occur is due to vertical Doppler-shifting (Fig. 1B).

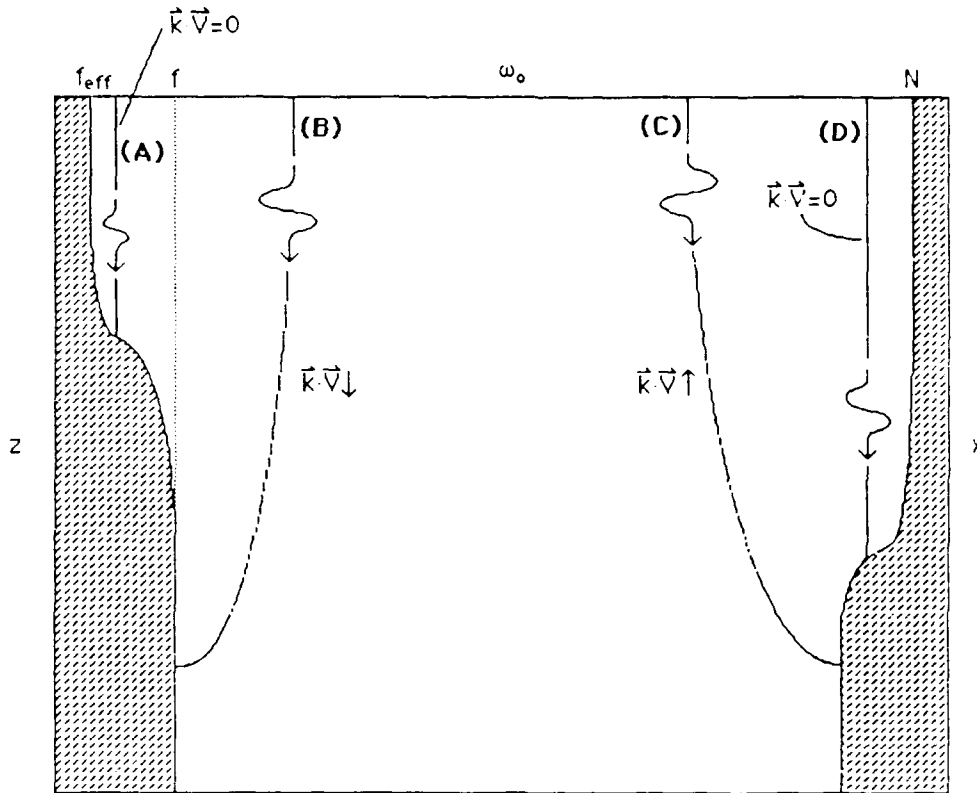


Figure 1. Schematic illustrating how internal waves can encounter critical-layers in a rotating, stratified ocean. Vertical critical-layers will occur if either (A) the lower bound of the internal waveband,  $f_{\text{eff}} = f + \zeta/2$ , rises above a wave's intrinsic frequency  $\omega_0$ , or (B) the wave's intrinsic frequency is shifted down toward the lower bound by changes in the magnitude of the mean flow with depth,  $(\mathbf{k} \cdot \mathbf{V})$ . Horizontal critical-layers can occur if (C) the upper bound of the internal waveband,  $N$ , decreases, or (D) the wave's intrinsic frequency is shifted toward  $N$  by horizontal changes in  $(\mathbf{k} \cdot \mathbf{V})$ .

The intrinsic frequency following the mean flow,  $\omega_0 = \omega - (\mathbf{k} \cdot \mathbf{V})$ , where the Eulerian frequency  $\omega$  is invariant in a time-independent mean flow. As a wave propagates down from the surface, the change in the geostrophic velocity,  $\Delta U = (\partial U_0 / \partial z) \Delta z$ , will result in a corresponding change of  $k_x \Delta U$  to its intrinsic frequency. A critical-layer will be encountered at the depth where  $k_x \Delta U_c = (\omega_0 - f)$  (e.g., Olbers, 1983). Therefore,  $\Delta U_c = (\omega_0 - f) / k_x$ , differing from the  $\Delta U_c = c = \omega_0 / k_x$  for the irrotational case. While, for much of the internal wave spectrum,  $\omega_0 \gg f$  so that this distinction does not matter, a large fraction of the internal wave variance is near-inertia, in the ocean and it is this part of the spectrum that is most sensitive to critical-layers.

## FORMULATION OF PROBLEM

The Boussinesq, hydrostatic,  $f$ -plane equations of motion describing the effect of internal waves on a mean assuming (i) a background geostrophic flow  $U_0(y, z)$  obeying the thermal-wind relation  $f \partial U_0 / \partial z = \partial B_0 / \partial y$  (2), (ii)  $\partial / \partial x = 0$  and (iii) the wave-induced means are weak so that their nonlinear interactions can be neglected, are

$$\begin{aligned} \frac{D\bar{u}}{Dt} + \bar{w} \frac{\partial U_0}{\partial z} - (f - \frac{\partial U_0}{\partial y}) \bar{v} &= - \frac{\partial \langle u'v' \rangle}{\partial y} - \frac{\partial \langle u'w' \rangle}{\partial z} \\ \frac{D\bar{v}}{Dt} + f U_0 &= - \frac{\partial P_0}{\partial y} - \frac{\partial \langle v'v' \rangle}{\partial y} - \frac{\partial \langle v'w' \rangle}{\partial z} \\ 0 &= - \frac{\partial P}{\partial z} - B \\ \frac{D\bar{b}}{Dt} + \bar{v} \frac{\partial B_0}{\partial y} - \bar{w} N^2 &= - \frac{\partial \langle v'b' \rangle}{\partial y} \\ \frac{\partial \bar{v}}{\partial y} + \frac{\partial \bar{w}}{\partial z} &= 0 \end{aligned} \quad (5)$$

where  $\langle w'b' \rangle = 0$  identically for internal waves so has been excluded. The background buoyancy frequency squared  $N^2 = -\partial B / \partial z$  and includes variations due to the geostrophic flow. The momentum-flux divergence  $\partial \langle u'w' \rangle / \partial z$  represents a weak perturbation from hydrostatic balance and has been neglected. The timescale of the wave-induced mean will prove to be much longer than that of the fluctuations. Variables have been separated into a background mean  $\Psi$  associated with the vertical stratification, a geostrophic mean  $\Psi_0$ , an internal wave-induced mean  $\psi$ , and a fluctuating wave component  $\psi'$ . For a horizontally quaquaversal (pointing equally in all directions) wave spectrum, the momentum-flux divergences  $\partial \langle v'w' \rangle / \partial z$  and  $\partial \langle v'b' \rangle / \partial y$  vanish for the above example because the effects of waves propagating toward the left and right of the flow direction cancel out. The only remaining driving force for the wave-induced mean is the momentum-flux divergence  $\partial \langle u'w' \rangle / \partial z$  in the  $u$ -momentum equation. In an irrotational system, this would be balanced by an acceleration of the mean flow  $Du/Dt$ . This will *not* be the case in a rotating system. *By analogy to surface wind-stress forcing, the momentum-flux divergence will be balanced by the Coriolis acceleration to produce an 'Ekman' flow  $v = (1/f) \partial \langle u'w' \rangle / \partial z$  perpendicular to the geostrophic flow.* This simple conclusion is in part due to the absence of horizontal gradients in the geostrophic flow. For example, horizontal gradients  $\partial U_0 / \partial y$  will result in momentum-flux divergence curl  $\partial^2 \langle u'w' \rangle / \partial y \partial z$ , driving Ekman divergences  $\partial v / \partial y$ . These in turn will produce vertical motions  $w$ . The interaction of this wave-induced 'Ekman' circulation with the background and geostrophic gradients will modify the geostrophic flow <sup>2</sup>

According to Jones (1967) and Bretherton (1969), the appropriate Lagrangian momentum-flux following a water parcel in a rotating system is not  $\langle u'w' \rangle$  but

$$\langle u'w' \rangle - f \langle \eta'w' \rangle = \langle u'w' \rangle + i \frac{f}{\omega} \langle v'w' \rangle$$

which they identify as the angular momentum flux. However, as already pointed out, in a horizontally isotropic internal wave field  $\partial \langle v'w' \rangle / \partial z$  vanishes, so can be neglected here.

There will be a nonvanishing  $f\partial\langle u'w' \rangle/\partial z$  in the  $v$ -momentum equation, where  $u' = i\omega\chi'$ . This will degrade the geostrophic balance, but for realistic momentum-flux divergences this effect is so small that it can be neglected without consequences.

For the remainder of this paper, we will focus on the case of a purely vertical geostrophic shear so that  $\partial/\partial y = 0$  (except for the geostrophic  $\partial B_0/\partial y$ ) and re-evaluate the critical-layer problem described by Andrews (1980) for more realistic oceanic conditions. By neglecting horizontal geostrophic shears, we assume that  $\partial v/\partial y = 0$ , so  $\partial w/\partial z = w = 0$ . The equations of motion (5) then simplify to

$$\begin{aligned} f\tilde{v} &= -\frac{\partial\langle u'w' \rangle}{\partial z} \\ fU_0 &= -\frac{\partial P_0}{\partial y} \\ \frac{D\tilde{h}}{Dt} + \tilde{v}\frac{\partial B_0}{\partial y} &= 0 \end{aligned} \tag{6}$$

where the  $v$ -momentum equation is the zeroth-order geostrophic balance. To first order, the  $u$ -momentum equation is an 'Ekman' balance, and to second order the buoyancy (density) equation is driven by advection of the geostrophic buoyancy gradients by the wave-induced 'Ekman' flow.

## A QUANTITATIVE EXAMPLE

To test the consequences of (6) under realistic oceanic conditions, we choose a realistic stratification  $N(z) = N_0 + \delta N e^{-kz}$  (where  $N_0 = 10^{-3}/s$ ,  $\delta N = 10^{-2}/s$  and  $k = \pi/1300$  m; Fig. 2a), and let the background geostrophic flow be a first baroclinic mode  $U_0(z)$  (Fig. 2b) in a 5000-m deep ocean with a surface magnitude of 30 cm/s.

A horizontally isotropic internal wave field radiating down from the surface will produce a net momentum-flux divergence  $\partial\langle u'w' \rangle/\partial z$  due to the increasing fraction of the internal wave spectrum lost to critical-layers with depth. We will use the Garrett and Munk (1979) model spectrum except for the assumed vertical asymmetry (considering only downward-propagating waves). The GM momentum-flux (or Reynolds-stress) co-spectrum  $\langle u'w' \rangle$  for downgoing waves travelling against the flow is shown versus  $\log(\omega_0)$  in loglog and variance-preserving formats in Fig. 3. The variance-preserving spectrum is flat; the nonvanishing value as  $\omega_0$  approaches  $f$  is due to the integrable singularity at the Coriolis frequency Garrett and Munk include in their horizontal velocity spectrum. The vertical wavenumber-dependence is  $k_z^{-2}$  so that low-wavenumber waves dominate the total momentum-flux.

As the geostrophic velocity difference  $\Delta U$  increases with depth, so does the portion of internal wave energy-flux and momentum-flux blocked by critical-layers (Fig. 4). Waves with frequencies near  $f$  or with high wavenumbers are most strongly affected. For  $\Delta U = 1$  cm/s, waves with  $\lambda_z < 20$  m encounter critical-layers; for  $\Delta U = 5$  cm/s, this extends to  $\lambda_z < 60$  m. We will assume that all the trapped energy-flux is lost to turbulence in the vicinity of the critical-layer. The resulting energy-flux divergence

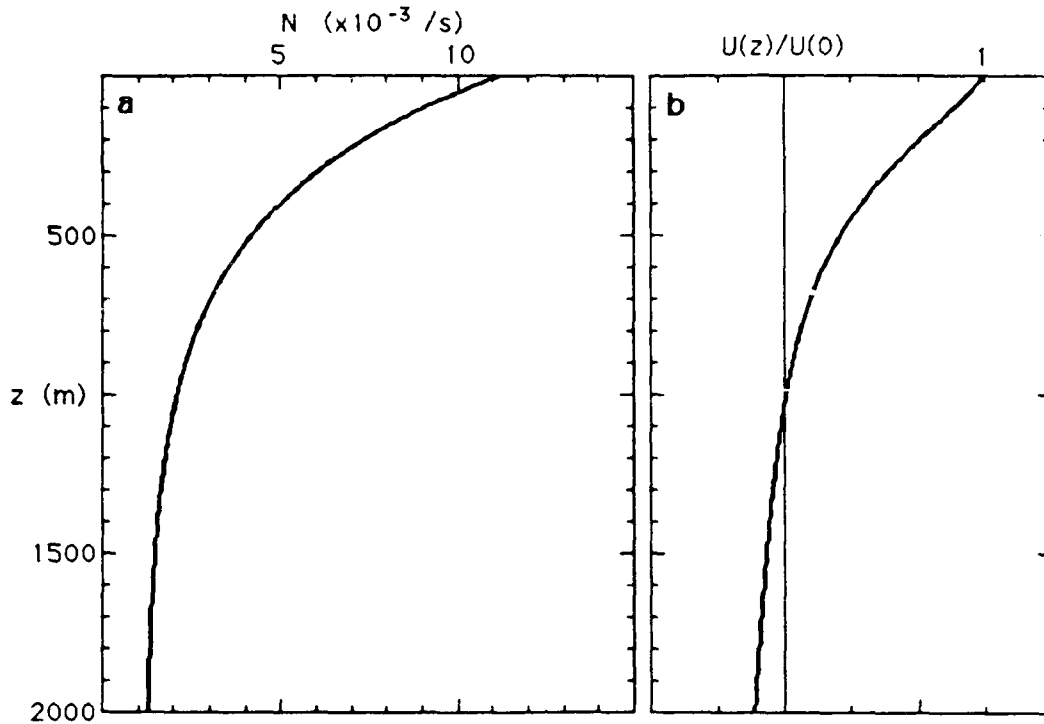


Figure 2. Vertical profiles of (a) buoyancy frequency  $N$  and (b) first baroclinic mode velocity structure  $U_0(z)$  for the geostrophic flow in a 5000-m deep ocean used for the simulation. Shear is concentrated in the upper 500 m of the ocean.

$\partial F_E / \partial z$  will be lost to turbulent dissipation  $\epsilon$  with maximum magnitudes of  $\sim 6 \times 10^{-9}$  W/kg at 700-m depth (Fig. 5a). This value could be measured with present-day microstructure shear probes to test the hypothesis that all the trapped variance is being dissipated provided that turbulence generated by random internal wave breaking does not mask the signal. Gregg (1989) reports enhanced internal wave shear and dissipation rates ( $\epsilon \sim 100\nu N^2 \sim 4 \times 10^{-9}$  W/kg) in a jet off northern California.

Turbulence will result in eddy viscosities and diffusivities. The internal wave shear should be  $\geq 2N$  ( $Ri \sim 0.25$ ) for shear-generated turbulence, so the eddy viscosity will be  $\epsilon / (V_z \cdot V_z) \leq \epsilon / 4N^2 = 5 \times 10^{-5}$  m<sup>2</sup>/s acting on the internal waves. The eddy diffusivity depends on the mixing efficiency  $e \leq 0.2$  (Osborn, 1980) and will be  $e\epsilon / N^2 \leq 4 \times 10^{-5}$  m<sup>2</sup>/s. Internal wave breaking due to the random superposition of waves will also contribute to the turbulent dissipation  $\epsilon$ , eddy viscosity and eddy diffusivity.

The 'Ekman' flow  $v$  driven by the momentum-flux divergence (6) is shown in Fig. 5b. It has maximum velocities of  $\sim 0.01$  cm/s to the right of the geostrophic flow at  $\sim 400$ -m depth.

The 'Ekman' flow interacts with the geostrophic horizontal buoyancy gradients. Substituting for  $v$  and  $\partial B_0 / \partial y$  from the 'Ekman' and geostrophic balances in the buoyancy equation in (6) and taking the vertical derivative leads to an expression for the change in the buoyancy frequency in time

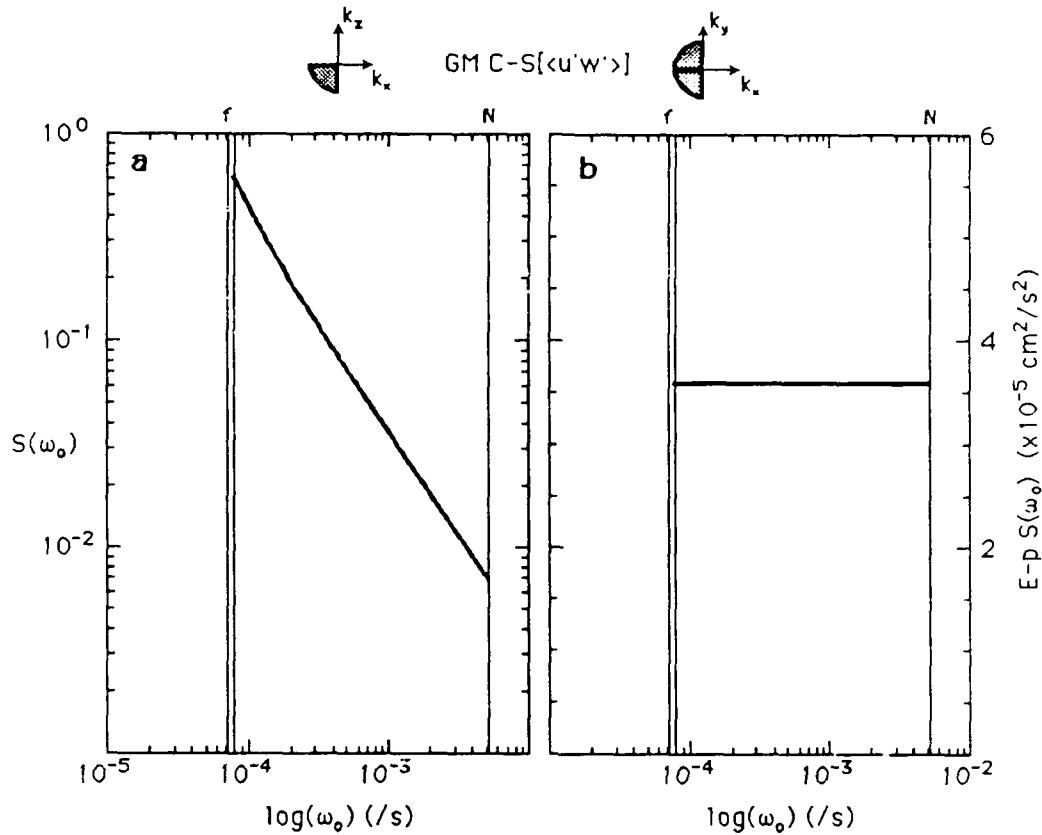


Figure 3. The  $\langle u'w' \rangle$  co-spectrum for the downward-propagating portion of the Garrett and Munk model travelling in the positive  $x$ -direction in (a) loglog and (b) variance-preserving formats. All frequencies contribute significantly to  $\langle u'w' \rangle$ . The nonvanishing value as  $\omega_0$  approaches  $f$  is a consequence of the integrable singularity in the Garrett and Munk horizontal velocity spectrum.

$$\frac{DN^2}{Dt} = \frac{\partial}{\partial z} \left[ \frac{\partial \langle u'w' \rangle}{\partial z} \frac{\partial U_0}{\partial z} \right]. \quad (7)$$

The buoyancy frequency will decrease in time because of the vertical shear  $\partial v / \partial z$  tilting the isopycnal surfaces to the vertical (Fig. 6). This also implies a reduction of the background potential vorticity  $fN^2$ . The horizontal buoyancy gradient (and so the geostrophic shear) is unaffected in the purely vertical shear case because  $\partial \langle u'w' \rangle / \partial y = 0$  and  $\partial U_0 / \partial y = 0$  so  $D(\partial B_0 / \partial y) / Dt = 0$ . Therefore, the geostrophic potential vorticity does not change.

The buoyancy frequency will be reduced to zero (7) in  $\sim O(100 \text{ yrs})$  (Fig. 7). As pointed out by Frank Henyey (personal communication, 1989), this timescale is comparable to the  $e$ -folding time for an eddy diffusivity of  $10^{-4} \text{ m}^2/\text{s}$  (Munk, 1966) to diffuse away the pycnocline. We now know that this value of the eddy diffusivity is far too large (e.g., Garrett, 1989; Gregg, 1989). Figure 7 suggests that, rather than the advective-diffusion balance for the thermocline proposed by Munk (1966)

$$w \frac{\partial T}{\partial z} = D \frac{\partial^2 T}{\partial z^2} \quad (8)$$

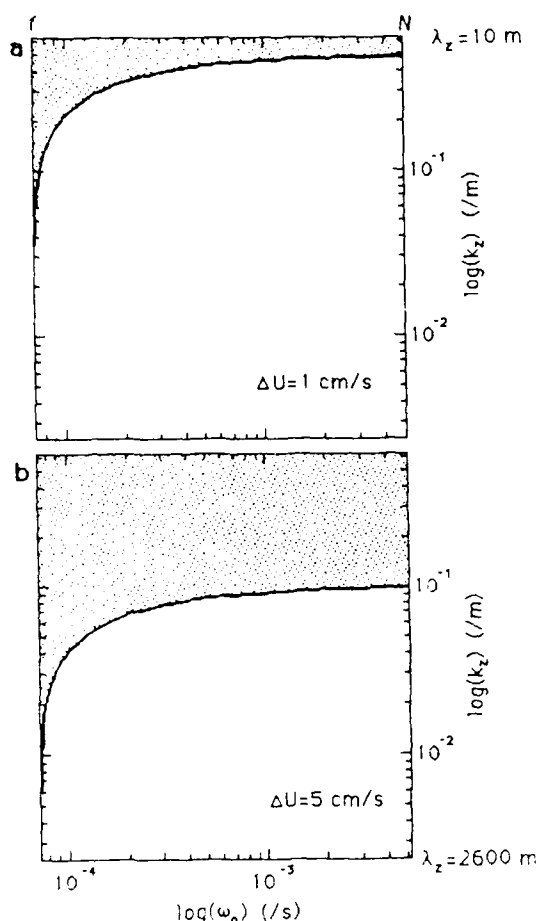


Figure 4. The portion of vertical wavenumber/frequency space affected by critical-layers (stippled) for velocity differences of (a)  $\Delta U_0 = 1$  cm/s and (b)  $\Delta U_0 = 5$  cm/s. The near-inertial and high wavenumber parts of the spectrum are lost to critical-layers first.

with the diffusion  $D$  produced by breaking internal waves, an advective balance

$$w \frac{\partial T}{\partial z} = - \langle \bar{v} \frac{\partial T}{\partial y} \rangle, \quad (9)$$

with  $\bar{v}$  induced by internal wave momentum flux divergences in geostrophic shear associated with  $\partial T / \partial y$ , needs to be considered. This naive view would imply either larger vertical velocities or larger vertical gradients in regions of strong geostrophic shear.

## PARAMETERIZATION

The effect of internal waves can be parameterized in eddy-resolving models without resolving the internal waves themselves. In the past the forcing terms have been assumed to be of an eddy viscosity form (e.g., Flierl and Mied, 1985). Figure 8 displays the momentum-flux lost from waves to critical-layers  $\Delta \langle u'w' \rangle$  as a function of the parameter  $(N_0/N)^{0.7} \Delta U_0$ , where  $\Delta U_0$  is the geostrophic velocity difference from the

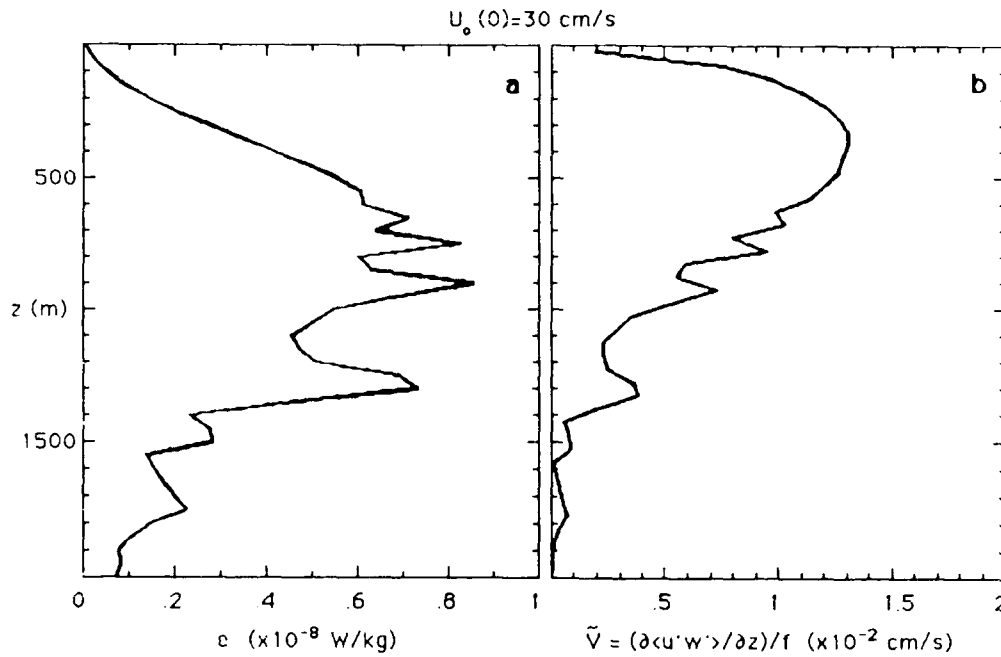


Figure 5. (a) Energy-flux divergence and (b) momentum-flux divergence for a 30-cm/s surface velocity. The energy-flux divergence is balanced by turbulent dissipation  $\epsilon$ . It has maximum values of  $\sim 5 \times 10^{-9}$  W/kg, which is measurable with present microstructure shear probes. The momentum-flux divergence drives an 'Ekman' mean flow  $v = (1/f)\partial\langle u'w' \rangle/\partial z$  of up to 0.01 cm/s (10 m/day), which is not measurable.

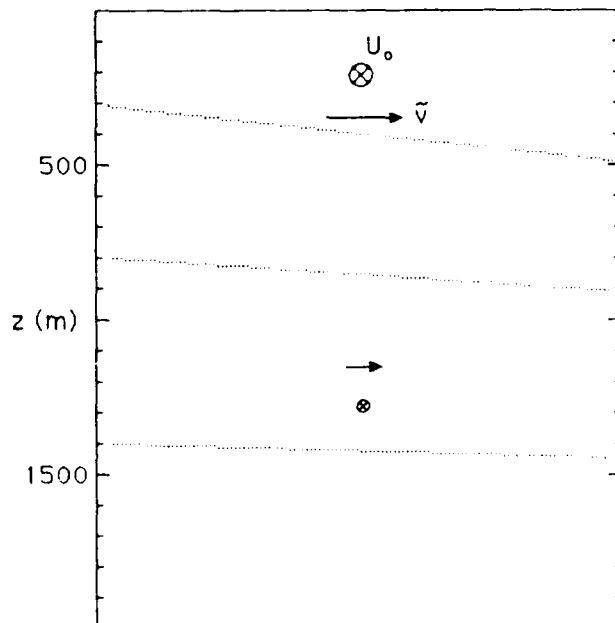


Figure 6. Cartoon illustrating the interaction of a wave-induced 'Ekman' shear  $\partial v/\partial z$  with the tilted isopycnals associated with a purely vertical geostrophic shear. The geostrophic flow  $U_0(z)$  is into the page ( $\otimes$ ). The wave-induced 'Ekman' flow is to the right. It will tilt the isopycnals into the vertical, reducing the vertical gradients (buoyancy frequency) but not affecting the horizontal gradients (geostrophy).

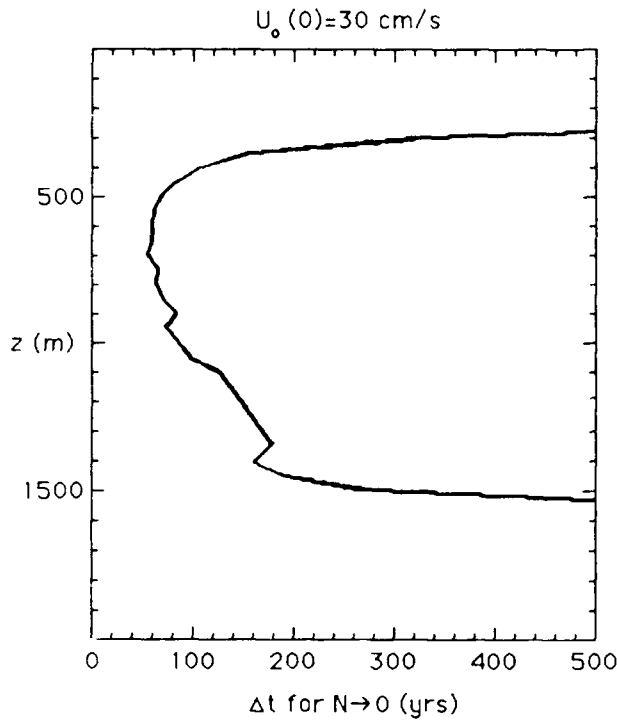


Figure 7. The timescale for reduction of the buoyancy frequency to zero due to tilting of the isopycnals by the 'Ekman' shear  $\partial v / \partial z$  acting on the geostrophic buoyancy-gradient  $\partial B_0 / \partial y$ . The minimum time is  $\sim O(100 \text{ yrs})$ .

surface,  $N$  is the local buoyancy frequency and  $N_0 = 5 \times 10^{-3} / \text{s}$ . The scaling does a good job of collapsing the curves for various stratification and flow structures provided  $(N_0/N)^{0.7} \Delta U_0 < 0.5 \text{ m/s}$ . (For higher values, there is an increased sensitivity to  $N$  as one runs out of spectrum.) This implies a simple scaling for the internal wave momentum-flux divergence

$$\frac{\partial \langle u'w' \rangle}{\partial z} = -1.5 \times 10^{-5} \left( \frac{N_0}{N} \right)^{0.7} \left( \frac{E}{E_{GM}} \right) \frac{\partial U_0}{\partial z} \quad (10)$$

where  $E/E_{GM}$  is the ratio of variance in the internal wave field compared to the Garrett and Munk model. There is evidence that  $E$  scales with the wind-forcing from observations of a seasonal dependence of internal wave variance (Briscoe and Weller, 1984). Note that (10) is not an eddy viscosity scaling. Past investigators (e.g., Ruddick, 1980 whose Fig. 3 is equivalent to our Fig. 8) have equated the momentum-flux divergence with an eddy viscous term  $\nu \partial^2 U_0 / \partial z^2$  to estimate an eddy viscosity  $\langle u'v' \rangle / (\partial U_0 / \partial z) \sim 2 \times 10^{-2} \text{ m}^2/\text{s}$ , much larger than the  $5 \times 10^{-5} \text{ m}^2/\text{s}$  found here. This suggests that the momentum-flux divergence will have a much greater influence on the mean flow than the turbulent dissipation. Also the eddy viscosity parameterization suggests a need for mean flow curvature whereas (10) indicates that all that is needed is shear. More significantly, it has been common to neglect the Coriolis acceleration, which is no more justified in this problem than it is for the surface wind-forced problem.

Substituting (10), (3) and (6) into (9), one can obtain an expression relating the upwelling velocity and the geostrophic Richardson number

$$w = -1.5 \times 10^{-5} (N_0/N)^{0.7} (E/E_{GM}) \text{ Ri}^{-1} \quad (11)$$



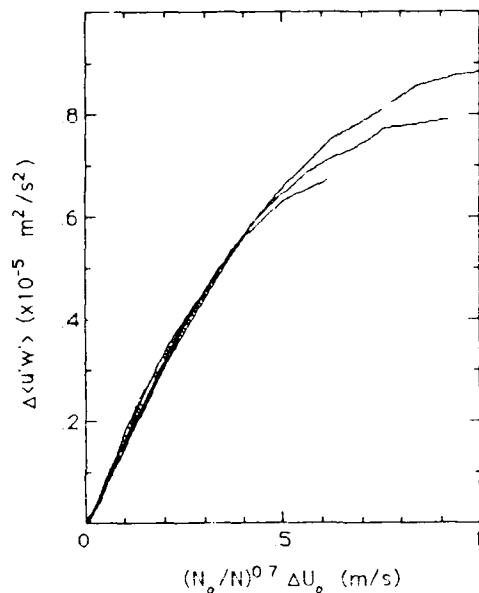


Figure 8. The internal wave momentum-flux lost to critical-layers  $\Delta\langle u'w' \rangle$  as a function of the geostrophic velocity difference scaled by the local buoyancy frequency for a variety of monotonic geostrophic shears. The scaling collapses the variance for  $(N_0/N)^{0.7} \Delta U_0 < 0.5$  m/s, allowing the momentum-flux to be parameterized in terms of the largescale properties.

which, for an upwelling velocity of 1.2 cm/day, implies geostrophic Richardson numbers of 100–400, corresponding to baroclinic velocity of  $\sim 15$  cm/s in the deep water and 25 cm/s in the main pycnocline. While these velocities appear to be overly large, this mechanism cannot be discarded outright.

While the parameterization (10) is of a form that could be readily included in numerical models, it is not clear whether the effect of this momentum flux divergence would be felt in the presence of the large numerical diffusivities/viscosities needed to maintain numerical stability in these models.

## DISCUSSION

A few cautionary remarks are in order concerning the assumptions that went into this model and the consequences of relaxing them. These include:

- neglect of upward-propagating waves.
- assuming all of trapped internal waves are lost to irreversible processes. Instabilities at the critical-layer generate untrapped waves that carry away the momentum-flux.
- assuming horizontal isotropy.
- assuming that the high-frequency, high-wavenumber motions are internal waves and are adequately described by the Garrett and Munk model.

Upgoing waves have been ignored under the assumption that the strongest source of internal waves is atmospheric forcing at the surface. In general, the momentum-flux

divergence of upgoing waves will act in the opposite sense to that of the downgoing waves so that the momentum-flux divergence and its associated 'Ekman' flow may have been overestimated or even assigned the wrong sign here. While the Garrett and Munk model is vertically symmetric at all frequencies, observations have found a dominance of downgoing energy-flux in the near-inertial peak (Sanford, 1975; Leaman, 1976; Kase and Olbers, 1980; D'Asaro and Perkins, 1984) and low-frequency part of the internal waveband (Müller *et al.*, 1978). Vertical symmetry at high frequencies was found in IWEX (Müller *et al.*, 1978) but Pinkel (1984) reported net upward propagation in one instance off California. These results are associated with low vertical wavenumbers. Whether there is vertical asymmetry at the high vertical wavenumbers that the momentum-flux divergences are most sensitive to is not known.

If some of the trapped wave momentum-flux escapes to untrapped waves through wave/wave interactions or instability at the critical-layer, the estimate here will also be an overestimate. However, instability and wave/wave interactions are likely to produce other high-wavenumber waves which will also be trapped (Fig. 4). It has been assumed that wave/wave interactions do not refill the part of the spectrum depleted by critical-layers. While lower wavenumbers might transfer energy to high wavenumbers, such interactions *must* conserve momentum-flux. In particular, an anisotropic internal wave field cannot be isotropized by wave/wave interactions. Thus, the momentum-flux in any direction can only be redistributed in frequency/vertical wavenumber-space. Past parameterizations of the relaxation of an internal wave field from a perturbed state back to equilibrium (e.g., Müller, 1976) have not preserved momentum-flux so have overestimated the vertical eddy viscosity ( $0.4 \text{ m}^2/\text{s}$ ), as has been demonstrated observationally ( $<10^{-2} \text{ m}^2/\text{s}$ , Frankignoul and Joyce, 1979; Ruddick and Joyce, 1979;  $\sim 10^{-4} \text{ m}^2/\text{s}$ , Lueck and Osborn, 1986).

The assumption of horizontal isotropy is of little concern for the vertical sheared case presented here. Anisotropy would have introduced a momentum-flux divergence  $\partial \langle v'w' \rangle / \partial z$  in the  $v$ -momentum equation (5), but with little effect (factor of 0.0003) on the geostrophic flow. In a problem including horizontal geostrophic shears, horizontal anisotropy in the internal wave field will lead to a net  $\partial \langle u'v' \rangle / \partial y$  and  $\partial \langle v'v' \rangle / \partial y$  due to horizontal critical-layers. Since weather patterns are carried eastward in the Westerlies and westward in the Trades, there may be significant anisotropy in the atmospherically forced wave field. This is consistent with the southeastward propagation observed in IWEX in the low-frequency part of the internal band (Müller *et al.*, 1978).

As already pointed out (Fig. 4), the momentum- and energy-flux divergences contain significant contributions from the high-wavenumber, high-frequency part of the spectrum which is not well-known. Because of the small amplitudes of these waves and the ease with which they can be Doppler-shifted in frequency-space, there are few reliable estimates of this part of the spectrum. Both shear and strain frequency slopes become less steep at high wavenumber (Pinkel, 1984). Moored measurements consistently find more shear variance in the high-wavenumber, high-frequency band than can be accounted for by the strain assuming linear internal waves (Müller *et al.*, 1978; Briscoe, 1977; Pinkel, 1984). This excess shear may be due to Doppler-shifted motions associated with finescale vortices (Müller *et al.*, 1988) or near-inertial waves (Kunze *et al.*, 1989). Recent work (Sherman and Pinkel, personal communication, 1989) suggests that, in the isopycnal-following (or Lagrangian) frame that is appropriate for an intrinsic frequency description, the strain spectrum is described by the Garrett and Munk model. The applicability of internal wave dynamics on these scales remains to be established.

## SUMMARY

Exchange of energy and momentum between internal waves and the geostrophic flow is constrained by conservation of potential vorticity to sites of irreversible dissipation and mixing. For a horizontally isotropic but vertically-asymmetric internal wave field, there will be no net momentum exchange due to random superpositions of internal wave breaking; only breaking at critical-layers will make a net contribution.

By analogy to wind stress forcing, the momentum-flux divergence  $\partial \langle u'w' \rangle / \partial z$  will be balanced by the Coriolis acceleration  $f v$  to drive an 'Ekman' flow  $v$  without accelerating the geostrophic mean; to modify the potential vorticity there must be a *curl* to the momentum-flux divergence. This, of course, does not prevent loss of mean energy to internal waves when geostrophic flow evolves from a higher to lower energy state with the same potential vorticity.

For a first baroclinic mode geostrophic shear with a surface velocity 30 cm/s in an exponentially stratified ocean, the wave-driven 'Ekman' flow  $v \leq 0.01$  cm/s. If the energy-flux divergence is lost to turbulence, then the maximum dissipation rate  $\epsilon = 6 \times 10^{-9}$  W/kg.

The shear associated with the 'Ekman' flow  $\partial v / \partial z$  will act on the geostrophic buoyancy-gradient  $\partial B_0 / \partial y$ , tilting the isopycnals into the vertical and reducing the background buoyancy frequency on a timescale of  $\sim O(100 \text{ yrs})$ . While long, this is comparable to the time it would take an abyssal recipes  $10^{-4} \text{ m}^2/\text{s}$  vertical eddy diffusivity (Munk, 1966) to homogenize the pycnocline. It is now known that this eddy viscosity is too large. If we still demand a Stommel-Arons (1960a,b) upwelling  $w$  over the world ocean, some other term must balance the resulting  $-v \partial T / \partial z$ . The possibility suggested here is a wave-induced advection of geostrophic gradients  $\langle v \partial T / \partial y \rangle$  acts to reduce the vertical gradients.

It is possible to parameterize the effect of internal wave momentum-flux divergences on the mean flow for eddy-resolving numerical models (10) but whether the effects can be felt in these models over that of the large numerical diffusivities/viscosities required to maintain numerical stability is not known. The results here suggest that internal waves may contribute significantly on climatological timescales.

Finally, we caution the reader that the purely vertical shear example presented here is an unrealistic simplification in the sense that it produces no 'Ekman' divergences  $\partial v / \partial y$ . These *would* occur in horizontally sheared currents and lead to modification of the geostrophic flow. Horizontal shear is important in the ocean. Rossby numbers are almost always larger than the inverse geostrophic Richardson number (4). The full consequences of including horizontal shear are beyond the scope of this note but the subject of continuing research. Interested readers are referred to Eliassen and Palm (1961), Andrews and McIntyre (1976) and Garrett (1982) for some discussion on this topic.

Acknowledgments: Comments from Chris Garrett, Frank Henyey, Peter Killworth and Lew Rothstein have been helpful. Peter Rhines generously provided funds from JRI contract N00014-86-K-0690#1 allowing Eric Kunze to undertake this research. Peter Müller is supported by the Office of Naval Research.

## REFERENCES

- Andrews, D.G., 1980: On the mean motion induced by transient inertio-gravity waves. *Pure Appl. Geophys.*, 118, 177-188.
- Andrews, D.G., and M.E. McIntyre, 1976: Planetary waves in horizontal and vertical shear: The generalized Eliassen-Palm relation and the mean zonal acceleration. *J. Atmos. Sci.*, 33, 2049-2053.
- Bretherton, F.P., 1969: Momentum transport by gravity waves. *Quart. J. Roy. Met. Soc.*, 95, 213-243.
- Briscoe, M.G., 1977: On current finestructure and moored current-meter measurements of internal waves. *Deep-Sea Res.*, 24, 1121-1131.
- Briscoe, M.G., and R.A. Weller, 1984: Preliminary results from the Long-Term Upper Ocean Study (LOTUS). *Dyn. Atmos. Ocean*, 8, 243-265.
- D'Asaro, E.A., and H. Perkins, 1984: The near-inertial internal wave spectrum in the late summer Sargasso Sea. *J. Phys. Oceanogr.*, 14, 489-505.
- Eliassen, A., and E. Palm, 1961: On the transfer of energy in stationary mountain waves. *Geophys. Publ.*, 22, 1-23.
- Ertel, H., 1942: Ein neuer hydrodynamischer Wirbelsatz. *Meteorol. Z.*, 59, 277-281.
- Flierl, G.R., and R.P. Mied, 1985: Frictionally-induced circulations and spindown of a warm-core ring. *J. Geophys. Res.*, 90, 8917-8927.
- Frankignoul, C., and T.M. Joyce, 1979: On internal wave variability during the Internal Wave Experiment (IWEX). *J. Geophys. Res.*, 84, 769-776.
- Gargett, A.E., 1989: Ocean turbulence. *Ann. Rev. Fluid Mech.*, 21, 419-451.
- Garrett, C., 1982: On spindown in the ocean interior. *J. Phys. Oceanogr.*, 12, 989-993.
- Garrett, C., and W. Munk, 1979: Internal waves in the ocean. *Ann. Rev. Fluid Mech.*, 11, 339-369.
- Gregg, M.C., 1989: Scaling turbulent dissipation in the thermocline. *J. Geophys. Res.* (in press).
- Hall, M.M., 1985: Horizontal and vertical structure of velocity, potential vorticity, and energy in the Gulf Stream. Ph.D. thesis, MIT/WHOI, WHOI-85-16, 165 pp.
- Jones, W.L., 1967: Propagation of internal gravity waves in fluids with shear flow and rotation. *J. Fluid Mech.*, 30, 439-448.
- Kase, R.H., and D.J. Olbers, 1980: Wind-driven inertial waves observed during phase III of CATE. *Deep-Sea Res.*, 26 (Suppl.), 191-216.
- Kunze, E., 1985: Near-inertial wave propagation in geostrophic shear. *J. Phys. Oceanogr.*, 15, 544-565.
- Kunze, E., M.G. Briscoe and A.J. Williams, 1989: Interpreting velocity finestructure from a neutrally-buoyant float. in preparation.
- Leaman, K.D., 1976: Observations of the vertical polarization and energy flux of near-inertial waves. *J. Phys. Oceanogr.*, 6, 894-908.
- Lueck, R., and T. Osborn, 1986: The dissipation of kinetic energy in a warm-core ring. *J. Phys. Oceanogr.*, 91, 803-818.
- McFarlane, N.A., 1987: The effect of orographically-excited gravity wave drag on the general circulation of the lower stratosphere and troposphere. *J. Atmos. Sci.*, 44, 1775-1785.
- Miroshnikov, Yu.Z., N.I. Solntseva and B.N. Filyuskin, 1976: On horizontal variability of Brunt-Vaisala frequency in the ocean. *Oceanology* (English version), 15, 15-20.
- Mooers, C.N.K., 1975: Several effects of a baroclinic current on the cross-stream propagation of inertial-internal waves. *Geophys. Fluid Dyn.*, 5, 245-275.
- Müller, P., 1976: On the diffusion of momentum and mass by internal gravity waves. *J. Fluid Mech.*, 77, 789-823.
- Müller, P., D.J. Olbers and J. Willebrand, 1978: The IWEX spectrum. *J. Geophys. Res.*, 83, 479-500.

- Müller, P., R.-C. Lien and R. Williams, 1988: Estimates of potential vorticity at small scales in the ocean. *J. Phys. Oceanogr.*, 18, 401-416.
- Munk, W.H., 1966: Abyssal recipes. *Deep-Sea Res.*, 13, 707-730.
- Munk, W., 1981: Internal waves and smallscale processes. *Evolution of Physical Oceanography*, B.A. Warren and C. Wunsch, Eds., The MIT Press, 264-291.
- Olbers, D.J., 1981: The propagation of internal waves in a geostrophic current. *J. Phys. Oceanogr.*, 11, 1224-1233.
- Olbers, D.J., 1983: Models of the oceanic internal wave field. *Rev. Geophys. Space Phys.*, 21, 1567-1606.
- Osborn, T.R., 1980: Estimates of the local rate of vertical diffusion from dissipation measurements. *J. Phys. Oceanogr.*, 10, 83-89.
- Pedlosky, J., 1979: *Geophysical Fluid Dynamics*. Springer-Verlag, 624 pp.
- Pinkel, R., 1984: Doppler sonar observations of internal waves: the wavenumber-frequency spectrum. *J. Phys. Oceanogr.*, 14, 1249-1270.
- Rossby, C.-G., 1938: On the mutual adjustment of pressure and velocity distributions in the certain simple current systems, II. *J. Mar. Res.*, 1, 239-263.
- Ruddick, B.R., 1980: Critical-layers and the Garrett-Munk spectrum. *J. Mar. Res.*, 38, 135-145.
- Ruddick, B.R., and T.M. Joyce, 1979: Observations of interaction between the internal wave field and low-frequency flows in the North Atlantic. *J. Phys. Oceanogr.*, 9, 498-517.
- Sanford, T. B., 1975: Observations of the vertical structure of internal waves. *J. Geophys. Res.*, 80, 3861-3871.
- Stommel, H., and A.B. Arons, 1960a: On the abyssal circulation of the world ocean—I. Stationary planetary flow patterns on a sphere. *Deep-Sea Res.*, 6, 140-154.
- Stommel, H., and A.B. Arons, 1960b: On the abyssal circulation of the world ocean—II. An idealized model of the circulation pattern and amplitude in oceanic basins. *Deep-Sea Res.*, 6, 217-233.

## DIANEUTRAL ADVECTION

Trevor J McDougall

CSIRO Division of Oceanography, GPO Box 1538, Hobart, TAS 7001, Australia.

### ABSTRACT

The nonlinear nature of the in situ density of seawater as a function of the potential temperature, pressure and salinity causes two vertical advection processes (thermobaricity and cabbeling) and also complicates the use of microstructure data to deduce upwelling velocities. In most of the ocean thermobaricity and cabbeling are weak, but where there is a significant epineutral gradient of potential temperature, the downwelling due to cabbeling is quite large. In the Southern Ocean, where the neutral surfaces have large slopes, thermobaricity causes a larger downwelling velocity than cabbeling and the two processes together cause a dianeutral velocity of about  $-2 \times 10^{-7} \text{ m s}^{-1}$ . The complementary roles of vertical mixing and vertical advection in achieving water-mass conversion are demonstrated, since maps of the dianeutral motion caused by vertical mixing are quite different to maps of water-mass conversion caused by the same process. This emphasizes the need to include both vertical advection and vertical mixing in ocean models. The method used to infer the upwelling velocity from microstructure dissipation measurements is also significantly affected by the nonlinear nature of the equation of state. The extra term that needs to be included in this method is a strong function of depth, changing sign at a depth of about 1500 m. The differences between interior mixing and boundary mixing are explored using the conservation statements for buoyancy and volume in the turbulent boundary layers. It is shown that the deep circulation driven by boundary mixing is quite different to that of Stommel and Arons. Interestingly, seamounts are, on average, sinks for the lateral flow, with downwelling in the turbulent boundary region surrounding each seamount.

### INTRODUCTION

The starting point for this paper is the conservation equations for scalars. For salinity,  $S$ , and potential temperature,  $\theta$ , the conservation equations are

$$\theta_t|_n + \left[ \mathbf{V}_n - \frac{1}{h} \nabla_n(hK) \right] \cdot \nabla_n \theta + e\theta_z = K \nabla_n^2 \theta + [D\theta_z]_z, \quad (1)$$

$$S_t|_n + \left[ \mathbf{V}_n - \frac{1}{h} \nabla_n(hK) \right] \cdot \nabla_n S + eS_z = K \nabla_n^2 S + [DS_z]_z, \quad (2)$$

where  $\mathbf{V}_n$  is the Lagrangian two-dimensional lateral velocity vector,  $u\mathbf{i} + v\mathbf{j}$ ,  $e$  is the velocity of fluid through a neutral surface (dianeutral velocity),  $h$  is the height between adjacent neutral surfaces,  $K$  is the epineutral diffusivity,  $D$  is the dianeutral (or vertical) diffusivity and  $\nabla_n$  is the lateral gradient operator in a neutral surface. These conservation equations have been

previously explained by McDougall (1987a); the only additional feature now is that the lateral variations of  $h$  have been included. The two terms in these equations that contain the epineutral diffusivity,  $K$ , can be derived by taking the epineutral divergence,  $(\nabla_n \cdot)$ , of the total flux of heat between two adjacent neutral surfaces,  $-hK\nabla_n\theta$ . The spatial gradients of  $\theta$  and  $S$  along neutral surfaces and also their temporal derivatives are related through the thermal expansion coefficient,  $\alpha$ , and the saline contraction coefficient,  $\beta$ , so that

$$\alpha\theta_t|_n = \beta S_t|_n, \quad \text{and} \quad \alpha\nabla_n\theta = \beta\nabla_n S. \quad (3)$$

Combining Eqs (1) – (3), one finds

$$\begin{aligned} \theta_t|_n + \left[ \mathbf{V}_n - \frac{1}{h}\nabla_n(hK) \right] \cdot \nabla_n\theta &= K\nabla_n^2\theta + D\frac{g}{N^2}\theta_z^3\beta\frac{d^2S}{d\theta^2} \\ &+ K\frac{g}{N^2}\theta_z\left\{ \frac{\partial\alpha}{\partial\theta}\nabla_n\theta \cdot \nabla_n\theta + \frac{\partial\alpha}{\partial p}\nabla_n\theta \cdot \nabla_n p \right\}, \end{aligned} \quad (4)$$

and

$$[e - D_z] \frac{N^2}{g} = D[\alpha\theta_{zz} - \beta S_{zz}] - K\left\{ \frac{\partial\alpha}{\partial\theta}\nabla_n\theta \cdot \nabla_n\theta + \frac{\partial\alpha}{\partial p}\nabla_n\theta \cdot \nabla_n p \right\}, \quad (5)$$

where  $\partial\alpha/\partial\theta$  and  $\partial\alpha/\partial p$  are given by Eq. (8) below. Equation (4) is sometimes called the water-mass transformation equation, since temporal changes of potential temperature on a neutral surface imply changes to the  $S$ - $\theta$  curve of a water-mass. An important point to note in Eq. (4) is that the total effect of the vertical diffusivity,  $D$ , on the  $\theta$  conservation equation is proportional to  $d^2S/d\theta^2$ , the "curvature" of the  $S$ - $\theta$  curve formed from a vertical CTD cast. As first pointed out by McDougall (1984), if either the dianeutral advective term or the vertical diffusive term in Eq. (1) is omitted in a diagnostic model, then the term in the conservation equations due to vertical turbulent mixing must take the form on the right-hand side of Eq. (4), namely,  $DgN^{-2}\theta_z^3\beta d^2S/d\theta^2$ . The corresponding equations for salinity,  $S$ , and another passive tracer,  $C$ , are obtained by eliminating  $[e - D_z]$  between Eqs (5) and (2) (and similarly for  $C$ ), obtaining

$$\begin{aligned} S_t|_n + \left[ \mathbf{V}_n - \frac{1}{h}\nabla_n(hK) \right] \cdot \nabla_n S &= K\nabla_n^2 S + D\frac{g}{N^2}\theta_z^3\alpha\frac{d^2S}{d\theta^2} \\ &+ K\frac{g}{N^2}S_z\left\{ \frac{\partial\alpha}{\partial\theta}\nabla_n\theta \cdot \nabla_n\theta + \frac{\partial\alpha}{\partial p}\nabla_n\theta \cdot \nabla_n p \right\}, \end{aligned} \quad (6)$$

and

$$\begin{aligned} C_t|_n + \left[ \mathbf{V}_n - \frac{1}{h}\nabla_n(hK) \right] \cdot \nabla_n C &= K\nabla_n^2 C + D C_z \frac{g}{N^2}\theta_z^2\beta\frac{d^2S}{d\theta^2} + D\theta_z^2\frac{d^2C}{d\theta^2} \\ &+ K\frac{g}{N^2}C_z\left\{ \frac{\partial\alpha}{\partial\theta}\nabla_n\theta \cdot \nabla_n\theta + \frac{\partial\alpha}{\partial p}\nabla_n\theta \cdot \nabla_n p \right\}. \end{aligned} \quad (7)$$

If the tracer  $C$  is consumed or produced, either biologically or radioactively, a suitable term can be added to Eq. (7) in the normal way; for example, radioactive decay requires an additional term,  $\lambda C$ , on the left-hand side.

## THERMOBARICITY AND CABELLING

The terms that appear in the conservation equations (4) to (7) that are proportional to  $\partial\alpha/\partial\theta$  and  $\partial\alpha/\partial p$  are the dianeutral advection processes of cabbelling and thermobaricity respectively. The parcel-mixing argument of Fig. 1 illustrates that when two water parcels that initially lie on a neutral surface are brought together without mixing, the temperature-dependence of the compressibility causes the parcels to move vertically off the neutral surface. This vertical advection process is thermobaricity. Once the two fluid parcels mix intimately, cabbelling causes an increase in density and a further vertical motion through neutral surfaces, as indicated in the figure. Both processes are proportional to the lateral flux of heat,  $-K\nabla_n\theta$ , cabbelling always producing a downwelling velocity through neutral surfaces, while thermobaricity can cause either upwelling or downwelling. Interestingly, while the dianeutral motion achieved by cabbelling and thermobaricity is quite significant, the dianeutral *diffusion*, or *mixing*, is negligible (McDougall 1987a). The partial derivatives,  $\partial\alpha/\partial\theta$  and  $\partial\alpha/\partial p$  that appear in the above equations are in fact shorthand expressions for

$$\left[ \frac{\partial\alpha}{\partial\theta} + 2\frac{\alpha}{\beta}\frac{\partial\alpha}{\partial S} - \frac{\alpha^2}{\beta^2}\frac{\partial\beta}{\partial S} \right] \quad \text{and} \quad \left[ \frac{\partial\alpha}{\partial p} - \frac{\alpha}{\beta}\frac{\partial\beta}{\partial p} \right] \quad (8)$$

respectively. These expressions are called the cabbelling and thermobaric parameters and are graphed in figure 9 of McDougall (1987a). Typical values are  $10^{-5} \text{ K}^{-2}$  for the cabbelling parameter and  $2.6 \times 10^{-8} \text{ K}^{-1} (\text{db})^{-1}$  for the thermobaric parameter.

Vertical mixing and advection processes are usually inferred from measurements of the dissipation rate of mechanical energy,  $\epsilon$ . However, the magnitudes of thermobaricity and cabbelling are determined by the *epineutral* heat flux and are not limited by the strength of vertical mixing processes. Hence neither thermobaricity nor cabbelling has a detectable signature in  $\epsilon$  measurements, and the strengths of these dianeutral advective processes must be inferred from information on the mesoscale lateral eddy field.

In order to map the cabbelling and thermobaric velocities in the ocean, a value of  $1000 \text{ m}^2 \text{ s}^{-1}$  was chosen for the epineutral diffusivity  $K$ . Freeland et al. (1975) used the statistics of float displacements to find the lateral diffusivity to be about this size at a depth of 1500 m in the relatively quiet MODE region, while Rossby et al. (1983) found  $K$  to be 50% larger than this at a depth of 1300 m in the region of the Local Dynamics Experiment. Estimates nearer the sea-surface are generally larger. Hence we believe that by taking a value of  $1000 \text{ m}^2 \text{ s}^{-1}$  we have erred on the side of being conservative, so that the strengths of cabbelling and thermobaricity are probably underestimated here. The combined contributions to the dianeutral velocity from cabbelling ( $e^{cabb}$ ) and thermobaricity ( $e^{tb}$ ), are (from Eq. 5),

$$e^{cabb} + e^{tb} = -\frac{g}{N^2} K \left\{ \frac{\partial\alpha}{\partial\theta} \nabla_n\theta \cdot \nabla_n\theta + \frac{\partial\alpha}{\partial p} \nabla_n\theta \cdot \nabla_n p \right\} \quad (\text{m s}^{-1}). \quad (9)$$



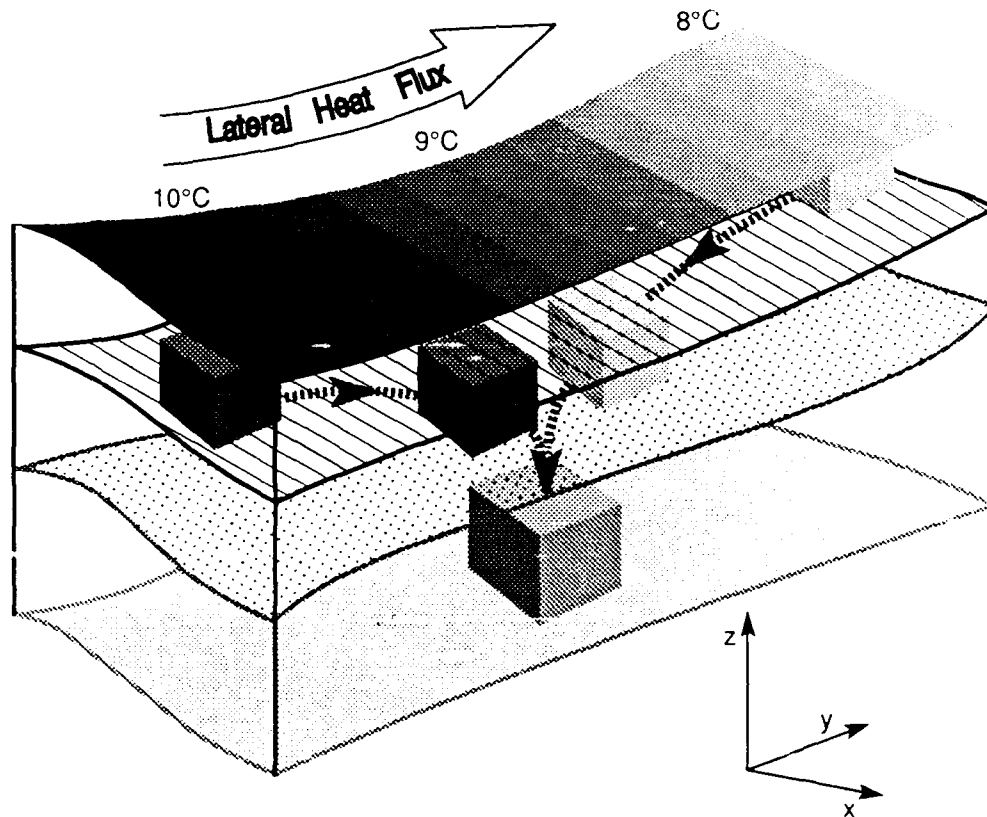


Fig. 1. A diagram illustrating the physical causes of thermobaricity and cabbeling. The upper surface depicts a neutral surface along which the pressure and potential temperature vary. A warm and a cool water parcel are moved together without doing any work against gravity and without exchanging heat or salt with their surroundings. When these two parcels meet they are allowed to mix completely. The lateral heat flux,  $\overline{V_n' \theta'}$ , can be imagined to be due to many such combinations of lateral stirring followed by intimate mixing. Along the path towards the central point, each water parcel has a different potential temperature to that on the original neutral surface at this location, and so the compressibility of the water parcel is different to that of fluid on the neutral surface. Because of the difference in compressibilities, the pressure excursions associated with the lateral motion cause the water parcels to move off the original neutral surface as shown. This process is called thermobaricity, as it is caused by the second-order partial derivative of in situ density with respect to potential temperature (thermo-) and pressure (baric). Once the two fluid parcels mix intimately, there is an increase of density and consequent dianeutral motion caused by cabbeling.

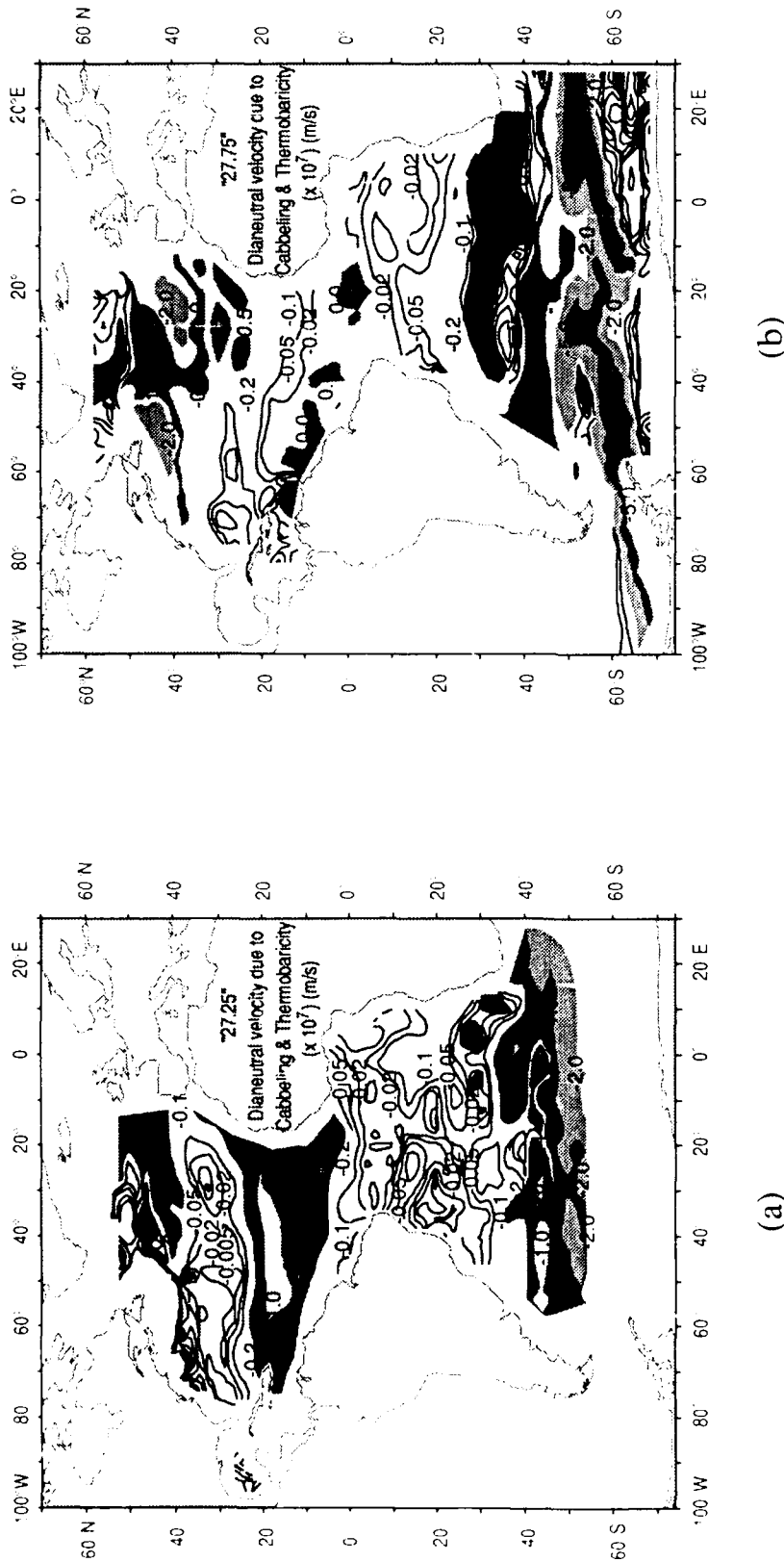


Fig. 2. The dianeutral velocity due to cabbeling and thermobaricity (assuming an epineutral diffusivity of  $1000 \text{ m}^2 \text{ s}^{-1}$ ), in the North and South Atlantic Ocean and in the Southern Ocean in the Atlantic sector, on two neutral surfaces. Fig (a) is for the "27.25°" neutral surface which has a potential density of 27.25 (referred to 0 db) in mid-ocean on the equator; its average pressure is about 650 db. Fig (b) is for the "27.75°" neutral surface which has a potential density of 27.75 (referred to 0 db) in mid-ocean on the equator; its average pressure is about 1500 db.

Fig. 2 shows the combined dianeutral velocity from thermobaricity and cabbeling on two neutral surfaces in the North and South Atlantic, labeled "27.25" and "27.75", respectively. These and other figures in this paper were derived from the Levitus (1982) data set. The nomenclature 'neutral surface "27.25"' means that the surface has a potential density, referred to the sea-surface, of 27.25 in mid-ocean on the equator. At other locations the potential density is different, as explained by You and McDougall (1989). A large proportion of the low-latitude region of the North Atlantic on the "27.25" neutral surface has downwelling larger than  $0.5 \times 10^{-7} \text{ m s}^{-1}$ . On much of the mid- and high-latitude region of the North Atlantic's "27.75" neutral surface, the downwelling due to cabbeling exceeds  $0.5 \times 10^{-7} \text{ m s}^{-1}$ , while in the Southern Ocean on this figure the downwelling is primarily caused by thermobaricity and is as large as  $5 \times 10^{-7} \text{ m s}^{-1}$ . There is also a small region of net upwelling near  $33^\circ\text{S}$  where thermobaricity is larger than cabbeling and of opposite sign.

It is clear that thermobaricity and cabbeling need to be included in inverse models of tracer data in regions where these processes cause significant water-mass conversion. The rate of water-mass conversion is given by the dianeutral velocity multiplied by the vertical tracer gradient. It is interesting to note that general circulation models that carry salinity as well as temperature, and therefore use the full equation of state, automatically include cabbeling and thermobaricity. To date, the contribution of these processes to the total upwelling of Bottom Water has not been separately determined in these models. Note that as a general rule, thermobaricity and cabbeling will be unimportant in shallow water where  $N^2$  is large (see Eq. 9).

It is very tempting to believe that cabbeling, or "densification on mixing", (and perhaps thermobaricity too) is partly caused by small-scale turbulent mixing as parameterized by the dianeutral diffusivity,  $D$ . This is not the case. That vertical mixing does not contribute to cabbeling or thermobaricity can be seen from the form of Eqs (4) to (7). In particular, from Eq. (5), the dianeutral motion caused by the vertical diffusivity,  $gN^{-2}D[\alpha\theta_{zz} - \beta S_{zz}]$  is independent of the nonlinearity of the equation of state. Rather, this expression depends only on the local values of  $\alpha$  and  $\beta$ . Similarly, in Eqs (4), (6) and (7), the terms multiplying  $D$  do not depend on the nonlinear terms of the equation of state. This means that neither cabbeling nor thermobaricity is assisted by vertical mixing processes to produce either upwelling (Eq. 5) or water mass conversion (Eqs (4), (6) and (7)). If one could (by magic) make the equation of state twice as nonlinear as it actually is, the vertical mixing terms on the right-hand sides of Eqs (4) - (7) would not change.

## DEDUCING DIANEUTRAL ADVECTION FROM THE BUOYANCY FLUX

In this section, only that part of the dianeutral velocity that is caused by small-scale turbulent mixing is considered. The dianeutral fluxes caused by this mixing are parameterized by a dianeutral diffusivity,  $D$ , and its contribution to dianeutral advection is

$D_z + DgN^{-2}[\alpha\theta_{zz} - \beta S_{zz}]$ . This can be expressed in terms of the vertical derivative of  $N^2$  as

$$eN^2 = [DN^2]_z - [DN^2] \frac{R_\rho}{R_\rho - 1} \left[ \frac{\alpha_z}{\alpha} - \frac{\beta_z}{\beta} \frac{1}{R_\rho} \right]. \quad (10)$$

or,

$$\begin{aligned}
 N^{-2} N_z^2 - g N^{-2} [\alpha \theta_{zz} - \beta S_{zz}] &= \frac{R_\rho}{R_\rho - 1} \left[ \frac{\alpha_z}{\alpha} - \frac{\beta_z}{\beta} \frac{1}{R_\rho} \right] \\
 &= \frac{[DN^2]_z}{DN^2} - \frac{e}{D} \quad (11)
 \end{aligned}$$

Since  $N_z^2$  is not equal to  $g[\alpha\theta_{zz} - \beta S_{zz}]$ , the dianeutral velocity is not simply proportional to the vertical divergence of the turbulent buoyancy flux,  $[DN^2]_z$ . The dissipation method of Osborn (1980) is commonly used to estimate the dianeutral diffusivity from microstructure measurements of the dissipation rate of mechanical energy,  $\epsilon$ , using the formula  $DN^2 = \Gamma' \epsilon$ , where  $\Gamma'$  is a constant, usually taken to be 0.2. Equation (11) shows that  $e/D$  is not simply equal to  $\epsilon_z/\epsilon$ . The additional term is shown in Figs. 3(a) and (b) on the "27.25" neutral surfaces in the Atlantic and Indian oceans. Using a value for  $D$  of  $10^{-4} \text{ m}^2 \text{ s}^{-1}$ , a contoured value of 100 in these figures implies that the dianeutral velocity is  $10^{-7} \text{ m s}^{-1}$  less than the estimate  $D\epsilon_z/\epsilon$  that one would infer from the microstructure data alone. It is seen that there are significant regions of the shallow neutral surfaces in each ocean where this correction term approaches or exceeds  $10^{-7} \text{ m s}^{-1}$ .

Figure 4 shows how the expression in Eq. (11) varies in the vertical at a variety of locations in different oceans. The nonlinear term in the above equations is positive and quite significant in the top kilometer of these profiles, thereafter changing sign in the deeper ocean. This can

be understood by examining the bracket  $\left[ \frac{\alpha_z}{\alpha} - \frac{\beta_z}{\beta} \frac{1}{R_\rho} \right]$  which may be approximated by  $\left[ \frac{1}{\alpha} \frac{\partial \alpha}{\partial \theta} \theta_z + \frac{1}{\alpha} \frac{\partial \alpha}{\partial p} p_z \right]$ , where  $p_z$  is simply  $-1 \text{ db m}^{-1}$ . Since the terms  $\frac{\partial \alpha}{\partial \theta}$  and  $\frac{\partial \alpha}{\partial p}$  are about  $1 \times 10^{-5} \text{ K}^{-2}$  and  $2.6 \times 10^{-8} \text{ K}^{-1} (\text{db})^{-1}$  respectively, the nonlinear term in the above equations is zero when  $\theta_z \cong 2.6 \times 10^{-3} \text{ K m}^{-1}$ ; a typical gradient of potential temperature at a depth of about 1500 m in the ocean. Deeper than this, the positive  $\theta_z$  term becomes dominated by the negative  $p_z$  term, and at a depth of 4000 m, Eq. (11) asymptotes to about  $-20 \times 10^{-5} \text{ m}^{-1}$ . McDougall (1988a) used a very simple model of one-dimensional upwelling in the deep ocean to demonstrate the importance of even this small negative value of Eq. (11). The vertical variation of  $N^2$  was taken to be exponential with an e-folding height of 1000 m, and Bottom Water was assumed to upwell at the depth-independent velocity of  $10^{-7} \text{ m s}^{-1}$ . Using Osborn's (1980) formula for  $DN^2$ , Eq. (11) becomes a first-order differential equation for  $\epsilon$ . This equation was integrated vertically to find that the nonlinear terms caused a doubling of the dianeutral diffusivity between 1500 m and 4000 m.

It is emphasized that the contribution of these nonlinear terms of the equation of state to the dianeutral velocity is by way of interpretation only. As explained above, vertical mixing processes do not contribute to thermobaricity or cabbeling. It is only if one chooses to find the dianeutral velocity from the vertical variations of the turbulent buoyancy flux that the grouping of nonlinear terms appears in Eq. (11). A very similar nonlinear term must be added to the conservation equation of potential density if the flux divergence of potential density is represented by the normal term,  $\partial\{D \partial \rho_\theta / \partial z\} / \partial z$ . The full conservation equation of

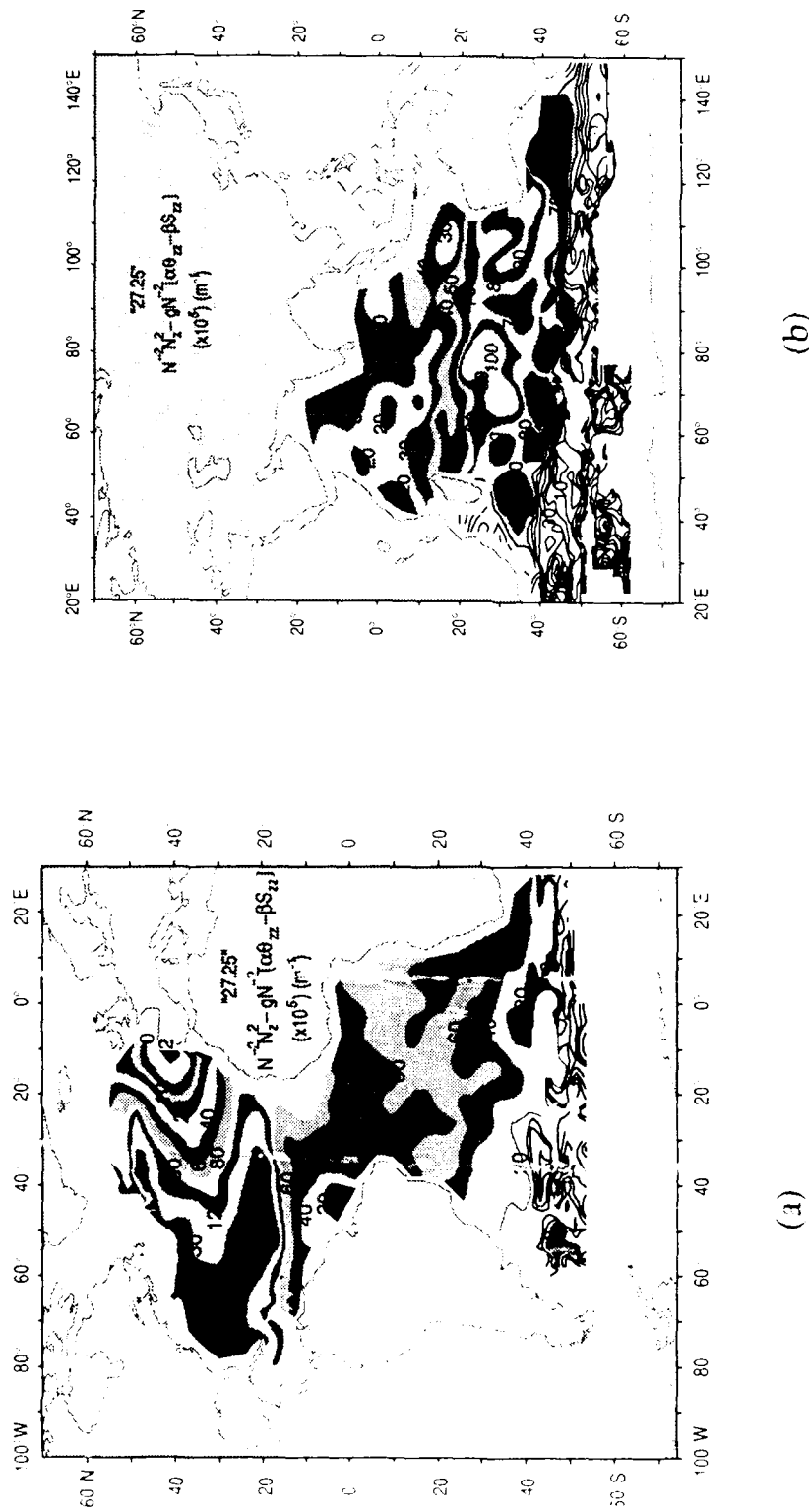


Fig. 3. These figures illustrate the difference of the dianeutral velocity between (i) that estimated from the vertical divergence of the buoyancy flux, and (ii), the true dianeutral velocity,  $e$ , given by Eq. (5) in the Atlantic and the Indian Oceans. When multiplied by the vertical diffusivity,  $D$ , the values from these figures give this difference in dianeutral velocity.

potential density is given by Eq. (70) of McDougall (1988b) and ignoring thermobaricity, cabbeling and the fact that there is a non-zero epineutral gradient of potential density, the vertical advective diffusive balance is given by

$$\begin{aligned} |w^d - D_z| \left[ -\frac{1}{\rho_\theta} \frac{\partial \rho_\theta}{\partial z} \right] &= D [\hat{\alpha}_{\theta_{zz}} - \hat{\beta}_{s_{zz}}] \\ &= -D \frac{1}{\rho_\theta} \frac{\partial^2 \rho_\theta}{\partial z^2} - D \left. \frac{\partial \alpha}{\partial \theta} \right|_{s, p, p_r} e_z^2. \end{aligned} \quad (12)$$

Here the diapycnal velocity is  $w^d$  and the thermal expansion and haline contraction coefficients are evaluated at the reference pressure of the potential density variable,  $p_r$ . The extra term that appears on the right-hand side of Eq. (12) is very similar to that discussed above: the difference being that now there is no contribution from  $[\partial \alpha / \partial p] p_z$ . In the upper ocean the change in the diapycnal velocity due to the nonlinear term in Eq. (12) is very similar to that estimated from Figs. 3 and 4. It is concluded that serious errors are occurring in the conservation equation of potential density in present inverse models since the two terms on the right-hand side of Eq. (12) are of the same magnitude, both being responsible for a contribution to the diapycnal velocity of order  $10^{-7} \text{ m s}^{-1}$ .

### One-dimensional Advection-Diffusion Balances

Gargett (1984) has suggested that the vertical diffusivity,  $D$ , may vary as the reciprocal of the buoyancy frequency,  $N$ , and that if  $N$  varies exponentially with depth,  $z$ , mixing would drive an equatorward interior flow in the deep ocean, in contrast to the poleward flow of the Stommel-Arons (1960) theory. Here I wish to make two points in relation to this one-dimensional view of the deep ocean. Firstly, this argument has ignored the non-linear terms of the equation of state that appear in Eq. (11), and it can be seen from Fig. 4 that at a depth of 1000 m, these terms can cause a vertical gradient of the diapycnal velocity larger than  $4 \times 10^{-10} \text{ s}^{-1}$ , or a change of the diapycnal velocity of  $4 \times 10^{-7} \text{ m s}^{-1}$  over a depth change of 1000 m. At this magnitude, the non-linear terms dominate the contribution to  $e_z$  calculated from the vertical buoyancy flux. These terms become smaller with depth, but they are probably not negligible in the abyssal ocean. Secondly, I wish to point out that the argument is quite sensitive to the assumed vertical variation of the buoyancy frequency.

For simplicity of argument, the non-linear terms in Eq. (11) are ignored, and so the diapycnal velocity is given by  $eN^2 = [DN^2]_z$ , and using Gargett's suggestion that  $D = AN^{-1}$ , where  $A$  is a constant, gives

$$e_z = -A [N^{-1}]_{zz}. \quad (13)$$

For an exponential  $N(z)$  profile,  $e_z < 0$ , implying an equatorward flow, but for other vertical distributions of  $N$ ,  $e_z$  can be positive. For example, the general  $N(z)$  profile that gives  $e_z = 0$  is

$$N(z) = \frac{1}{[a - bz]}, \quad (14)$$

where  $a$  and  $b$  are positive constants. This functional form may be indistinguishable from an exponential shape over much of the ocean's depth (see Fig. 5).

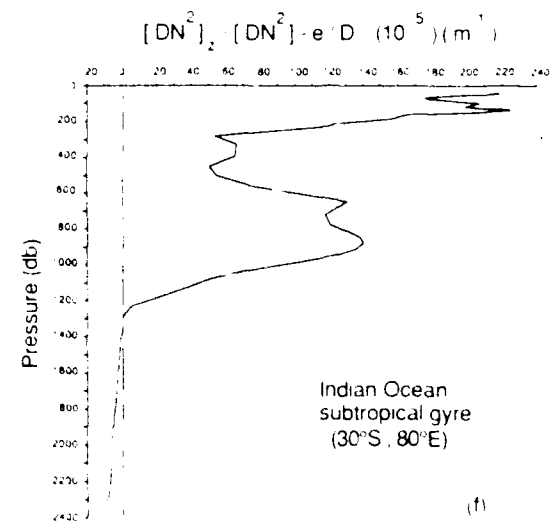
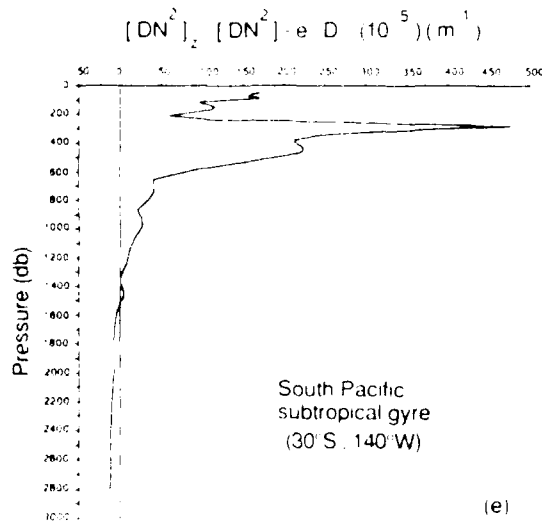
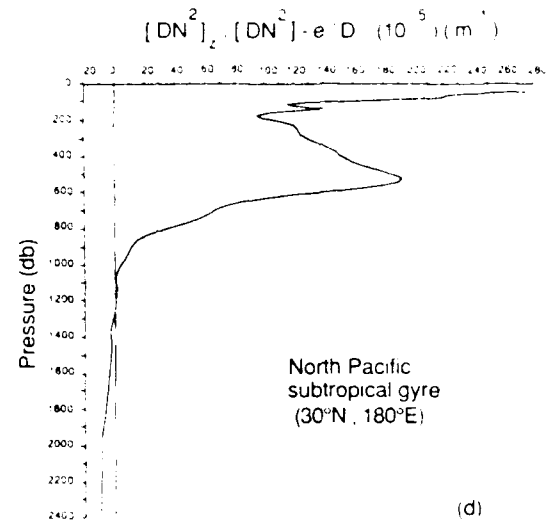
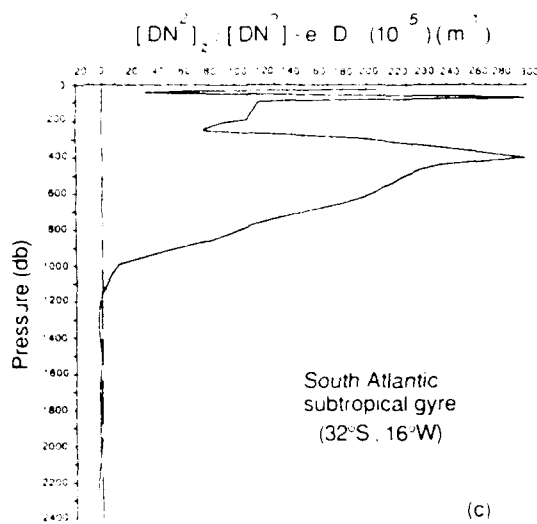
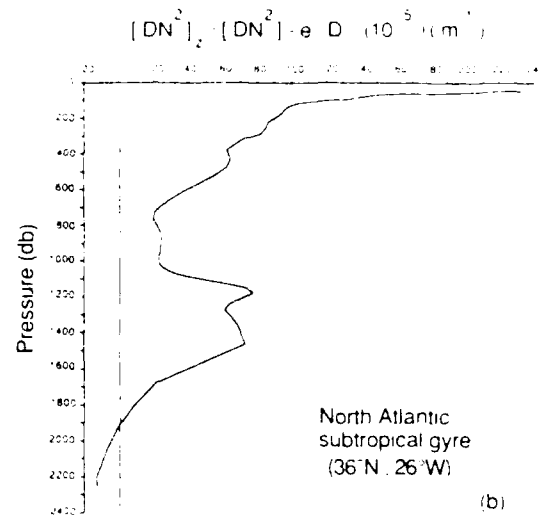
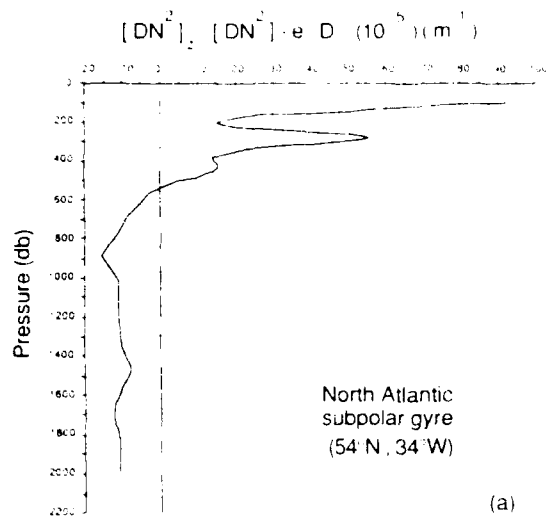


Fig. 4. Vertical mixing causes dianeutral advection to occur at the rate

$D_z + gN^{-2}D [\alpha\theta_{zz} - \beta S_{zz}]$  rather than  $N^{-2}[DN^2]_z$ , as one may guess at first. These vertical profiles show the difference between these two expressions (divided by  $D$ ) at six different places in the world's oceans. The same terms are shown as contour maps in Figs. 3(a) and (b) on a neutral surface in each of the Atlantic and Indian Oceans.

Another aspect of a one-dimensional advective-diffusive balance is the influence of (i) the entrainment into sinking Bottom Water plumes and (ii) the variation of the ocean's area with depth, on the sense of  $e_z$  and hence of the sign of the poleward velocity,  $v$ . Consider the situation depicted in Fig. 6 where a dense plume of Bottom Water sinks to the ocean floor, entraining fluid from the interior as it sinks. The downward volume flux of the sinking plume,  $Q(z)$ , must equal the upwelling of interior fluid in our one-dimensional ocean of area  $A(z)$ , so that

$$Q(z) = e(z)A(z). \quad (15)$$

Differentiating this equation with respect to  $z$ , we find that

$$e_z = \frac{Q_z}{A} - \frac{Q}{A^2}A_z. \quad (16)$$

Both parts of the right-hand side of this equation are negative, so that both physical processes argue for a deep interior ocean circulation in the opposite sense to that of Stommel and Arons (1960). A different flow pattern must exist very near the ocean floor where the flow must

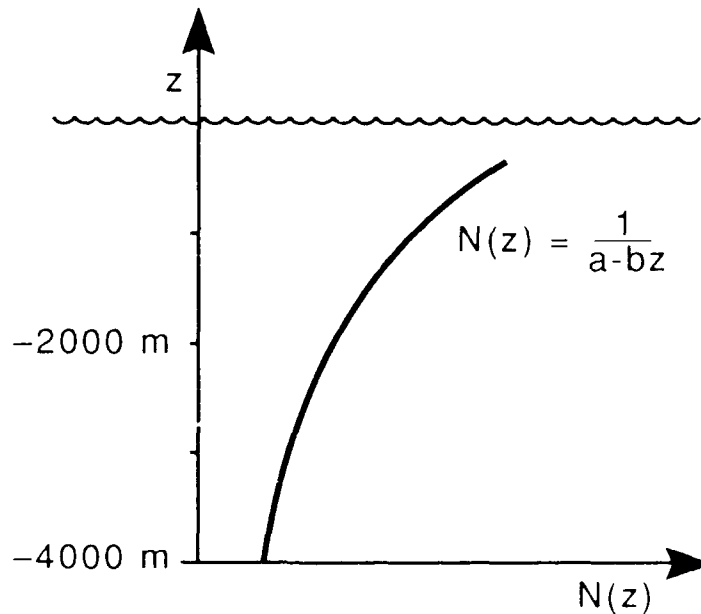


Fig. 5. Sketch of the buoyancy frequency  $N(z) = [a - bz]^{-1}$  (where  $a$  and  $b$  are both positive) for which the vertical diffusivity may vary as  $N^{-1}$  and yet  $e_z$  is zero.



leave the ocean boundary and fill the interior. Perhaps the Stommel-Arons circulation applies to the vertically-integrated flow, with most of the interior going in the opposite direction to the deep boundary layer. Note that the argument based on Fig. 6 and Eqs (15) and (16) does not depend on the magnitude or the vertical variation of the vertical diffusivity. Rather, the argument has relied only on the conservation of volume: the vertical diffusivity and the vertical density stratification must arrange themselves to be consistent with the volume fluxes in the steady state. Perhaps the weakest part of this argument is the fact that only one source of Bottom Water is considered, whereas in reality, many sources of various density must exist. The simple remarks presented here on one-dimensional advective-diffusive balances are meant mainly to reinforce our feeling of ignorance about the deep ocean circulation; we have not come very far since 1960!

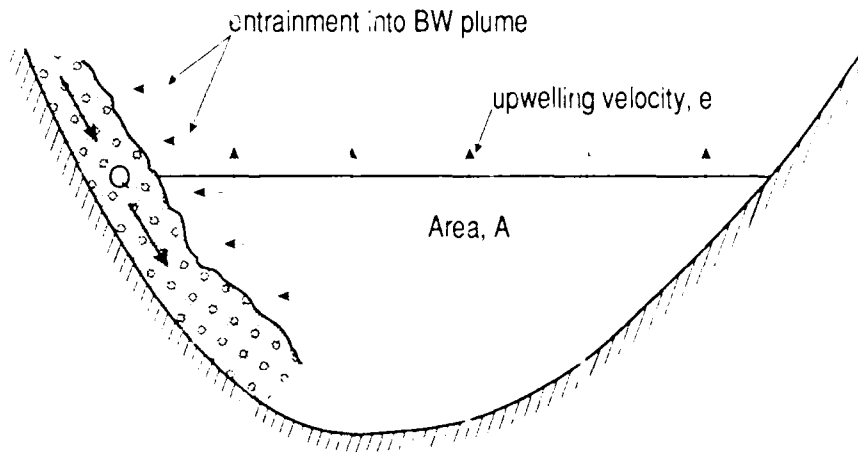


Fig. 6. Sketch of a plume of Bottom Water descending into an ocean of area  $A(z)$ . The volume flux in the descending plume,  $Q(z)$ , must be equal to that due to upwelling in the ocean interior.

## DIANEUTRAL ADVECTION VERSUS DIANEUTRAL DIFFUSION

Equation (5) shows that the contribution of vertical mixing processes, as parameterized by a vertical diffusivity,  $D$ , to dianeutral advection is equal to  $gN^{-2}D[\alpha\theta_{zz} - \beta S_{zz}]$ . Fig. 7 shows  $gN^{-2}[\alpha\theta_{zz} - \beta S_{zz}]$  contoured on the "27.25" neutral surface in the Pacific Ocean. A vertical diffusivity,  $D$ , of  $10^{-4} \text{ m}^2 \text{ s}^{-1}$ , together with a contoured number of 10 on this figure implies a dianeutral velocity,  $e$ , of the canonical value,  $10^{-7} \text{ m s}^{-1}$ . This is the contribution to the dianeutral velocity of the vertical turbulent mixing process. Other contributions occur through the vertical variation of the vertical diffusivity,  $D_z$ , cabbeling, thermobaricity, and other mixing processes that have not been included in our analysis (such as double-diffusive convection, double-diffusive interleaving and the dianeutral advection of submesoscale coherent vortices). Some of the patchiness in these maps is undoubtedly due to the difficulty in estimating second order vertical derivatives from the data set. There is however a striking pattern in Fig. 7 showing upwelling in the North Pacific and downwelling in the South Pacific. A similar clear pattern of positive and negative values is seen on the "27.25" surface in the Indian Ocean, with upwelling between  $10^\circ\text{S}$  and  $30^\circ\text{S}$ , and predominantly downwelling in the other regions (Fig. 8(a)).

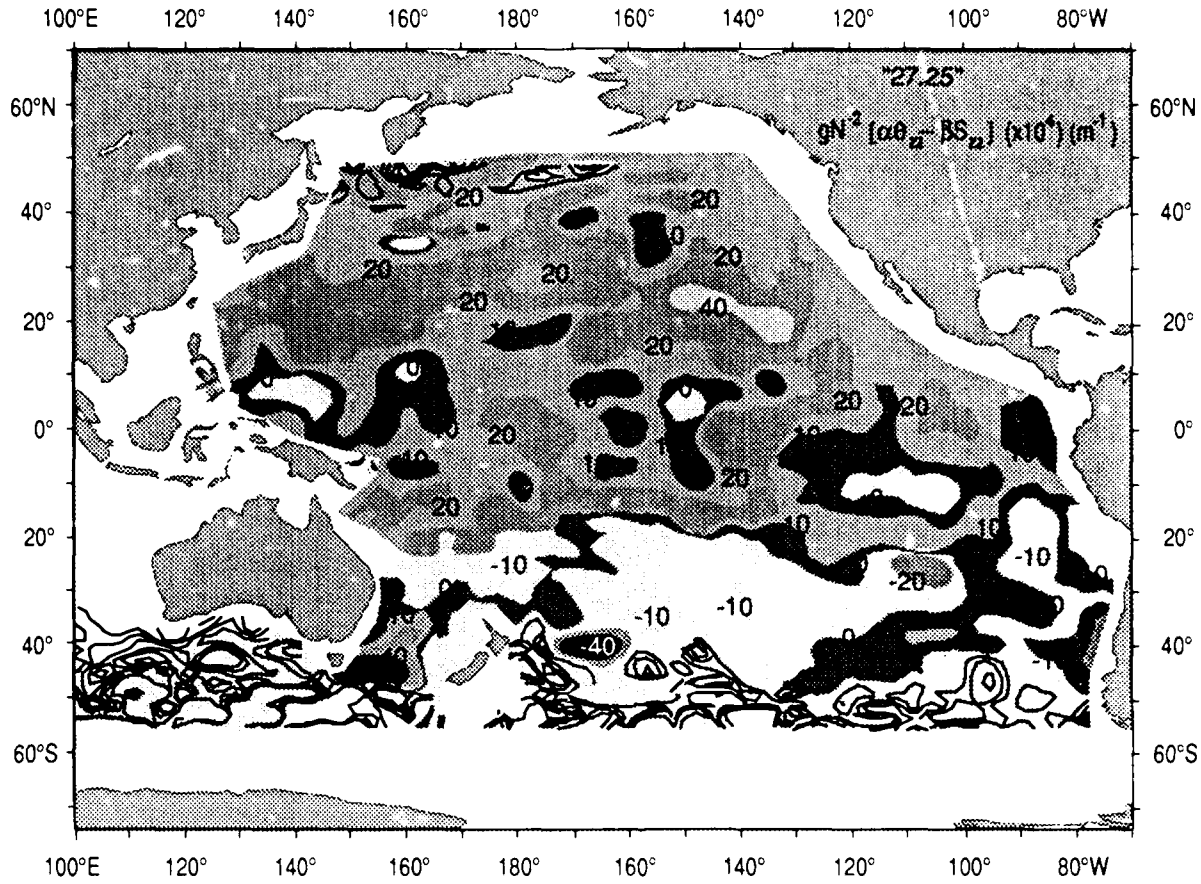


Fig. 7. Contour map on the "27.25" neutral surface in the Pacific Ocean of the term that when multiplied by the diapycnal diffusivity,  $D$ , is the part of the diapycnal velocity caused by vertical mixing processes.

The contribution of vertical mixing processes to water-mass conversion is given by  $D$  multiplied by  $gN^{-2}\theta_z^3\beta d^2S/d\theta^2$ . This term is the sum of the diffusive flux divergence of potential temperature and the advective term, all divided by  $D$ , i.e.,

$$\frac{g}{N^2}\theta_z^3\beta\frac{d^2S}{d\theta^2} = \frac{(D\theta_z)_z - e\theta_z}{D} = \frac{\beta(\theta_z S_{zz} - S_z\theta_{zz})}{(\alpha\theta_z - \beta S_z)}, \quad (17)$$

where the last part of this expression indicates how it is evaluated from the data, using first and second order vertical derivatives of  $S$  and  $\theta$ . The sign of this term is governed by that of  $d^2S/d\theta^2$ , as  $\theta_z$  is positive on the surfaces presented here. Water-mass conversion caused by vertical mixing on the shallow neutral surfaces in the Atlantic and Pacific tends to increase the potential temperature and the salinity, while deeper in the water column, vertical mixing has a cooling and freshening tendency. On the "27.25" neutral surface in the Indian Ocean, vertical mixing cools and freshens the water-mass in the equatorial region, while at mid-latitudes, the opposite tendency is evident (Fig 8(b)).

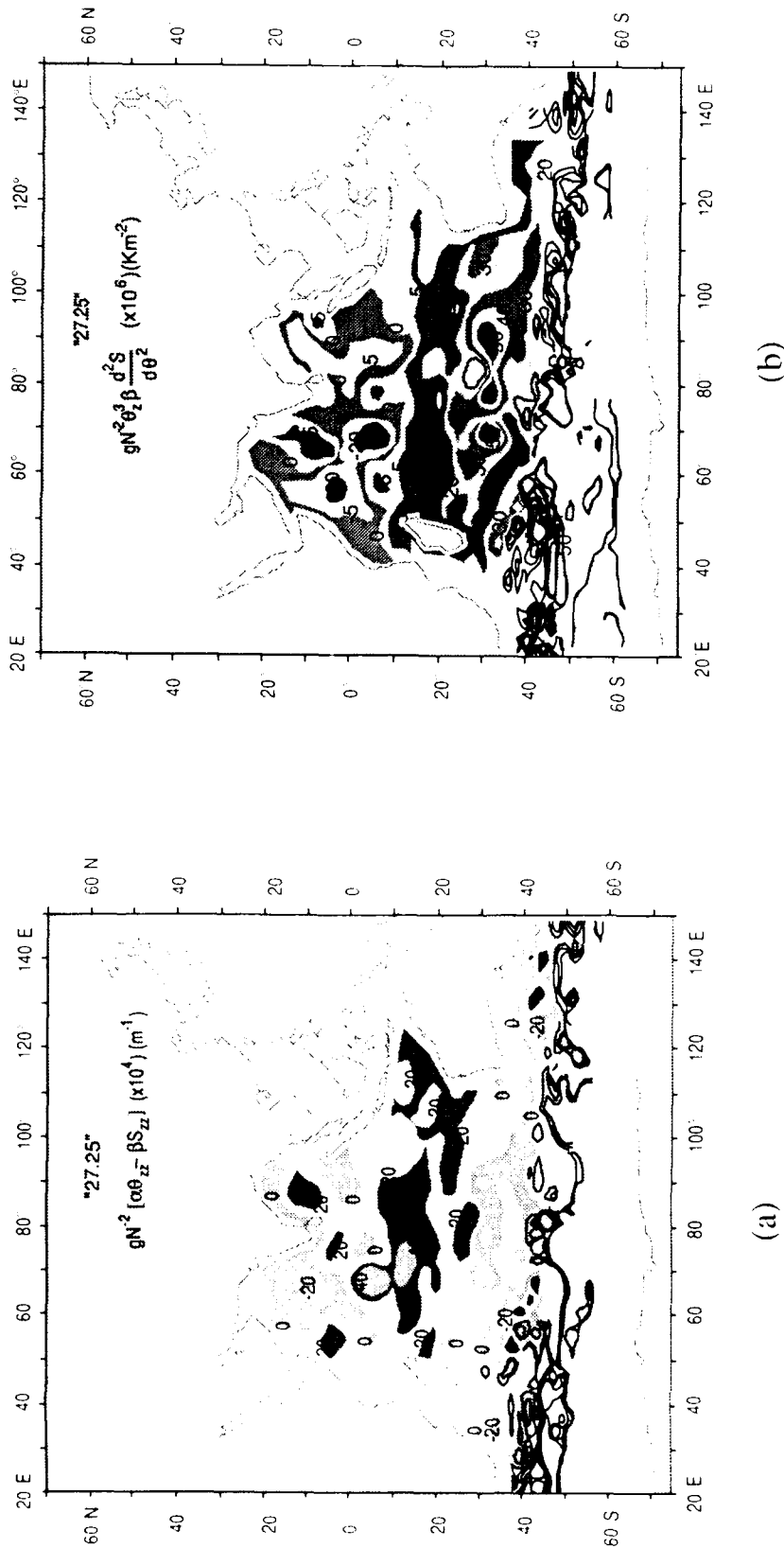


Fig. 8. (a) Contour map on the "27.25" neutral surface in the Indian Ocean of the term that when multiplied by the dianeutral diffusivity,  $D$ , is the part of the dianeutral velocity caused by vertical mixing processes. (b) Contour map on the "27.25" neutral surface in the Indian Ocean of the term that when multiplied by the dianeutral diffusivity,  $D$ , is the rate at which vertical mixing changes the potential temperature on a neutral surface (this is called "water-mass conversion").

Inverse models of the ocean circulation often take dianeutral advection as the only vertical process in the conservation equations for scalars. Fig. 8(a) and (b) allow us to estimate the error associated with this procedure. In the conservation equation of potential temperature, the ratio of the total water-mass conversion caused by the vertical diffusivity,  $D$ , to that caused by only the dianeutral advective term is

$$\frac{D \frac{g}{N^2} \theta_z^3 \beta \frac{d^2 S}{d\theta^2}}{-\theta_z D \frac{g}{N^2} [\alpha \theta_{zz} - \beta S_{zz}]} = \frac{\{Fig. 8(b)\}}{-\theta_z \{Fig. 8(a)\}} \quad (18)$$

On virtually the whole of this neutral surface the quantities mapped in Figs. 8(a) and 8(b) have the same sign so that the ratio of Eq. (18) is negative. This implies that existing box inverse models cannot find the correct sign for both the interfacial volume flux ( $e$  times the horizontal area of a box) and the total effect of vertical mixing processes in the conservation equation for potential temperature. Since the dianeutral velocity affects the linear vorticity equation, it is clear that by using only interfacial advection, one cannot simultaneously model the influence of vertical mixing processes on both this equation and the heat equation.

Of equal concern are the errors caused by such over-simplified physics when more than one passive tracer is considered. For example, if conservation equations are written for both salinity and potential temperature, vertical advection affects these equations in the ratio  $\theta_z/S_z$ , whereas in reality, the total effect of vertical diffusion and advection occurs in the ratio  $\beta/\alpha$  (compare the  $D$  terms in Eqs (4) and (6)). The relative changes in the inverse model's  $\theta$  and  $S$  equations are then in error by  $R_\rho = \alpha\theta_z/\beta S_z$ ; a ratio that is about 2 in the Central Water and is often negative in the Intermediate Water and below. Similarly, the ratio of the relevant two terms in the  $C$  equation, (7), to the corresponding term in the  $S$  equation will not resemble  $C_z/S_z$  which it is forced to do by ignoring dianeutral diffusion and considering only dianeutral advection.

These remarks apply particularly to inverse models such as that of Wunsch (1984a) where the aim was to find the strength of equatorial upwelling using radiocarbon and other tracer data. One cannot expect to even find the correct sign for such upwelling/downwelling if one ignores an inherent aspect of dianeutral mixing, namely dianeutral diffusion. Similarly, Wunsch (1984b), in an eclectic model of the North Atlantic, found a "highly energetic convective, or thermohaline, mode of motion", displayed in the streamlines of the zonally averaged overturning flow in the meridional sections of his figures 8b and 9. The above discussion, and the corresponding figures for the Atlantic (which are not shown here) shows that if the dianeutral motion of these figures had the correct sign, the concomitant water-mass conversion is modelled with an incorrect magnitude, and also the wrong sign in some of the North Atlantic. In an inverse model of the Deep Water in the Eastern Atlantic, Schlitzer (1987) included both interfacial mixing and advection, but without an equation like Eq. (5) above to link them together. In one of his solutions, he finds a zero vertical diffusivity and a downwelling velocity through his  $\sigma_4$  surface of  $13 \times 10^{-7} \text{ m s}^{-1}$ ! Such a large interfacial velocity must be caused by a correspondingly large vertical diffusivity. It is hoped that the step-by-step derivation of the appropriate conservation equations (4, 6 and 7) will assist in the design of future inverse models so that the elegant mathematical machinery developed by Wunsch and others can be used in a consistent fashion. Equation (6) has already been used successfully by Bauer and Siedler (1988). This paper and one by Hogg (1987) demonstrate that the second order vertical derivatives that are required can be evaluated with sufficiently

little noise. Bauer and Siedler (1988) found that the diffusivities could be determined quite accurately, and in particular, both lateral and vertical diffusivities were positive even when the model was perturbed substantially by doubling the lateral advection term. This study provides real hope that once mixing processes are included in diagnostic models (including inverse models) in a consistent fashion, we may expect that not only will the strength of mixing processes be a well-determined model output, but that such mixing processes will provide useful constraints on the reference level velocities and hence the magnitude of the mean circulation.

Table 1 shows the relative roles of diapycnal diffusion and advection for a variety of mixing processes in the ocean. The columns labeled "Diffusion" and "Advection" are the two contributions of the mixing processes to the right-hand side of the conservation equation for potential temperature, Eq. (4), and the sum of these columns appears at the right of the table, labeled "Water-Mass Conversion". The first row is concerned with small-scale turbulent mixing as parameterized by a vertical diffusivity,  $D$ , and this process has been discussed in

Table 1. Diapycnal Diffusion Versus Diapycnal Advection

Process :	Diffusion	+	Advection	=	Water - Mass Conversion
Small - scale turbulent mixing	$(D\theta_z)_z$		$-D_z\theta_z - \theta_z g N^{-2} D(\alpha\theta_{zz} - \beta S_{zz})$		$D g N^{-2} \theta_z \beta \frac{d^2 S}{d\theta^2}$
Double - diffusive convection	$-F_z^\theta$		$-F_z^\theta \left[ \frac{1}{\gamma} - 1 \right] \frac{R_\rho}{[R_\rho - 1]}$		$-F_z^\theta \left[ \frac{R_\rho/\gamma - 1}{[R_\rho - 1]} \right]$
Cabbeling	$\rightarrow 0$		$\theta_z K g N^{-2} \frac{\partial \alpha}{\partial \theta} V_n \theta \cdot V_n \theta$		$\theta_z K g N^{-2} \frac{\partial \alpha}{\partial \theta} V_n \theta \cdot V_n \theta$
Thermobaricity	$\rightarrow 0$		$\theta_z K g N^{-2} \frac{\partial \alpha}{\partial p} V_n \theta \cdot V_n p$		$\theta_z K g N^{-2} \frac{\partial \alpha}{\partial p} V_n \theta \cdot V_n p$
Double - diffusive interleaving	$-(B\theta_z)_z$ (negative sign)		$\theta_z g N^{-2} \alpha (B\theta_z)_z$		$\frac{1}{[R_\rho - 1]} (B\theta_z)_z$ (positive sign)
SCV motion	small ?		significant ?		significant ?
Helicity of neutral trajectories	? , but small		proportional to $\oint_A V_n \theta \times V_n p dA$ , small		? , but small

this section. The second is double-diffusive convection, where the ratio of the vertical flux divergences of heat and salt (in buoyancy units) is  $\gamma$ . This case has been discussed in detail by McDougall (1987a). Double-diffusive convection changes the potential temperature of a water-mass at a rate that is larger than the diffusive contribution,  $-F_z^\theta$ , by the ratio  $[R_\rho/\gamma - 1]/[R_\rho - 1]$  which is often greater than 3. Cabbeling and thermobaricity are the next entries in the table. As explained above, these processes are advective by nature and they do negligible amounts of vertical diffusion (see also McDougall, 1987a).

Double-diffusive intrusions are commonly observed at thermocline fronts and are expected to be responsible for a significant amount of water-mass conversion in these locations. The total dianeutral fluxes of properties by double-diffusive interleaving are due to (i) the "diffusive" and "salt-finger" fluxes across the quasi-horizontal double-diffusive interfaces, and (ii), the dianeutral advection of the intrusions themselves. Garrett (1982) and McDougall (1985) have shown that the dianeutral advective contribution is often as large as that directly caused by the driving interfacial fluxes. The vertical fluxes of  $\theta$  and  $S$  due to salt-fingering are down their respective vertical gradients, while for positive  $\theta_z$  and  $S_z$  (such as in the Central Water of the World's oceans), the dianeutral advective fluxes are up their gradients. The advective contributions to the fluxes of  $\theta$  and  $S$  almost balance in buoyancy terms, while the salt-fingers transport twice as much salt as heat, and there are also small vertical fluxes due to the "diffusive" interfaces. The total dianeutral flux of heat is up the potential temperature gradient while the effective vertical diffusivity of salt is smaller and may be either positive or negative depending on the exact conditions and on the model assumptions that are not now well-determined. This suggests that a convenient way to parameterize double-diffusive interleaving is to take the vertical salt flux to be zero and the vertical flux of potential temperature to be given by a negative vertical diffusivity,  $-B$ , where  $B$  is positive. This simple parameterization scheme should preserve the flavour of what is now known about double-diffusive interleaving. Since dissolved substances are fluxed by salt-fingers in a similar fashion to salt (the fluxes are proportional to the respective vertical gradients), the effective vertical diffusivity of tracer  $C$  should also be taken to be zero. With this parameterization of double-diffusive interleaving, the conservation equation (1) for potential temperature has the term  $-(B\theta_z)_z$  on the right-hand side. The contribution of double-diffusive interleaving to the dianeutral velocity is shown in the table and the total effect on water-mass conversion acts like a positive diffusivity,  $B$ , with a weighting function  $[R_\rho - 1]^{-1}$ . The positive nature of this effective diffusivity arises because the advective contribution outweighs the negative diffusive contribution.

The last two processes in Table 1 are concerned with less well known dianeutral processes, namely the dianeutral motion of submesoscale coherent vortices (SCVs) and the vertical advection caused by the ill-defined nature of neutral surfaces. Submesoscale coherent vortices move vertically through both potential-density surfaces and neutral surfaces (McDougall, 1987b) and this contribution to the average dianeutral motion in an ocean basin will be significant if submesoscale coherent vortices make a significant contribution to the epineutral fluxes of scalars. Since this has not yet been proven, a temporary conclusion is that the dianeutral motion of submesoscale coherent vortices is probably small. Because neutral surfaces are formally ill-defined, neutral trajectories are helicoidal in nature, and the lateral motion along neutral trajectories necessarily involves vertical advection (McDougall and Jackett, 1988). This vertical advection does not rely on vertical mixing processes per se. Recent work (Jackett and McDougall, manuscript in preparation) has shown that this process does not cause significant vertical motion in any part of the main thermocline in any of the world's oceans.

## BOUNDARY MIXING VERSUS INTERIOR MIXING

Bottom Water is formed each year and yet the ocean is not believed to become continually more dense so it is clear that there must be a mean upwelling of water through neutral surfaces. It is not yet known where this upwelling occurs. The Stommel-Arons (1960) theory for the circulation of the deep ocean is driven by an upwelling velocity field that is

uniform in latitude and longitude and increases linearly with height,  $z$ , from zero at the ocean bottom. Partly fuelled by the lower-than-expected observed levels of ocean microstructure in mid-ocean, some authors have suggested that a large part of the required mixing activity may occur at the ocean's boundaries.

Armi (1978) stresses that mixed layers on seamounts or continental boundaries are periodically injected into the ocean interior by unsteady meso-scale eddies, thereby increasing the efficiency of boundary mixing above the level that would apply if the ocean were steady, while Garrett (1979) has argued that the mixing in bottom boundary layers is often quite inefficient in that where the energy available for mixing is the largest, there is a vanishingly small density gradient (i.e. the flux Richardson number is small where the overall Richardson number is small). Eriksen (1985), and more recently, Garrett and Gilbert (1988) have studied a different type of "near-boundary" mixing that is based on the relaxation of the internal wave field to the Garrett & Munk spectrum after internal waves are reflected off the sloping ocean floor. These theories can give quite large vertical diffusivities and the elevated mixing activity occurs within 100 m to 200 m of the ocean floor, which is quite a large distance compared with the typical bottom mixed-layer depth of about 35 m.

Early research on boundary mixing concentrated on the along-slope flow produced because of the vanishing density gradient normal to the slope (Phillips, 1970, and Wunsch, 1970). However, Thorpe (1987) has considered a fully turbulent boundary layer structure and has shown that this process leads to net motion along the slope that is proportional to the vertical diffusivity *outside* the boundary layer. Phillips et al. (1986) have analyzed the motion adjacent to a sloping turbulent boundary layer in a stratified fluid and have shown that the diffusion of material along the slope is due to three quite separate processes. First, the diffusivity in the boundary layer, second a counter-flowing velocity field in the boundary region, and third, a mean convergent flow toward a depth of maximum buoyancy frequency. In their terminology, if  $\kappa_e$  is the diffusivity in the boundary layer,  $\theta$  is the angle of the slope to the horizontal and  $\delta$  the boundary layer thickness, the magnitude of the up- and down-slope velocities in the counter-flowing structure is  $v' = \delta^{-1} \kappa_e \cot \theta$  and the buoyancy perturbation between the counter-flowing cells is  $b' = N^2 \delta \cos \theta$ . The vertical velocity of each cell is of magnitude  $w' = \delta^{-1} \kappa_e \cos \theta$  so that the effective vertical diffusivity of this counter-flowing structure is of order  $[w'b']/N^2 = \kappa_e \cos^2 \theta \approx \kappa_e$ , so that this counter-flowing convection process is quite weak. Here we will not be concerned with the detailed processes that cause diapycnal fluxes of properties in the boundary or "near-boundary" region, nor the detailed structure of the boundary layer. Rather, boundary mixing or near-boundary mixing will be simply regarded as a normal vertical mixing process, parameterized by a vertical turbulent diffusivity,  $D$ , which is simply enhanced near ocean boundaries.

Laboratory studies by Thorpe (1982) and Ivey (1987a) show that when a stratified fluid is mixed at a side boundary, there is a continual bi-directional exchange of fluid between the interior and the boundary layer. This exchange amounts to an efficient means of mixing passive tracers into the interior but does not cause significant diapycnal transport (Ivey and Corcos, 1982). This observation has led to the common belief that strong mixing in the relatively small area of the ocean near boundaries is equivalent to a much weaker mixing intensity distributed evenly throughout the ocean. This assumption is often written in the form

$$D_i^{eff} = D_b \frac{A_b}{A_i}, \quad (19)$$

(see for example, Ivey, 1987a,b), where  $D_i^{eff}$  is the effective interior diapycnal diffusivity caused by the boundary mixing,  $A_i$  is the area of the ocean measured along a particular isopycnal and  $A_b$  is the area of this same isopycnal surface that is inside turbulent boundary regions where the diapycnal diffusivity is  $D_b$  (see Fig. 9). In this section of the paper, it will be shown that if most mixing happened near boundaries, the circulation of the deep ocean would be profoundly affected. Interior and boundary mixing may have similar effects on the distributions of passive tracers but the mean circulation driven by the two types of mixing could hardly be more different.

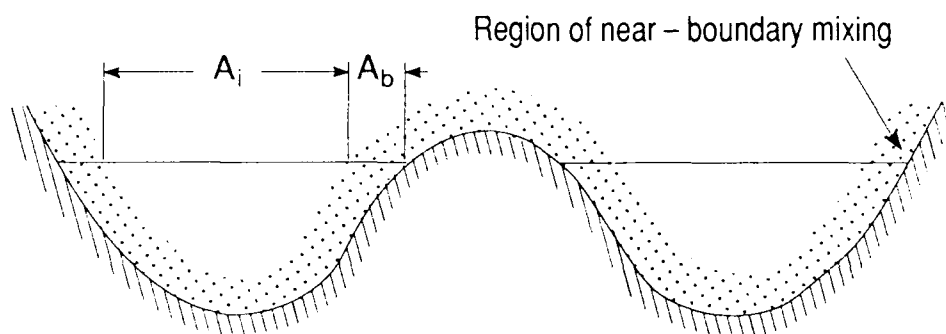


Fig. 9. A schematic cross-section showing four near-boundary mixing regions of total area  $A_b$ , and the total lateral area,  $A_i$ , of a particular isopycnal.

### A Single Side-wall

A steady-state ocean is considered in which there is boundary mixing but no interior mixing. Initially mixing is considered to be present at only one side boundary, and then the discussion is broadened to include the more general cases of many actively mixing boundaries and also the implications of mixing at seamounts. In a steady-state, the depths of all the neutral surfaces are constant and so the volume between pairs of neutral surfaces is constant. In an ocean with no interior mixing, there can be no diapycnal motion and so there is not net exchange of volume between the turbulent boundary region of Fig. 10 and the interior. All the upwelling of Bottom Water occurs in the turbulent boundary region. In the steady state, the area of the boundary region,  $A_b$ , the vertical density gradient and the mixing intensity,  $D$ , must have adjusted so that the buoyancy flux and the volume flux in the boundary region are both independent of height. The side-walls in Fig. 10 need not be vertical. This simple case demonstrates that a totally quiescent interior ocean is consistent with no interior vertical mixing.

### Several Side-walls

The situation with two separate turbulent boundary regions is shown in Fig. 11. Since there is no diapycnal motion and the volume between neutral surfaces is constant (under the steady state assumption), there is still no net flow into or out of the interior. However there can now



be flow in the ocean interior as fluid moves from one boundary region to the other. Where there is increased mixing activity at a particular depth in one boundary layer, the vertical buoyancy flux is locally enhanced, leading to a negative value of  $e_z$  in the boundary region and a consequent loss of fluid from the boundary layer to the quiescent interior. This is indicated graphically in Fig 12. In a steady state, the volume flux lost from one boundary is gained by another. The implication of these simple arguments of buoyancy and volume conservation is that a deep ocean that is mixed only at its boundaries will not display the smoothly varying mean flows of the Stommel-Arcs type. Rather, mean flows will occur in a more random pattern and probably with a smaller amplitude. These mean flows have the rather passive job of simply moving fluid from one boundary layer to another: all the action occurs in the boundary regions.

### Seamounts

Seamounts are worthy of special consideration because the area available for boundary mixing is a strong function of height. The conservation equations for buoyancy and volume are

$$AeN^2 = [ADN^2]_z \quad (20)$$

and

$$Cu = -[Ae]_z, \quad (21)$$

where the subscript  $b$  has been dropped from the area,  $C$  is the circumference around the seamount on a neutral surface, and  $u$  is the horizontal velocity leaving the boundary layer and entering the non-turbulent interior ocean. (Of course, the non-linear equation of state term from Eq. (11) should also appear in Eq. (20), but is excluded here for convenience).

Assuming that the dominant contribution to  $[ADN^2]_z$  at a seamount comes from the comparatively rapid variation of  $A$  with  $z$ , one finds that

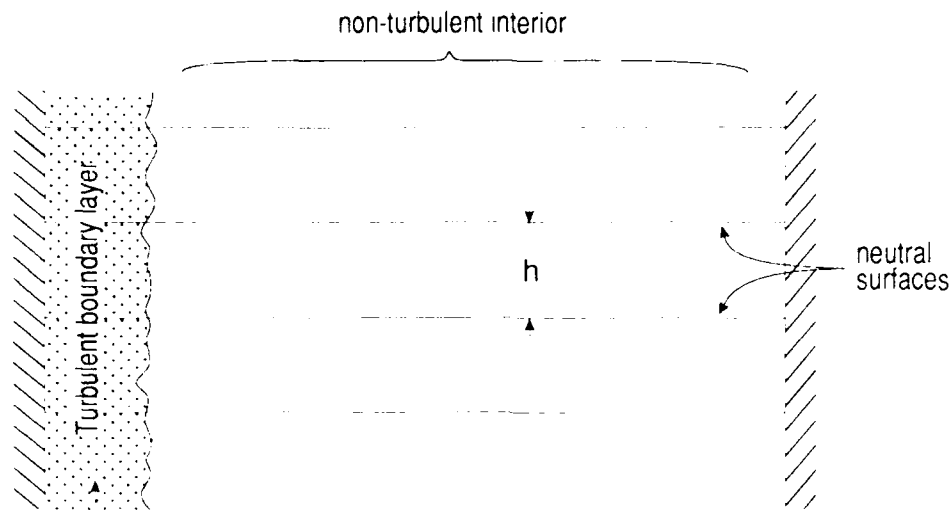
$$Ae \approx DA_z, \quad (22)$$

and

$$Cu \approx -[DA_z]_z \approx -DA_{zz}. \quad (23)$$

The area available for mixing at a seamount is a decreasing function of height,  $z$ , and so from Eq. (22), the vertical motion in the turbulent boundary layer is downwards, implying that above this depth, the seamount is (on average) acting as a sink for the lateral flow field. It is interesting to consider some simple geometrical shapes to see how the ocean may choose to achieve the local balances described by Eqs (22) and (23).

Consider first a conical seamount. The lateral width of the boundary layer and the vertical diffusivity,  $D$ , are assumed to be independent of depth and so the area,  $A$ , the circumference,  $C$ , and the radius of the seamount are all proportional to  $(z_0 - z)$ , where  $z_0$  is the height of the top of the seamount.  $A_z$  is negative and constant along the cone so that the downwelling volume flux,  $Ae$ , is depth-independent and the horizontal velocity outside of the boundary layer,  $u$ , is zero. From where does the downwelling volume flux in the turbulent boundary layer originate? The answer lies in a singularity at the apex of the cone, as is indicated in Fig. 13 (a). The real ocean does not of course exhibit such singular behaviour, but it is not obvious how things will adjust. Perhaps the density gradient near the apex will change sufficiently in the vicinity of the seamount to ensure a smoother velocity structure near the apex.



$Q$ , Bottom Water volume flux

Fig. 10. Sketch of an ocean in steady state with no interior mixing and with boundary mixing occurring at only one side-wall. All the upwelling of Bottom Water occurs in the turbulent boundary layer, and there is no net exchange of volume between the boundary region and the ocean interior.

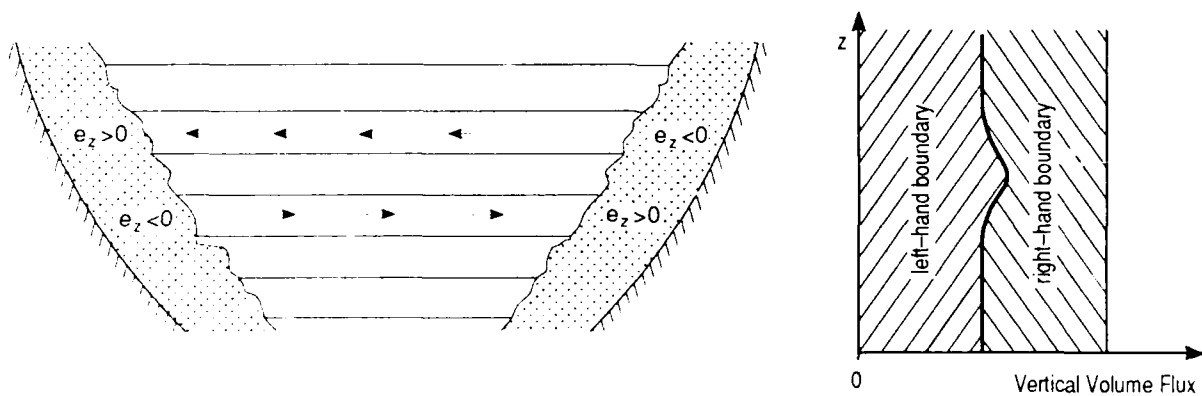


Fig. 11. Two turbulent boundary regions can share the task of upwelling the Bottom Water. The volume flux divergence in one boundary layer is matched by the convergence at the other. There is still no divergence in the interior, although there must now be a mean flow there to effect the exchange of mass between the different boundary layers.

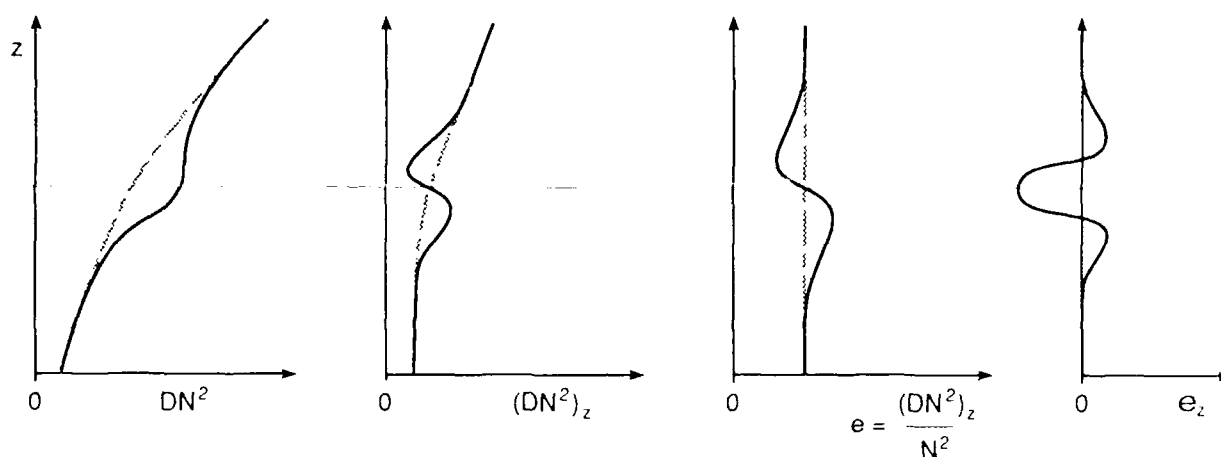


Fig. 12. These graphs indicate how increased vertical mixing near one boundary leads to outflow from that boundary. The area of the boundary mixing is assumed constant with height so that the diapycnal velocity is given by  $eN^2 = [DN^2]_z$ . The dashed lines are for a depth-independent upwelling velocity,  $e$ , that would apply if the vertical diffusivity,  $D$ , were not locally enhanced at the depth indicated.

Two other seamount geometries are considered in Fig. 13 (b) and (c): the seamount radius proportional to  $(z_0 - z)^2$  and  $(z_0 - z)^{0.5}$ . The pinnacle shape of Fig. 13 (b) does not require any singularities, while the more realistic geometry of Fig. 13 (c) has an infinitely large downwelling flow at the apex and a corresponding singularity in the horizontal inflowing mass flux to match (F. Henyey, private communication, 1989). Of the three geometries considered here, all have downwelling in the boundary layer, but the lateral volume flux,  $Cu$ , is quite different in the three cases. The pinnacle (Fig. 13b) acts as a sink at all depths whereas the cone is a strong sink (a delta function) at the apex and thereafter does not exchange fluid with the ocean interior. The most realistic shape for the top of a seamount, Fig. 13c, has a strong double singularity at its highest point with alternating inflow and outflow. The volume flux of the inflow must be larger than that of the outflow because the turbulent boundary layer carries fluid downward at all depths.

One can imagine constructing a model of a realistic seamount by having the geometry of Fig. 13 (c) at the summit, a straight-sided seamount like Fig. 13(a) near the mid-depth, and a flared section like Fig. 13(b) at the base. The downwelling volume flux in the boundary layer would then be large near the summit, decrease to a constant value on the conical section and then increase on the flared section at the base of the seamount. Meanwhile, the very top of the seamount would act like a sink to the exterior fluid, followed by a source of fluid which decreased to zero on the conical section and then became a sink of constant strength on the flared section.

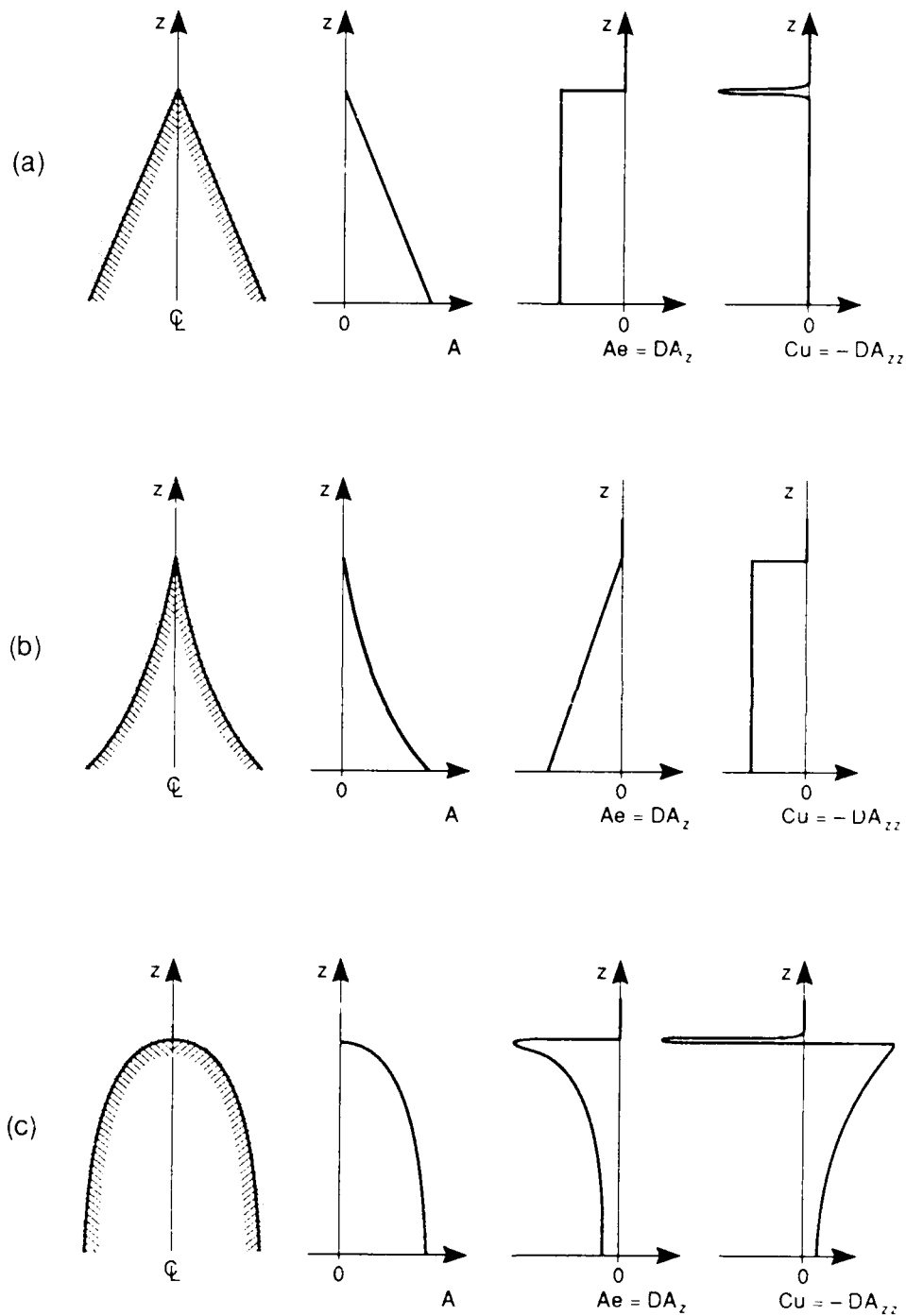


Fig. 13. Sketches of the seamount cross-section, the area of the boundary mixing,  $A$ , as a function of height,  $z$ , the diapycnal volume flux,  $Ae$ , and the lateral outflowing volume flux,  $Cu$ , for three different seamount geometries. Fig (a) is a cone, Fig (b) has the radius of the seamount proportional to  $(z_0 - z)^2$  and Fig (c) has the radius proportional to  $(z_0 - z)^{0.5}$ .

It is clear from these simple geometrical examples that the implications of mixing near the top of seamounts are far from solved. Nevertheless, one can reach some useful conclusions about seamounts without a detailed knowledge of the mixing-induced flows near the summit. This is because Eqs. (22) and (23) apply at each depth,  $z$ , independent of our ignorance of the near-summit region where extra physical processes seem to be needed. From Eq. (22) it is concluded that because  $A_z$  is always negative at a seamount, the fluid in the turbulent boundary moves downward so that, on average, seamounts are sinks for the deep ocean. From Eq. (23) it is concluded that the lateral flow into or out of the boundary is governed by the curvature of the seamount profile. A convex region with  $A_{zz} < 0$  is a source for the deep ocean, while a concave region where  $A_{zz} > 0$  is a sink. Since on average seamounts are sinks for the lateral flow field of the deep ocean, the fluid that is downwelled in the seamount boundary layers must make its way to continental boundaries or to mid-ocean ridges, where, on average, it is upwelled.

The picture that emerges for the deep circulation driven by boundary mixing is quite different to that of Stommel and Arons (1960) where the spatially uniform upwelling must be driven by interior mixing. Instead of broad smooth regions of poleward flow, we have found that the interior deep ocean is quiescent except for the need to transfer fluid from one turbulent boundary layer to another, and for the tendency for seamounts to act as sinks for the horizontal circulation. The contrasting deep circulation patterns are shown schematically in Fig. 14. It is concluded that while it may be satisfactory to regard boundary mixing in terms of an equivalent interior diffusivity for the purpose of understanding the mean distributions of passive tracers, the two types of mixing processes have very different dynamical implications for the mean circulation in the deep ocean.

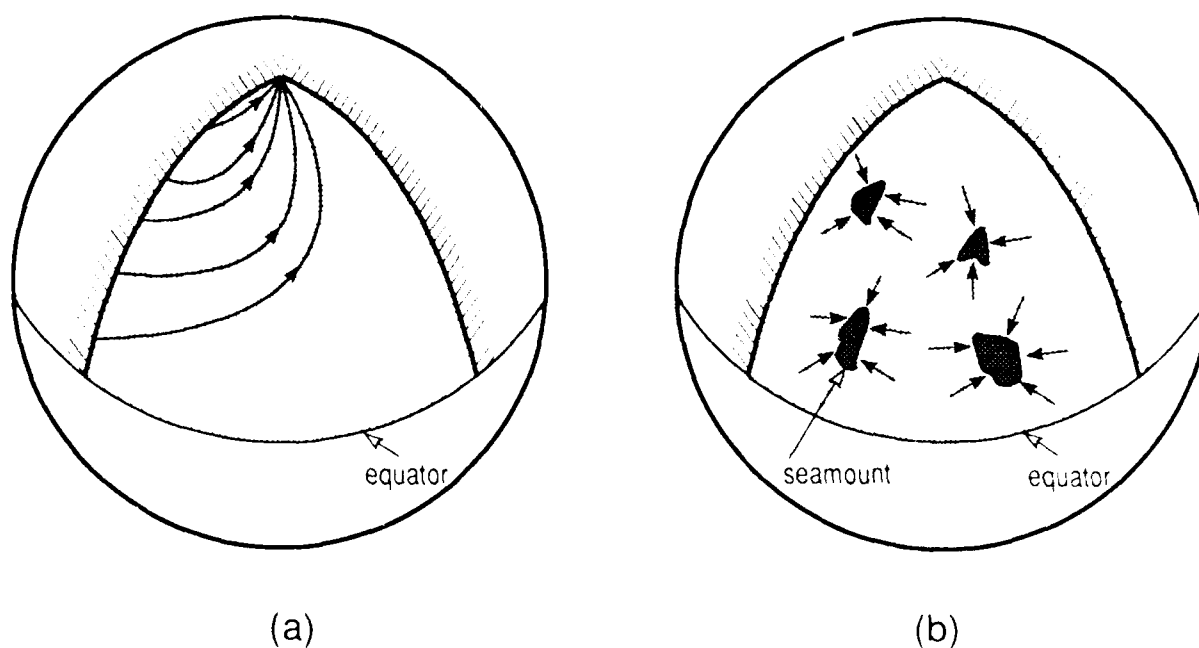


Fig. 14. Sketches of the Stommel-Arons (1960) circulation (Fig a), and a circulation caused by boundary mixing at continental margins and seamounts. The boundary layers adjacent to continents must upwell not only the Bottom Water flux, but also the water that is pumped down at the boundaries of seamounts.

## CONCLUSIONS

The importance of the vertical velocity to the general circulation of the ocean provides much of the incentive for measuring the strength of ocean microstructure and thereby deducing the vertical advection through neutral surfaces (i.e. dianeutral advection). The separate roles of dianeutral advection and dianeutral mixing in causing water-mass conversion have been illustrated in this paper by maps of the relevant vertical derivatives of hydrographic variables on some neutral surfaces from each of the world's oceans. For example, maps of the upwelling (dianeutral advection) caused by small-scale mixing are presented, normalized by the vertical diffusivity. These maps show that there is considerable variability in the magnitude and sign of such upwelling at different depths and at different locations on a neutral surface. Vertical diffusion and vertical advection have no strong tendency to be correlated for any given tracer, and so the common practice in inverse models of lumping the effects of dianeutral advection and diffusion into a single interfacial volume flux is unacceptable. This practice often forces the vertical processes to contribute a term of the wrong sign to the conservation equations.

Two processes – thermobaricity and cabbeling – achieve dianeutral advection without relying on vertical mixing processes, and so this part of the total vertical velocity is invisible to microstructure instruments that measure the dissipation rate of mechanical energy,  $\epsilon$ . Thermobaricity and cabbeling are quite strong in the North Atlantic and Southern Oceans, causing contributions to the dianeutral downwelling velocity of order  $-1 \times 10^{-7} \text{ m s}^{-1}$ . These in turn make a large impact on the conservation equations of scalars in these regions. Of the two processes, thermobaricity is rather smaller than cabbeling except in the Antarctic Circumpolar Current where it is at least as large as cabbeling and also of the same sign.

It is common to use the dissipation rate of mechanical energy,  $\epsilon$ , to infer the vertical diffusivity through Osborn's (1980) formula,  $D = \Gamma^t \epsilon N^{-2}$ . The nonlinearity of the equation of state means that in the thermocline, the real dianeutral velocity will often be  $10^{-7} \text{ m s}^{-1}$  less than the estimate,  $D \epsilon_z / \epsilon$ , that one would infer from the microstructure data alone.

It is shown that vertical mixing processes do not contribute to cabbeling or thermobaricity. The opposite side of this coin is that when a conservation equation is written for potential density, the contribution of the vertical diffusivity acting on the nonlinear terms of the equation of state must be subtracted from the normal diffusive flux divergence of potential density. Failure to do this in inverse models to date has undoubtedly led to significant errors in the diapycnal velocities of such models.

The final section of the paper considers the contrasting dynamical implications of interior mixing and boundary mixing in the deep ocean. Simple arguments, based largely on the conservation of volume in a steady ocean, have shown that it is quite misleading to regard boundary mixing as equivalent to an "effective interior diffusivity." In an ocean with no interior mixing, Bottom Water is upwelled only in the turbulent boundary layers on continental boundaries, with the interior ocean being largely stagnant, and seamounts causing a local sinking of fluid in their vicinity.

## Acknowledgments

Dr Frank Henyey is thanked for first pointing out to the author the singularity in the flow field, due to boundary mixing, that occurs at the apex of any smoothly shaped seamount.

## REFERENCES

- Armi, L., 1978: Some evidence of boundary mixing in the deep ocean. *J. Geophys. Res.*, **83**, 1971-1979.
- Bauer, E. and G. Siedler, 1988: The relative contributions of advection and isopycnal and diapycnal mixing below the subtropical salinity maximum. *Deep-Sea Res.*, **35**, 811-837.
- Eriksen, C. C., 1985: Implications of ocean bottom reflections for internal wave spectra and mixing. *J. Phys. Oceanogr.*, **15**, 1145-1156.
- Freeland, H.J., P. Rhines and H. T. Rossby, 1975: Statistical observations of trajectories of neutrally buoyant floats in the North Atlantic. *J. Mar. Res.*, **33**, 383-404.
- Gargett, A. E., 1984: Vertical eddy diffusivity in the ocean interior. *J. Mar. Res.*, **42**, 359-393.
- Garrett, C., 1979: Comment on 'some evidence for boundary mixing in the deep ocean' by Laurence Armi. *J. Geophys. Res.*, **84**, 5095-5098.
- Garrett, C., 1982: On the parameterization of diapycnal fluxes due to double-diffusive intrusions. *J. Phys. Oceanogr.*, **12**, 954-959.
- Garrett, C. and D. Gilbert 1988: Estimates of vertical mixing by internal waves reflected off a sloping bottom, in *Small-scale turbulence and mixing in the ocean*, edited by J. C. J. Nihoul and B. M. Jamart, Elsevier, Amsterdam, 405-423.
- Hogg, N. G., 1987: A least-squares fit of the advective-diffusive equations to Levitus atlas data, *J. Mar. Res.*, **45**, 347-375.
- Ivey, G. N., 1987a: Boundary mixing in a rotating, stratified fluid. *J. Fluid Mech.*, **183**, 25-44.
- Ivey, G. N., 1987b: The role of boundary mixing in the deep ocean. *J. Geophys. Res.*, **92**, 11,873-11,878.
- Ivey, G. N. and G. M. Corcos, 1982: Boundary mixing in a stratified fluid. *J. Fluid Mech.*, **121**, 1-26.
- Levitus, S., 1982: Climatological atlas of the world ocean, *Prof. Pap. 13*, Natl. Oceanic and Atmos. Admin., US. Dep. of Commer., Washington D. C.
- McDougall, T.J., 1984: The relative roles of diapycnal and isopycnal mixing on subsurface water-mass conversion. *J. Phys. Oceanogr.*, **14**, 1577-1589.
- McDougall, T.J., 1985: Double-diffusive interleaving. II: Finite amplitude, steady state interleaving. *J. Phys. Oceanogr.*, **15**, 1542-1556.
- McDougall, T.J., 1987a: Thermobaricity, cabbeling, and water-mass conversion. *J. Geophys. Res.*, **92**, 5448-5464.
- McDougall, T.J., 1987b: The vertical motion of submesoscale coherent vortices across neutral surfaces. *J. Phys. Oceanogr.*, **17**, 2334-2342.
- McDougall, T. J., 1988a: Some implications of ocean mixing for ocean modelling, in *Small-scale turbulence and mixing in the ocean*, edited by J. C. J. Nihoul and B. M. Jamart, Elsevier, Amsterdam, 21-36.
- McDougall, T. J., 1988b: Neutral-surface potential vorticity. *Prog. Oceanog.* **20**, 185-221.
- McDougall, T. J. and D. R. Jackett, 1988: On the helical nature of neutral trajectories in the ocean. *Prog. Oceanog.*, **20**, 153-183.
- Osborn, T.R., 1980: Estimates of the local rate of vertical diffusion from dissipation measurements. *J. Phys. Oceanogr.*, **10**, 83-89.
- Phillips, O. M., 1970: On flows induced by diffusion in a stably stratified fluid. *Deep-Sea Res.*, **17**, 435-443.
- Phillips, O. M., J. -H. Shyu and H. Salmon, 1986: An experiment on boundary mixing: mean circulation and transport rates. *J. Fluid Mech.*, **173**, 473-499.

- Rossby, H. T., S. C. Riser and A. J. Mariano, 1983: The western North Atlantic - A Lagrangian viewpoint, in *Eddies in Marine Science*, edited by A. R. Robinson, Springer Verlag, New York.
- Schlitzer, R., 1987: Renewal rates of East Atlantic Deep Water estimated by inversion of  $^{14}\text{C}$  data. *J. Geophys. Res.*, **92**, 2953-2969.
- Stommel, H. and A. B. Arons, 1960: On the abyssal circulation of the world ocean. I. Stationary planetary flow patterns on a sphere. *Deep-Sea Res.*, **6**, 140-154.
- Thorpe, S. A., 1982: On the layers produced by rapidly oscillating a vertical grid in a uniformly stratified fluid. *J. Fluid Mech.*, **124**, 391-409.
- Thorpe, S. A., 1987: Current and temperature variability on the continental slope. *Phil. Trans. R. Soc. Lond. A* **323**, 471-517.
- Wunsch, C., 1970: On oceanic boundary mixing. *Deep-Sea Res.*, **17**, 293-301.
- Wunsch, C., 1984a: An estimate of the upwelling rate in the equatorial Atlantic based on the distribution of bomb radiocarbon and quasi-geostrophic dynamics. *J. Geophys. Res.*, **89**, 7971-7978.
- Wunsch, C., 1984b: An eclectic Atlantic Ocean circulation model. I. The meridional flux of heat. *J. Phys. Oceanogr.*, **14**, 1712-1732.
- You, Y. and T. J. McDougall, 1989: Neutral surfaces and potential vorticity in the world's oceans. submitted to *J. Geophys. Res.*



## ARE DIAPYCINAL FLUXES LINKED TO LATERAL STIRRING RATES?

Chris Garrett

Department of Oceanography, Dalhousie University, Halifax, N.S. B3H 4J1, Canada

### ABSTRACT

The correct parameterisation of diapycnal mixing in the ocean requires that we identify the rate-limiting processes. In some parts of the ocean the process governing fluxes across mean isopycnals may be baroclinic instability, with the fluxes requiring, but independent of the magnitude of, smaller scale water mass modification processes. Even if the stirring by mesoscale eddies does not cause a diapycnal flux directly, it should create thermohaline fronts at which double diffusive intrusions are associated with diapycnal mixing. Simple formulae for the effective diapycnal diffusivity in these two cases are reviewed.

Near-boundary mixing by the breaking of internal waves reflected off a sloping bottom may be the dominant diapycnal mixing mechanism in the abyssal ocean; this is reviewed. A simple mechanistic argument for the connection between Thorpe and Ozmidov scales is also presented.

### 1. INTRODUCTION

A couple of decades ago it seems to have been thought computationally convenient, and philosophically acceptable, to parameterise the mixing of scalars in the ocean using an eddy diffusivity tensor that was diagonal with respect to horizontal and vertical axes. The horizontal mixing coefficient  $K_H$  was taken to represent the stirring effect of mesoscale eddies and so was several orders of magnitude greater than the vertical coefficient  $K_V$  which represented mixing associated with processes such as breaking internal waves.

It became recognized, though, that a horizontal diffusivity  $K_H$  would produce a flux across the positions of mean isopycnals (surfaces of equal potential density, based on the average temperature and salinity resolved by the model) that was equivalent to a diapycnal diffusivity  $K_H s^2$ , where  $s$  is the slope of the isopycnal. Veronis (1975) pointed out that, in regions of large  $s$ , this might be considerably larger than  $K_V$  and that the associated flux might force a model to produce a compensating mean circulation of a magnitude and even direction that was implausible.

The horizontal/vertical split has thus fallen into disfavour, though its use appears to have persisted long enough for McDougall and Church (1986) to launch a fresh attack. It seems to have become a matter of faith that eddies in the ocean stir scalars along isopycnals rather than horizontally, so that the diffusivity tensor is diagonal in a coordinate frame defined by the isopycnal surface and the normal to it.

Contributing to this belief was the argument that mesoscale eddies carry the potential density field adiabatically with them and so cannot produce a flux across the potential density surface (e.g., McDougall and Church, 1986). The fundamental flaw in this argument, though, is that, for a model in which the eddies are not resolved, the appropriate density surfaces are those associated with the *mean* temperature and salinity fields, averaged over several eddy space or time scales. It is quite possible that a water mass, advected by eddy motion across a mean isopycnal, undergoes sufficient modification, by mixing or air-sea interaction, that the eddying return flow has different properties, thus giving rise to a net eddy flux across the mean isopycnal.

In the troposphere, for example, it is quite clear that there is a net flux of heat, across the sloping surfaces of equal average potential temperature, associated with the combined processes of baroclinic instability and air mass modification by a variety of diabatic effects. It seems quite likely that the net diapycnal flux may be controlled by the baroclinic instability rather than the smaller scale diabatic processes, provided only that the latter exist and perhaps have a strength greater than some minimum. On the other hand, tracers in the stratosphere seem to be generally stirred along mean isentropic surfaces (e.g., Andrews et al., 1987), much as is fashionably assumed for the ocean.

It thus seems quite likely that, in the ocean too, there will be regions where eddies do merely stir scalars along neutral surfaces based on the mean temperature and salinity, but there may well be others where they provide the dominant flux across these surfaces. This possibility has, in fact, been recognized for some time; a review of ocean mixing (Garrett, 1979) ascribes the suggestion to Peter Rhines (personal communication), but there do not appear to have been any definitive assessments of its importance. Section 2 of this paper merely raises the issue again, pointing out its potential quantitative importance, particularly in the Antarctic Circumpolar Current.

In Section 3 a different relationship between lateral stirring and diapycnal mixing is reviewed. As eddies stir temperature and salinity gradients on mean neutral surfaces they presumably create thermohaline fronts at which double diffusive intrusions will appear and cause diapycnal fluxes. Simple formulae for the effective eddy diffusivity, and for other measures indicative of this process, are reviewed and evaluated for a few locations.

In Section 4 it is suggested that, once mixing coefficients have been determined, the most straightforward way of incorporating them into a numerical model may just be in the (horizontal, vertical) coordinate frame, rather than attempting to use potential density as the vertical coordinate.

Section 5 provides a brief review of the role of near-boundary mixing by breaking internal waves, a process that may turn out to be of major importance. Attention is also drawn to the possibility that very different circulation patterns may be associated with near-boundary, rather than interior, mixing.

Section 6, on a somewhat different topic, presents a simple mechanistic derivation of the expected proportionality of Thorpe and Ozmidov scales in a stratified ocean in which intermittently breaking internal waves are the dominant cause of mixing. Section 7 presents brief conclusions.

## 2. FLUXES ACROSS MEAN ISOPYCNALS BY BAROCLINIC INSTABILITY

We consider first a two-layer situation, sketched in Fig. 1, in which warm and cold core rings are formed at a front through baroclinic instability. If both rings blend into their new surroundings by mixing processes, then the correct parameterisation will be as a diffusion process across mean isopycnals. On the other hand, if only the warm core ring blends into its new surroundings, perhaps through air-sea interaction, whereas the cold core ring spins down viscously without any exchange of scalar properties with the warm water around it, the correct parameterisation of the exchange will be as a mean flow from the warm water to the cold.

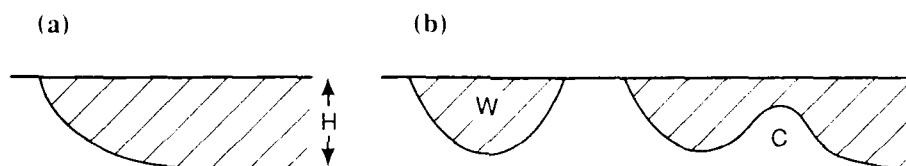


Fig. 1. (a) Schematic of a front in a two-layer ocean. (b) The same front after baroclinic instability has led to the formation of warm-core (W) and cold-core (C) rings; the shaded area denotes the warm water.

In both these scenarios the net transfer is associated with the original baroclinic instability rather than with the small-scale dissipative processes; if the strengths of the latter are halved there will just be twice as many rings present at any given time. The parameterisation of the flux in this scenario is usually taken to be  $\alpha (g' H)^{1/2} H$  with  $g'$  the reduced gravity and  $\alpha \approx 5 \times 10^{-3}$  (Green, 1970; Pingree, 1979), although this is likely to be a gross oversimplification in many cases. Of course if the warm core rings have the possibility of rejoining the front, the net flux may depend on the small scale processes that produce some changes in the ring before it rejoins.

The case of continuous stratification (Fig. 2) is of rather more interest. The flux parameterisation adopted by Bryden (1979) and Johnson and Bryden (1989) from meteorological studies by Stone (1974) is

$$F_T = \overline{u' T'} = CH^2 (N/f) \overline{U_z} \overline{T_y} \quad (1)$$

where  $C$  is a constant of about 0.2. This flux can be regarded as  $C$  times a velocity scale  $H \overline{U_z}$  times a mixing length  $NH/f$  (the Rossby radius of deformation) times the mean temperature gradient  $\overline{T_y}$ . The effective horizontal diffusivity is  $CH^2 (N/f) \overline{U_z}$ , and so,

after multiplying by the square of the geostrophically balanced isopycnal slope  $f \bar{U}_z / N^2$ , the effective diapycnal diffusivity can be written

$$K_d = CH^2 f Ri^{-3/2} \quad (2)$$

where  $Ri = N^2 / \bar{U}_z^2$  is the Richardson number of the mean flow. For Bryden's (1979) and Johnson and Bryden's (1989) analysis of the Antarctic Circumpolar Current, which does seem to be baroclinically unstable,  $Ri \approx 10^3$  and a  $K_d$  of between  $10^{-3}$  and  $10^{-2} \text{ m}^2 \text{ s}^{-1}$  seems quite possible if we take  $H \approx 4000 \text{ m}$ . Regions with such large effective diapycnal diffusivities do not have to be very numerous or extensive to have a major impact on overall diapycnal fluxes.

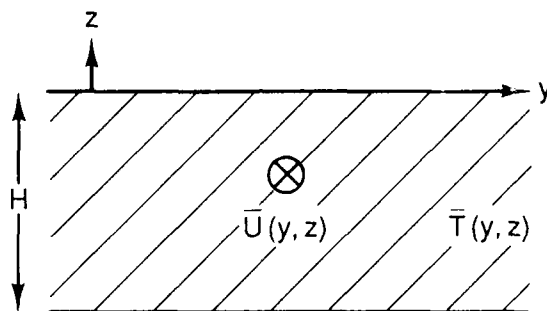


Fig. 2. Sloping isotherms in an ocean of depth  $H$ .

Small-scale processes such as mixing or air-sea interaction must act in series, of course, otherwise the Charney-Drazin nonacceleration theorem (e.g., Andrews et al., 1987) tells us that the eddy fluxes of heat and momentum would be opposed by a mean flow, with no net change in  $\bar{T}$  and  $\bar{U}$ . However, as long as these small-scale processes do eventually operate, the net diapycnal flux may well be controlled by baroclinic instability, rather than the small-scale processes; maybe the Southern Ocean more resembles the troposphere than the stratosphere.

The above discussion is undoubtedly rather superficial; what is required is a series of numerical model experiments, using an eddy-resolving model, in which the sensitivity of fluxes across mean isopycnals to the parameterisation of sub-grid-scale processes is investigated.

### 3. DIAPYCNAL FLUXES FROM ISOPYCNAL STIRRING

Surfaces of constant in-situ potential density (neutral surfaces) may be defined in terms of the temperature and salinity fields averaged over eddy space or time scales. Such surfaces will have compensating gradients of potential temperature and salinity on them, and stirring by mesoscale eddies will create thermohaline fronts at which double-diffusive intrusions can be expected to form (Fig. 3), as described by Stern (1967),

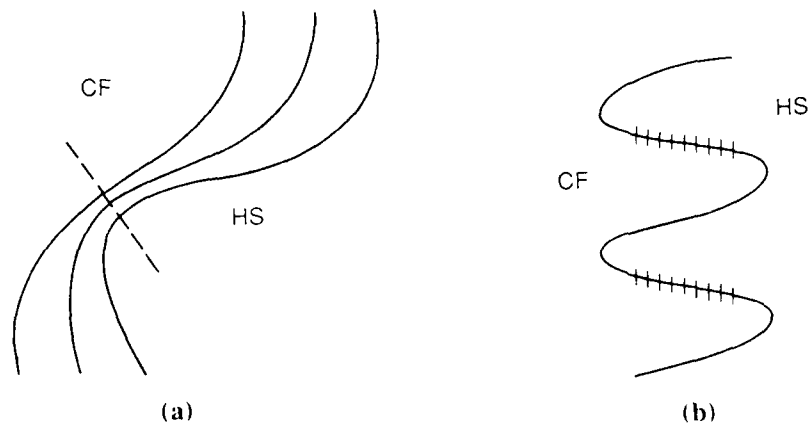


Fig. 3. Schematic of (a) lines of constant potential temperature and salinity on a neutral surface, and (b) thermohaline intrusions at a front. (a) is a plan view with (b) an elevation of a section along the dashed line in (a). HS, CF refer to "hot, salty" and "cold, fresh" water, respectively; the short vertical lines in (b) denote salt fingers.

Ruddick and Turner (1979) and others. As diapycnal fluxes are associated with such intrusions, it seems that the final stages of *isopycnal* stirring inevitably lead to *diapycnal* mixing.

Garrett (1982) made a crude attempt to evaluate the importance of this mechanism, deriving very approximate formulae for the large-scale average diapycnal diffusivities  $K_S$ ,  $K_T$  and  $K_\rho$  for salinity, temperature and density that should be used in a model that does not attempt to deal with the intrusions explicitly. He found that  $K_\rho < 0$  (as is appropriate for a mechanism that draws on the potential energy of the ocean),  $K_T$  may take either sign and  $K_S$  is given by

$$K_S \approx 10^{-3} L^2 N (g \beta |\nabla S| N^{-2})^3 \quad (3)$$

with  $L$  a measure of eddy diameter,  $|\nabla S|$  the large-scale isopycnal salinity gradient and  $\beta = \rho^{-1} \partial \rho / \partial S$ . Taking  $L = 100$  km, Table 1 shows typical input parameters and the resulting  $K_S$  for three regions using the maps of Reid (1981) for the abyssal South Pacific and Armi and Stommel (1983) for the "Beta Triangle" region of the Atlantic.

It appears that obtaining a significant value of  $K_S$ , which is the average diapycnal diffusivity rather than the larger value applicable within regions of frontal intrusions, depends on having a fairly large isopycnal salinity gradient and weak vertical stratification. While generally rather weak, the mechanism appears to warrant further attention. Relevant to this, Table 1 also shows the associated predictions for intrusion height  $h$  (actually this is the Ruddick and Turner, 1979, scale for a pair of hot-salty and cold-fresh intrusions), the width  $W$  of frontal regions containing active intrusions (so that  $W/L = W/100$  km is the predicted fraction of the surface area, or of hydrographic casts,

Table 1. Parameter values associated with isopycnal stirring of lateral temperature and salinity gradients.

Region	$ \nabla S  (\text{‰ m}^{-1})$	$N (\text{s}^{-1})$	$g\beta  \Delta S  N^{-2}$	$K_S (\text{m}^2 \text{s}^{-1})$	$h (\text{m})$	$W (\text{km})$	$L  \nabla S  (\text{‰})$
Abyssal S. Pacific	$10^{-7}$	$10^{-3}$	$10^{-3}$	$10^{-5}$	50	8	$10^{-2}$
Beta triangle	$3 \times 10^{-7}$	$3 \times 10^{-3}$	$3 \times 10^{-4}$	$10^{-6}$	15	7	$3 \times 10^{-2}$
Mediterranean salt tongue	$10^{-6}$	$2 \times 10^{-3}$	$2 \times 10^{-3}$	$2 \times 10^{-4}$	100	30	$10^{-1}$

that should contain intrusions) and the salinity amplitude  $L |\nabla S|$  of the intrusions. The numbers are based on exceedingly approximate arguments and, for the Mediterranean tongue particularly, may overestimate layer thickness and  $K_S$  if one examines Niino's (1986) criterion for the formation of thinner layers in a wider front, but the results here may provide some guidance.

#### 4. OVERALL PARAMETERISATION

Suppose that we have sorted out the problems discussed in the preceding two sections and also know the diapycnal mixing rates associated with more conventional processes such as breaking internal waves and double diffusion; how are all the parameterisations best used in a numerical model of the ocean for which these processes are all sub-grid-scale?

In his interesting and careful studies of the effect of nonlinearities in the equation of state, McDougall (e.g., 1988) has generally recommended working with respect to neutral surfaces, i.e., using potential density as the vertical coordinate. There can occasionally be advantages to this, but in general it seems that numerical modelers might prefer to stick to coordinates  $(x, y, z, t)$  with  $z$  vertically upwards. The diffusivity tensor may be better known with respect to neutral surfaces (and may include the skew diffusion tensor discussed by Haidvogel and Rhines, 1983), but can readily be rotated to a coordinate frame with vertical and horizontal axes (Solomon, 1971; Redi, 1982).

With respect to the  $(x, y, z, t)$  reference frame the cabbeling process, or densification on mixing, leads to extra terms on the right-hand side of the equation for  $\partial \rho / \partial t$ , with the dominant being  $-\frac{1}{2} \rho_{TT} \chi$  where  $\chi = 2\kappa \nabla T \cdot \nabla T$  is the dissipation rate of temperature variance (Garrett and Horne, 1978; McDougall, 1984). We note that all of  $\chi$  is included here, whereas with potential density as a vertical coordinate only that part of  $\chi$  associated with the lateral production of temperature variance enters the water mass conversion equation (McDougall, 1984). It is clear that cabbeling thus does have a microstructure signal. Also, of course, densification on mixing, or cabbeling, is automatically allowed for if the temperature and salinity equations are solved separately.

## 5. NEAR-BOUNDARY MIXING BY BREAKING INTERNAL WAVES

Data on the depth dependence of turbulent energy dissipation in the ocean interior, as well as various theories, suggest that the diapycnal diffusivity  $K_V$  may be independent of  $N$  and hence also of depth (Gregg, 1989). Diffusivities of a few  $\times 10^{-4} \text{ m}^2 \text{ s}^{-1}$  inferred for some abyssal basins from heat budgets thus seem incompatible with values of less than  $10^{-5} \text{ m}^2 \text{ s}^{-1}$  inferred from dissipation measurements in the thermocline, and one seeks mixing mechanisms associated with the sloping boundaries of the basins.

Eriksen (1982, 1985) has drawn attention to the major changes that occur in a typical internal wave spectrum on reflection from a plane sloping sea floor, and has suggested that significant energy dissipation and mixing near the boundary might ensue. Garrett and Gilbert (1988) attempted to quantify the process by integrating the shear spectrum of the reflected waves out to a vertical wavenumber such that the integrated shear gave a Richardson number of about 1. They argued that reflected waves with higher wavenumbers should undergo shear instability and hence give up their energy flux to dissipation and mixing. The energy flux thus calculated is a function of bottom slope and the frequency ratio  $f/N$  but can exceed  $1 \text{ mW m}^{-2}$  for reasonable bottom slopes and could be associated with an effective interior vertical eddy diffusivity of  $O(10^{-4}) \text{ m}^2 \text{ s}^{-1}$  in the abyssal ocean.

One shortcoming of their calculations was that they assumed an infinite plane slope. Gilbert and Garrett (1989) have discussed the effects of finite topographic scale, using the results of the diffraction theories of Baines (1971, 1974) and others. Their conclusions can be summarised through discussion of Figure 4.

In general some of the incident wave energy is back-scattered, reducing the energy flux into the shorter forward-reflected waves. This effect is small, however, if the radius of curvature of the topography is not much less than the wavelength of the incident waves.

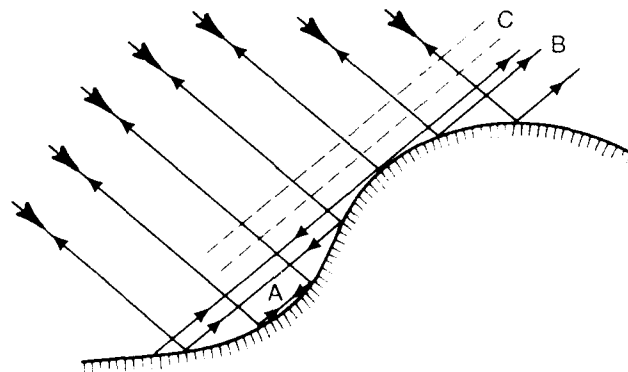


Fig. 4. Schematic of internal wave rays incident on irregular bottom topography (large arrows) and being reflected (small arrows). Regions A, B, C are discussed in the text.

Hence in region B the solution for an infinite plane slope may be used. In region A, however, the internal wave shear is generally small due to destructive interference of the waves after their first reflection; after the second reflection the energy is all reflected back in the direction opposite to that of the incident waves. Region C contains a pattern of weak standing waves associated with the diffraction.

A very approximate rule of thumb is thus that significant mixing, at a rate derived from the formulae of Garrett and Gilbert (1988), may be expected above convex topography, but that little near-boundary mixing due to breaking internal waves is to be expected above concave topography. Further mixing might arise as a consequence of wave-wave interactions within the residual wave spectrum that remains after the initial shear instability; the magnitude of this effect remains to be calculated.

The consequences for ocean circulation of near-boundary, rather than interior, mixing also need to be investigated. Phillips et al. (1986) have shown that a convergence or divergence of buoyancy flux in the boundary layer will drive upwelling or downwelling there and that, if the resulting flow is itself convergent or divergent, it will drive fluid into, or out of, the interior and modify its stratification. In principle, knowing boundary mixing rates (which may depend on the bottom slope and other parameters) and the interior stratification, one can evaluate this exchange with the interior. The consequences in a rotating system may require a numerical model; even if not, an investigation of how circulation patterns change in response to near-boundary, rather than internal, mixing represents an opportunity for models already in existence.

## 6. THE PROPORTIONALITY OF THORPE AND OZMIDOV SCALES

Thorpe (1977) suggested the possibility of estimating vertical mixing rates from the scale of observed overturns in a vertical density profile. Later Dillon (1982) was able to demonstrate, from microstructure data, a strong correlation between the Thorpe scale  $L_T$  (the rms particle displacement from a re-ordered stable profile) and the Ozmidov scale  $L_R = (\epsilon/N^3)^{1/2}$ , with  $L_R \approx 0.8 L_T$ .

Most theoretical derivations predicting the proportionality of  $L_R$  and  $L_T$  are based on ideas of continuous, stationary, stratified turbulence, whereas in reality the mixing in the ocean may primarily be associated with intermittent shear instability of internal waves. In that case, one might ask whether the ratio  $L_R/L_T$  could depend on the dimensionless ratio  $f/N$ , as the wave shear might have a time scale related to  $f^{-1}$  whereas the collapse of an overturn would occur in a frame proportional to  $N^{-1}$ .

It thus seems worthwhile to present an extremely simple argument connecting  $L_R$  and  $L_T$  for an ocean in which the mixing mechanism is intermittent overturns of vertical scale  $H$ . In each overturn the displacement varies linearly between  $-H$  and  $+H$ , so that the mean square is  $\frac{1}{3}H^2$ . If each overturn persists for a time  $T_o$  and the time between overturns is  $T_e$ , the expected squared Thorpe scale is

$$L_T^2 = \frac{1}{3} H^2 (T_o/T_e) \quad . \quad (4)$$



On the other hand, the vertical eddy diffusivity  $K_V$  can be related to the overturns by  $K_V = \frac{1}{12} \alpha H^2 T_e^{-1}$ , where perfect homogenisation leads to  $\alpha = 1$  and  $\alpha < 1$  if the mixing is incomplete. If we also assume that a fraction  $\Gamma$  of the average energy dissipation rate  $\epsilon$  ends up as potential energy, then  $K_V = \Gamma \epsilon / N^2$ . Hence

$$L_R^2 = \epsilon / N^3 = \frac{1}{12} \alpha \Gamma^{-1} H^2 (N T_e)^{-1} \quad (5)$$

and so

$$L_R^2 / L_T^2 = \frac{1}{4} \alpha \Gamma^{-1} (N T_o)^{-1} \quad (6)$$

Here one might expect  $\Gamma \approx 0.2$  (e.g., Oakey, 1982),  $\alpha$  not much less than 1 and  $NT_o$  also  $O(1)$ . Hence a ratio  $L_R/L_T$  close to 1 is not unexpected. More interestingly, the ratio  $f/N$  can only affect  $L_R/L_T$  via  $\alpha$  and  $\Gamma$ . Such a dependence might be weak, consistent with Crawford's (1986) finding of the same ratio of  $L_R$  to  $L_T$  on the equator as found by Dillon (1982) at mid-latitude.

## 7. CONCLUSIONS

There is a need to determine the rate-controlling processes for diapycnal fluxes in the ocean. We do not know whether breaking internal waves and other small-scale processes are the rate-controlling process, or whether, in some parts of the ocean, they merely serve to remove the variance produced by baroclinic instability which is the rate-controlling process. Investigation of this, and determination of the correct parameterisation, will require extensive sensitivity studies with eddy-resolving models using different parameterisations of the mass and momentum transfers that are sub-grid-scale.

The parameterisation of diapycnal mixing may also depend on mesoscale eddies if it is associated with thermohaline fronts and intrusions that are caused by the stirring of temperature and salinity on neutral surfaces. The process does not appear to be very significant, but some formulae have been presented and could form the basis of further work.

One clear opportunity for numerical models lies in the investigation of the consequences of spatially variable diapycnal diffusivity, particularly if this diffusivity is taken to be large close to boundaries or frontal regions, small elsewhere.

In any of the investigations proposed above it is important to recognize the value of over-idealized intuition-building models as well as more elaborate, and potentially more realistic, simulations.

*Acknowledgements.* I thank Mike Gregg, Trevor McDougall, Barry Ruddick and other colleagues for discussions, and the Applied Physics Laboratory of the University of Washington for hospitality. The Office of Naval Research and the Natural Sciences and Engineering Research Council provided support.

## REFERENCES

- Andrews, D.G., J.R. Holton, and C.B. Leovy, 1987: *Middle Atmosphere Dynamics*. Academic Press, 489 pp.
- Armi, L., and H. Stommel, 1983: Four views of a portion of the North Atlantic subtropical gyre. *J. Phys. Oceanogr.*, **13**, 828–857.
- Baines, P.G., 1971: The reflexion of internal/inertial waves from bumpy surfaces. Part 2. Split reflexion and diffraction. *J. Fluid Mech.*, **49**, 113–131.
- Baines, P.G., 1974: The generation of internal tides over steep continental shelves. *Phil. Trans. Roy. Soc. London, Ser. A*, **277**, 27–58.
- Bryden, H., 1979: Poleward heat flux and conversion of available potential energy in Drake Passage. *J. Mar. Res.*, **37**, 1–22.
- Crawford, W.R., 1986: A comparison of length scales and decay times of turbulence in stably stratified flows. *J. Phys. Oceanogr.*, **16**, 1847–1854.
- Dillon, T.M., 1982: Vertical overturns: a comparison of Thorpe and Ozmidov length scales. *J. Geophys. Res.*, **87**, 9601–9613.
- Eriksen, C.C., 1982: Observations of internal wave reflection off sloping bottoms. *J. Geophys. Res.*, **87**, 525–538.
- Eriksen, C.C., 1985: Implications of ocean bottom reflection for internal wave spectra and mixing. *J. Phys. Oceanogr.*, **15**, 1145–1156.
- Garrett, C., 1979: Mixing in the ocean interior. *Dynamics of Oceans and Atmospheres*, **3**, 239–265.
- Garrett, C., 1982: On the parameterization of diapycnal fluxes due to double diffusive intrusions. *J. Phys. Oceanogr.*, **12**, 952–959.
- Garrett, C., and E. Horne, 1978: Frontal circulation due to cabbeling and double diffusion. *J. Geophys. Res.*, **83**, 4651–4656.
- Garrett, C., and D. Gilbert, 1988: Estimates of vertical mixing by internal waves reflected off a sloping bottom. In *Small Scale Turbulence and Mixing in the Ocean, Proceedings of the 19th Liège Colloquium on Ocean Hydrodynamics*, J.C.J. Nihoul and B.M. Jamart, Eds., Elsevier, 405–424.
- Gilbert, D., and C. Garrett, 1989: Implications for ocean mixing of internal wave scattering off irregular topography. *J. Phys. Oceanogr.* (submitted).
- Green, J.S.A., 1970: Transfer properties of large-scale eddies and the general circulation of the atmosphere. *Q. J. Roy. Met. Soc.*, **96**, 157–185.
- Gregg, M.C., 1989: Scaling turbulent dissipation in the thermocline. *J. Geophys. Res.* (in press).
- Haidvogel, D.B., and P.B. Rhines, 1983: Waves and circulation driven by oscillatory winds in an idealized ocean basin. *Geophys. Astrophys. Fluid Dyn.*, **25**, 1–63.
- Johnson, G.C., and H. Bryden, 1989: On the size of the Antarctic Circumpolar Current. *Deep-Sea Res.* (in press).
- McDougall, T.J., 1984: The relative roles of diapycnal and isopycnal mixing on subsurface water mass conversion. *J. Phys. Oceanogr.*, **14**, 1577–1589.

- McDougall, T.J., 1988: Some implications of ocean mixing for ocean modelling. In *Small Scale Turbulence and Mixing in the Ocean, Proceedings of the 19th Liège Colloquium on Ocean Hydrodynamics*, J.C.J. Nihoul and B.M. Jamart, Eds., Elsevier, 21–35.
- McDougall, T.J., and J.A. Church, 1986: Pitfalls with the numerical representation of isopycnal and diapycnal mixing. *J. Phys. Oceanogr.*, **16**, 196–199.
- Niino, H., 1986: A linear stability theory of double-diffusive horizontal intrusions in a temperature-salinity front. *J. Fluid Mech.*, **171**, 71–100.
- Oakey, N.S., 1982: Determination of the rate of dissipation of turbulent energy from simultaneous temperature and velocity shear microstructure measurements. *J. Phys. Oceanogr.*, **12**, 256–271.
- Phillips, O.M., J.-H. Shyu, and H. Salmun, 1986: An experiment on boundary mixing: mean circulation and transport rates. *J. Fluid Mech.*, **173**, 473–499.
- Pingree, R.T., 1979: Baroclinic eddies bordering the Celtic Sea in late summer. *Jour. Mar. Biol. Assoc. U.K.*, **59**, 689–698.
- Redi, M., 1982: Oceanic isopycnal mixing by coordinate rotation. *J. Phys. Oceanogr.*, **12**, 1154–1158.
- Reid, J.L., 1981: On the mid-depth circulation of the world ocean. In *Evolution of Physical Oceanography*, MIT Press, 70–111.
- Ruddick, B.R., and J.S. Turner, 1979: The vertical scale of double-diffusive intrusions. *Deep-Sea Res.*, **26A**, 903–913.
- Solomon, H., 1971: On the representation of isentropic mixing in ocean circulation models. *J. Phys. Oceanogr.*, **1**, 233–234.
- Stern, M.E., 1967: Lateral mixing of water masses. *Deep-Sea Res.*, **14**, 747–753.
- Stone, P.H., 1974: The meridional variation of the eddy heat fluxes and their parameterization. *J. Atmos. Sci.*, **31**, 444–456.
- Thorpe, S.A., 1977: Turbulence and mixing in a Scottish loch. *Phil. Trans. Roy. Soc. London, Ser. A*, **286**, 125–181.
- Veronis, G., 1975: The role of models in tracer studies. In *Numerical Models of Ocean Circulation*, National Academy of Science, 133–146.

## RELATING TURBULENCE DISSIPATION MEASUREMENTS TO OCEAN MIXING

Greg Holloway

School of Oceanography, University of Washington, Seattle, Washington, USA 98195  
and  
Institute of Ocean Sciences, Sidney BC, Canada V8L4B2

### ABSTRACT

Dissipation observations, both of temperature variance and of velocity variance, have been used to infer rates of turbulent transport in the ocean interior. Arguments supporting such inference depend upon assumed balances between gradient transport production and direct dissipation. It is suggested that these arguments may be not merely inaccurate but grossly uncertain in the sense of orders of magnitude or even sign. Three different theoretical accounts, each consistent with observed spectra, support very different possible transport rates.

### INTRODUCTION

This note only elaborates upon a topic that arose during workshop discussion. The concern, expressed most graphically by Moum, is that what we can measure in the ocean (dissipation rates of temperature or velocity variance) is not what we want to parameterize in ocean models (usually property fluxes). Possibilities to make direct measurements of property fluxes, either by an instrument such as Moum describes or by tracer release experiments such as described by Ledwell, hold attractive promise that remains to be realized in the typical open ocean environment. On the other hand, microstructure dissipation measurements such as described by Gregg are quite advanced. So then *the* question is: do these dissipation measurements imply property fluxes?

A host of uncertainties arise when any kind of measurement is used to imply something else. *Caveats* pertaining to dissipation measurements (e.g., matters of intermittency, anisotropy, etc.) have been discussed in detail elsewhere. What is important here is to determine whether we are dealing only with tolerable uncertainty (perhaps at the level of a few tens % or maybe 100% ) or whether the uncertainty is truly gross (like orders of magnitude or sign.) The comment I'll try to demonstrate is this: From observations of small scale variance spectra (including dissipation rates as moments of those spectra), the inference of property fluxes is *grossly* uncertain. This is not to say that the inference is wrong. The comment is that arguments based on the equations of motion appear to admit wildly different property fluxes for observed spectra or dissipation rates.

WHAT HAPPENS TO  $\nabla \cdot \mathbf{u} T'^2$  ?

Inferences of oceanic vertical diffusivity  $K_v$  for heat or salt have been made from dissipation observations of temperature variance following the argument of Osborn and Cox (1972) or from velocity variance dissipation following the argument of Lilly *et al.* (1974). In order to isolate the term leading to purported gross uncertainty, consider a much simplified temperature variance equation (omitting compressibility, salinity effects, non-constant thermal conductivity, mean horizontal gradients, vertical mean motion):

$$\partial/\partial t (T'^2) + \nabla \cdot \mathbf{u} T'^2 + 2wT'\partial/\partial z T = 2T'\kappa \nabla^2 T' = -\chi \quad (1)$$

Averaged over time, we may omit the  $\partial/\partial t$  term. The right side is nearly negative definite at dissipation rate  $\chi$ . Then the "classical" assumption is to ignore  $\nabla \cdot \mathbf{u} T'^2$  so that  $wT'$  can then be estimated from observables. If we define  $K_v$  from  $wT' = -K_v \partial/\partial z T$ , then  $2K_v = \chi/(\partial/\partial z T)^2$ . The question is: why ignore  $\nabla \cdot \mathbf{u} T'^2$  ?

Sundry reasons have been given for ignoring  $\nabla \cdot \mathbf{u} T'^2$ . Assume statistical homogeneity, for instance. Of course that will work; but what supports such an assumption? The ocean is principally forced from above, is dissipative in its interior, and suffers a poorly understood benthic boundary interaction. (With so much inhomogeneity in the vertical, I hesitate to mention also horizontal inhomogeneity.)

Alright then, how about saying "Well  $\mathbf{u} T'^2$  is a *turbulent* transport of  $T'^2$ , and it just doesn't *make sense* that small scale turbulence, which is quite patchy after all, can be very effective at redistributing  $T'^2$  over vertical scales of km."

That is a semantic dodge, masquerading as dynamics. It depends upon an even more mischievous (if venerated) ploy: to somehow separate "waves" from "turbulence". How do we know what scales (or "kinds") of motion support  $\mathbf{u} T'^2$ ? Although (1) is written in a form that suggests "turbulence-like" ideas, the nonlinear term  $\nabla \cdot \mathbf{u} T'^2$  together with corresponding nonlinear terms in the momentum equation would be just the terms that support nonlinear wave-wave interactions. Then we might discuss how  $T'$  fluctuations in larger scale waves are transferred by wave-wave interaction down to  $T'$  fluctuations at shorter scale waves and so on to yet shorter scale waves until the waves "break". After that, the turbulence takes  $T'$  on down to smaller scales and so on to  $\chi$ . Whether we talk "waves" or "turbulence", we see that nonlinear transfer from large to small scales may support  $\chi$ . However, this need not be the case, and I will return (below) to an argument which could as well send  $T'$  fluctuations the other way, from small to larger scales, enhancing the burden that must be born by  $wT'$  in (1). For the present, the only comment is that  $\nabla \cdot \mathbf{u} T'^2$  appears to be the "loose cannon on deck".

Can we rule out  $\nabla \cdot \mathbf{u} T'^2$  from "back of the envelope" scale analysis? Expressed in terms of (available potential) energy units, the dissipation rate for  $T'^2$  may be written  $N^2 \zeta^2 / \tau$ , where  $\zeta$  is a characteristic vertical displacement and  $\tau$  is a residence time that may be estimated from observed  $\chi$ . Likewise in energy units  $\nabla \cdot \mathbf{u} T'^2$  might be expressed  $C u \zeta^2 N^2 / Z$  with  $C$  an unknown correlation coefficient and  $Z$  a scale depth for variation of  $\mathbf{u} T'^2$ . On the conservative side, suppose we replace  $u'$  by  $N \zeta$ . Then for  $\nabla \cdot \mathbf{u} T'^2$  to

balance  $\chi$ , we need the magnitude of  $C$  to approximate  $Z/(\zeta N\tau)$ . The reader will likely choose numbers to insert; it seems to me that  $Z/\zeta$  needn't be larger than 100 while  $N\tau$  may be of order  $10^4$ . Given the kind of uncertainty of such analysis, it appears that  $\nabla \cdot \mathbf{u} T'^2$  can comfortably manage with  $C$  of order  $10^{-2}$ . But is  $10^{-2}$  actually a large number? After all, at the more wavelike scales that dominate  $w'$  or  $T'$ , the second order correlation coefficient for  $wT'$  may already be smaller than  $10^{-2}$ . And third order correlation coefficients must be smaller yet. Really? If this is a proposition only at the level of kinematics, it is demonstrably false. One can readily enough construct fields with vanishingly small second order correlations but quite significant third order correlations. On the other hand, so far as I'm aware, there's no dynamical reason why the correlation coefficient for  $\mathbf{u} T'^2$  should be small, however small the coefficient for  $wT'$ .

THEN HOW ABOUT  $K_v = \gamma \epsilon N^{-2}$  ?

An increasingly popular alternative to estimation of  $K_v$  from  $K_v = \chi/(\partial/\partial z T)^2$  is by observing the rate  $\epsilon$  of dissipation of kinetic energy (approximately, from observations of one or two components of shear variance and from assumed dissipation scale isotropy.) After Lilly *et al.* (1974), the suggestion is  $K_v = \gamma \epsilon N^{-2}$  where  $\gamma$  is a "mixing efficiency" related to a flux Richardson number  $R_f$  as  $\gamma = R_f/(1-R_f)$ , following Osborn (1980). The usual suggestion is that  $\gamma$  isn't bigger than about 0.2, based upon  $R_f$  of about 0.15, and  $\gamma$  may be rather smaller. If so, this can be quite useful just as an upper bound. Can we say *with confidence* that  $K_v$  is *no larger* than  $0.2\epsilon N^{-2}$ ? No, and not even "approximately". The first of **Three Theories** to be described below implies quite the contrary: the theory in fact depends upon  $K_v \gg \epsilon N^{-2}$ ! Perhaps this theory will turn out to be false; but we may only know that by establishing that  $K_v < \epsilon N^{-2}$  from direct or indirect determination of  $K_v$ . Another awful possibility, which is admitted but not implied by the third of Three Theories, is  $\gamma < 0$  hence  $K_v < 0$ ! In each case we only need to recognize that third order correlations, from both the temperature and momentum equations, will support transfers of  $T'^2$  and of  $u'^2$  across scales of motion. Arguments given in the previous section for  $T'^2$  could be repeated for  $u'^2$ , suggesting that  $\epsilon$  might be supported entirely by transfer of  $u'^2$  from larger scales. Indeed that is roughly the conventional wisdom, with only a little (like 15% or less) of the  $u'^2$  being given up by working against gravity under  $wT' < 0$ .

But how inconsistent we are! The kinetic energy (KE) equation in stratified fluid is

$$\partial/\partial t (u^2/2) + \nabla \cdot (\mathbf{u}'p' + \mathbf{u}'u'^2/2) + \rho'w'g = -\epsilon \quad (2)$$

where  $u^2 = \mathbf{u}' \cdot \mathbf{u}'$ ,  $p'$  is pressure fluctuation,  $\rho'$  is the fractional density fluctuation due to  $T'$ ,  $g$  is gravity, and  $\epsilon$  is viscous dissipation of KE. Customarily, one discards the second term in Eq. (2) as being the divergence of a turbulent flux. However, we would next notice that, if  $\rho'w' > 0$  (as, of course, it must be!), and with  $\epsilon > 0$  (as it is), then Eq. (2) has no production term for KE. Clearly I have forgotten to include the Reynolds stress term  $\mathbf{u}'w'\partial U/\partial z$ . In fact I did not forget. Rather I only admit that I do not know how to separate mean flow  $U$  from fluctuating flow  $u'$  and so resort to calling it all "fluctuation". Then the Reynolds stress production term *is* present in Eq. (2); only it is part of the divergence of a triple correlation which, by custom, we would have discarded! Apparently we are content here that triple correlations (choosing, as we may, not to separate  $\mathbf{u}$  into mean and fluctuation parts) can support all of  $\epsilon$ , with even some

extra left over, yet we abhor the idea that such triple correlations might support  $\chi$ . *Why?! (Expressed in terms of energetics,  $\chi$  is even smaller than  $\varepsilon$  according to Oakey, 1982, or Gregg, 1987).*

If we should admit that triple correlations can support  $\varepsilon$  or  $\chi$ , why not turn the table: perhaps  $\nabla \cdot \mathbf{u} \mathbf{T}^2$  supports all of  $\chi$  with some extra to give up by  $w \mathbf{T}' > 0$  as a contribution to  $\varepsilon$ ? Then  $K_v < 0$ .

### DO WE NEED A FRESH CHAMPION?

Following custom, we've imagined rejecting the second term in Eq. (2). However, as the previous paragraph has indicated, it is just that second term that contains what--*customarily*--would have been the Reynolds stress working term. But there's more. As well we should reconsider the divergence of pressure work

$$\nabla \cdot (\mathbf{u} p') = \nabla \cdot (\mathbf{u}' \nabla^{-2} (g \partial / \partial z \rho' + \nabla \cdot (\nabla \cdot \mathbf{u}') \mathbf{u}')) \quad (3)$$

in Eq. (2), where  $\nabla^{-2}$  is the inverse Laplacian. In part, Eq. (3) expresses further contribution from triple correlations  $\mathbf{u}' \mathbf{u}' \mathbf{u}'$ . As well there is the contribution  $\mathbf{u}' \nabla^{-2} (g \partial / \partial z \rho')$ . Very importantly, this is the wave-born energy flux. Does this term tip the balance to favor KE supply? If so, it might even turn out that  $K_v = 0.2 \varepsilon N^{-2}$  is right after all. The Lilly-Osborn argument might well be saved--but only on account of a term that Lilly-Osborn rejected.

### THREE THEORIES

#### Theory Number One

For each of the theories, let me be brief while only pointing to their published accounts. The main comment to make here is that each of these theories appear to do a good job of predicting variance spectra, both of temperature and of velocity, in excellent agreement with observations. Yet the theories support wildly different  $w \mathbf{T}'$ , hence different  $K_v$ .

The first theory is sometimes termed "Buoyancy Subrange" and follows Lumley (1964). The idea is that at some sufficiently small scale one finds ordinary turbulence of a kind described asymptotically by Kolmogorov (1941). Below a transitional wavenumber  $k_b = (N^3/\varepsilon)^{1/2}$ , the spectrum is modified by the stable stratification. This modification is a result of  $w \mathbf{T}' < 0$  extracting kinetic energy (in turn generating  $\mathbf{T}^2$ .) The resulting theoretical prediction for the kinetic energy spectrum

$$E(k) = \varepsilon^{2/3} k^{-5/3} [A + B(k_b/k)^{4/3}] \quad (4)$$

turns out to be in good agreement with oceanic observations (Gargett *et al.*, 1981) and with a host of recent observations in the middle atmosphere, with order unity coefficients A and B in fact taking values of order unity. In this case  $k$  is understood as vertical wavenumber  $k_z$  while the theory did not attempt to address possible anisotropy.

At high wavenumbers, the spectrum is a familiar  $A\epsilon^{2/3}k^{-5/3}$ . Below  $k_b$  the spectrum approaches  $BN^2k^{-3}$ .

Lucky? Maybe. Lumley's theory also has implications for the temperature variance spectrum, as developed by Weinstock (1985). The resulting theoretical temperature spectrum  $T(k)$  has an expression very similar (though not identical) to Eq. (4). This also turns out to agree with oceanic spectra reported by Gregg (1977) and with spectra from balloon soundings reported by Dalaudier and Sidi (1987). We appear to have a theory that very well predicts *both* the velocity and temperature spectra (the amplitudes as well as shapes of spectra) in both the ocean and atmosphere. That should seem encouraging. So what's  $K_v$ ?

On the  $BN^2k^{-3}$  range, spectra are controlled by the strong conversion of kinetic to potential energy by means of  $wT' < 0$ . Vastly more kinetic energy is removed by  $wT'$  than ever reaches dissipation scales to appear as  $\epsilon$ . Hence  $K_v \gg \epsilon N^{-2}$ . This is the theory alluded to previously. Immediately we can ask where all that energy has gone. Why doesn't it turn up as an enormous dissipation rate  $\chi$  for  $T'^2$ ? Here again the theory (Weinstock, 1985) has ready answers: the triple correlations in the  $T'^2$  equation do *not* transfer  $T'$  fluctuations from large to small scales but rather go just the other way, pumping  $T'$  fluctuations up to ever larger scales. (What happens to  $T'$  at the larger scales is then someone else's department.) The result is that most velocity variance that starts out at large scales never gets down to  $\epsilon$  while  $T'^2$  gets sent back out to large scales with only a little going on down to  $\chi$ . Therefore one can have huge  $K_v$  with hardly any  $\epsilon$  or  $\chi$ . Is that crazy? Or it just doesn't "feel" right? Maybe so. But if we don't want to do science by "feels good", then we would have to make arguments based on dynamics to disprove the theory or else go and observe  $K_v$  somehow.

## Theory Number Two

This is the theory usually termed "Saturation", following Fritts (1984) or Dewan and Good (1986). Here I'll be especially brief insofar as I don't very well understand this idea. The reader is better advised to turn to Fritts' contribution in these proceedings. My perception is that one considers various models of mechanisms that may limit internal wave amplitude, leading to breaking and dissipation. No matter which particular mechanism is considered, so long as  $N$  is the only dimensional parameter that one permits, any resulting energy spectrum must have the form  $N^2k^{-3}$ . As well, so long as one has a reasonably plausible "breaking" scenario in mind, a coefficient in front of  $N^2k^{-3}$  will tend to be some fraction of unity, whether individual waves "saturate" or if it is more of a collective phenomenon. At some sufficiently high wavenumber, more nearly classical turbulence of  $\epsilon^{2/3}k^{-5/3}$  kind takes over, implying a transitional wavenumber near  $k_b$ . Velocity and temperature spectra are both expected to follow the same rules. Indeed this appears to agree with observed spectra in both the ocean and atmosphere. The advantage of this approach is that one is not compelled to treat the large scale waves as if they are "turbulent". In particular, one is not obliged to expect enormous  $wT'$  dominating the  $k^{-3}$  subrange. On the other hand, to my limited perception I don't know what to expect for  $wT'$  depending on which particular wave "breaking" model one chooses from among a variety that are tolerably consistent with the observed spectra. Maybe  $K_v = 0.2\epsilon N^{-2}$  is just right. It's hard to say.



What I find disturbing is that the "turbulence" appears to be only stuck onto the end of the "saturation" range; it would be nice if the theory actually *put* it there. As well, if the idea of "saturation" is that wave breaking (*i.e.*, overturning?) governs the entire  $k^{-3}$  subrange, then one might expect to observe overturns of several meters height in the typical open ocean internal wave field with overturns of several km in the middle atmosphere. These are not usually observed, I think. Nonetheless, "Saturation" appears to be an idea that is consistent with observed spectra and which admits (but does not confidently predict?) that  $K_v$  may be related to  $\varepsilon$  or  $\chi$  in about the ways that are commonly assumed.

### Theory Number Three

The best theory, only coincidentally due to Holloway (1983), doesn't have any special label. (*Well intended* reader suggestions are welcome. I like simply "Best".) The underlying premise is that energy (both kinetic and available potential) somehow gets into the ocean at large scales. How that energy gets there is "someone else's department". "Large" means at least hundreds of meters or kilometers or more. Then, by wave-wave interaction, those large scale reservoirs of energy are transferred down to shorter scales and so on to dissipation. I don't use the label "turbulent" at any stage because that seems to connote some different kind of dynamics. Simply, wave-wave interactions may be relatively weak at large scales (in a sense of interaction time long compared with wave period) while gradually becoming stronger at smaller scales (interaction times shorter than wave periods). The motivation is to retain one overall view of fluid dynamics without getting involved in delicate *ad hoc* procedures for somehow separating motions into their "turbulent" and "nonturbulent" parts. Why do that anyway? (I think this crutch only frustrates quantitative theory.) If there are scales of motion at which nonlinear interactions are much faster than wave periods--or perhaps we elect to consider neutrally stratified flow, hence without wave periods--then one might like to call the motion "turbulent". Only we may wish that such "turbulence" simply result as a limiting case of more general "wave-wave" interaction theory. At the limit of weak interaction, we may hope to approach resonant wave interaction theory in the sense of Hasselman (1962). Formalism to accomplish such unified treatment has been developed in Kadomtsev (1965) and in Holloway (1979).

Actually to carry out this formalism for a system of internal gravity waves + vortical modes has not been done to date, so far as I know. (Only as an exercise, the formalism was evaluated in two dimensional (vertical planar) geometry, without vortical modes, as reported in Holloway, 1988.) Nonetheless, without actually carrying out the fully three-dimensional calculation, one can roughly "guess" how it might come out. Very simply we only suppose a transfer  $\varepsilon(k)$  of kinetic energy from wavenumbers  $<k$  to wavenumbers  $>k$ , likewise with transfer  $\chi(k)$  of available potential energy also from  $<k$  to  $>k$ . Conjecturing that this transfer depends locally in  $k$  upon the shape of the energy spectrum  $E(k)$ , the implication is

$$\varepsilon(k) = - \mu^2 \theta k^{r+1} \partial^r E / \partial k^r \quad (5)$$

where  $\mu(k)$  is a nonlinear interaction rate (yet to be determined), while the "waves"- "turbulence" character enters only through the parameter

$$\theta(k) = \mu / (\mu^2 + N^2) \quad (6)$$

The form for  $\theta(k)$  follows more careful theory from Holloway (1979) but is grossly abbreviated for purpose of tractability in the present context. Then the rest of Eq. (5) is required from dimensional consistency. Interestingly, one can pick any value of  $r$  that one likes (even fractional values!)--it won't matter to the outcome. We are left only to address  $\mu(k)$ . The argument that I offer is that the role of nonlinearity is to support energy transfer across the spectrum--whether that be "wavelike" or "turbulent". Since  $\epsilon(k)$  is such a transfer, a local scaling hypothesis and dimensional consistency oblige

$$\mu(k) = \epsilon^{1/3} k^{2/3} \quad (7)$$

Substituting Eq. (6) and (7) into Eq. (5), resulting  $E(k)$  is just as Eq. (4). *Again!* Order unity coefficients  $A$  and  $B$  would enter due to the imprecision of "equalities" (5), (6) and (7). The same arguments apply to the available potential energy (or temperature variance) equation, likewise producing spectra that are indistinguishable from what is observed. However, the key to Theory Number Three ("Best") is that buoyancy flux plays *no dynamically significant role* at all--precisely the opposite of Theory Number One ("Buoyancy Subrange"). Thus "Best" is entirely consistent with  $K_v = 0$ , hence certainly with  $K_v \ll \epsilon_0 N^{-2}$ . As well, "Best" is entirely consistent with larger scale motion appearing to be dominantly "wavelike", since it is just wave-wave interactions that support transfer  $\epsilon(k)$ . Unlike Theory Number Two ("Saturation"), "Best" naturally includes the "turbulent" spectrum in  $k > k_b$ . As well, "Best" doesn't imply overturning on height scales characteristic of the  $k^{-3}$  range.

## LABORATORY EVIDENCE

If we are unable to decide among the Three Theories just mentioned on a basis either of dynamical reasoning or of field observation, perhaps laboratory experiments offer the alternative approach. Focusing on the question of turbulent mixing in stably stratified fluids, possible laboratory approaches might consist of forcing a stably stratified fluid through a grid, e.g., as Itsweire *et al.* (1986), or dropping a grid through a stably stratified fluid as Dickey and Mellor (1980), or in a way such as described in these proceedings by Fernando. Another approach is to excite internal waves to the point of breaking, as McEwan (1983). With respect to the ocean--and to the numerical modeling thereof--the question we must ask of each of these laboratory experiments is "To what extent are the lab results dependent upon the particular mechanism of forcing?" It would be nice to think that there's something "universal" about small scale turbulence, so that how it gets there is largely irrelevant. However, there's not a good argument (so far as I know) why that should be so; and there is numerical experimental indication (Holloway, 1988) that the nature of buoyancy flux is strongly dependent upon the nature of forcing even when velocity and buoyancy variance spectra are quite similar. So we are cautioned: Are the lab results applicable to open ocean turbulence? Surely the grid turbulence experiments *are* applicable to sites where one drops or drags a large grid through the ocean; but what about the rest? Perhaps the experiments that may appear most directly applicable are the internal wave breaking studied by McEwan.

Here let me recall only very briefly the experiments of McEwan, referring the interested reader to the full published account (McEwan, 1983). In his experiments, McEwan gently excited internal waves in a continuously stratified fluid by means of a sidewall paddle. Energy input by the paddle could be carefully calculated; likewise energy loss to

frictional boundary layers on the walls was estimated. When the waves became sufficiently steep, intermittent spilling was observed, resulting in localized turbulent patches that McEwan terms "traumata". It seems to me that this provides a very plausible picture appropriate to what may lead to mixing events in the ocean interior or in the middle atmosphere. Therefore let us look more closely at the outcome and interpretation of the experimental results.

After some number of traumata were observed, and the sidewall forcing was stopped, the fluid settled down. Then density profiling allowed a calculation of the overall work against gravity by raising the center of mass (CM). Having estimated energy input to the tank and energy loss to friction at the tank walls, one could estimate what fraction of internal wave energy was expended by irreversible buoyancy flux on account of the traumata. The fraction turned out to be 0.23, very happily in agreement with the values of  $\gamma$  or  $R_f$  mentioned previously, considering the uncertainty in all such things. Evidently this is not  $\gamma \gg 1$  according to Theory Number One, but neither would the lab experiment develop nearly the range of scales over which a buoyancy subrange would develop. The lab experiments seem to me to be broadly consistent with Theory Number Two, at least at the descriptive level since questions of spectral shape are not accessible in these experiments. Can we, however, rule out Theory Number Three ("Best") ? Apparently the traumata do yield  $\gamma$  which are some significant fraction of unity.

An observation needs to be made about the outcome (and interpretation thereof) from these experiments. Were the traumata in fact making any net conversion from kinetic to potential energy? Clearly, after the experiment has completed, some fluid has been mixed and the CM is raised by about 1/4 of the energy supplied to the wave field. *How* was that CM raised? In fact it must have been raised well in advance of any traumata at all. The sidewall paddle, while putting energy into the fluid through pressure-velocity work, *c.f.* Eq. (2) and (3), excited an internal *gravity wave* field, with frequencies sufficiently above  $f$  that one may suppose kinetic : potential energy equipartition. (Some vortical kinetic energy was surely excited as well, although one guesses from the manner of forcing that this part would have been quite small.) So we have approximately that 1/2 of the input energy was present as elevated CM before any wave breaking at all. Then, after traumata, mixing and settling down, only 1/4 of input energy is left in elevated CM. It therefore seems to me that the actual traumata (*i.e.* localized regions of overturning, disturbed flow) may have been more nearly involved with mass *falling down*--although this did lead to thermodynamic mixing which eventually shows up in the elevated CM of the fluid. However, if one had been able to calculate buoyancy ("heat") flux  $wT'$  over the regions of traumata, my guess is that would have turned out to be counter-gradient (*i.e.* upward or restratifying). Hence  $\gamma < 0$  or, if one imagined representing traumata as subgrid-scale to a coarsely resolved model,  $K_v < 0$  !

#### PUTTING IT ALL TOGETHER

When results are as confusing--and perhaps frustrating--as all of the above, one must ask if a more sensible person would just step back and think "How *could* an ocean work really?" If a theory such as "Best" even admits the possibility that internal wave breaking might yield systematically counter-gradient  $wT'$ , isn't that immediately and obviously silly--if one *thinks* about it? Let's see. Figure 1 is only a free hand sketch. At some large scale, systematic differences in windstress curl induce differential Ekman pumping. We may imagine the contrast between subtropical and subpolar gyres, or

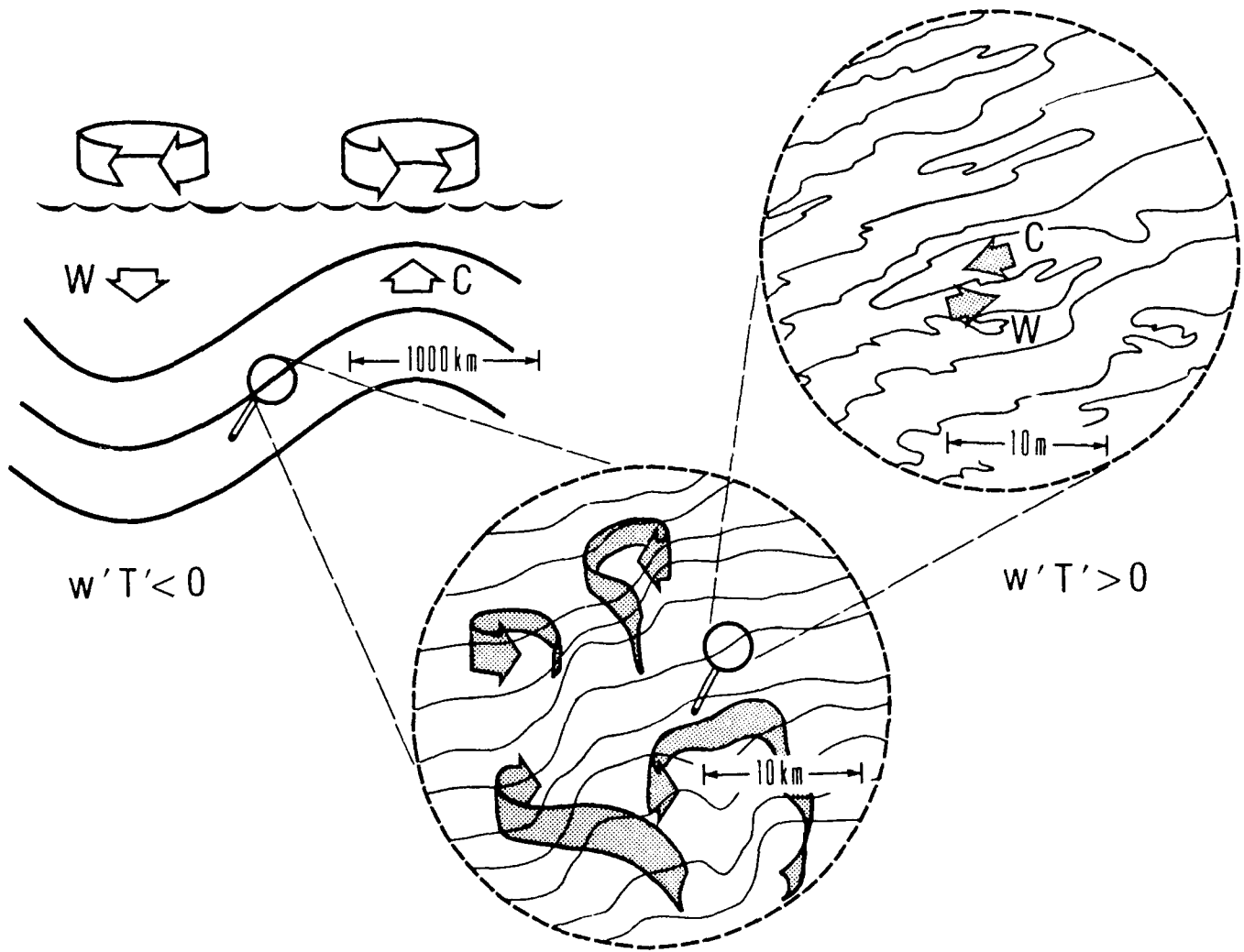


Figure 1. A sketch depicts processes in a hypothesized ocean.

perhaps only consider transient weather. In many circumstances (though not invariably so), downwelling occurs over regions of relatively warmer water while upwelling pumps cooler water. The main thermocline is deformed. Zooming to somewhat smaller scales, eddies further deform the thermohaline features. Here, while we're only going Sacred Cows anyway, let's hypothesize that eddies stir predominantly in the horizontal (level  $z$ ) rather than along mean isopycnals. (In truth, the one hypothesis seems fully as reasonable to me as the other, with some "half-way" hypothesis perhaps even better.) Quasi-random straining by the eddy field acts to generate variance of the local slopes of isopycnals.

Zooming to yet smaller scales, we encounter internal wave breaking: heavier water being spilled over patches of lighter water. Here it is supposed to be obvious that lifting up heavy water while plunging down the lighter water, one must clearly perform work against gravity. *Everyone* knows that! Only maybe I didn't draw the sketch so well because it *looks* as if the scales of internal wave breaking sustain mean  $wT' > 0$ , i.e. gravitational energy is being *released*. Again, Figure 1 is only a free hand sketch. Surely I don't know whether the ocean works this way.

A query is to the reader: Can you see why the ocean *cannot* work this way? Perhaps there is one answer: Simply, the ocean cannot work this way because none of the models work this way! If the large scales with their Ekman pumping and main thermocline shape are resolved, and if eddies are resolved or maybe even parameterized as simple horizontal (level  $z$ ) "eddy diffusion", then should we be obliged to put in  $K_v < 0$  for our vertical subgrid-scale parameterization?

To close, let us reconsider briefly the question of appropriate field observations. The main thrust of this note has been to argue that we have no dynamical basis for believing that dissipation observations are related in any simple way to ocean mixing. Three different theories have been found to agree quite adequately with observed small scale spectra while admitting grossly different implications for vertical transport. Apparently we need to observe that transport directly. The instrument Moum has described offers one approach to measuring  $wT'$  directly, out to scales of a meter or more until the vehicle motion becomes a problem. Although initial test results are from regions chosen for their higher turbulence levels, hence greater likelihood of an observable and (presumably!) down-gradient transport, for now we can only speculate whether the ambient open ocean may yield ambiguous or even counter-gradient results--especially if one entertains a picture such as Figure 1. On the other hand, there are already Ledwell's tracer release results from Santa Monica Basin. There the stuff *did* flux down-gradient under conditions of a tolerably gentle ocean environment. Surely this refutes Figure 1, doesn't it?

#### ACKNOWLEDGMENTS

Crystal Miles and Peter Müller made this workshop both delightful and stimulating. I am grateful to the Office of Naval Research which sponsored this engaging workshop and to the National Science Foundation which supported the preparation of this article. Patricia Kimber provided the artwork for Figure 1. Trevor McDougall offered helpful, critical comment.

## REFERENCES

- Dalaudier, F. and C. Sidi : 1987. Evidence and interpretation of a spectral gap in the turbulent atmospheric temperature spectra. *J. Atmos. Sci.*, 44, 3121-26.
- Dewan, E. M. and R. E. Good : 1986. Saturation and universal spectrum for vertical profiles of horizontal scalar winds in the atmosphere. *J. Geophys. Res.*, 91, 2742-48.
- Dickey, T. D. and G. L. Mellor : 1980. Decaying turbulence in neutral and stratified fluids. *J. Fluid Mech.*, 99, 13-31.
- Fritts, D. C.: 1984. Gravity wave saturation in the middle atmosphere: a review of theory and observations. *Rev. Geophys. Space Phys.*, 22, 275-308.
- Gargett, A. E., P. J. Hendricks, T. B. Sanford, T. R. Osborn and A. J. Williams III : 1981. A composite spectrum of vertical shear in the upper ocean. *J. Phys. Oceanogr.*, 11, 1258-71.
- Gregg, M. C.: 1977. A comparison of fine-structure spectra from the main thermocline. *J. Phys. Oceanogr.*, 7, 33-40.
- Gregg, M. C.: 1987. Diapycnal mixing in the thermocline: a review. *J. Geophys. Res.*, 92, 5249-86.
- Hasselmann, K.: 1962. On the nonlinear energy transfer in a gravity spectrum. Part 1. General theory. *J. Fluid Mech.*, 12, 481-500.
- Holloway, G.: 1979. On the spectral evolution of strongly interacting waves. *Geophys. Astrophys. Fluid Dyn.*, 11, 271-287.
- Holloway, G.: 1983. A conjecture relating oceanic internal waves and small scale processes. *Atmos.-Ocean*, 21, 107-122.
- Holloway, G.: 1988. The buoyancy flux from internal gravity wave breaking. *Dyn. Atmos. Oceans*, 12, 107-125.
- Itsweire, E. C., K. N. Helland and C. W. Van Atta: 1986. The evolution of grid generated turbulence in a stably stratified fluid. *J. Fluid Mech.*, 162, 299-338.
- Kadomtsev, B. B.: 1965. *Plasma Turbulence*. London: Academic. 149 pp.
- Kolmogorov, A. N.: 1941. The local structure of turbulence in an incompressible viscous fluid for very large Reynolds numbers. *C. R. Akad. Nauk, SSSR*, 30, 301-305.
- Lilly, D. K., D. E. Waco and S. I. Adelfang: 1974. Stratospheric mixing estimated from high-altitude turbulence measurements. *J. Applied Meteorology*, 13, 488-493.
- Lumley, J. L.: 1964. The spectrum of nearly inertial turbulence in a stably stratified fluid. *J. Atmos. Sci.*, 21, 99-102.
- McEwan, A. D.: 1983. Internal mixing in stratified fluids. *J. Fluid Mech.*, 128, 59-80.
- Oakey, N. S.: 1982. Determination of the rate of dissipation of turbulent energy from simultaneous temperature and velocity shear microstructure measurements. *J. Phys. Oceanogr.*, 12, 256-271.
- Osborn, T. R. and C. S. Cox: 1972. Oceanic fine structure. *Geophys. Fluid Dyn.*, 3, 321-345.
- Osborn, T. R.: 1980. Estimates of the local rate of vertical diffusion from dissipation measurements. *J. Phys. Oceanogr.*, 10, 83-89.
- Weinstock, J.: 1985. On the theory of temperature spectra in a stably stratified fluid. *J. Phys. Oceanogr.*, 15, 475-477.

## PARAMETERIZATION OF SMALL-SCALE PROCESSES

Peter Müller

Department of Oceanography and Hawaii Institute of Geophysics  
University of Hawaii, Honolulu, HI 96822

Greg Holloway

Institute of Ocean Sciences, Sidney, BC V8L 4B2

Oceanic general circulation models must parameterize the effect of subgrid-scale motions and generally do so with diffusion terms. The questions then arise:

- do oceanic observations allow inferences about mixing and diffusion coefficients; if so,
- how do "observed" coefficients compare with those used in numerical models;
- can mixing rates be predicted from an understanding of the processes involved; and finally,
- does it matter? Are the results of numerical models sensitive to the choice of the diffusion coefficients?

To discuss these and related questions the fifth 'Aha Huliko'a Hawaiian Winter Workshop brought together numerical modelers, theoreticians, and small-scale observers. The focus was on general circulation models, both coarse resolution and eddy resolving, and on the diapycnal or vertical mixing caused by small-scale turbulence. The overall conclusions that emerged from the lectures and discussions are:

- Oceanic fine- and microstructure measurements do not determine mixing rates unambiguously. Direct flux measurements are needed.
- Diffusion coefficients in numerical models must often be chosen for numerical stability rather than physical reasons.
- Prediction of mixing rates is hampered by a wide range of unsolved issues: the diffusion concept, conservation of potential vorticity, horizontal versus isopycnal mixing, interior versus boundary mixing, and the rate control of mixing.
- Yes, numerical models are sensitive to the way subgrid-scale processes are parameterized, but systematic exploration of the parameter space is complicated by implicit diffusion, computational modes, and the delicately tuned state of the models.

This report elaborates on these conclusions and highlights major difficulties.

## OCEANIC CIRCULATION MODELS

*Coarse resolution models.* The development of computers provided a tool for physical oceanographers which was quickly applied to modeling the oceanic general circulation. Through experimentation with various numerical schemes and parameter choices, the numerical modeling community has arrived at a set of standard coarse resolution oceanic general circulation models (OGCMs). These models typically have a spatial resolution of a few degrees and therefore must parameterize mesoscale eddies and smaller scale motions. OGCMs reproduce many of the features of the general circulation. However, the models have to use very large diffusion coefficients in order to assure numerical stability. Details of the circulation therefore cannot be resolved and all the major fronts (e.g., the Gulf Stream and the permanent pycnocline) are too broad. The models are too diffusive, and do not allow any inertial enhancement or recirculation.

Numerical modelers have not yet (for reasons discussed below) explored the sensitivity of OGCMs to the values of the diffusion coefficients in a thorough systematic manner. The few sensitivity studies that have been carried out do show that OGCMs are sensitive to the diffusion coefficients. The standard OGCMs use a lateral momentum diffusion coefficient larger than the lateral heat diffusion coefficient. The resulting meridional circulation consists of downwelling in polar convection regions and a broad upwelling in the Sverdrup interior. Reducing the momentum diffusion changes this circulation completely with upwelling occurring primarily in the western boundary current. A narrow boundary current, required by vorticity dynamics, can only support a large transverse heat flux by upwelling (W. Holland, National Center for Atmospheric Research, Boulder, CO).

OGCMs are also sensitive to the diapycnal heat diffusivity. The poleward heat flux increases by an order of magnitude when the diffusivity is changed from  $0.1$  to  $2.5 \cdot 10^{-4} \text{ m}^2 \text{ s}^{-1}$  (F. Bryan, National Center for Atmospheric Research, Boulder, CO, Figure 1). Surprisingly, OGCMs are less sensitive to the vertical dependence of the diapycnal diffusivity. A reversal of the deep thermohaline circulation, anticipated for a coefficient inversely proportional to the buoyancy frequency, is not observed (A. Gargett, Institute of Ocean Sciences, Sidney, British Columbia) since the vertical advective-diffusive balance is not valid. Furthermore, explicit diapycnal mixing is overridden in some areas by implicit diapycnal mixing due to horizontal diffusion across sloping isopycnals. Decreasing the horizontal diffusion coefficient sometimes enhances this effect.

Sensitivity studies, insightful and desirable as they are, are difficult to perform and interpret:

- Diffusion sensitivity studies are complicated by the fact that some of the numerical algorithms for approximating the advection operator contain *implicit* diffusion terms. A central difference scheme with explicit diffusion, an upwind scheme with no explicit (but implicit) diffusion, and a flux corrected transport scheme all result in different thicknesses of the thermocline and different magnitudes of the abyssal circulation (R. Gerdes, Princeton University, Princeton, NJ).



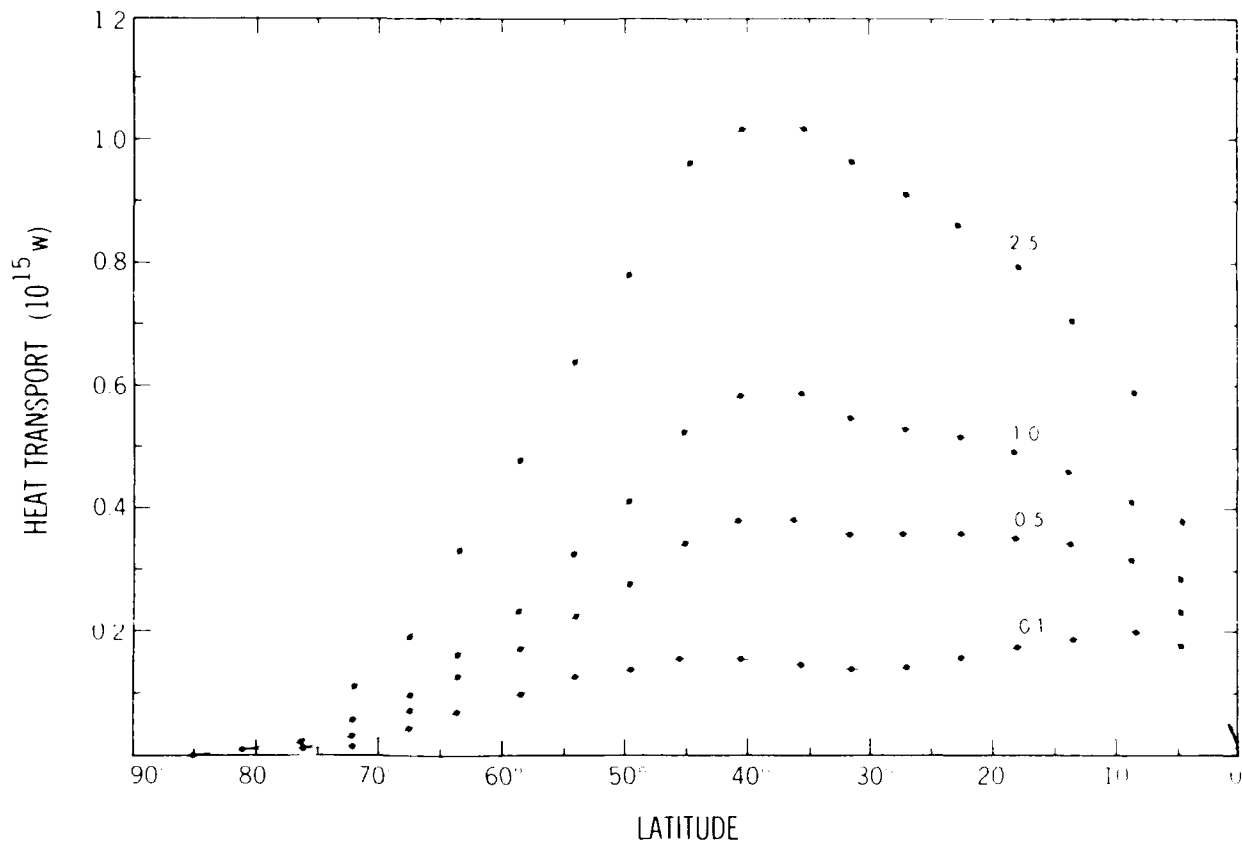


Fig. 1. Poleward heat transport in a coarse resolution general circulation model as a function of latitude for various values of the vertical diffusivity ranging from  $0.1$  to  $2.5 \cdot 10^{-4} \text{ m}^2 \text{ s}^{-1}$ . From Bryan (1987).

- If diffusion coefficients are lowered such that advection becomes dominant, then numerical schemes start to produce "computational modes" with local extrema (in violation of the second law of thermodynamics). These computational modes might arise in unexpected places. In a particular model run, local temperature minima appear in the ocean interior which are caused by a computational mode in the convection region of the model. The usual signature of the mode is, however, masked by the convective adjustment scheme used in that model (P. Killworth, Hooke Institute for Atmospheric Research, Oxford, UK).
- The parameter space of OGCMs is multidimensional. Changing one parameter affects many aspects of the models. Furthermore, the models are in such a finely-tuned balance that small parameter changes might completely upset their performance. For these reasons potential users were warned not to regard OGCMs as black boxes whose inner workings need not be understood in order to perform sensitivity studies.

*Eddy resolving models.* With the availability of ever more powerful computers, efforts are under way to resolve the mesoscale eddy field and study its effects explicitly. These high resolution, eddy resolving general circulation models (EGCMs)

can use smaller diffusion coefficients because they have to parameterize less of the eddy field. A state-of-the-art model (a component of the World Ocean Circulation Experiment's Community Modeling Effort) is a primitive equation model of the Equatorial and North Atlantic at  $1/3$  degree resolution (F. Bryan and W. Holland, Figure 2). The model reproduces dynamical details of the circulation and eddy field extremely well, including such phenomena as the deep recirculation under the Gulf Stream.

- At present EGCMs require so much computing power that they cannot be integrated long enough to study the large-scale thermodynamically driven circulation and the distribution of water masses and tracers.

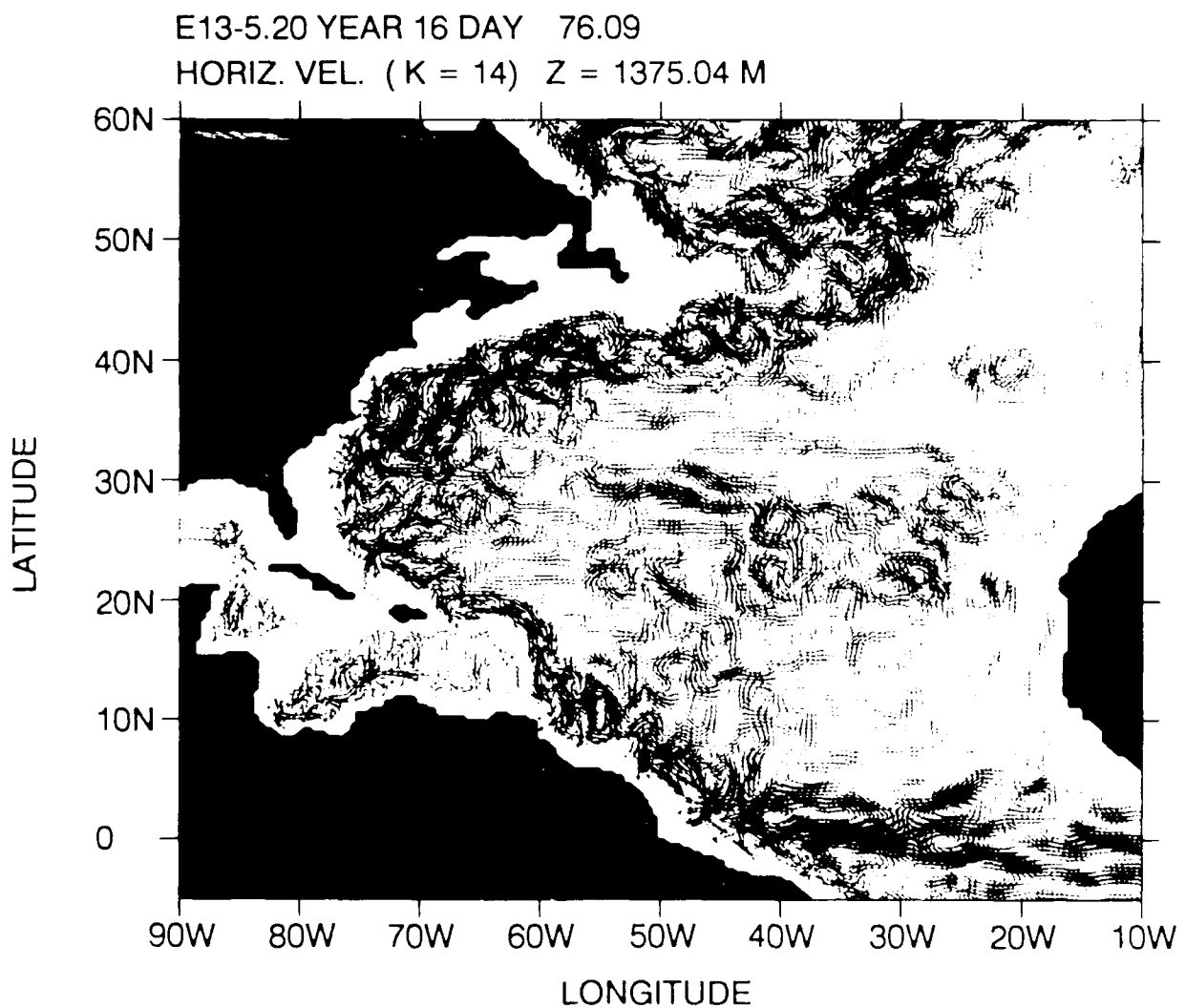


Fig. 2. WOCE community model. Map of the instantaneous horizontal velocity field at 1375 m depth after 16 years of integration. Note the rich and detailed structure of the field. Courtesy of F. Bryan and W. Holland.

- Systematic sensitivity studies with respect to diffusion coefficients, forcing fields and numerical algorithms, are also beyond present computing capabilities.

However, longer integrations and sensitivity studies will become feasible once more powerful computers are available. Nevertheless, coarse resolution models will remain the main tool in many research areas, notably climate research. A more troubling consequence of EGCN experiments then is:

- EGCNs show that mesoscale eddies play an important role in the dynamics of the general circulation and that this role is complex and cannot be parameterized in terms of simple diffusion coefficients. The effect of mesoscale eddies is hence incorrectly parameterized in coarse resolution models and it is unclear what can be inferred from sensitivity studies carried out with these coarse models.

## OBSERVATIONS OF DIAPYCNAL MIXING

Diapycnal diffusion coefficients have been inferred primarily from oceanic dissipation measurements and from inverse calculation.

*Dissipation measurements.* The development of fine- and microstructure instruments and their deployment in major experiments is leading to a quantitative characterization of small-scale fields and parameters. The dissipation rates of kinetic energy and temperature variance are the primary means of inferring the vertical buoyancy flux and hence the vertical or diapycnal diffusivity. The observed microstructure is interpreted as being caused by internal wave breaking or double diffusive processes.

Results from six experiments suggest that the kinetic energy dissipation rate in the main thermocline is proportional to the buoyancy frequency squared and to the 10 m vertical internal wave shear to the fourth power (M. Gregg, University of Washington, Seattle, WA, Figure 3). The inclusion of the shear scaling reduces the observed variability from a factor 58 to a factor 2. This scaling has also been found with eikonal and resonant interaction calculations of the internal wave energy flux to high wavenumbers. When the observed shear matches the Garrett and Munk level, the scaling implies a vertical diffusivity of  $5 \cdot 10^{-6} \text{ m}^2 \text{ s}^{-1}$ , independent of depth and smaller than Munk's (1966) abyssal recipe value of  $10^{-4} \text{ m}^2 \text{ s}^{-1}$ .

Double diffusive salt-fingering might also be coupled to the internal wave field. There are indications that the wave shear creates finestructure in the density ratio and therefore modulates the growth rate and flux of salt fingers (R. Schmitt, Woods Hole Oceanographic Institution, MA).

The interpretation of dissipation measurements is, however, not straightforward:

- The relation between vertical buoyancy flux (or vertical diffusivity) and the dissipation rate of temperature variance or kinetic energy depends on various efficiency, homogeneity, isotropy and intermittency assumptions that are not well justified and are the subject of controversies. There is the even more

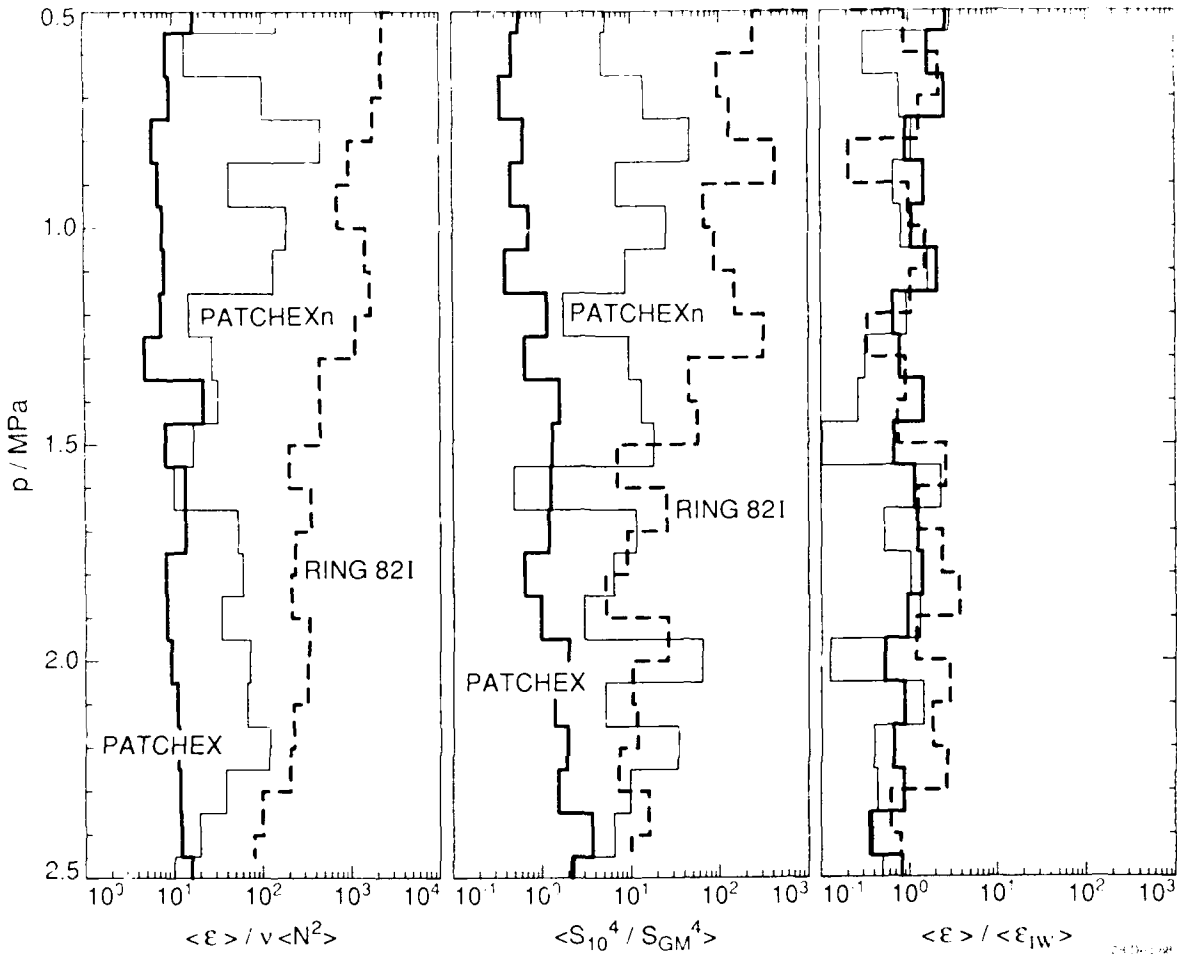


Fig. 3. Comparison of three different mid-latitude sites: PATCHEX, PATCHEXn, RING82I. The three panels show, as a function of pressure, the dissipation rate  $\epsilon$  normalized by the buoyancy frequency  $N$ , the 10 m vertical shear  $S$  normalized by the 10 m shear of the Garrett and Munk model, and the dissipation rate normalized by buoyancy frequency and shear. Note that the shear scaling greatly reduces the large differences when  $\epsilon$  is scaled only by  $N$ . Courtesy of M. Gregg.

troubling suggestion that dissipation measurements might not even provide an upper bound for the diffusivity. Different theories, each consistent with dynamics as far as we understand at present, admit a range of possibilities from zero (or even negative) diffusion up through arbitrarily large diffusion while reproducing the observed velocity and temperature spectra within observational uncertainty (G. Holloway, Institute of Ocean Sciences, Sidney, British Columbia). For example, a downward buoyancy flux, which converts kinetic to potential energy, might exist without any dissipation, if the generated potential energy is cascaded up-scale to low wavenumbers.

- The measured dissipations can be generated by breaking internal waves, or by salt-fingering, if the stratification is double-diffusively unstable. Salt fingers

diffuse salt and heat at different rates than the turbulence caused by breaking internal waves. Interpretation of dissipation measurements requires identification of the mechanism at work.

- Estimates of diffusion coefficients also depend on the assumed underlying statistical distribution of measured parameters. The analysis of rapidly repeated CTD profiles showed that the vertical strain is lognormally distributed. Therefore, the mean, median and most probable values differ widely. The mean strain is made up of very few high strain "events" or, as it was put succinctly: "Isopycnals avoid the water" (R. Pinkel, Scripps Institution of Oceanography, La Jolla, CA).

Direct flux measurements are needed. They have been attempted by measuring the vertical velocity-temperature correlation, inferring the vertical velocity from the dynamic pressure via Bernoulli's theorem (J. Moum, Oregon State University, Corvallis, OR). Preliminary results from the upper ocean indicate that the scales of the buoyancy flux are in the decimeter range while the dissipation scales are in the centimeter range. Mixing coefficients can also be directly inferred from the diffusion of artificial tracers released into the ocean (J. Ledwell, Lamont-Doherty Geological Observatory, Palisades, NY). The two such releases, one in the Santa Monica and one in the Santa Cruz Basin, suggest diapycnal diffusivities of approximately  $3 \cdot 10^{-5} \text{ m}^2 \text{ s}^{-1}$  and  $10^{-4} \text{ m}^2 \text{ s}^{-1}$ , respectively.

*Inverse methods.* Diffusion coefficients can also be inferred from large-scale hydrographic and tracer data using inverse methods. Applying the "beta-spiral" method to Southern Ocean data, unexpectedly large values of the diapycnal heat diffusivity ( $10^{-3} \text{ m}^2 \text{ s}^{-1}$ ) are found in the Antarctic Circumpolar Current (D. Olbers, Alfred Wegener Institute for Polar and Marine Research, Bremerhaven, West Germany, Figure 4). These values are nearly two orders of magnitude larger than the currently accepted values of about  $10^{-5} \text{ m}^2 \text{ s}^{-1}$  for the mid-latitude main pycnocline.

Although inverse methods are an important complement to the direct dissipation measurements, they are limited.

- The inverse problem is often ill-conditioned and care must be taken to avoid unreliable results.
- More importantly, the estimated diffusion coefficients are those needed to "explain" large-scale smoothed hydrographic data. The relation of these coefficients to those inferred from small-scale measurements, which are the ones needed to "explain" the actual instantaneous ocean state, is unclear. EGCMS might elucidate this relation if diffusion coefficients inferred from the averaged circulation by inverse methods were compared with those used to run the model.

## LABORATORY AND ATMOSPHERIC FLOWS

Because of the tremendous difficulties in making direct measurements, help is being sought from laboratory experiments and atmospheric observations.

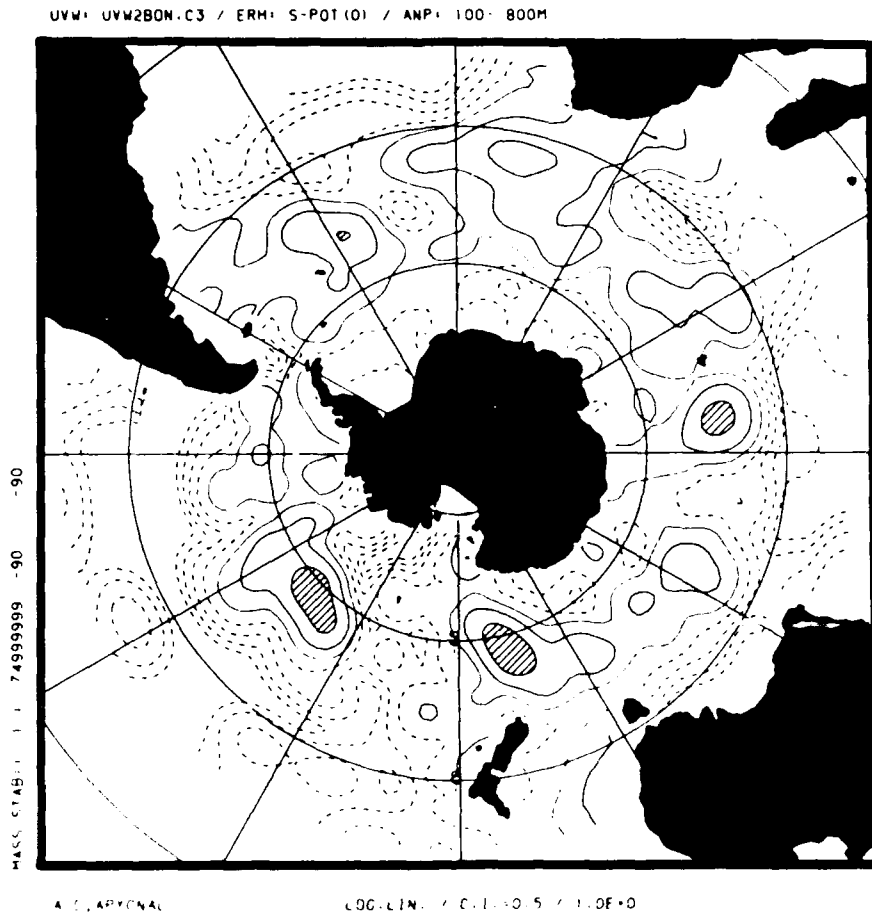


Fig. 4. Diapycnal diffusivity in the Antarctic Circumpolar Current for the depth range from 100 to 800 m, as inferred from beta-spiral calculations. Contours are logarithmically spaced with interval 0.5. Contours which are larger than  $10^{-4} \text{ m}^2 \text{ s}^{-1}$  are full. Areas with values larger than  $10^{-3} \text{ m}^2 \text{ s}^{-1}$  are shaded. Courtesy of D. Olbers.

*Laboratory experiments.* Unlike the ocean, the laboratory allows the study of isolated processes in detail and a fairly complete visualization of the flow field. Hence laboratory experiments have been the major source for identifying processes and building intuition. Laboratory work on mixing across density surfaces with and without shear and across double diffusively unstable interfaces has provided many of the parameters and efficiency factors used in the interpretation of oceanic measurements (H. Fernando, Arizona State University, Tempe, AZ), though more work is needed, especially on stratified shear flows. Furthermore, laboratory results are not always directly applicable to the ocean:

- The source of turbulence in the laboratory is often grid stirring whereas mixing in the ocean interior is assumed to be caused by sporadic internal wave breaking.
- Laboratory experiments may not be able to reproduce all the non-dimensional parameter values of the ocean.

Laboratory flows also provide an analogue to large scale geophysical flows. An experiment, designed to study the driving of a stratified fluid by bottom Ekman layers in a bowl-shaped container, revealed a startling difference between the spin-up and spin-down phase of the experiment (P. Rhines, University of Washington, Seattle, WA) with the bottom Ekman layer becoming unstable in the spin-down phase. This experiment questions our conventional wisdom about Ekman layers on sloping surfaces and their parameterization by bottom friction coefficients.

*Atmospheric measurements.* Both in the ocean and atmosphere the internal gravity wave field is assumed to play a role in the transport of momentum and heat. There are, however, important differences:

- In the atmosphere, there are clearly identified sources and sinks for the internal gravity wave field. The waves are believed to be generated primarily as lee or mountain waves by mean flows passing over topography, and by convection and wind shear. As they propagate upwards they rapidly increase their amplitude (due to decreasing density) and break near the tropopause and throughout the middle atmosphere. The waves hence show a strong up-down asymmetry and are short-lived, on the order of a few hours (D. Fritts, University of Alaska, Fairbanks, AK). In the ocean, a nearly universal, horizontally isotropic and vertically symmetric wave field is observed, with no single clearly identifiable source or sink and a lifetime on the order of 100 days.
- In the atmosphere, the major role of internal gravity waves is momentum transport. The waves transport momentum from source regions, primarily in the lower atmosphere, to levels at which the waves undergo dissipation, accelerating or decelerating the mean flow there. Indeed, incorporation of momentum transport by mountain waves (in parameterized form) considerably improves the climatology of an atmospheric general circulation model (N. McFarlane, Canada Climate Centre, Downsview, Ontario, Figure 5). In the ocean, momentum transfer from the wave field to the mean flow is regarded as small. Mixing of heat, salt and other tracers induced by breaking waves is the major concern.
- In the atmosphere, the wave spectrum is viewed as a saturation spectrum. Each wave component propagates upwards, reaches its critical amplitude, and breaks. The oceanic view is that breaking occurs as the result of a random superposition of many subcritical waves and that energy is cascaded down the spectrum to the dissipation scales by wave-wave interactions.

## THE MAJOR ISSUES

Despite all the information about diapycnal mixing provided by direct and indirect observations in the ocean, laboratory and atmosphere, several basic issues remain unresolved.

*Diffusion concept.* Oceanic general circulation models parameterize subgrid-scale mixing processes by diffusion terms. This concept requires, among other things, a scale separation between the "turbulence" that does the mixing and the mean properties that are being mixed (F. Henyey, Areté Associates and La Jolla Institute, La Jolla, CA). It is unclear to what extent such a scale-gap exists in the ocean.

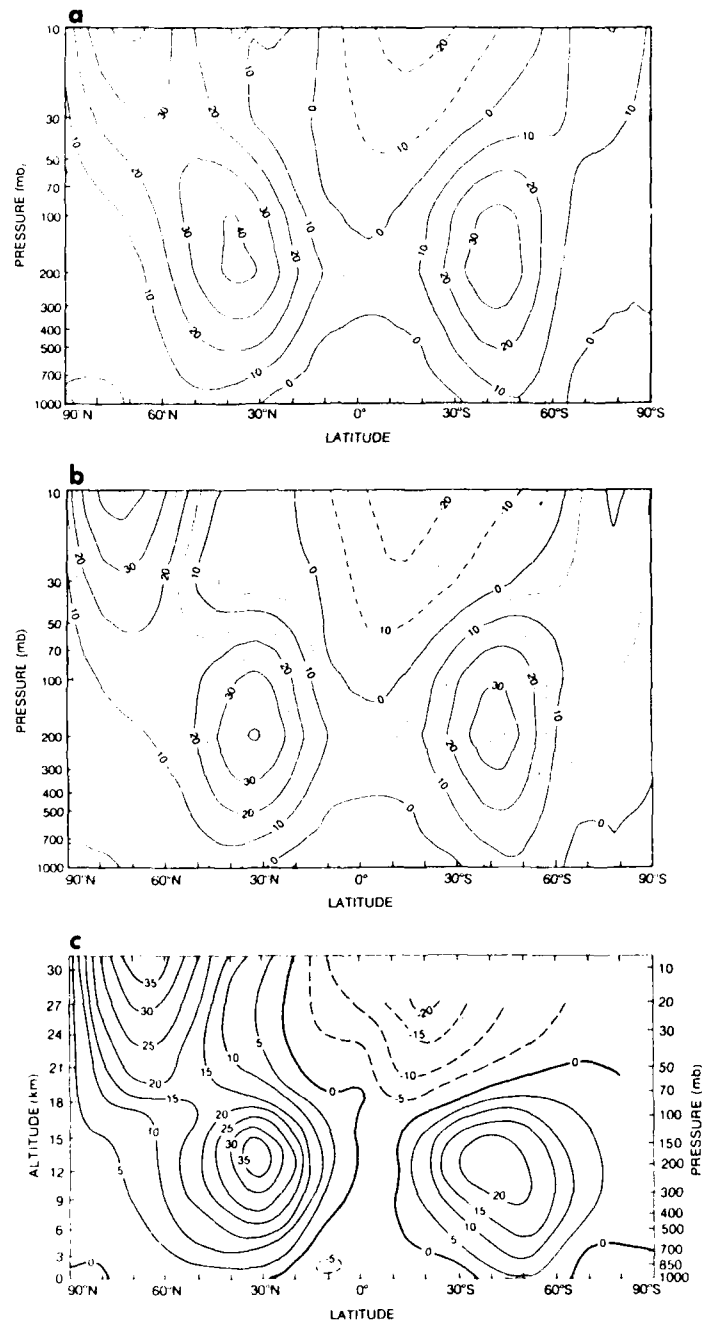


Fig. 5. The effect of orographic gravity-wave drag on zonally averaged westerly winds as simulated by the Canadian Climate Centre atmospheric GCM for the Dec.-Feb. season. (a) Control simulation without wave drag. (b) Simulation with wave drag. (c) Observed climatological mean zonal flow (Newell et al., 1972). Note the effect of wave drag in reducing the westerly bias in the upper troposphere and lower stratosphere (50-150 mb) in the northern hemisphere so as to provide a more realistic separation between the tropospheric jet and the lower part of the polar night westerly flow. From McFarlane (1987).



The parameterizations used in general circulation models are technically first-order closure schemes. For boundary layers, second-order closure models have been very successful (G. Mellor, Princeton University, Princeton, NJ). In second-order closure models, the diffusion coefficients depend on the kinetic energy and on the length scale of the subgrid turbulence. The energy and length scale are determined by additional prognostic equations. It seems premature at this point to extend such higher-order schemes to the general circulation of the ocean interior with its different subgrid-scale processes.

*Potential vorticity conservation.* In the absence of molecular diffusion, Ertel's potential vorticity of a fluid parcel is conserved. This conservation law severely constrains the interaction between geostrophic flows (which carry potential vorticity) and internal gravity waves (which do not). In the absence of molecular diffusion, internal gravity waves will only redistribute the potential vorticity. Internal wave induced diffusion coefficients are inadequate to describe this interaction since they inherently dissipate potential vorticity variance. If molecular diffusion is taken into account, internal gravity waves can modify the geostrophic flow in regions of wave breaking where molecular processes are enhanced. However, considering critical layer absorption, it is found that internal gravity waves produce Ekman mean flows which tilt isopycnals without modifying the geostrophic flow, unless this flow is horizontally sheared (E. Kunze, University of Washington, Seattle, WA). For a realistic oceanic wave spectrum, the tilting reduces the buoyancy frequency on a time scale of  $O(100 \text{ y})$ , comparable to the time it would take the classical diffusion coefficient of  $10^{-4} \text{ m}^2 \text{ s}^{-1}$  to diffuse away the pycnocline.

*Horizontal versus isopycnal mixing.* Diffusion in three-dimensional physical space requires specification of a diffusion tensor. The orientation of this tensor is not known, a priori. The principal axes may lie in and orthogonal to the geopotential, isopycnal, neutral or any other surface (T. McDougall, Commonwealth Scientific and Industrial Research Organization, Hobart, Tasmania). The orientation is important. Horizontal diffusion across sloping isopycnal surfaces becomes cross-isopycnal diffusion.

Most numerical models use a diagonal diffusivity tensor in the horizontal/vertical coordinate system, with the vertical diffusivity much smaller than the horizontal one. This choice is based on the rationale that horizontal mixing by mesoscale eddies is much more efficient than vertical mixing by small scale turbulence. Since mesoscale eddies mix or rather stir along isopycnal surfaces, some researchers argue that horizontal mixing should refer to isopycnal mixing and that the diffusivity tensor should be diagonal in the isopycnal/diapycnal system. This idea receives additional support from the fact that exchange of water particles on isopycnals does not require any work against gravity. However, neither argument is fully convincing. Mesoscale eddies can transport properties across *mean* isopycnals, as they are resolved in coarse models, by processes such as baroclinic instability. Secondly, exchange of water parcels on horizontal (i.e., geopotential) surfaces also does not require any work. Furthermore, potential energy is released when two water parcels are exchanged within the wedge between the horizontal and isopycnal surface (D. Olbers). At present, there is no convincing theoretical argument for any specific orientation of the diffusion tensor.

*Interior versus boundary mixing.* Diapycnal mixing coefficients in the main pycnocline have been inferred from dissipation measurements, the probability of internal gravity wave breaking, the internal gravity wave energy flux to high wavenumbers and inverse calculations. In the main pycnocline, all these estimates fall consistently in the range from  $5 \cdot 10^{-6}$  to  $5 \cdot 10^{-5} \text{ m}^2 \text{ s}^{-1}$ , an order of magnitude smaller than the abyssal recipe value  $10^{-4} \text{ m}^2 \text{ s}^{-1}$  required to satisfy abyssal heat and fresh water budgets with a vertical advective/diffusive balance. A possible resolution of this discrepancy is that vigorous diapycnal mixing at the side-wall boundaries of the ocean, in combination with along-isopycnal advection and stirring, causes an effective diapycnal mixing of the required value of  $10^{-4} \text{ m}^2 \text{ s}^{-1}$ . Internal waves reflecting off a sloping bottom might provide the energy source for such vigorous sidewall mixing. Assuming that the higher wavenumber reflected waves break and produce mixing, an energy flux is calculated that might sustain an abyssal equivalent diffusivity of the required magnitude (C. Garrett, Dalhousie University, Halifax, Nova Scotia). This mechanism favors low latitudes and steep slopes.

Though interior and boundary mixing may have similar effects on the distribution of passive tracers, the dynamics of the flow are profoundly altered. If all mixing happened near the boundaries all the bottom water would be upwelled in the boundary layers. The interior of the ocean would be quiescent except for the need to transfer fluid from one boundary layer to another (T. McDougall). This circulation differs from the smooth poleward flow of Stommel and Arons (1960) where the spatially uniform upwelling must be driven by interior mixing. If the deep circulation is not controlled by mixing at all but solely by the shape (hypsometry) of the basins, then an anticyclonic circulation with equatorward interior flow is predicted (P. Rhines).

*Rate control.* Molecular diffusion is the ultimate agent of diapycnal mixing. Only molecular diffusion transports tracers across actual instantaneous density surfaces; mesoscale eddies, internal gravity waves and small-scale turbulence do not. However, all these motions can move tracers across *mean* isopycnal surfaces, and it is the flux across such mean isopycnals that is relevant in general circulation models. The question then arises: what controls this flux or the rate of diffusion? It may well be that this flux is set by the mesoscale eddy field and that all the other smaller scale motions "just do what needs to be done" (C. Garrett), similar to the classical example of three-dimensional turbulence in a homogeneous, non-rotating fluid where energy is cascaded to the dissipation scales without any back-effect on the larger scales. However, the flux across mean isopycnals might equally well be set by the nature of diapycnal mixing, with mesoscale eddies just doing what needs to be done. If much more powerful computers were available it would be a simple task to integrate an eddy resolving model on thermodynamic time scales, calculate the mean isopycnals and the fluxes across them, and check whether or not these fluxes depend on the value of the diffusivity.

## CONSENSUS

This was an opportunity for numerical modelers and small-scale observers to sit in the same room and compare observations of small-scale processes with their representation in models. Many questions came up; only a few could be answered. It

is apparent that we are just beginning to scratch the surface of this important problem. Although many issues remain unresolved, a consensus was reached on what we need to do next:

Foremost, we need to *identify the physical mechanisms* that lead to mixing. "Tuning," i.e., choosing coefficients such that the models best reproduce a particular data set, is not sufficient. A model with such tuned parameters does not have any predictive value and provides no assurance that it will perform properly in other dynamical regimes. The same is true for the diffusion coefficients derived from inverse methods, since these coefficients only "explain" a specific data set and different coefficients may be required for altered circumstances.

Increasing the resolution, though important, is also not sufficient. It must be accompanied by a proper and adjusted representation of the newly resolved and still unresolved physical processes. Atmospheric models show that certain systematic errors not only remain but become accentuated with increased resolution. Only the inclusion of specific physical processes, such as momentum transfer by gravity waves, leads to further improvement.

Second, there was agreement that we need to continue the ongoing efforts:

- to make direct flux measurements by either the correlation method or by tracer release experiments to validate our indirect estimates from dissipation measurements,
- to assess the relationship between directly measured diffusion coefficients and those inferred by inverse methods,
- to further resolve the mesoscale eddy field in primitive equation models to explicitly calculate their effect, and
- to explore the parameter dependence of general circulation models by carrying out more sensitivity studies.

With respect to diapycnal mixing, the participants perceived as the major physical issues, with far-reaching consequences for observational and modeling programs:

- interior versus boundary mixing, and
- rate control by mesoscale eddies.

The parameterization of small-scale processes in numerical models is a basic issue. It will only be resolved as numerical modelers, theoreticians and small-scale observers collaborate, pooling their expertise and resources and providing essential cross-checks for each other. The meeting in Honolulu was an attempt to stimulate such collaboration and it is encouraging that many of the participants left the meeting with joint projects on their minds - in the best of the Aloha spirit.

The names in parentheses refer to lectures given at the meeting. These lectures will be published in the proceedings of the workshop. We thank all participants of the workshop for their input into this report and for their permission to quote

unpublished material and Crystal Miles is thanked for expert editorial advice. Copies of the proceedings are available from Peter Müller, Department of Oceanography, University of Hawaii, 1000 Pope Road, MSB 429, Honolulu, HI 96822.

The fifth 'Aha Huliko'a Hawaiian Winter Workshop was held from January 17 to 20, 1989, in Honolulu and is supported by Department of Navy Grant N00014-89-J-1226 issued by the Office of Naval Research. The United States Government has a royalty-free license throughout the world in all copyrightable material contained herein. This report is Hawaii Institute of Geophysics Contribution No. 1949.

## REFERENCES

- Bryan, F., 1987. Parameter sensitivity of primitive equation ocean general circulation models. *J. Phys. Oceanogr.*, 17, 970-985.
- McFarlane, N. A., 1987. The effect of orographically excited gravity wave drag on the general circulation of the lower stratosphere and troposphere. *J. Atmos. Sci.*, 14, 1775-1800.
- Munk, W. H., 1966. Abyssal recipes. *Deep Sea Res.*, 13, 707-730.
- Newell, R. E., J. W. Kidson, D. G. Vincent and G. J. Boer, 1972. *The general circulation of the tropical atmosphere and interactions with extratropical latitudes*. Vol. 1, The MIT Press, 258 pp.
- Stommel, H. and A. B. Arons, 1960. On the abyssal circulation of the world ocean. I. Stationary planetary flow patterns on a sphere. *Deep Sea Res.*, 6, 140-154.

# REPORT DOCUMENTATION PAGE

1a REPORT SECURITY CLASSIFICATION <b>Unclassified</b>		1b RESTRICTIVE MARKINGS	
2a SECURITY CLASSIFICATION AUTHORITY		3 DISTRIBUTION/AVAILABILITY OF REPORT Approved for public release; distribution unlimited	
2b DECLASSIFICATION/DOWNGRADING SCHEDULE		5 MONITORING ORGANIZATION REPORT NUMBER(S)	
4 PERFORMING ORGANIZATION REPORT NUMBER(S)		7a NAME OF MONITORING ORGANIZATION Office of Naval Research	
6a NAME OF PERFORMING ORGANIZATION Hawaii Institute of Geophysics	6b OFFICE SYMBOL (If applicable)	7b ADDRESS (City, State, and ZIP Code) Department of the Navy 800 N. Quincy Street Arlington, Virginia 22217	
6c ADDRESS (City, State, and ZIP Code) 2525 Correa Road Honolulu, Hawaii 96822	8a NAME OF FUNDING/SPONSORING ORGANIZATION	8b OFFICE SYMBOL (If applicable)	9. PROCUREMENT INSTRUMENT IDENTIFICATION NUMBER N00014-89-J-1226
8c ADDRESS (City, State, and ZIP Code)	10 SOURCE OF FUNDING NUMBERS		
	PROGRAM ELEMENT NO	PROJECT NO 4229013-01	TASK NO WORK UNIT ACCESSION NO
11 TITLE (Include Security Classification) Parameterization of Small-Scale Processes			
12. PERSONAL AUTHOR(S) Müller, Peter and Henderson, Diane (eds.)			
13a TYPE OF REPORT Workshop Proceedings	13b TIME COVERED FROM 12/1/88 TO 1/30/89	14 DATE OF REPORT (Year, Month, Day) September 1989	15 PAGE COUNT 362
16. SUPPLEMENTARY NOTATION Proceedings, 'Aha Huliko'a, Hawaiian Winter Workshop, January 1989, Honolulu, Hawaii			
17 COSATI CODES		18 SUBJECT TERMS (Continue on reverse if necessary and identify by block number)	
FIELD	GROUP	SUB-GROUP	
		general circulation models, eddy resolving models, parameterization, subgrid-scale processes, parameter sensitivity, mixing (diapycnal, isopycnal, interior,	
19 ABSTRACT (Continue on reverse if necessary and identify by block number) These proceedings contain the lectures given at the fifth 'Aha Huliko'a Hawaiian Winter Workshop on the "Parameterization of Small-Scale Processes" and a summary of the workshop, which appeared in EOS (Transactions, American Geophysical Union). The lectures and the summary cover the major aspects and issues of representing subgrid-scale mixing processes in oceanic general circulation models.			
20 DISTRIBUTION/AVAILABILITY OF ABSTRACT <input checked="" type="checkbox"/> UNCLASSIFIED/UNLIMITED <input type="checkbox"/> SAME AS RPT <input type="checkbox"/> OTIC USERS		21. ABSTRACT SECURITY CLASSIFICATION Unclassified	
22a NAME OF RESPONSIBLE INDIVIDUAL		22b TELEPHONE (Include Area Code)	22c OFFICE SYMBOL

18. Subject Terms (continued)

→ boundary), diffusion, stirring, finestructure, microstructure,  
dissipation, JZJ